Isotopic constraints on the palaeoenvironmental conditions during the Cambrian radiation of animals

Thesis by
Tianchen He

A dissertation submitted to University College London
in accordance with the requirements for award of the degree of
Doctor of Philosophy

Department of Earth sciences

Author's Declaration

I, Tianchen He, confirm that the work presented in this thesis is my own. Where information has been derived from other sources, I confirm that this has been indicated in the thesis.

Abstract

Debates around the triggers for the Cambrian radiation have long focused on oxygenation events, weathering history and marine chemistry during the Ediacaran–Cambrian transition. However, high-resolution palaeoenvironmental constraints remain unsatisfactory regarding both long-term evolution and short-term shifts that directly tie into the early Cambrian fossil records and geological events. In the following thesis, a multi-proxy approach combining stratigraphic and geochemical analyses is presented that investigates the marine successions in Siberia and China, and draws on the environmental backdrop and triggers during the animal radiation events and Botomian–Toyonian extinction. This study miniaturises and validates the existing carbonate-associated sulphate (CAS) extraction methods, and suggests that a thorough leaching in NaCl solution reduces the risk of contamination from non-CAS sulphur phases. Applying high-fidelity geochemical methods and rigid screening techniques for diagenesis evaluation, this thesis presents paired, continuous and high-resolution carbonate carbon, CAS sulphur and carbonate strontium isotope trends for the Cambrian stages 2-4. These new data suggest that cyclical redox fluctuations exerted a direct control on the episodic pattern of early animal radiations, while low oceanic sulphate concentrations below modern levels likely persisted through the early Cambrian. High continental weathering flux may have dominated through Cambrian stages 2 and 3, implying high marine ion (e.g. Ca^{2+}) and nutrient availability in the coeval oceans that could have facilitated animal diversification and calcium-favouring biomineralisation. This thesis also reports the first global seawater LOWESS-fitted $^{87}Sr/^{86}Sr$ curve from the latest Ediacaran to Cambrian Stage 4. New stratigraphic interpretations and detrital zircon ages provide the first robust constraints on the timing and position of the 'Great Unconformity' on the North China Craton (NCC). Provenance analysis further demonstrates the affinity between NCC and eastern Gondwana during the Cambrian Period.

Acknowledgements

I am particularly grateful to my PhD supervisors Prof Graham A. Shields and Dr Philip Pogge von Strandmann. They gave so much guidance and helped with both my academic and daily life in London.

I would like to thank the following people for their support, without whose help this thesis would never have been possible: Dr Peter M. Wynn, Dr Rosalie Tostevin, Gary Tarbuck and Prof John McArthur gave much valuable advice for the development of CAS extraction method and suggestions on the CAS sulphur isotope studies. The Sr isotope studies were made possible benefited from the support from Prof Matthew F. Thirlwall, Dr Christina J. Manning and Dr Ying Zhou. Dr Pieter Vermeesch, Dr Martin Rittner and Prof Andrew Carter provided technical assistance in all the detrital zircon dating work.

Support was also given by the institutes in Nanjing and my Chinese supervisors and collaborators Prof Maoyan Zhu, Prof Hongfei Ling and Dr Da Li, who partly funded the work in the initial sampling stages and contributed to the discussions in this thesis. I am also indebted to my research comrades Rosalie Tostevin, Rehemat Bhatia, Ying Zhou, Long Yu, Lanyun Miao, Jieming Niu, Ahai Chen and Liu Liu who worked alongside me in the last wonderful four years.

I also thank my thesis examiners Prof Bridget Wade and Dr Tais W. Dahl for their valuable suggestions and discussions.

Finally, I am grateful to have the trust and unconditional support from my parents and my beloved wife Hepin Wu.

I dedicate this thesis to my family

Glossary of common abbreviations

AECE	Archaeocyathid Extinction Carbon isotope Excursion
AVS	Acid volatile sulphur
BACE	BAse of Cambrian isotope Excursion
BTE	Botomian–Toyonian extinction
CARE	Cambrian Arthropod Radiation isotope Excursion
CAS	Carbonate-associated sulphate
CIs	Confidence intervals
DIC	Dissolved inorganic carbon
DICE	DrumIan Carbon isotope Excursion
DOC	Dissolved organic carbon
EA-IRMS	Elemental analysis-isotope ratio mass spectrometer
FAD	First appearance datum
GSSP	Global boundary stratotype section and point
HBRE	Hawke bay regression event
ICP-MS	Inductively coupled plasma mass spectrometer
ICP-OES	Inductively coupled plasma optical emission spectrometer
LIP	Large igneous province
LOWESS	LOcally Weighted scatterplot smoothing
MICE	MIngxinsi Carbon Isotope Excursion
MSR	Microbial sulphate reduction
NCC	North China Craton
NOE	Neoproterozoic oxygenation event
PAL	Present atmospheric levels
ROECE	*Redlichiid-Olenellid* Extinction Carbon isotope Excursion
SAS	Secondary atmospheric sulphate
SCC	South China Craton
SIS	Strontium isotope stratigraphy
SPICE	Steptoean Positive Carbon Isotope Excursion
SSFs	Small shelly fossils
TIMS	Thermal ionization mass spectrometer
TOCE	Top of Cambrian Excursion
TTG	Tonalite-Trondhjemite-Granodiorite
VCDT	Vienna-Canyon Diablo Troilite
ZHUCE	ZHUjiaqing Carbon isotope Excursion
$\delta^{13}C_{carb}$	Carbon isotopic composition of carbonate
$\delta^{18}O_{carb}$	Oxygen isotopic composition of carbonate
$\delta^{34}S_{SW}$	Sulphur isotopic composition of seawater sulphate
$\delta^{34}S_{CAS}$	Sulphur isotopic composition of carbonate-associated sulphate
$\delta^{34}S_{pyr}$	Sulphur isotopic composition of pyrite
$^{34}\varepsilon_{mic}$	Sulphur isotope fractionation during microbial sulphate reduction
$\Delta^{34}S_{SW\text{-}pyr}$	Sulphur isotope fractionation between pyrite and seawater sulphate

Contents

List of Figures

List of Tables

Chapter 1

Introduction

Author Contributions: This chapter benefitted from discussions with Graham A. Shields, Philip Pogge von Strandmann and Maoyan Zhu.

1.1. Thesis aims and outline

The aim of this thesis is to establish a high-resolution and high-fidelity isotopic chemostratigraphic framework (C, S and Sr isotope stratigraphy) of the lower Cambrian for global stratigraphic correlation reference, to provide up-to-date chronological and stratigraphic constraints on the key geological and biological events in the early Cambrian, and then to combine these geochemical proxies to reconstruct the long-term marine redox conditions and continental weathering history during the Cambrian radiation of animals and early Cambrian extinction events. The studies within this thesis are presented as a series of independent research chapters, some of which have been published, submitted or are due to be submitted, as publications.

Chapter 1 reviews and appraises the triggers for the Cambrian radiation and Botomian-Toyonian extinction, and presents the geological background and stratigraphic settings for the investigated sections and samples.

Chapter 2 presents a miniaturised and high-fidelity method for carbonate-associated sulphate (CAS) extraction. The refined method ensures the extraction of primary seawater sulphate sulphur isotope signals from ancient bulk carbonate precipitates, and provides a protocol for future sulphur isotope stratigraphy study. This Chapter also validates the method by testing carbonate samples of the late Ediacaran Nama Group.

Chapter 3 applies the CAS extraction method developed in *Chapter 2* to the early Cambrian carbonate samples of the Siberian Aldan-Lena Rivers sections and Xiaotan section, South China. The study reports paired carbonate carbon and CAS sulphur isotope data, which represents the first, continuous, high-resolution and high-fidelity sulphur isotope record in the Cambrian stages 2-4. The results also provide insight into both long-term evolution and short-term shift in marine redox structure and pattern that accompanied the Cambrian radiation and Botomian–Toyonian extinction.

Chapter 4 presents new analyses of carbonate strontium isotope of the Siberian Aldan-Lena Rivers sections. The study applies sequential leaching and rigid screening technique to

minimise the diagenetic imprints on the seawater strontium isotopic signals. The study also resolves the early Cambrian seawater strontium isotope trends into an up-to-date LOWESS-fitted $^{87}Sr/^{86}Sr$ curve calibrated using a consistent age model. The plausible relationship between early Cambrian geological events (e.g. sea-level change, large igneous province eruption) and $^{87}Sr/^{86}Sr$ trends are also discussed.

Chapter 5 presents new stratigraphic evidence of the Cambrian 'Great Unconformity' in Huaibei and Dalian regions of North China. This chapter reports new analyses of U-Pb detrital zircon dating from Tonian–Cambrian successions of the southeastern North China Craton (NCC). Together with constraints by maker fossils and radiometric ages of diabase intrusions, the study provides a firm chronological framework for the position and duration of the 'Great Unconformity' on the NCC. The study also discusses the provenance affinity between the NCC and East Gondwana in the early-mid Cambrian.

Chapter 6 is the synthesis of these individual investigations, and seeks to highlight the questions raised in this thesis. Conclusions and concepts for further work are also included in this chapter.

1.2. Definition of the lower/early Cambrian

The Cambrian refers to the first period of the Phanerozoic Eon or Paleozoic Era, spanning a geological time interval approximately from 541 to 485.4 Ma. Historically, it was subdivided into early, middle, and upper parts (Peng, Babcock and Cooper, 2012). Then a new fourfold chronostratigraphic scheme (corresponding to series/epochs) rather than the threefold one, emerged from the International Commission on Stratigraphy (Fig. 1.1). However, the 'lower/early Cambrian' mentioned in the current thesis includes the first two series/epochs (Terreneuvian and Series 2) or four stages/ages (Fortunian–Stage 4) in the new scheme of the geological timescale. The duration of the early Cambrian in this study is thereby regarded as about 33 Myr, ranging from 541 to ~509 Ma as shown in Fig. 1.1.

The base of the Fortunian Stage is defined by the first appearance datum (FAD) of the ichnofossil *Treptichnus pedum* in Newfoundland (Narbonne *et al*., 1997). It reflects the first appearance of complex sediment-disturbing or bioturbation behaviour by animals. However, since the time of boundary ratification, it has been shown that the lowest occurrence of *T. pedum* is below the stratigraphic horizon of the Global boundary Stratotype Section and Point (GSSP) (Gehling *et al*., 2001). Besides, a regional unconformity and its unique siliciclastic facies at this section hinder the stratigraphic correlation among carbonate successions using small shelly fossils (SSFs) and carbon isotope records, respectively. As an alternative, the BACE (BAse of Cambrian isotope Excursion), which is a globally correlated negative $\delta^{13}C$ excursion, has been recently proposed to be a more reliable non-biostratigraphic marker for the base of the Cambrian System (Li *et al*., 2009; Landing *et al*., 2013; Li *et al*., 2013).

On the other hand, the base of Cambrian stages 2, 3 and 4 have not been formally defined. The FAD of the small shelly fossils *Watsonella crosbyi* or *Aldanella attleborensis*, which have a wide distribution in pre-trilobitic strata and occur in both carbonate and siliciclastic successions globally (Babcock, 2005), are being considered as suitable candidates for marking the base of Stage 2. However, Landing *et al*. (2013) suggest that FAD of *W. crosbyi* and *A. attleborensis* are diachronous while the positive $\delta^{13}C$ ZHUjiaqing Carbon isotope Excursion (ZHUCE) (see Fig. 1.1 and Fig 3.5 of studied Xiaotan section, South China), which is bracketed by the lower ranges of the above two SSF species, would be a better definition of the base of Stage 2.

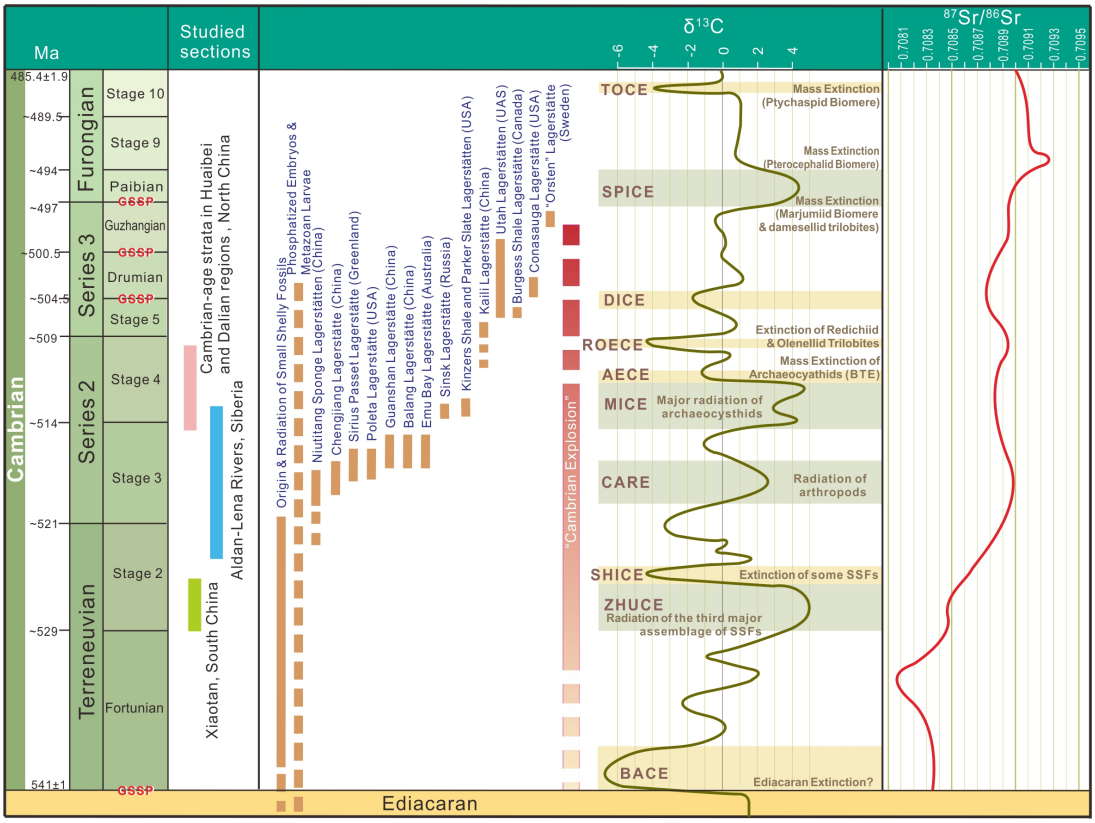

Figure. 1.1: Compilation of chronostratigraphy and chemostratigraphy of the Cambrian System and comparison to major biotic events. Modified from Peng, Babcock and Cooper (2012). $\delta^{13}C$ records and comparison to extinction events are modified from Miller *et al*. (2006) and Zhu, Babcock and Peng (2006). BACE: BAsal Cambrian Carbon isotope Excursion; ZHUCE: ZHUjiaqing Carbon isotope Excursion; SHICE: SHIyantou Carbon isotope Excursion; CARE: Cambrian Arthropod Radiation isotope Excursion; MICE: MIngxinsi Carbon Isotope Excursion; AECE: Archaeocyathid Extinction Carbon isotope Excursion; ROECE: *Redlichiid-Olenellid* Extinction Carbon isotope Excursion; DICE: DrumIan Carbon isotope Excursion; SPICE: Steptoean Positive Carbon Isotope Excursion; TOCE: Top of Cambrian Excursion; BTE: Botomian-Toyonian extinction. The strontium isotope trend ($^{87}Sr/^{86}Sr$) is a composite curve derived from data for the Upper Terreneuvian and lower Series 2 (Derry *et al*., 1994); Upper Series 2 through Series 3 (Montañez *et al*., 1996); the Furongian (Saltzman *et al*., 1995; Kouchinsky *et al*., 2008) and the uppermost part of Stage 10 (Ebneth *et al*., 2001). The time interval of sampled geological sections in this thesis, including Xiaotan (~528.7-526.7 Ma), Aldan-Lena Rivers (~523-513 Ma), Cambrian-age strata in Huaibei and Dalian regions (~515-510 Ma), are marked with green, blue and pink rectangle respectively.

The base of Stage 3 has traditionally been taken to approximate the FAD of the first trilobite, which is equivalent to the base of Siberian Atdabanian Stage. But for the same reason of diachroneity, the positive $\delta^{13}C$ peak (IV) within the Siberian lower Atdabanian Stage is also suggested as an auxiliary marker for the base of Stage 3 (see Fig. 3.4 of studied Siberian Aldan-Lena Rivers sections for details). The subcommission has favoured placing the base of

Stage 4 at a stratigraphic level coincident with the FAD of a single trilobite genus such as *Olenellus*, *Redlichia* or *Judomia*, while the positive $\delta^{13}C$ MIngxinsi Carbon isotope Excursion (MICE, equivalent to VII at the Siberian lower Botomian Stage; see Fig. 1.1 and Fig. 3.4 for details) might also serve as an auxiliary boundary marker.

Hence, globally correlated carbon isotope excursions have been applied in defining the lower Cambrian stage GSSPs. This emphasises the importance of high-resolution muti-proxy chemostratigraphic study (e.g. C, S and Sr isotopes in this thesis) at suitable sections worldwide to confirm the reliability of isotope signals as global Cambrian stratigraphic markers.

1.3. Radiation of early animals: Cambrian Explosion

The early Cambrian is remarkable for recording a widespread radiation of skeletal animals, known as the Cambrian Explosion or Cambrian radiation. The Cambrian radiation is a long-standing macro-evolutionary phenomenon, which marks the abrupt rises of different, morphologically distinctive bilaterians in the fossil record during the first four ages of the Cambrian Period, including representatives of most of the major animal groups that now exist on Earth. Recent analyses revealed that the divergence of major bilaterian animal clades was in an episodic and step by step fashion. For instance, lophotrochozoans and ecdysozoans diversified during the Cambrian Fortunian, while deuterostomes diversified within the Stage 3 (Erwin *et al*., 2011; Zhang *et al*., 2014). On the other hand, it has been difficult since Darwin's time to determine the fossil record lineages between early Cambrian phyla and their late Ediacaran ancestors, possibly due to the poor preservation and recognisable potential of small, soft-bodied Ediacaran faunas.

Many studies proposed that a significant end-Ediacaran mass extinction wiped out the entire Ediacaran soft-bodied macroscopic organisms. But a recent study by Zhu *et al*. (2017) suggests it was rather a gradual replacement than a sudden extinction event, evidenced by the co-occurrence of both Ediacaran-type and Cambrian-type skeletal fossils in the uppermost Ediacaran strata from Siberia. Moreover, as shown in Fig. 1.1, the exceptionally preserved Fossil-Lagerstätten of the early Cambrian and nearly all major animal radiation events coincide with positive carbon isotope excursions, which are demonstrably global phenomena (Zhu, Babcock and Peng, 2006; Peng, Babcock and Cooper, 2012). Minor or mass extinction events appear to be associated with the negative excursions. The coincident pattern is predicted to reflect a cause-and-effect relationship between the early Cambrian biological and environmental perturbations (Zhu, Babcock and Peng, 2006; Zhu, 2010), but no study has constrained this issue yet.

1.4. Causes of the Cambrian radiation of animals

1.4.1. Developmental and ecological innovations

A wide range of plausible triggers has been proposed to cause the Cambrian radiation (Maloof *et al*., 2010; Erwin and Valentine, 2013; Smith and Harper, 2013; Zhang *et al*., 2014). These include genetic developmental explanations, such as the evolution of Hox genes which could have controlled the body plan diversification of Cambrian bilateral animals (de Rosa *et al*., 1999). However, molecular biology clocks predicted that the genetic developmental system of bilateral animals was already established in the Cryogenian Period about 100 Ma before the actual animal divergence in the Cambrian fossil records (Erwin *et al*., 2011; Zhang and Shu, 2013; Zhang *et al*., 2014). This contradiction suggests an evolutionary lag in the timing of bilateral animal radiation. Other factors such as controls of physical environment could be responsible for such delay (Erwin and Valentine, 2013). The catastrophic Snowball Earth event, which persisted through the Cryogenian, could have interrupted the macroscopic evolutionary processes and delayed the emergence of animals until the latest Ediacaran.

Ecological innovations concerning new trophic capacities such as predation arms race, which describes the first establishment of the ecological relationship between predators and prey. The preceding Ediacaran ocean has few predation activities (Fox, 2016). The Ediacaran macroscopic organisms were largely soft-bodied. They mainly fed from grazing and absorbing on the seafloor or simply filtering the seawater (Erwin and Valentine, 2013). But the Cambrian ocean witnessed a dramatic rise in the predation intensity, evidenced by the first appearance of 'shell-crushing' behaviours (Morris, 1989). Both predators and prey were fighting to survive. And this pressure would force both sides to adapt to each other, evolve simultaneously and become a possible driving force of animal morphological diversification (Sperling, Frieder, *et al*., 2013). Predator-prey relationships would also change dramatically after eyesight (Zhao *et al*., 2013) and skeletonisation evolved for the first time in the early Cambrian (Maloof *et al*., 2010). Both biological developments would have significantly altered the life habit, food webs, and introduced new ecological niches and evolutionary opportunities.

Another important ecological innovation is epitomised by the Cambrian substrate revolution, which describes a transition to intense animal burrowing and sediment-mixing (bioturbation) behaviours on the surface of the ocean floor in the early Cambrian (Bottjer, Hagadorn and

Dornbos, 2000; Boyle *et al*., 2014; Mángano and Buatois, 2014). The development of this function oxygenated the seafloor sediments, increased the food sources, and expanded living habitat for bottom-dwelling lifeforms.

1.4.2. Environmental triggers

Interacting processes within the biosphere and new ecological feedbacks would have in part accelerated the rate of animal radiations in the early Cambrian. But external environmental factors are also crucial to provide a permissive environment before the emergence of animals.

1.4.2.1. Rise in oxygen levels

One environmental trigger that has received much attention, however, is the Neoproterozoic oxygenation event (NOE) (Maloof *et al*., 2010; Shields-Zhou and Och, 2011; Och and Shields-Zhou, 2012). It is known that more complex and advanced animals that are motile or produce biominerals demand higher oxygen concentrations for the intense metabolism, and their evolution throughout Ediacaran and Cambrian shows broad correlations with rising oxygen concentrations (Och and Shields-Zhou, 2012). The NOE occurred between the end of the catastrophic Marinoan glaciation (~635 Ma) and the Cambrian radiation, oxygenated the ocean and atmosphere to 40% of present atmospheric levels (PAL) after the Great Oxidation Event (Canfield, 2005). The NOE has been reconstructed using a combination of different geochemical systems, including the Fe, C and S cycles, rare earth elements, redox-sensitive trace elements (reviewed by Maloof *et al*., 2010; Shields-Zhou and Och, 2011; Och and Shields-Zhou, 2012) and novel chromium and selenium isotope systems (Frei *et al*., 2009; Pogge von Strandmann *et al*., 2015). New molybdenum isotope and concentration data confirmed that at least part of the early Cambrian ocean was well-oxygenated to modern-levels, coinciding with the early Cambrian animal radiation at ~521 Ma (Chen *et al*., 2015).

On the other hand, increase in the bioturbation intensity and areal extent during the Cambrian substrate evolution could regulate the overall phosphorus fixation rate, and thus operated a negative feedback on the nutrient availability in the ocean. As a result, the same process places a negative feedback on the marine organic productivity and oxygen production (Lenton and

Watson, 2000; Algeo and Ingall, 2007; Shields-Zhou and Zhu, 2013). Boyle *et al*. (2014) proposed that dramatic increase in the bioturbation intensity limited the oxygen production during the Cambrian stages 2-4 and resulted in ocean deoxygenation in the stages 3-4. However, a recent study challenged the idea by providing the evidence that mid-depth waters in South China transitioned from anoxic conditions in the Stage 2 to widespread oxic conditions until the Stage 4 (Li *et al*., 2017).

Mills *et al*. (2014) proposed that the last common ancestor of animals could have thrived in oxygen levels as low as 0.5% PAL. And more recent studies reveal that many basins of the late Precambrian ocean might have exceeded requisite oxygen thresholds with well-oxygenated surface layer well before the Cambrian radiation (Sperling, Halverson, *et al.*, 2013; Zhang *et al.*, 2016), which is consistent with quantitative constrains on Proterozoic oxygen level being greater than 1% PAL (Lyons, Reinhard and Planavsky, 2014). Although these redox constraints could merely report localised conditions, it still reveals that low oxygen levels would have only constrained early animal to very small and thin body plans with little metabolic scope, but the Cambrian radiation of early animals was possibly not limited by the oxygen thresholds alone.

Therefore, convincing links between oxygenation and the early Cambrian bio-radiations have hitherto been lacking, pending the arrival of high fidelity geochemical records (e.g. carbon and sulphur isotopes) that tie directly into the fossil record. This thesis aims to address this knowledge gap by correlating the oceanic redox evolutionary pattern with the paired palaeontological data, and to explore the relationship between oxygenation/deoxygenation pattern and radiation/extinction events in the early Cambrian.

1.4.2.2. Shift in seawater chemistry

The questioning of the hypothesis of 'high oxygen level'-induced Cambrian radiation encourages us to reconsider other environmental causes. Many studies have suggested the shifts in seawater composition during the Ediacaran–Cambrian transition as one plausible trigger for the Cambrian radiation. These hypotheses include high weathering rate on the trans-Gondwana mountains (Brasier and Lindsay, 2001), shift from aragonite to calcite seas (Porter, 2007), and 'Great Unconformity' effect (Peters and Gaines, 2012).,

Assembly of Gondwana is involved in the polyphase accretion of formerly disparate blocks (Fig. 1.2), which is accomplished along East Africa, Brasiliano, Kuungan and Damaran orogenies and resulted in an extensive mountain chain by the earliest Cambrian (541-530Ma) (Li and Powell, 2001; Meert, 2003; Campbell and Squire, 2010). Erosion of these elevated trans-Gondwana mountains would have had a significant impact on seawater chemistry and global climate, providing nutrients (e.g. phosphorus) to boost marine primary production during the Cambrian Explosion. Analyses of primary fluid inclusions from terminal Proterozoic (ca. 544 Ma) and early Cambrian (ca. 515 Ma) marine halites indicate that seawater Ca^{2+} concentrations increased approximately threefold in the early Cambrian (Berner, 2004; Brennan, Lowenstein and Horita, 2004). This shift facilitated the first utilisation of calcite production by biomineralisation during the Cambrian radiation. The calcium-favouring skeletonisation is also supported by the evolution of the Mg/Ca ratio of seawater, as it exhibits a shift from aragonite to calcite seas during Cambrian Stage 2 (Porter, 2007).

A novel hypothesis links the 'Great Unconformity' to the Cambrian Explosion (Peters and Gaines, 2012; He *et al*., 2016). The 'Great Unconformity' separates Precambrian continental crystalline basement rock from much younger Cambrian shallow marine sedimentary deposits in several palaeocontinents. It involved the widespread continental denudation followed by an extensive physical reworking of soil, regolith and basement rock, and enhanced chemical weathering of continental crust during the first continental-scale marine transgression in the early Cambrian (Brasier and Lindsay, 2001; Haq and Schutter, 2008). These processes could also serve as mechanisms to affect seawater chemistry, e.g. increase of Ca^{2+} concentrations and nutrient availability in seawater, and thus promoting biomineralisation among the first calcium-dominated skeletal animals in the Cambrian Stage 2 (Porter, 2007).

Although early Cambrian animal radiation has long been recognised as the most important step in animal evolution, poorly constrained chemostratigraphic correlation and chronological uncertainties have hindered its detailed palaeoenvironmental study. An additional problem is that recent research has tended to focus on the late Ediacaran rather than the interval during the Cambrian radiation. Consequently, this study understands that a permissive environment (e.g. breaching oxygen and nutrient thresholds) was already established in the late Ediacaran for the emergence of earliest animals, but there is still considerable ambiguity with regard to the environmental explanation of the timing, radiation pattern and scale of Cambrian radiation.

1.5. Botomian–Toyonian extinction

Subsequently after the remarkable early animal diversification occurred between the Cambrian Fortunian and Stage 3, there followed a global generic diversity fall among archaeocyaths, other reef-associated and many trilobite faunas (Zhuravlev and Wood, 1996). Echinoderms and lingulid brachiopods, by contrast, passed through this event relatively unscathed. This bio-crisis, known as the Botomian–Toyonian extinction (BTE), occurred from the mid Stage 3 and through the early-mid Stage 4, and is stratigraphically best constrained on the Cambrian Siberian platform (Brasier, Corfield, *et al*., 1994; Fig. 1.7).

The BTE includes two episodes of major archaeocyathan and trilobite extinctions. The first one is Sinsk event, which occurred during the mid Stage 3 (corresponding to Botomian in Siberia), which is noted on all major palaeocontinents in the early Cambrian (Zhuravlev and Wood, 1996). The cause of the Sinsk event in Siberia has been linked to marine anoxia by Zhuravlev and Wood, (1996), who suggested that it was triggered by an extensive encroachment of anoxic deep water into the shallow-water environment during the Botomian transgression based on sedimentary observations of widespread accumulation of non-bioturbated laminated black shales in tropical shallow-water settings. These black shales are commonly enriched in pyrite, and organic matter which is typical of anoxic conditions. On the other hand, the anoxia has also been attributed to eutrophication and resultant phytoplankton blooms. The stratigraphy on the Siberian platform suggests that phosphate-rich horizons noted by Cook and Shergold (1984) occur at stratigraphic horizons two trilobite biozones above and three zones below the Sinsk Formation (Brasier, Corfield, *et al*., 1994). Phosphorus should have been present in excess relative to normal nutrient requirements, and lead to persistent phytoplankton blooms, resulting in anoxia. This ‘eutrophication-induced’ hypothesis is also supported by the presence of abundant fleshy algae (e.g. chlorophytes) in Sinsk Formation. Isotopic anomalies characterise the BTE-Sinsk event include $\delta^{13}C$ spikes (MICE and AECE; Brasier, Corfield, *et al*., 1994) as well as low $^{87}Sr/^{86}Sr$ values compared to the earlier record (Derry *et al*., 1994), but none of them have been discussed by geochemical constraints.

Another major extinction episode of BTE occurred during the subsequent Hawke bay regression event (HBRE) in the early Stage 4 (corresponding to early Toyonian in Siberia) (Zhuravlev and Wood, 1996; Rowland and Shapiro, 2002). The HBRE represents a global

marine regression event (Hallam and Wignall, 1999), and is possibly bracketed by a series of high-frequency sea-level oscillations at Milankovitch scale (Haq and Schutter, 2008). The timing of the HBRE in Siberia, western and eastern Laurentia is poorly defined and possibly diachronous (Dilliard *et al*., 2007). Globally chemostratigraphic correlation for this event is also poorly constrained. Some late episodes of the BTE might be linked to the eruption of the Kalkarindji large igneous province (LIP) of northern Australia in the latest early Cambrian (Hough *et al*., 2006). LIP-induced extreme hothouse conditions and oceanic anoxia provides a compatible environmental model to explain the BTE, but recent high-precision dating work reveals that Kalkarindji LIP occurred at ca. 510.7 ± 0.6 Ma in the late Stage 4 (Jourdan *et al*., 2014), suggesting a later event proceeding the BTE. Therefore, the age correlation between BTE (mid Stage 3–mid Stage 4) and LIP remains to be tested.

Although many causes have been proposed to trigger the BTE, all these hypotheses derived from lithological, sedimentological and quantitative palaeontological data, thus awaiting detailed palaeoenvironmental analysis using geochemical proxies to explore the possible mechanisms responsible for the extinction. This thesis will address the issue by providing detailed geochemical constraint on the redox conditions, continental weathering extent and oceanic chemistry during this crucial interval.

1.6. Geology of studied sites and samples

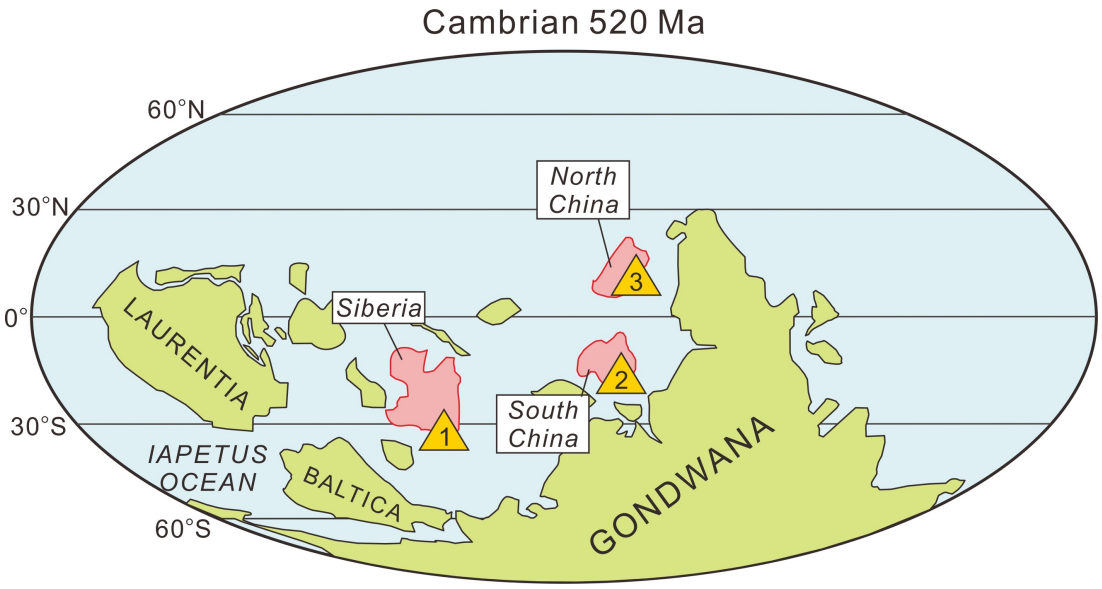

Figure. 1.2: Early Cambrian palaeogeographic reconstruction at ~520 Ma and locations for the studied sites. Modified after Torsvik and Cocks (2013). The location for North China Craton relative to Gondwana supercontinent is modified to match the reconstruction by new detrital zircon data in Chapter 5 although the exact location is still debatable. Yellow triangles mark the locations of stratigraphic sections at the 1-Aldan-Lena Rivers (eastern Siberia); 2-Xiaotan (South China); 3-Cambrian-age strata in Huaibei and Dalian regions (North China). Locations for the Laurentia, Baltica palaeocontinents and Iapetus Ocean are also shown on the map. Location for the late Ediacaran-age Namibian Zebra River section is not shown, but Namibia was probably located at the core of Gondwana during the early Cambrian as part of the Damara and Gariep belt in the Pan-African Orogeny (Gresse and Germs, 1993).

A summary of the sampling positions of Cambrian materials relative to an absolute timescale, biological events, long-term isotope trends and palaeogeographic reconstruction in the early Cambrian is illustrated in Fig. 1.1 and Fig. 1.2. Field collections of marine carbonate for chemostratigraphic study and siliciclastic rocks for detrital zircon dating were conducted as part of this study. Samples were obtained at four globally separated sites from southern Namibia (Nama Group at Zebra River section), South China (Dahai Member at Xiaotan section), eastern Siberia (Aldan-Lena Rivers sections) and southeastern North China Craton (Tonian-Cambrian successions in Huaibei and Dalian regions). Geological settings and sample descriptions of these sections are given in chronostratigraphic order as follow.

1.6.1. Tonian–Cambrian successions in Huaibei and Dalian regions, North China Craton

The Huaibei and Dalian regions are geologically situated at the southeastern margin of the North China Craton (NCC), and are located along the rims of the Jiao-Liao-Ji belt (Fig. 1.3a), which is a Paleoproterozoic orogenic belt (~1.9 Ga) that divides the eastern Block of the NCC into two sub-blocks in the northwest (Longgang Block) and southeast (Langrim Block) (Zhao *et al*., 2005). Neoproterozoic–Cambrian successions are well exposed, including the Huaibei Group in Huaibei region (Fig. 1.3b) and Jinxian Group in Dalian region (Fig. 1.3c). Given that both regions were contiguous during the Neoproterozoic–Cambrian transition, they share a similar litho- and biostratigraphic record (Wang *et al*., 1984; Hong, Huang and Liu, 1991; Xiao *et al*., 2014). However, neither of these formal lithostratigraphic groups follow the international standard practice in that their included formations, although contiguous, do not have 'significant and diagnostic lithologic properties in common' (Murphy and Salvador, 1999). In both regions, one could easily argue that the topmost formation has more in common with overlying Cambrian units, which are characterised by a reddish colour, evaporite pseudomorphs and planar-bedded mottle limestone, than with those beneath, which are characterised by stromatolitic build-ups and molar-tooth structure.

In *Chapter 5*, the study focuses on the upper parts of the Huaibei and Jinxian groups and their adjacent Cambrian strata. Thirteen siliciclastic samples, which are ideal for U-Pb detrital zircon dating, were collected from five sections in the two regions (Fig. 1.3d), including Heifengling section, Gouhou section, Jinshanzhai section, Longwangmiao section and Manjiatan section. Samples were collected by Tianchen He and Ying Zhou (UCL) during two field trips to Huaibei and Dalian regions in 2013 and 2014. Stratigraphic context of these sections is reported in *Chapter 5* as part of the supporting evidences to the discussion. A compilation of samples and U-Pb ages is shown in Appendix F.

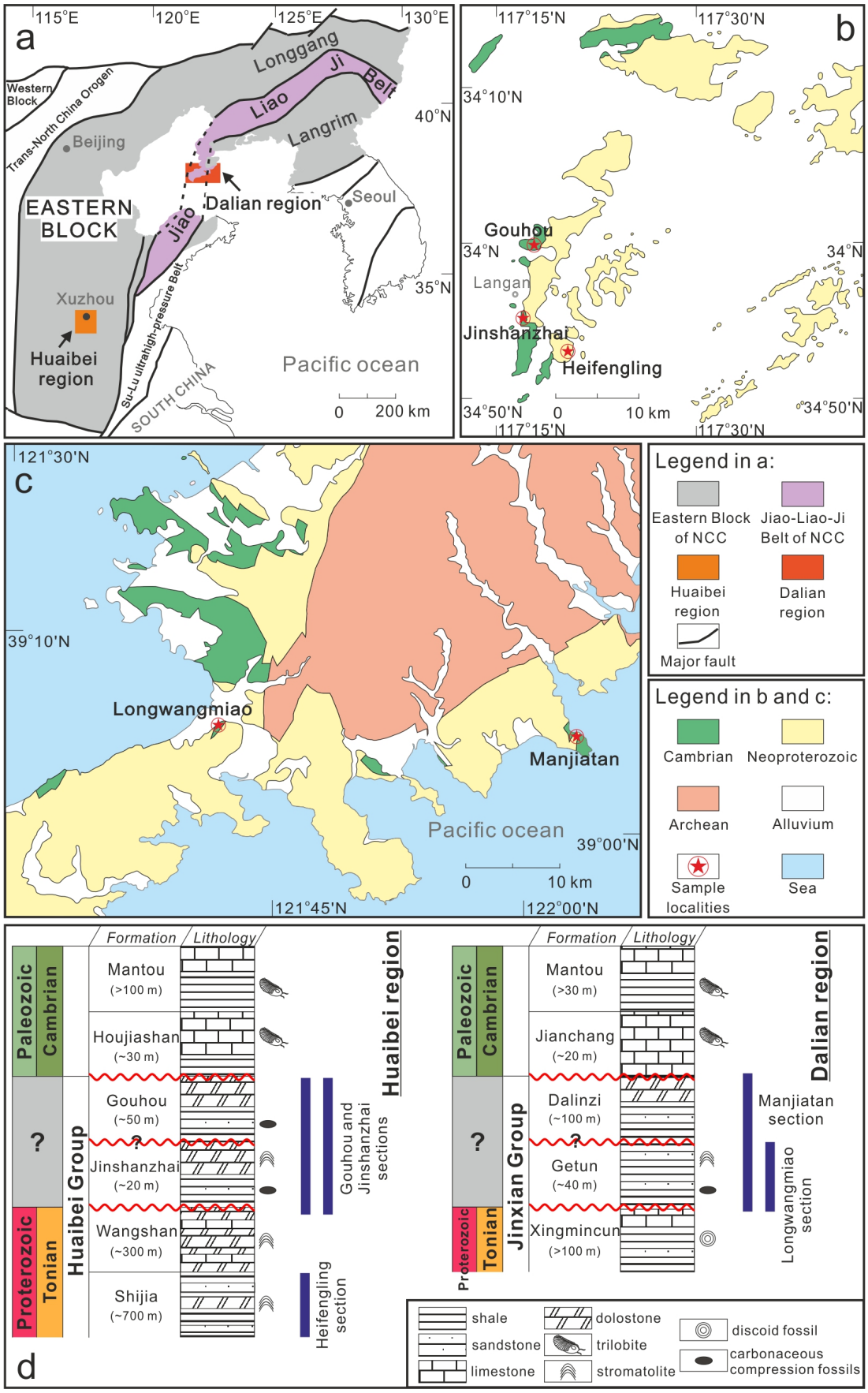
a
115°E
120°E
125°E
130°E
40°N
35°N
Western Block
Trans-North China Orogen
Beijing
Longgang
Ji
Belt
Liao
Langrim
Dalian region
Seoul
EASTERN BLOCK
Jiao
Xuzhou
Huaibei region
Su-Lu ultrahigh-pressure Belt
SOUTH CHINA
Pacific ocean
0
200 km
b
117°15'N
117°30'N
34°10'N
Gouhou
34°N
Langan
Jinshanzhai
Heifengling
34°50'N
0
10 km
c
121°30'N
39°10'N
Longwangmiao
Manjiatan
Pacific ocean
39°00'N
121°45'N
122°00'N
Legend in a:
Eastern Block of NCC
Jiao-Liao-Ji Belt of NCC
Huaibei region
Dalian region
Major fault
Legend in b and c:
Cambrian
Neoproterozoic
Archean
Alluvium
Sample localities
Sea
d
Formation
Lithology
Paleozoic
Cambrian
Mantou
(>100 m)
Houjiashan
(~30 m)
?
Gouhou
(~50 m)
Jinshanzhai
(~20 m)
Wangshan
(~300 m)
Proterozoic
Tonian
Huaibei Group
Shijia
(~700 m)
Huaibei region
Gouhou and Jinshanzhai sections
Heifengling section
Mantou
(>30 m)
Jianchang
(~20 m)
Dalinzi
(~100 m)
Getun
(~40 m)
Xingmincun
(>100 m)
Jinxian Group
Dalian region
Manjiatan section
Longwangmiao section
shale
sandstone
limestone
dolostone
trilobite
stromatolite
discoid fossil
carbonaceous compression fossils

Figure. 1.3: Overview geological map showing the eastern North China Craton and adjacent terranes, simplified from Zhao *et al*. (2005). (b) Geological map of Huaibei region with sample localities. (c) Geological map of Dalian region with sample localities. NCC: North China Craton. (d) Lithostratigraphic column of the investigated Tonian–Cambrian successions in Huaibei and Dalian regions. Names and distribution of investigated sections are marked next to the sample localities in b, c and next to the stratigraphic column in d, respectively.

1.6.2. Nama Group, Zebra River section, Namibia

The Namibian Nama Group is a mixed carbonate-siliciclastic sequence deposited in a ramp system, which hosts terminal Ediacaran fauna, including soft-bodied fossils belonging to the Ediacaran biota and the skeletal metazoans, *Cloudina*, *Namacalathus* and *Namapoikia* (Grant, 1990; Grotzinger, Watters and Knoll, 2000; Wood, 2002; Hall *et al*., 2013; Penny *et al*., 2014). The Nama Group spans from the late Ediacaran to early Cambrian, and includes three Subgroups (Kuibis, Schwarzrand, and Fish River Subgroup in ascending stratigraphic order; Fig. 1.4a). Trace fossils have been reported from the Omkyk Member of Kuibis Subgroup (Macdonald, Pruss and Strauss, 2014), consistent with the beginnings of infaunal bioturbation noted globally during this time (McIlroy and Logan, 1999).

The investigated Zebra River section is situated in the Zaris basin from southern Namibia. Nama Group of this section spans the Kuibis Subgroup, and includes the late Ediacaran Omkyk and Hoogland Members in ascending stratigraphic order (see Fig. 1.4b). Zebra River is a distal inner ramp section, hosting laterally extensive microbial reef systems, and associated skeletal fossils, <35 mm (Wood, 2011). An ash bed in the lowermost Hoogland Member of the Kuibis Subgroup provides robust U–Pb zircon age constraints at 548.8 ± 1 Ma (Grotzinger *et al*., 1995), revised to 547.36 ± 0.31 Ma by Bowring *et al*. (2007).

In *Chapter 2*, fifty-one well-preserved carbonate samples from the Omkyk and Hoogland members at Zebra River section, were used in the validation test study for carbonate-associated sulphate (CAS) extraction method. Samples were collected by Dr Rosalie Tostevin (University of Oxford). A summary of paired CAS and pyrite sulphur isotope data is shown in Table 2.5.

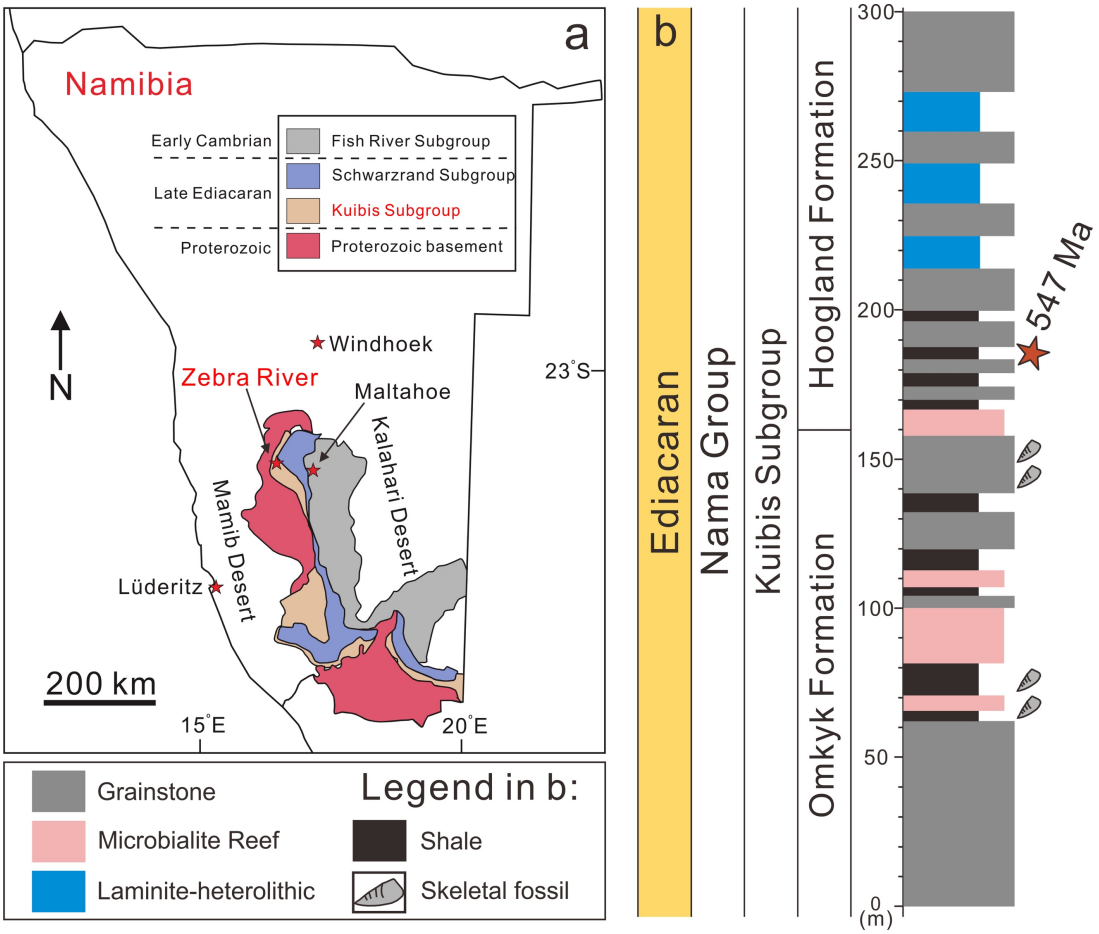

Figure. 1.4: Simplified geological map of Namibia (a), showing the location of Zebra River section in the Kuibis Subgroup of the Nama Group; litho- and biostratigraphy (b) of Zebra River section. Modified from Tostevin *et al*. (2017). The age for lower Hoogland Formation is given at 547.36 ± 0.31 Ma by ash bed U-Pb zircon dating from Bowring *et al*. (2007).

1.6.3. Dahai Member, Xiaotan section, South China

The Xiaotan section is situated on the southern bank of the Jinsha River in Yunnan Province, South China. It exhibits a stratigraphic column spanning an interval from the late Ediacaran to Cambrian Stage 3. This study focuses on the limestone horizons (Dahai Member of Zhujiaqing Formation) of Xiaotan section, covering the lower part of Cambrian Stage 2 (Fig. 1.5b). The Dahai Member comprises pale, thickly bedded limestone, underlain by phosphatic Zhongyicun Member and overlain by siliciclastic Shiyantou Formation. Sedimentary and lithofacies evolution of the Xiaotan section indicates that the upper Ediacaran and lower Cambrian successions in NE Yunnan Province were deposited in an offshore intra-basin and shallow water setting within the Yangtze Platform (Fig. 1.5a). And the gradual transition from

thinly bedded Zhongyicun phosphorite layers to thickly bedded Dahai limestone represents a rise in sea-level and a consequent increase of sedimentary rate (Li *et al*., 2013).

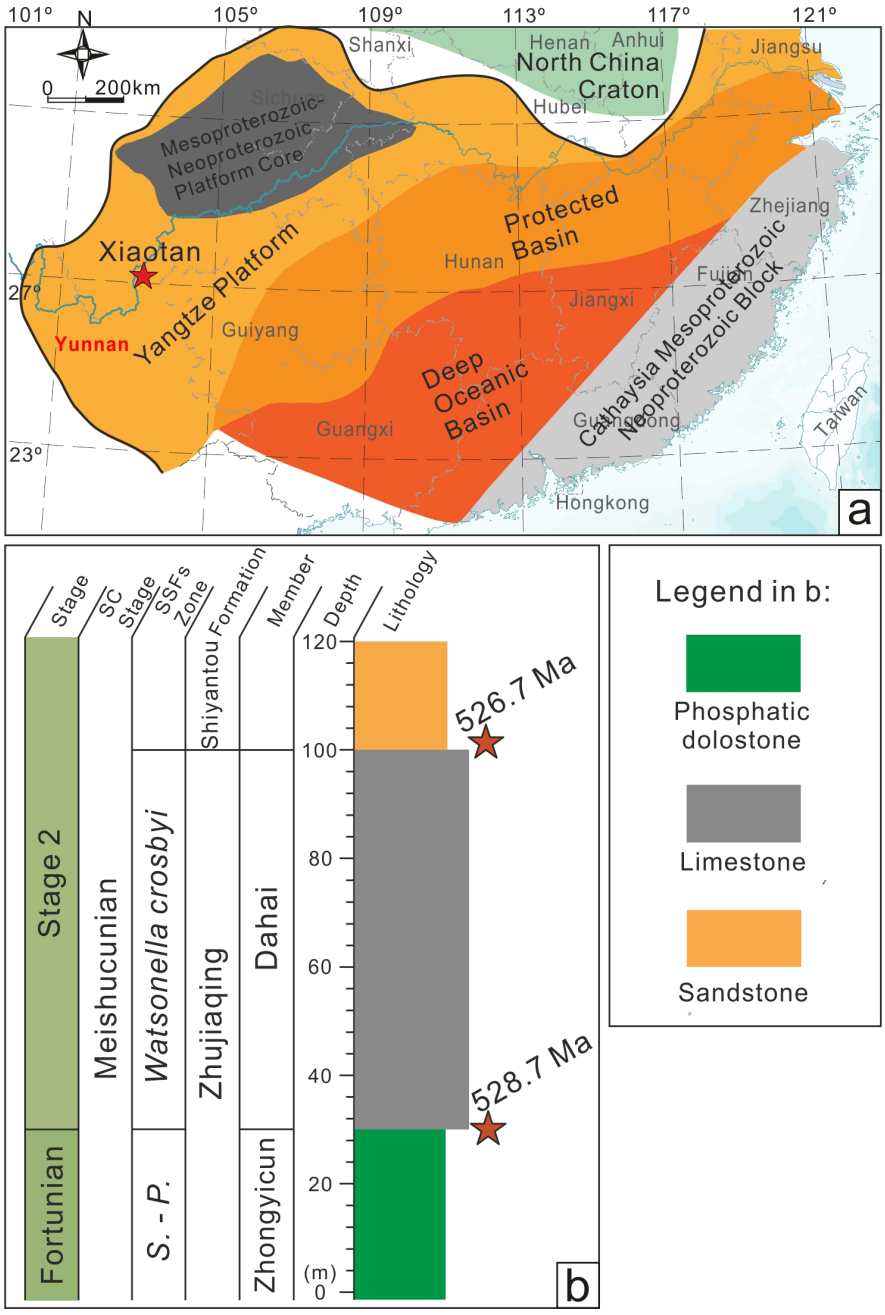

Figure. 1.5: Simplified geological map of South China (a), showing the location of Xiaotan section in Yunnan Province, modified after Och *et al*. (2013); litho- and biostratigraphy (b) of Xiaotan section, modified after Li *et al*. (2013). SC Stage: South China Stage subdivision; SSFs: Small Shelly Fossils; *S*. – *P*.: *Siphogonuchites triangularis* – *Paragloborilus subglobosus*. Ages for the base and top of Dahai Member are given by tuffs zircon SIMS U-Pb dating at ~528.7 Ma and 526.7 Ma respectively.

No large fossils have been discovered at Xiaotan and the known fossil record is limited to small shelly fossils. Three SSFs assemblage biozones are preserved in Zhongyicun Member (*Anabarites trisulcatus - Protohertzina anabarica* zone in the lower part and *Siphogonuchites triangularis - Paragloborilus subglobosus* zone in the upper part), Dahai Member (*Watsonella crosbyi*) and Shiyantou Formation (*Sinosachites - Tannuolina* zone in its upper part).

Importantly, the Dahai Member preserves the small shelly fossil zone *Watsonella crosbyi* and an uninterrupted positive $\delta^{13}C$ ZHUjiaqing Carbon isotope Excursion (ZHUCE) (Li *et al*., 2013; see Fig. 3.5 for details of $\delta^{13}C$ data), of which both were suggested as potential global stratigraphic markers for the base of the Cambrian Stage 2 (Landing *et al*., 2013; Li *et al*., 2013). U-Pb tuffs zircon dating gives absolute age constraints at the base and top of Dahai Member with ~528.7 Ma and ~526.7 Ma respectively (personal communication with Dr Chuan Yang from Institute of Geology and Geophysics, Chinese Academy of Sciences).

In *Chapter 3*, twenty-three well-preserved limestone samples from the Dahai Member at Xiaotan section, were used in the study for carbonate-associated sulphate sulphur isotope analysis. Samples were collected by Graham Shields. A summary of sulphur isotope data is shown in Appendix A. Carbonate strontium isotope data reported by Li *et al*. (2013) at the Xiaotan section are also integrated into the discussion of *Chapter 4*.

1.6.4. Aldan-Lena Rivers sections, eastern Siberia

The region of the type sections of the lower Cambrian subdivisions and their lower boundaries occupies the southeastern part of the Siberian Platform. The main sections are observable along the Aldan and Lena rivers (Fig. 1.6), and were suggested to have formed in normal-salinity, shallow-water, open marine environment (Varlamov *et al*., 2008). Samples were collected from seven lower Cambrian carbonate-dominated sections along the Aldan and Lena rivers, and in ascending Siberia Stage stratigraphic order include Dvortsy section, Isit section, Zhurinsky Mys section, Ulakhan-kyyry-Taas section, Ulakhan-Tyoidukh section, Labaia section and Titary section. These sections are the stratotype type sections for the lower Cambrian stages used in Russia, and a total thickness of the Lower Cambrian sequences is ~600 m spanning an interval from the Cambrian Stage 2 to Stage 4 (Fig. 1.7).

Importantly, the GSSPs of the Cambrian stages 2-4 are not determined, but the provisional international subdivision is mainly based on fossil distribution and the stages established in these Siberian sections. Moreover, since the Aldan-Lena Rivers sections are unique in the abundance of archaeocyathan and trilobite fossils, and many forms were found in different regions of the world, the subdivision of the lower Cambrian stages is mainly based on their distribution and the stages established here which are globally recognised. Stratigraphic correlations among sections are well-established and were examined by the Sino-Russian international working group on the 'Subdivision of the lower Cambrian' (Rozanov *et al.*, 2008), based on lithologic markers, archaeocyathid/trilobite biozones and carbon isotope stratigraphy (Brasier, Rozanov, *et al.*, 1994; Varlamov *et al.*, 2008) (details shown in Fig. 1.7).

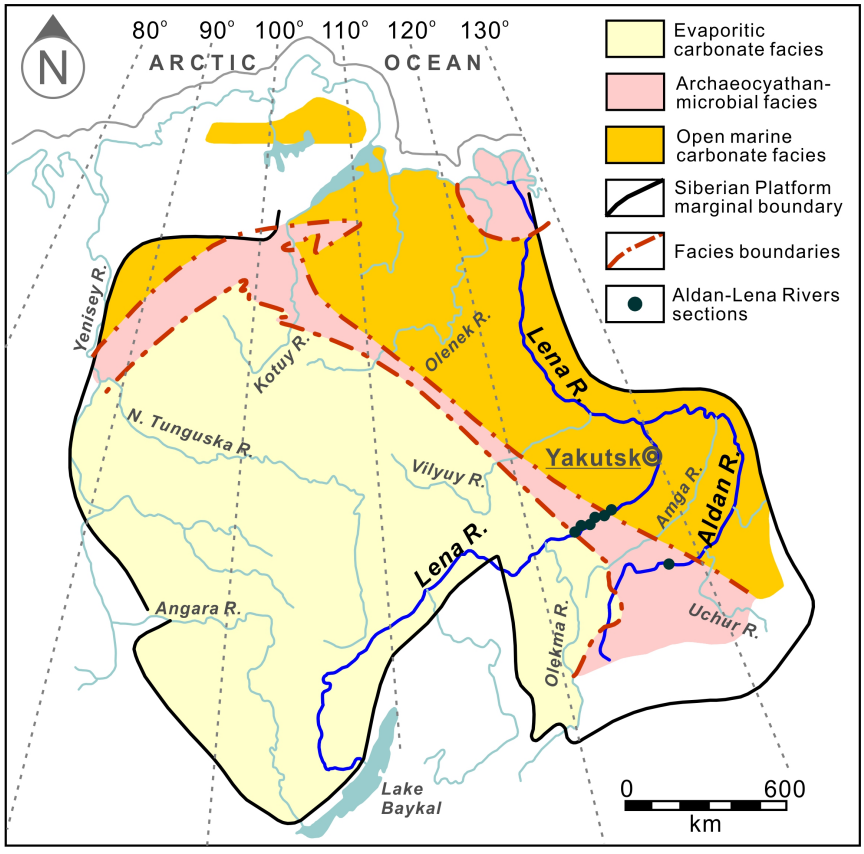

Figure. 1.6: Simplified geological map of the Siberian Platform in the early Cambrian (Brasier, Corfield, *et al.*, 1994), showing modern rivers (R.: river), the distribution of major sedimentary facies and localities of studied sections.

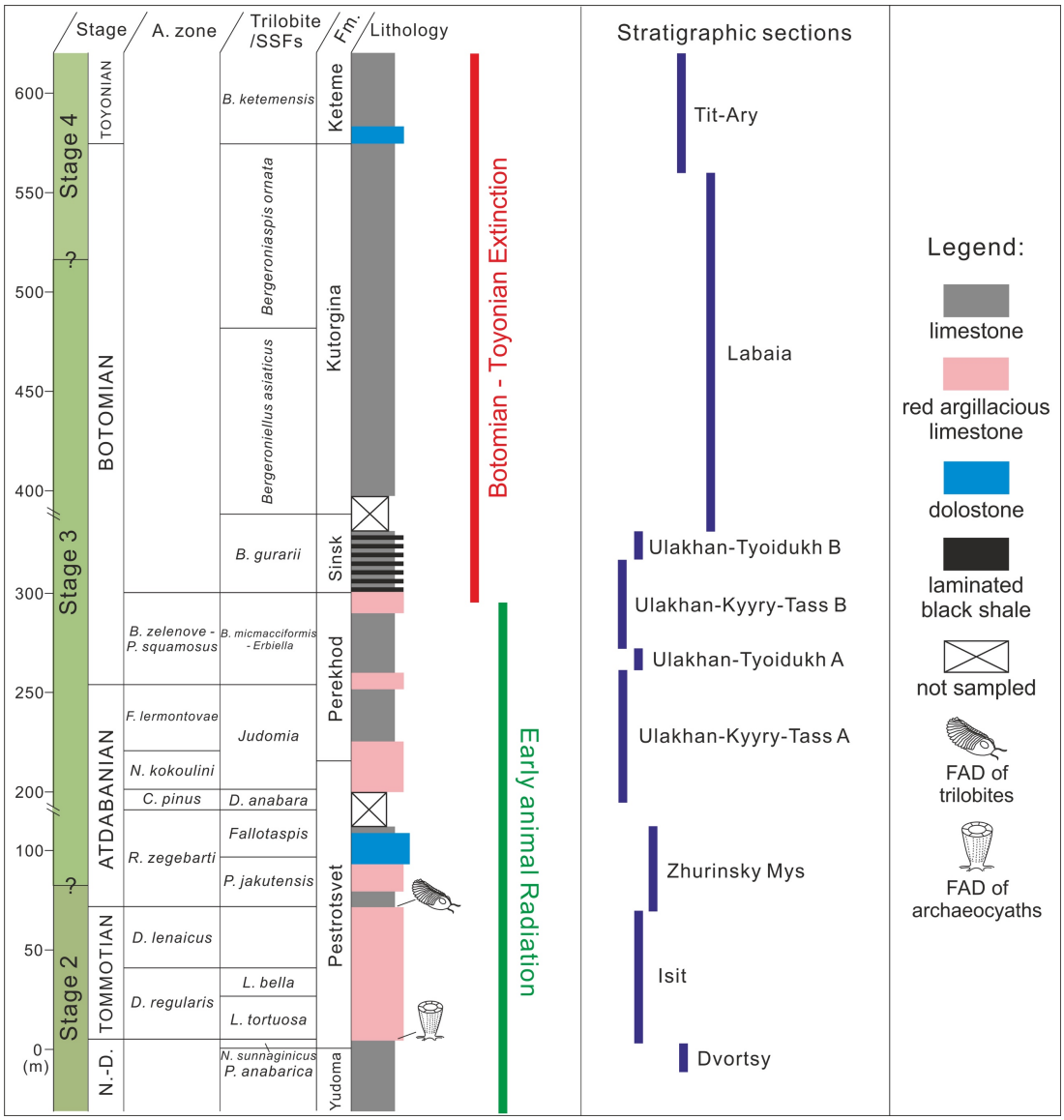

Figure. 1.7: Litho- and biostratigraphy from the Cambrian Stage 2 to Stage 4 of Siberian Aldan-Lena Rivers sections. Regional Siberian stages subdivision is shown next to the global subdivision plan for comparison (Brasier, Corfield, *et al.*, 1994). N.-D.: Nemakit-Dalaynian; A. zone: Archaeocyathid zone; Fm.: Formation; SSFs: small shelly fossils; FAD: first appearance datum. Distribution and covered intervals for the seven studied stratigraphic sections are shown.

Nearly 400 well-preserved carbonate samples were systematically collected following the regional stratigraphic guidebook for the 'Subdivision of the Siberian Lower Cambrian' (Varlamov *et al.*, 2008), with a sampling resolution of roughly 50cm-1m. Samples were collected by Maoyan Zhu (Nanjing Institute of Geology and Palaeontology, Chinese Academy of Sciences) and Aihua Yang (Nanjing University) during the field trip in 2008 following the 2nd Sino-Russian symposium on the lower Cambrian subdivision.

The investigated samples cover a continuous record through the major early animal radiations (Cambrian Explosion) and the first mass extinction event (Botomian–Toyonian extinction) of the Phanerozoic Eon (Brasier, Corfield, *et al.*, 1994; Zhuravlev and Wood, 1996). In *Chapter 2* and *Chapter 3*, some 352 samples were analysed for carbon isotopes and 142 samples for sulphur isotope study. In *Chapter 4*, forty-eight limestone samples were used for strontium isotope and elemental analysis. A detailed compilation of sample list, litho-, bio- and chemostratigraphy of Aldan-Lena Rivers sections is shown in Appendix B, C and D.

Chapter 2

Validating and refining carbonate-associated sulphate extraction method

ABSTRACT

The sulphur isotopic composition of carbonate-associated sulphate (CAS) is widely used to estimate ancient seawater $\delta^{34}S_{sw}$. However, there are concerns about the extraction of pristine marine sulphate from bulk carbonates and associated isotope signatures during cleaning and acid dissolution. CAS is commonly extracted by acid digestion of carbonate after pre-leaching treatment. A major concern is the release and subsequent oxidation of sulphur phases during pre-leaching (e.g. pyrite), as many studies use bleaches such as NaOCl and H_2O_2, which can act as effective oxidants. Before acid dissolution, samples are commonly pre-leached to remove contaminant sulphur, which may include atmospheric sulphate, organic sulphur, or the products of pyrite weathering. Multiple pre-leaches in 10% NaCl solution is considered to provide effective cleaning. In this Chapter, methods for sample pre-treatment as well as barium sulphate precipitation are compared. This study also test the efficiency of consecutive NaCl leaching based on sulphur concentration and isotope composition of NaCl leachates and CAS. Improvements are made to miniaturise conventional CAS extraction procedures. The modified method uses <10g of carbonate per analysis compared to as high as ~250g in previous approaches. Five thorough NaCl pre-leaches are shown to be effective in eliminating contaminated sulphur for carbonates from the investigated geological sections. This study also discusses the new $\delta^{34}S$ data of carbonate-associated sulphate and pyrite from the late Ediacaran-age lower Nama Group, Namibia (~550 to <547 Ma), and use these data to

interrogate terminal Ediacaran sulphur cycle dynamics. Data produced with the improved extraction method show $\delta^{34}S_{CAS}$ as much as 12‰ higher ($\delta^{34}S_{CAS}$-enriched) than previously reported which suggests a re-evaluation of the phenomenon of 'Superheavy' pyrite.

Author Contributions: Tianchen He designed and implemented the CAS extraction method development with supervision from Graham A. Shields and Peter M. Wynn (Lancaster University), and technical assistance from Gary Tarbuck and John McArthur at Wolfson laboratory for environmental geochemistry, University College London. Sulphur isotope analysis was undertaken at Lancaster Environment Centre, Lancaster University (by Tianchen He) and University of Cambridge (by Rosalie Tostevin). The full compilation of $\delta^{34}S_{CAS}$ data and discussion of the Nama Group were reported in Rosalie Tostevin's thesis, but re-evaluated here as part of the CAS extraction method development. The discussion benefitted from helpful conversations with Rosalie Tostevin, Graham A. Shields, Peter M. Wynn, John McArthur, and Philip A. E. Pogge von Strandmann. Some of the text and discussion within this Chapter is adapted from Tostevin et al. (2017).

CHAPTER 2. CAS EXTRACTION

2.1. Introduction

Marine sulphate preserved as carbonate-associated sulphate (CAS) in bulk carbonate precipitates or calcified skeletons is widely used to reconstruct the primary seawater sulphate sulphur isotope composition ($\delta^{34}S_{sw}$) through Earth history. CAS is thought to form when a sulphate ion replaces a carbonate ion in the calcium carbonate mineral structure, whereby sulphur isotopic fractionation during incorporation should be negligible (Staudt and Schoonen, 1995). Metastable carbonate minerals undergo recrystallisation during diagenesis, and so may lose their associated sulphate in terms of CAS concentration, but original CAS sulphur isotope composition ($\delta^{34}S_{CAS}$) are likely retained under most conditions (Kah, Lyons and Frank, 2004; Gill, Lyons and Frank, 2008; Gill *et al*., 2011; Rennie and Turchyn, 2014; Fichtner *et al*., 2017). However, recent studies suggest that the rate and extent of early diagenetic alteration is in part controlled by the sedimentation rate, the recrystallisation rate of unstable carbonate minerals, as well as the relative concentration of sulphate in the pore fluid versus the concentration in the carbonate minerals (Rennie and Turchyn, 2014; Present *et al*., 2015). Although the mechanisms of sulphate incorporation as well as possible diagenetic effects are incompletely understood, efforts have been taken to establish better extraction procedures for the extraction of CAS (Gill, Lyons and Frank, 2008; Wotte, Shields-Zhou and Strauss, 2012).

There are two major aspects that could affect the sulphur isotopic composition of CAS. The first one is host rock diagenetic alteration, which could be constrained by petrographic screening, and geochemical evaluation by analysing carbonate $\delta^{13}C$, $\delta^{18}O$, and diagnostic elemental concentrations (Ca, Mg, Fe, Mn, Sr) as recently summarized by Wotte *et al*. (2012) and Wotte, Shields-Zhou and Strauss (2012). Even if $\delta^{34}S_{CAS}$ is faithfully preserved in the carbonate record, there is the other concern in the analytical aspect about the effective extraction of pristine marine phases and imparted contamination during cleaning and mineral extraction (Wotte, Shields-Zhou and Strauss, 2012; Peng *et al*., 2014). Carbonate samples selected for CAS-extraction may be pre-leached to remove matrix-bound contaminant sulphur-bearing phases from a bulk rock carbonate, which may include secondary atmospheric sulphate (SAS), organic sulphur, or disseminated pyrite, and these generally have a lower $\delta^{34}S$. Of these various contaminants, one major concern is the oxidation of reduced sulphur phases such as pyrite, as many studies use bleaches such as NaOCl and H_2O_2, which can act as effective oxidants (Marenco *et al*., 2008). It was recently suggested that SAS results in widespread contamination of $\delta^{34}S_{CAS}$, particularly in outcrop samples from arid or heavily

polluted regions, as SAS forms a significant component of water leachable sulphate (Peng *et al*., 2014). Multiple pre-leaches in 10% NaCl solution are now suggested for effective cleaning (Wotte, Shields-Zhou and Strauss, 2012; Theiling and Coleman, 2015), but the pre-leaching procedure is not yet standardised. Pre-leaching that is less thorough may not eliminate contaminants before the acid-leaching stage, resulting in acid-leachable sulphate that does not represent primary $\delta^{34}S_{sw}$. On the other hand, most CAS extractions used unreasonably large portions of sample (50-250g) per analysis (Gill, Lyons and Frank, 2008; Luo *et al*., 2010; Gill *et al*., 2011; Wotte *et al*., 2012; Osburn *et al*., 2015), although <10g would generally have enough CAS for analysis. Excessive use of large samples would increase the difficulty of handing during experiment, and thereby higher the possibility of non-CAS sulphur contamination due to inadequate leaching. The intention of this study is to further develop and miniaturise the HCl-$BaCl_2$ sulphate extraction protocol (Wotte, Shields-Zhou and Strauss, 2012) in order to establish guidelines for future CAS studies. Existing methods are evaluated for their efficacy in eliminating non-CAS sulphur phases. The revised method is then tested with randomly selected samples from two Ediacaran–Cambrian carbonate successions including the Ediacaran Zebra River section of Namibia and Cambrian Aldan-Lena Rivers sections of eastern Siberia. Finally, the issues of possible contamination of CAS by present-day secondary atmospheric sulphate are also discussed here (Peng *et al*., 2014).

The $\delta^{34}S_{sw}$ has varied over Earth history as a result of changes in the riverine sulphate flux (e.g. oxidative weathering flux of continental pyrite), the sulphur isotope composition of the riverine sulphate, the sulphur isotope composition of pyrite ($\delta^{34}S_{pyr}$) and the amount of pyrite buried (Claypool *et al*., 1980; Garrels and Lerman, 1981; Berner, 1989). Of these various fluxes, the sulphur isotope composition of pyrite and the amount of pyrite buried remain both the largest lever on $\delta^{34}S_{sw}$ and the closest link to Earth's surface redox state. Sulphate is respired by sulphate reducing microbes in anoxic environments, producing sulphide which is enriched in ^{32}S by up to 47‰ or possibly more (Wortmann, Bernasconi and Böttcher, 2001; Canfield, Farquhar and Zerkle, 2010; Sim, Bosak and Ono, 2011; Leavitt *et al*., 2013). In the modern ocean, the $\delta^{34}S_{sw}$ is globally homogeneous (21.1 ± 0.8‰; Rees, 1978; Johnston *et al*., 2014). $\delta^{34}S_{sw}$ is elevated over riverine input (which is between 3 and 8‰, Canfield, 2013) because of the burial of ^{32}S-enriched pyrite.

Therefore, measurements of $\delta^{34}S_{sw}$ may provide more interpretative power when paired with coeval pyrite $\delta^{34}S_{pyr}$, which preserves the $\delta^{34}S$ signature of the net reduced sulphur produced

during microbial sulphate reduction. Sulphur isotope fractionation during microbial sulphate reduction, $^{34}\varepsilon_{mic}$, depends largely on the rate of microbial sulphate reduction, which is impacted by other environmental factors, including temperature, sulphate concentration, the microbial community and organic carbon source (D.E. Canfield, 2001; Habicht and Canfield, 2001; Wortmann, Bernasconi and Böttcher, 2001; Canfield, Farquhar and Zerkle, 2010; Sim, Bosak and Ono, 2011; Leavitt *et al*., 2013; Bradley *et al*., 2016). Pyrite preserves the apparent sulphur isotope fractionation, $\Delta^{34}S_{sw\text{-}pyr}$, which may differ from $^{34}\varepsilon_{mic}$, and is controlled by sedimentary parameters including sedimentation rate, porosity, and the availability of reactive organic carbon and reactive iron oxides (Fike, Bradley and Rose, 2015).

The Nama Group, Namibia is a well-preserved terminal Ediacaran mixed clastic and carbonate succession, deposited between ~550 and 541 Ma (Grotzinger *et al*., 1995). Previous reports of $\delta^{34}S_{CAS}$ from the Nama Group reveal an unexpected observation, also known as the phenomenon of 'Superheavy' pyrite, whereby the sulphur isotope composition of sedimentary sulphide/pyrite ($\delta^{34}S_{pyr}$) in the bulk rock carbonate is commonly higher than coeval $\delta^{34}S_{CAS}$ (Ries *et al*., 2009). This result does not fit within the accepted frameworks for interpreting marine $\delta^{34}S$, as sedimentary pyrite typically exhibits lower $\delta^{34}S$ compared with coeval sulphate. Abiotic sulphide oxidation produces oxidized sulphate that is depleted in ^{34}S by 4–5‰ (Fry *et al*., 1988), and < 2‰ when microbially mediated (but see Kaplan and Rittenberg, 1964 for fractionations up to 18‰), which could in theory leave the residual sulphide pool 'heavy', but in most natural environments this signal would be overprinted by the larger sulphur isotope fractionation during microbial sulfate reduction which should result in higher $\delta^{34}S_{sw}$ and $\delta^{34}S_{CAS}$ than $\delta^{34}S_{pyr}$ (Canfield, 2001). Here, this study discusses the high-resolution paired CAS-pyrite sulphur isotope data for the Kuibis Subgroup (~550 to <547 Ma) of the Nama Group, from Zebra River section, near Maltahoe, Hardap, Namibia. By applying improved methodologies that minimise the chance of contamination during the cleaning and leaching of carbonate, it produces an improved $\delta^{34}S_{CAS}$ record for the Nama Group. The thorough elimination of contaminants allows this study to verify the presence of any 'superheavy' pyrite.

2.2. Methods

2.2.1. Samples and materials

Eight carbonate samples from the Siberian Aldan-Lena Rivers sections and Namibian Zebra River section were used to test the method for CAS extraction. Descriptions of these samples are given in Table 2.1. Details for geological and stratigraphic settings of these sections and samples are discussed in sections 1.6.2 and 1.6.4. Additionally, fifty-one carbonate samples from the Ediacaran Zebra River section of Namibia were investigated to validate the refined CAS extraction method.

Table. 2.1: List of test samples analysed in this study with ages, sampling locations and lithology.

Sample	Age	Location	Lithology
IST28	early Cambrian	Aldan-Lena Rivers sections/Siberia	Limestone
UKT028	early Cambrian	Aldan-Lena Rivers sections/Siberia	Limestone
UKT043	early Cambrian	Aldan-Lena Rivers sections/Siberia	Limestone
UKT068	early Cambrian	Aldan-Lena Rivers sections/Siberia	Limestone
UT36	early Cambrian	Aldan-Lena Rivers sections/Siberia	Limestone
OS2-1	late Ediacaran	Zebra River section/Namibia	Limestone
OS2-2	late Ediacaran	Zebra River section/Namibia	Limestone
OS2-4	late Ediacaran	Zebra River section/Namibia	Limestone

Large blocks (>200 g) of these carbonates were targeted for sampling, and were cut and polished under the presence of water, in order to trim the weathering surfaces prior to powdering. Then they were cut down into small rock slabs using a water-cooled, diamond tipped bench circular saw. Rock chips were then ground to a fine powder until a few microns in size (flour-like consistency, <10 μm) using a *Retsch*® Agate Mortar grinder. Sample powder was then treated with procedures designed to miniaturise the extraction methods and eliminate any water-soluble non-CAS sulphur contaminant (see in section 2.2.2).

2.2.2. Sample pretreatment

2.2.2.1. Total HCl-leachable sulphur concentration

A large amount of carbonate rock powder (50-250g) per analysis was used for CAS extraction in previous studies (Gill, Lyons and Frank, 2008; Luo *et al*., 2010; Gill *et al*., 2011; Wotte *et al*., 2012; Osburn *et al*., 2015). This not only brings difficulties to the handling of experiments, but also significantly increases the risk of contamination by water-soluble sulphur phases due to inadequate cleaning. However, this study adopted 'small sample volume' (< 10g) to explore and miniaturise the sulphate extraction procedures. To roughly determine the amount of sample required and understand the process of multiple NaCl pre-leaches steps from the beginning, 6M HCl was utilised to dissolve the eight test carbonate samples. The total HCl-leachable sulphur concentration was then analysed. The type and concentration of the acid used here are identical to the one used for CAS extraction after the multiple NaCl pre-leaches.

2.2.2.2. Multiple NaCl leaching technique

Before liberating CAS from the calcite lattice through acid digestion, removing the non-CAS sulphur-bearing compounds or potentially soluble sulphate is essential. Different methods have been developed, primarily using solutions of NaCl (Burdett, Arthur and Richardson, 1989) or simply rinsing with deionised water (Ries *et al*., 2009). Other approaches include using oxidising agents such as NaOCl and H_2O_2 to remove pyrite and organic matter (Shen *et al*., 2011; Xiao *et al*., 2012). However, Wotte, Shields-Zhou and Strauss (2012) have demonstrated that leaching with deionised water does not eliminate non-CAS sulphate, while a single leaching step with NaCl, NaOCl or H_2O_2 is not sufficient to completely remove the non-CAS fraction in a carbonate sample. Thus, repeated pre-leaching is required. On the other hand, in terms of using oxidants, experiments show that leaching with NaOCl and H_2O_2 will generally not remove all pyrite, while both methods may substantially alter the final $\delta^{34}S_{pyr}$ values of reducible sulphur species in a bulk carbonate extracted from chromium reduction procedures (Wotte, Shields-Zhou and Strauss, 2012). The alterations suggest considerable release of NaCl-insoluble sulphur derived from oxidation of reduced sulphur species, and this can overwhelm the relatively small amounts of CAS and thus alter $\delta^{34}S_{CAS}$ values. As a result, recommend consecutive NaCl leaching as future standard protocol, which is applied and verified in this study.

In theory, the required number of pre-leaches depend on the amount and particle size of rock powder, as well as the amount of non-CAS sulphate or readily oxidisable sulphide in a bulk carbonate. Besides, as it is illustrated in Wotte, Shields-Zhou and Strauss (2012)'s results, the non-CAS phases would normally have a lower $\delta^{34}S$ value and much higher sulphate concentration in the NaCl leachate than CAS. Nevertheless, there is still no systematic test to report on this issue. To achieve this purpose, approximately 8-10 g of the fine powder for each sample was leached in 50 ml of 10% NaCl solution for 24 hours to remove the non-CAS sulphur-bearing compounds or potentially soluble sulphate. Importantly, this step was replicated 12 times. Also, to enhance the efficiency of all leaching steps, samples were constantly agitated using a roller mixer at room temperature. Leachates from each step were collected, while remains were rinsed with ultrapure water four times between each leaching and five times after the final leaching. An aliquot of NaCl leachate from each pre-leach was analysed for sulphur concentration. After each leach, the presence of sulphate released in leachates was also tested by adding saturated barium chloride solution to precipitate barite. Barite from the first two pre-leaches of three samples (OS2-1, OS2-2 and OS2-4) were collected for sulphur isotope analysis.

2.2.2.3. Liberation of CAS: acid digestion

All pre-leached carbonate samples were treated with 6M HCl, which was added in calculated aliquots based on total HCl-leachable $CaCO_3$ content. It is noteworthy that this step was completed within 30 mins to minimise the potential for oxidation of reducible sulphur species (e.g. acid volatile sulphur and iron sulphide minerals, including pyrite) during dissolution. Instead of using the complicated, time-consuming vacuum filtration system, the insoluble residue was separated from the solution by centrifugation in the 50ml tube with filtration through *VWR*® 0.2 μm Polypropylene membrane syringe filters (Fig. 2.1).

2.2.2.4. Collection of CAS: barium sulphate precipitation

A method for concentrating CAS as barium sulphate precipitates for sulphur isotope analysis was suggested by Wotte *et al*. (2012). The filtrate after acid digestion was first acidified to a pH below 2, then heated until boiling. Excess 8.5% $BaCl_2$ solution (10% of filtrate volume) was subsequently added to trigger the precipitation. Then the solution was heated three hours at 80°C, cooling overnight, and precipitated at room temperature. These steps were applied to reach the best precipitation conditions within the solution, but may increase the risk of

contamination as the solution is exposed to the air during the long experimental process. However, Wynn *et al*. (2008) used a different but simpler technique. Saturated barium chloride solution (~250 g/L) was added to the filtered carbonate digesting solution using a cleaned polyethylene syringe. Samples were then left to precipitate within the housing of a sealed tube for 2-3 days at room temperature. If there are no visible precipitates seen in the solution after 24 hours, ~2 mg sulphur-free quartz powder (*EuroVector*® isotopic-grade) was added. The quartz powder serves as an inert medium onto which barium sulphate could precipitate, thus increasing the mass of product and enabling ease of handling (Fig. 2.1).

In order to evaluate the two different approaches, duplicate test samples OS2-1, OS2-2 and OS2-4 from the Namibian Zebra River section were directly treated with 6M HCl without consecutive NaCl leaching. A small aliquot of digestion solution (total HCl-leachable) was analysed for sulphur concentration while the rest followed the two precipitation methods respectively. Finally, precipitates were dried and collected in a tin capsule prior to $\delta^{34}S$ analysis via Elemental Analysis-Isotope Ratio Mass Spectrometry (EA-IRMS).

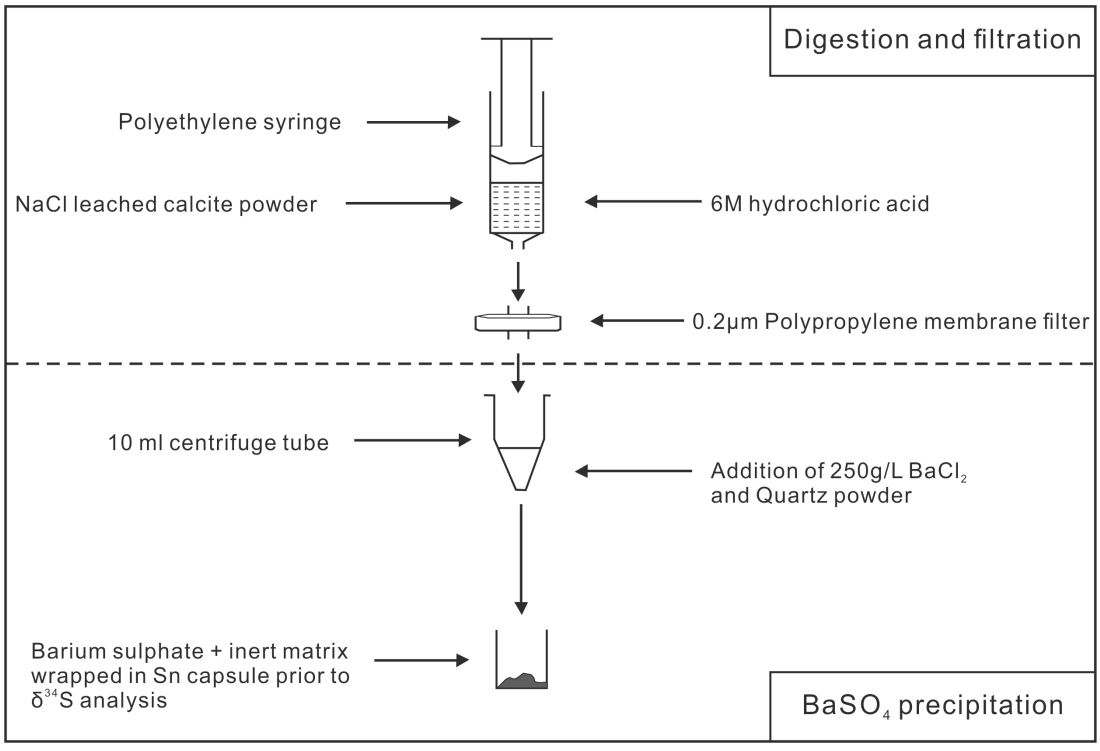

Figure. 2.1: Diagram showing the approaches to extract and concentrate sulphate as barium sulphate prior to $\delta^{34}S$ analysis. The diagram is modified after Wynn *et al*. (2008), illustrating procedures includes the filtration step of acid digestion solution and precipitation of barium sulphate.

2.2.3. Analytical techniques

2.2.3.1. Sulphur concentration analysis

The concentration of CAS and sulphur content in different pre-leaches were measured in aliquots of the filtered acid digestion solution using a *Varian*® 720 Inductively Coupled Plasma Optical Emission Spectrometer (ICP-OES) at the London Geochemistry and Isotope Centre (LOGIC), University College London. Wavelength 182.5 nm was selected to minimise the interference with calcium ions, and analysis was conducted using the N_2-purging polyboost function to avoid the oxygen interference in the system. Detection limit for sulphur in NaCl-matrix is 3 μg/L.

2.2.3.2. Sulphur isotope analysis

The sulphur isotopic composition of test samples OS2-1, OS2-2 and OS2-4 were analysed in Lancaster University. These include $\delta^{34}S$ values in different stages of CAS extraction and comparative $\delta^{34}S$ results from the two precipitation methods. $^{34}S/^{32}S$ analysis of product barium sulphate was undertaken using a *EuroVector*® elemental analyser linked to *Isoprime*® 100 Dual-Inlet mass spectrometer at the Lancaster Environment Centre, Lancaster University. Pellets of $BaSO_4$ precipitate resulting from sulphate extraction with or without the addition of quartz powder were combusted in tin capsules in the presence of excess vanadium pentoxide (V_2O_5) at 1030°C to yield SO_2 for the determination of $\delta^{34}S$. Values were normalised to Vienna-Canyon Diablo Troilite (VCDT) using within-run analyses of international standards NBS-127 and SO5 (assuming $\delta^{34}S$ values of +20.3‰ and +0.49‰, respectively). Within-run standard replication (1sd) was below 0.3‰. Procedural standard solutions of calcium sulphate precipitated as barium sulphate were used to test the integrity of the method. These yielded $\delta^{34}S$ values of +2.7‰ (0.3‰, 1sd, n=12) compared to values of +3.0‰ (0.3‰, 1sd, n=13) for analysis of the raw calcium sulphate powder. Blank contamination associated with $\delta^{34}S$ determination was zero.

Regarding the CAS extraction application to fifty-one samples from Ediacaran Zebra River section, paired $\delta^{34}S$ values of carbonate CAS and chromium reduction pyrite were analysed in University of Cambridge. Acid volatile sulphur (AVS) and iron sulphide minerals, including pyrite, were chemically extracted using HCl and chromous chloride distillation, respectively.

The gas generated during distillation was bubbled through silver nitrate solution to precipitate Ag_2S (Canfield *et al*., 1986). Where sufficient precipitate formed, both AVS and sulphide mineral fractions were retained for analysis. The barite from CAS extraction and silver sulphide from pyrite extraction were weighed into tin cups with an excess of vanadium pentoxide for sulphur isotope analysis at the University of Cambridge. Samples were combusted in a Flash EA coupled through the continuous flow through a magnesium perchlorate trap and gas chromatograph before the gas was introduced to a Delta-Advantage mass spectrometer. $\delta^{34}S$ is reported versus the VCDT standard using within-run analyses of international standards NBS-127 (certified as 20.3‰). Within-run standard replication had an average standard deviation of 0.18‰ (1sd). $\delta^{34}S$ values were corrected for machine drift using this bracketing standard NBS-127.

2.3. Results and discussions

2.3.1. Efficacy of multiple NaCl leaching

As it is shown in Table 2.2 and Fig. 2.2, tested carbonate samples have higher sulphur concentration in the total HCl-leachable solution than in the NaCl pre-leaches. However, combining sulphur contents from all pre-leaches together still gives much lower sulphur content than in the total HCl-leachable solution. This behaviour demonstrates that most sulphur phases sit in the calcite lattice as carbonate-associated sulphate while losing water-soluble sulphur contaminants (e.g. gypsum and anhydrite) during NaCl-leaching. Besides, sulphur concentrations in the NaCl-leachates experienced a dramatic decline through sequential leaching and reached the blank level in the 4th pre-leach (Fig. 2.2), suggesting a guaranteed removal of soluble sulphur contaminants from 10g carbonate power after the 5th leach.

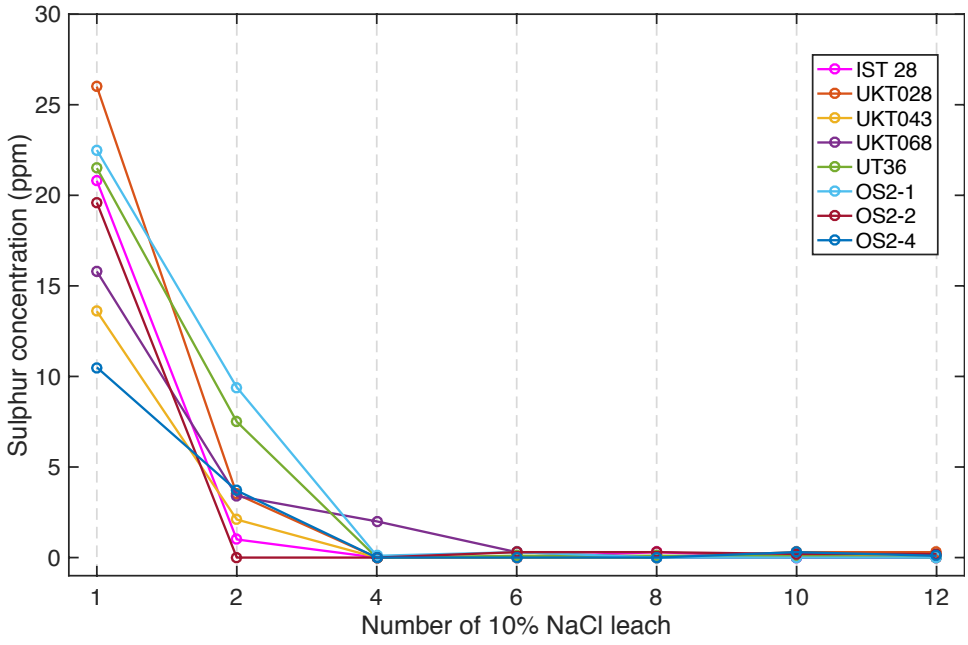

Figure 2.2: Sulphur concentration (ppm) variations in 10% sodium chloride leached solution from different stages of multiple leaching (leach 1, 2, 4, 6, 8, 10, 12). Sulphur concentration levels for blank and 6M HCl in 10% NaCl matrix are normalised to 0 ppm. Test samples IST28, UKT028, UKT043, UKT068, UT36 are Cambrian carbonate from the Siberian Aldan-Lena Rivers sections. OS2-1, OS2-2, OS2-4 are tested Ediacaran carbonate from Nama Group for comparison.

Table. 2.2: Sulphur concentration in the total HCl-leachable phases and sodium chloride leachates from different stages of multiple leaching. Pre-leaches show higher sulphur content in the first two leaches, but nearly no sulphur is observed in leachates after the 4th leach. Results of sulphur concentration are reported as parts per million (ppm). b.d.l.-below detection limit.

Sample	IST28	UKT028	UKT043	UKT068	UT36	OS2-1	OS2-2	OS2-4
HCl-leachable	289.0	220.5	434.2	122.6	166.1	391.2	267.7	506.5
Leach 1	20.8	26.0	13.6	15.8	21.5	22.5	19.6	10.5
Leach 2	1.0	3.5	2.1	3.4	7.5	9.4	b.d.l.	3.7
Leach 4	b.d.l.	b.d.l.	b.d.l.	2.0	b.d.l.	0.1	b.d.l.	b.d.l.
Leach 6	b.d.l.	b.d.l.	b.d.l.	0.3	0.1	0.3	0.3	b.d.l.
Leach 8	0.3	b.d.l.	b.d.l.	b.d.l.	0.1	b.d.l.	0.3	b.d.l.
Leach 10	b.d.l.	0.3	0.1	b.d.l.	0.1	b.d.l.	0.2	0.3
Leach 12	b.d.l.	0.3	0.2	b.d.l.	b.d.l.	b.d.l.	0.2	0.1

This study also measured the sulphur isotope compositions in total HCl-leachable sulphur phases, initially in two pre-leached solutions and carbonate-associated sulphate for three Namibian samples (OS2-1, OS2-2 and OS2-4). Results show much lower $\delta^{34}S$ in HCl-leachable solution by as much as 15.8‰ when compared with $\delta^{34}S_{CAS}$ of carbonate-associated sulphate (Table 2.3 and Fig. 2.3). These results confirm previous findings by Wotte, Shields-Zhou and Strauss (2012) that multiple leaching in 10% NaCl is effective in removing contaminant sulphur, and unremoved would lower the resultant $\delta^{34}S_{CAS}$. The other following pre-leaches did not result in sufficient $BaSO_4$ precipitate for sulphur isotope analysis, suggesting water-soluble contaminant sulphur was removed effectively within the first two pre-leaches for the Namibian test samples. However, it is shown in Fig. 2.3 that there is a decline in $\delta^{34}S$ between the 1st and 2nd leachates. This is probably due to the solubility of different sulphur phases. All in all, these results demonstrated that repeated 10% NaCl pre-leaching with careful water-rinsing between leaches is efficient in eliminating the NaCl-soluble non-CAS phases.

Table. 2.3: Sulphur isotope ratios, $\delta^{34}S$, of the bulk carbonate total HCl-leachable sulphur and first two sodium chloride leachates compared with CAS for three selected samples. Leaches 3–5 did not produce sufficient precipitate for isotopic analysis. Pre-leaches show lower $\delta^{34}S$ compared with final CAS values, consistent with previous method development work by Wotte, Shields-Zhou and Strauss (2012) and Peng *et al*. (2014). Results of $\delta^{34}S$ value are reported as per mil (‰). CAS: carbonate-associated sulphate.

Sample	**OS2-1**	**OS2-2**	**OS2-4**
HCl-leachable	21.5	35.4	14.8
Leach 1	33.1	36.9	20.5
Leach 2	25.4	29.7	16.4
CAS	35.0	40.1	29.5

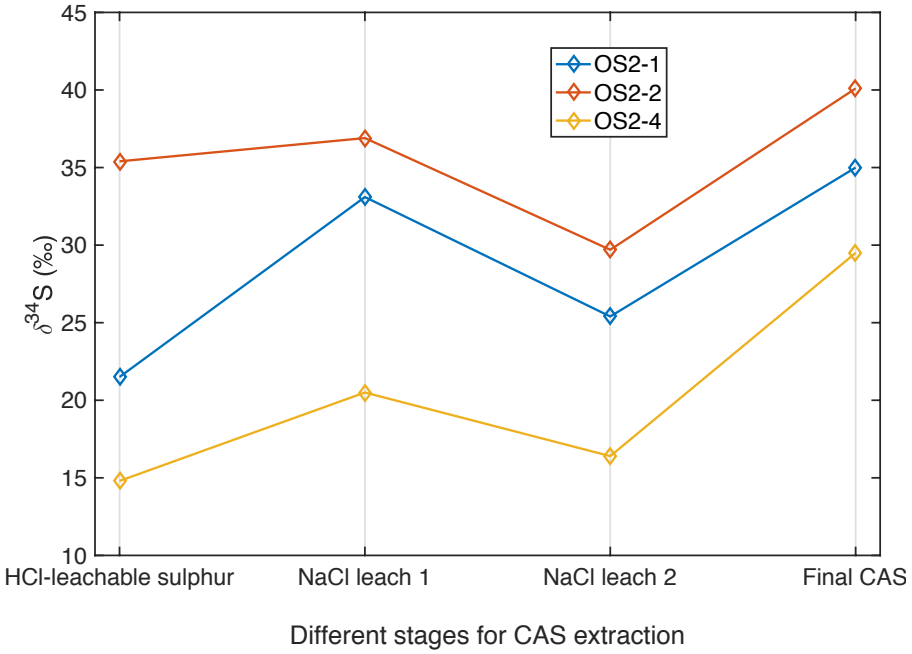

Figure. 2.3: Sulphur isotope ratios, $\delta^{34}S$, of the first two sodium chloride leachates compared with CAS and HCl-leachable sulphur for three selected samples (OS2-1, OS-2 and OS2-4). Pre-leaches (Leach 1 and 2) show lower $\delta^{34}S$ compared with final CAS values. The standard/sample replication were below 0.3‰, and thereby analytical error bars are too small to show on the graph.

2.3.2. Comparison between CAS concentrating and precipitation methods

In the total HCl-leachable sulphur extracted from tested samples, no difference is observed in the amount or qualitative character of the barium sulphate precipitates from the two compared concentrating methods introduced in section 2.2.2.4. Besides, as it is indicated from Table 2.4, there is no variation in sulphur isotope compositions from the precipitates collected by the methods. Comparing both techniques with respect to efficacy and contamination, this study recommends the simplified method by Wynn *et al*. (2008).

Table. 2.4: Sulphur isotope ratios, $\delta^{34}S$, of barium sulphate from two different CAS concentrating and precipitation techniques by Wotte *et al*. (2012) and Wynn *et al*. (2008) respectively. Results of $\delta^{34}S$ value are reported as per mil (‰).

CAS concentrating methods	OS2-1	OS2-2	OS2-4
Wotte, Shields-Zhou and Strauss (2012)	22.5	35.4	14.8
Wynn *et al*. (2008)	22.5	35.7	14.9

2.3.3. Present-day secondary atmospheric sulphate (SAS) contamination

Peng *et al*. (2014) suggested that extracted CAS could be contaminated by present-day secondary atmospherically sulphate (SAS). They applied triple oxygen isotope analyses of sequentially extracted NaCl-leachable sulphate and acid-leachable sulphate (corresponding to CAS) and they blamed the positive $\Delta^{17}O$ signatures as consequences of present-day SAS contamination based on the fact that SAS is the only source of sulphate known to bear positive ^{17}O anomalies. However, as it is illustrated in their dataset, $\Delta^{17}O$ experienced a dramatic decline during sequential NaCl leaching, while the positive $\Delta^{17}O$ anomaly disappeared in acid-leachable sulphate (CAS) in most of the studied samples. Coincidently, this trend is also associated with declining of sulphur concentration and increasing $\delta^{34}S$ in leachates, reaching much higher $\delta^{34}S$ values in acid-leachable sulphate CAS. This may reveal the fact that recent SAS contaminants within a bulk rock carbonate are leachable, and could be eliminated via consecutive NaCl cleaning. Present-day SAS should only incorporate into the bulk rock via weathering, and it may not stand a chance to affect the firm fresh calcite lattices where hold

CAS. Besides, it is noteworthy that the Neoproterozoic–Cambrian samples in their dataset with positive $\Delta^{17}O$ values are always associated with relatively low $\delta^{34}S_{CAS}$ values (< 20‰), while samples with higher $\delta^{34}S_{CAS}$ (> 20‰) values have no positive ^{17}O anomalies or no $\Delta^{17}O$ data at all in their study. This may suggest that their studied samples suffered a great degree of weathering or alteration and are not suitable for CAS study. However, the current study applied great care in rinsing the tested samples, and $\delta^{34}S_{CAS}$ data from two application of samples from Ediacaran Zebra River section (see in section 2.4) and Cambrian Aldan-Lena Rivers sections (Chapter 3) are characteristically heavy and thus inconsistent with the much lighter putative SAS contaminants from multiple locations suggested by Peng *et al*. (2014), indicating that possible SAS contamination can be minimized to not affect the primary $\delta^{34}S_{CAS}$.

2.3.4. A refined protocol for CAS extraction

The conditional experiments and tested results outlined above demonstrate that the water-soluble, non-CAS sulphur phases in a bulk carbonate can be effectively removed via thorough leaching by 10% NaCl solution. Other refinements including method miniaturisation and $BaSO_4$ precipitation are also suggested in this study as illustrated in Fig. 2.4. Apart from these, when CAS is used for reconstructing sulphur isotopic records of seawater, it should ideally be extracted from carbonate samples with minimal diagenetic overprint. A standard way to evaluate diagenesis is to apply $\delta^{13}C_{carb}$, $\delta^{18}O_{carb}$, diagnostic elemental concentrations (Ca, Mg, Fe, Mn, Sr) and rare earth elements pattern of the carbonate host rock to scrutinise the potential alteration effects on the measured $\delta^{34}S_{CAS}$. Such evaluation procedure is also recommended to screen carbonate samples prior to future CAS study. A case study of the geochemical evaluation protocol is shown in section 3.3.1.

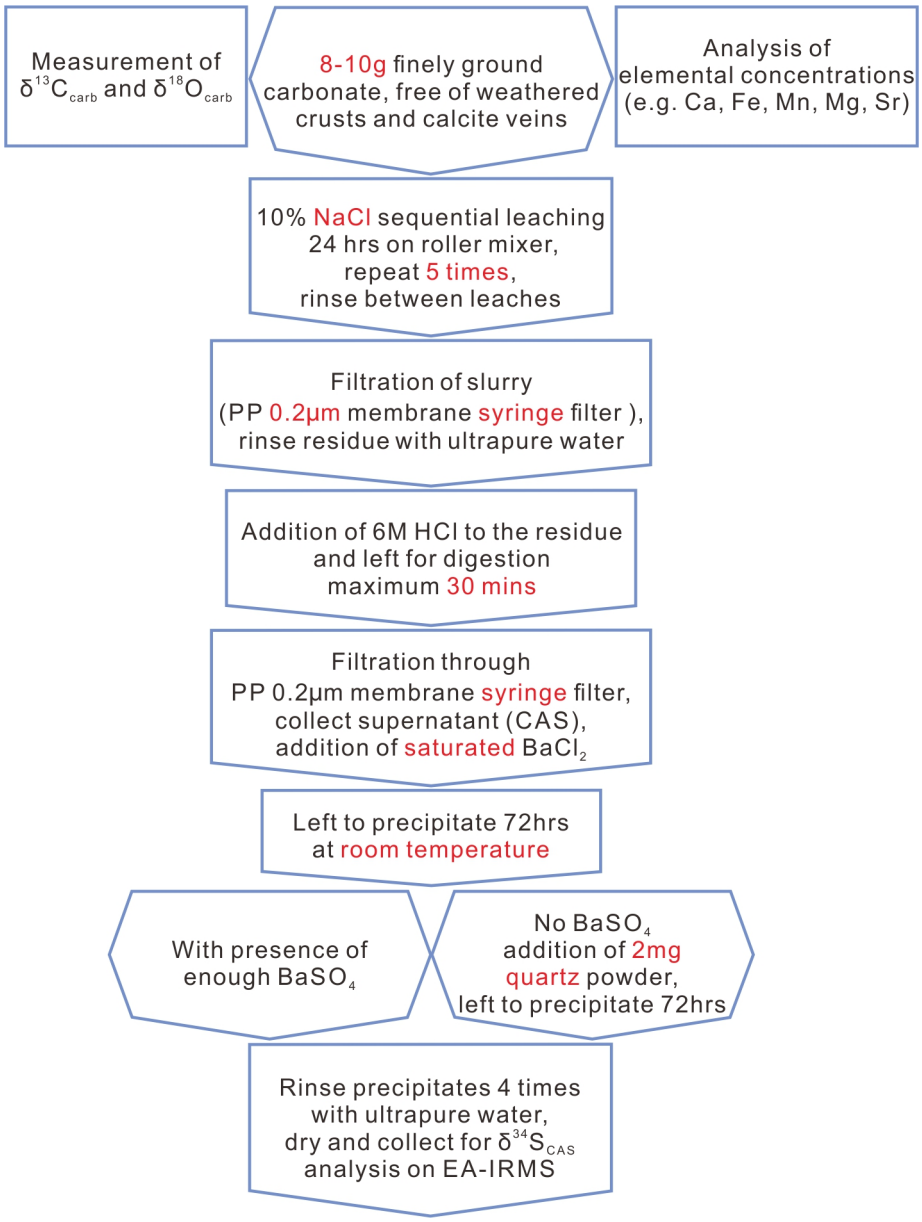

Figure. 2.4: Refined protocol for carbonate-associated sulphate extraction and sulphur isotope analysis, modified after Wotte, Shields-Zhou and Strauss (2012). Note that 0.2µm filter is used in the current protocol instead of conventional 0.45µm to ensure through filtration.

2.4. Application to the Ediacaran Nama Group, Zebra River section, Namibia

2.4.1. Comparing new $\delta^{34}S_{CAS}$ data with published CAS data from Nama Group

Organic sulphur, the products of oxidative pyrite weathering and secondary atmospheric sulphate (SAS) must all be removed before carbonates are dissolved with acid to extract CAS. Previous studies have suggested that the sulphur extracted during pre-leaching can be as much as 24‰ lower in $\delta^{34}S$ than CAS (Peng *et al*., 2014). Cleaning in water has been shown to be inadequate for removing this contaminant matrix-bound sulphur (Wotte, Shields-Zhou and Strauss, 2012; Peng *et al*., 2014). In this study, care has been taken to minimise the possibility of contamination during the extraction of CAS from fifty-one samples from Nama Group. Samples were pre-leached five times in 10% NaCl solution under constant agitation, with three rinses in ultrapure water in between each NaCl leach. Small amounts of powder (8–10g) in enclosed vessels to minimise any possibility of contamination from within the laboratory. However, prior studies on samples from the Nama Group cleaned large amounts of powder (~300 g) only once with Milli-Q water for 24 h before acid leaching (Ries *et al*., 2009).

Here, this study presents average $\delta^{34}S_{CAS}$ 12.4‰ higher than equivalent samples reported in Ries *et al*. (2009) for the lower Omkyk member (Table. 2.5). A common concern during CAS extraction is the inadvertent oxidation of sulphide minerals through the use of oxidants (e.g. NaOCl and H_2O_2), or inclusion of matrix-bound contaminant sulphur derived from weathered pyrite (Marenco *et al*., 2008). Disseminated sulphide minerals must have been present in the original rock in concentrations equivalent to or higher than those extracted. Given that measured $\delta^{34}S_{pyr}$ is similar to or even heavier than $\delta^{34}S_{CAS}$, analytical contamination from pyrite oxidation is unable to lower measured $\delta^{34}S_{CAS}$ by 12‰. The lower apparent CAS values in the Ries *et al*. (2009) study must therefore originate from the inclusion of the contaminant sulphur that the current study eliminated during the pre-leaching stage. This ^{32}S enriched contaminant sulphur (up to 16‰ lower than resultant CAS, Table 2.4), must derive from sources other than pyrite weathering (e.g. SAS). In cases where this sulphate is not effectively removed during pre-leaching, it would contribute to the lower measured CAS sulphur isotope composition.

Table. 2.5: Average sulphur isotope composition of CAS and pyrite in each member from this study and Ries *et al*. (2009), where 'n' indicates the number of analyses. Errors are one standard deviation. In the lower Omkyk, this study presents higher $\delta^{34}S_{CAS}$ than Ries *et al*. (2009). Results of $\delta^{34}S$ value are reported as per mil (‰).

Member	Study	$\delta^{34}S$ CAS	$\delta^{34}S$ Pyrite
Lower *Omkyk*	This study	30.1 ± 5.1‰ (n = 11)	36.3 ± 1.8‰ (n = 5)
	Ries *et al*. (2009)	17.7 ± 3.6‰	28.7 ± 4.0‰
Upper *Omkyk*	This study	32.5 ± 3.8‰ (n = 20)	31.7 ± 2.2‰ (n = 3)
	Ries *et al*. (2009)	31.4 ± 5.9‰	29.9 ± 5.9‰
Hoogland	This study	38.0 ± 4.3‰ (n = 20)	40.4 ± 1.5‰ (n = 3)
	Ries *et al*. (2009)	38.6 ± 9.1‰	40.9 ± 12.7‰

The new average $\delta^{34}S_{CAS}$ data is consistent with Ries *et al*. (2009) for the upper Omkyk and Hoogland members, but with overall lower standard deviations (Table 2.5). The scatter in their $\delta^{34}S_{CAS}$ may partly result from differing contributions from contaminant phases. There remains significant scatter in the new data, however, which is common in CAS data (Kampschulte and Strauss, 2004; Newton *et al*., 2004; Bottrell and Newton, 2006; Rennie and Turchyn, 2014). SAS, a common contaminant in CAS studies, can accumulate on outer surfaces and micro-cracks within outcrops, particularly in arid regions such as southern Namibia, and this SAS may be removed by effective cleaning (Peng *et al*., 2014). However, if SAS is incorporated into secondary carbonate in micro-veins that are impossible to identify and exclude during the powdering process, the contaminant signal would not be removed by pre-leaching and would be included in the acid leachable sulphate fraction. This, along with variable early diagenetic alteration, may explain the remaining scatter in the new $\delta^{34}S_{CAS}$ data.

2.4.2. 'Superheavy' pyrite or contaminated CAS?

Several studies investigating the $\delta^{34}S$ of various Late Neoproterozoic sedimentary successions report pyrite enriched in ^{34}S relative to the global average for seawater sulphate at that time, which is also ^{34}S-enriched relative to other times in the Proterozoic or Phanerozoic (Bottomley *et al*., 1992; Strauss *et al*., 1992; Tie-bing, Maynard and Alten, 2006; Shen, Zhang and Hoffman, 2008). This 'superheavy' pyrite has also been observed a few times in the Phanerozoic and modern environments, but the $\delta^{34}S_{pyr}$ is only slightly elevated compared with

$\delta^{34}S_{CAS}$ (Goodfellow and Jonasson, 1984; Aller *et al*., 2010; Ferrini *et al*., 2010). On the whole, the occurrence of 'superheavy' pyrite involves a small number of anomalously ^{34}S enriched samples within a larger $\delta^{34}S_{pyr}$ dataset, which in some cases are not reported alongside coeval $\delta^{34}S_{CAS}$ (e.g. Bottomley *et al*., 1992, n= 1; Shen, Zhang and Hoffman, 2008, n= 4). In particular, Ries *et al*. (2009) report some extremely ^{34}S-enriched pyrite in the Hoogland member (9 samples > 45.0‰, reaching 80.2‰), but the current study does not reproduce these in our more limited pyrite data set. Although our highest reported $\delta^{34}S_{CAS}$ is 45.4‰, Ries *et al*. (2009) report some extremely enriched $\delta^{34}S_{CAS}$, up to 64.2‰, from the same part of the stratigraphy as the 'superheavy' pyrite.

An apparent 'superheavy' pyrite effect may result from normal marine $\delta^{34}S_{pyr}$, in the presence of $\delta^{34}S_{CAS}$ that is low compared with contemporaneous local or global sections as a result of contamination during CAS extraction. Our average $\delta^{34}S_{CAS}$ is 12.4‰ higher than equivalent samples reported in Ries *et al*. (2009) for the lower Omkyk member (Table 2.5). Significantly, the lower Omkyk member is one section of the Nama Group where Ries *et al*. (2009) describe the phenomenon of 'superheavy' pyrite (highlighted by the grey box in Table 2.5). This study did not sample the exact same section as Ries *et al*. (2009), and so lateral variability in pyrite sulphur isotope composition or $\delta^{34}S_{CAS}$ across the basin remains a possible explanation (Hurtgen *et al*., 2006).

In the current study, pyrite $\delta^{34}S$ remains higher than $\delta^{34}S_{CAS}$ for two samples in the lower Omkyk member and this could point to the presence of genuine 'superheavy' pyrite. Alternately, it could indicate diagenetic alteration of $\delta^{34}S_{CAS}$ to lower values, or the presence of small amounts of contaminant sulphur even after extensive cleaning. In general, the new CAS dataset suggests that 'superheavy' pyrite may not be as widespread in the Nama Group as previously thought (Ries *et al*., 2009), and that where it does occur, the offset between seawater sulphate and pyrite $\delta^{34}S$ may be smaller and therefore easier to explain. While some of the offset reported in Ries *et al*. (2009) could have arisen from artefacts during CAS extraction, there remains some extraordinarily high $\delta^{34}S_{pyr}$ in the Nama Group that needs to be addressed. 'Superheavy' pyrite has been attributed to decoupling of surface and bottom water sulphur reservoirs in a stratified ocean, where bottom waters produce enriched $\delta^{34}S_{pyr}$ via Rayleigh distillation, and surface waters record undistilled $\delta^{34}S_{CAS}$ (Liu, Maynard and Alten, 2006). This model cannot explain observations in the Nama Group, because there is sedimentological evidence for storm driven mixing in parts of the basin, and iron speciation data suggests there are no sulphidic bottom waters (Ries *et al*., 2009; Wood *et al*., 2015). Ries *et al*. (2009) suggest

that under low sulphate conditions, small sulphur isotope fractionations during sulphide oxidation could deplete seawater $\delta^{34}S_{SW}$ or seawater sulphate $\delta^{34}S_{CAS}$ in ^{34}S relative to $\delta^{34}S_{pyr}$ via Rayleigh-type distillation within pore waters. This interpretation requires minimal sulphur isotope fractionation during microbial sulphate reduction, which may be achieved through very low sulphate concentrations or high rates of sulphate reduction. If pore water sulphide is partially re-oxidised, aided by storm-driven reworking or bioturbation beneath aerobic bottom waters, the residual sulphide pool may be left heavy compared with seawater sulphate. Within the Zebra River section, previous work has identified a spectrum of fully anoxic (ferruginous), low oxygen (manganous) and well-oxygenated bottom waters (Wood *et al.*, 2015; Tostevin *et al.*, 2016). But current study notes that $\delta^{34}S_{CAS}$ and $\delta^{34}S_{pyr}$ data show no clear correspondence to inferred local bottom water redox conditions.

On the other hand, pyrite generally forms within the sediments and so reflects pore water chemistry, whereas carbonate forms close to the sediment-water interface in contact with the marine sulphate reservoir (Gomes and Hurtgen, 2013). $\delta^{34}S_{CAS}$, therefore, forms in different environments to $\delta^{34}S_{pyr}$, possibly decoupling the actual sulphur isotope fractionation between seawater and pyrite ($\Delta^{34}S_{SW\text{-}pyr}$) from the fractionation during microbial sulphate reduction, $^{34}\varepsilon_{mic}$, which depends largely on the rate of microbial sulphate reduction. $\delta^{34}S_{pyr}$ thus may evolve towards parent sulphate $\delta^{34}S$ in closed systems, lowering the apparent $\Delta^{34}S_{SW\text{-}pyr}$. The presence of superheavy pyrite may indicate shallow, high energy depositional environments characterised by partial sulphide oxidation during frequent sedimentary reworking, rather than low concentrations of seawater sulphate (Fike, Bradley and Rose, 2015). Regardless of the exact mechanism, simple models struggle to explain extremely high $\delta^{34}S_{pyr}$ (>50‰), wide ranges in $\delta^{34}S_{pyr}$, and the absence of complementary low $\delta^{34}S_{pyr}$, and so the genesis of 'superheavy' pyrite remains enigmatic (Aller *et al.*, 2010; Ferrini *et al.*, 2010; Fike, Bradley and Rose, 2015).

2.5. Conclusions

This study evaluates procedures for 10% NaCl leaching, CAS extraction and barium sulphate precipitation from previous studies. Efficacy of multiple NaCl leaching is evaluated based on sulphur concentration and isotope composition of NaCl leachates and CAS. This study miniaturises the experimental setup, and recommends the following protocol for future studies that seek to extract and analyse CAS: 1) To avoid risk of sample heterogeneity and contamination, total HCl-leachable sulphur concentration can be helpful when considering the amount of rock powder required for CAS extraction; 2) Repeated 10% NaCl leaching is effective in eliminating all soluble non-CAS sulphur proportions, while the numbers of pre-leaches required can be tested by investigating sulphur concentration in the leachates; 3) Samples with extremely low acid-leachable $\delta^{34}S$ would possibly suffer great degree of SAS contamination, but thorough NaCl leaching would possibly minimise such effect; 4) This study recommends 5-10g sample with at least 10-20ppm CAS concentration for future analysis. This study also discusses the new $\delta^{34}S_{CAS}$ data from the Ediacaran-age lower Nama Group, Namibia as the first validation study for the refined CAS extraction method. The data show higher $\delta^{34}S_{CAS}$ than previous studies, which could be attributed to improved cleaning procedures and reduced contributions from contaminant sulphur. The phenomenon of 'superheavy' pyrite, previously reported from these sections, may in part be an artefact of contamination due to inadequate cleaning procedures, and that true $\delta^{34}S_{CAS}$ and $\delta^{34}S_{SW}$ is close to coeval $\delta^{34}S_{pyr}$.

Chapter 3

Extreme redox oscillations due to coupling of the marine sulphur and carbon cycles during the Cambrian Explosion

ABSTRACT

Understanding the coupling of marine carbon and sulphur cycles in deep time is crucial for reconstructing the history of redox variations and ocean chemistry. Extreme carbon isotope fluctuations have long been known to characterise the Cambrian radiation of animals, but it is commonly assumed that any excess oxidant generated by organic carbon burial (generating higher carbonate $\delta^{13}C_{carb}$) will be balanced by reduced pyrite burial (lower seawater sulphate $\delta^{34}S_{CAS}$), and vice-versa. On the other hand, some recent studies suggest that organic carbon and pyrite sulphur burial may be positively correlated during the early Cambrian IV and late Cambrian SPICE (Steptoean Positive Carbon Isotope Excursion) event, leading to two pulses in oxygenation (Gill *et al*., 2011; Dahl *et al*., 2017). Using a new, high-fidelity analytical approach, this study reports 352 analyses of carbonate carbon isotope and 165 analyses of carbonate-associated sulphate sulphur isotope in samples from the Aldan-Lena Rivers sections (eastern Siberia) and Xiaotan section (South China). Results demonstrate a convincing positive correlation between carbonate $\delta^{13}C_{carb}$ and carbonate-associated sulphate $\delta^{34}S_{CAS}$ through at least six isotope cycles during the canonical explosive phase of the Cambrian radiation from

~529 to ~516.5 Myr ago. This isotopic coupling reflects periodic oscillations in ocean redox that shed light on the episodic radiations of major animal phyla with which they coincide. Conversely, by contrast, the Botomian–Toyonian extinction events coincide with decoupled isotope records that evidence a shrinking marine sulphate reservoir and a shoaling of marine anoxia through this later interval (~516.5-~513 Ma). These new data demonstrate a tight relationship between environmental and biological evolution during one of the most fundamental transitions towards the modern biosphere.

Author Contributions: Maoyan Zhu provided the samples. Carbon isotope analysis was undertaken at Nanjing Institute of Geology and Palaeontology, Chinese Academy of Sciences with technical assistance from Xiaoming Chen. Sulphur isotope analysis was undertaken at Lancaster Environment Centre, Lancaster University with assistance from Peter Wynn. Benjamin Mills from the University of Leeds supervised the development of numerical models. The discussion benefitted from helpful conversations with Graham Shields, Benjamin Mills, Maoyan Zhu, Rosalie Tostevin, Peter Wynn, Philip Pogge von Strandmann and Andrey Yu. Zhuravlev. Carbon isotope record and elemental data of Xiaotan section are obtained from Li *et al*. (2013)

3.1. Introduction

The early Cambrian witnessed dramatic diversification of animal body plans and behaviours, with ocean oxygenation being a commonly invoked environmental trigger (Shields-Zhou and Och, 2011; Boyle *et al*., 2014; Lenton *et al*., 2014; Chen *et al*., 2015). However, more recent but challenging studies reveal that the late Precambrian ocean might have exceeded requisite oxygen thresholds well before the Cambrian Period (Mills *et al*., 2014; Zhang *et al*., 2016), leading to a more nuanced understanding of the relationship between redox conditions and early animal evolution. To be specific, the precise timing, pattern and mechanism for the redox shifts, and any causal relationship with animal radiation and extinction events, remains controversial. Convincing links between oxygenation history and the early Cambrian geo-, biological events have hitherto been lacking, pending the arrival of high-fidelity geochemical records that tie directly into the fossil record.

Carbonate carbon isotope oscillations are characteristic of the early Cambrian (Brasier, Corfield, *et al*., 1994; Brasier *et al*., 1996; Brasier and Sukhov, 1998; Maloof, Porter, *et al*., 2010). These globally reproducible $\delta^{13}C_{carb}$ excursions exhibit a periodicity of ~1-2 Myr with magnitudes of ~2‰-~4‰ in the Tommotion–Botomian stages in Siberia and Morroco (Brasier, Corfield, *et al*., 1994; Maloof, Ramezani, *et al*., 2010). Under steady-state conditions, the cause of the $\delta^{13}C_{carb}$ fluctuation through geologic time can be explained by variations in organic carbon burial fraction, isotopic composition of the carbon input flux to the ocean and fractionation between carbonate and organic carbon, all of which could be directly or indirectly controlled by variations in the size of seawater dissolved organic carbon reservoir and changes in marine redox conditions (Shields-Zhou and Zhu, 2013; Shields, 2017).

The marine biogeochemical sulphur and carbon cycles connect via their respective redox-sensitive reservoirs and fluxes. Both elements have a single, large oxidised oceanic reservoir (dissolved sulphate and inorganic carbon, respectively), the isotopic composition of which is governed by organically mediated isotopic fractionation of the reduced sink (pyrite and organic carbon, respectively). The redox sensitivity of both output and input fluxes (due to oxidative weathering) means that redox imbalances should imprint on both the seawater sulphate sulphur ($\delta^{34}S_{CAS}$ of carbonate-associated sulphate) and carbon isotope ($\delta^{13}C_{carb}$ of carbonate) records, allowing us to trace oceanic redox behaviour through geologic time. Therefore, if the secondary diagenetic alteration can be eliminated, the same fluctuation

pattern in $\delta^{13}C_{carb}$ record is predicted to exist in the seawater sulphate sulphur isotope record, based on the theory that both marine carbon and sulphur cycles should respond and behave simultaneously due to their paired control from connected redox-sensitive reservoirs and fluxes.

On the other hand, two of the key fluxes that control the concentration of sulphate in the ocean include riverine sulphate derived from oxidative weathering of pyrite, and microbial reduction of sulphate to sedimentary sulphide/pyrite. These fluxes depend indirectly on oxygen concentrations in the atmosphere and oceans, respectively. But flux of pyrite burial in the sediments regulates the oceanic sulphate concentration, and represents an important source of oxygen release to the atmosphere over long timescales in the biogeochemical sulphur cycle (Berner, 1989). Although higher marine sulphate concentrations might be expected to correlate with generally increased oxygen availability in the early Cambrian (Canfield and Farquhar, 2009), many studies have inferred short-term low-sulphate conditions during extreme palaeoenvironmental incidences (Hough *et al*., 2006; Gill *et al*., 2011; Loyd *et al*., 2012), and the sulphate concentration of the early Cambrian ocean remains unresolved.

$\delta^{34}S_{CAS}$ of carbonate-associated sulphate, which represents the sulphur isotope composition of marine sulphate, tracks changes in the sources and sinks within the biogeochemical sulphur cycle (Claypool *et al*., 1980). Modern marine sulphate has a concentration of ~29 mM, and a residence time of 10–20 million years, which far exceeds the mixing time of the ocean (Paytan and Gray, 2012). At high sulphate concentrations, $\delta^{34}S_{CAS}$ should provide a globally integrated archive of the relative sources and sinks of sulphur to the global ocean. Marine sulphate concentrations, however, have likely varied widely through Earth history (Algeo *et al*., 2015). When the residence time of sulphate is reduced, the concentration and isotope composition of sulphate may vary within and among marine basins (Kah, Lyons and Frank, 2004).

Few studies have been published on the early Cambrian $\delta^{34}S_{CAS}$ record, while research has tended to focus on the sections in Siberia due to its exceptional preservation of continuous carbonate successions (Kampschulte and Strauss, 2004; Wotte, T. , Strauss, H., Sundaberg, 2011). The main limitation of previous datasets lies in poor data resolution, and unreliable CAS extraction due to inadequate washing of water-soluble sulphur contaminants. Larger datasets are required to increase the data resolution and fill in the data gaps in the Cambrian stages 2-3 (Paytan and Gray, 2012). In a major advance during the writing of this thesis, Dahl *et al*. (2017) reported a paired $\delta^{13}C_{carb}$ and $\delta^{34}S_{CAS}$ record for the isotope excursion IV of Cambrian

Stage 3 in Siberia. Their data for the first time draw our attention to the coupling behaviour of $\delta^{13}C_{carb}$ and $\delta^{34}S_{CAS}$ in the early Cambrian. New data in the current thesis reproduced and echo the results of Dahl *et al*. (2017), but our data covers a longer period with five more excursions, revealing a long-term covariant history of marine carbon and sulphur cycles.

Using the refined carbonate-associated sulphate (CAS) extraction method introduced in *Chapter 2*, this study generated high-fidelity $\delta^{34}S_{CAS}$ data from the lower Cambrian carbonate samples of the Aldan-Lena Rivers sections (eastern Siberia) and Xiaotan section (South China). Together with paired carbonate carbon isotope data, this study presents a continuous, high-resolution, paired isotope record, from Cambrian Stage 2 through to Stage 4 (circa 529-513 Ma), in the context of an integrated litho- and biostratigraphic framework with a new age model. The goals were to investigate the marine redox variations and oxygenation history associated with the Cambrian radiation and Botomian–Toyonian extinction, and to test the hypothesis and quantitatively constrain the local marine sulphate concentrations using numerical isotope mass balance models.

3.2. Methods

3.2.1. Samples

Carbonate samples collected from the Siberian Aldan-Lena Rivers sections and South China Xiaotan section underwent carbonate-associated extraction and paired sulphur-carbon isotope analyses. The samples cover the interval of Cambrian stages 2-4. Details of the geological and stratigraphic settings are given in section 1.6.3 for the Xiaotan section and in section 1.6.4 for the Aldan-Lena Rivers sections. For samples from the Aldan-Lena Rivers sections, 352 well-preserved carbonates were analysed for carbon and oxygen isotopes. Some 142 samples were analysed for CAS sulphur isotopes, concentrations of diagenetic-diagnostic elements and [CAS]. For samples from the Xiaotan section, 23 limestone samples of the Dahai Member were analysed for CAS sulphur isotopes and CAS concentration. Sample descriptions and data compilation are shown in Appendix B and C. A composite litho-, bio- and chemostratigraphic framework is shown in Fig. 3.4 and 3.5.

3.2.2. Analytical techniques

3.2.2.1. Extraction of carbonate-associated sulphate, measurement of CAS concentration and $\delta^{34}S_{CAS}$ analysis

The miniaturised CAS extraction protocol presented in *Chapter 2*, which is an extension of two published approaches (Wynn *et al*., 2008; Wotte, Shields-Zhou and Strauss, 2012), was applied in this study. Samples followed strict pretreatment procedures, including rock grinding, multiple NaCl leaching (5 pre-leaches), acid digestion and collection of carbonate-associated sulphate prior to $\delta^{34}S_{CAS}$ analysis. Sulphur isotope analysis of CAS was conducted using a *EuroVector*® elemental analyser linked to *Isoprime*® 100 Dual-Inlet mass spectrometer at the Lancaster Environment Centre, Lancaster University. The concentrations of carbonate-associated sulphate were measured in aliquots of the filtered acid digestion solution. The analytical methods for sulphur isotope and [CAS] are described in sections 2.2.3.1 and 2.2.3.2.

3.2.2.2. Carbonate carbon and oxygen isotopes

About 20 mg of the rock powder that was drilled from a rock slab of each Siberian sample was used for analysis. Limestone samples were reacted with 100% H_3PO_4 at 25°C for more than 12h, and dolostone samples were reacted with 100% H_3PO_4 at 50°C for more than 24h. Prepared gas samples were analysed for $^{13}C/^{12}C$ and $^{18}O/^{16}O$ using the Chinese national standard, an Ordovician carbonate from a site near Beijing (reference number GBW04405: $\delta^{13}C$= 0.57 ± 0.03‰ VPDB; $\delta^{18}O$= −8.49 ± 0.13‰ VPDB). The analyses were performed using the *Finnegan*® MAT 253 mass spectrometers at the Nanjing Institute of Geology and Palaeontology, Chinese Academy of Sciences.

3.2.2.3. Elemental analysis

For concentrations of diagenesis-diagnostic elements, including Ca, Mg, Mn and Sr, an aliquot of approximately 50mg of the rock power was micro-drilled of each sample and pre-treated with excess (about 3ml) 6M hydrochloric acid at room temperature for at least 12h. The concentration of the acid used here is identical to the one used for CAS extraction after NaCl leaching. The reaction was facilitated through frequently using an ultrasonic bath and roller mixer. After centrifugation, aliquots of the supernatant were then analysed for sulphate concentration using the *Varian*® 720 ICP-OES at University College London. All analyses for major and minor elements were done using certified reference materials: SRM1c (Argillaceous limestone), SRM120b (Florida phosphate rock). Solution standards were run at the start of the analyses along with a blank to monitor the accuracy of the bulk elemental analysis. Laboratory control solution standards were also run after every batch of 20 samples to monitor the drift and precision of the machinery.

3.2.3. Biogeochemical models

3.2.3.1. 'Rate method' model

Maximum seawater sulphate concentrations are calculated using the published 'rate method' (Algeo *et al*., 2015). The model was constructed based on the observed rate of change in

seawater sulphate $\delta^{34}S_{CAS}$, fractionation between oxidised (sulphate) and reduced sulphur (pyrite) reservoirs and the equation (Eqn. 3.1) that connect the two parameters:

$$\frac{d\delta^{34}S_{CAS}}{dt} = \frac{\left(\left(F_Q \times \Delta^{34}S_{Q-SW}\right) - \left(F_{PY} \times \Delta^{34}S_{CAS-PY}\right)\right)}{M_{SW}} \qquad (Eqn.\ 3.1)$$

$$M_{SW} = \frac{F_{PY} \times \Delta^{34}S_{CAS-PY}}{\frac{d\delta^{34}S_{CAS}}{dt}} \qquad (Eqn.\ 3.2)$$

where F_x represents the input and output fluxes, $\Delta^{34}S_x$ represents isotopic difference of $\delta^{34}S$ between fluxes (Q = total input flux of sulphur, PY = pyrite burial, SW = seawater/sulphate deposition) and MSW represents the mass of sulphate in the ocean.

The maximum rates of $\delta^{34}S_{CAS}$ change are attained when sulphur input flux to the ocean approaches zero ($F_Q = 0$), and the standing oceanic sulphate reservoir is removed as pyrite. The Eqn. 3.1 is then transformed to Eqn. 3.2 to calculate the size of seawater sulphate reservoir. Because that the observed rates of $\delta^{34}S_{CAS}$ change in a normal marine environment should never exceed the theoretical maximum rates of change ($d\delta^{34}S_{CAS}/dt$), the calculation using Eqn. 3.1 should provide the maximum estimate of seawater sulphate concentration. The definition of F_{PY}, $\Delta^{34}S_{CAS\text{-}PY}$, and unit-conversion constants (gram to mM) are consistent with the values applied for the long-term secular variation study of seawater sulphate concentration (Algeo *et al.*, 2015). $F_{PY} = 4 \times 10^{13}$ g yr^{-1} is suggested for a normal oxygenated marine environment. $\Delta^{34}S_{CAS\text{-}PY}$ = 35‰.

3.2.3.2. Coupled carbon and sulphur cycles model

A simple model of the global carbon and sulphur cycles was applied to explore the proposed mechanisms for isotopic variations in the system. This follows the work of Garrels and Lerman (Garrels and Lerman, 1984), Berner (Berner, 2006) and Bergman *et al.* (Bergman, Lenton and Watson, 2004). The model calculates the global rate of organic carbon burial using isotope mass balance, and then attempts to predict the operation of the sulphur system based on the supply of organic matter. Fig. 3.1 shows the model processes as a diagram, Table 3.1 shows the model flux and parameter values, and Fig. 3.8 shows the model output.

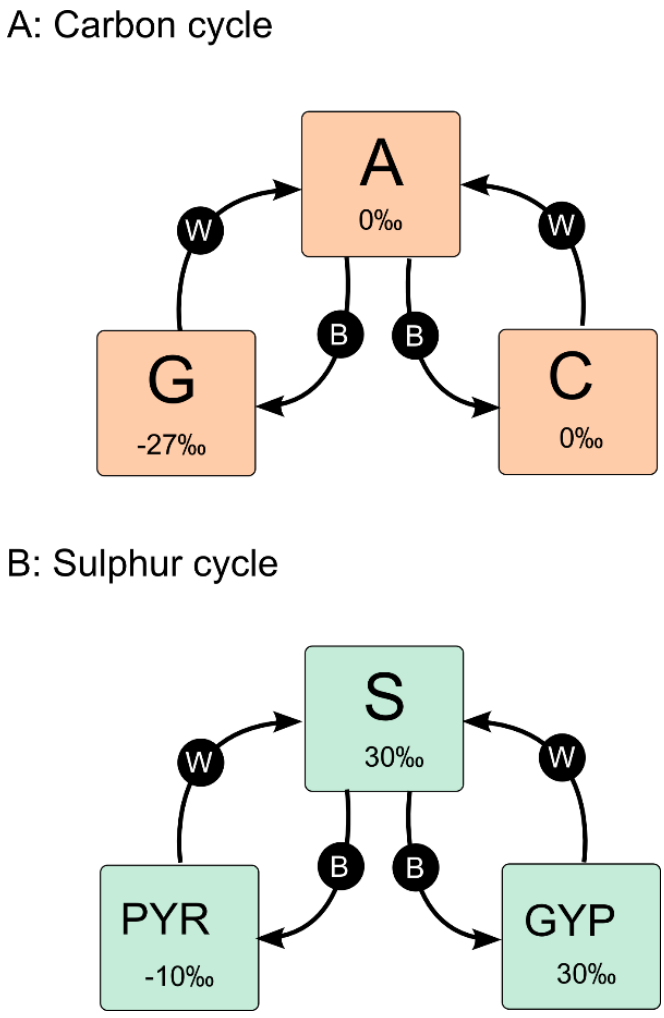

Figure. 3.1: Coupled C-S cycles model diagram. Boxes show reservoirs and arrows show fluxes. Burial fluxes are denoted 'B' and weathering fluxes are denoted 'W'. A denotes atmosphere and ocean carbon, S denotes oceanic sulphate. G is buried organic carbon, C is buried carbonate, PYR is buried pyrite and GYP is buried gypsum. ΔB and ΔS are the fractionation factors associated with the burial of organic carbon (G) and pyrite (PYR) relative to the ocean/atmosphere fractionation. Assumed isotopic composition of reservoirs for the standard model run are shown underneath the reservoir titles.

The model estimates long-term fluxes between the ocean and sediments for both carbon and sulphur. Carbon is modelled as CO_2 in the atmosphere and ocean (A), and will be buried either as organic carbon (G) or carbonate (C). Similarly, sulphur can exist as oceanic sulphate (S), and will be buried as pyrite (PYR) or gypsum (GYP). Weathering (and metamorphism) constitutes the return flux from the sediments to the ocean and atmosphere. This study set the weathering inputs to constant values, which are chosen in line with previous models (Bergman, Lenton and Watson, 2004; Berner, 2006). Here in this study, the model allows around half of

present total organic carbon burial (and weathering) due to the absence of land plants, and an enhanced burial flux of pyrite sulphur due to anoxia. The weathering rate of gypsum is held constant, but the burial rate is adjusted so that the model maintains a constant sulphate concentration. Due to the relatively short model timeframe, the sedimentary reservoirs are assumed to have a fixed isotopic composition and are assumed not to vary in size. The ocean and atmosphere reservoirs are allowed to vary in size and isotopic composition.

Table. 3.1: List of Coupled C-S cycles model fluxes and parameters.

Flux	**Symbol**	**Rate**
Organic C weathering	W(G)	$4\times10^{12}\ mol\ yr^{-1}$
Organic C burial	B(G)	Calculated from isotope mass balance
Carbonate weathering	W(C)	$12\times10^{12}\ mol\ yr^{-1}$
Carbonate burial	B(C)	$12\times10^{12}\ mol\ yr^{-1}$
Pyrite weathering	W(PYR)	$2\times10^{12}\ mol\ yr^{-1}$
Pyrite burial	B(PYR)	Calculated from organic C availability
Gypsum weathering	W(GYP)	$1\times10^{12}\ mol\ yr^{-1}$
Gypsum burial	B(GYP)	Calculated to maintain steady state
Parameter	**Symbol**	**Value**
Ocean/atmosphere carbon	A	$3.3\times10^{18}\ mol$
Ocean sulphate	S	Varied, present day = $42\times10^{18}\ mol$
Isotopic composition of A	δA	Data in this study
Isotopic composition of S	δS	Predicted from model
Isotopic composition of G	δG	Varied, average = $-27‰$
Isotopic composition of C	δC	Varied, average = 0‰
Isotopic composition of PYR	δPYR	-10
Isotopic composition of GYP	δGYP	30
Fractionation factor: carbon	ΔB	27
Fractionation factor: sulphur	ΔS	40

Organic carbon burial is calculated using isotope mass balance (Garrels and Lerman, 1984; Berner, 2006), which uses the total carbon input fluxes and isotopic composition of seawater (δA) to calculate the required burial rate of isotopically depleted organic carbon (Eqn. 3.3):

$$B(G) = \frac{1}{\Delta B}\{W(G)(\delta A - \delta G) + W(C)(\delta A - \delta C)\} \qquad (Eqn.\ 3.3)$$

It is assumed that pyrite burial is governed by the supply rate of organic carbon to microbial sulphate reducers, and therefore scales with the burial rate of organic carbon. The proportionality constant (0.5) is chosen to balance pyrite weathering (Eqn. 3.4).

$$B(PYR) = 0.5\,B(G) \qquad (Eqn.\,3.4)$$

Variation in the ocean and atmosphere carbon is calculated as (Eqn. 3.5):

$$\frac{dA}{dt} = W(G) + W(C) - B(G) - B(C) \qquad (Eqn.\,3.5)$$

Variation in ocean sulphate is calculated as (Eqn. 3.6):

$$\frac{dS}{dt} = W(PYR) + W(GYP) - B(PYR) - B(GYP) \qquad (Eqn.\,3.6)$$

Variation in the isotopic composition of ocean sulphate is calculated as (Eqn. 3.7):

$$\frac{d(S\times\delta S)}{dt} = W(PYR)\delta PYR + W(GYP)\delta GYP - B(PYR)(\delta S - \Delta S) - B(GYP)\delta S \qquad (Eqn.\,3.7)$$

The model is solved in MATLAB using the ODE suite. Code is available in Appendix G.

3.3. Results

3.3.1. Evaluating diagenesis

It is important to constrain the degree to which carbonate rocks have been altered to establish whether geochemical trends are likely to be representative of syn-depositional oceanic values. For example, primary depositional fluids have the potential to result in dissolution and recrystallization of carbonate phases. Such diagenetic alteration of carbonates simultaneously lowers $\delta^{13}C_{carb}$ and $\delta^{18}O_{carb}$ values of carbonate rocks (Brand and Veizer, 1981; Allan and Matthews, 1982; Banner and Hanson, 1990). Therefore, positive correlation between $\delta^{13}C$ and $\delta^{18}O$ is often considered to be diagnostic of diagenetic alteration by primary depositional fluids (e.g. seawater $CaCO_3$). As it is shown is Fig. 3.2 and 3.3, the cross-plots of $\delta^{13}C_{carb}$ and $\delta^{18}O_{carb}$ results of Aldan-Lena Rivers sections and Xiaotan section exhibit very weak to moderate positive correlation ($R^2 = 0.213$ and $R^2 = 0.504$, respectively), which could indicate diagenesis imprints. However, non-diagenetic covariations are evident in many cases such as in the long-term Ordovician $\delta^{13}C_{carb}$ and $\delta^{18}O_{carb}$ records (Shields *et al.*, 2003). Besides, the $\delta^{13}C_{carb}$ records as shown in Fig. 3.2 and 3.3 exhibit a gradual and extremely smooth curve, and both the long-term trends and short-term $\delta^{13}C_{carb}$ excursions are globally identical (Maloof, Porter, *et al.*, 2010; Peng, Babcock and Cooper, 2012), which is a robust indication of its primary nature. Therefore, $\delta^{13}C_{carb}$ and $\delta^{18}O_{carb}$ systematics of the Aldan-Lena Rivers section and Dahai Member of Xiaotan section are likely the signatures of coeval seawater rather than alteration during diagenesis.

Post-depositional and early diagenetic reactions with pore water solutions could also produce changes in the isotopic composition and abundance of carbonate-associated sulphate (e.g. dolomitisation). Regarding the results of carbonate-associated sulphate sulphur isotope analysis ($\delta^{34}S_{CAS}$) of Aldan-Lena Rivers sections, cross-plots of $\delta^{34}S_{CAS}$ show no correlation with traditional indicators of diagenesis, carbonate-associated sulphate (CAS) concentration ($R^2 = 0.025$), Mn/Sr ($R^2 < 0.0001$), Mg/Ca ($R^2 = 0.003$) or $\delta^{18}O_{carb}$ ($R^2 = 0.008$) (Fig. 3.2), indicating that 142 $\delta^{34}S_{CAS}$ values might not have been affected by significant diagenetic alteration. In addition, alteration of CAS signal may be related to variation among different lithologies. But no correlation is observed between $\delta^{34}S_{CAS}$, HCl-leachable carbonate content and Mg/Ca for these data, indicating $\delta^{34}S_{CAS}$ values may not vary between minor changes in carbonate lithologies.

For samples from the Dahai Member of the Xiaotan section, cross-plots of $\delta^{34}S_{CAS}$ show no correlation with CAS concentration, Mg/Ca or $\delta^{18}O_{carb}$ (Fig. 3.3). However, a moderate negative correlation is observed between $\delta^{34}S_{CAS}$ and Mn/Sr. Mn/Sr has been widely used to evaluate carbonate diagenesis and the fidelity of carbonate isotopic compositions (e.g. Sr, C isotopes) (Veizer *et al*., 1983; Derry *et al*., 1994). It is based on the theory that dissolution and recrystallization of carbonate phases during diagenesis generally raise Mn contents and simultaneously lowers Sr contents. But there is no supporting evidence that such diagenesis processes would affect the isotopic composition of carbonate-associated sulphate. Besides, Mn/Sr values could also differ with variation in lithologies of carbonate. In the Dahai Member, samples with low $\delta^{34}S_{CAS}$ values below 20‰ exhibit low carbonate contents (< 85%) and high Mn/Sr (> 0.3) (Fig. 3.3c), but these samples are all derived from stratigraphic horizons that are close to the lithological or sequence boundaries at the bottom and top of Dahai Member (Fig. 3.5). This coincidence implies that low carbonate contents and elevated Mn/Sr could merely reflect transitional lithology changes of phosphorite-limestone and limestone-siltstone close to a lithological boundary, rather than diagenetic alteration of carbonate-associated sulphate. No correlation is observed between $\delta^{34}S_{CAS}$ and other indicators of diagenesis (Fig. 3.3), suggesting $\delta^{34}S_{CAS}$ values of Dahai Member are likely recording primary seawater sulphate isotopic features.

A recent approach by Fichtner *et al*. (2017) suggests that concentrations of carbonate-associated sulphate can be directly affected by burial diagenesis. CAS concentrations generally decrease with increasing degree of burial depth and temperature when exposed to burial fluids. However, by contrast, there is no variation in the CAS sulphur isotopic composition during progressive burial diagenesis. Their results suggest that $\delta^{34}S_{CAS}$ is highly resistant to late diagenetic processes. Carbonate-associated sulphate should preserve the pristine sulphur isotope records of ambient seawater sulphate, but analysed CAS concentration from a bulk carbonate cannot be considered as a reliable indicator of original seawater sulphate. Therefore, the observed $\delta^{34}S_{CAS}$ trends and excursions in the current study are likely to represent primary signatures of Cambrian seawater sulphate, but the CAS concentrations are likely to have been altered.

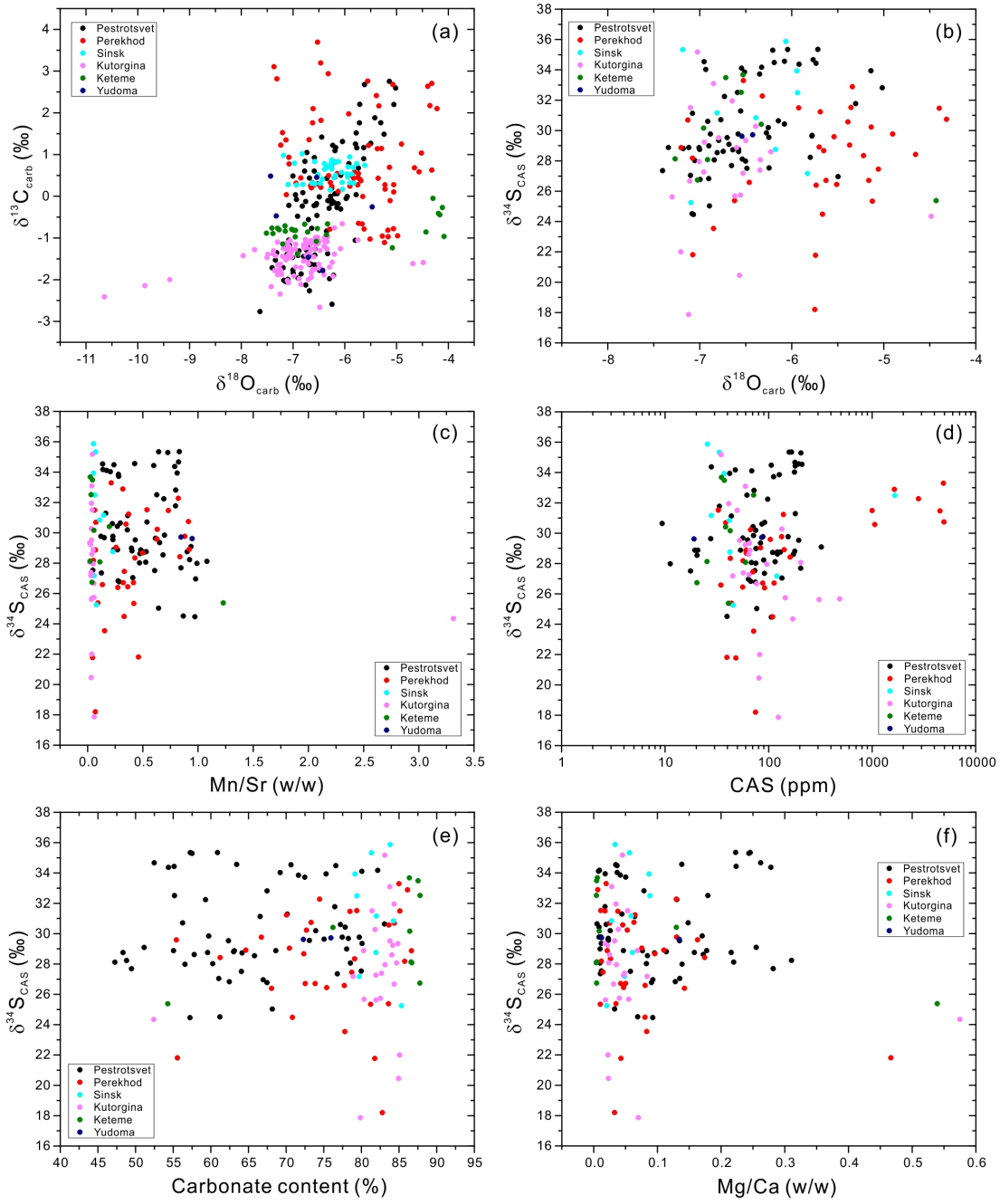

Figure. 3.2: Cross-plots of (a) $\delta^{18}O_{carb}$ (‰)-$\delta^{13}C_{carb}$ (‰) ($R^2 = 0.213$); (b) $\delta^{34}S_{CAS}$(‰)- $\delta^{18}O_{carb}$ (‰) ($R^2 = 0.008$); (c) $\delta^{34}S_{CAS}$(‰)-Mn/Sr (w/w) ($R^2 < 0.0001$); (d) $\delta^{34}S_{CAS}$ (‰)-CAS (ppm) ($R^2 = 0.025$); (e) $\delta^{34}S_{CAS}$ (‰)-carbonate content (%) ($R^2 = 0.002$); and (f) $\delta^{34}S_{CAS}$ (‰)-Mg/Ca (w/w) ($R^2 = 0.003$) of carbonates from the Aldan-Lena Rivers sections. Results are separated into groups by formations. Carbonate content (%): weight percentages of HCl-leachable $CaCO_3$ and $CaMg(CO_3)_2$ in the carbonate samples. CAS: carbonate-associated sulphate; carb: carbonate. Different colours represent different stratigraphic formations of the Aldan-Lena Rivers sections.

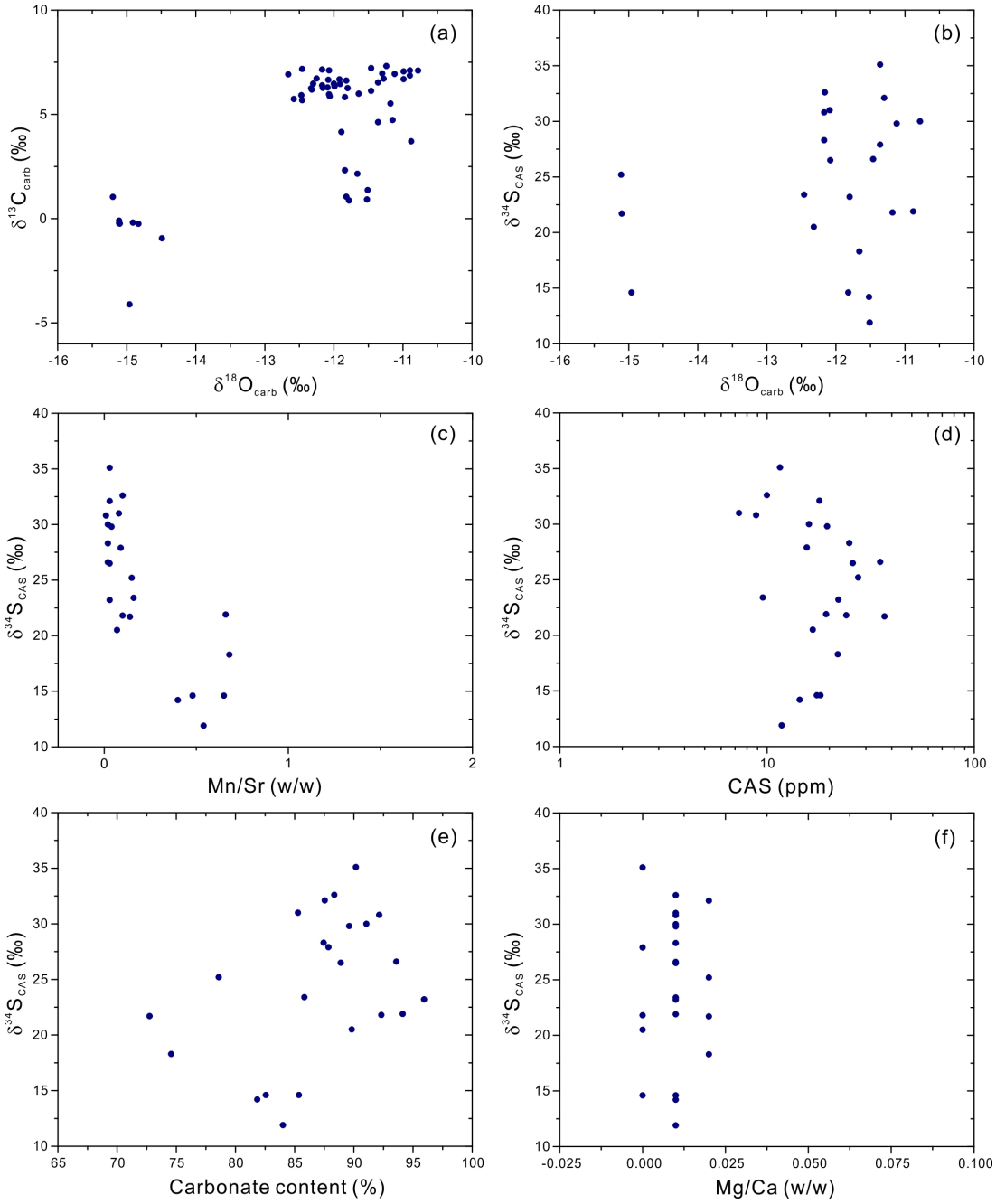

Figure. 3.3: Cross-plots of (a) $\delta^{18}O_{carb}$ (‰)-$\delta^{13}C_{carb}$ (‰) ($R^2 = 0.504$); (b) $\delta^{34}S_{CAS}$(‰)- $\delta^{18}O_{carb}$ (‰) ($R^2 = 0.049$); (c) $\delta^{34}S_{CAS}$(‰)-Mn/Sr (w/w) ($R^2 = 0.583$); (d) $\delta^{34}S_{CAS}$ (‰)-CAS (ppm) ($R^2 = 0.018$); (e) $\delta^{34}S_{CAS}$ (‰)-carbonate content (%) ($R^2 = 0.154$); and (f) $\delta^{34}S_{CAS}$ (‰)-Mg/Ca (w/w) ($R^2 < 0.001$) of carbonates from the Dahai Member of Xiaotan section. Results are separated into groups by formations. Carbonate content (%): weight percentages of HCl-leachable $CaCO_3$ and $CaMg(CO_3)_2$ in the carbonate samples. CAS: carbonate-associated sulphate; carb: carbonate.

3.3.2. $\delta^{13}C_{carb}$ records and age models

3.3.2.1. Aldan-Lena Rivers sections (late Stage 2–early Stage 4)

The new high-resolution carbon isotope results shown in Appendix C and Fig. 3.4 confirm the long-term $\delta^{13}C_{carb}$ trend, values and amplitudes of all short-term carbon-isotope oscillations presented in previous studies at the Aldan-Lena Rivers sections (Brasier, Corfield, *et al*., 1994; Brasier, Rozanov, *et al*., 1994, Dahl *et al*., 2017). The current study recovered three full $\delta^{13}C_{carb}$ positive excursions (III, VI, VII), the rising limb of IV and the falling limb of V (Fig. 3.4).

$\delta^{13}C_{carb}$ variability from the Tommotian to Botomian at the Aldan-Lena Rivers sections and Moroccan sections can be matched peak for peak without violating biostratigraphic or geochronologic constraints (Maloof *et al*., 2005; Maloof, Porter, *et al*., 2010; Peng, Babcock and Cooper, 2012). Therefore, an age model of Tommotian–Botomian stages can be applied in this study, based on the Moroccan radiometric ages presented in Fig. 3.4. The consistent reproducibility of $\delta^{13}C_{carb}$ across large environmental and sedimentation-rate gradients, ~50 m/Myr in Siberia and ~200 m/Myr in Morocco, may suggest that these carbonates are recording primary $\delta^{13}C_{carb}$ signals in well-mixed dissolved inorganic carbon (DIC) of the global ocean.

Age tie points were selected at the peaks of prominent and globally recognised $\delta^{13}C_{carb}$ excursions between the Siberian Aldan-Lena Rivers sections and Moroccan sections. The correlation scheme assumes constant sediment accumulation rates between tie points. These tie points include positive and negative excursions at 523.7 Ma, 522.9 Ma, 521.6 Ma, 520.6 Ma and 517 Ma (Maloof, Ramezani, *et al*., 2010). Age constraints on the topmost stratigraphic horizon in this study were calculated using the radiometric age for the Toyonian Stage (Landing *et al*., 1998). The age of 511 ± 1 Ma derives from a correlative trilobite-bearing (*Ovatoryctocara granulata* zone) stratigraphic horizon in Avalon. Accordingly, the sediment accumulation rate is calculated between *Ovatoryctocara granulata* zone (~511 Ma) and topmost *Fansycyathus lermontovae* zone (~517 Ma) at the Siberian Aldan-Lena Rivers sections based on the previously reported stratigraphic thickness in between (Brasier, Corfield, *et al*., 1994). Estimated ages are then assigned to our new data during this interval. Because the *O. granulata* zone in eastern Siberia is younger than the highest stratigraphic horizon (*Bergeroniellus ketemensis* zone) investigated in the current study (Peng, Babcock and Cooper,

2012), an age of 513 Ma is accordingly suggested for the early Toyonian as shown in Fig. 3.4 based on the calculation. The age for each sample and its correlation with archaeocyathid and/or trilobite biozones are shown in Appendix B.

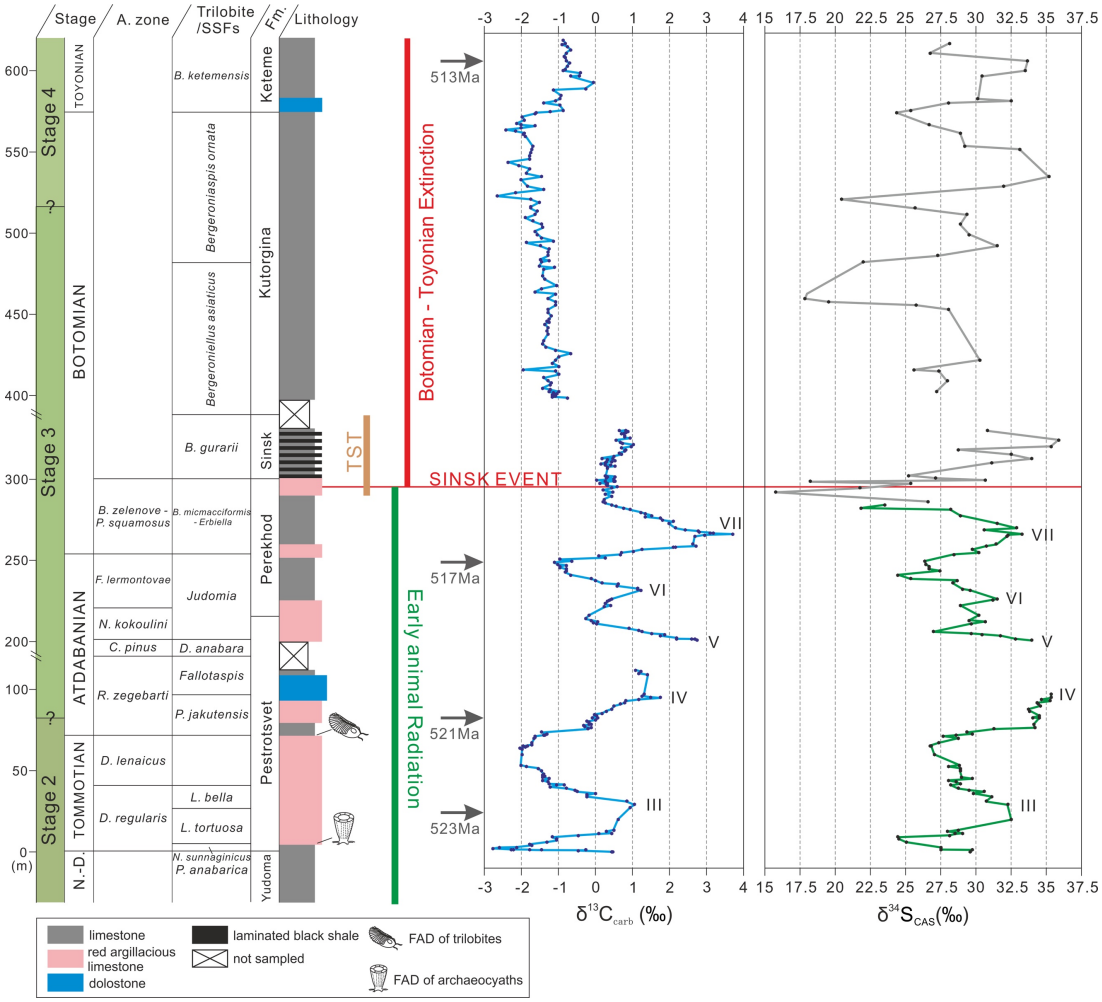

Figure. 3.4: High-resolution carbonate carbon ($\delta^{13}C_{carb}$) and carbonate-associated sulphate sulphur isotope ($\delta^{13}S_{CAS}$) records from Cambrian Stage 2 to Stage 4 of Siberian Aldan-Lena Rivers sections. Regional Stage subdivision is shown next to the global subdivision plan for comparison (Brasier, Corfield, *et al*., 1994) (N.-D.–Nemakit–Dalaynian; TST–Transgressive System Tract (Zhuravlev, 1998); A. zone–Archaeocyathid zone; SSFs–small shelly fossils; Fm.–Formation). Age assignments are deduced from carbon isotope stratigraphic correlations and U-Pb radiometric ages of tuffs of correlative strata in Morocco (Maloof, Ramezani, *et al*., 2010; Peng, Babcock and Cooper, 2012) and Avalon (Landing *et al*., 1998) (see details in Appendix B). Names for the positive $\delta^{13}C$ peaks (III, IV, V, VI, VII) are consistent with those of previously suggested $\delta^{13}C$ curves (Brasier, Corfield, *et al*., 1994; Brasier, Rozanov, *et al*., 1994).

3.3.2.2. Xiaotan section (early Stage 2)

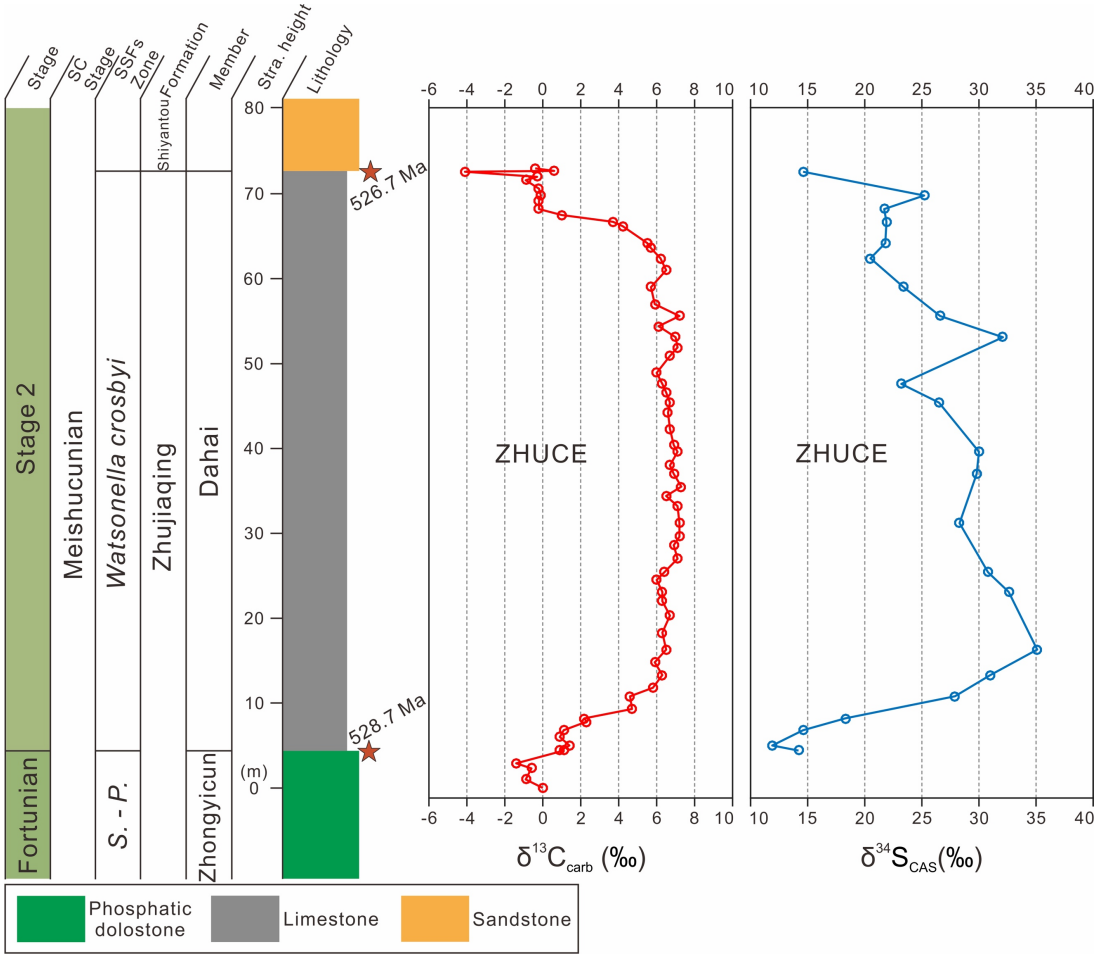

Figure. 3.5: High-resolution carbonate carbon ($\delta^{13}C_{carb}$) and carbonate-associated sulphate sulphur isotope ($\delta^{13}S_{CAS}$) records of early Cambrian Stage 2 at South China Xiaotan section. $\delta^{13}C_{carb}$ data are derived from Li *et al*. (2013). Regional Stage subdivision is shown next to the global subdivision plan for comparison (Li *et al*., 2013). SC Stage: South China Stage; SSFs: small shelly fossils. *S*. – *P*.: *Siphogonuchites triangularis* – *Paragloborilus subglobosus*. Age assignments are deduced from U-Pb radiometric ages of tuffs at the bottom and top horizon of Dahai Member. ZHUCE: ZHUjiaqing Carbon isotope Excursion. Stra. height: Stratigraphic height.

Carbonate carbon isotope results of the Dahai Member at the Xiaotan section are derived from previous studies by Li *et al*. (2013). The Dahai Member comprises the positive $\delta^{13}C_{carb}$ ZHUjiaqing Carbon isotope Excursion (ZHUCE), which is globally recognised in Cambrian Stage 2. U-Pb tuffs zircon dating gives absolute age constraints at the base and top of the Dahai Member with ~528.7 Ma and ~526.7 Ma, respectively (personal communication with Dr Chuan Yang of Institute of Geology and Geophysics, Chinese Academy of Sciences). The

peak of the positive $\delta^{13}C_{carb}$ excursion in Dahai Member is then estimated as at 527.3 Ma assuming a constant sediment accumulation rate within the member. The age for each sample and its correlation with small shelly fossils biozones are given in Appendix A.

3.3.3. $\delta^{34}S_{CAS}$ records

3.3.3.1. Aldan-Lena Rivers sections (late Stage 2–early Stage 4)

The stratigraphic distribution of $\delta^{34}S_{CAS}$ values of 142 carbonate samples from the Siberian Aldan-Lena Rivers sections is shown in Fig. 3.4. These data provide the first, continuous, high-resolution and high-fidelity carbonate-associated sulphate $\delta^{34}S_{CAS}$ record, from the late Stage 2 through to early Stage 4 (circa 524-513 Ma), exhibiting values between 16‰ and 36‰, averaging 29.1‰ ± 3.8‰ (1σ). Wotte, T. , Strauss, H., Sundberg (2011) reported seven $\delta^{34}S_{CAS}$ values from the Ulakhan-Kyyry-Taas section, which is one of the sub-sections and comprises the middle Stage 3 succession along the Aldan-Lena Rivers. Their results display $\delta^{34}S_{CAS}$ data between 27.7‰ and 30.6‰ averaging 29.3‰ ± 1.3‰ (1σ), matching the range of our new dataset. Although our data only cover the rising limb of positive $\delta^{34}S_{CAS}$ excursion IV, both values and magnitude of this excursion are consistent with Dahl et al. (2017)'s findings.

Our new dataset has also demonstrated that $\delta^{34}S_{CAS}$ fell from generally high values (mostly ~40-50‰) during the late Ediacaran (Cui *et al*., 2016) to lower values (~30‰) by the early Cambrian in Siberia, which confirm the drawdown of seawater sulphate $\delta^{34}S$ during the Ediacaran–Cambrian transition elsewhere on the other early Cambrian palaeocontinents (Fike, Bradley and Rose, 2015).

Strikingly, $\delta^{34}S_{CAS}$ data of Aldan-Lena Rivers sections exhibit a steadily evolving trend from the Tommotian (late Stage 2) to early Botomian (mid Stage 3), with positive excursions simultaneously coinciding with positive $\delta^{13}C_{carb}$ spikes (Fig. 3.4). Statistical correlation parameters show good positive correlation in both the trends and isotopic excursions from ~524 to ~516.5 Ma (Table 3.2). The coupled trends coincide with most of the reef-building organisms and arthropod radiation events on the Siberian Platform (Brasier, Corfield, *et al*., 1994; Varlamov *et al*., 2008), from where these biotic events are globally recognised (Zhu, Babcock and Peng, 2006; Zhu, 2010; Peng, Babcock and Cooper, 2012). By contrast, $\delta^{34}S_{CAS}$

data of ~516.5-~513 Ma are decoupled from the $\delta^{13}C_{carb}$ data, and show unsystematic scattering compared to its relatively stable $\delta^{13}C_{carb}$ trend. The decoupled trends approximately coincide with the interval of the Botomian–Toyonian extinction.

Table. 3.2: Statistical correlation parameters for paired short-term $\delta^{13}C_{carb}$ and $\delta^{34}S_{CAS}$ excursions and long-term trends in Fig. 3.4 and 3.5. The goodness of fit is indicated by the Pearson index, coefficient of determination (R^2) and root mean square error (*RMSE*). For Pearson (*P*) and R-square (R^2), closer to 1 indicate a better correlation between C-S isotopic data; For *RMSE*, smaller number indicate better correlation. ~524-516.5 Ma: interval when $\delta^{13}C_{carb}$ and $\delta^{34}S_{CAS}$ records are positively correlated at Aldan-Lena Rivers sections; ~516.5-513 Ma: interval when $\delta^{13}C_{carb}$ and $\delta^{34}S_{CAS}$ records decoupled at Aldan-Lena Rivers sections. ~528.7-526.7 Ma: interval when $\delta^{13}C_{carb}$ and $\delta^{34}S_{CAS}$ records are positively correlated in Dahai Member of Xiaotan section. ZHUCE: ZHUjiaqing Carbon isotope Excursion.

Isotope excursions/trends	*P*	R^2	*RMSE*	Regions
III	0.54	0.32	1.64	Aldan-Lena Rivers, Siberia
IV	0.94	0.92	0.96	Aldan-Lena Rivers, Siberia
V	0.60	0.73	1.21	Aldan-Lena Rivers, Siberia
VI	0.64	0.53	1.57	Aldan-Lena Rivers, Siberia
VII	0.74	0.55	2.14	Aldan-Lena Rivers, Siberia
~524-~516.5 Ma	0.50	0.26	2.53	Aldan-Lena Rivers, Siberia
~516.5-~513 Ma	0.076	0.001	4.9	Aldan-Lena Rivers, Siberia
ZHUCE / ~528.7-~526.7 Ma	0.74	0.50	5.1	Xiaotan, South China

3.3.3.2. Xiaotan section (early Stage 2)

The stratigraphic distribution of $\delta^{34}S_{CAS}$ values of 23 carbonate samples from the Xiaotan section is shown in Fig. 3.5. Only limestone samples ($CaCO_3$ content > 70%) of the Dahai Member (Li *et al*., 2013) are analysed because other stratigraphic horizons are characterised by either phosphatic dolostone or dolostone, which may have had their isotope signals altered during diagenesis and dolomitisation.

$\delta^{34}S_{CAS}$ data exhibit values between 12‰ and 35‰, averaging 24.4‰ ± 6.6‰ (1σ). These data provide the first high-resolution $\delta^{34}S_{CAS}$ record pairing the ZHUjiaqing Carbon isotope Excursion (ZHUCE) and associated small shelly fossil radiation event in the early Stage 2 (Zhu, Babcock and Peng, 2006; Peng, Babcock and Cooper, 2012). Paired $\delta^{34}S_{CAS}$ and $\delta^{13}C_{carb}$ records of Dahai Member also show strong positive correlations according to the statistical correlation parameters in Table 3.2, consistent with the findings in the younger isotope

excursions at the Siberian Aldan-Lena Rivers sections.

Considering the strict CAS extraction method and data diagenetic evaluation applied in the current study, the new $\delta^{34}S_{CAS}$ dataset from Siberia and South China provides hitherto the first, continuous, high-resolution and high-fidelity sulphur isotopic constraints on the long-term evolution of early Cambrian seawater sulphate, while structured cycles are obvious in the records where sampling resolution is high enough (Fig. 3.4 and 3.5).

3.4. Discussions

3.4.1. Estimation of early Cambrian seawater sulphate concentrations

The rate of change of seawater sulphate sulphur isotope ratio, using the 'rate method' model (Song *et al*., 2014; Algeo *et al*., 2015), allows us to estimate the size of the marine sulphate reservoir ($[SO_4^{2-}]$) through the Cambrian stages 2-4 in eastern Siberia and South China. The descriptions and parameters of the model are shown in section 3.2.3.1.

The variation of seawater sulphate concentrations between 529 Ma and 513 Ma is provided based on a point-to-point calculation on the rates of $\delta^{34}S_{CAS}$ change between samples (Fig. 3.6). However, the maximum concentration for an individual point could be under- or overestimated due to fluctuation and anomalies in the rate of $\delta^{34}S_{CAS}$ changes. To overcome this bias, the resulting $[SO_4^{2-}]$ data are binned into 0.5-Myr bands. The lower envelope of the $[SO_4^{2-}]$ curves, which links the lowest value for each band, is expected to represent the maximum rates of $\delta^{34}S_{CAS}$ change and thus the theoretical estimate of maximum seawater sulphate concentration through time. The results are presented by using three different data smoothing grids at 0.1 (red), 0.5 (blue) and 1 (black) Myr respectively. Although the age difference between samples is generally below 0.1 Myr (see Appendix A and C), a conservative $[SO_4^{2-}]$ ranges between the 0.1- and 0.5-Myr gridded curves (shaded area in Fig. 3.6) are suggested here to avoid influence by $\delta^{34}S_{CAS}$ data variation anomalies due to sample quality and analytical uncertainties.

The maximum seawater sulphate concentrations ($[SO_4^{2-}]$) in eastern Siberia are constrained as ~2.3-11.7 mM for the interval c. 524-516.5 Ma (late Stage 2–late Stage 3), and ~1.0-5.1 mM for the interval c. 516.5-513 Ma (late Stage 3–early Stage 4), if taking the average values from the 0.1- and 0.5-Myr gridded curves (Fig. 3.6). Additional $[SO_4^{2-}]$ data from the South China Xiaotan section yields ~1.5-7.5 mM for the interval c. 524-516.5 Ma (early Stage 2), consistent with the ranges of Siberia. These $[SO_4^{2-}]$ results are consistent with previously modelled estimates of ~5 to ~10 mM for the early Cambrian (Algeo *et al*., 2015), ~2 to ~12 mM for the late Cambrian (Gill, Lyons and Saltzman, 2007; Gill *et al*., 2011), and fluid inclusion-based estimates of ~4.5 to ~11 mM for the early Cambrian (Brennan, Lowenstein and Horita, 2004; Petrychenko, Peryt and Chechel, 2005). Thus, the early Cambrian ocean, at

least in eastern Siberia and South China, was characterised by a relative paucity of sulphate, when compared with the modern ocean (~29 mM).

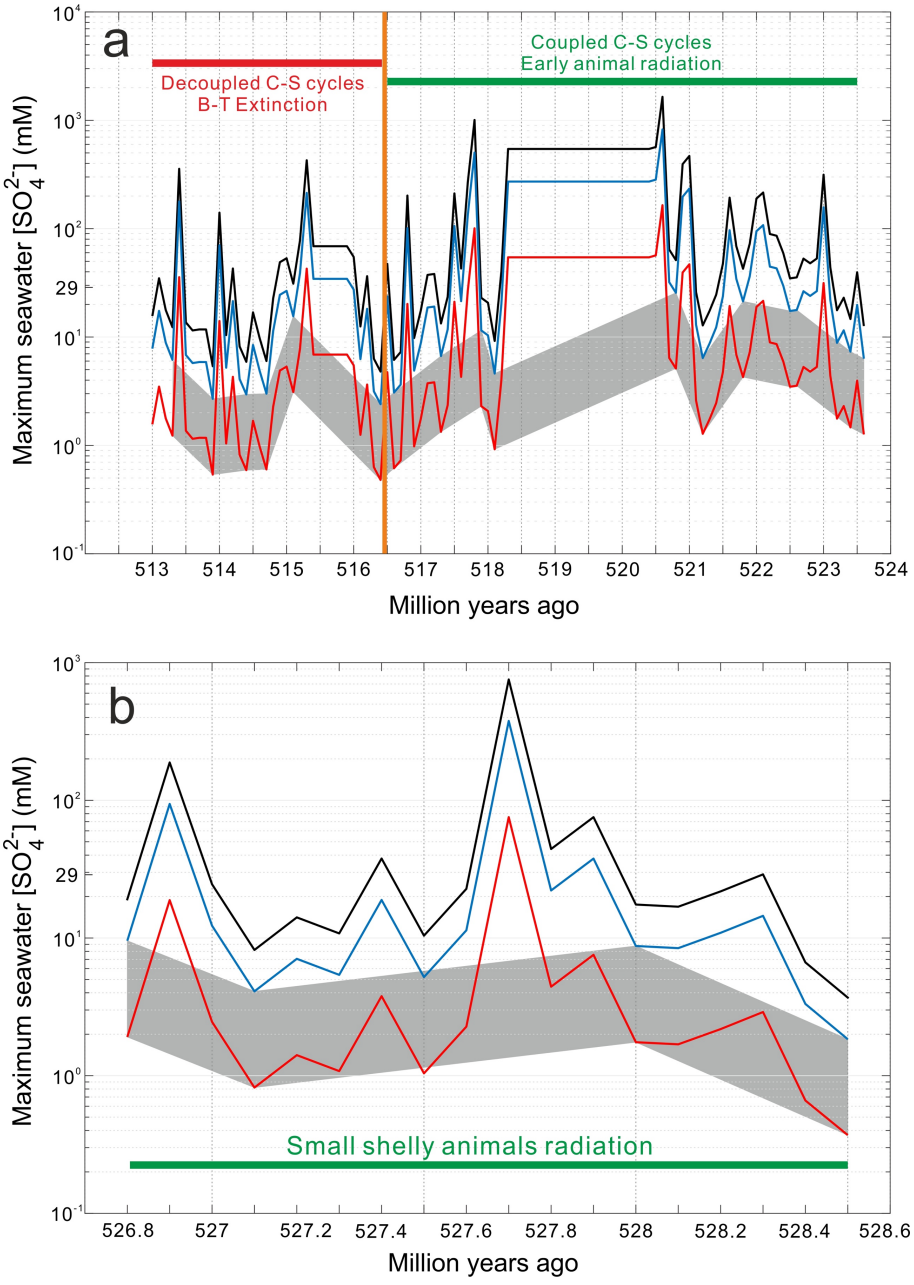

Figure. 3.6: Secular variation of maximum seawater [SO_4^{2-}] from the Cambrian Stage 2 to Stage 4 (~529-~513 Ma) for eastern Siberia (a) and South China (b) platforms. The curves yield the maximum possible seawater [SO_4^{2-}] with data smoothing grids at 0.1 (red), 0.5 (blue) and 1 (black) Myr respectively. The shaded area represents the best estimate of the variation of sulphate concentration. Coupled C-S cycles: interval when $\delta^{13}C_{carb}$ and $\delta^{34}S_{CAS}$ records are positively correlated; Decoupled C-S cycles: interval when $\delta^{13}C_{carb}$ and $\delta^{34}S_{CAS}$ records are decoupled; B-T Extinction: Botomian-Toyonian Extinction.

The new modelled results are also consistent with a rise in seawater sulphate concentrations from the late Neoproterozoic (< 5 mM) (Algeo *et al*., 2015) to the early Cambrian, possibly mirroring the Neoproterozoic oceanic oxygenation event at the Ediacaran–Cambrian transition (Shields-Zhou and Och, 2011; Och and Shields-Zhou, 2012). Additionally, on the eastern Siberian Platform, the rate of $\delta^{34}S_{CAS}$ change during the Botomian–Toyonian Extinction (~516.5-~513 Ma) is higher than that in the preceding radiation interval (~524-~516.5 Ma). By the calculation above, a significant drawdown of more than half of the sulphate pool by ~516.5 Ma is seen to coincide with the major extinction point-Sinsk event of Botomian–Toyonian extinction (Fig. 3.4).

3.4.2. Modelling the causes for the coupled sulphur and carbon isotopic records

The covariant behaviour of the marine carbon and sulphur isotope systems of interval c. 529-513 Ma is observed in the Siberian and South China oceans (Fig. 3.4&3.5). The positively correlated carbonate carbon and sulphate sulphur isotope records can be explained by coupled burial of pyrite and organic carbon in marine sediments under anoxic, productive settings (Berner and Raiswel, 1983). Under deep-water anoxic, highly productive conditions, organic matter preservation potential will be high, but increased export to the seafloor will also enhance microbial sulphate reduction (MSR), resulting in increased pyrite formation due to the production of H_2S from MSR. Because pyrite and organic carbon are enriched in the lighter isotopes ^{32}S and ^{12}C, respectively, elevated removal rates of both of these reduced species on a global scale would leave seawater higher in $\delta^{34}S$ and $\delta^{13}C$.

A simple biogeochemical box model (Garrels and Lerman, 1984; Bergman, Lenton and Watson, 2004; Berner, 2006) was applied to test whether measured trends in S isotopes can be reproduced from the coupled burial of pyrite sulphur and organic carbon (see Methods for details of coupled C-S cycles model). The model infers the rate of organic carbon burial using the $\delta^{13}C_{carb}$ record and an isotopic mass balance (Garrels and Lerman, 1984), while the rate of pyrite burial is calculated assuming a linear relationship with organic carbon burial (relative to initial burial rate), allowing prediction of coeval seawater sulphate $\delta^{34}S$ values (corresponding to $\delta^{34}S_{CAS}$ in this study).

Results (Fig. 3.7) show that both the amplitudes of positive sulphur isotope excursions and their long-term trend from c. 524-516.5 Ma can be replicated. The absolute $\delta^{34}S_{CAS}$ values are not replicated perfectly in this simplified model: the assumed constancy of parameters such as the isotopic composition of carbon and sulphur inputs ($\delta^{13}C_{in}$, $\delta^{34}S_{in}$), and the background carbon and sulphur cycle input fluxes through weathering and metamorphism is likely an oversimplification. The shaded area in Fig. 3.7 shows the results of varying $\delta^{13}C_{in}$ between ~-5‰ and ~-8‰ as an example of how this may shift the curve. The model requires a low concentration of sulphate in seawater (best-fit ~1 mM), in order to match the rate and amplitude of $\delta^{34}S_{CAS}$ variations. The ~1 mM constraint is consistent with the lower end of maximum estimates derived from the 'rate method' model.

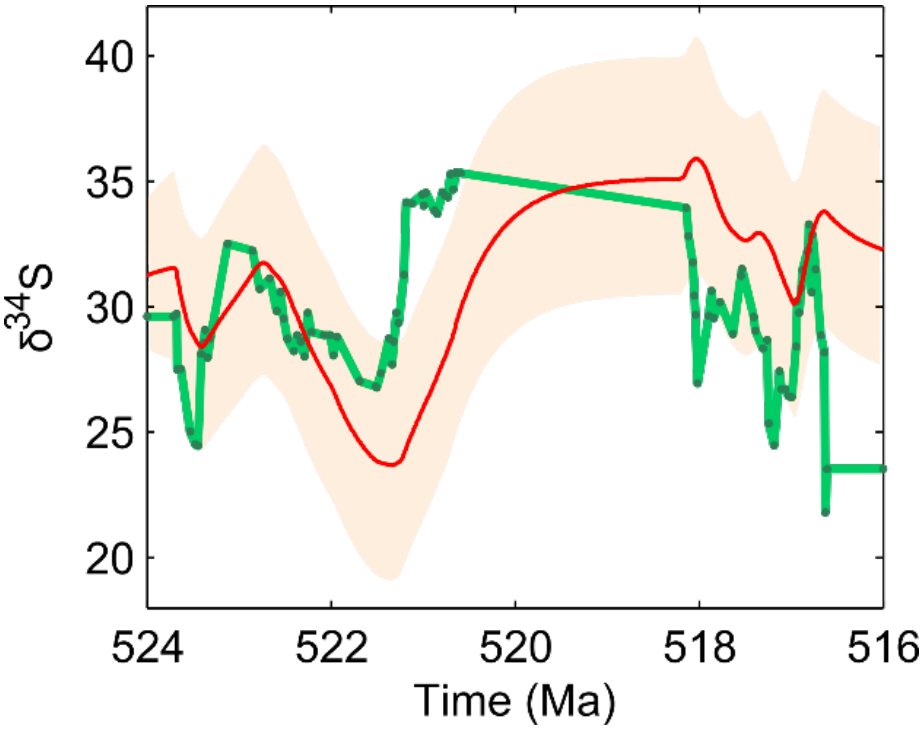

Figure. 3.7: Comparison between analysed $\delta^{34}S_{CAS}$ data (green curve) and simulated sulphur isotope curve of seawater sulphate (red) which utilises $\delta^{13}C$ data of carbonate to drive a coupled C-S cycle model (see in extended data). Faint uncertainty window represents changing the $\delta^{13}C$ value of carbon inputs between ~-5‰ and ~-8 ‰. The modelled interval is associated with the positively correlated $\delta^{34}S_{CAS}$ and $\delta^{13}C_{carb}$ records and most of the early animal radiations.

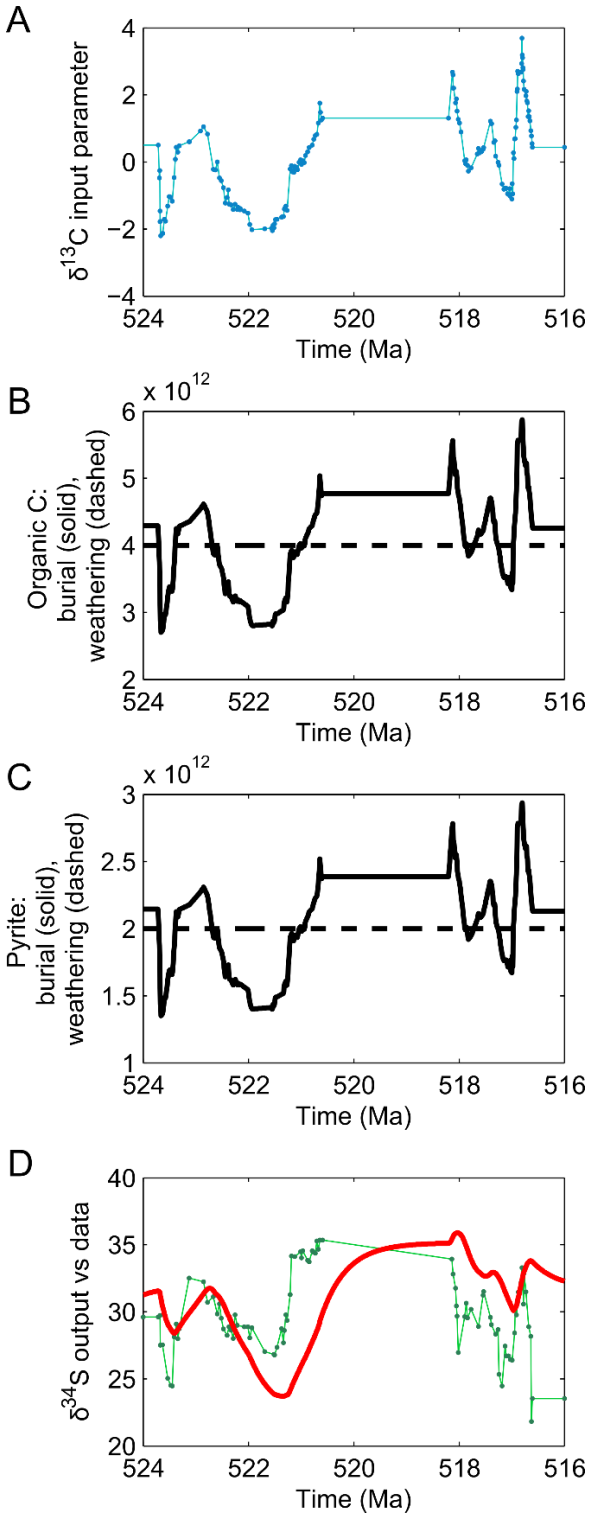

Figure. 3.8: Coupled C-S cycle model output. A: $\delta^{13}C$ of carbonate used as model input parameter. B: Organic carbon burial rate (solid line) and weathering rate (dashed line) predicted from the model. C: Pyrite sulphur burial rate (solid line) and weathering rate (dashed line) predicted from the model. D: Model $\delta^{34}S$ of seawater sulphate output (red) compared to data from this study (green). This shows model run where the average composition of carbon inputs is -6.75‰, which is the red line in Fig. 3.7.

The coupled carbon and sulphur isotope swings show an apparent periodicity of approximately 1-2 Myr duration that reflects cyclical changes in the burial rates of organic carbon and pyrite, respectively, which could be ultimately induced by the expansion of deep-water anoxia or euxinia (Gomes and Johnston, 2017). Coupled burial of both reduced species in the marine sediments also results in the release of oxygen and other marine oxidants. Each peak of the positive isotope swing thus represents the peak of an oceanic oxygenation event and/or a pulse of atmospheric oxygen production (Gill, Lyons and Saltzman, 2007; Saltzman *et al*., 2011). Accordingly, the falling limbs of the positive isotope excursions represent periods of increased organic carbon remineralization rate and decreased MSR intensity during more oxygenated deep-water conditions.

Such redox and oxygenation oscillations could also relate to regulation of the size of a marine dissolved organic carbon (DOC) reservoir. High marine productivity accompanying the Cambrian radiation would have promoted organic carbon/matter production. A stepwise building DOC reservoir exhausted the oxidants and surpassed the oxygen production rate via marine photosynthesis that resulted in widespread anoxia, enhanced organic carbon burial and facilitated the pyrite production/burial via MSR on the seafloor. On the other hand, enhanced organic production would have induced the negative feedback on the benthic oxygen production, but promoted the phosphorous diffusion into the seawater and thereby nutrient availability to facilitate the radiations in the shallow marine animal habitat. (Shields-Zhou and Zhu, 2013).

3.4.3. Decoupling the marine carbon and sulphur cycles in the late Stage 3–Stage 4

In sharp contrast to the coupled trends during interval of animal radiations, $\delta^{34}S_{CAS}$ values across most of the Botomian to early Toyonian (late stage 2–early Stage 4; c. 516.5-513 Ma), which coincides with the Botomian–Toyonian extinction (BTE), are decoupled from the $\delta^{13}C_{carb}$ record, and are characterised by rapid rhythmic fluctuations of large magnitude (Fig. 3.4). As evidenced by the increased rapidity of $\delta^{34}S_{CAS}$ change, the 'rate method' suggests a considerable decline in the size of the oceanic sulphate reservoir during this interval. This is based on the theory that changes in global or regional marine sulphate concentrations will change the

sensitivity of sulphate isotope compositions to water mass exchange rates (Newton *et al*., 2011).

A drop in oceanic sulphate concentration is generally assigned to enhanced evaporite deposition or widespread anoxia. There are no obvious evaporite deposits in the local rock record during this period. The cause of the major extinction event (Sinsk event; Fig. 3.4) at the beginning of the BTE has been linked to shoaling of oxygen-depleted water during a major transgressive event (Zhuravlev and Wood, 1996; Mángano and Buatois, 2014). Anoxic/euxinic conditions likely prevailed in the Siberian shallow marine realm during the BTE. Short-term variability in the $\delta^{34}S_{CAS}$ record thus could be explained by rhythmic oxidation of a ^{34}S-depleted reactive, deep ocean HS^- reservoir. The repeated fluctuations thereby represent an alternation between enhanced MSR that pushed the seawater sulphate $\delta^{34}S$ to high values, and enhanced reoxidation of the marine HS^- to lower values in a sulphate-limited ocean.

3.4.4. Correlating the oceanic redox pattern with the early Cambrian biological events

Some preliminary work suggested that the exceptionally preserved Fossil-Lagerstätten of the early Cambrian and major animal radiation events coincide with the five positive isotope excursions of our study that, in the case of $\delta^{13}C_{carb}$, are demonstrably global phenomena (Zhu, Babcock and Peng, 2006; Maloof, Porter, *et al*., 2010; Peng, Babcock and Cooper, 2012). For example, positive excursion-IV coincides with the major arthropod radiations as evident in Chengjiang and Sirius Passet Lagerstätten. Excursion-VII coincides with a global radiation of archaeocyathids. By contrast, minor extinction events appear to be associated with the negative excursions (Zhu, Babcock and Peng, 2006; Peng, Babcock and Cooper, 2012). However, palaeontological data would always generate animal diversity anomalies at intervals with the presence of Fossil-Lagerstätten. Further correlation between isotope excursions and radiation events remains to be elucidated.

To investigate the direct relationship between the isotopic cycles and radiation pattern, this study uses the paired animal diversity data at the Aldan-Lena Rivers sections. As illustrated in Fig. 3.9, these data quantitatively resolve the diversity trends and radiation peaks of total marine animal species and reefal communities through time (Zhuravlev and Wood, 1996;

Zhuravlev and Naimark, 2005). The correlation between the diversity data and $\delta^{13}C_{carb}$ curve applies a consistent age model, and is achieved by matching the trilobite/archaeocyathid zones.

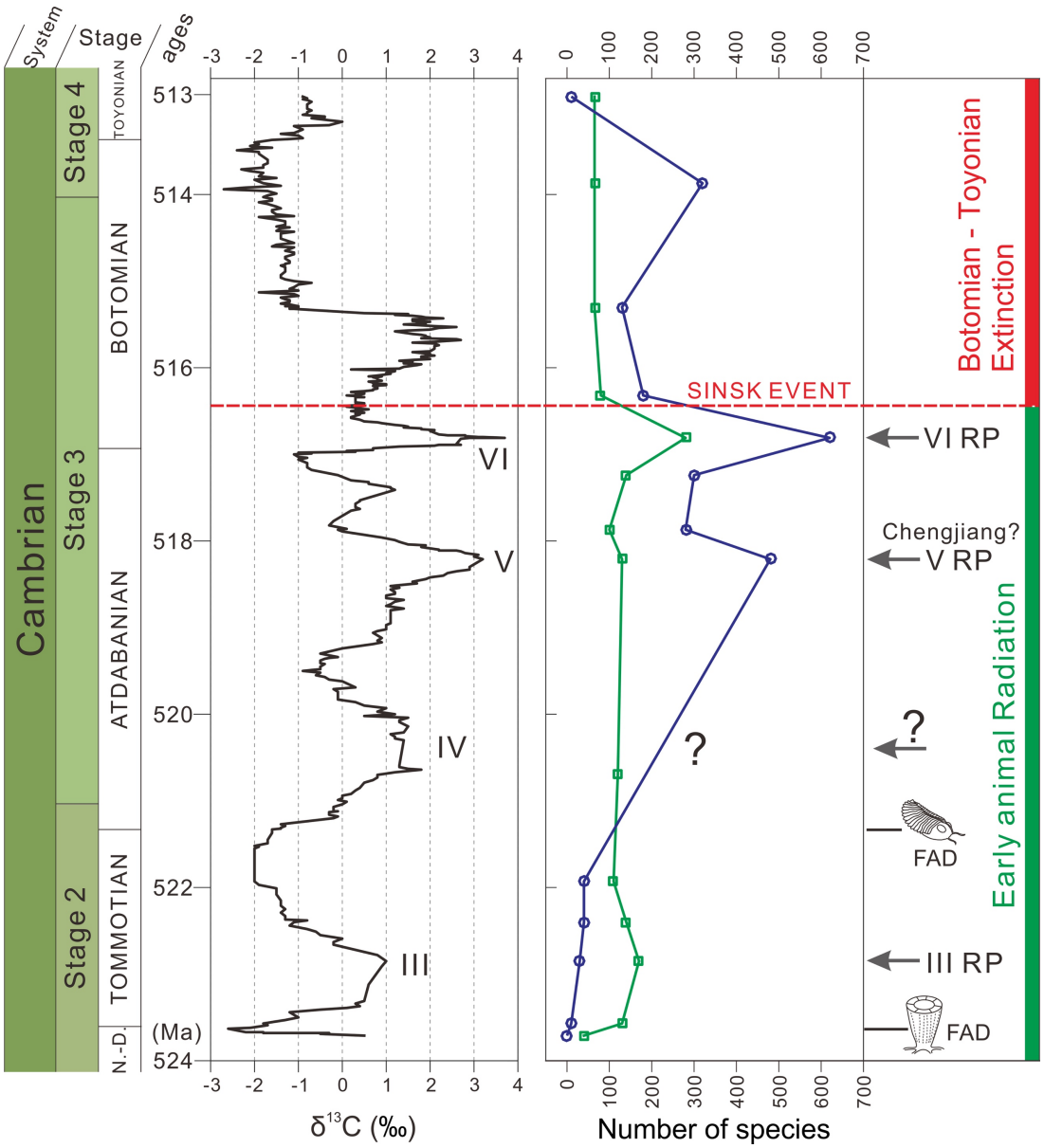

Figure. 3.9: Summary of the Siberian animal species diversity, biological events and their correlation to the carbonate carbon isotope record in the Cambrian stages 2-4. Regional Stage subdivision is shown next to the global subdivision plan for comparison; N.-D.–Nemakit–Dalaynian. $\delta^{13}C_{carb}$ data are obtained from the current study and Brasier, Corfield, *et al.* (1994) using the age model discussed in section 3.3.2.1; Names for the positive $\delta^{13}C_{carb}$ peaks (III, IV, V, VI, VII) are consistent with those of previously suggested $\delta^{13}C_{carb}$ curves (Brasier, Corfield, *et al.*, 1994; Brasier, Rozanov, *et al.*, 1994). The animal diversity curves are expressed as mean number of species per sampling unit at the Siberian Aldan-Lena Rivers sections; Green curve: total animal species diversity including reef-building archaeocyath (Zhuravlev and Wood, 1996); Blue curve: archaeocyath species diversity based on an updated database after

the 1996-version (Zhuravlev and Naimark, 2005). RP: radiation peak; FAD: first appearance datum; Chengjiang?: timing of the Chengjiang Fossil-Lagerstätten in Yunnan Province, South China (Zhu, Babcock and Peng, 2006).

Strikingly, three positive isotopic excursions (III, V, VI) coincide closely with three prominent animal diversity/radiation peaks at the Aldan-Lena Rivers sections (Fig. 3.9). With only one exception, there is no radiation peak associated with the IV $\delta^{13}C_{carb}$ excursion. However, this missing link could have been overshadowed by the continuous building up of archaeocyathid diversity through the interval between IV and V or simply due to the lack of data. Nevertheless, the rising limb of excursion-IV can still be approximately correlated with the first emergence of trilobites, which was a key arthropod radiation event in early Stage 3. The positive isotopic excursion-ZHUCE at the South China Xiaotan section also coincides with the biggest diversity peak of small shelly animal species in the mid Stage 2 (Li *et al*., 2007), suggesting a covariant relationship between the isotope cycles and animal diversification pattern.

The coupled behaviour in the $\delta^{13}C_{carb}$ and $\delta^{34}S_{CAS}$ cycles has revealed that episodic pulses of atmospheric oxygenation events correspond to the peaks of positive isotope swings. These isotopic cycles thereby reflect an oscillating pattern in the marine redox condition and net oxygen production, which further leads to a tight correlation with the rise and fall in animal diversity. Therefore, this study proposes that perturbations in deep-water redox and atmospheric oxygenation of the Cambrian stages 2-3 would seem to have governed the origination rate and diversification pattern of animals, and so provides a direct environmental explanation for the episodic nature of early animal radiation. The periodic oxygenation of the ocean would have introduced new ecological niches and radiation opportunities, which could facilitate the periodic increase in the rate and extent of animal forms and behaviours (e.g. bioturbation).

However, these episodic oxygenation events could also be in part the consequence of animal radiations. It seems that the return to more oxygenated conditions corresponds to a system response to excess oxidant production via increased burial of reduced carbon and sulphur species. But such a negative feedback loop between long-term oxygen release and burial of reduced species might be related to an increase in bioturbation intensity and areal extent, such as happened during Cambrian stages 2-3 (Boyle *et al*., 2014; Mángano and Buatois, 2014). It has also been hypothesised by Dahl *et al*. (2017) that enhanced biological pump by larger zooplankton increased the bioturbation, and thereby benthic oxygen production, which could

briefly stabilise the oceanic oxygen levels. But the subsequent benthic oxygen consumption due to organic carbon remineralisation and high bioturbation rate would have lowered the oxygen levels (Dahl *et al*., 2017). Therefore, this ecological feedback serves as a possible mechanism to explain the episodic marine redox perturbation in the early Cambrian ocean. But whether such feedback could have continuously controlled the periodic oxygenations through at least five cycles in the Cambrian stages 2-3 remains unclear. Further high-resolution data collection of bioturbation intensity would be needed to confirm this ecological explanation.

On the other hand, there was a major drawdown in the animal diversity by the early Botomian (Fig. 3.9), coinciding the decoupled $\delta^{13}C_{carb}$ and $\delta^{34}S_{CAS}$ cycles (Fig. 3.7). The timing of this diversity decline is consistent with the initiation of Botomian–Toyonian extinction and Sinsk transgression event in eastern Siberia (Zhuravlev and Wood, 1996). The Sinsk transgression could possibly induce the significant decline in the marine sulphate concentration and shoaling of anoxic/euxinic deep-water to the animal habitat, resulting in the temporary interruption of the early Cambrian animal diversification.

3.5. Conclusions

Using paired $\delta^{13}C_{carb}$ and $\delta^{34}S_{CAS}$ records, this study reveals covariant behaviour between the marine carbon and sulphur cycles via coupled burial of pyrite sulphur and organic carbon. Results also demonstrate a periodicity with at least six isotopic cycles in the Cambrian stages 2-3, suggesting extreme redox fluctuations and episodic oxygenation events in the ocean. These pulses of oxygenation correspond perfectly to the animal diversity peaks through this interval in Siberia, thereby providing the first environmental explanation for the episodic nature of Cambrian animal radiation pattern. By contrast, the subsequent Botomian-Toyonian extinction evidenced a decline in the marine sulphate concentration and decoupling of $\delta^{13}C_{carb}$ and $\delta^{34}S_{CAS}$ records, likely triggered by widespread shoaling of anoxic/euxinic deep-water to the shallow marine animal habitat.

Chapter 4

Strontium isotope evidence for high continental weathering flux during the Cambrian radiation of animals

ABSTRACT

New $^{87}Sr/^{86}Sr$ data from eastern Siberia are integrated with existing lower Cambrian data from China, Mongolia and Morocco in this study. New analyses of 48 carbonate rocks from the Siberian Aldan-Lena Rivers sections reveal a rapid monotonous climb in seawater $^{87}Sr/^{86}Sr$ ratios by ~0.0006 from the Cambrian Stage 2 minimum (~0.7081) to Stage 3 maximum (~0.7087). Utilising a new age model and integrated dataset, the rate of change of seawater $^{87}Sr/^{86}Sr$ was 0.00008/Myr at approximately 523.5-517.5 Ma. Modelling results suggest that the increase of seawater $^{87}Sr/^{86}Sr$ in Cambrian stages 2-3 coincided with major radiations of animal phyla in the early Cambrian and was due primarily to an elevated flux and/or $^{87}Sr/^{86}Sr$ ratio of continental crust weathering. Enhanced denudation and chemical weathering of exposed continental materials (e.g. Pan-African orogeny on the Gondwana, regolith on the 'Great Unconformity' surface) could have resulted in a high nutrient flux into the ocean, fuelling the marine biotic diversification. This study also provides the first LOWESS-fitted (LOcally Weighted scatterplot smoothing) seawater $^{87}Sr/^{86}Sr$ curve for the first two series of the Cambrian System. Secular evolution of early Cambrian seawater $^{87}Sr/^{86}Sr$ exhibits a first-order decline starting from the late Ediacaran to late Cambrian Stage 2, followed by a long-term increase towards the Phanerozoic maximum (~0.7092) in Cambrian Stage 5. However, a retardation at

ca. 517-512 Ma is superimposed on the long-term increase, with the beginning and end of this $^{87}Sr/^{86}Sr$ plateau coinciding with two global sea-level change/extinction events, respectively: the Sinsk transgression event at ~516 Ma and the Hawke Bay regression event at ~512 Ma. Sea-level fluctuations could have altered the contribution of radiogenic Sr from the continental weathering flux, providing a possible mechanism to explain the 4-Myr interruption of the Cambrian stages 2-5 $^{87}Sr/^{86}Sr$ increase and associated Botomian–Toyonian extinction.

Author Contributions: Matthew F. Thirlwall, Christina J. Manning, Ying Zhou supervised or assisted Sr isotopic analysis at Royal Holloway, University of London. Major and trace element data presented here were obtained with technical assistance from Gary Tarbuck, University College London. The discussion benefitted from helpful conversations with Graham Shields, Philip Pogge von Strandmann, Benjamin Mills and John McArthur.

4.1. Introduction

Diversification of early animals, including skeletonised arthropods and advanced reef-building animals, reached its apex during Cambrian stages 2-4. A wide range of plausible environmental triggers is surmised to have been linked to the events. The most favoured ideas focus on changes in the chemical composition of seawater, due to exceedingly high rates of continental weathering of elevated trans-Gondwanan mountain chains and exposed 'Great Unconformity' surface during the interval. Enhanced weathering of the continental crust would have boosted transport fluxes of cations and life-bearing nutrients (e.g. phosphorus) to the oceans thereby playing a potentially critical role in fuelling the Cambrian radiation of animals (Brasier and Lindsay, 2001; Zhang *et al*., 2014). On the other hand, after the radiation events, there followed a dramatic biotic crisis around late Stage 3 to early Stage 4 (Brasier, Corfield, *et al*., 1994; Zhuravlev and Wood, 1996), known as the Botomian-Toyonian extinction (BTE). Two major extinction phases bracket this period, and coincide with the Sinsk transgression and Hawke Bay regression events, respectively (Zhuravlev, 1996; Zhuravlev and Wood, 1996; Dilliard *et al*., 2007). The cause and effect of these sea-level changes are poorly constrained, but such global-scale sea-level fluctuations should impact on the surface area of the exposed continental crust and weathering flux of source materials.

To resolve the continental weathering history and related bio- and geological events at this crucial juncture, the marine strontium isotopic system is selected as a focus of the study. Modern seawater $^{87}Sr/^{86}Sr$ is primarily determined by fluxes from continental weathering via river runoff and seafloor hydrothermal circulation at mid-ocean ridges (Palmer and Edmond, 1989; Vance, Teagle and Foster, 2009). Continents are enriched in radiogenic ^{87}Sr, whereas the mantle and oceanic crust have a lower $^{87}Sr/^{86}Sr$ ratio. This is due their contrasting, initial Rb/Sr ratios and ages. As a consequence of this dual control, the $^{87}Sr/^{86}Sr$ ratio of seawater is predicted to rise if the relative contribution from continental silicate weathering to the oceans increases. On the other hand, an increase in mantle Sr input and/or seafloor-spreading rates would lower seawater $^{87}Sr/^{86}Sr$. Therefore, the balance between the continents and the mantle input flux is crucial in understanding the Sr isotopic evolution of seawater, allowing us to evaluate both continental and hydrothermal activities through geological time. Diagenetically least-altered marine carbonate, which is considered as preserving primary seawater isotopic signals, can be used to determine the seawater $^{87}Sr/^{86}Sr$ of the coeval ocean (McArthur, Howarth and Shields-Zhou, 2012). Derry *et al*. (1994) first reported a carbonate-based $^{87}Sr/^{86}Sr$ curve for

the Aldan-Lena River sections from the eastern Siberian Platform. $^{87}Sr/^{86}Sr$ rose steadily from Cambrian Stage 2 to Stage 3, then decreased in early Stage 4 but rose again in late Stage 4. However, their data only exhibited low-resolution sampling and applied an estimated timescale, thus was unable to determine the timing and duration of the rate of changes in $^{87}Sr/^{86}Sr$. An additional problem is that data presented in Derry's work used inadequate criteria to distinguish carbonate diagenetic alteration and so the fidelity of their primary seawater signature needs testing.

Variation of seawater $^{87}Sr/^{86}Sr$ as a function of geological time is widely applied to date and to correlate stratigraphic horizons between sedimentary sections (McArthur, Howarth and Shields-Zhou, 2012; Korte and Ullmann, 2017). This rests on the assumption that the mixing time of the oceans with respect to Sr is significantly shorter (1 kyr) compared to its residence time (~3 Myr) (Palmer and Edmond, 1989; Pearce *et al*., 2015). This means that oceans are thoroughly mixed and homogeneous with respect to $^{87}Sr/^{86}Sr$ on time scales that are short relative to the rates of input and output of strontium. However, resolving the Cambrian $^{87}Sr/^{86}Sr$ calibration curve is problematic due to unreliable relative and absolute age constraints as well as the poor global stratigraphic correlation for the lower Cambrian strata. It is also hampered by the fact that many of the published carbonate $^{87}Sr/^{86}Sr$ data did not apply a thorough analysis of diagenetic alteration. As a result, the previous compilation of data produces a scattering dataset through geological time rather than a tightly defined curve (Maloof, Porter, *et al*., 2010). Moreover, the timing and tempo of the rise and fall of seawater $^{87}Sr/^{86}Sr$ during the early Cambrian are not well-constrained, and the current study attempts to improve that chronological constraint.

This study presents a new high-resolution $^{87}Sr/^{86}Sr$ profile for the Siberian Aldan-Lena River sections, in the context of an integrated litho- and biostratigraphic framework and new age model. These new data establish the best available constraints on seawater $^{87}Sr/^{86}Sr$ evolution from the late Stage 2 to early Stage 4. The goals were to evaluate the reliability of previously published carbonate $^{87}Sr/^{86}Sr$, and to test whether the seawater $^{87}Sr/^{86}Sr$ record can resolve continental weathering history and tectonic backdrop during the animal radiation events and Botomian–Toyonian extinction of the Cambrian stages 2-4. This study also provides a compilation of carbonate $^{87}Sr/^{86}Sr$ data for the lower Cambrian series. A LOWESS-fitted calibration curve based on least-diagenetically altered carbonate is given here constraining the evolution of seawater $^{87}Sr/^{86}Sr$ during ca. 546-511 Ma.

4.2. Methods

4.2.1. Samples

Samples collected from the Siberian Aldan-Lena rivers sections are utilised for a strontium isotope stratigraphy (SIS) study from the Cambrian Stage 2 to Stage 4. Details of geological and stratigraphic settings are discussed in section 1.6.4. Forty-eight well-preserved carbonate samples were selected following the petrographic and carbonate (total HCl-leachable) geochemical selection criteria set out in section 4.2.2.

4.2.2. Analytical techniques

Prior to the Sr isotope analysis, procedures of sample preparation derive from protocols for Strontium Isotope Stratigraphy (SIS) study in two publications (Bailey *et al*., 2000; Li *et al*., 2011). Application of these protocols would help target the least-altered components in bulk rock carbonate. Thin-sections of the sample rock slabs were firstly scrutinised to identify the best-preserved rock components destined for Sr isotope analyses. Carbonate rock powders were then drilled on the counterpart of the rock slabs using a tungsten carbide tipped drill. Care was taken to avoid sampling areas near cross-cutting, late stage calcitic micro-veins and interstitial cements, visible alteration zones and zones where fine-grained microspar was intermixed with coarse-grained sparry phases. However, some low-quality samples were also analysed for comparison (see discussion in section 4.3.2).

Samples screened by petrographic evaluation were further screened based on rigid bulk carbonate (total HCl-leachable) geochemical selection criteria (Li *et al*., 2011, 2013). An aliquot of the powder (~50 mg) was dissolved in excess (about 3ml) 10% hydrochloric acid at room temperature for at least 12h. Reaction was facilitated using an ultrasonic bath and roller mixer. After centrifugation, aliquots of supernatant were then analysed using a *Varian*® 720-ES Inductively Coupled Plasma Optical Emission Spectrometer (ICP-OES) at the Cross-Faculty Elemental Analysis Facility, University College London. Only samples with [Sr] > 150 ppm, carbonate content > 70%, [Al] < 0.1 %, [Rb] < 10 ppm and Mn/Sr < 1 were chosen. This is because that best-preserved carbonates for SIS study are often characterised by high Sr and carbonate concentrations, low clay content (Low [Al] and [Rb]) and minimal diagenetic

alteration (e.g. low Mn/Sr).

Fine powders (100-200 mg) of selected samples were pre-leached (1st leach) with 0.00013 M acetic acid by calculated volume to dissolve roughly 30% of the carbonate by applying the total HCl-leachable carbonate content data (reported in Appendix C). This step is designed to remove ions (e.g. Rb and radiogenic Sr) from exchangeable or leachable sites within or on clay-bound and altered carbonate phases. Water-rinsed residues were then leached by another 40% of carbonate (2nd leach), of which the portion is expected to represent the primary carbonate component (Li *et al*., 2011). Sr was separated from the 2nd leachate solution using *Eichrom*® Sr-spec resin. Sr isotopes were analysed by Thermal Ionization Mass Spectrometer (TIMS) on an *Isotopx*® *Phoenix* system at Royal Holloway, University of London. Isotope ratios and concentrations were determined using a multi-dynamic method modified from Thirlwall (1991). The accuracy and reproducibility of Sr isotope data were monitored using the external standard NIST SRM987. $^{87}Sr/^{86}Sr$ of SRM987 yielded 0.710234 ± 0.000008 (2sd, n=76) during the analysis. Data mentioned in the text have been normalised to the SRM 987 standard value of 0.710248 (McArthur, Howarth and Shields-Zhou, 2012).

Acetic leachate solution from the 2nd leaching step was also analysed for the concentration of carbonate diagenesis-diagnostic elements, including Ca, Mg, Mn, Sr, Rb. Ca and Mg were analysed using the *Varian*® 720-ES ICP-OES, and other elements (Mn, Sr, Rb) using a *Bruker*® M90 Inductively Coupled Plasma Mass Spectrometer (ICP-MS) at the Cross-Faculty Elemental Analysis Facility, University College London. All elemental analyses were conducted using certified reference materials: SRM1c (Argillaceous limestone), SRM120b (Florida phosphate rock). Solution standards were run at the start of the analyses along with a blank to monitor the accuracy of the bulk elemental analysis. Laboratory control solution standards were also run after every batch of 20 samples to monitor the drift and precision of the machinery.

4.2.3. Fitting the early Cambrian seawater $^{87}Sr/^{86}Sr$ curve

Due to high resistance to diagenesis, least-altered skeletal materials (e.g. foraminifera, brachiopods and belemnites) are regarded as microscopically well-preserved low Mg biogenic calcite, and thus contain fewer impurities to affect measured $^{87}Sr/^{86}Sr$ (McArthur, Howarth and Shields-Zhou, 2012). However, regarding Strontium Isotope Stratigraphy (SIS) study for early Cambrian materials, it is particularly important to target the least altered components in bulk rock carbonate. This is because there is no proven suitable skeletal material older than Ordovician and least-diagenetic altered bulk micrite is thought to retain the seawater $^{87}Sr/^{86}Sr$ signature. Rigid geochemical screening criteria is thus applied in this study to filter the least-altered $^{87}Sr/^{86}Sr$ data from the current study and published dataset (Derry *et al*., 1994; Brasier *et al*., 1996; Maloof, Porter, *et al*., 2010; Li *et al*., 2013). Although few studies applied the sequential leaching technique discussed in section 4.2.2, which could minimise the influence of diagenetic alteration to $^{87}Sr/^{86}Sr$ signatures, data were screened using HCl-leachable elemental cut-offs at Mn/Sr <0.2 (w/w), Mg/Ca <0.05 (w/w), [Sr] > 150 ppm, and [Al] <0.1%, Rb/Sr <0.002 (w/w) where possible. Additionally, for comparing results from different studies and laboratories, screened $^{87}Sr/^{86}Sr$ data are adjusted to international standard NIST SRM 987, which gives $^{87}Sr/^{86}Sr$ ratios of 0.710248 (McArthur, Howarth and Shields-Zhou, 2012).

Reconstruction of the seawater $^{87}Sr/^{86}Sr$ curve for the early Cambrian has been difficult because both the relative and absolute ages of lower Cambrian strata remain poorly constrained (McArthur, Howarth and Shields-Zhou, 2012). Only one chronologic framework with absolute ages is reported for the interval of Fortunian-Stage 3 at the lower Cambrian successions of Morocco (Maloof, Ramezani, *et al*., 2010). Among the investigated sections with carbonate Sr isotope data, merely Siberian Aldan-Lena Rivers sections (Brasier, Corfield, *et al*., 1994; Varlamov *et al*., 2008) and South China Xiaotan section (Li *et al*., 2013) possess detailed and global correlative biostratigraphic framework. However, proposed marker fossils for the lower Cambrian tend to be asynchronous or endemic to specific regions and facies (McArthur, Howarth and Shields-Zhou, 2012). For instance, some small shelly fossils (e.g. *Watsonella crosbyi*), which are identical in sections of South China, have a wider range of distribution on other continents (Peng, Babcock and Cooper, 2012; Landing *et al*., 2013). Benthic trilobites also yielded significant geographic and chronologic differentiation in Cambrian Stage 3 between Laurentia and Gondwana, possibly due to the opening of the lapetus ocean (Fortey, Briggs and Wills, 1996; B S Lieberman, 2003; Bruce S Lieberman, 2003; Dalziel, 2014). Therefore, no relative time scale using biostratigraphic zonal schemes

can perfectly resolve global stratigraphic calibration for $^{87}Sr/^{86}Sr$ data.

As an alternative solution, this study utilised the Moroccan age model (Maloof, Ramezani, *et al*., 2010) and high-resolution $\delta^{13}C_{carb}$ features (Maloof *et al*., 2005; Maloof, Porter, *et al*., 2010) for global stratigraphic calibration from the Cambrian Fortunian to Stage 3, supplemented by biostratigraphic schemes. Age tie points were selected at the peaks of prominent and globally recognised $\delta^{13}C$ excursions, and the scheme assumes constant sediment accumulation rates between tie points. These peaks include both positive and negative ones at 541.0 Ma, 527.3 Ma, 525.5 Ma, 523.7 Ma, 522.9 Ma, 521.6 Ma, 520.6 Ma and 517 Ma (Maloof, Porter, *et al*., 2010).

$^{87}Sr/^{86}Sr$ data fitted into the global seawater curve are obtained from the Siberian Aldan-Lena Rivers section (this study and Derry *et al*., 1994), Moroccan sections (Maloof, Porter, *et al*., 2010), Mongolian sections (Brasier *et al*., 1996), and South China Xiaotan section (Li *et al*., 2013). The Mongolian and Siberian data of Cambrian Fortunian–Stage 3 are assigned into a consistent timescale with Moroccan data based on chemostratigraphic correlation using $\delta^{13}C_{carb}$ excursions peaks and age tie points discussed above. Correlation between my new $^{87}Sr/^{86}Sr$ data and previously reported Siberian data is achieved by matching the lithostratigraphic, biostratigraphic zonal marker beds as well as $\delta^{13}C_{carb}$ excursions (Brasier, Corfield, *et al*., 1994; Brasier, Rozanov, *et al*., 1994; Derry *et al*., 1994). Only data from Dahai Member of Xiaotan section (Li *et al*., 2013) is incorporated in my compilation because other stratigraphic horizons at the section are characterised by either phosphorite or dolostone, and so $^{87}Sr/^{86}Sr$ were likely altered during diagenesis. U-Pb zircon dating of tuffs gives absolute age constraints at the base and top of Dahai Member with ~528.7 Ma and ~526.7 Ma respectively (personal communication with Dr Chuan Yang). The peak of the positive $\delta^{13}C$ excursion (ZHUCE) in Dahai Member is then estimated as at 527.3 Ma assuming a constant sediment accumulation rate within the member, which is consistent with its correlative $\delta^{13}C$ excursion (527.34 Ma) at the Moroccan Qued Sdas section (Maloof, Porter, *et al*., 2010). The available $^{87}Sr/^{86}Sr$ data of late Cambrian Stage 3-early Stage 4 are reported from the Siberian sections (Brasier, Corfield, *et al*., 1994; Derry *et al*., 1994). However, the unique absolute age for mid Cambrian Stage 4/Toyonian, which yielded 511±1 Ma, is reported at a correlative trilobite-bearing (*Ovatoryctocara granulata* zone) stratigraphic horizon from Avalon (Landing *et al*., 1998). A probable constant sediment accumulation rate of 0.01116 m/Myr is then calculated between *Bergeroniellus micmacciformis – Erbiella* zone of mid Stage 3 and *Ovatoryctocara granulata* zone of late Stage 4 at the Siberian Aldan-Lena Rivers sections, based on previously reported

stratigraphic thickness between the two zones (Brasier, Corfield, *et al*., 1994). Estimated ages are then assigned to the current Siberian $^{87}Sr/^{86}Sr$ data during this interval. Because the *O. granulata* zone in eastern Siberia is younger than the highest stratigraphic horizon (*Bergeroniellus ketemensis* zone) investigated in my study, an age of 513 Ma is calculated for the lower Toyonian as shown in Fig. 4.3.

A full compilation of the latest Ediacaran–early Cambrian $^{87}Sr/^{86}Sr$ data with estimated ages is summarised in Appendix E. Data are calibrated applying the numerical age model and global stage subdivision plan suggested by GTS2012 time scale (Gradstein *et al*., 2012). A nonparametric LOWESS fitting method (LOcally Weighted scatterplot smoothing) is applied to produce the best-fit curve for the global seawater $^{87}Sr/^{86}Sr$ curve as a function of geological time. LOWESS was suggested as the standard technique in GTS2012 for $^{87}Sr/^{86}Sr$ calibration curve production (Howarth and McArthur, 1997; McArthur, Howarth and Bailey, 2001; McArthur, Howarth and Shields-Zhou, 2012). Unlike the traditional parametric smoothing processes (e.g. Linear, Polynomial, Exponential, Moving average) which often yield unrealistic sloping from the fitting curves, smoothed $^{87}Sr/^{86}Sr$ values by LOWESS are determined by neighbouring screened $^{87}Sr/^{86}Sr$ data points defined within the time window/span (Howarth and McArthur, 1997; Zhang *et al*., 2004). The smoothing is weighted because a regression weight function is defined for the data points contained within the time span, thereby ensuring the trending process is transitional and resistant to influence by data points from neighboured time span. The time span is set to 0.2, which accounts for 20% of the total number of the $^{87}Sr/^{86}Sr$ data points. 'Robust' regression weight function and quadratic polynomial differentiation are applied to the calculation in this study to optimise the curving through the unevenly spaced data points (Howarth and McArthur, 1997). Importantly, the LOWESS solution is resistant to unrealistic data anomalies (probably altered samples) in the dataset, therefore capable of producing a best-fitted curve that most likely match the 'observation' or 'expected' trend through geological time.

The LOWESS-fitted curve is given a two-sided, 95% Confidence Intervals (*CIs*) as the local minima and maxima constraints for each time span. Rather than the standard deviation, CIs are calculated as the standard error of the mean (s_m), which provides a confidence for any designated position (data point) on the mean line (Howarth and McArthur, 1997; McArthur, Howarth and Shields-Zhou, 2012). Analytical uncertainties (s_c) from different referenced studies are also incorporated into the calculations of CIs using the Eqn. 4.1 (McArthur, Howarth and Shields-Zhou, 2012):

$$CIs = \sqrt{s_m^2 + s_c^2} \qquad (Eqn.\ 4.1)$$

Calculation and visualisation of the LOWESS fitting and CIs were performed by the author using *MathWorks*® MATLAB R2016a. Fitted curves for the interval at 546-511 Ma are illustrated in Fig. 4.4 and Fig. 4.6

4.2.4. Strontium cycle model

An isotope mass balance box model, based on a modification of previous studies (Pogge von Strandmann, Jenkyns and Woodfine, 2013; Lechler *et al*., 2015), was applied to the LOWESS-fitted $^{87}Sr/^{86}Sr$ data derived from this study and previously published analyses (Derry *et al*., 1994; Brasier *et al*., 1996; Maloof, Porter, *et al*., 2010) to model the Sr cycle across the Cambrian stages 2-3 interval, and hence to explore the geological interpretation of the increasing trend at ca. 523.6-517.4 Ma as shown in Fig. 4.4. The model was constructed from the mass-balance differential equation with respect to geological time (t) (Eqn. 4.2):

$$\frac{dN_{Sr}}{dt} = F_{cw} + F_{hydr} + F_{diag} - F_{carb} \qquad (Eqn.\ 4.2)$$

where N_{sr} is the total inventory of seawater Sr reservoir, and F_x represents the input and sink fluxes (*cw* = continental weathering via riverine input; *hydr* = hydrothermal system/mantle input; *diag* = diagenetic back flux from deep-sea sediments; *carb* = marine carbonate sink). The isotopic balance equation is then given by Eqn. 4.3:

$$N_{Sr}\frac{dR_{SW}}{dt} = F_{cw}(R_{cw} - R_{SW}) + F_{hydr}\left(R_{hydr} - R_{SW}\right) + F_{diag}\left(R_{diag} - R_{SW}\right) - F_{carb}(R_{carb} - R_{SW}) \qquad (Eqn.\ 4.3)$$

where R_x represents the isotopic ratio of the different input and sink fluxes. As Sr isotopes are not fractionated during the uptake into marine carbonate, R_{carb} is assumed as equal to contemporaneous seawater $^{87}Sr/^{86}Sr$ (R_{SW}).

Calculation of the marine carbonate sink (F_{carb}) from seawater assumes that partitioning of Sr into the sink has a constant partition coefficient $k = 3.25 \times 10^{-7}$, which is determined by Eqn.

4.4 using the initial model input parameters listed in Table 5.1:

$$F_{carb} = k \times N_{Sr} \qquad (Eqn. 4.4)$$

Then the initial Sr residence time (T_{res}) in the modelled Cambrian ocean is given by 3.08×10^6 years (Eqn. 4.5), which is similar to the residence time of Sr in the ocean today of $\sim 3 \times 10^6$ years (Hodell, Mueller and Garrido, 1991):

$$T_{res} = \frac{N_{Sr}}{F_{carb}} = \frac{1}{k} = 3.08 \times 10^6 \; years \qquad (Eqn. 4.5)$$

Regarding the model input parameters, initial conditions are set at steady state with present-day parameters, including N_{Sr}, R_{hydr}, F_{diag}, R_{diag} and R_{cw} (Elderfield and Gieskes, 1982; Palmer and Edmond, 1989; Hodell, Mueller and Garrido, 1991; Davis, Bickle and Teagle, 2003; Vance, Teagle and Foster, 2009). The initial hydrothermal input flux (F_{hydr}) is estimated based on the mid-ocean ridge volume constraints by paleo-sea level inversion modelling, which gives a degassing input rate of 1.7 times of the present day value at ca. 520 Ma (Berner, 1994). The initial F_{cw} is calculated to match the actual seawater $^{87}Sr/^{86}Sr$ value (0.70815) from the LOWESS-fitted curve at 523.6 Ma (Fig. 4.4). Applying the initial input parameters shown in Table 4.1, Sr isotope record at 523.6-517.4 Ma was forward modelled at a step of 10 kyr by either varying the continental weathering input flux (F_{cw}) or residence time of Sr in the Cambrian ocean (T_{res}). Modelling results are shown in Fig. 4.5.

Table. 4.1: Initial model input parameters (t=0). Values sources: N_{Sr}, R_{cw} (Vance, Teagle and Foster, 2009); R_{hydr} (Davis, Bickle and Teagle, 2003); F_{diag}, R_{diag} (Elderfield and Gieskes, 1982; Palmer and Edmond, 1989).

Flux/inventory size		**$^{87}Sr/^{86}Sr$ of fluxes**	
F_{cw}	2.32×10^{10} mol yr^{-1}	R_{cw}	0.71144
F_{hydr}	1.4×10^{10} mol yr^{-1}	R_{hydr}	0.7025
F_{diag}	0.34×10^{10} mol yr^{-1}	R_{diag}	0.7084
F_{carb}	4.06×10^{10} mol yr^{-1}	R_{carb}	0.70815
N_{sr}	1.25×10^{17} mol	R_{sw}	0.70815

4.3. Results

4.3.1. Petrographic screening

A growing amount of literature has revealed that it is crucial to target the primary and least-altered carbonate components for SIS study (Bailey *et al*., 2000; Li *et al*., 2011; McArthur, Howarth and Shields-Zhou, 2012). Either recrystallisation or dolomitisation during carbonate diagenesis would alter the syn-depositional $^{87}Sr/^{86}Sr$ values retained from coeval seawater. Besides, post-depositional alteration through interaction with detrital components would generally increase $^{87}Sr/^{86}Sr$ ratios, while contamination of clay minerals and tiny silicate minerals originating from basaltic rocks decrease $^{87}Sr/^{86}Sr$ values. Therefore, microscopic investigation is essential for recognising the primary and secondary carbonate phases, and for filtering the purest carbonate for Sr isotope analysis.

Typical photomicrographs from individual formations and Siberian stages at Aldan-Lena Rivers sections are presented in Fig. 4.1. The Pestrotsvet Formation contains micrite, sparite and biosparite (Fig. 4.1a-f), but some samples from the lower Pestrotsvet Formation (Fig. 4.1b-e) are characteristic of recrystallised spars and abundant siliciclastic content in brown colour, which possibly indicate enrichment in iron-oxides. The Perekhod Formation comprises of microsparite, sparite and biosparite (Fig. 4.1g-k), and some dolomitic stratigraphic horizons with recrystallised dolosparite (Fig. 4.1i). Samples from Sinsk, Kutorgina, and Keteme (Fig. 4.1l-o) are typical well-preserved microsparite carbonate, but rare in bioclasts. In general, sparitic or micritic samples with minimal neomorphism, dolomitisation and siliciclastic content would be suggested for SIS study. Samples of these qualities in this study, with their paired thin-sections presented here, for instance include IST03, ZHU09, UKT032, UT03, UKT101, UT27, LAB56 and TA28.

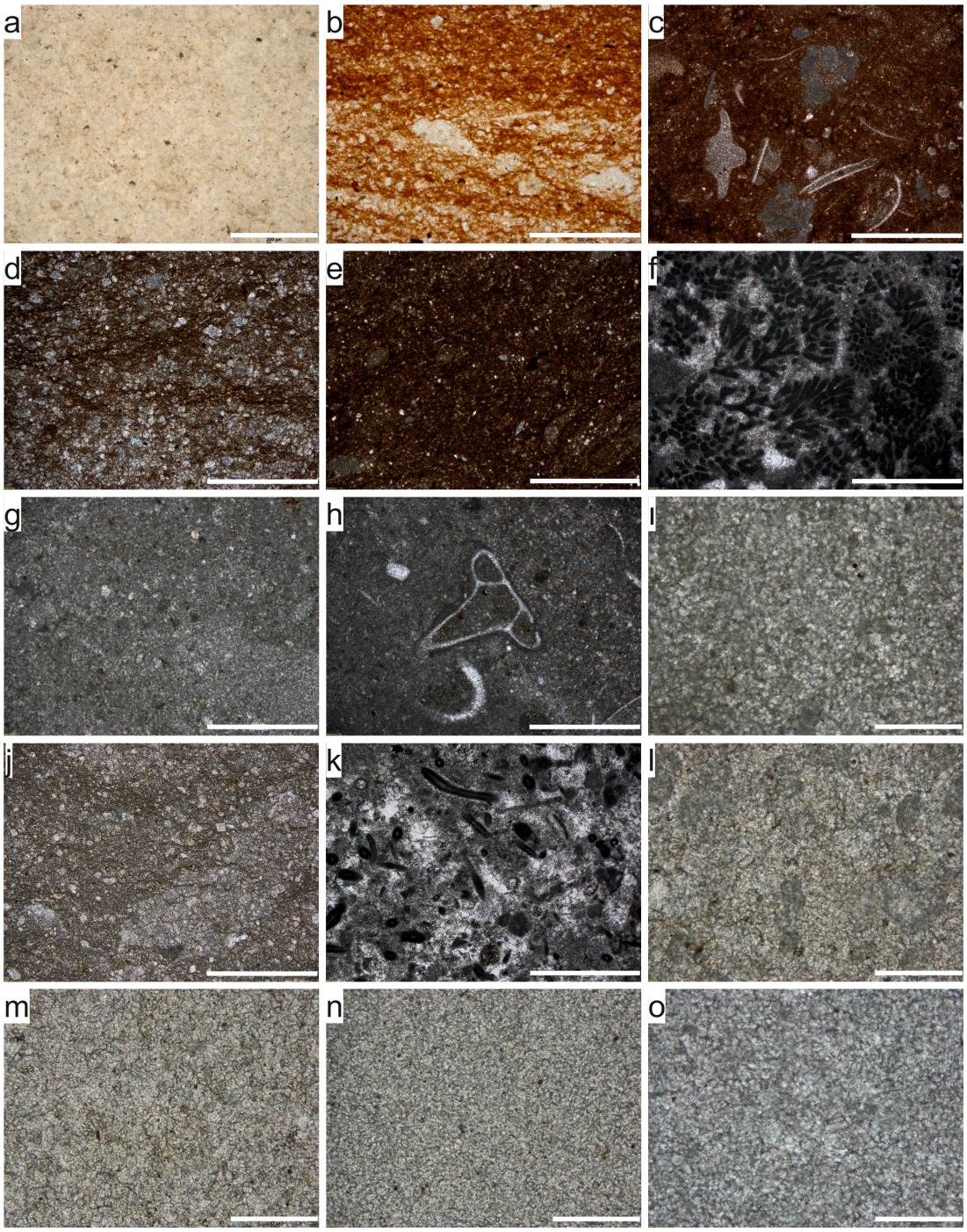

Figure. 4.1: Thin-section photomicrograph (plane-polarised light) of carbonate samples used for SIS study. (a) micritic sample (IST03, Pestrotsvet Formation, Tommotian) showing fine-grained calcite with minimal siliciclastic content, scale bar = 200 µm. (b) sparitic sample (IST19, Pestrotsvet Formation, Tommotian) with partially recrystallised spars, scale bar = 500 µm. (c) biosparite (IST26, Pestrotsvet Formation, Tommotian) with abundant small shelly fossils and iron-rich siliciclastic content, scale bar = 1 mm. (d) sparitic sample (IST47, Pestrotsvet Formation, Tommotian) with partially recrystallised spars, scale bar = 500 µm. (e) sparitic sample (ZHU01, Pestrotsvet Formation, Atdabanian) with partially recrystallised spars and iron-rich siliciclastic content, scale bar = 1 mm. (f) micritic carbonate (ZHU09,

Pestrotsvet Formation, Atdabanian) with abundant calcimicrobe or microproblematic framework organism, *Epiphyton*, scale bar = 1 mm. (g-h) microsparite (UKT032, Perekhod Formation, Atdabanian) with the presence of likely chambered mollusc *Chancelloriids*, scale bar = 500 μm. (i) coarsely grained dolostone (UKT043, Perekhod Formation, Atdabanian) , scale bar = 200 μm. (j) sparitic sample (UKT051, Perekhod Formation, Botomian) with partially recrystallised spars and siliciclastic content, scale bar = 500 μm. (k) biosparitic carbonate (UT03, Perekhod Formation, Botomian) with probable abundant trilobite spines, scale bar = 1 mm. (l) microsparite sample (UKT101, Sinsk Formation, Botomian Stage) contained fine-grained calcite and probable algae fragments, scale bar = 200 μm. (m) microsparite sample (UT27, Sinsk Formation, Botomian) contained fine-grained calcite, scale bar = 200 μm. (n) microsparite sample (LAB56, Kutorgina Formation, Botomian) contained fine-grained calcite, scale bar = 200 μm. (o) microsparite sample (TA28, Keteme Formation, Toyonian) contained fine-grained calcite, scale bar = 200 μm.

4.3.2. Evaluating diagenesis

It is important to determine the degree to which carbonate rocks have been altered during diagenesis, and to identify whether individual $^{87}Sr/^{86}Sr$ data and overall trends are representative of syn-depositional oceanic values. Late diagenesis is believed to alter rock chemistry by fluid interaction, which can change Sr isotope ratios to either higher (more radiogenic) or lower values. In section 3.2.1, $\delta^{13}C_{carb}$ and $\delta^{18}O_{carb}$ systematics of the Aldan-Lena Rivers section were argued to be likely the signatures of primary depositional fluids rather than alteration during diagenesis. No obvious correlation between $^{87}Sr/^{86}Sr$ and $\delta^{13}C_{carb}$ is observed in Fig. 4.2a, but $^{87}Sr/^{86}Sr$ values of Pestrotsvet and Perekhod formations exhibit higher variability than the other formations, suggesting possible greater degree of alteration in these two units.

In addition to petrographic screening, results of [Sr], Mn/Sr, Mg/Ca, and Rb/Sr derived from the second leachate solution are utilised here to test the $^{87}Sr/^{86}Sr$ data fidelity as primary ancient seawater signatures. Primary depositional fluids have the potential to result in dissolution and recrystallization of carbonate phases. Such diagenetic alteration of carbonates generally raises Mn contents and simultaneously lowers Sr contents (Veizer *et al*., 1983; Derry *et al*., 1994). Besides, Rubidium isotope of ^{87}Rb decays to ^{87}Sr, and as time passed this decay will alter $^{87}Sr/^{86}Sr$ during diagenesis especially in those samples with high Rb or clay content (Brasier *et al*., 1996). Cross-plots of $^{87}Sr/^{86}Sr$ versus Mn/Sr, Sr/Ca and Rb/Sr ratio of carbonate show strong correlations (Fig. 4.2b,c,d), indicating that samples with low Sr and high Rb concentrations are more likely to be subjected to alteration. $^{87}Sr/^{86}Sr$ values that obviously deviate from the major data group ($Sr/Ca < 0.0005$, $Mn/Sr > 0.2$, $Rb/Sr > 0.002$) are therefore omitted to obtain the least-altered samples. Moreover, low Rb/Sr ratio (< 0.02) in both total HCl-leachable

carbonate and 2nd leachate solution analysis indicates no need for Rb correction for $^{87}Sr/^{86}Sr$ values when comparing to the Rb correction table (McArthur, 1994).

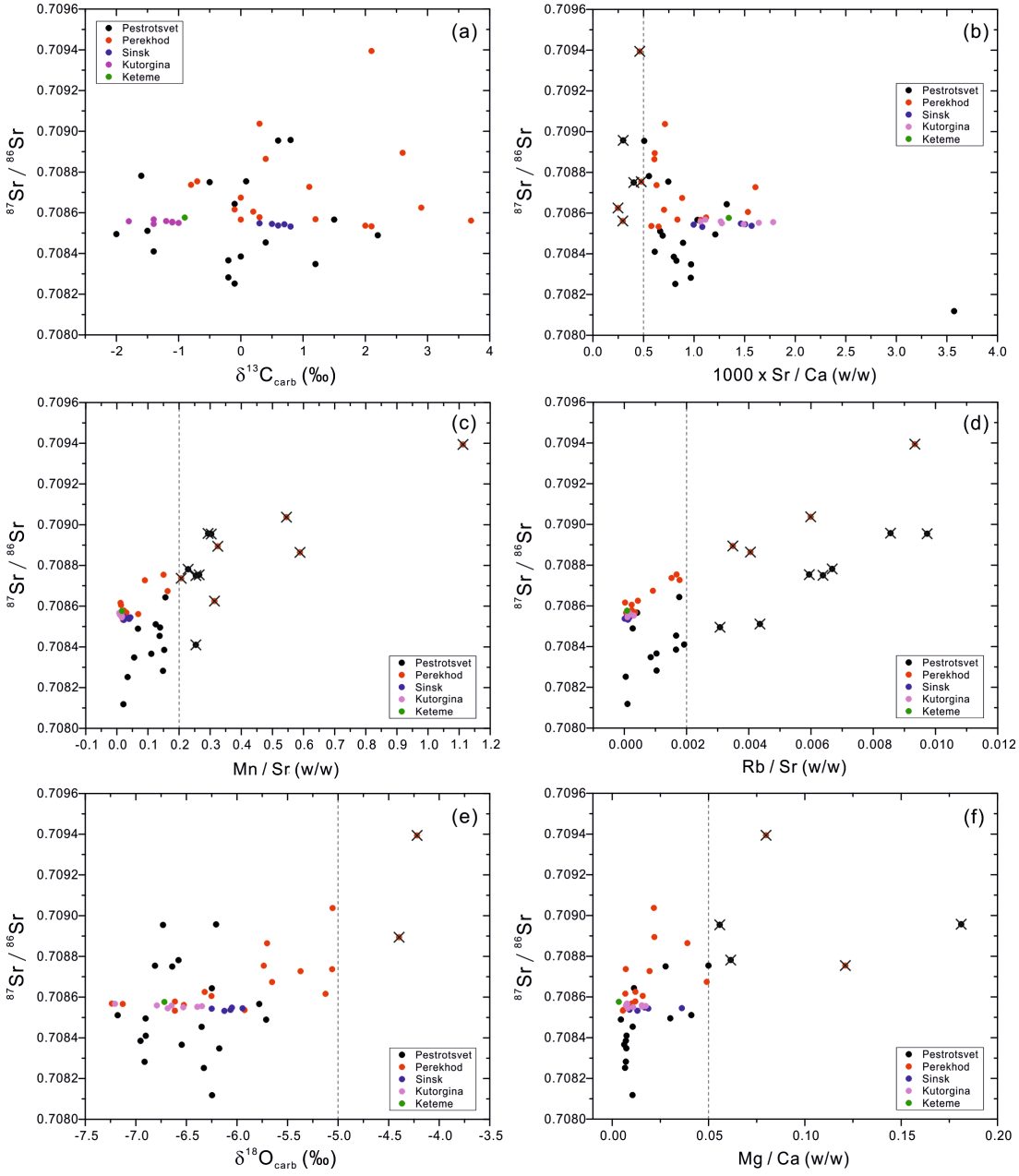

Figure. 4.2: Cross-plots of (a) $^{87}Sr/^{86}Sr - \delta^{13}C_{carb}$ (‰) ($R^2 = 0.083$), (b) $^{87}Sr/^{86}Sr$ – 1000×Sr/Ca (w/w; 2nd leach) ($R^2 = 0.217$), (c) $^{87}Sr/^{86}Sr$ – Mn/Sr (w/w; 2nd leach) ($R^2 = 0.583$), (d) $^{87}Sr/^{86}Sr$ – Rb/Sr (w/w; 2nd leach) ($R^2 = 0.540$), (e) $^{87}Sr/^{86}Sr - \delta^{18}O_{carb}$ (‰) ($R^2 = 0.296$), and (f) $^{87}Sr/^{86}Sr$ – Mg/Ca (w/w; 2nd leach) ($R^2 = 0.325$) of carbonates from the Aldan-Lena River sections. Results are grouped into different colours by stratigraphic formations. Unscreened data dots are crossed-out for those laid outside the cut-offs (dotted line) for least-altered carbonate.

Dolomitisation is believed to alter the original seawater-equivalent $^{87}Sr/^{86}Sr$ values during carbonate diagenesis (Derry *et al*., 1994; Li *et al*., 2013). Five samples of Pestrotsvet and Perekhod formations with Mg/Ca ratio above 0.05 are excluded from the least-altered dataset (Fig. 4.2f). Although $\delta^{18}O_{carb}$ could be either deceased or elevated due to low-temperature equilibrium isotopic fractionation during dolomitisation (Li *et al*., 2011), two excluded samples from Pestrotsvet Formation exhibit obviously elevated $^{87}Sr/^{86}Sr$, higher $\delta^{18}O_{carb}$ (> -5‰), high Rb, Mn and low Sr concentrations (Fig. 4.2e), and so were probably affected by late diagenesis fluid alteration (e.g. meteoric or high-temperature fluid).

4.3.3. New carbonate $^{87}Sr/^{86}Sr$ data of Aldan-Lena Rivers sections

The stratigraphic distribution of $^{87}Sr/^{86}Sr$ values of 48 carbonate samples from the Siberian Aldan-Lena Rivers sections is shown in Fig. 4.3 and Appendix D. Sr isotopic change of the screened data through the Cambrian stages 2-4 can be divided into three phases. The first phase is characterised by a steep climb in $^{87}Sr/^{86}Sr$ ratios, from 0.70812 in the mid Stage 2/late Tommotian to 0.70873 in the mid Stage 3/late Atdabanian. The $^{87}Sr/^{86}Sr$ maximum of investigated interval at Aldan-Lena Rivers sections thus lies within the lowermost Perekhod Formation, coinciding with the *F. lermontovae* zone (archaeocyathid) and *Judomia* zone (trilobite). The increasing trend is also accompanied by high $\delta^{13}C_{carb}$ variability (Fig. 4.3) and most of the reef-building organisms and arthropod radiation events on the Siberian Platform (Brasier, Corfield, *et al*., 1994; Varlamov *et al*., 2008), from where these biotic events are globally recognised (Zhu, Babcock and Peng, 2006; Zhu, 2010; Peng, Babcock and Cooper, 2012). In the second phase, the $^{87}Sr/^{86}Sr$ ratio quickly declines to ~0.70855 by the end of the Atdabanian. $^{87}Sr/^{86}Sr$ ratios in the last phase yield no variability at ~0.70855, showing stable record through mid Stage 3 to early Stage 4, coinciding the Botomian–Toyonian extinction.

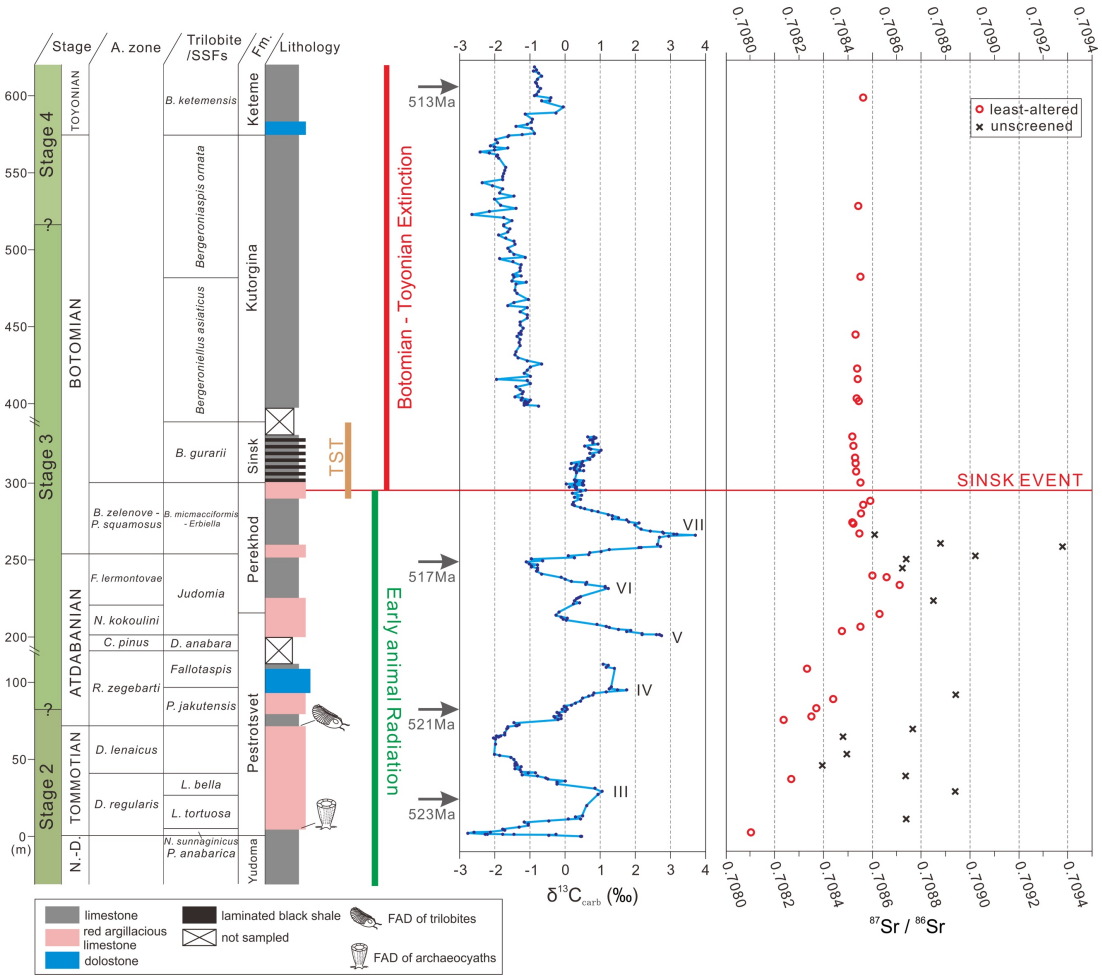

Figure. 4.3: High-resolution carbonate carbon ($\delta^{13}C_{carb}$) and strontium isotope ($^{87}Sr/^{86}Sr$) records from Cambrian Stage 2 to Stage 4 at Aldan-Lena Rivers sections. Regional Stage subdivision is shown next to the global subdivision plan for comparison (Brasier, Corfield, *et al*., 1994). N.-D.: Nemakit-Dalaynian Stage; TST: Transgressive System Tract (Zhuravlev, 1998); A. zone: Archaeocyathid zone; Fm.: Formation). Age constraints are deduced from U-Pb zircon ages of tuffs of correlative strata in Morocco (Maloof, Ramezani, *et al*., 2010; Peng, Babcock and Cooper, 2012) and Avalon (Landing *et al*., 1998). Names for the positive $\delta^{13}C_{carb}$ peaks are consistent with those of previously suggested $\delta^{13}C_{carb}$ curve (Brasier, Corfield, *et al*., 1994; Brasier, Rozanov, *et al*., 1994). Unscreened Sr isotope data points are crossed-out following the criteria discussed in 4.3.2.

4.4. Discussions

4.4.1. Compilation of $^{87}Sr/^{86}Sr$ data through the Cambrian stages 2-4

Fig. 4.4 shows a global marine $^{87}Sr/^{86}Sr$ trend from the late Cambrian Stage 2 to mid Stage 4. Utilising a consistent time scale, new results from the Aldan-Lena Rivers sections match with those from least-altered carbonates of Derry *et al*. (1994) regarding the increasing trend of $^{87}Sr/^{86}Sr$ at 523-517 Ma and the stranded interval at 517-512 Ma. However, the current study significantly improves the resolution of least-altered data and positions the Stage 3 $^{87}Sr/^{86}Sr$ maximum (~0.70864) at ~517.5 Ma. Although one least-altered sample falls within the CIs ranges of the calibrated LOWESS-fitted curve at ~520.5 Ma, most of the $^{87}Sr/^{86}Sr$ data from the Moroccan sections (Maloof, Porter, *et al*., 2010) yields high variability likely because of severe diagenetic alteration (Fig. 4.6). Two additional least-altered samples from the Mongolian sections also fit the Siberian trend and confirm the positioning of the Stage 2 $^{87}Sr/^{86}Sr$ minimum (~0.7081) at ~523.5 Ma (Brasier *et al*., 1996).

Accepting the early Cambrian age model of Maloof, Porter, *et al*. (2010), the average rate of increase of $^{87}Sr/^{86}Sr$ ratios at 523.6-517.4 is about 8.0×10^{-5} Myr^{-1} (0.00050 in 6.2 Myr). This is in agreement with the estimated rate calculated in Derry *et al*. (1994)'s model (0.0001/Myr) even though they used a less accurate timescale. Comparing with other equivalent steep slopes in the Phanerozoic Eon, the rate of increase through the late Eocene to early Miocene was 4.1×10^{-5} Myr^{-1} (~0.0009 in 22 Myr), through mid-Miocene to present day was 3.1×10^{-5} Myr^{-1} (~0.0005 in 16 Myr) (Hess, Bender and Schilling, 1986; McArthur, Howarth and Shields-Zhou, 2012). However, the early Cambrian $^{87}Sr/^{86}Sr$ rise is less significant when compared to the unprecedented steep climb in the Early Triassic (3.3×10^{-4} Myr^{-1}; (0.00125 in 3.8 Myr) subsequently after the end-Permian extinction (Song *et al*., 2015).

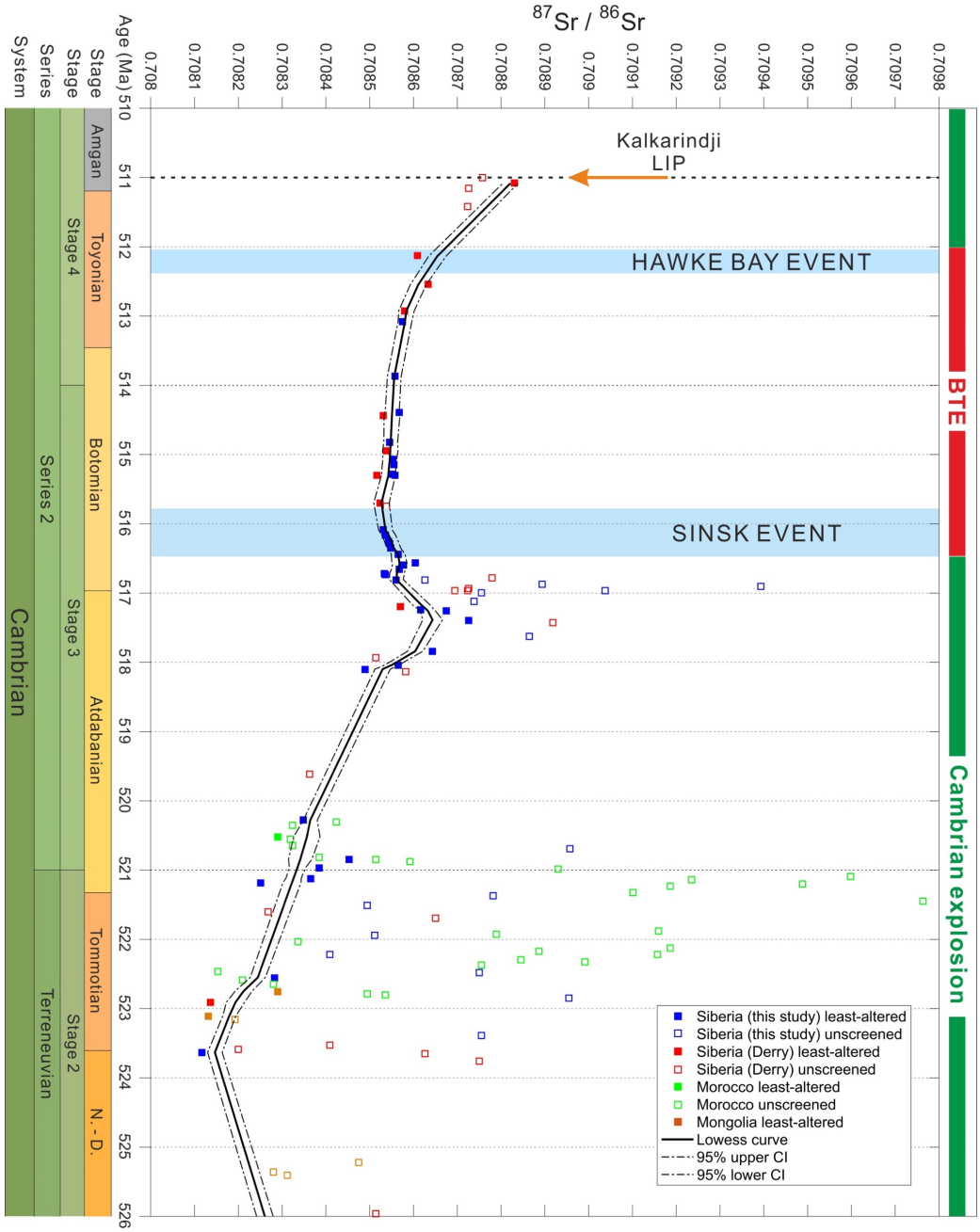

Figure. 4.4: Carbonate $^{87}Sr/^{86}Sr$ (this study) in comparison to literature data derived from carbonate samples of Siberia (Derry *et al*., 1994), Morocco (Maloof, Porter, *et al*., 2010) and Mongolia (Brasier *et al*., 1996). N.-D.: Nemakit–Dalaynian; Open square: unscreened carbonate; solid square: screened and least-altered carbonate; All data are assigned to a consistent timescale by applying the age model from Morocco (Maloof, Ramezani, *et al*., 2010) and tie points of $\delta^{13}C$ excursions between sections. All data are adjusted to NIST SRM 987 = 0.710248 (McArthur, Howarth and Shields-Zhou, 2012), and recalculated to the Geologic Time Scale 2012 (Gradstein *et al*., 2012). Solid black curve: mean LOWESS-fitted line; dotted line: two-sided 95% confidence intervals. Timing of Sinsk transgression and Hawke Bay regression events are deduced from previous suggestion at Siberian Aldan-Lena Rivers sections (Zhuravlev and Wood, 1996; Dilliard *et al*., 2007). The brief emplacement for the Australian Kalkarindji Large igneous province is given at ca. 511 Ma (Jourdan *et al*., 2014).

4.4.2. Modelling the causes for the Cambrian stages 2-3 seawater $^{87}Sr/^{86}Sr$ increase

The marine $^{87}Sr/^{86}Sr$ record reflects the balance between isotope ratios and fluxes of various inputs and sinks. Input flux of diagenetic recrystallisation after deep-sea sediment burial is generally considered to have only a minor effect on the modern oceanic Sr budget (Elderfield and Gieskes, 1982; Palmer and Edmond, 1989). The diagenetic input has a relatively radiogenic $^{87}Sr/^{86}Sr$ ratio (0.7084) and a flux of ~10 times less than the hydrothermal input flux. It is impossible to solely boost diagenetic flux to generate the rapid rise in seawater $^{87}Sr/^{86}Sr$ at 523.6-517.4 Ma (Fig. 4.4). The steep climb of seawater $^{87}Sr/^{86}Sr$ ratios during the Cambrian stages 2-3 interval thus could be attributed to either a quick decline of less-radiogenic mantle Sr flux, an increase in riverine $^{87}Sr/^{86}Sr$ ratios or/and increase in continental weathering run-off.

Calculations using the Sr cycle model reveals that a reduction of 27.3% of the total mantle Sr flux is required to produce the increasing $^{87}Sr/^{86}Sr$ trend. However, the $^{87}Sr/^{86}Sr$ record exhibits a long-term decline from the late Ediacaran until the $^{87}Sr/^{86}Sr$ turnover at 523.6 Ma (Fig. 4.4). The declining trend is interpreted as best explained by enhanced hydrothermal activity associated with the mid-ocean ridge growth during the extension of the lapetus ocean between Laurentia, Baltica and young Gondwana (Maloof, Porter, *et al*., 2010; Dalziel, 2014). Additional subaerial weathering of the rift-related igneous rocks (e.g. basalts) would presumably have a greater effect on the oceanic unradiogenic Sr input flux. However, because the lapetus extension continued until the mid-Ordovician, hydrothermal Sr input flux would have been strengthened rather than significantly reduced by nearly 30% during the Cambrian Stage 2-3. On the basis of this argument, reduction in hydrothermal flux alone is unrealistic to reverse the $^{87}Sr/^{86}Sr$ trend by the mid Stage 2, thereby leaving the continental weathering/riverine Sr flux as a designated player to explain the increasing trend.

Modelling results suggest that riverine $^{87}Sr/^{86}Sr$ would have had to increase by ~0.00099 and last for 6.2 Ma if the sole cause of the shift in seawater $^{87}Sr/^{86}Sr$ was due to the rise in the $^{87}Sr/^{86}Sr$ ratio of continental weathering flux. However, the deduced rapid change of riverine $^{87}Sr/^{86}Sr$ for the early Cambrian is greater than the shift (< 0.0005) for the interval from 40 Ma to present day as possibly a result of enhanced erosion of the Himalayas and Tibetan Plateau (Richter, Rowley and DePaolo, 1992). Besides, as already pointed out by Derry *et al*. (1994), no other calculated range or rate of riverine $^{87}Sr/^{86}Sr$ change in the Phanerozoic would measure

up to the shift of ~0.00099 in a < 10 Myr interval (Kump, 1989). These findings thereby refute the possibility that the $^{87}Sr/^{86}Sr$ increase was solely caused by elevated riverine $^{87}Sr/^{86}Sr$.

Therefore, it is likely that the rapid increase in early Cambrian seawater $^{87}Sr/^{86}Sr$ could have resulted from enhanced continental weathering flux. The Sr cycle model is applied to simulate the dynamic influence of the continental weathering/riverine flux (Fcw) on the seawater $^{87}Sr/^{86}Sr$. Modern values were set as the initial parameters for various inputs and sink in the model. The initial ocean $^{87}Sr/^{86}Sr$ is set to 0.70815 as consistent with the value at 523.6 Ma. The model was generated by increasing the Fcw through 6.2 Myr to reach the Cambrian Stage 3 maximum (0.70864), but assuming constant isotopic ratios and flux for all other inputs (e.g. hydrothermal/mantle input flux). The results suggest that a persistent elevated riverine flux of ~1.4 times the initial level is required (Fig. 4.5a) to produce the increasing trend in the Cambrian Stage 2-3 seawater $^{87}Sr/^{86}Sr$ record (Fig. 4.4). Besides, the degree of the increase in riverine flux should also be dependent on estimates of oceanic Sr residence time (Pogge von Strandmann, Jenkyns and Woodfine, 2013). However, given that the long present-day residence time of Sr of $\sim 3 \times 10^6$ yr, only a minor change is observed when double or half the oceanic Sr residence time relative to the present day (Fig. 4.5b). Moreover, note that influence of lapetus extension and contemporaneous could enhance hydrothermal input flux in the early Cambrian, which would be expected to drive down seawater $^{87}Sr/^{86}Sr$ (Maloof, Porter, *et al.*, 2010), to some extent could buffer the rapid climb in the Cambrian Stage 2-3 seawater $^{87}Sr/^{86}Sr$. As a result, the constraints of riverine flux increase (by ~1.4 times) in this study represent a minimum estimate of such increase.

Although the Cambrian Stage 2-3 $^{87}Sr/^{86}Sr$ increase was likely driven by high continental weathering flux, other contributions from plausible elevated riverine $^{87}Sr/^{86}Sr$ ratios and diagenetic flux still cannot be excluded. An additional ambiguity derives from the fact that riverine $^{87}Sr/^{86}Sr$ ratios are strongly affected by the isotopic composition of rocks exposed to weathering. It has been shown, for example, that carbonates can gain silicate-rock-like isotope ratios through metamorphism, while weathering of relatively unradiogenic juvenile volcanic rocks would tend to lower seawater $^{87}Sr/^{86}Sr$. Hence, changes in seawater $^{87}Sr/^{86}Sr$ could simply reflect a significant change in the age and type of rocks and minerals undergoing weathering, rather than a change in the weathering flux. Clearly, additional information (e.g. a seawater lithium isotope record) is crucial to establish whether continental weathering flux was indeed anomalously high in the early Cambrian that is independent of Sr isotopes.

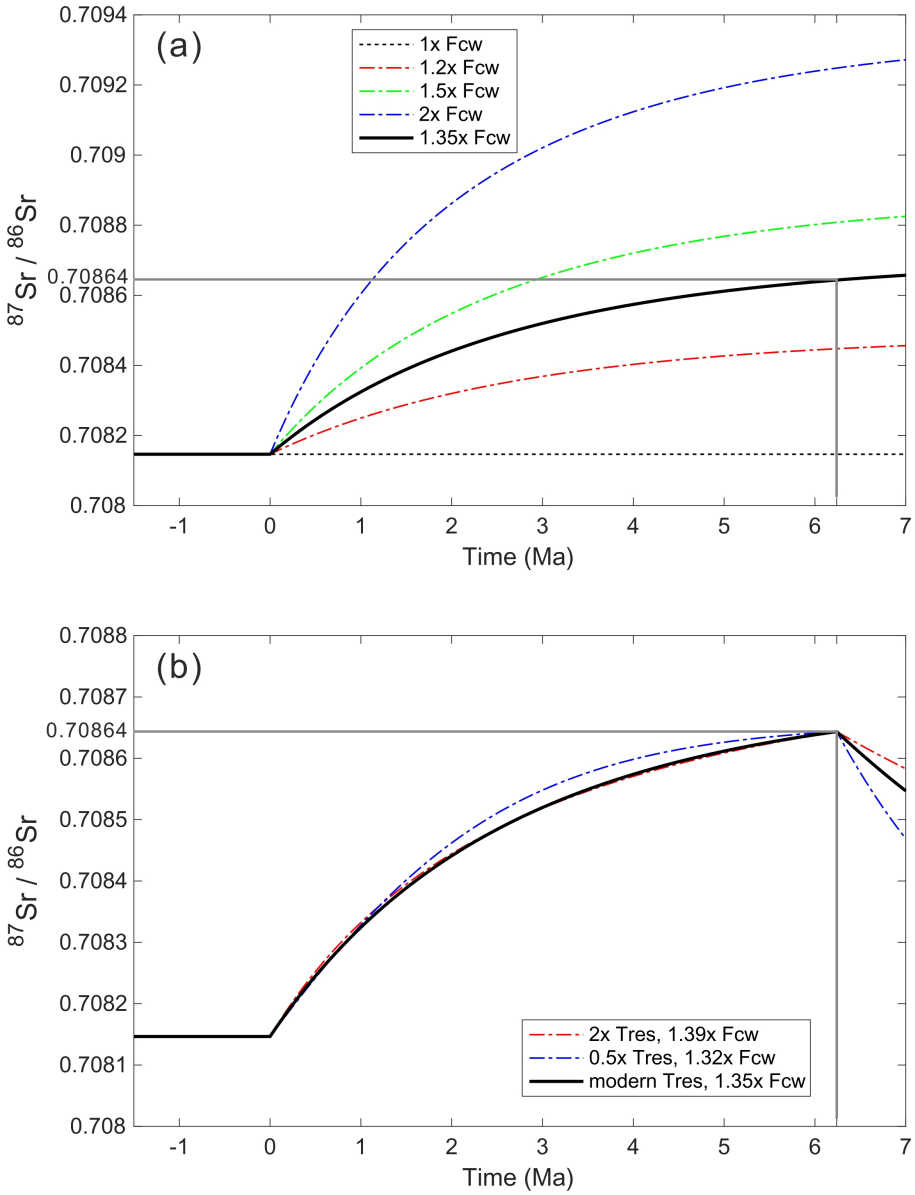

Figure. 4.5: Numerical model simulating the dynamic influence of the continental weathering (riverine) flux (Fcw) on the ocean $^{87}Sr/^{86}Sr$. The initial ocean $^{87}Sr/^{86}Sr$ is set to 0.70815 as consistent with the value at 523.6 Ma. The model was generated by varying the F_{cw} through 7 Myr, but assuming a constant hydrothermal/mantle input flux. Sensitivity test (a) shows effect of a transitory 1.2, 1.35, 1.5, 2 times increase in F_{cw} for 6.2 Myr on ocean $^{87}Sr/^{86}Sr$. Modelling results (b) show variations of increase rate and required F_{cw} at different Sr isotope residence time, if boost $^{87}Sr/^{86}Sr$ to 0.70864 by 6.2 Ma. (T_{res} = modern residence time of Sr, ~3×10^6 yrs)

4.4.3. Early Cambrian $^{87}Sr/^{86}Sr$ trend and geological interpretations

The integrated global marine $^{87}Sr/^{86}Sr$ data for the latest Ediacaran–Cambrian Stage 4 are plotted in Figure 4.4 and 4.6. Two data gaps are observed at 532-529 Ma and 527-524 Ma, therefore awaiting more data of least-altered samples from possibly the Mongolian sections (Brasier *et al*., 1996; Smith *et al*., 2016) and other correlative carbonate successions that cover the gaps. It is also important to note that although samples were screened following the rigid elemental criteria, the $^{87}Sr/^{86}Sr$ values of some contemporaneous samples show larger range than the LOWESS-fitted CIs, indicating that even apparently least-altered samples can deviate from their primary seawater values. The LOWESS-fitted curve of least-altered samples shows 1) a plausible $^{87}Sr/^{86}Sr$ plateau at ~0.7085 from the late Ediacaran (Cox *et al*., 2016) to at least mid Fortunian at ca. 532 Ma; 2) a declining trend from 532 Ma to 523.5 Ma; 3) a long-term increasing trend from the late Stage 2 to Stage 4, interrupted by a 4-myr plateau across the stages 3-4 boundary. These overall trends are resolved here based on rigid screened least-altered carbonate data from worldwide successions with consistent chronologic constraints (Appendix E).

4.4.3.1. Latest Ediacaran–mid Fortunian $^{87}Sr/^{86}Sr$ plateau

Maloof, Porter, *et al*. (2010) argued that the marine $^{87}Sr/^{86}Sr$ decreased monotonically by ~0.0006 starting from the late Ediacaran and through the entire Terreneuvian Series (541-521 Ma). However, the reconstruction in this study does not corroborate their observation (Fig. 4.6). In contrast, the seawater $^{87}Sr/^{86}Sr$ acquired a steady state (~0.7085) at 546-532 Ma, followed by the gradual decline to ~0.7081 by 523.5 Ma. Data from late Ediacaran Nama Group, Namibia (Kaufman, Jacobsen and Knoll, 1993) and Central Iberia (Valladares *et al*., 2006) confirms the stabilising of the seawater $^{87}Sr/^{86}Sr$ at ~0.7085 in the latest Ediacaran. The contradiction could be explained by false interpretation from unscreened and thus scattered $^{87}Sr/^{86}Sr$ data in the previous compilations (Halverson *et al*., 2010; Maloof, Porter, *et al*., 2010; Peng, Babcock and Cooper, 2012). Utilising the rigid diagenesis-screening criteria, it reveals the fact that the unscreened data show a disturbing variability (Fig. 4.6) and thereby considerably deviate from the smoothed $^{87}Sr/^{86}Sr$ curve and the true seawater trend. The late Ediacaran–Fortunian interval is characterised by the transition from mostly soft-bodied

Ediacaran biotas to the first diversification of skeletal biotas (Maloof, Porter, *et al*., 2010; Wood *et al*., 2016; Zhu *et al*., 2017). This $^{87}Sr/^{86}Sr$ plateau possibly reflects an interval of equilibrium state between continental weathering and mantle input, mimicking unperturbed seawater chemistry (e.g. Mg/Ca) through this interval.

4.4.3.2. Late Fortunian–late Stage 2 $^{87}Sr/^{86}Sr$ decrease and the Stage 2 minimum

New constraints in this study reveal that the late Fortunian–late Stage 2 $^{87}Sr/^{86}Sr$ decrease started no earlier than ca. 532 Ma (Fig. 4.6). Interpretations of this declining trend include a decrease in continental weathering flux, and/or a probable reduction in radiogenic riverine Sr flux, but no geological evidence indicates a significant switch in lithologies in the weathering of rocks. As the early Cambrian is generally known as an interval with 'Greenhouse' or 'Hothouse' conditions (Brasier and Sukhov, 1998) and a long-term rise in the global sea-level (Miller, 2005; Haq and Schutter, 2008), it is unlikely that Cambrian Terreneuvian experienced a prolonged cooling event, which could hinder continental weathering. On the other hand, a previous modelling study put forward enhanced seafloor spreading and less Sr-radiogenic hydrothermal flux during the opening of the Iapetus ocean as the major control (Maloof, Porter, *et al*., 2010). Seafloor spreading centres cycle seawater through hydrothermal vents, reducing the ratio of magnesium to calcium in the seawater through metamorphism of calcium-rich minerals in basalt to magnesium-rich clays. While the reduction in the Mg/Ca ratio favours the precipitation of calcite over aragonite, the decrease in seawater $^{87}Sr/^{86}Sr$ signals a rise in hydrothermal flux and reduction Mg/Ca in the ocean that should have had an vital impact on the skeletal mineralogy of animals that evolved in the early Cambrian. Indeed, the late Stage 2 witnessed a dramatic switch from aragonite to calcite skeletonisation in early Cambrian animals (Porter, 2007) as well as an increase of seawater Ca^{2+} concentrations as imprinted in the fluid inclusion records (Berner, 2004; Brennan, Lowenstein and Horita, 2004; Porter, 2007). Importantly, the actual turning point of shifts in both skeletal mineralogy and seawater chemistry towards Ca enrichment coincides with the Stage 2 $^{87}Sr/^{86}Sr$ minimum (~0.7081) close to the base of the Tommotian at ca. 523.5 Ma (Fig. 4.4&4.6). The $^{87}Sr/^{86}Sr$ minimum thereby pinpoints the timing of the final overcoming of the Mg/Ca threshold for the first shift from aragonite sea to calcite sea in the Phanerozoic. In theory, the timing of the shift to high $^{87}Sr/^{86}Sr$ values is possibly related to the initiation of a brief cessation or deceleration of the lapetus extension and reduction of associated hydrothermal flux, but this explanation remains

speculative without detailed palaeogeographic and palaeoclimatic data. On the other hand, a dramatic increase in continental weathering flux could also turn the seawater $^{87}Sr/^{86}Sr$ towards high values even presuming the hydrothermal input remained unchanged.

4.4.3.3. Late Stage 2–Stage 4 trend

There is a generally increasing trend in $^{87}Sr/^{86}Sr$ in Cambrian stages 2-4, which follows the decline in the Fortunian–Stage 2 (Fig. 4.6). As it is discussed in 4.4.2, this rise in seawater $^{87}Sr/^{86}Sr$ ratio can be attributed to enhanced continental weathering relative to hydrothermal input of ocean crust alteration. The argument becomes more robust when considering the impact of the shift from 'Aragonite sea' to 'Calcite sea' immediately preceding the $^{87}Sr/^{86}Sr$ increase trend. This is because that 'Calcite sea' is usually accompanied by rapid seafloor spreading rates and enhanced hydrothermal input of less radiogenic Sr. To shift the seawater $^{87}Sr/^{86}Sr$, continental weathering flux is predicted as high to offset the 'Calcite sea' effect. The final formation of the Gondwana supercontinent was just prior to or nearly synchronous with the Cambrian radiations (Li and Powell, 2001; Meert, 2003; Campbell and Squire, 2010). The uplift and erosion of trans-Gondwana orogenies could be the major source of radiogenic Sr (Derry *et al*., 1994), and thus the driving force of the global rising seawater $^{87}Sr/^{86}Sr$ in this period. Another plausible alternative involves the physical reworking of soil, regolith and ^{87}Sr-rich granitic basement rock that was progressively exposed on the 'Great Unconformity' as a result of continental crust denudation (Brasier and Lindsay, 2001; Peters and Gaines, 2012; He *et al*., 2016). It is also argued that enhanced chemical weathering of these fresh materials on the continental crust during the Cambrian Sauk transgression could be a major contribution to the elevated seawater $^{87}Sr/^{86}Sr$ (Peters and Gaines, 2012). On the other hand, although uncertainty remains surrounding the initiation of this first continental-scale marine transgression of the Phanerozoic, the weathering process on the flooded continents would affect seawater chemistry by increasing the Ca^{2+} concentrations in seawater, and thus could have triggered the shift to 'Calcite sea' and calcium-favouring biomineralisation from the beginning of the Tommotian (Fig. 4.4). Moreover, Stage 2-3 coincides closely with the animal radiation events (Fig. 4.4). Enhanced continental erosion during this interval should exert a significant influence on the seawater composition and global climate, and provide numerous life-bearing nutrients such as phosphorus to the coeval oceanic realm.

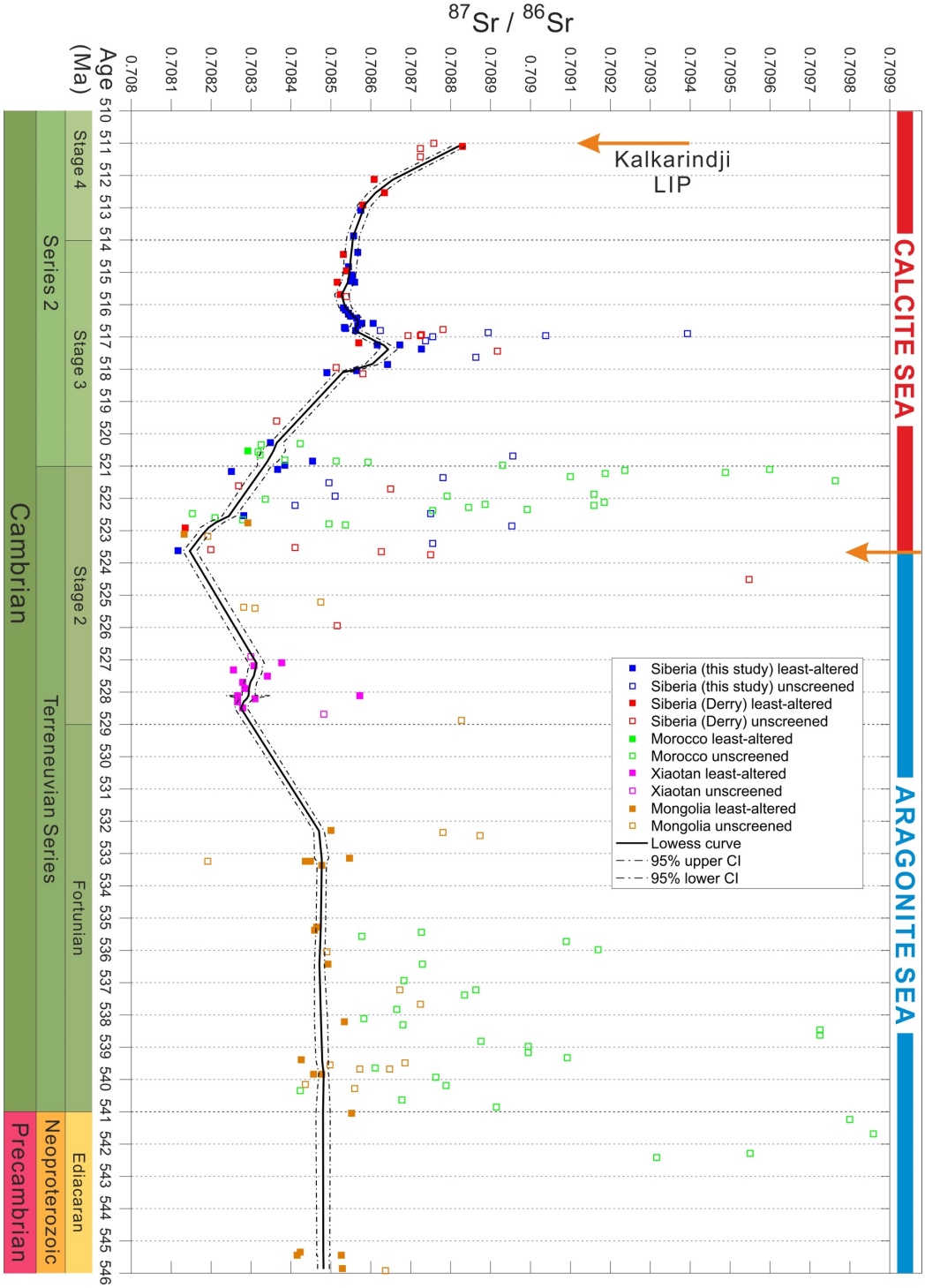

Figure. 4.6: Details of carbonate $^{87}Sr/^{86}Sr$ record through the Ediacaran–Cambrian boundary to the Cambrian Stage 4. Data are derived from carbonate samples of South China Xiaotan section (Li *et al*., 2013), Siberia (this study and Derry *et al*., 1994), Morocco (Maloof, Porter, *et al*., 2010) and Mongolia (Brasier *et al*., 1996). Open square: unscreened carbonate; solid square: screened and least-altered carbonate; All data are assigned to a consistent timescale by applying the high-resolution carbon isotope chemostratigraphy between sections, age constraints from Morocco (Maloof, Ramezani, *et al*., 2010) and South China (Appendix E). All data are adjusted to NIST SRM 987 = 0.710248 (McArthur, Howarth and Shields-Zhou,

2012), and recalculated to the Geologic Time Scale 2012 (Gradstein *et al*., 2012). Solid black curve: mean LOWESS fitted line; dotted line: two-sided 95% confidence intervals. The switch on seawater chemistry between 'Aragonite Sea' and 'Calcite Sea' is given at ca. 523.5 Ma (base of Tommotian Stage) based on previous statistical constraints by lithology change of early Cambrian skeletal fossils and fluid inclusions-based data (Porter, 2007). The brief emplacement for the Australian Kalkarindji Large igneous province is given at ca. 511 Ma (Jourdan *et al*., 2014).

Against the backdrop of an increasing trend, the $^{87}Sr/^{86}Sr$ record witnessed a short-term decline in seawater $^{87}Sr/^{86}Sr$ of 0.0001 at ca. 517.5 Ma and a subsequent stable $^{87}Sr/^{86}Sr$ record through the late Stage 3–early Stage 4 (Botomian–early Toyonian in Siberia Stage) (Fig. 4.4). The seawater $^{87}Sr/^{86}Sr$ reversal and retardation coincide with the Botomian–Toyonian extinction (BTE), and could be attributed to the following hypotheses either independently or combined: 1) Reduced rates of tectonically driven uplift or climate change may have resulted in a temporary decline in global silicate weathering rates. However, there is no direct evidence suggesting a short-term change in uplift rate nor global temperature drop. 2) A change in the type of crust undergoing weathering could have driven a significant drop in the mean riverine $^{87}Sr/^{86}Sr$ ratios. It was proposed that the eruption of north Australian flood basalts of the Kalkarindji Large Igneous Province (LIP) was likely the trigger of the BTE. This event could be the ideal unradiogenic Sr source in the early–mid Cambrian that lowered the seawater $^{87}Sr/^{86}Sr$ significantly. But more recent high-precision dating work by Jourdan *et al*. (2014) suggest that Kalkarindji LIP occurred at ca. 510.7 ± 0.6 Ma, which is at least 5 Myr later than the initiation of the seawater $^{87}Sr/^{86}Sr$ reversal (Fig. 4.4&4.6). However, a major phase of riftogenic extension and dispersal of the continents is known to have taken place during the early Cambrian. The dispersal is indicated by conjugate rift systems (Dalziel, 1991, 1997). Products of rift-related magmatism such as volcanism and alkali basalts would in part contribute to the ^{87}Sr-depleted source. 3) Increase in mid-ocean-ridge length owing to higher ocean spreading rates would contribute additional less radiogenic hydrothermal Sr source to the ocean. Although the timing and mechanism remain unclear, the development of the Iapetus-Pacific oceanic gateway might involve considerable increase in the length of young spreading ridges. 4) Chemical weathering of low $^{87}Sr/^{86}Sr$ materials (e.g. carbonate dissolution) during the transgression might have been sufficient to reverse temporarily the upward trend of seawater $^{87}Sr/^{86}Sr$.

The $^{87}Sr/^{86}Sr$ retardation is bracketed by two global events in sea-level change before rising again at ca. 512.5 Ma (Fig.4.4). The Sinsk transgression event approximately matches the initiation of the $^{87}Sr/^{86}Sr$ plateau. Subaqueous carbonate dissolution should keep pace with the

transgression. Earlier formed carbonate, such as the underlying late Ediacaran age limestone of lower $^{87}Sr/^{86}Sr$ value (0.7080-0.7086; Kaufman, Jacobsen and Knoll, 1993; Melezhik *et al*., 2009), would buffer the seawater $^{87}Sr/^{86}Sr$ value and possibly reverse the increasing trend. Coincidently, the Hawke Bay regression event marked the termination of the seawater $^{87}Sr/^{86}Sr$ retardation, which can be explained by recovery of exposed continental crust following the regression event. Although the global correlation of both sea-level change events remains problematic (Zhuravlev and Wood, 1996; Dilliard *et al*., 2007), the BTE on the Siberian Platform was interpreted as triggered by extensive encroachment of anoxic deep water to shallow environment during the Sinsk transgression event. The sea-level change model thus offers a novel mechanism that stranding both the seawater $^{87}Sr/^{86}Sr$ record and Cambrian radiations simultaneously.

4.5. Conclusions

New $^{87}Sr/^{86}Sr$ measurements based on least-altered carbonate samples from the Siberian Aldan-Lena Rivers sections evaluate the fidelity of both long-term trends and short-term turnovers from previous studies (Derry *et al*., 1994; Nicholas, 1996), addressing the necessity of diagenesis evaluation of $^{87}Sr/^{86}Sr$ data. Using a consistent age model based on Moroccan absolute U-Pb ages and high-resolution $\delta^{13}C_{carb}$ features, a calibrated LOWESS-fitted curve is proposed here as the best estimate of the seawater $^{87}Sr/^{86}Sr$ trend for the first two series of Cambrian System. The data compilation of least-altered carbonate shows that the early Cambrian is marked by a gradual decline (532-523.5 Ma), two plateaus (546-532 Ma and 517-512Ma) and two steep increase (523.5-517.5 Ma and 513-511 Ma). The rapid climb of seawater $^{87}Sr/^{86}Sr$ from ~0.7081 to 0.7087 in the mid Stage 2–early Stage 3 is associated with the major animal radiation events, and probably caused by a rapid increase of continental weathering flux. A combination of trans-Gondwana orogenies denudation and enhanced chemical weathering on the 'Great Unconformity' during the Sauk transgression would contribute to the high continental weathering flux. The Cambrian $^{87}Sr/^{86}Sr$ minimum is positioned at ca. 523.5 Ma, coinciding with the turning point for the 'Aragonite sea' to 'Calcite sea' transition, while the plateau at ca. 517-512 Ma is interpreted here as responsive to global sea-level changes. This study also resolves possible mechanisms for other temporary $^{87}Sr/^{86}Sr$ retardation or turnovers in the early Cambrian, but conclusions await confirmation from additional weathering-related proxies such as Ca, Os and Li isotopes.

Chapter 5

Measuring the 'Great Unconformity' on the North China Craton

ABSTRACT

The 'Great Unconformity' effect offers one of the plausible mechanisms to explain the 'Cambrian Explosion'. It involves the idea that enhanced weathering on this trans-global stratigraphic marker facilitated the high nutrient flux to the ocean realm that accommodated the early Cambrian biotic community. Ages and correlations of the Neoproterozoic–Cambrian sedimentary successions in North China, which preserve a slice of the 'Great Unconformity', are not well constrained and have been the subjects of recent debate. New detrital zircon ages presented in this chapter confirm that Neoproterozoic strata of the southeastern North China Craton (NCC) are mostly of early Tonian age, but that the Gouhou Formation, previously assigned to the Tonian, is Cambrian in age. A discordant hiatus of >150-300 million years occurs across the NCC, spanning most of the late Tonian, Cryogenian, Ediacaran and early Cambrian periods. This widespread unconformable surface is akin to the 'Great Unconformity' seen elsewhere in the world, and highlights a major shift in depositional style from largely erosional, marked by low rates of net deposition, during the mid-late Neoproterozoic to high rates of transgressive deposition during the mid-late Cambrian. Comparison between age spectra for southeastern NCC and northern India are consistent with a provenance affinity linking the NCC and East Gondwana by ~510 Ma.

Author Contributions: Andrew Carter and Martin Rittner supervised and assisted with the U-Pb isotopic analysis at London geochronology Centre, University College London. Pieter Vermeesch helped with the data visualisation. Ying Zhou contributed two samples of Gouhou Formation. The discussion benefitted from helpful conversations with Graham A. Shields, Ying Zhou, Pieter Vermeesch, Martin Rittner, Andrew Carter, Lanyun Miao, Maoyan Zhu and Philip A. E. Pogge von Strandmann. Some of the text and discussion within this Chapter is adapted from He et al. (2016).

5.1. Introduction

It has long been recognized that the traditional Precambrian–Cambrian (Ediacaran–Cambrian) boundary interval is characterized worldwide by low rates of deposition and/or a major unconformity, known as the 'Great Unconformity' (Brasier and Lindsay, 2001; Peters and Gaines, 2012). Global eustatic sea-level rise and widespread orogenesis accompanied the Cambrian bioradiation, and have both been linked to unprecedented high flux rates of nutrients and other dissolved ions during the late Neoproterozoic and early Paleozoic (Squire *et al*., 2006; Campbell and Allen, 2008; Meert and Lieberman, 2008). Enhanced chemical weathering on the 'Great Unconformity' during transgression has been causally linked to the Cambrian radiation of animals (Peters and Gaines, 2012), in particular the introduction of skeletal biomineralisation. In support of this, Brasier and Lindsay (2001) identified a number of regions of the world where deposition rates increased remarkably after the Ediacaran–Cambrian boundary, in a transgressive episode marked by widespread phosphogenesis. One such area is the southeastern North China Craton (NCC), which possesses well-exposed Neoproterozoic–Cambrian marine successions with astonishingly well-preserved, organic-walled fossils (Zang and Walter, 1992; Dong *et al*., 2008; Xiao *et al*., 2014; Tang *et al*., 2015). However, the full potential of these exceptional paleontological archives cannot be realized until uncertainties in the depositional ages and stratigraphic correlations across the NCC are resolved (Xiao *et al*., 2014).

The 'Great Unconformity' is unambiguously recognised in large parts of the world where this contact is represented by a nonconformity. However, it is much more challenging to identify this contact in other regions, including the Canadian Rocky Mountains (Aitken, 1969), South Australia (Nedin, Jenkins and Mount, 1991) and the NCC, where this surface is commonly preserved as a cryptic disconformity, separating thick successions of Neoproterozoic strata from overlying Cambrian ones. Uncertainty remains surrounding the stratigraphic level of the lowermost Cambrian as well as the positioning of the major break that is regionally traceable along the southeastern margin of the NCC. Precise age constraints on individual formations are needed to locate the position of this significant gap in successions that potentially may exhibit a number of disconformable levels (Wang *et al*., 1984; Hong, Huang and Liu, 1991) and to resolve the timing and duration of the coeval uplift events and/or sea-level fluctuations. In addition, recent palaeogeographic reconstructions, e.g. in which the NCC was attached to East Gondwana (McKenzie, Hughes, Myrow, Choi, *et al*., 2011; Han *et al*., 2016) or was an

isolated continent (Wilhem, Windley and Stampfli, 2012; Cocks and Torsvik, 2013; Li, Evans and Halverson, 2013; Torsvik and Cocks, 2013) during the Cambrian, are not yet fully grounded.

Detrital zircon is highly refractory and commonly distributed in sedimentary clastic deposits, which could provide a critical overview of the detrital source history of a deposit. Utilising the U-Pb radiometric ages of these zircons, we can determine the maximum depositional age from the youngest detrital zircon of a deposit, and quantitatively identify the source components based on the age distribution and populations of these zircons. Therefore the detrital zircon analysis can be used to address these uncertainties to 1) establish the maximum depositional age of sedimentary units; 2) identify the missing age interval such as depositional breaks in stratigraphic successions in the absence of a robust biostratigraphic framework; 3) use provenance comparison of age modes to build up interbasinal stratigraphic correlations and 4) reconstruct the fragmentation and affinity history of different continental plates of the geological past (Fedo, 2003).

This study presents new detrital zircon U-Pb age data for thirteen Neoproterozoic–Cambrian samples from the Huaibei and Dalian regions, which are situated along the southeastern margin of the NCC. Combining the new age constraints with published radiometric ages of detrital zircons and intrusive diabase sills, the results provide refined age constraints on stratigraphic successions and attempt to resolve the major depositional breaks in Neoproterozoic–Cambrian successions of the southeastern NCC. The provenance of age components identified in these samples is also interpreted with respect to regional stratigraphic correlation and palaeogeographic reconstruction.

5.2. Regional stratigraphic context

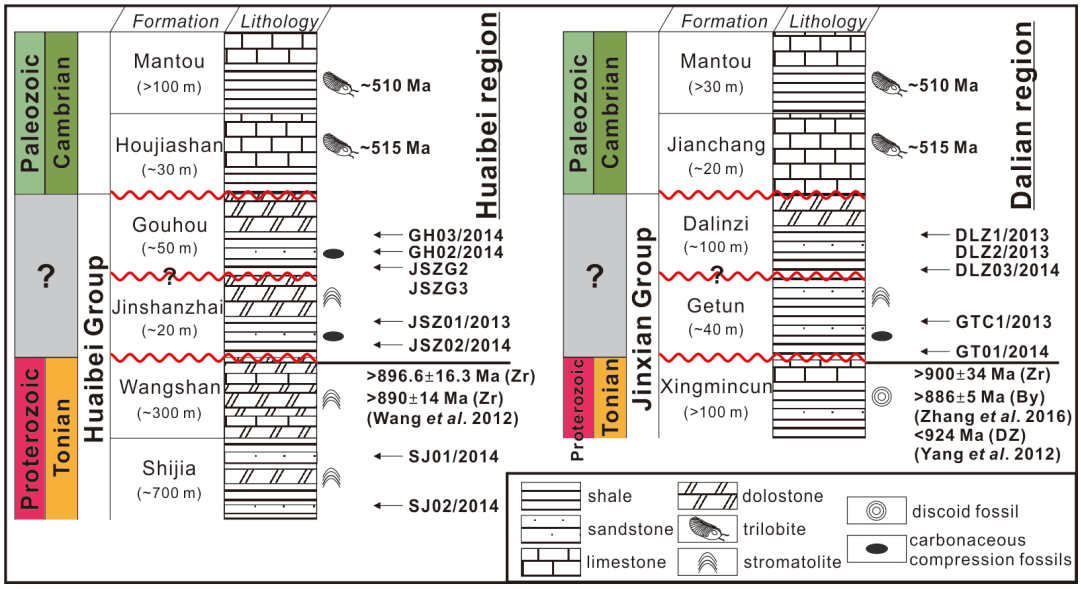

Figure 5.1: Stratigraphic columns showing the investigated Tonian–Cambrian successions in Huaibei and Dalian regions. Columns are not to scale but thickness of individual formations at investigated sections is shown in bracketed under the formation name. Published fossil occurrences (Zhang and Zhu, 1979; Hong, Huang and Liu, 1991; Zang and Walter, 1992; Qian *et al*., 2002; Dong *et al*., 2008; Xiao *et al*., 2014; Tang *et al*., 2015; Luo, Zhu and Reitner, 2016), minimum depositional age constraints for Wangshan and Xingmincun formations by U-Pb baddeleyite (By) or zircon (Zr) dating of cross-cutting diabase sills (Wang, Yang and Xu, 2012; Zhang *et al*., 2016), maximum depositional age (DZ) for Xingmincun Formation using the youngest cluster of detrital zircon ages (Yang *et al*., 2012) are marked next to the stratigraphic column. Arrows point out the sampling horizons for detrital zircon dating in this study. Wave lines represent proposed unconformities.

5.2.1. Huaibei region

In general, the upper part of the Huaibei Group constitutes a sequence of carbonate and siliciclastic deposits, including the Shijia, Wangshan, Jinshanzhai and Gouhou formations in ascending stratigraphic order (Fig. 5.1). The Shijia Formation was sampled at the Heifengling section (Fig. 1.3), and is characterized by pale yellowish green and reddish purple shale with interbeds of quartz sandstone and stromatolitic dolostone. The succeeding Wangshan, Jinshanzhai and Gouhou formations were investigated at Gouhou and Jinshanzhai sections (Fig. 1.3). The Wangshan Formation is dominated by dolomitic or cherty limestone with the presence of abundant ‘molar tooth’ structures and stromatolite forms, including *Acaciella*,

Anabaria, *Inzeria* that would be consistent with a pre-Cryogenian age (Qian *et al*., 2002). The Jinshanzhai Formation consists of green and reddish purple shale interbedded with glauconitic quartz sandstone in the lower part, while the upper part is characterized by purple stromatolitic dolostone with stromatolite forms, including *Boxonia*, *Linella* and *Xiejiella* (Qian *et al*., 2002). The Gouhou Formation, which is the uppermost unit of the Huaibei Group, is subdivided into two parts in this study. The lower 'member' is dominated by red clastic rocks, while the upper 'member' consists of pale grey, cherty dolostone (Fig. 5.2e, g & h). Halite pseudomorphs are present in both clastic (Fig. 5.2f) and carbonate intervals, which together with abundant mud cracks in the lower member indicate an evaporitic, likely marginal marine environment was maintained throughout deposition of the Gouhou Formation. Algal fossils are reported from the Jinshanzhai and Gouhou formations in the form of carbonaceous compressions of the genera *Protoarenicola* (Jinshanzhai Fm.) and *Chuaria*, *Ellipsophysa* and *Tawuia* (Gouhou Fm.), respectively (Zang and Walter, 1992; Dong *et al*., 2008).

The lower contacts of the Jinshanzhai and Gouhou formations have both been suggested to coincide with the Precambrian–Cambrian boundary in the Huaibei region (Qian *et al*., 2001). However, these two formations are now thought to have been deposited during the Tonian Period based on the co-occurrence of a possible 'Tonian-age' acritarch organic-walled microfossil assemblage that includes *Trachyhystrichosphaera*, *Valeria*, and *Dictyosphaera* at a single level within the lower Gouhou Formation (Tang *et al*., 2015). Although this Tonian assignment is consistent with reports of a *Chuaria-Tawuia* association in the same formation (Xiao *et al*., 2014; Tang *et al*., 2015), the validity of acritarch biostratigraphy for age determination in the Precambrian is less well established than for the Phanerozoic, and may have limitations due to relatively poor species classification and long-range distribution in the geological record. Moreover, as shown in Fig. 5.2g & h, some beds within the upper Gouhou Formation, in which halite pseudomorphs are conspicuously absent, are characterised by mottled fabrics that this study compare with the pervasive bioturbation that is characteristic of the Phanerozoic, although no nameable ichnofossils have yet been identified. Given that the oldest ichnofabrics are no older than Late Ediacaran in age (Rogov *et al*., 2012), it seems reasonable to question the assigned Tonian affinity of the Gouhou Formation. The unambiguously Cambrian Houjiashan and Mantou formations overlie the Huaibei Group with apparent conformity at Gouhou and Jinshanzhai sections. The Houjiashan Formation consists of yellowish dolomitic shale at the base, followed by extensively bioturbated thick-bedded, intrasparitic limestone. The trilobites *Estaingia* and *Redlichia* characterize the Houjiashan Formation, indicative of the Canglangpuan Stage = lower part of Cambrian Stage 4, (~515

Ma) (Zhang and Zhu, 1979; Miao, 2014). The Mantou Formation overlies the Houjiashan Formation, and its lower part is characterized by red shale and *Redlichia*, consistent with the Longwangmiaoan Stage = upper part of Cambrian Stage 4 (~510 Ma).

5.2.2. Dalian region

The upper part of the Jinxian Group consists of the Xingmincun, Getun and Dalinzi formations in ascending stratigraphic order (Fig. 5.1). The Xingmincun Formation comprises glauconite-bearing clastic rocks in the lower to middle parts, and dark grey thin-medium bedded limestone in the upper part (Fig. 5.3a & b). Discoid fossils of probable pre-Ediacaran age are reported in shale of the middle part of the formation (Hong, Huang and Liu, 1991; Luo, Zhu and Reitner, 2016), while recently published radiometric ages confirm that the Xingmincun Formation was deposited in the Tonian Period (Yang *et al*., 2012; Zhang *et al*., 2016). The Getun and Dalinzi formations were sampled at Manjiatan and Longwangmiao sections (Fig. 1.3). The Getun Formation is dominated by clastic rocks (Fig. 5.3c, d & e) with some stromatolitic horizons and the carbonaceous compression fossils *Chuaria* and *Tawuia* (Hong, Huang and Liu, 1991). *Archaeostracods* (*bradoriids*) were reported from the upper part of the Getun Formation, implying a Qiongzhusinian or Cambrian Stage 3 affinity (~520-515 Ma) (Wang and Yang, 1986), but these findings have not been confirmed. The Dalinzi Formation consists of yellowish green and reddish purple sandstone (Fig. 5.3f) with thin-bedded light grey dolostone in the topmost beds (Fig. 5.3h). The small shelly fossil *Sachites* of Cambrian Fortunian-Stage 3 affinity was reported from the red shale of the upper Dalinzi Formation (Hong, Huang and Liu, 1991). Mud cracks, halite casts (Fig. 5.3g), thin-layered gypsum deposits and cross-bedding are all observed in both the Getun and Dalinzi formations, suggesting that the units were probably formed in a shallow marine evaporitic environment. Indeed, the Getun and Dalinzi facies have been interpreted to represent a lagoonal and playa lake or other evaporative setting, respectively (Fairchild *et al*., 2000). Also noteworthy is the observation that these features are also found in the Gouhou Formation (Huaibei region), which is dominated in its lower-middle part by clastic rocks, which are gradually replaced by dolostone in the upper part, possibly due to a widespread marine transgression that resumes through the overlying formations. The Cambrian Jianchang and Mantou formations overlie the Jinxian Group. The Jianchang Formation is dominated by dark grey medium-thick bedded limestone. Co-occurrence of the *Latipalaeolenus* trilobite assemblage (Hong, Huang and Liu, 1991; Liu, 2012) and archaeocyath assemblages (Hong, Yang and Liu, 1990) indicates that

the unit can be approximately correlated with the Houjiashan Formation in the Huaibei region (Fig. 5.5). The overlying Mantou Formation is characterized by red shale and *Redlichia*, and so is consistent with the Mantou Formation in the Huaibei region.

Importantly, many hypotheses regarding the placement of the Neoproterozoic–Cambrian boundary in the region appear to be debatable. Some propose the Getun Formation (also referred to as 'Gejiatun Formation') as the lowermost Cambrian unit (Wang and Yang, 1986; Duan and An, 1994; Qiao, 2002), while others favour a boundary at the top of the Dalinzi Formation (Hong, Huang and Liu, 1991; Xue *et al*., 2001). However, these arguments are largely based on the unsubstantiated occurrence of Cambrian ichnofossils and small shelly fossils, highlighting the importance of precise and accurate radiometric dating of these formations.

5.2.3. Unconformable stratigraphic contacts

Various observations have been made regarding the possible location of the major unconformity among multiple candidates between Neoproterozoic and Cambrian strata on the southeastern NCC. In the Huaibei region, the Jinshanzhai Formation sits with clear erosional unconformity on top of the Wangshan Formation, evidenced at its base by a widespread conglomeratic bed that marks an abrupt lithological change from carbonate to siliciclastic rocks (Fig. 5.2a & b). Another abrupt change in lithology and a conglomerate bed can be observed between the Gouhou and Jinshanzhai formations (Fig. 5.2c), indicating the existence of a second possible depositional gap, although the clasts in this case are smaller, more angular and potentially derived from underlying strata at the Jinshanzhai section (Fig. 5.2d). Regional mapping reveals that the Houjiashan Formation overlies various Neoproterozoic formations, which are reddened at their tops, identifying its base as a major transgressive surface (Li, Qian and Jiang, 2013; Xiao *et al*., 2014), but without clear indication of an erosional unconformity. At sections where the Houjiashan Formation overlies the Gouhou Formation, there is no reddening or other sign of surface exposure at the top of the Gouhou Formation. However, the top of the Jinshanzhai Formation comprises reddened stromatolites, which directly underlie the red beds of the lower Gouhou Formation.

In the Dalian region, potentially significant erosional disconformities are reported overlying the Xingmincun (Fig. 5.3a), Getun and Dalinzi formations (Fig. 5.3h), respectively (Hong,

Huang and Liu, 1991). By contrast, others have observed no major lithological or facies changes between the Getun and Dalinzi formations, implying a conformable contact (Wang and Yang, 1986; Duan and An, 1994; Qiao, 2002). The Getun/Xingmincun boundary is marked in the field by the abrupt appearance of black shale overlying a basal lag conglomerate (Fairchild, Einsele and Song, 1997; Fairchild *et al*., 2000), which lies directly on top of bluish dolomitic limestone of the upper Xingmincun Formation (Fig. 5.3a & b). The Getun Formation is not always well exposed in the Dalian region and is interrupted by diorite sills at Manjiatan section, where there are potentially significant erosional surfaces within it (Fig. 5.3c). A transitional contact is suggested between the fine-grained, shaly upper Getun and sandy lower Dalinzi formations (Fig. 5.3d). However, black chert lonestones are exposed near the contact (Fig. 5.3e), indicating another possible erosional surface. Despite equivocal support for major disconformable surfaces from sedimentary evidence, the timing and duration of these proposed hiatus surfaces remain unresolved due to a lack of a reliable chronostratigraphic framework and to some extent the lack of regional continuity of outcrop due in part to recent urban development and widespread igneous intrusions of Neoproterozoic–Mesozoic age.

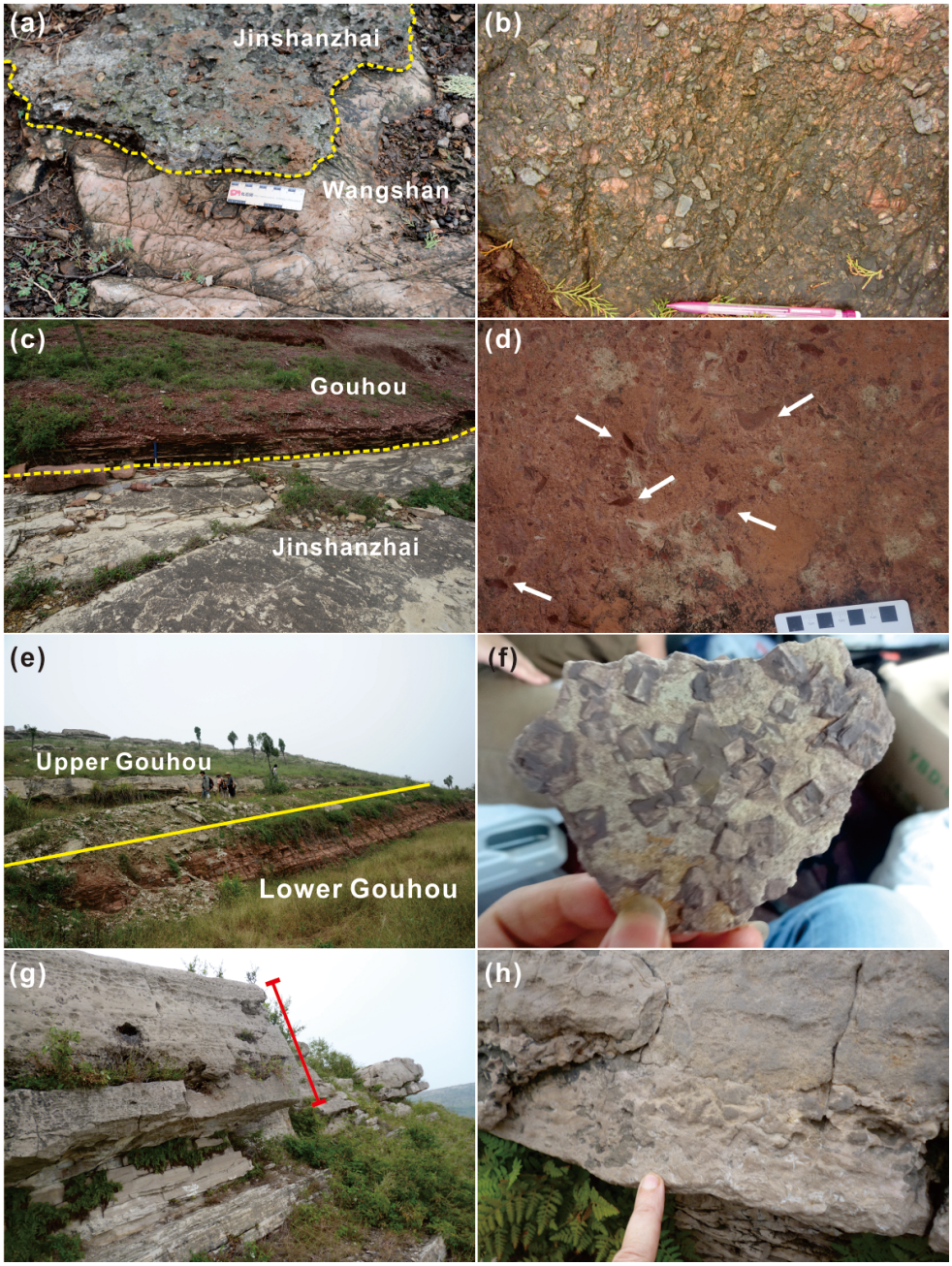

Figure 5.2: Outcrop photos from Huaibei region: (a) unconformable contact between Wangshan and Jinshanzhai formations, Jinshanzhai section; (b) conglomerate bed exposed at the base of Jinshanzhai Formation, Jinshanzhai section; (c) unconformable contact between Gouhou and Jinshanzhai formations, Jinshanzhai section; (d) conglomerate bed exposed at the base of Gouhou Formation, Jinshanzhai section; clasts of stromatolite fragments possibly sourced from underlying Jinshanzhai Formation are marked by white arrows; (e) red clastic rocks in the lower part of Gouhou Formation and carbonate in the upper part, Gouhou section; (f) halite pseudomorphs in the lower part of Gouhou Formation, Gouhou section; (g) Mottled (bioturbated) dolostone beds (bracketed by red bar) in the upper part of Gouhou Formation, Gouhou section; (h) Burrows in the upper part of Gouhou Formation, Gouhou section. Yellow lines illustrate the formation or member boundaries.

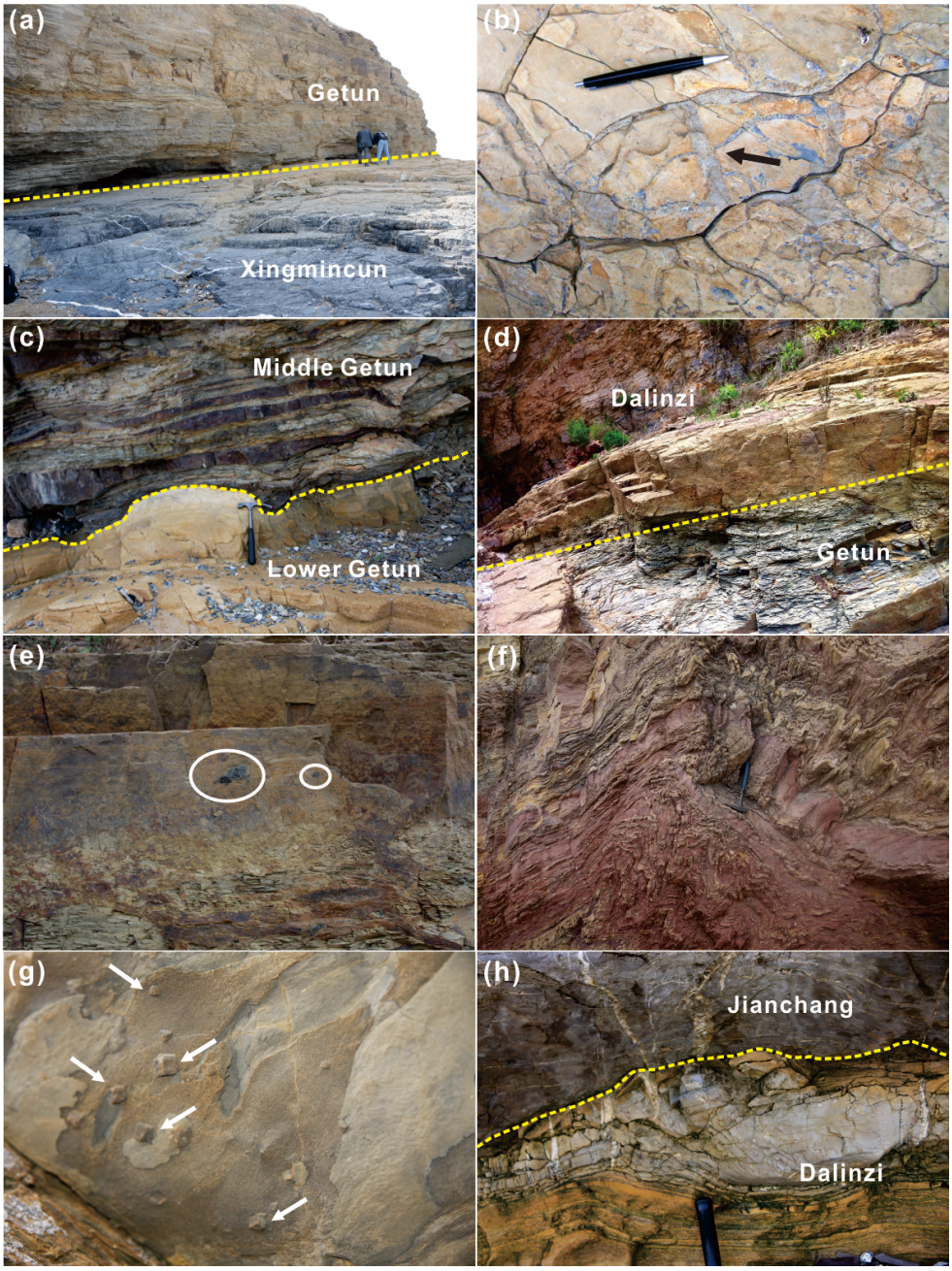

Figure 5.3: Outcrop photos from Dalian region: (a) Disconformity between Xingmincun and Getun formations, Manjiatan section; (b) exposure cracks (marked by black arrow) in the topmost bed of the Xingmincun Formation, Manjiatan section; (c) erosional surface between lower and middle parts of Getun Formation, Manjiatan section; (d) apparently transitional contact between Getun and Dalinzi formations, Manjiatan section; (e) black chert clasts near the contact between Getun and Dalinzi formations, Manjiatan section; (f) yellowish green and reddish purple sandstone of the Dalinzi Formation, contorted by evaporite dissolution and fluid escape, Manjiatan section; (g) halite pseudomorphs marked by white arrows in the Dalinzi Formation, Manjiatan section; (h) unconformable contact between Jianchang and Dalinzi formations, Manjiatan section; Yellow lines illustrate the formation or member boundaries.

5.3. Materials and methods

Details for regional geological and stratigraphic settings of the studied sections are discussed in sections 1.6.1 and 5.2. Thirteen samples of siliciclastic rock from the Shijia, Jinshanzhai, Gouhou, Getun and Dalinzi formations were taken at different stratigraphic intervals within the individual formations. Poorly sorted and coarser samples were selected in the field as they likely represent better mixed detrital sources, and zircons of larger grain size are preferred for laser ablation and dating precision. Sample lithologies, GPS locations and a compiled U-Pb age dataset are reported in *Appendix F*.

Zircon grains were separated using standard mineral separation procedures, which include jaw crushing, sieving, magnetic and heavy liquids separation. Handpicked zircons were then mounted in epoxy and polished prior to analysis. In-situ zircon U-Pb dating was carried out at the London Geochronology Centre, University College London, using a *New Wave®* 193 nm excimer laser ablation system, coupled to an *Agilent®* 7700x quadrupole ICP-MS. Real time data were processed using GLITTER 4.4 data reduction software, which enables selection of the best intervals for background and signal measurement during the analysis. Repeat measurements of external zircon standard *Plešovice* (TIMS reference age 337.13 ± 0.37 Ma) (Sláma *et al*., 2008) and NIST 612 silicate glass (Pearce *et al*., 1997) were used to correct for instrumental mass bias and depth-dependent inter-element fractionation of Pb, Th and U. Around 150 grains were analysed for each sample in order to meet established requirements for provenance studies as suggested in Vermeesch (2004).

A -15/+5% discordance limit was used to filter out discordant data. $^{206}Pb/^{238}U$ age was chosen if the age is younger than 1100 Ma, otherwise a $^{207}Pb/^{206}Pb$ age was used. Normalized age kernel density estimate plots (Fig. 5.4) were produced utilizing software package 'provenance' (Vermeesch, Resentini and Garzanti, 2016). Maximum deposition ages in Fig. 5.4 were calculated by the youngest cluster in the detrital zircon U-Pb age spectra using the minimum age algorithm (random effects model) with normal errors Galbraith (2005) as implemented in the 'DensityPlotter' software (Vermeesch, 2012). Statistically, the algorithm advances by providing the common age of the youngest age mode rather than the central age of all grains (Galbraith, 2005), especially helpful when analysed ages are over-dispersed.

5.4. U-Pb data

Detrital zircon U-Pb results from Dalian and Huaibei regions are presented separately as Kernel density estimate plots (Fig. 5.4).

In Huaibei Group, the Shijia Formation zircons exhibit a broad range of ages between 0.9 Ga and 2.0 Ga, with the main peak at ca. 1.2 Ga. The Jinshanzhai Formation yielded no grains younger than 0.8 Ga, with an age distribution dominated by a large population with peak centring at ca. 2.1 Ga. The overlying Gouhou Formation exhibits a broad population of zircons, with an isolated age population of around 0.5 Ga, two prominent peaks at approximately 1.85 Ga and 2.5 Ga as well as a smaller population of Neoproterozoic to Mesoproterozoic age. The Cambrian-age group comprises 8 concordant zircon grains from three samples that were collected at different stratigraphic horizons within the Lower Gouhou Formation from two separate sections (see Appendix F). Ages of these grains range from 490.4 ± 5.9 Ma to 519.2 ± 5.9 Ma. Utilizing the minimum age algorithm, a statistical estimate age of 518.4 ± 2.9 Ma for the youngest age mode is suggested here to represent the maximum depositional age for the Gouhou Formation. Previously reported age spectra for the Jinshanzhai Formation shows peaks centred at 1.85 Ga and 2.5 Ga (Yang *et al*., 2012), similar to the patterns from my Gouhou Formation samples. However, both samples of the Jinshanzhai Formation in my study show distinctive 2.1 Ga peaks, which are strikingly absent in the published study. The contradiction would result from false sampling or different definition of the boundary between Jinshanzhai and Gouhou formations.

For the Jinxian Group, the Xingmincun Formation yielded prominent populations of around 0.9-1.1 Ga and 1.5-1.8 Ga (Yang *et al*., 2012). The overlying Getun Formation yielded a considerable number of grains between 0.7 Ga and 1.0 Ga. As with the Gouhou Formation, the Dalinzi Formation contains one prominent peak at 1.85 Ga and two smaller peaks at ca. 0.7 Ga and 2.5 Ga. Published data from the adjacent Korea terrain are also discussed here for comparison. The lowermost Cambrian Myeonsan Formation from eastern Korea yielded similar age spectra to Gouhou and Dalinzi formations with dominant peaks at 1.85 Ga and 2.5 Ga (Cho and Cheong, 2016; Kim and Ree, 2016; Lee *et al*., 2016).

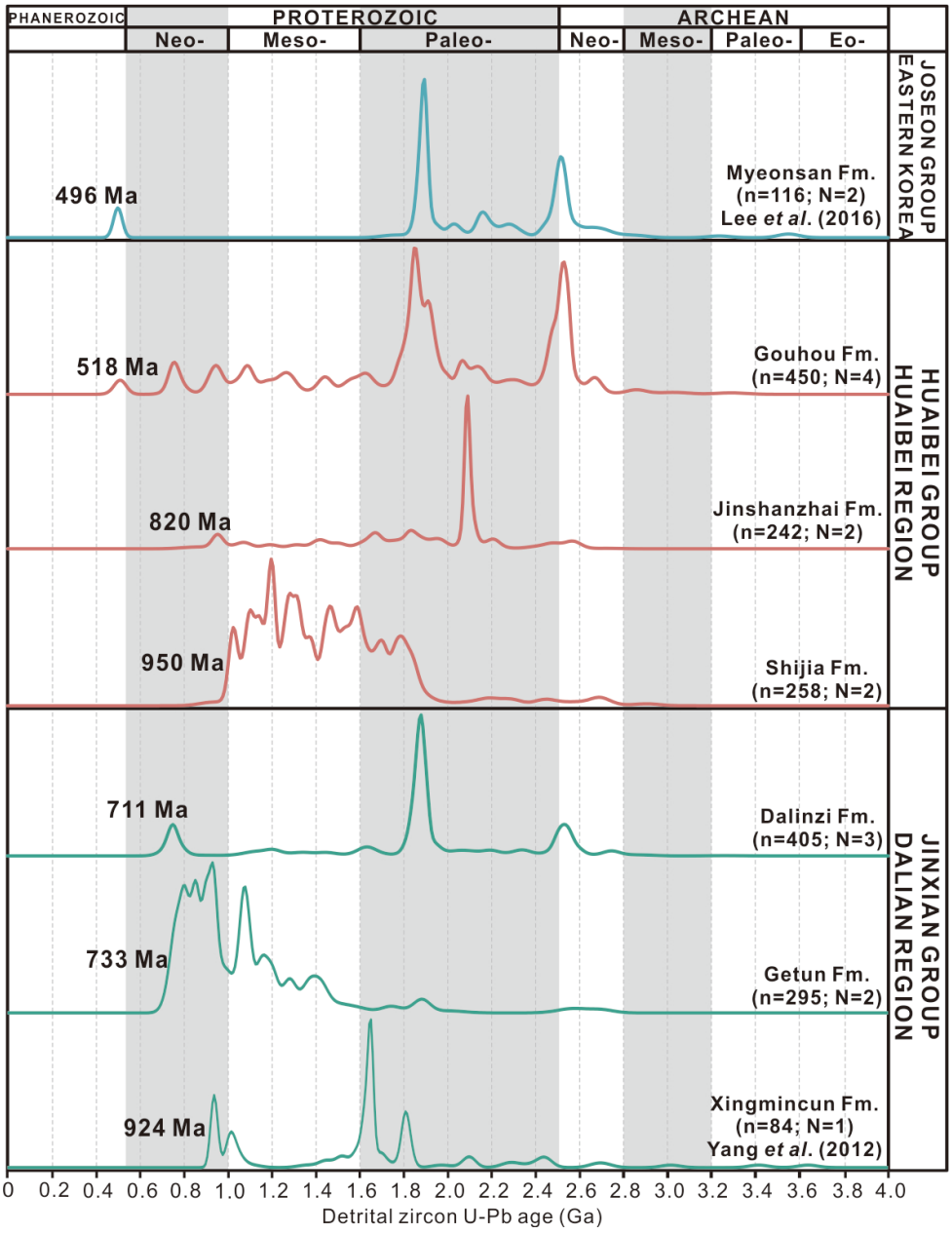

Figure 5.4: Normalized kernel density estimate plots showing detrital zircon U-Pb ages from Tonian–Cambrian successions in southeastern North China Craton and eastern Korea. Maximum depositional ages of individual formations are illustrated. n: total number of zircon grains analysed. N: numbers of samples analysed. Raw data is reported in Appendix F.

5.5. Discussion

5.5.1. Depositional age constraints

New and compiled detrital zircon U-Pb age populations in Fig. 5.4 likely reflect the ages of dominant magmatism in the southeastern NCC. Maximum depositional ages of each formation are determined by the ages of the youngest group of detrital zircons. In addition, minimum depositional ages are constrained by U-Pb baddeleyite or zircon crystallization ages of cross-cutting diabase sills (Fig. 5.1). In the Huaibei region, detrital zircon data show that the Shijia and Wangshan formations were most likely deposited between 950 Ma and 820 Ma; zircon data from sills and likely correlation with correlative strata in the Dalian region indicate a depositional age most probably closer to the older end of that age range (Zhang *et al*., 2016). There is no general agreement regarding the depositional age of the Jinshanzhai and Gouhou formations of the uppermost Huaibei Group, with diverse interpretations from Cambrian (Zang and Walter, 1992; Xing, 1996), Cryogenian–Ediacaran (Wang *et al*., 1984; Cao, 2000) to Tonian ages (Xiao *et al*., 2014). However, given that the youngest zircon grains yield a maximum depositional age of 518 Ma (Fig. 5.4), the Gouhou Formation, consistent with evidence for possible bioturbation and burrows (Fig. 5.2g & h), appears to be of similar mid-Cambrian age to the overlying trilobite-bearing Houjiashan Formation. This conclusion would appear to contradict the evidence from the acritarchs, including *Trachyhystrichosphaera aimika* and *Valeria lophostriata*, that would indicate a Tonian age (Tang *et al*., 2015). Possible explanations for this include an unexpectedly long-range distribution for several typically Tonian acritarchs and reworking of fossil fragments from older sediments. Neither of these possibilities seems perfectly satisfactory as the reported Tonian assemblage is both diverse and apparently well preserved. Our results also argue against correlating the negative $\delta^{13}C_{carb}$ excursion in the Gouhou Formation with the Tonian Bitter Springs anomaly in South Australia (Xiao *et al*., 2014) as this interval, ~0.8-0.9 Ga, would seem to be entirely missing on the North China Craton. Although the Jinshanzhai Formation can only be constrained with a maximum depositional age of ca. 820 Ma (Fig. 5.4), the current study consider that the Jinshanzhai Formation was deposited significantly before the Gouhou Formation, due to its entirely different character, with as much as 300 million years between them.

In the Dalian region, the depositional age of the Xingmincun Formation is approximately constrained as between 924 Ma and 886 Ma (Yang *et al*., 2012; Zhang *et al*., 2016), and is

thus confirmed as Tonian in age, which refutes the official interpretation, which assigns the entire Jinxian Group, including the Xingmincun Formation, to the Ediacaran System (National Commission on Stratigraphy of China and China Geological Survey, 2014). On the other hand, these data indicate that the overlying Getun and Dalinzi formations of the uppermost Jinxian Group formed much later than the Tonian with maximum depositional ages of 733 Ma and 711 Ma, respectively. Importantly, this compiled age framework confirms that most of the Neoproterozoic strata in southeastern NCC were deposited no later than the early Tonian Period (Xiao *et al*., 2014), and thus are considerably older than the Neoproterozoic successions of South China (Shields-Zhou, Hill and Macgabhann, 2012; Xiao, Narbonne and Shields-Zhou, 2012), with which they have traditionally been compared (Zang and Walter, 1992). Cryogenian–Ediacaran age strata that might be correlative with the South China successions may be absent, but if present could conceivably be represented by the highly localised, glaciogenic Fengtai and Luoquan formations of Anhui and Henan provinces, respectively (Fig. 5.5).

5.5.2. Where is the major hiatus between the Neoproterozoic and Cambrian on the NCC?

A major depositional hiatus was proposed above the Gouhou Formation in the Huaibei region, implying a time gap spanning almost 300 million years between the Tonian (~0.8 Ga) to the Cambrian (~0.5 Ga) interval (Xiao *et al*., 2014; Tang *et al*., 2015). However, new age constraints here reveal that the Gouhou Formation and the overlying Houjiashan Formation are both Cambrian in age, with a more likely major depositional gap being placed between the Jinshanzhai and Gouhou formations, but involving an equivalently large depositional hiatus of up to 300 million years. A minor disconformity may still exist between the Gouhou and Houjiashan formations – the transition between them is commonly poorly exposed in the region - but based on the ages presented here it is unlikely to be significant.

In the Dalian region, utilizing the minimum depositional age of the Xingmincun Formation and the maximum age of the Getun Formation, the hiatus in between can be constrained to a minimum time gap of roughly 150 million years. In this regard, it should be noted that much of the Tonian–Cambrian interval witnessed global-scale glaciations (Fig. 5.5), while the North China craton was subject to regional glaciation possibly during the Ediacaran Period, all of

which makes it seem unlikely that the Getun and Dalinzi formations were deposited earlier than 635 Ma. This would make the hiatus at least as long as ~250 million years, and possibly much longer. Although some suggest that the Getun and Dalinzi formations are in conformable contact (Wang and Yang, 1986; Duan and An, 1994; Qiao, 2002), it is still plausible that a second hiatus could be situated between them as suggested by the clast-enriched horizon near the Dalinzi/Getun boundary (Fig. 5.3e) and other studies (Hong, Huang and Liu, 1991; Xiao *et al*., 2014; Luo, Zhu and Reitner, 2016). A more satisfactory resolution of their depositional ages awaits more convincing fossil evidence and improved age constraints. Notwithstanding the lack of detrital zircon grains younger than ~0.7 Ga in the Getun and Dalinzi formations, putative age-diagnostic fossils could place their ages as young as Early Cambrian (Wang and Yang, 1986; Hong, Huang and Liu, 1991). Thus, both formations could still represent transgressive lower Cambrian strata overlying a great hiatus, thus allowing approximate temporal correlation with the lithologically similar Gouhou Formation of the Huaibei region. As argued above, the Dalinzi and Gouhou formations are significantly different in a lithological sense from underlying formations of the same group which raises question about the traditional definitions of the Huaibei and Jinxian groups.

It is noteworthy that the age spectra of the Dalinzi and Gouhou formations are similar to each other, with peaks at ca. 1.85 Ga and 2.5 Ga, and are thus distinct from other formations of the Huaibei and Jinxian groups (Fig. 5.4). The apparent change in detrital zircon sources coincides with the regionally expressed unconformity outlined above, reflecting perhaps a major tectonic uplift event, which affected the southeastern margin of the NCC during the Neoproterozoic–Cambrian transition. Furthermore, as illustrated in Fig. 5.5, this unconformable surface is ubiquitously developed over the NCC and adjacent eastern Korea terrain. It is always underlain by Precambrian rocks and overlain by Cambrian-age strata that yield trilobite (Zhang and Zhu, 1979; Liu, 2012; Miao, 2014), archaeocyathid (Hong, Yang and Liu, 1990) and small shelly fossils (Pei and Feng, 2005) of approximate Cambrian Age 4 (~515-510 Ma) affinity. The widespread erosion surface developed across southeastern NCC is considered equivalent to the globally recognized ‘Great Unconformity’ that separates Cambrian-aged sediments (~510 Ma) from underlying Precambrian units elsewhere in the world (Brasier and Lindsay, 2001; Peters and Gaines, 2012).

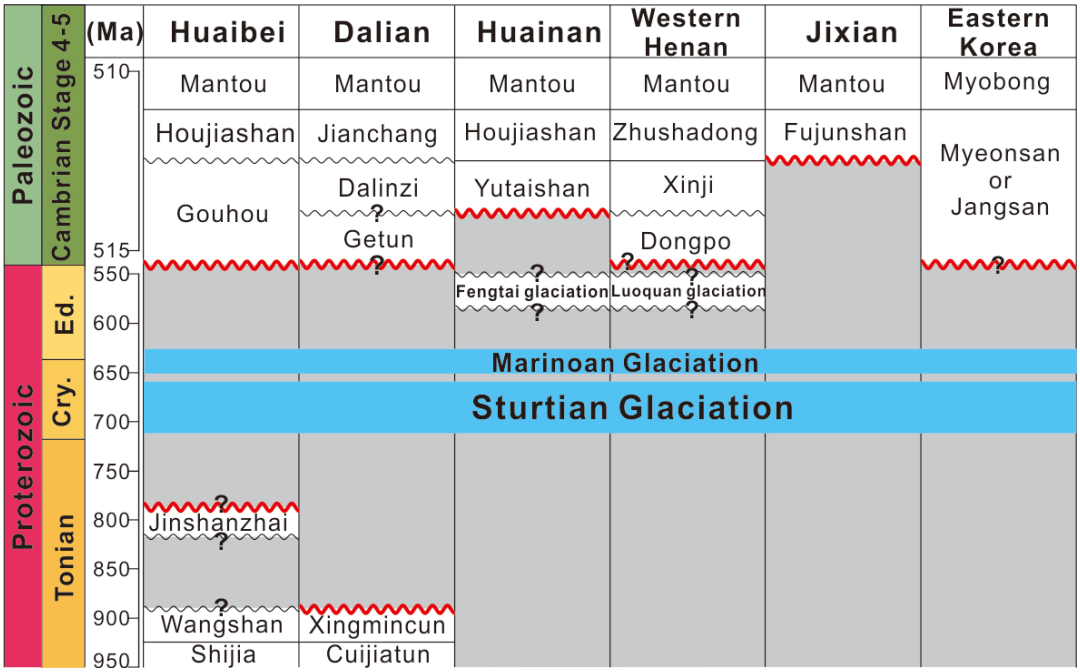

Figure 5.5: Simplified chronostratigraphy with stratigraphic formations of the Neoproterozoic–Cambrian successions in southeastern North China Craton and eastern Korea, showing the regional unconformities at the Neoproterozoic–Cambrian transition. Red wave lines illustrate the unconformable contacts ('Great Unconformity') in contact with the major hiatus (grey area). Blue bands represent the intervals of major Cryogenian glaciations including Sturtian glaciation of ca. 717-662 Ma and Marinoan glaciation of ca. 645-635 Ma (Rooney *et al*., 2015; Shields-Zhou, Porter and Halverson, 2016). Question marks represent debatable unconformable contacts or undated boundaries. Ed. – Ediacaran; Cry. – Cryogenian;

5.5.3. Detrital zircon provenance and palaeogeographic implications

All samples of NCC share a common age-population around 0.9-1.0 Ga. Grains of this age in the Tonian clastic units could be sourced from the Early Neoproterozoic large igneous province (LIP), which is evidenced by the widespread mafic sills and dykes (0.92-0.85 Ga) in southeastern NCC (Wang, Yang and Xu, 2012; Zhai *et al*., 2015; Zhang *et al*., 2016). However, mafic magmatism is generally not associated with zircon mineralisation. The Jinshanzhai and Xingmincun formations yielded additional, distinct peaks at approximately 2.1 Ga and 1.7 Ga, respectively. These ages probably include the reworking of mineral grains formed during the Early Paleoproterozoic rifting magmatism (2.2-1.9 Ga) on the eastern continental margin of the NCC (Zhao *et al*., 2005) and the ~1.72 to 1.62 Ga anorogenic magmatic association that affected the NCC (Zhai *et al*., 2015).

Distinctively, the Cambrian Dalinzi and Gouhou formations exhibit prominent zircon clusters of 1.8-1.9 Ga and 2.5 Ga that are absent in their respective underlying formations. Voluminous granitoids, TTG (Tonalite-Trondhjemite-Granodiorite) gneiss and mafic volcanic rocks with ages of about 2.5 Ga are known to be widespread and account for 90% of the total exposure of Archean basement on the NCC (Zhao, 2013), while the 1.8-1.9 Ga events are consistent with the assemblage of Longgang and Langrim blocks to form Jiao-Liao-Ji belt as well as the collision of the eastern and western Blocks that resulted in the final amalgamation of the NCC at ca. 1.85 Ga (Zhao *et al*., 2005; Yang *et al*., 2012; Zhao, 2013).

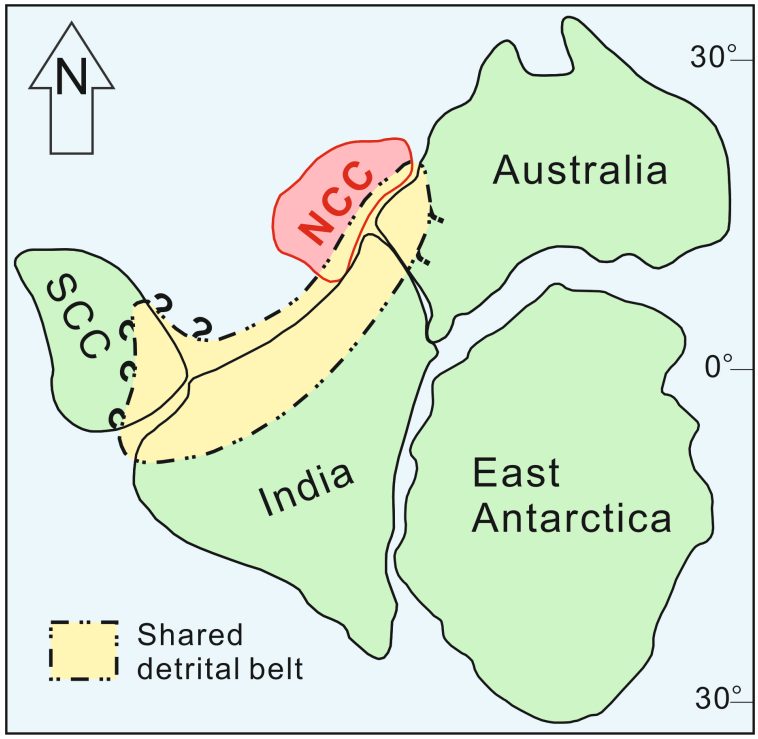

Figure 5.6: Simplified palaeogeographic map of eastern Gondwana terranes and adjacent SCC and NCC cratons at ~510 Ma showing the probable location of NCC. Modified from McKenzie, Hughes, Myrow, Choi, *et al*. (2011). NCC: North China Craton; SCC: South China Craton. The map illustrates the shared detrital source between eastern Gondwana and NCC.

Zircons of ~0.7 Ga age are only recovered in strata (including Getun, Dalinzi and Gouhou formations), which overlie the major hiatus in their respective regions. However, no Cryogenian igneous sources are known from the NCC, which possibly indicates that an exterior source supplied these detrital minerals. Previous studies proposed that the NCC was approaching northern India or western Australia during the Neoproterozoic–Cambrian interval (Lin, Fuller and Zhang, 1985; McKenzie, Hughes, Myrow, Choi, *et al*., 2011; Myrow *et al*.,

2015), and possibly collided with northern margin of East Gondwana in the Late Cambrian at ca. 500 Ma (Han *et al*., 2016). There is also strong trilobite faunal evidence, which suggests biogeographic links between NCC and East Gondwana (McKenzie, Hughes, Myrow, Choi, *et al*., 2011; Miao, 2014). Western Australia and northern India, which occupied the northern margin of East Gondwana during the Cambrian, were apparently affected by Cryogenian magmatism during the breakup of Rodinia (Hoffman, 1999; Van Lente *et al*., 2009; Hofmann *et al*., 2011; Rao *et al*., 2012). The occurrence of ca. 0.7 Ga detrital zircons on the southeastern NCC supports proximity to Gondwana much earlier than the eventual collision in the Cambrian. Additionally, zircons of 0.9-1.0 Ga age are a characteristic of source regions in East Gondwana and are found in blocks that lay adjacent to this margin of Gondwana such as South China (Cawood *et al*., 2013). This also raises the possibility that East Gondwana served as an additional source of the zircon grains of early Tonian age in the Cambrian clastic units of the southeastern NCC.

Comparing with their equivalent strata in northern India (Hughes *et al*., 2010), clastic rocks of Cambrian stages 4-5 from southern NCC (McKenzie, Hughes, Myrow, Choi, *et al*., 2011) and eastern Korea (Lee *et al*., 2016) show strong similarity in age spectra with a dominant age population of 0.5-1.0 Ga, confirming the close affinity between NCC and East Gondwana in the Cambrian (McKenzie, Hughes, Myrow, Choi, *et al*., 2011). Note that these samples include those from Cambrian stages 4-5 Mantou Formation that is stratigraphically younger than the Gouhou and Dalinzi formations of the NCC, as well as from the Myobong Formation that overlies the Myeonsan Formation in eastern Korea (Fig. 5.5). Gouhou, Dalinzi and Myeonsan formations, which lie directly above the regional unconformity and represent the lowermost Cambrian strata, share similar age spectra patterns with a dominant age population of 1.8-1.9 Ga (Fig. 5.4), but do not match the lowermost Cambrian strata from northern India, which show a widespread and distinctive population of 1.7-1.8 Ga instead (Myrow *et al*., 2010; McKenzie, Hughes, Myrow, Xiao, *et al*., 2011; Turner *et al*., 2014). The similarities of age spectra of Cambrian stages 4-5 strata between southeastern NCC and northern India possibly imply that the East Gondwana provided detritus to the southeastern NCC in the Cambrian (Fig. 5.6). On the other hand, inconsistencies at the lowermost Cambrian horizons indicate that local Archean–Paleoproterozoic basement sources appear still to have dominated the southeastern margin of the NCC at ca. 515 Ma, but these sources were replaced by shared trans-Gondwanan Neoproterozoic–Cambrian sources following the final collision of the NCC and East Gondwana, probably during the late Cambrian Stage 4 to early Cambrian Stage 5 (Han *et al*., 2016).

5.6. Conclusions

This study provides a refined geochronological framework for the upper Huaibei and Jinxian groups overlying the southeastern North China Craton. The results confirm that the Neoproterozoic units were deposited during the early Tonian Period, while the Gouhou Formation of the uppermost Huaibei Group is shown to be Cambrian in age. A regional unconformity is revealed between the Gouhou and the Jinshanzhai formations of the Huaibei region as well as between the Getun and Xingmincun formations of the Dalian region. This vast erosional surface can be traced across the craton and is interpreted here to be equivalent to the 'Great Unconformity' that marks the regional base of the Cambrian System, and neither of the Huaibei and Jinxian groups follow international standard practice in that their included formations, although contiguous, do not have 'significant and diagnostic lithologic properties in common' (Murphy and Salvador, 1999). The magnitude of this depositional gap is constrained to be greater than 150 to 300 million years. Provenance analysis of the detrital zircon age spectra suggests that, during the Neoproterozoic–Cambrian transition, the southeastern NCC experienced exposure and weathering of the Archean–Paleoproterozoic basement, possible denudation of a Tonian large igneous province as well as a possible contribution from Gondwana sources some time during the Cryogenian–Cambrian interval. These data also suggest that the detrital provenance of southeastern NCC did not fully overlap with that of northern margin of East Gondwana until ca. 510 Ma.

Chapter 6

Conclusions and future perspectives

This thesis demonstrates a high-resolution and high-fidelity carbonate C-Sr-S isotopic chemostratigraphic framework of the lower Cambrian in Siberia and South China. Together with a well-established biostratigraphic framework, these isotopic trends could be readily utilised as reliable references for future global stratigraphic correlation. The findings of this study also update our understanding regarding the relationship between marine redox evolution, continental weathering history, palaeogeography and early Cambrian biological events. Results also highlight potential directions for further research.

Chapter 2 validate conventional methodologies of carbonate-associated sulphate (CAS) extraction. Progress has been made to miniaturise the experimental setup to improve efficiency. Results have provided evidence that multiple pre-leaches by 10% NaCl guarantee the removal of water-soluble sulphur contaminants and maximise the recovery of primary CAS sulphur isotopic signals. New $\delta^{34}S_{CAS}$ results from the Ediacaran Nama Group show higher values than the previously reported data, suggesting that 'superheavy' pyrite can be the result of inadequate cleaning of non-CAS contaminants. However, the refined CAS extraction method was still unable to prevent contamination from carbonate-associated pyrite oxidation during the liberation of CAS (HCl digestion). The method is thereby limited by carbonate lithologies, specifically when dealing with samples with abundant presence of pyrite. Further experimental tests are needed to eliminate the risk of reduced sulphur-phase oxidation during CAS extraction. One solution is to allow HCl digestion to occur in an oxygen-free environment, for instance, in sealed tubes filled with nitrogen gas. On a wider level, further method miniaturisation can be achieved by using smaller sample amounts (<100mg) and column chromatography to purify sulphur and multicollector-ICPMS for isotopic analysis.

Chapter 3 of this thesis provides the first, continuous, high-resolution carbonate carbon and CAS sulphur isotopic trends for the interval of Cambrian stages 2-4. Results from Siberian and South China reveal an unprecedented positive correlation between $\delta^{13}C_{carb}$ and $\delta^{34}S_{CAS}$ records through six isotope cycles in the Cambrian stages 2-3, suggesting intervals of coupled burial of organic carbon and pyrite in the marine sediments. This coupling behaviour would seem to reflect redox oscillations in the ocean with a periodicity of 1-2 Myr. This study proposes that these covariant phenomena represent periodic oxygenation events, which can be correlated with pulses of animal radiation event in Siberia. However, this argument is still limited by the age model and resolution in the current animal diversity database for the early Cambrian. I recommend further palaeontological research should be undertaken to integrate global animal diversity data using an age model consistent with the chemostratigraphic record. Using

biogeochemical models, this study also presents constraints on the early Cambrian seawater sulphate concentration in Siberia and evidenced a significant drawdown of oceanic sulphate pool during the Botomian–Toyonian extinction (BTE). But these modelled results await confirmation from more fluid inclusion constraints at different early Cambrian intervals in Siberia. The decoupling of $\delta^{13}C_{carb}$ and $\delta^{34}S_{CAS}$ during the BTE was suggested as a result of localised shoaling of anoxic/euxinic deep-water and reduction of seawater sulphate concentration. This finding provides preliminary geochemical evidence of an oceanic anoxic event during the BTE, but more data and additional proxies (e.g. Fe speciation, carbonate-associated Uranium isotopes) are needed to review the redox conditions at different water-depths in Siberia and other platforms.

Using least diagenetically-altered carbonate samples, *Chapter 4* revisits the lower Cambrian $^{87}Sr/^{86}Sr$ record at the Siberian Aldan-Lena Rivers sections and updates the early Cambrian seawater $^{87}Sr/^{86}Sr$ record. This study recognises a sharp increasing $^{87}Sr/^{86}Sr$ trend from the mid Stage 2 to mid Stage 3, which possibly represents a period of enhanced continental weathering flux. Importantly, this period coincides closely with most of the animal radiation events. The evidence of enhanced erosion and chemical weathering may imply high Ca^{2+} concentration and nutrient availability to facilitate the emergence of calcium biomineralisation and animal diversification in the early Cambrian oceans. However, an additional ambiguity derives from the fact that contemporaneous riverine and seawater $^{87}Sr/^{86}Sr$ ratios are strongly affected by the isotopic composition of rocks exposed to weathering. Anomalously high seawater $^{87}Sr/^{86}Sr$ in the Cambrian Stage 3 thereby might not represent a high continental weathering flux. To further this research, I intend to apply the carbonate lithium isotopes, which are robust tracers of overall silicate weathering, to evaluate the palaeoenvironmental interpretations deduced from the Sr isotopes. This study also presents the first LOWESS-fitted seawater $^{87}Sr/^{86}Sr$ curve from the latest Ediacaran to Cambrian Stage 4. But more least-altered data are needed to fill the gaps in the late Fortunian and mid Stage 2.

The key outcome of *Chapter 5* is identifying the 'Great Unconformity' in the southeastern North China Craton (NCC) that separates the Cambrian from the underlying Tonian-age strata. Using both maximum and minimal depositional ages from detrital zircons and intrusive diabase sills respectively, this study obtains a chronostratigraphic framework for the Tonian-Cambrian successions in Dalian and Huaibei regions. These new age constraints outline the duration and position of a significant depositional gap of 150-300 Ma. This hiatus is suggested here as corresponding to the 'Great Unconformity', which is stratigraphically similar in many

parts of the world. This study also provides evidence that the NCC was closely in palaeogeographic affinity with Gondwana during Cambrian stages 4-5. Although there are limitations due to the lack of absolute age (e.g. tuffs zircon dating) for each stratigraphic unit, I believe this work could be the basis for defining and correlating the Precambrian-Cambrian boundary in North China and regional/global stratigraphic correlation. However, the findings might not be transferable to regions in Huainan and western NCC as the durations of the gap there seem to be longer than 500 million years. Age and stratigraphic constraints are also needed to resolve the equivocal Ediacaran-age glaciations. Future work will also concentrate on the chemostratigraphic study of the Cambrian-age carbonate successions in North China (e.g. carbonate C and Sr isotope stratigraphy).

References

Aitken, J. D. (1969) 'Documentation of the sub-Cambrian unconformity, Rocky Mountains Main Ranges, Alberta', *Canadian Journal of Earth Sciences*, 6(2), pp. 193–200. doi: 10.1139/e69-018.

Algeo, T. J. and Ingall, E. (2007) 'Sedimentary Corg:P ratios, paleocean ventilation, and Phanerozoic atmospheric pO_2', *Palaeogeography, Palaeoclimatology, Palaeoecology*, 256(3–4), pp. 130–155. doi: 10.1016/j.palaeo.2007.02.029.

Algeo, T. J., Luo, G. M., Song, H. Y., Lyons, T. W. and Canfield, D. E. (2015) 'Reconstruction of secular variation in seawater sulfate concentrations', *Biogeosciences*, 12(7), pp. 2131–2151. doi: 10.5194/bg-12-2131-2015.

Allan, J. R. and Matthews, R. K. (1982) 'Isotope signatures associated with early meteoric diagenesis', *Sedimentology*, 29(6), pp. 797–817. doi: 10.1111/j.1365-3091.1982.tb00085.x.

Aller, R. C., Madrid, V., Chistoserdov, A., Aller, J. Y. and Heilbrun, C. (2010) 'Unsteady diagenetic processes and sulfur biogeochemistry in tropical deltaic muds: Implications for oceanic isotope cycles and the sedimentary record', *Geochimica et Cosmochimica Acta*, 74(16), pp. 4671–4692. doi: 10.1016/j.gca.2010.05.008.

Babcock, L. E. (2005) 'Interpretation of biological and environmental changes across the Neoproterozoic–Cambrian boundary: developing a refined understanding of the radiation and preservational record of early multicellular organisms', *Palaeogeography, Palaeoclimatology, Palaeoecology*, 220(1–2), pp. 1–5. doi: 10.1016/j.palaeo.2004.09.013.

Bailey, T. R., McArthur, J. M., Prince, H. and Thirlwall, M. F. (2000) 'Dissolution methods for strontium isotope stratigraphy: Whole rock analysis', *Chemical Geology*, 167(3–4), pp. 313–319. doi: 10.1016/S0009-2541(99)00235-1.

Banner, J. L. and Hanson, G. N. (1990) 'Calculation of simultaneous isotopic and trace element variations during water-rock interaction with applications to carbonate diagenesis', *Geochimica et Cosmochimica Acta*, 54(11), pp. 3123–3137. doi: 10.1016/0016-7037(90)90128-8.

Bergman, N. M., Lenton, T. M. and Watson, A. J. (2004) 'COPSE: A new model of biogeochemical cycling over phanerozoic time', *American Journal of Science*, 304(5), pp. 397–437. doi: 10.2475/ajs.304.5.397.

Berner, R. A. and Raiswel, R. (1983) 'Burial of organic carbon and pyrite sulfur in sediments over Phanerozoic time: a new theory', *Geochemica et Cosmochimica Acta*, 47, pp. 855–862. doi: 10.1016/0016-7037(83)90151-5.

Berner, R. A. (1989) 'Biogeochemical cycles of carbon and sulfur and their effect on atmospheric oxygen over phanerozoic time', *Global and Planetary Change*, 1(1–2), pp. 97–122. doi: 10.1016/0921-8181(89)90018-0.

Berner, R. A. (1994) 'GEOCARB II: a revised model of atmospheric CO_2 over Phanerozoic time', *American Journal of Science*, 294(1), pp. 56–91. doi: 10.2475/ajs.294.1.56.

Berner, R. A. (2004) 'A model for calcium, magnesium and sulfate in seawater over Phanerozoic time', *American Journal of Science*, 304(5), pp. 438–453. doi: 10.2475/ajs.304.5.438.

Berner, R. A. (2006) 'GEOCARBSULF: A combined model for Phanerozoic atmospheric O_2 and CO_2', *Geochimica et Cosmochimica Acta*, 70(23), pp. 5653–5664. doi: 10.1016/j.gca.2005.11.032.

Bottjer, D. J., Hagadorn, J. W. and Dornbos, S. Q. (2000) 'The Cambrian substrate revolution', *GSA Today*, 10(9), pp. 1–7. doi: 10.1130/GSAT01707GW.1.

Bottomley, D. J., Veizer, J., Nielsen, H. and Moczydlowska, M. (1992) 'Isotopic composition of disseminated sulfur in Precambrian sedimentary rocks', *Geochimica et Cosmochimica Acta*, 56(8), pp. 3311–3322. doi: 10.1016/0016-7037(92)90307-5.

Bottrell, S. H. and Newton, R. J. (2006) 'Reconstruction of changes in global sulfur cycling from marine sulfate isotopes', *Earth-Science Reviews*, 75(1–4), pp. 59–83. doi: 10.1016/j.earscirev.2005.10.004.

Bowring, S. A., Grotzinger, J. P., Condon, D. J., Ramezani, J., Newall, M. J. and Allen, P. A. (2007) 'Geochronologic constraints on the chronostratigraphic framework of the Neoproterozoic Huqf Supergroup, Sultanate of Oman', *American Journal of Science*, 307(10), pp. 1097–1145. doi: 10.2475/10.2007.01.

Boyle, R. A., Dahl, T. W., Dale, A. W., Shields-Zhou, G. A., Zhu, M., Brasier, M. D., Canfield, D. E. and Lenton, T. M. (2014) 'Stabilization of the coupled oxygen and phosphorus cycles by the evolution of bioturbation', *Nature Geoscience*, 7(9), pp. 671–676. doi: 10.1038/ngeo2213.

Bradley, A. S., Leavitt, W. D., Schmidt, M., Knoll, A. H., Girguis, P. R. and Johnston, D. T. (2016) 'Patterns of sulfur isotope fractionation during microbial sulfate reduction', *Geobiology*, 14(1), pp. 91–101. doi: 10.1111/gbi.12149.

Brand, U. and Veizer, J. (1981) 'Chemical diagenesis of a multicomponent carbonate system -2: stable isotopes', *Journal of Sedimentary Research*, 51(3), pp. 987–997.

Brasier, M. D., Corfield, R. M., Derry, L. A., Rozanov, A. Y. and Zhuravlev, A. Y. (1994) 'Multiple $\delta^{13}C$ excursions spanning the Cambrian explosion to the Botomian crisis in Siberia', *Geology*, 22(5), pp. 455–458. doi: 10.1130/0091-7613(1994)022<0455:MCESTC>2.3.CO;2.

Brasier, M. D., Rozanov, a. Y., Zhuravlev, A. Y., Corfield, R. M. and Derry, L. A. (1994) 'A carbon isotope reference scale for the Lower Cambrian succession in Siberia: report of IGCP Project 303', *Geological Magazine*, 131(6), pp. 767–783. doi: 10.1017/S0016756800012851.

Brasier, M. D., Shields, G., Kuleshov, V. N. and Zhegallo, E. A. (1996) 'Integrated chemo- and biostratigraphic calibration of early animal evolution: Neoproterozoic–early Cambrian

of southwest Mongolia', *Geological Magazine*, 133(4), pp. 445–485. doi: 10.1017/S0016756800007603.

Brasier, M. D. and Sukhov, S. S. (1998) 'The falling amplitude of carbon isotopic oscillations through the Lower to Middle Cambrian: northern Siberia data', *Canadian Journal of Earth Sciences*, 35(4), pp. 353–373. doi: 10.1139/e97-122.

Brasier, M. D. and Lindsay, J. F. (2001) 'Did supercontinental amalgamation trigger the "Cambrian explosion"?', in Zhuravlev, A. Y. and Riding, R. (eds) *The ecology of the Cambrian radiation*. New York: Columbia University Press, pp. 69–89.

Brennan, S. T., Lowenstein, T. K. and Horita, J. (2004) 'Seawater chemistry and the advent of biocalcification', *Geology*, 32(6), pp. 473–476. doi: 10.1130/G20251.1.

Burdett, J. W., Arthur, M. A. and Richardson, M. (1989) 'A Neogene seawater sulfur isotope age curve from calcareous pelagic microfossils', *Earth and Planetary Science Letters*, 94(3–4), pp. 189–198. doi: 10.1016/0012-821X(89)90138-6.

Campbell, I. H. and Allen, C. M. (2008) 'Formation of supercontinents linked to increases in atmospheric oxygen', *Nature Geoscience*, 1(8), pp. 554–558. doi: 10.1038/ngeo259.

Campbell, I. H. and Squire, R. J. (2010) 'The mountains that triggered the Late Neoproterozoic increase in oxygen: The Second Great Oxidation Event', *Geochimica et Cosmochimica Acta*, 74(15), pp. 4187–4206. doi: 10.1016/j.gca.2010.04.064.

Canfield, D. E., Raiswell, R., Westrich, J. T., Reaves, C. M. and Berner, R. A. (1986) 'The use of chromium reduction in the analysis of reduced inorganic sulfur in sediments and shales', *Chemical Geology*, 54(1–2), pp. 149–155. doi: 10.1016/0009-2541(86)90078-1.

Canfield, D. E. (2001) 'Biogeochemistry of sulfur isotopes', *Reviews in Mineralogy and Geochemistry*, 43(1), pp. 607–636. doi: 10.2138/gsrmg.43.1.607.

Canfield, D. E. (2001) 'Isotope fractionation by natural populations of sulfate-reducing bacteria', *Geochimica et Cosmochimica Acta*, 65(7), pp. 1117–1124. doi: 10.1016/S0016-7037(00)00584-6.

Canfield, D. E. (2005) 'The early history of atmospheric oxygen: Homage to Robert M. Garrels', *Annual Review of Earth and Planetary Sciences*, 33(1), pp. 1–36. doi: 10.1146/annurev.earth.33.092203.122711.

Canfield, D. E. and Farquhar, J. (2009) 'Animal evolution, bioturbation, and the sulfate concentration of the oceans', *Proceedings of the National Academy of Sciences*, 106(20), pp. 8123–8127. doi: 10.1073/pnas.0902037106.

Canfield, D. E., Farquhar, J. and Zerkle, A. L. (2010) 'High isotope fractionations during sulfate reduction in a low-sulfate euxinic ocean analog', *Geology*, 38(5), pp. 415–418. doi: 10.1130/G30723.1.

Canfield, D. E. (2013) 'Sulfur isotopes in coal constrain the evolution of the Phanerozoic sulfur cycle', *Proceedings of the National Academy of Sciences*, 110(21), pp. 8443–8446. doi: 10.1073/pnas.1306450110.

Cao, R. (2000) 'Discussion on some problems in the Mesoproterozoic and Neoproterozoic stratigraphical study in China', *Journal of Stratigraphy*, 24, pp. 1–7.

Cawood, P. A., Wang, Y., Xu, Y. and Zhao, G. (2013) 'Locating South China in Rodinia and

Gondwana: A fragment of greater India lithosphere?', *Geology*, 41(8), pp. 903–906. doi: 10.1130/G34395.1.

Chen, X., Ling, H.-F., Vance, D., Shields-Zhou, G. A, Zhu, M., Poulton, S. W., Och, L. M., Jiang, S.-Y., Li, D., Cremonese, L. and Archer, C. (2015) 'Rise to modern levels of ocean oxygenation coincided with the Cambrian radiation of animals', *Nature Communications*, 6, pp. 1–7. doi: 10.1038/ncomms8142.

Cho, M. and Cheong, W. (2016) 'Comments on "Detrital zircon geochronology and Nd isotope geochemistry of the basal succession of the Taebaeksan Basin, South Korea: Implications for the Gondwana linkage of the Sino-Korean (North China) Block during the Neoproterozoic–early Cambrian", *Palaeogeography, Palaeoclimatology, Palaeoecology*, 459, pp. 606–609. doi: 10.1016/j.palaeo.2016.04.024.

Claypool, G. E., Holser, W. T., Kaplan, I. R., Sakai, H. and Zak, I. (1980) 'The age curves of sulfur and oxygen isotopes in marine sulfate and their mutual interpretation', *Chemical Geology*, 28, pp. 199–260. doi: 10.1016/0009-2541(80)90047-9.

Cocks, L. R. M. and Torsvik, T. H. (2013) 'The dynamic evolution of the Palaeozoic geography of eastern Asia', *Earth-Science Reviews*, 117, pp. 40–79. doi: 10.1016/j.earscirev.2012.12.001.

Cook, P. J. and Shergold, J. H. (1984) 'Phosphorus, phosphorites and skeletal evolution at the Precambrian-Cambrian boundary', *Nature*, 308(5956), pp. 231–236. doi: 10.1038/308231a0.

Cox, G. M., Halverson, G. P., Stevenson, R. K., Vokaty, M., Poirier, A., Kunzmann, M., Li, Z.-X., Denyszyn, S. W., Strauss, J. V. and Macdonald, F. A. (2016) 'Continental flood basalt weathering as a trigger for Neoproterozoic Snowball Earth', *Earth and Planetary Science Letters*, 446, pp. 89–99. doi: 10.1016/j.epsl.2016.04.016.

Cui, H., Grazhdankin, D. V., Xiao, S., Peek, S., Rogov, V. I., Bykova, N. V., Sievers, N. E., Liu, X.-M. and Kaufman, A. J. (2016) 'Redox-dependent distribution of early macro-organisms: Evidence from the terminal Ediacaran Khatyspyt Formation in Arctic Siberia', *Palaeogeography, Palaeoclimatology, Palaeoecology*, 461, pp. 122–139. doi: 10.1016/j.palaeo.2016.08.015.

Dahl, T. W., Connelly, J. N., Kouchinsky, A., Gill, B. C., Mansson, S. F. and Bizzarro, M. (2017) 'Reorganisation of Earth's biogeochemical cycles briely oxygenated the oceans 520 Myr ago', *Geochemical Perspectives Letters*, pp. 210–220. doi: 10.7185/geochemlet.1724.

Dalziel, I. W. D. (1991) 'Pacific margins of Laurentia and East Antarctica-Australia as a conjugate rift pair: Evidence and implications for an Eocambrian supercontinent', *Geology*, 19(6), pp. 598–601. doi: 10.1130/0091-7613(1991)019<0598:PMOLAE>2.3.CO;2.

Dalziel, I. W. D. (1997) 'Neoproterozoic-Paleozoic geography and tectonics : Review, hypothesis, environmental speculation', *Geological Society of America Bulletin*, 109(1), pp. 16–42. doi: 10.1130/0016-7606(1997)109<0016:ONPGAT>2.3.CO;2.

Dalziel, I. W. D. (2014) 'Cambrian transgression and radiation linked to an Iapetus-Pacific oceanic connection?', *Geology*, 42(11), pp. 979–982. doi: 10.1130/G35886.1.

Davis, A. C., Bickle, M. J. and Teagle, D. A. H. (2003) 'Imbalance in the oceanic strontium budget', *Earth and Planetary Science Letters*, 211(1–2), pp. 173–187. doi: 10.1016/S0012-821X(03)00191-2.

REFERENCES

De Rosa, R., Grenier, J. K., Andreeva, T., Cook, C. E., Adoutte, A., Akam, M., Carroll, S. B. and Balavoine, G. (1999) 'Hox genes in brachiopods and priapulids and protostome evolution', *Nature*, 399(6738), pp. 772–776. doi: 10.1038/21631.

Derry, L. A., Brasier, M. D., Corfield, R. M., Rozanov, A. Y. and Zhuravlev, A. Y. (1994) 'Sr and C isotopes in Lower Cambrian carbonates from the Siberian craton: A paleoenvironmental record during the "Cambrian explosion"', *Earth and Planetary Science Letters*, 128(3–4), pp. 671–681. doi: 10.1016/0012-821X(94)90178-3.

Dilliard, K. A., Pope, M. C., Coniglio, M., Hasiotis, S. T. and Lieberman, B. S. (2007) 'Stable isotope geochemistry of the lower Cambrian Sekwi Formation, Northwest Territories, Canada: Implications for ocean chemistry and secular curve generation', *Palaeogeography, Palaeoclimatology, Palaeoecology*, 256(3–4), pp. 174–194. doi: 10.1016/j.palaeo.2007.02.031.

Doglioni, C., Pignatti, J. and Coleman, M. (2016) 'Why did life develop on the surface of the Earth in the Cambrian?', *Geoscience Frontiers*, 7(6), pp. 865–873. doi: 10.1016/j.gsf.2016.02.001.

Dong, L., Xiao, S., Shen, B., Yuan, X., Yan, X. and Peng, Y. (2008) 'Restudy of the worm-like carbonaceous compression fossils Protoarenicola, Pararenicola, and Sinosabellidites from early Neoproterozoic successions in North China', *Palaeogeography, Palaeoclimatology, Palaeoecology*, 258(3), pp. 138–161. doi: 10.1016/j.palaeo.2007.05.019.

Duan, J. and An, S. (1994) 'On the subdivision and correlation for upper Precambrian System in south Liaoning Province, China', *Liaoning Geology*, 1–2, pp. 30–43.

Ebneth, S., Shields, G. A., Veizer, J., Miller, J., and Shergold, J. (2001) 'High-resolution strontium isotope stratigraphy across the Cambrian-Ordovician transition', *Geochimica et Cosmochimica Acta*, 65(14), pp. 2273–2292. doi: 10.1016/S0016-7037(01)00580-4.

Elderfield, H. and Gieskes, J. M. (1982) 'Sr isotopes in interstitial waters of marine sediments from Deep Sea Drilling Project cores', *Nature*, 300(5892), pp. 493–496. doi: 10.1038/300493a0.

Erwin, D. H., Laflamme, M., Tweedt, S. M., Sperling, E. A., Pisani, D. and Peterson, K. J. (2011) 'The Cambrian Conundrum: early divergence and later ecological success in the early history of animals', *Science*, 334(6059), pp. 1091–1097. doi: 10.1126/science.1206375.

Erwin, D. and Valentine, J. (2013) *The Cambrian Explosion: The Construction of Animal Biodiversity*. Greenwood Village: Roberts and Company.

Fairchild, I. J., Einsele, G. and Song, T. (1997) 'Possible seismic origin of molar tooth structures in Neoproterozoic carbonate ramp deposits, north China', *Sedimentology*, 44(4), pp. 611–636. doi: 10.1046/j.1365-3091.1997.d01-40.x.

Fairchild, I. J., Spiro, B., Herrington, P. M. and Song, T. (2000) 'Controls on Sr and C isotope compositions of Neoproterozoic Sr-rich limestones of East Greenland and North China', in Grotzinger, J. P. and James, N. P. (eds) *Carbonate Sedimentation and Diagenesis in the Evolving Precambrian World*. SEPM (Society for Sedimentary Geology), pp. 297–313.

Fedo, C. M. (2003) 'Detrital Zircon Analysis of the Sedimentary Record', *Reviews in Mineralogy and Geochemistry*, 53(1), pp. 277–303. doi: 10.2113/0530277.

Ferrini, V., Fayek, M., De Vito, C., Mignardi, S. and Pignatti, J. (2010) 'Extreme sulphur isotope fractionation in the deep Cretaceous biosphere', *Journal of the Geological Society*, 167(5), pp. 1009–1018. doi: 10.1144/0016-76492009-161.

Fichtner, V., Strauss, H., Immenhauser, A., Buhl, D., Neuser, R. D. and Niedermayr, A. (2017) 'Diagenesis of carbonate associated sulfate', *Chemical Geology*, 463, pp. 61–75. doi: 10.1016/j.chemgeo.2017.05.008.

Fike, D. A., Bradley, A. S. and Rose, C. V. (2015) 'Rethinking the ancient sulfur cycle', *Annual Review of Earth and Planetary Sciences*, 43(1), pp. 593–622. doi: 10.1146/annurev-earth-060313-054802.

Fortey, R., Briggs, D. E. G. and Wills, M. A (1996) 'The Cambrian evolutionary "explosion": decoupling cladogenesis from morphological disparity', *Biological Journal of the Linnean Society*, 57(1), pp. 13–33. doi: 10.1111/j.1095-8312.1996.tb01693.x.

Fox, D (2016) 'What sparked the Cambrian Explosion?', *Nature*, 530(7590), pp. 268–270. doi: 10.1038/530268a.

Frei, R., Gaucher, C., Poulton, S. W. and Canfield, D. E. (2009) 'Fluctuations in Precambrian atmospheric oxygenation recorded by chromium isotopes', *Nature*, 461(7261), pp. 250–253. doi: 10.1038/nature08266.

Fry, B., Ruf, W., Gest, H. and Hayes, J. M. (1988) 'Sulfur isotope effects associated with oxidation of sulfide by O_2 in aqueous solution', *Chemical Geology: Isotope Geoscience section*, 73(3), pp. 205–210. doi: 10.1016/0168-9622(88)90001-2.

Galbraith, R. F. (2005) *Statistics for fission track analysis*. London: CRC Press.

Garrels, R. M. and Lerman, A. (1981) 'Phanerozoic cycles of sedimentary carbon and sulfur', *Proceedings of the National Academy of Sciences*, 78(8), pp. 4652–4656. doi: 10.1073/pnas.78.8.4652.

Garrels, R. M. and Lerman, A. (1984) 'Coupling of the sedimentary sulfur and carbon cycles; an improved model', *American Journal of Science*, 284(9), pp. 989–1007. doi: 10.2475/ajs.284.9.989.

Gehling, J. G., Jensen, S., Droser, M. L., Myrow, P. M. and Narbonne, G. M. (2001) 'Burrowing below the basal Cambrian GSSP, Fortune Head, Newfoundland', *Geological Magazine*, 138(2), pp. 213–218. doi: 10.1017/S001675680100509X.

Gill, B. C., Lyons, T. W. and Saltzman, M. R. (2007) 'Parallel, high-resolution carbon and sulfur isotope records of the evolving Paleozoic marine sulfur reservoir', *Palaeogeography, Palaeoclimatology, Palaeoecology*, 256(3–4), pp. 156–173. doi: 10.1016/j.palaeo.2007.02.030.

Gill, B. C., Lyons, T. W. and Frank, T. D. (2008) 'Behavior of carbonate-associated sulfate during meteoric diagenesis and implications for the sulfur isotope paleoproxy', *Geochimica et Cosmochimica Acta*, 72(19), pp. 4699–4711. doi: 10.1016/j.gca.2008.07.001.

Gill, B. C., Lyons, T. W., Young, S. A, Kump, L. R., Knoll, A. H. and Saltzman, M. R. (2011) 'Geochemical evidence for widespread euxinia in the later Cambrian ocean.', *Nature*, 469(7328), pp. 80–83. doi: 10.1038/nature09700.

REFERENCES

Gomes, M. L. and Hurtgen, M. T. (2013) 'Sulfur isotope systematics of a euxinic, low-sulfate lake: Evaluating the importance of the reservoir effect in modern and ancient oceans', *Geology*, 41(6), pp. 663–666. doi: 10.1130/G34187.1.

Gomes, M. L. and Johnston, D. T. (2017) 'Oxygen and sulfur isotopes in sulfate in modern euxinic systems with implications for evaluating the extent of euxinia in ancient oceans', *Geochimica et Cosmochimica Acta*, 205, pp. 331–359. doi: 10.1016/j.gca.2017.02.020.

Goodfellow, W. D. and Jonasson, I. R. (1984) 'Ocean stagnation and ventilation defined by $\delta^{34}S$ secular trends in pyrite and barite, Selwyn Basin, Yukon', *Geology*, 12(10), pp. 583–586. doi: 10.1130/0091-7613(1984)12<583:OSAVDB>2.0.CO;2.

Grant, S. W. F. (1990) 'Shell structure and distribution of Cloudina, a potential index fossil for the terminal Proterozoic', *American Journal of Science*, 290-A, pp. 261–294.

Gradstein, F. M., Ogg, J. G., Schmitz, M. D., Ogg, G. M., Gradstein, F. M. and All, A. (2012) *The Geologic Time Scale 2012*, Elsevier Science Limited.

Gresse, P. G. and Germs, G. J. B. (1993) 'The Nama foreland basin: sedimentation, major unconformity bounded sequences and multisided active margin advance', *Precambrian Research*, 63(3–4), pp. 247–272. doi: 10.1016/0301-9268(93)90036-2.

Grotzinger, J. P., Bowring, S. A., Saylor, B. Z. and Kaufman, A. J. (1995) 'Biostratigraphic and Geochronologic Constraints on Early Animal Evolution', *Science*, 270(5236), pp. 598–604. doi: 10.1126/science.270.5236.598.

Grotzinger, J. P., Watters, W. A. and Knoll, A. H. (2000) 'Calcified metazoans in thrombolite-stromatolite reefs of the terminal Proterozoic Nama Group, Namibia', *Paleobiology*, 26(3), pp. 334–359. doi: 10.1666/0094-8373(2000)026<0334:CMITSR>2.0.CO;2.

Habicht, K. S. and Canfield, D. E. (2001) 'Isotope fractionation by sulfate-reducing natural populations and the isotopic composition of sulfide in marine sediments', *Geology*, 29(6), pp. 555–558. doi: 10.1130/0091-7613(2001)029<0555:IFBSRN>2.0.CO;2.

Hall, M., Kaufman, A. J., Vickers-Rich, P., Ivantsov, A., Trusler, P., Linnemann, U., Hofmann, M., Elliott, D., Cui, H., Fedonkin, M., Hoffmann, K.-H., Wilson, S. A., Schneider, G. and Smith, J. (2013) 'Stratigraphy, palaeontology and geochemistry of the late Neoproterozoic Aar Member, southwest Namibia: Reflecting environmental controls on Ediacara fossil preservation during the terminal Proterozoic in African Gondwana', *Precambrian Research*, 238, pp. 214–232. doi: 10.1016/j.precamres.2013.09.009.

Hallam, A. and Wignall, P. B. (1999) 'Mass extinctions and sea-level changes', *Earth-Science Reviews*, 48(4), pp. 217–250. doi: 10.1016/S0012-8252(99)00055-0.

Halverson, G. P., Wade, B. P., Hurtgen, M. T. and Barovich, K. M. (2010) 'Neoproterozoic chemostratigraphy', *Precambrian Research*, 182(4), pp. 337–350. doi: 10.1016/j.precamres.2010.04.007.

Han, Y., Zhao, G., Cawood, P. A., Sun, M., Eizenhöfer, P. R., Hou, W., Zhang, X. and Liu, Q. (2016) 'Tarim and North China cratons linked to northern Gondwana through switching accretionary tectonics and collisional orogenesis', *Geology*, 44(2), pp. 95–98. doi: 10.1130/G37399.1.

Haq, B. U. and Schutter, S. R. (2008) 'A Chronology of Paleozoic Sea-Level Changes', *Science*, 322(5898), pp. 64–68. doi: 10.1126/science.1161648.

He, T., Zhou, Y., Vermeesch, P., Rittner, M., Miao, L., Zhu, M., Carter, A., Pogge von Strandmann, P. A. E. and Shields, G. A. (2016) 'Measuring the 'Great Unconformity' on the North China Craton using new detrital zircon age data', *Geological Society, London, Special Publications*, 448, p. SP448.14. doi: 10.1144/SP448.14.

Hess, J., Bender, M. L. and Schilling, J.-G. (1986) 'Evolution of the Ratio of Strontium-87 to Strontium-86 in Seawater from Cretaceous to Present', *Science*, 231(4741), pp. 979–984. doi: 10.1126/science.231.4741.979.

Hodell, D. A., Mueller, P. A. and Garrido, J. R. (1991) 'Variations in the strontium isotopic composition of seawater during the Neogene', *Geology*, 19(1), pp. 24–27. doi: 10.1130/0091-7613(1991)019<0024.

Hoffman, P. F. (1998) 'A Neoproterozoic Snowball Earth', *Science*, 281(5381), pp. 1342–1346. doi: 10.1126/science.281.5381.1342.

Hoffman, P. F. (1999) 'The break-up of Rodinia, birth of Gondwana, true polar wander and the snowball Earth', *Journal of African Earth Sciences*, 28(1), pp. 17–33. doi: 10.1016/S0899-5362(99)00018-4.

Hofmann, M., Linnemann, U., Rai, V., Becker, S., Gärtner, A. and Sagawe, A. (2011) 'The India and South China cratons at the margin of Rodinia - Synchronous Neoproterozoic magmatism revealed by LA-ICP-MS zircon analyses', *Lithos*, 123(1–4), pp. 176–187. doi: 10.1016/j.lithos.2011.01.012.

Hong, Z., Yang, Y. and Liu, X. (1990) 'Archaeocyathid fossils from the lower Cambrian Jianchang Formation of the southern Liaodong Peninsula', *Geological Review*, 36(6), pp. 558–565.

Hong, Z., Huang, Z. and Liu, X. (1991) 'Geology of Upper Precambrian in southern Liaodong Peninsula', in Xu, G. and Lun, Z. (eds) *Special Reports on Geology from the Ministry of Geology and Mineral Resources, People's Republic of China*. Beijing: Geological Publishing House.

Hough, M. L., Shields, G. A., Evins, L. Z., Strauss, H., Henderson, R. A. and Mackenzie, S. (2006) 'A major sulphur isotope event at c. 510 Ma: a possible anoxia-extinction-volcanism connection during the Early-Middle Cambrian transition?', *Terra Nova*, 18(4), pp. 257–263. doi: 10.1111/j.1365-3121.2006.00687.x.

Howarth, R. and McArthur, J. (1997) 'Statistics for strontium isotope stratigraphy: a robust LOWESS fit to the marine Sr-isotope curve for 0 to 206 Ma, with look-up table for derivation of numeric age', *The Journal of Geology*, 105(4), pp. 441–456. doi: 10.1086/515938.

Hughes, N., Myrow, P., Mckenzie, N., Harper, D., Bhargava, O., Tangri, S., Ghalley, K. and Fanning, C. (2010) 'Cambrian rocks and faunas of the Wachi La, Black Mountains, Bhutan', *Geological Magazine*, 148(3), pp. 351–379. doi: 10.1017/S0016756810000750.

Hurtgen, M. T., Halverson, G. P., Arthur, M. A. and Hoffman, P. F. (2006) 'Sulfur cycling in the aftermath of a 635-Ma snowball glaciation: Evidence for a syn-glacial sulfidic deep ocean', *Earth and Planetary Science Letters*, 245(3–4), pp. 551–570. doi: 10.1016/j.epsl.2006.03.026.

Johnston, D. T., Gill, B. C., Masterson, A., Beirne, E., Casciotti, K. L., Knapp, A. N. and Berelson, W. (2014) 'Placing an upper limit on cryptic marine sulphur cycling', *Nature*,

513(7519), pp. 530–533. doi: 10.1038/nature13698.

Jourdan, F., Hodges, K., Sell, B., Schaltegger, U., Wingate, M. T. D., Evins, L. Z., Soderlund, U., Haines, P. W., Phillips, D. and Blenkinsop, T. (2014) 'High-precision dating of the Kalkarindji large igneous province, Australia, and synchrony with the Early-Middle Cambrian (Stage 4-5) extinction', *Geology*, 42(6), pp. 543–546. doi: 10.1130/G35434.1.

Kah, L. C., Lyons, T. W. and Frank, T. D. (2004) 'Low marine sulphate and protracted oxygenation of the Proterozoic biosphere', *Nature*, 431(7010), pp. 834–838. doi: 10.1038/nature02974.

Kampschulte, A. and Strauss, H. (2004) 'The sulfur isotopic evolution of Phanerozoic seawater based on the analysis of structurally substituted sulfate in carbonates', *Chemical Geology*, 204(3–4), pp. 255–286. doi: 10.1016/j.chemgeo.2003.11.013.

Kaplan, I. R. and Rittenberg, S. C. (1964) 'Microbiological fractionation of sulphur isotopes.', *Journal of general microbiology*, 34(1958), pp. 195–212. doi: 10.1099/00221287-34-2-195.

Kaufman, A. J., Jacobsen, S. B. and Knoll, A. H. (1993) 'The Vendian record of Sr and C isotopic variations in seawater: Implications for tectonics and paleoclimate', *Earth and Planetary Science Letters*, 120(3–4), pp. 409–430. doi: 10.1016/0012-821X(93)90254-7.

Kim, H. S. and Ree, J.-H. (2016) 'Comments on "Detrital zircon geochronology and Nd isotope geochemistry of the basal succession of the Taebaeksan Basin, South Korea: Implications for the Gondwana linkage of the Sino-Korean (North China) Block during the Neoproterozoic–early Cambrian", *Palaeogeography, Palaeoclimatology, Palaeoecology*, 459, pp. 610–612. doi: 10.1016/j.palaeo.2016.04.031.

Korte, C. and Ullmann, C. V (2017) 'Permian strontium isotope stratigraphy', *Geological Society, London, Special Publications*, 450, p. SP450.5. doi: 10.1144/SP450.5.

Kouchinsky, A., Bengtson, S., Gallet, Y., Korovnikov, I., Pavlov, V., Runnegar, B., Shields, G., Veizer, J., Young, E. and Ziegler, K. (2008) 'The SPICE carbon isotope excursion in Siberia: a combined study of the upper Middle Cambrian–lowermost Ordovician Kulyumbe River section, northwestern Siberian Platform', *Geological Magazine*, 145(5), pp. 609–622. doi: 10.1017/S0016756808004913.

Kump, L. R. (1989) 'Alternative modeling approaches to the geochemical cycles of carbon, sulfur, and strontium isotopes', *American Journal of Science*, 299, pp. 390–410. doi: 10.2475/ajs.289.4.390.

Landing, E., Bowring, S. A., Davidek, K. L., Westrop, S. R., Geyer, G. and Heldmaier, W. (1998) 'Duration of the Early Cambrian: U-Pb ages of volcanic ashes from Avalon and Gondwana', *Canadian Journal of Earth Sciences*, 35(4), pp. 329–338. doi: 10.1139/e97-107.

Landing, E., Geyer, G., Brasier, M. D. and Bowring, S. A. (2013) 'Cambrian Evolutionary Radiation: Context, correlation, and chronostratigraphy-Overcoming deficiencies of the first appearance datum (FAD) concept', *Earth-Science Reviews*, 123, pp. 133–172. doi: 10.1016/j.earscirev.2013.03.008.

Leavitt, W. D., Halevy, I., Bradley, A. S. and Johnston, D. T. (2013) 'Influence of sulfate reduction rates on the Phanerozoic sulfur isotope record.', *Proceedings of the National Academy of Sciences*, 110(28), pp. 11244–11249. doi: 10.1073/pnas.1218874110.

Lechler, M., Pogge von Strandmann, P. A. E., Jenkyns, H. C., Prosser, G. and Parente, M. (2015) 'Lithium-isotope evidence for enhanced silicate weathering during OAE 1a (Early Aptian Selli event)', *Earth and Planetary Science Letters*, 432, pp. 210–222. doi: 10.1016/j.epsl.2015.09.052.

Lee, Y. Il, Choi, T., Lim, H. S. and Orihashi, Y. (2016) 'Detrital zircon geochronology and Nd isotope geochemistry of the basal succession of the Taebaeksan Basin, South Korea: Implications for the Gondwana linkage of the Sino-Korean (North China) block during the Neoproterozoic–early Cambrian', *Palaeogeography, Palaeoclimatology, Palaeoecology*, 441, pp. 770–786. doi: 10.1016/j.palaeo.2015.10.025.

Lenton, T. M. and Watson, A. J. (2000) 'Redfield revisited: 2. What regulates the oxygen content of the atmosphere?', *Global Biogeochemical Cycles*, 14(1), pp. 249–268. doi: 10.1029/1999GB900076.

Lenton, T. M., Boyle, R. A., Poulton, S. W., Shields-Zhou, G. A. and Butterfield, N. J. (2014) 'Co-evolution of eukaryotes and ocean oxygenation in the Neoproterozoic era', *Nature Geoscience*. Nature Publishing Group, a division of Macmillan Publishers Limited. All Rights Reserved., 7(4), pp. 257–265. doi: 10.1038/ngeo2108.

Li, C., Jin, C., Planavsky, N. J., Algeo, T. J., Cheng, M., Yang, X., Zhao, Y., Xie, S. (2017) 'Coupled oceanic oxygenation and metazoan diversification during the early–middle Cambrian?', *Geology*, 45(7), p. 743-746. doi: 10.1130/G39208.1.

Li, D., Ling, H.-F., Jiang, S.-Y., Pan, J.-Y., Chen, Y.-Q., Cai, Y.-F. and Feng, H.-Z. (2009) 'New carbon isotope stratigraphy of the Ediacaran–Cambrian boundary interval from SW China: implications for global correlation', *Geological Magazine*, 146(4), p. 465–484. doi: 10.1017/S0016756809006268.

Li, D., Shields-Zhou, G. A., Ling, H.-F. and Thirlwall, M. (2011) 'Dissolution methods for strontium isotope stratigraphy: Guidelines for the use of bulk carbonate and phosphorite rocks', *Chemical Geology*, 290(3–4), pp. 133–144. doi: 10.1016/j.chemgeo.2011.09.004.

Li, D., Ling, H.-F., Shields-Zhou, G. A., Chen, X., Cremonese, L., Och, L., Thirlwall, M. and Manning, C. J. (2013) 'Carbon and strontium isotope evolution of seawater across the Ediacaran–Cambrian transition: Evidence from the Xiaotan section, NE Yunnan, South China', *Precambrian Research*, 225, pp. 128–147. doi: 10.1016/j.precamres.2012.01.002.

Li, J., Qian, M. and Jiang, Y. (2013) 'Overlapping of the Lower Cambrian Houjiashan Formation over the Pre-Cryogenian sequences in the Northern Jiangsu and Anhui Provinces', *Journal of Stratigraphy*, 37(2), pp. 232–241.

Li, Z. X. and Powell, C. M. (2001) 'An outline of the palaeogeographic evolution of the Australasian region since the beginning of the Neoproterozoic', *Earth Science Reviews*, 53(3–4), pp. 237–277. doi: 10.1016/S0012-8252(00)00021-0.

Li, Z. X., Evans, D. A. D. and Halverson, G. P. (2013) 'Neoproterozoic glaciations in a revised global palaeogeography from the breakup of Rodinia to the assembly of Gondwanaland', *Sedimentary Geology*, 294, pp. 219–232. doi: 10.1016/j.sedgeo.2013.05.016.

Lieberman, B. S. (2003) 'Biogeography of the trilobita during the Cambrian radiation: Deducing geological processes from trilobite evolution', in *Trilobites and Their Relatives*, pp. 59–72.

Lieberman, B. S. (2003) 'Taking the Pulse of the Cambrian Radiation', *Integrative and*

Comparative Biology, 43(1), pp. 229–237. doi: 10.1093/icb/43.1.229.

Lin, J.-L., Fuller, M. and Zhang, W.-Y. (1985) 'Paleogeography of the North and South China Blocks during the Cambrian', *Journal of geodynamic*, 2, pp. 91–114.

Liu, T., Maynard, J. B. and Alten, J. (2006) 'Superheavy S isotopes from glacier-associated sediments of the Neoproterozoic of south China: Oceanic anoxia or sulfate limitation?', in *Memoir 198: Evolution of Early Earth's Atmosphere, Hydrosphere, and Biosphere - Constraints from Ore Deposits*. Geological Society of America, pp. 205–222. doi: 10.1130/2006.1198(12).

Liu, Y. (2012) *Restudy on Jianchang Formation and trilobite fauna of the early Cambrian in eastern Liaoning*. Shenyang Normal University.

Loyd, S. J., Marenco, P. J., Hagadorn, J. W., Lyons, T. W., Kaufman A. J., Sour-Tovar, F. and Corsetti, F. A. (2012) 'Sustained low marine sulfate concentrations from the Neoproterozoic to the Cambrian: Insights from carbonates of northwestern Mexico and eastern California', *Earth and Planetary Science Letters*, 339-340, pp. 79-94. doi: 10.1016/j.epsl.2012.05.032.

Luo, G., Kump, L. R., Wang, Y., Tong, J., Arthur, M. A., Yang, H., Huang, J., Yin, H. and Xie, S. (2010) 'Isotopic evidence for an anomalously low oceanic sulfate concentration following end-Permian mass extinction', *Earth and Planetary Science Letters*, 300(1–2), pp. 101–111. doi: 10.1016/j.epsl.2010.09.041.

Luo, C., Zhu, M. and Reitner, J. (2016) 'The Jinxian Biota revisited: taphonomy and body plan of the Neoproterozoic discoid fossils from the southern Liaodong Peninsula, North China', *Paläontologische Zeitschrift*. doi: 10.1007/s12542-016-0289-5.

Lyons, T. W., Reinhard, C. T. and Planavsky, N. J. (2014) 'The rise of oxygen in Earth's early ocean and atmosphere.', *Nature*, 506(7488), pp. 307–315. doi: 10.1038/nature13068.

Macdonald, F. A., Pruss, S. B. and Strauss, J. V. (2014) 'Trace fossils with spreiten from the Late Ediacaran Nama Group, Namibia: complex feeding patterns five million years before the Precambrian–Cambrian boundary', *Journal of Paleontology*, 88(2), pp. 299–308. doi: 10.1666/13-042.

Maloof, A. C., Schrag, D. P., Crowley, J. L. and Bowring, S. A. (2005) 'An expanded record of Early Cambrian carbon cycling from the Anti-Atlas Margin, Morocco', *Canadian Journal of Earth Sciences*, 42(12), pp. 2195–2216. doi: 10.1139/e05-062.

Maloof, A. C., Ramezani, J., Bowring, S. A., Fike, D. A., Porter, S. M. and Mazouad, M. (2010) 'Constraints on early Cambrian carbon cycling from the duration of the Nemakit-Daldynian-Tommotian boundary ^{13}C shift, Morocco', *Geology*, 38(7), pp. 623–626. doi: 10.1130/G30726.1.

Maloof, A. C., Porter, S. M., Moore, J. L., Dudas, F. O., Bowring, S. A., Higgins, J. A., Fike, D. A. and Eddy, M. P. (2010) 'The earliest Cambrian record of animals and ocean geochemical change', *Geological Society of America Bulletin*, 122(11–12), pp. 1731–1774. doi: 10.1130/B30346.1.

Mángano, M. G. and Buatois, L. A. (2014) 'Decoupling of body-plan diversification and ecological structuring during the Ediacaran-Cambrian transition: evolutionary and geobiological feedbacks.', *Proceedings. Biological sciences / The Royal Society*, 281(1780), pp. 2014-2038. doi: 10.1098/rspb.2014.0038.

Marenco, P. J., Corsetti, F. A., Hammond, D. E., Kaufman, A. J. and Bottjer, D. J. (2008) 'Oxidation of pyrite during extraction of carbonate associated sulfate', *Chemical Geology*, 247(1–2), pp. 124–132. doi: 10.1016/j.chemgeo.2007.10.006.

McArthur, J. M. (1994) 'Recent trends in strontium isotope stratigraphy', *Terra Nova*, 6(4), pp. 331–358. doi: 10.1111/j.1365-3121.1994.tb00507.x.

McArthur, J. M., Howarth, R. J. and Bailey, T. R. (2001) 'Strontium isotope stratigraphy: LOWESS version 3: best fit to the marine Sr-isotope curve for 0-509 Ma and accompanying look-up table for deriving numerical age', *The Journal of Geology*, 109(2), pp. 155–170. doi: 10.1086/319243.

McArthur, J. M., Howarth, R. J. and Shields-Zhou, G. A. (2012) 'Strontium Isotope Stratigraphy', in Gradstein, F. M., Ogg, J. G., Schmitz, M. D., and Ogg, G. M. (eds) *The Geologic Time Scale 2012*. Elsevier Science Limited, pp. 127–144.

McIlroy, D. and Logan, G. A. (1999) 'The impact of bioturbation on infaunal ecology and evolution during the Proterozoic–Cambrian transition', *Palaios*, 14(1), pp. 58–72. doi: 10.2307/3515361.

McKenzie, N. R., Hughes, N. C., Myrow, P. M., Choi, D. K. and Park, T. -Y. (2011) 'Trilobites and zircons link north China with the eastern Himalaya during the Cambrian', *Geology*, 39(6), pp. 591–594. doi: 10.1130/G31838.1.

McKenzie, N. R., Hughes, N. C., Myrow, P. M., Xiao, S. and Sharma, M. (2011) 'Correlation of Precambrian–Cambrian sedimentary successions across northern India and the utility of isotopic signatures of Himalayan lithotectonic zones', *Earth and Planetary Science Letters*, 312(3–4), pp. 471–483. doi: 10.1016/j.epsl.2011.10.027.

Meert, J. G. (2003) 'A synopsis of events related to the assembly of eastern Gondwana', *Tectonophysics*, 362(1–4), pp. 1–40. doi: 10.1016/S0040-1951(02)00629-7.

Meert, J. G. and Lieberman, B. S. (2008) 'The Neoproterozoic assembly of Gondwana and its relationship to the Ediacaran–Cambrian radiation', *Gondwana Research*, 14(1–2), pp. 5–21. doi: 10.1016/j.gr.2007.06.007.

Melezhik, V. A., Pokrovsky, B. G., Fallick, A. E., Kuznetsov, A. B. and Bujakaite, M. I. (2009) 'Constraints on $^{87}Sr/^{86}Sr$ of Late Ediacaran seawater: insight from Siberian high-Sr limestones', *Journal of the Geological Society*, 166(1), pp. 183–191. doi: 10.1144/0016-76492007-171.

Miao, L. (2014) *Biostratigraphy of the basal Cambrian Xinji Formation and the Houjiashan Formation from the southern Noth China plate*. University of Chinese Academy of Sciences.

Miller, K. G. (2005) 'The Phanerozoic record of global sea-level change', *Science*, 310(5752), pp. 1293–1298. doi: 10.1126/science.1116412.

Miller, J. F., Ethington, R. L., Evans, K. R., Holmer, L. E., Loch, J. D., Popov, L. E., Repetski, J. E., Ripperdan, R. L. and Taylor, J. F. (2006) 'Proposed stratotype for the base of the highest Cambrian stage at the first appearance datum of Cordylodus andresi, Lawson Cove section, Utah, USA', *Palaeoworld*, 15(3–4), pp. 384–405. doi: 10.1016/j.palwor.2006.10.017.

Mills, D. B., Ward, L. M., Jones, C., Sweeten, B., Forth, M., Treusch, A. H. and Canfield, D.

E. (2014) 'Oxygen requirements of the earliest animals.', *Proceedings of the National Academy of Sciences*, 111(11), pp. 4168–4172. doi: 10.1073/pnas.1400547111.

Morris, S. C. (1989) 'Burgess shale faunas and the Cambrian Explosion', *Science*, 246(4928), pp. 339–346. doi: 10.1126/science.246.4928.339.

Montañez, I. P., Banner, J. L., Osleger, D. A., Borg, L. E. and Bosserman, P. J. (1996) 'Integrated Sr isotope variations and sea-level history of Middle to Upper Cambrian platform carbonates: Implications for the evolution of Cambrian seawater $^{87}Sr/^{86}Sr$', *Geology*, 24(10), pp. 917–920. doi: 10.1130/0091-7613(1996)024<0917:ISIVAS>2.3.CO;2.

Murphy, M. A. and Salvador, A. (1999) 'International stratigraphic guide - an abridged version', *Episodes*, 22(4), pp. 255–271.

Myrow, P. M., Chen, J., Snyder, Z., Leslie, S., Fike, D. A., Fanning, M., Yuan, J., Tang, P., Fanning, C. M., Yuan, J. and Tang, P. (2015) 'Depositional history, tectonics, and provenance of the Cambrian-Ordovician boundary interval in the western margin of the North China block', *Geological Society of America Bulletin*, 127(9–10), pp. 1174–1193. doi: 10.1130/B31228.1.

Myrow, P. M., Hughes, N. C., Goodge, J. W., Fanning, C. M., Williams, I. S., Peng, S., Bhargava, O. N., Parcha, S. K. and Pogue, K. R. (2010) 'Extraordinary transport and mixing of sediment across Himalayan central Gondwana during the Cambrian-Ordovician', *Geological Society of America Bulletin*, 122(9–10), pp. 1660–1670. doi: 10.1130/B30123.1.

Narbonne, G. M., Myrow, P. M., Landing, E. and Anderson, M. M. (1997) 'A candidate stratotype for the Precambrian–Cambrian boundary, Fortune Head, Burin Peninsula, southeastern Newfoundland', *Canadian Journal of Earth Sciences*, 24, pp. 1277–1293. doi: 10.1139/e87-124.

National Commission on Stratigraphy of China and China Geological Survey (2014) *The stratigraphic chart of China (2014)*. Beijing: Geological Publishing House.

Nedin, C., Jenkins, R. J. F. and Mount, J. F. (1991) 'Re-evaluation of unconformities separating the "Ediacaran" and Cambrian systems, South Australia', *Palaios*, 6(1), p. 102. doi: 10.2307/3514959.

Newton, R. J., Pevitt, E. L., Wignall, P. B. and Bottrell, S. H. (2004) 'Large shifts in the isotopic composition of seawater sulphate across the Permo-Triassic boundary in northern Italy', *Earth and Planetary Science Letters*, 218(3–4), pp. 331–345. doi: 10.1016/S0012-821X(03)00676-9.

Newton, R. J., Reeves, E. P., Kafousia, N., Wignall, P. B., Bottrell, S. H. and Sha, J.-G. (2011) 'Low marine sulfate concentrations and the isolation of the European epicontinental sea during the Early Jurassic', *Geology*, 39(1), pp. 7–10. doi: 10.1130/G31326.1.

Nicholas, C. J. (1996) 'The Sr isotopic evolution of the oceans during the "Cambrian Explosion"', *Journal of the Geological Society*, 153(2), pp. 243–254. doi: 10.1144/gsjgs.153.2.0243.

Och, L. M. and Shields-Zhou, G. A. (2012) 'The Neoproterozoic oxygenation event: Environmental perturbations and biogeochemical cycling', *Earth-Science Reviews*, 110(1–4), pp. 26–57. doi: 10.1016/j.earscirev.2011.09.004.

Och, L. M., Shields-Zhou, G. A., Poulton, S. W., Manning, C., Thirlwall, M. F., Li, D., Chen, X., Ling, H., Osborn, T. and Cremonese, L. (2013) 'Redox changes in Early Cambrian black shales at Xiaotan section, Yunnan Province, South China', *Precambrian Research*, 225, pp. 166–189. doi: 10.1016/j.precamres.2011.10.005.

Osburn, M. R., Owens, J., Bergmann, K. D., Lyons, T. W. and Grotzinger, J. P. (2015) 'Dynamic changes in sulfate sulfur isotopes preceding the Ediacaran Shuram Excursion', *Geochimica et Cosmochimica Acta*, 170, pp. 204–224. doi: 10.1016/j.gca.2015.07.039.

Palmer, M. R. and Edmond, J. M. (1989) 'The strontium isotope budget of the modern ocean', *Earth and Planetary Science Letters*, 92(1), pp. 11–26. doi: 10.1016/0012-821X(89)90017-4.

Paytan, A. and Gray, E. T. (2012) 'Sulfur Isotope Stratigraphy', in Gradstein, F. M., Ogg, J. G., Schmitz, M. D., and Ogg, G. M. (eds) *The Geologic Time Scale 2012*. Elsevier Science Limited, pp. 167–180. doi: 10.1016/B978-0-444-59425-9.00009-3.

Pearce, N. J. G., Perkins, W. T., Westgate, J. A., Gorton, M. P., Jackson, S. E., Neal, C. R. and Chenery, S. P. (1997) 'A Compilation of New and Published Major and Trace Element Data for NIST SRM 610 and NIST SRM 612 Glass Reference Materials', *Geostandards and Geoanalytical Research*, 21(1), pp. 115–144. doi: 10.1111/j.1751-908X.1997.tb00538.x.

Pearce, C. R., Parkinson, I. J., Gaillardet, J., Charlier, B. L. A., Mokadem, F. and Burton, K. W. (2015) 'Reassessing the stable ($\delta^{88/86}$Sr) and radiogenic (^{87}Sr/^{86}Sr) strontium isotopic composition of marine inputs', *Geochimica et Cosmochimica Acta*, 157, pp. 125–146. doi: 10.1016/j.gca.2015.02.029.

Pei, F. and Feng, W. (2005) 'Discovery of the Molluscan fauna from the lower Cambrian Xinji Formation of Zhuyang, Lingbao of Henan', *Journal of Stratigraphy*, S1, pp. 458–461.

Peng, S., Babcock, L. E. and Cooper, R. A. (2012) 'The Cambrian Period', in Gradstein, F. M., Ogg, J. G., Schmitz, M. D., and Ogg, G. M. (eds) *The Geologic Time Scale 2012*. Elsevier Science Limited, pp. 437–488.

Peng, Y., Bao, H., Pratt, L. M., Kaufman, A. J., Jiang, G., Boyd, D., Wang, Q., Zhou, C., Yuan, X., Xiao, S. and Loyd, S. (2014) 'Widespread contamination of carbonate-associated sulfate by present-day secondary atmospheric sulfate: Evidence from triple oxygen isotopes', *Geology*, 42(9), pp. 815–818. doi: 10.1130/G35852.1.

Penny, A. M., Wood, R., Curtis, A., Bowyer, F., Tostevin, R. and Hoffman, K.-H. (2014) 'Ediacaran metazoan reefs from the Nama Group, Namibia', *Science*, 344(6191), pp. 1504–1506. doi: 10.1126/science.1253393.

Peters, S. E. and Gaines, R. R. (2012) 'Formation of the 'Great Unconformity' as a trigger for the Cambrian explosion', *Nature*, 484(7394), pp. 363–366. doi: 10.1038/nature10969.

Petrychenko, O. Y., Peryt, T. M. and Chechel, E. I. (2005) 'Early Cambrian seawater chemistry from fluid inclusions in halite from Siberian evaporites', *Chemical Geology*, 219(1–4), pp. 149–161. doi: 10.1016/j.chemgeo.2005.02.003.

Pogge von Strandmann, P. A. E., Jenkyns, H. C. and Woodfine, R. G. (2013) 'Lithium isotope evidence for enhanced weathering during Oceanic Anoxic Event 2', *Nature Geoscience*, 6(8), pp. 668–672. doi: 10.1038/ngeo1875.

REFERENCES

Pogge von Strandmann, P. A. E., Stüeken, E. E., Elliott, T., Poulton, S. W., Dehler, C. M., Canfield, D. E. and Catling, D. C. (2015) 'Selenium isotope evidence for progressive oxidation of the Neoproterozoic biosphere', *Nature Communications*, 6, pp. 1–10. doi: 10.1038/ncomms10157.

Porter, S. M. (2007) 'Seawater chemistry and early carbonate biomineralization', *Science*, 316(5829), pp. 1302–1302. doi: 10.1126/science.1137284.

Present, T. M., Paris, G., Burke, A., Fischer, W. W. and Adkins, J. F. (2015) 'Large carbonate associated sulfate isotopic variability between brachiopods, micrite, and other sedimentary components in Late Ordovician strata', *Earth and Planetary Science Letters*, 432, pp. 187–198. doi: 10.1016/j.epsl.2015.10.005.

Qian, M., Yuan, X., Li, J., Yan, Y. and Wang, P. (2001) 'Comments on the Cambrian–Neoproterozoic boundary in Huaibei district, northern Anhui-Jiangsu', *Journal of Stratigraphy*, (25), pp. 135–143.

Qian, M., Yuan, X., Xu, X., Hu, J. and Li, J. (2002) 'An assemblage of the Neoproterozoic stromatolites from the Xuzhou-Huainan region', *Acta Palaeontologica Sinica*, 41(3), pp. 403–418.

Qiao, X. (2002) 'Seismic event, sequence and tectonic significance in Canglangpu Stage in Paleo-Tanlu Fault Zone', *Science in China Series D*, 45(9), p. 781–791. doi: 10.1360/02yd9078.

Rao, D. C. V, Santosh, M., Kim, S. W., Rao, C. V. D., Santosh, M. and Kim, S. W. (2012) 'Cryogenian volcanic arc in the NW Indian Shield: Zircon SHRIMP U–Pb geochronology of felsic tuffs and implications for Gondwana assembly', *Gondwana Research*, 22(1), pp. 36–53. doi: 10.1016/j.gr.2011.10.014.

Rees, C. E. (1978) 'Sulphur isotope measurements using SO_2 and SF_6', *Geochimica et Cosmochimica Acta*, 42(4), pp. 383–389. doi: 10.1016/0016-7037(78)90269-7.

Rennie, V. C. F. and Turchyn, A. V. (2014) 'The preservation of $\delta^{34}S_{SO4}$ and $\delta^{18}O_{SO4}$ in carbonate-associated sulfate during marine diagenesis: A 25 Myr test case using marine sediments', *Earth and Planetary Science Letters*, 395(0), pp. 13–23. doi: 10.1016/j.epsl.2014.03.025.

Richter, F. M., Rowley, D. B. and DePaolo, D. J. (1992) 'Sr isotope evolution of seawater: the role of tectonics', *Earth and Planetary Science Letters*, 109(1–2), pp. 11–23. doi: 10.1016/0012-821X(92)90070-C.

Ries, J. B., Fike, D. A., Pratt, L. M., Lyons, T. W. and Grotzinger, J. P. (2009) 'Superheavy pyrite ($\delta^{34}S_{pyr} > \delta^{34}S_{CAS}$) in the terminal Proterozoic Nama Group, southern Namibia: A consequence of low seawater sulfate at the dawn of animal life', *Geology*, 37(8), pp. 743–746. doi: 10.1130/G25775A.1.

Rogov, V., Marusin, V., Bykova, N., Goy, Y., Nagovitsin, K., Kochnev, B., Karlova, G. and Grazhdankin, D. (2012) 'The oldest evidence of bioturbation on Earth', *Geology*, 40(5), pp. 395–398. doi: 10.1130/G32807.1.

Rooney, A. D., Strauss, J. V., Brandon, A. D. and Macdonald, F. A. (2015) 'A Cryogenian chronology: Two long-lasting synchronous Neoproterozoic glaciations', *Geology*, 43(5), pp. 459–462. doi: 10.1130/G36511.1.

Rowland, S. M. and Shapiro, R. S. (2002) 'Reef patterns and environmental influences in the

Cambrian and earliest Ordovician', *SEPM Special Publication*, 72, pp. 95–128.

Rozanov, A. Y., Zhu, M.-Y., Pak, K. L. and Parkhaev, P. Yu. (2008) 'The 2nd Sino-Russian Symposium on the Lower Cambrian Subdivision', *Paleontological Journal*, 42(4), pp. 441–446. doi: 10.1134/S0031030108040151.

Saltzman, M. R., Davidson, J. P., Holden, P., Runnegar, B. and Lohmann, K. C. (1995) 'Sea-level-driven changes in ocean chemistry at an Upper Cambrian extinction horizon', *Geology*, 23(10), pp. 893-896. doi: 10.1130/0091-7613(1995)023<0893:SLDCIO>2.3.CO;2.

Saltzman, M. R., Young, S. a, Kump, L. R., Gill, B. C., Lyons, T. W. and Runnegar, B. (2011) 'Pulse of atmospheric oxygen during the late Cambrian.', *Proceedings of the National Academy of Sciences*, 108(10), pp. 3876–3881. doi: 10.1073/pnas.1011836108.

Shen, B., Xiao, S., Bao, H., Kaufman, A. J., Zhou, C. and Yuan, X. (2011) 'Carbon, sulfur, and oxygen isotope evidence for a strong depth gradient and oceanic oxidation after the Ediacaran Hankalchough glaciation', *Geochimica et Cosmochimica Acta*, 75(5), pp. 1357–1373. doi: 10.1016/j.gca.2010.12.015.

Shen, Y., Zhang, T. and Hoffman, P. F. (2008) 'On the coevolution of Ediacaran oceans and animals', *Proceedings of the National Academy of Sciences*, 105(21), pp. 7376–7381. doi: 10.1073/pnas.0802168105.

Shields-Zhou, G. and Och, L. (2011) 'The case for a Neoproterozoic Oxygenation Event: Geochemical evidence and biological consequences', *GSA Today*, 21(3), pp. 4–11. doi: 10.1130/GSATG102A.1.

Shields-Zhou, G. A., Hill, A. C. and Macgabhann, B. A. (2012) 'The Cryogenian Period', in Gradstein, F. M., Ogg, J. G., Schmitz, M. D., and Ogg, G. M. (eds) *The Geologic Time Scale 2012*. Elsevier Science Limited, pp. 393–411.

Shields-Zhou, G. A. and Zhu, M. (2013) 'Biogeochemical changes across the Ediacaran-Cambrian transition in South China', *Precambrian Research*, 225(0), pp. 1–6. doi: 10.1016/j.precamres.2012.10.011.

Shields-Zhou, G. A., Porter, S. and Halverson, G. P. (2016) 'A New Rock-Based Definition for the Cryogenian Period (Circa 720-635 Ma)', *Episodes*, 39(1), pp. 3–8. doi: 10.18814/epiiugs/2016/v39i1/89231.

Shields, G. A. (2017) 'Earth system transition during the Tonian–Cambrian interval of biological innovation : nutrients, climate, oxygen and the marine organic carbon capacitor', *Geological Society, London, Special Publications*, 448, p. SP448.17. doi: 10.1144/SP448.17.

Sim, M. S., Bosak, T. and Ono, S. (2011) 'Large sulfur isotope fractionation does not require disproportionation', *Science*, 333(6038), pp. 74–77. doi: 10.1126/science.1205103.

Sláma, J., Košler, J., Condon, D. J., Crowley, J. L., Gerdes, A., Hanchar, J. M., Horstwood, M. S. A., Morris, G. A., Nasdala, L., Norberg, N., Schaltegger, U., Schoene, B., Tubrett, M. N. and Whitehouse, M. J. (2008) 'Plešovice zircon — A new natural reference material for U–Pb and Hf isotopic microanalysis', *Chemical Geology*, 249(1–2), pp. 1–35. doi: 10.1016/j.chemgeo.2007.11.005.

Smith, M. P. and Harper, D. A. T. (2013) 'Causes of the Cambrian Explosion', *Science*,

341(6152), pp. 1355–1356. doi: 10.1126/science.1239450.

Smith, E. F., Macdonald, F. A., Petach, T. A., Bold, U. and Schrag, D. P. (2016) 'Integrated stratigraphic, geochemical, and paleontological late Ediacaran to early Cambrian records from southwestern Mongolias', *Geological Society of America Bulletin*, 128(3–4), pp. 442–468. doi: 10.1130/B31248.1.

Song, H., Tong, J., Algeo, T. J., Song, H., Qiu, H., Zhu, Y., Tian, L., Bates, S., Lyons, T. W., Luo, G. and Kump, L. R. (2014) 'Early Triassic seawater sulfate drawdown', *Geochimica et Cosmochimica Acta*, 128(0), pp. 95–113. doi: 10.1016/j.gca.2013.12.009.

Song, H., Wignall, P. B., Tong, J., Song, H., Chen, J., Chu, D., Tian, L., Luo, M., Zong, K., Chen, Y., Lai, X., Zhang, K. and Wang, H. (2015) 'Integrated Sr isotope variations and global environmental changes through the Late Permian to early Late Triassic', *Earth and Planetary Science Letters*, 424, pp. 140–147. doi: 10.1016/j.epsl.2015.05.035.

Sperling, E. A., Frieder, C. A., Raman, A. V., Girguis, P. R., Levin, L. A. and Knoll, A. H. (2013) 'Oxygen, ecology, and the Cambrian radiation of animals.', *Proceedings of the National Academy of Sciences*, 110(33), pp. 13446–51. doi: 10.1073/pnas.1312778110.

Sperling, E. A., Halverson, G. P., Knoll, A. H., Macdonald, F. A. and Johnston, D. T. (2013) 'A basin redox transect at the dawn of animal life', *Earth and Planetary Science Letters*, 371–372, pp. 143–155. doi: 10.1016/j.epsl.2013.04.003.

Squire, R. J., Campbell, I. H., Allen, C. M. and Wilson, C. J. L. (2006) 'Did the Transgondwanan Supermountain trigger the explosive radiation of animals on Earth?', *Earth and Planetary Science Letters*, 250(1–2), pp. 116–133. doi: 10.1016/j.epsl.2006.07.032.

Staudt, W. J. and Schoonen, M. A. A. (1995) 'Sulfate incorporation into sedimentary carbonates', *Geochemical Transformations of Sedimentary Sulfur*, 612(4), pp. 332–345. doi: 10.1021/bk-1995-0612.

Strauss, H., Bengtson, S., Myrow, P. M. and Vidal, G. (1992) 'Stable isotope geochemistry and palynology of the late Precambrian to Early Cambrian sequence in Newfoundland', *Canadian Journal of Earth Sciences*, 29(8), pp. 1662–1673. doi: 10.1139/e92-131.

Tang, Q., Pang, K., Yuan, X., Wan, B. and Xiao, S. (2015) 'Organic-walled microfossils from the Tonian Gouhou Formation, Huaibei region, North China Craton, and their biostratigraphic implications', *Precambrian Research*, 266, pp. 296–318. doi: 10.1016/j.precamres.2015.05.025.

Theiling, B. P. and Coleman, M. (2015) 'Refining the extraction methodology of carbonate associated sulfate: Evidence from synthetic and natural carbonate samples', *Chemical Geology*, 411, pp. 36–48. doi: 10.1016/j.chemgeo.2015.06.018.

Thirlwall, M. F. (1991) 'Long-term reproducibility of multicollector Sr and Nd isotope ratio analysis', *Chemical Geology: Isotope Geoscience section*, 94(2), pp. 85–104. doi: 10.1016/0168-9622(91)90002-E.

Torsvik, T. H. and Cocks, L. R. M. (2013) 'New global palaeogeographical reconstructions for the Early Palaeozoic and their generation', *Geological Society, London, Memoirs*. Edited by D. A. T. Harper and T. Servais. London: The Geological Society of London, 38(1), pp. 5–24. doi: 10.1144/M38.2.

Tostevin, R., Wood, R. A., Shields, G. A., Poulton, S. W., Guilbaud, R., Bowyer, F., Penny, A. M., He, T., Curtis, A., Hoffmann, K. H. and Clarkson, M. O. (2016) 'Low-oxygen waters limited habitable space for early animals', *Nature Communications*, 7, pp. 1–9. doi: 10.1038/ncomms12818.

Tostevin, R., He, T., Turchyn, A. V, Wood, R. A., Penny, A. M., Bowyer, F., Antler, G. and Shields, G. A. (2017) 'Constraints on the late Ediacaran sulfur cycle from carbonate associated sulfate', *Precambrian Research*, 290, pp. 113–125. doi: 10.1016/j.precamres.2017.01.004.

Turner, C. C., Meert, J. G., Pandit, M. K. and Kamenov, G. D. (2014) 'A detrital zircon U–Pb and Hf isotopic transect across the Son Valley sector of the Vindhyan Basin, India: Implications for basin evolution and paleogeography', *Gondwana Research*, 26(1), pp. 348–364. doi: 10.1016/j.gr.2013.07.009.

Valladares, M. I., Ugidos, J. M., Barba, P., Fallick, A. E. and Ellam, R. M. (2006) 'Oxygen, carbon and strontium isotope records of Ediacaran carbonates in Central Iberia (Spain)', *Precambrian Research*, 147(3–4), pp. 354–365. doi: 10.1016/j.precamres.2006.01.021.

Van Lente, B., Ashwal, L. D., Pandit, M. K., Bowring, S. A. and Torsvik, T. H. (2009) 'Neoproterozoic hydrothermally altered basaltic rocks from Rajasthan, northwest India: Implications for late Precambrian tectonic evolution of the Aravalli Craton', *Precambrian Research*, 170(3–4), pp. 202–222. doi: 10.1016/j.precamres.2009.01.007.

Vance, D., Teagle, D. A. H. and Foster, G. L. (2009) 'Variable Quaternary chemical weathering fluxes and imbalances in marine geochemical budgets', *Nature*, 458(7237), pp. 493–496. doi: 10.1038/nature07828.

Varlamov, A. I., Rozanov, A. Y., Khomentovsky, V. V., Shabanov, Y. Y., Abaimova, G. P., Demidenko, Y. E., Karlova, G. A., Korovnikov, I. V., Luchinina, V. A., Malakhovskaya, Y. E., Parkhaev, P. Y., Pegel, T. V., Skorlotova, N. A., Sundukov, V. M., Sukhov, S. S., Fedorov, A. B. and Kipriyanova, L. D. (2008) *The Cambrian System of the Siberian Platform Part 1 : The Aldan-Lena Region*. Edited by A. Y. Rozanov and A. I. Varlamov. Moscow: PIN RAS.

Veizer, J., Compston, W., Clauer, N. and Schidlowski, M. (1983) 'in Late Proterozoic carbonates: evidence for a 'mantle' event at ~900 Ma ago', *Geochimica et Cosmochimica Acta*, 47(2), pp. 295–302. doi: 10.1016/0016-7037(83)90142-4.

Vermeesch, P. (2004) 'How many grains are needed for a provenance study?', *Earth and Planetary Science Letters*, 224(3–4), pp. 441–451. doi: 10.1016/j.epsl.2004.05.037.

Vermeesch, P. (2012) 'On the visualisation of detrital age distributions', *Chemical Geology*, 312–313, pp. 190–194. doi: 10.1016/j.chemgeo.2012.04.021.

Vermeesch, P., Resentini, A. and Garzanti, E. (2016) 'An R package for statistical provenance analysis', *Sedimentary Geology*, 336, pp. 14–25. doi: 10.1016/j.sedgeo.2016.01.009.

Wang, G., Zhang, S., Li, S., Yan, Y., Dou, S. and Fang, D. (1984) *Research on the Upper Precambrian of Northern Jiangsu and Anhui Provinces*. Hefei: Anhui Press of Science and Technology.

Wang, M. and Yang, Z. (1986) 'Discovery of the lower Cambrian Qiongzhusi Stage in southern Liaodong Peninsula', *Liaoning Geology*, 1, pp. 1–7.

REFERENCES

Wang, Q., Yang, D. and Xu, W. (2012) 'Neoproterozoic basic magmatism in the southeast margin of North China Craton: Evidence from whole-rock geochemistry, U-Pb and Hf isotopic study of zircons from diabase swarms in the Xuzhou-Huaibei area of China', *Science China Earth Sciences*, 55(9), pp. 1461–1479. doi: 10.1007/s11430-011-4237-7.

Wilhem, C., Windley, B. F. and Stampfli, G. M. (2012) 'The Altaids of Central Asia: A tectonic and evolutionary innovative review', *Earth-Science Reviews*, 113(3–4), pp. 303–341. doi: 10.1016/j.earscirev.2012.04.001.

Wood, R. A. (2002) 'Proterozoic modular biomineralized metazoan from the Nama Group, Namibia', *Science*, 296(5577), pp. 2383–2386. doi: 10.1126/science.1071599.

Wood, R. A. (2011) 'Paleoecology of the earliest skeletal metazoan communities: Implications for early biomineralization', *Earth-Science Reviews*, 106(1–2), pp. 184–190. doi: 10.1016/j.earscirev.2011.01.011.

Wood, R. A., Poulton, S. W., Prave, A. R., Hoffmann, K.-H., Clarkson, M. O., Guilbaud, R., Lyne, J. W., Tostevin, R., Bowyer, F., Penny, A. M., Curtis, A. and Kasemann, S. A. (2015) 'Dynamic redox conditions control late Ediacaran metazoan ecosystems in the Nama Group, Namibia', *Precambrian Research*, 261, pp. 252–271. doi: 10.1016/j.precamres.2015.02.004.

Wood, R. A., Zhuravlev, A. Y., Sukhov, S. S., Zhu, M. and Zhao, F. (2016) 'Demise of Ediacaran dolomitic seas marks widespread biomineralization on the Siberian Platform', *Geology*, 45(1), pp. 27-30. doi: 10.1130/G38367.1.

Wortmann, U. G., Bernasconi, S. M. and Böttcher, M. E. (2001) 'Hypersulfidic deep biosphere indicates extreme sulfur isotope fractionation during single-step microbial sulfate reduction', *Geology*, 29(7), pp. 647–650. doi: 10.1130/0091-7613(2001)029<0647:HDBIES>2.0.CO;2.

Wotte, T. , Strauss, H., Sundberg, F. A. (2011) 'Carbon and sulfur isotopes from the Cambrian Series 2–Cambrian Series 3 of Laurentia and Siberia', *Museum of Northern Arizona Bulletin*, 67, pp. 43–63.

Wotte, T., Shields-Zhou, G. A. and Strauss, H. (2012) 'Carbonate-associated sulfate: Experimental comparisons of common extraction methods and recommendations toward a standard analytical protocol', *Chemical Geology*, 326–327, pp. 132–144. doi: 10.1016/j.chemgeo.2012.07.020.

Wotte, T., Strauss, H., Fugmann, A. and Garbe-Schönberg, D. (2012) 'Paired $\delta^{34}S$ data from carbonate-associated sulfate and chromium-reducible sulfur across the traditional Lower–Middle Cambrian boundary of W-Gondwana', *Geochimica et Cosmochimica Acta*, 85(0), pp. 228–253. doi: 10.1016/j.gca.2012.02.013.

Wynn, P. M., Fairchild, I. J., Baker, A., Baldini, J. U. L. and McDermott, F. (2008) 'Isotopic archives of sulphate in speleothems', *Geochimica et Cosmochimica Acta*, 72(10), pp. 2465–2477. doi: 10.1016/j.gca.2008.03.002.

Xiao, S., McFadden, K. A., Peek, S., Kaufman, A. J., Zhou, C., Jiang, G. and Hu, J. (2012) 'Integrated chemostratigraphy of the Doushantuo Formation at the northern Xiaofenghe section (Yangtze Gorges, South China) and its implication for Ediacaran stratigraphic correlation and ocean redox models', *Precambrian Research*, 192–195(1), pp. 125–141. doi: 10.1016/j.precamres.2011.10.021.

Xiao, S., Narbonne, G. M. and Shields-Zhou, G. A. (2012) 'The Ediacaran Period', in Gradstein, F. M., Ogg, J. G., Schmitz, M. D., and Ogg, G. M. (eds) *The Geologic Time Scale 2012*. Elsevier Science Limited, pp. 413–435.

Xiao, S., Shen, B., Tang, Q., Kaufman, A. J., Yuan, X., Li, J. and Qian, M. (2014) 'Biostratigraphic and chemostratigraphic constraints on the age of early Neoproterozoic carbonate successions in North China', *Precambrian Research*, 246, pp. 208–225. doi: 10.1016/j.precamres.2014.03.004.

Xing, Y. (1996) *Chinese Stratigraphy Catalog- Neoproterozoic*. Beijing: Geological Publishing House.

Xue, Y., Cao, R., Tang, T., Yin, L., Yu, C. and Yang, J. (2001) 'The Sinian stratigraphic sequence of the Yangtze region and correlation to the Late Precambrian strata of North China', *Journal of Stratigraphy*, 25(3), pp. 207–234.

Yang, D.-B., Xu, W.-L., Xu, Y.-G., Wang, Q.-H., Pei, F.-P. and Wang, F. (2012) 'U–Pb ages and Hf isotope data from detrital zircons in the Neoproterozoic sandstones of northern Jiangsu and southern Liaoning Provinces, China: Implications for the Late Precambrian evolution of the southeastern North China Craton', *Precambrian Research*, 216–219(0), pp. 162–176. doi: http://dx.doi.org/10.1016/j.precamres.2012.07.002.

Zang, W. and Walter, M. R. (1992) 'Late Proterozoic and Early Cambrian microfossils and biostratigraphy, northern Anhui and Jiangsu, central-eastern China', *Precambrian Research*, 57(3–4), pp. 243–323. doi: 10.1016/0301-9268(92)90004-8.

Zhai, M., Hu, B., Zhao, T., Peng, P. and Meng, Q. (2015) 'Late Paleoproterozoic–Neoproterozoic multi-rifting events in the North China Craton and their geological significance: A study advance and review', *Tectonophysics*, 662, pp. 153–166. doi: 10.1016/j.tecto.2015.01.019.

Zhang, M., Huang, S., Xie, G., Wang, Q. and Hou, J. (2004) 'Application of LOWESS fit to strontium isotope stratigraphy', *Journal of Earth Sciences and Environment*, 26(2), pp. 1–5.

Zhang, S., Wang, X., Wang, H., Bjerrum, C. J., Hammarlund, E. U., Costa, M. M., Connelly, J. N., Zhang, B., Su, J. and Canfield, D. E. (2016) 'Sufficient oxygen for animal respiration 1,400 million years ago', *Proceedings of the National Academy of Sciences*, p. 1713–1716. doi: 10.1073/pnas.1523449113.

Zhang, S.-H., Zhao, Y., Ye, H. and Hu, G.-H. (2016) 'Early Neoproterozoic emplacement of the diabase sill swarms in the Liaodong Peninsula and pre-magmatic uplift of the southeastern North China Craton', *Precambrian Research*, 272, pp. 203–225. doi: 10.1016/j.precamres.2015.11.005.

Zhang, W. and Zhu, Z. (1979) 'Notes on some trilobites from the lower Cambrian Houjiashan Formation in southern and southwestern parts of North China', *Acta Palaeontologica Sinica*, 18(6), pp. 513–526.

Zhang, X. and Shu, D. (2013) 'Causes and consequences of the Cambrian explosion', *Science China Earth Sciences*, 57(5), pp. 930–942. doi: 10.1007/s11430-013-4751-x.

Zhang, X., Shu, D., Han, J., Zhang, Z., Liu, J. and Fu, D. (2014) 'Triggers for the Cambrian explosion: Hypotheses and problems', *Gondwana Research*, 25(3), pp. 896–909. doi: 10.1016/j.gr.2013.06.001.

REFERENCES

Zhao, F., Bottjer, D. J., Hu, S., Yin, Z. and Zhu, M. (2013) 'Complexity and diversity of eyes in early Cambrian ecosystems.', *Scientific reports*, 3, pp. 1–6. doi: 10.1038/srep02751.

Zhao, G., Sun, M., Wilde, S. A. and Sanzhong, L. (2005) 'Late Archean to Paleoproterozoic evolution of the North China Craton: key issues revisited', *Precambrian Research*, 136(2), pp. 177–202. doi: 10.1016/j.precamres.2004.10.002.

Zhao, G. (2013) *Precambrian Evolution of the North China Craton*. Elsevier.

Zhu, M., Babcock, L. E. and Peng, S. C. (2006) 'Advances in Cambrian stratigraphy and paleontology: Integrating correlation techniques, paleobiology, taphonomy and paleoenvironmental reconstruction', *Palaeoworld*, 15(3–4), pp. 217–222. doi: 10.1016/j.palwor.2006.10.016.

Zhu, M. (2010) 'The origin and Cambrian explosion of animals: fossil evidences from China', *Acta Palaeontologica Sinica*, 49(3), pp. 269–287.

Zhu, M., Babcock, L. E. and Peng, S. C. (2006) 'Advances in Cambrian stratigraphy and paleontology: Integrating correlation techniques, paleobiology, taphonomy and paleoenvironmental reconstruction', *Palaeoworld*, 15(3–4), pp. 217–222. doi: 10.1016/j.palwor.2006.10.016.

Zhu, M., Zhuravlev, A. Y., Wood, R. A., Zhao, F. and Sukhov, S. S. (2017) 'A deep root for the Cambrian explosion : Implications of new bio- and chemostratigraphy from the Siberian Platform', *Geology*, 45(5), pp. 1–4. doi: 10.1130/G38865.1.

Zhuravlev, A. Y. and Wood, R. A. (1996) 'Anoxia as the cause of the mid-Early Cambrian (Botomian) extinction event', *Geology*, 24(4), pp. 311–314. doi: 10.1130/0091-7613(1996)024<0311:AATCOT>2.3.CO.

Zhuravlev, A. Y. (1996) 'Reef ecosytem recovery after the Early Cambrian extinction', *Geological Society, London, Special Publications*, 102(1), pp. 79–96. doi: 10.1144/GSL.SP.1996.001.01.06.

Zhuravlev, A. Y. (1998) 'Outlines of the Siberian platform sequence stratigraphy in the Lower and lower Middle Cambrian (Lena-Aldan area)', *Revista Española de Paleontología*, pp. 105–114.

Zhuravlev, A. Y. and Naimark, E. B. (2005) 'Alpha, beta, or gamma: Numerical view on the Early Cambrian world', *Palaeogeography, Palaeoclimatology, Palaeoecology*, 220(1–2), pp. 207–225. doi: 10.1016/j.palaeo.2004.08.009.

Appendix A

Isotopes, elemental data for Xiaotan section

SSFs: small shelly fossils; CAS: carbonate-associated sulphate; Carbonate%: total HCl-leachable carbonate content; *S.-P.*: *Siphogonuchites triangularis-Paragloborilus subglobosus*; Sulphur isotope and CAS concentrations were analysed in the current study. Litho-, biostratigraphy and all other geochemical data are obtained from paired study of Li *et al.* (2013). Age model is deduced from radiometric ages of Dahai Member from Yang Chuan (see section 1.6.3). Elemental analyses in this Appendix represent total HCl-leachable elemental contents of bulk carbonate samples;

Sample	Height (m)	Age (Ma)	South China Stage	SSFs biozones	Stratigraphic unit	Lithology	$\delta^{13}C$ (‰)	$\delta^{18}O$ (‰)	$\delta^{34}S_{CAS}$ (‰)	[CAS] ppm	Carbonate% (%)	Mg/Ca (w/w)	Mn/Sr (w/w)
XT-2	73	526.67	Meishucunian		Shiyantou Fm.	Siltstone	-0.4	-14.0					
XT-1	72.7	526.67	Meishucunian		Shiyantou Fm.	Siltstone	0.6	-14.7					
XT-101	72.6	526.67	Meishucunian	*Watsonella crosbyi*	Dahai Mb., Zhujiaqing Fm.	Limestone	-4.1	-15.0	14.6	18.11	82.6	0.01	0.48
XT-102	72	526.69	Meishucunian	*Watsonella crosbyi*	Dahai Mb., Zhujiaqing Fm.	Limestone	-0.3	-14.8					
XT-103	71.6	526.70	Meishucunian	*Watsonella crosbyi*	Dahai Mb., Zhujiaqing Fm.	Limestone	-0.9	-14.5					
XT-104	70.6	526.73	Meishucunian	*Watsonella crosbyi*	Dahai Mb., Zhujiaqing Fm.	Limestone	-0.2	-14.9					
XT-105	69.8	526.75	Meishucunian	*Watsonella crosbyi*	Dahai Mb., Zhujiaqing Fm.	Limestone	-0.1	-15.1	25.2	27.53	78.6	0.02	0.15
XT-106	69.2	526.77	Meishucunian	*Watsonella crosbyi*	Dahai Mb., Zhujiaqing Fm.	Limestone	-0.2	-15.1					
XT-107	68.2	526.80	Meishucunian	*Watsonella crosbyi*	Dahai Mb., Zhujiaqing Fm.	Limestone	-0.2	-15.1	21.7	36.89	72.7	0.02	0.14
XT-108	67.5	526.82	Meishucunian	*Watsonella crosbyi*	Dahai Mb., Zhujiaqing Fm.	Limestone	1.0	-15.2					
XT-109	66.7	526.85	Meishucunian	*Watsonella crosbyi*	Dahai Mb., Zhujiaqing Fm.	Limestone	3.7	-10.9	21.9	19.30	94.1	0.01	0.66
XT-110	66.2	526.86	Meishucunian	*Watsonella crosbyi*	Dahai Mb., Zhujiaqing Fm.	Limestone	4.2	-11.9					
XT-111	64.2	526.92	Meishucunian	*Watsonella crosbyi*	Dahai Mb., Zhujiaqing Fm.	Limestone	5.5	-11.2	21.8	24.12	92.3	0.00	0.10
XT-112	63.6	526.94	Meishucunian	*Watsonella crosbyi*	Dahai Mb., Zhujiaqing Fm.	Limestone	5.7	-12.6					
XT-113	62.4	526.97	Meishucunian	*Watsonella crosbyi*	Dahai Mb., Zhujiaqing Fm.	Limestone	6.2	-12.3	20.5	16.63	89.8	0.00	0.07
XT-114	61	527.01	Meishucunian	*Watsonella crosbyi*	Dahai Mb., Zhujiaqing Fm.	Limestone	6.5	-12.3					
XT-115	59	527.07	Meishucunian	*Watsonella crosbyi*	Dahai Mb., Zhujiaqing Fm.	Limestone	5.7	-12.5	23.4	9.54	85.8	0.01	0.16
XT-116	57	527.13	Meishucunian	*Watsonella crosbyi*	Dahai Mb., Zhujiaqing Fm.	Limestone	5.9	-12.5					
XT-117	55.6	527.17	Meishucunian	*Watsonella crosbyi*	Dahai Mb., Zhujiaqing Fm.	Limestone	7.2	-11.5	26.6	35.17	93.6	0.01	0.02
XT-118	54.4	527.21	Meishucunian	*Watsonella crosbyi*	Dahai Mb., Zhujiaqing Fm.	Limestone	6.1	-11.5					
XT-119	53.1	527.24	Meishucunian	*Watsonella crosbyi*	Dahai Mb., Zhujiaqing Fm.	Limestone	7.0	-11.3	32.1	17.91	87.5	0.02	0.03
XT-120	51.9	527.28	Meishucunian	*Watsonella crosbyi*	Dahai Mb., Zhujiaqing Fm.	Limestone	7.1	-11.0					
XT-121	50.9	527.31	Meishucunian	*Watsonella crosbyi*	Dahai Mb., Zhujiaqing Fm.	Limestone	6.7	-11.0					
XT-122	48.9	527.37	Meishucunian	*Watsonella crosbyi*	Dahai Mb., Zhujiaqing Fm.	Limestone	6.0	-11.6					
XT-123	47.6	527.40	Meishucunian	*Watsonella crosbyi*	Dahai Mb., Zhujiaqing Fm.	Limestone	6.3	-11.8	23.2	22.11	95.9	0.01	0.03
XT-124	46.6	527.43	Meishucunian	*Watsonella crosbyi*	Dahai Mb., Zhujiaqing Fm.	Limestone	6.5	-11.9					
XT-125	45.4	527.47	Meishucunian	*Watsonella crosbyi*	Dahai Mb., Zhujiaqing Fm.	Limestone	6.7	-12.1	26.5	25.93	88.9	0.01	0.03
XT-126	44.2	527.50	Meishucunian	*Watsonella crosbyi*	Dahai Mb., Zhujiaqing Fm.	Limestone	6.6	-11.8					
XT-127	42.3	527.56	Meishucunian	*Watsonella crosbyi*	Dahai Mb., Zhujiaqing Fm.	Limestone	6.7	-11.9					
XT-128	40.4	527.62	Meishucunian	*Watsonella crosbyi*	Dahai Mb., Zhujiaqing Fm.	Limestone	6.9	-10.9					
XT-129	39.6	527.64	Meishucunian	*Watsonella crosbyi*	Dahai Mb., Zhujiaqing Fm.	Limestone	7.1	-10.8	30.0	15.94	91.1	0.01	0.02
XT-130	38	527.69	Meishucunian	*Watsonella crosbyi*	Dahai Mb., Zhujiaqing Fm.	Limestone	6.7	-11.3					
XT-131	37	527.72	Meishucunian	*Watsonella crosbyi*	Dahai Mb., Zhujiaqing Fm.	Limestone	6.9	-11.1	29.8	19.50	89.6	0.01	0.04
XT-132	35.5	527.76	Meishucunian	*Watsonella crosbyi*	Dahai Mb., Zhujiaqing Fm.	Limestone	7.3	-11.2					
XT-133	34.4	527.79	Meishucunian	*Watsonella crosbyi*	Dahai Mb., Zhujiaqing Fm.	Limestone	6.5	-12.0					
XT-134	33.2	527.83	Meishucunian	*Watsonella crosbyi*	Dahai Mb., Zhujiaqing Fm.	Limestone	7.1	-12.1					
XT-135	31.2	527.89	Meishucunian	*Watsonella crosbyi*	Dahai Mb., Zhujiaqing Fm.	Limestone	7.2	-12.2	28.3	24.96	87.4	0.01	0.02
XT-136	29.6	527.93	Meishucunian	*Watsonella crosbyi*	Dahai Mb., Zhujiaqing Fm.	Limestone	7.2	-12.5					
XT-137	28.6	527.96	Meishucunian	*Watsonella crosbyi*	Dahai Mb., Zhujiaqing Fm.	Limestone	6.9	-12.7					
XT-138	27	528.01	Meishucunian	*Watsonella crosbyi*	Dahai Mb., Zhujiaqing Fm.	Limestone	7.1	-10.9					
XT-139	25.4	528.06	Meishucunian	*Watsonella crosbyi*	Dahai Mb., Zhujiaqing Fm.	Limestone	6.4	-12.2	30.8	8.86	92.1	0.01	0.01
XT-140	24.5	528.08	Meishucunian	*Watsonella crosbyi*	Dahai Mb., Zhujiaqing Fm.	Limestone	6.0	-12.1					
XT-141	23.1	528.12	Meishucunian	*Watsonella crosbyi*	Dahai Mb., Zhujiaqing Fm.	Limestone	6.3	-12.2	32.6	9.98	88.3	0.01	0.10
XT-142	22	528.15	Meishucunian	*Watsonella crosbyi*	Dahai Mb., Zhujiaqing Fm.	Limestone	6.3	-12.3					
XT-143	20.3	528.20	Meishucunian	*Watsonella crosbyi*	Dahai Mb., Zhujiaqing Fm.	Limestone	6.7	-12.3					

Sample	Height (m)	Age (Ma)	South China Stage	SSFs biozones	Stratigraphic unit	Lithology	$\delta^{13}C$ (‰)	$\delta^{18}O$ (‰)	$\delta^{34}S_{CAS}$ (‰)	[CAS] ppm	Carbonate% (%)	Mg/Ca (w/w)	Mn/Sr (w/w)
XT-144	18.3	528.26	Meishucunian	*Watsonella crosbyi*	Dahai Mb., Zhujiaqing Fm.	Limestone	6.3	-12.0					
XT-145	16.3	528.32	Meishucunian	*Watsonella crosbyi*	Dahai Mb., Zhujiaqing Fm.	Limestone	6.5	-11.4	35.1	11.55	90.2	0.00	0.03
XT-146	14.8	528.37	Meishucunian	*Watsonella crosbyi*	Dahai Mb., Zhujiaqing Fm.	Limestone	5.9	-12.1					
XT-147	13.3	528.41	Meishucunian	*Watsonella crosbyi*	Dahai Mb., Zhujiaqing Fm.	Limestone	6.3	-12.1	31.0	7.32	85.3	0.01	0.08
XT-148	11.8	528.45	Meishucunian	*Watsonella crosbyi*	Dahai Mb., Zhujiaqing Fm.	Limestone	5.8	-11.8					
XT-149	10.8	528.48	Meishucunian	*Watsonella crosbyi*	Dahai Mb., Zhujiaqing Fm.	Limestone	4.6	-11.4	27.9	15.57	87.9	0.00	0.09
XT-150	9.3	528.53	Meishucunian	*Watsonella crosbyi*	Dahai Mb., Zhujiaqing Fm.	Limestone	4.7	-11.2					
XT-151	8.2	528.56	Meishucunian	*Watsonella crosbyi*	Dahai Mb., Zhujiaqing Fm.	Limestone	2.2	-11.7	18.3	21.95	74.6	0.02	0.68
XT-152	7.8	528.57	Meishucunian	*Watsonella crosbyi*	Dahai Mb., Zhujiaqing Fm.	Limestone	2.3	-11.8					
XT-153	6.8	528.60	Meishucunian	*Watsonella crosbyi*	Dahai Mb., Zhujiaqing Fm.	Limestone	1.1	-11.8	14.6	17.40	85.4	0.00	0.65
XT-154	6	528.62	Meishucunian	*Watsonella crosbyi*	Dahai Mb., Zhujiaqing Fm.	Limestone	0.9	-11.8					
XT-155	5	528.65	Meishucunian	*Watsonella crosbyi*	Dahai Mb., Zhujiaqing Fm.	Limestone	1.4	-11.5	11.9	11.77	84.0	0.01	0.54
XT-156	4.4	528.67	Meishucunian	*Watsonella crosbyi*	Dahai Mb., Zhujiaqing Fm.	Limestone	0.9	-11.5	14.2	14.38	81.8	0.01	0.40
XT-157	4.4	528.67	Meishucunian	*S. – P.*	Zhongyicun Mb., Zhujiaqing Fm.	Phosphatic dolostone	1.1	-10.8					
XT-158	2.9	528.76	Meishucunian	*S. – P.*	Zhongyicun Mb., Zhujiaqing Fm.	Phosphatic dolostone	-1.4	-10.7					
XT-159	2.3	528.80	Meishucunian	*S. – P.*	Zhongyicun Mb., Zhujiaqing Fm.	Phosphatic dolostone	-0.6	-10.8					
XT-160	1	528.87	Meishucunian	*S. – P.*	Zhongyicun Mb., Zhujiaqing Fm.	Phosphatic dolostone	-0.9	-10.6					
XT-161	0	528.93	Meishucunian	*S. – P.*	Zhongyicun Mb., Zhujiaqing Fm.	Phosphatic dolostone	0.0	-10.5					

Appendix B

Stratigraphic context, age model and litho-, biostratigraphy for Aldan-Lena Rivers sections

SSFs: small shelly fossils. TA: Tit-Ary section; LAB: Labaia section; AT: Achchagy-Tuydakh section; UT: Ulakhan-Tyoidukh section; UKT: Ulakhan-Kyyry-Tass section; AKT: AchchagyKyyry-Taas section; Z Myrs and ZHU: Zhurinsky-Mys section; IST: Isit section; DVO: Dvortsy section. Data of AT, AKT, Z Mys sections along the Lena river are obtained from pioneering study of Brasier *et al*. (1994) to fill the sampling gap in the current study. Calculation of age model and sedimentation rates is discussed in section 3.3.2.1.

Sample	Height (m)	Age (Ma)	Sedimentation rate Myr/m	Siberian Stage	Formation	Archaeocyathid biozones	Trilobite and SSFs biozones
TA40	619.0	512.87	0.011	Toyonian	Keteme		*Bergeroniellus ketemensis*
TA39	617.0	512.89	0.011	Toyonian	Keteme		*Bergeroniellus ketemensis*
TA38	616.0	512.90	0.011	Toyonian	Keteme		*Bergeroniellus ketemensis*
TA37	615.0	512.91	0.011	Toyonian	Keteme		*Bergeroniellus ketemensis*
TA36	613.0	512.93	0.011	Toyonian	Keteme		*Bergeroniellus ketemensis*
TA35	611.0	512.96	0.011	Toyonian	Keteme		*Bergeroniellus ketemensis*
TA34	609.0	512.98	0.011	Toyonian	Keteme		*Bergeroniellus ketemensis*
TA33	608.0	512.99	0.011	Toyonian	Keteme		*Bergeroniellus ketemensis*
TA32	606.0	513.01	0.011	Toyonian	Keteme		*Bergeroniellus ketemensis*
TA31	604.5	513.03	0.011	Toyonian	Keteme		*Bergeroniellus ketemensis*
TA30	603.0	513.05	0.011	Toyonian	Keteme		*Bergeroniellus ketemensis*
TA29	601.0	513.07	0.011	Toyonian	Keteme		*Bergeroniellus ketemensis*
TA28	600.0	513.08	0.011	Toyonian	Keteme		*Bergeroniellus ketemensis*
TA27	598.5	513.10	0.011	Toyonian	Keteme		*Bergeroniellus ketemensis*
TA26	597.0	513.11	0.011	Toyonian	Keteme		*Bergeroniellus ketemensis*
TA25	596.5	513.12	0.011	Toyonian	Keteme		*Bergeroniellus ketemensis*
TA24	592.5	513.16	0.011	Toyonian	Keteme		*Bergeroniellus ketemensis*
TA22	589.1	513.20	0.011	Toyonian	Keteme		*Bergeroniellus ketemensis*
TA21	588.2	513.21	0.011	Toyonian	Keteme		*Bergeroniellus ketemensis*
TA20	584.7	513.25	0.011	Toyonian	Keteme		*Bergeroniellus ketemensis*
TA19	582.7	513.27	0.011	Toyonian	Keteme		*Bergeroniellus ketemensis*
TA18	581.4	513.29	0.011	Toyonian	Keteme		*Bergeroniellus ketemensis*
TA17	580.2	513.30	0.011	Toyonian	Keteme		*Bergeroniellus ketemensis*
TA16	578.7	513.32	0.011	Toyonian	Keteme		*Bergeroniellus ketemensis*
TA15	575.7	513.35	0.011	Toyonian	Keteme		*Bergeroniellus ketemensis*
TA14	574.7	513.36	0.011	Toyonian	Keteme		*Bergeroniellus ketemensis*
TA13	574.2	513.37	0.011	Botomian	Kutorgina		*Bergeroniaspis ornata*
TA12	573.7	513.37	0.011	Botomian	Kutorgina		*Bergeroniaspis ornata*
TA11	571.7	513.40	0.011	Botomian	Kutorgina		*Bergeroniaspis ornata*
TA10	569.7	513.42	0.011	Botomian	Kutorgina		*Bergeroniaspis ornata*
TA09	567.7	513.44	0.011	Botomian	Kutorgina		*Bergeroniaspis ornata*
TA08	566.7	513.45	0.011	Botomian	Kutorgina		*Bergeroniaspis ornata*
TA07	565.9	513.46	0.011	Botomian	Kutorgina		*Bergeroniaspis ornata*
TA06	564.7	513.47	0.011	Botomian	Kutorgina		*Bergeroniaspis ornata*
TA05	563.7	513.49	0.011	Botomian	Kutorgina		*Bergeroniaspis ornata*
TA04	562.7	513.50	0.011	Botomian	Kutorgina		*Bergeroniaspis ornata*
TA03	561.7	513.51	0.011	Botomian	Kutorgina		*Bergeroniaspis ornata*
TA02	560.7	513.52	0.011	Botomian	Kutorgina		*Bergeroniaspis ornata*
TA01	559.7	513.53	0.011	Botomian	Kutorgina		*Bergeroniaspis ornata*

Sample	Height (m)	Age (Ma)	Sedimentation rate Myr/m	Siberian Stage	Formation	Archaeocyathid biozones	Trilobite and SSFs biozones
LAB92	553.7	513.60	0.011	Botomian	Kutorgina		*Bergeroniaspis ornata*
LAB91	551.7	513.62	0.011	Botomian	Kutorgina		*Bergeroniaspis ornata*
LAB90	549.7	513.64	0.011	Botomian	Kutorgina		*Bergeroniaspis ornata*
LAB89	547.7	513.66	0.011	Botomian	Kutorgina		*Bergeroniaspis ornata*
LAB88	545.7	513.69	0.011	Botomian	Kutorgina		*Bergeroniaspis ornata*
LAB87	543.7	513.71	0.011	Botomian	Kutorgina		*Bergeroniaspis ornata*
LAB86	541.7	513.73	0.011	Botomian	Kutorgina		*Bergeroniaspis ornata*
LAB85	539.7	513.75	0.011	Botomian	Kutorgina		*Bergeroniaspis ornata*
LAB84	536.7	513.79	0.011	Botomian	Kutorgina		*Bergeroniaspis ornata*
LAB83	534.7	513.81	0.011	Botomian	Kutorgina		*Bergeroniaspis ornata*
LAB82	532.8	513.83	0.011	Botomian	Kutorgina		*Bergeroniaspis ornata*
LAB81	528.8	513.87	0.011	Botomian	Kutorgina		*Bergeroniaspis ornata*
LAB80	526.8	513.90	0.011	Botomian	Kutorgina		*Bergeroniaspis ornata*
LAB79	524.8	513.92	0.011	Botomian	Kutorgina		*Bergeroniaspis ornata*
LAB78	522.8	513.94	0.011	Botomian	Kutorgina		*Bergeroniaspis ornata*
LAB77	520.8	513.96	0.011	Botomian	Kutorgina		*Bergeroniaspis ornata*
LAB76	518.8	513.99	0.011	Botomian	Kutorgina		*Bergeroniaspis ornata*
LAB75	516.3	514.01	0.011	Botomian	Kutorgina		*Bergeroniaspis ornata*
LAB74	515.3	514.03	0.011	Botomian	Kutorgina		*Bergeroniaspis ornata*
LAB73	513.3	514.05	0.011	Botomian	Kutorgina		*Bergeroniaspis ornata*
LAB72	511.3	514.07	0.011	Botomian	Kutorgina		*Bergeroniaspis ornata*
LAB71	509.3	514.09	0.011	Botomian	Kutorgina		*Bergeroniaspis ornata*
LAB64	507.3	514.11	0.011	Botomian	Kutorgina		*Bergeroniaspis ornata*
LAB70	505.3	514.14	0.011	Botomian	Kutorgina		*Bergeroniaspis ornata*
LAB69	503.3	514.16	0.011	Botomian	Kutorgina		*Bergeroniaspis ornata*
LAB68	501.3	514.18	0.011	Botomian	Kutorgina		*Bergeroniaspis ornata*
LAB67	499.3	514.20	0.011	Botomian	Kutorgina		*Bergeroniaspis ornata*
LAB66	497.3	514.23	0.011	Botomian	Kutorgina		*Bergeroniaspis ornata*
LAB65	495.3	514.25	0.011	Botomian	Kutorgina		*Bergeroniaspis ornata*
LAB63	494.0	514.26	0.011	Botomian	Kutorgina		*Bergeroniaspis ornata*
LAB62	492.0	514.29	0.011	Botomian	Kutorgina		*Bergeroniaspis ornata*
LAB61	490.0	514.31	0.011	Botomian	Kutorgina		*Bergeroniaspis ornata*
LAB60	488.0	514.33	0.011	Botomian	Kutorgina		*Bergeroniaspis ornata*
LAB59	486.0	514.35	0.011	Botomian	Kutorgina		*Bergeroniaspis ornata*
LAB58	484.0	514.37	0.011	Botomian	Kutorgina		*Bergeroniaspis ornata*
LAB57	483.2	514.38	0.011	Botomian	Kutorgina		*Bergeroniaspis ornata*
LAB56	482.2	514.39	0.011	Botomian	Kutorgina		*Bergeroniaspis ornata*
LAB55	479.7	514.42	0.011	Botomian	Kutorgina		*Bergeroniellus asiaticus*
LAB54	478.7	514.43	0.011	Botomian	Kutorgina		*Bergeroniellus asiaticus*

Sample	Height (m)	Age (Ma)	Sedimentation rate Myr/m	Siberian Stage	Formation	Archaeocyathid biozones	Trilobite and SSFs biozones
LAB53	477.7	514.45	0.011	Botomian	Kutorgina		*Bergeroniellus asiaticus*
LAB51	473.7	514.49	0.011	Botomian	Kutorgina		*Bergeroniellus asiaticus*
LAB50	471.7	514.51	0.011	Botomian	Kutorgina		*Bergeroniellus asiaticus*
LAB48	467.7	514.56	0.011	Botomian	Kutorgina		*Bergeroniellus asiaticus*
LAB47	465.7	514.58	0.011	Botomian	Kutorgina		*Bergeroniellus asiaticus*
LAB46	463.7	514.60	0.011	Botomian	Kutorgina		*Bergeroniellus asiaticus*
LAB45	462.7	514.61	0.011	Botomian	Kutorgina		*Bergeroniellus asiaticus*
LAB44	459.7	514.65	0.011	Botomian	Kutorgina		*Bergeroniellus asiaticus*
LAB43	457.7	514.67	0.011	Botomian	Kutorgina		*Bergeroniellus asiaticus*
LAB42	455.7	514.69	0.011	Botomian	Kutorgina		*Bergeroniellus asiaticus*
LAB41	453.0	514.72	0.011	Botomian	Kutorgina		*Bergeroniellus asiaticus*
LAB40	451.0	514.74	0.011	Botomian	Kutorgina		*Bergeroniellus asiaticus*
LAB39	449.0	514.77	0.011	Botomian	Kutorgina		*Bergeroniellus asiaticus*
LAB38	447.0	514.79	0.011	Botomian	Kutorgina		*Bergeroniellus asiaticus*
LAB37	446.0	514.80	0.011	Botomian	Kutorgina		*Bergeroniellus asiaticus*
LAB36	445.0	514.81	0.011	Botomian	Kutorgina		*Bergeroniellus asiaticus*
LAB35	444.0	514.82	0.011	Botomian	Kutorgina		*Bergeroniellus asiaticus*
LAB34	442.0	514.84	0.011	Botomian	Kutorgina		*Bergeroniellus asiaticus*
LAB33	440.0	514.87	0.011	Botomian	Kutorgina		*Bergeroniellus asiaticus*
LAB32	438.0	514.89	0.011	Botomian	Kutorgina		*Bergeroniellus asiaticus*
LAB30	434.0	514.93	0.011	Botomian	Kutorgina		*Bergeroniellus asiaticus*
LAB29	432.0	514.96	0.011	Botomian	Kutorgina		*Bergeroniellus asiaticus*
LAB28	430.0	514.98	0.011	Botomian	Kutorgina		*Bergeroniellus asiaticus*
LAB27	428.0	515.00	0.011	Botomian	Kutorgina		*Bergeroniellus asiaticus*
LAB26	426.0	515.02	0.011	Botomian	Kutorgina		*Bergeroniellus asiaticus*
LAB25	424.0	515.04	0.011	Botomian	Kutorgina		*Bergeroniellus asiaticus*
LAB24	421.9	515.07	0.011	Botomian	Kutorgina		*Bergeroniellus asiaticus*
LAB23	419.9	515.09	0.011	Botomian	Kutorgina		*Bergeroniellus asiaticus*
LAB22	417.9	515.11	0.011	Botomian	Kutorgina		*Bergeroniellus asiaticus*
LAB21	415.9	515.13	0.011	Botomian	Kutorgina		*Bergeroniellus asiaticus*
LAB20	414.9	515.15	0.011	Botomian	Kutorgina		*Bergeroniellus asiaticus*
LAB19	412.9	515.17	0.011	Botomian	Kutorgina		*Bergeroniellus asiaticus*
LAB18	410.9	515.19	0.011	Botomian	Kutorgina		*Bergeroniellus asiaticus*
LAB17	408.9	515.21	0.011	Botomian	Kutorgina		*Bergeroniellus asiaticus*
LAB16	407.9	515.22	0.011	Botomian	Kutorgina		*Bergeroniellus asiaticus*
LAB15	406.7	515.24	0.011	Botomian	Kutorgina		*Bergeroniellus asiaticus*
LAB13	404.7	515.26	0.011	Botomian	Kutorgina		*Bergeroniellus asiaticus*
LAB12	403.7	515.27	0.011	Botomian	Kutorgina		*Bergeroniellus asiaticus*
LAB11	402.4	515.29	0.011	Botomian	Kutorgina		*Bergeroniellus asiaticus*

Sample	Height (m)	Age (Ma)	Sedimentation rate Myr/m	Siberian Stage	Formation	Archaeocyathid biozones	Trilobite and SSFs biozones
LAB10	402.2	515.29	0.011	Botomian	Kutorgina		*Bergeroniellus asiaticus*
LAB09	401.7	515.29	0.011	Botomian	Kutorgina		*Bergeroniellus asiaticus*
LAB08	401.3	515.30	0.011	Botomian	Kutorgina		*Bergeroniellus asiaticus*
LAB07	401.0	515.30	0.011	Botomian	Kutorgina		*Bergeroniellus asiaticus*
LAB06	400.5	515.31	0.011	Botomian	Kutorgina		*Bergeroniellus asiaticus*
LAB05	400.0	515.31	0.011	Botomian	Kutorgina		*Bergeroniellus asiaticus*
LAB04	399.7	515.32	0.011	Botomian	Kutorgina		*Bergeroniellus asiaticus*
LAB03	399.5	515.32	0.011	Botomian	Kutorgina		*Bergeroniellus asiaticus*
LAB02	399.2	515.32	0.011	Botomian	Kutorgina		*Bergeroniellus asiaticus*
LAB01	398.7	515.33	0.011	Botomian	Kutorgina		*Bergeroniellus asiaticus*
AT 20-141	395.2	515.37	0.011	Botomian	Kutorgina		*Bergeroniellus asiaticus*
AT 20-140	394.2	515.38	0.011	Botomian	Kutorgina		*Bergeroniellus asiaticus*
AT 20-139	393.2	515.39	0.011	Botomian	Kutorgina		*Bergeroniellus asiaticus*
AT 20-138	392.2	515.40	0.011	Botomian	Kutorgina		*Bergeroniellus asiaticus*
AT 20-137	391.2	515.41	0.011	Botomian	Kutorgina		*Bergeroniellus asiaticus*
AT 20-136	390.2	515.42	0.011	Botomian	Kutorgina		*Bergeroniellus asiaticus*
AT 20-135	389.2	515.43	0.011	Botomian	Kutorgina		*Bergeroniellus asiaticus*
AT 20-134	388.2	515.44	0.011	Botomian	Kutorgina		*Bergeroniellus asiaticus*
AT 20-133	387.2	515.46	0.011	Botomian	Kutorgina		*Bergeroniellus asiaticus*
AT 20-132	386.2	515.47	0.011	Botomian	Kutorgina		*Bergeroniellus asiaticus*
AT 19-131	385.2	515.48	0.011	Botomian	Kutorgina		*Bergeroniellus asiaticus*
AT 19-130	384.2	515.49	0.011	Botomian	Kutorgina		*Bergeroniellus asiaticus*
AT 19-129	383.2	515.50	0.011	Botomian	Kutorgina		*Bergeroniellus asiaticus*
AT 19-128	382.2	515.51	0.011	Botomian	Kutorgina		*Bergeroniellus asiaticus*
AT 18-127	381.2	515.52	0.011	Botomian	Kutorgina		*Bergeroniellus asiaticus*
AT 18-126	380.2	515.53	0.011	Botomian	Kutorgina		*Bergeroniellus asiaticus*
AT 18-125	379.2	515.54	0.011	Botomian	Kutorgina		*Bergeroniellus asiaticus*
AT 18-124	378.2	515.56	0.011	Botomian	Kutorgina		*Bergeroniellus asiaticus*
AT 18-123	377.2	515.57	0.011	Botomian	Kutorgina		*Bergeroniellus asiaticus*
AT 18-122	376.2	515.58	0.011	Botomian	Kutorgina		*Bergeroniellus asiaticus*
AT 17-121	373.7	515.61	0.011	Botomian	Kutorgina		*Bergeroniellus asiaticus*
AT 17-120	372.7	515.62	0.011	Botomian	Kutorgina		*Bergeroniellus asiaticus*
AT 17-119	371.7	515.63	0.011	Botomian	Kutorgina		*Bergeroniellus asiaticus*
AT 17-118	370.7	515.64	0.011	Botomian	Kutorgina		*Bergeroniellus asiaticus*
AT 17-117	369.7	515.65	0.011	Botomian	Kutorgina		*Bergeroniellus asiaticus*
AT 17-116	368.7	515.66	0.011	Botomian	Kutorgina		*Bergeroniellus asiaticus*
AT 17-115	367.7	515.67	0.011	Botomian	Kutorgina		*Bergeroniellus asiaticus*
AT 16-114	366.7	515.68	0.011	Botomian	Kutorgina		*Bergeroniellus asiaticus*
AT 16-113	365.7	515.70	0.011	Botomian	Kutorgina		*Bergeroniellus asiaticus*

Sample	Height (m)	Age (Ma)	Sedimentation rate Myr/m	Siberian Stage	Formation	Archaeocyathid biozones	Trilobite and SSFs biozones
AT 16-112	364.7	515.71	0.011	Botomian	Kutorgina		*Bergeroniellus asiaticus*
AT 16-111	363.7	515.72	0.011	Botomian	Kutorgina		*Bergeroniellus asiaticus*
AT 16-109	361.7	515.74	0.011	Botomian	Kutorgina		*Bergeroniellus asiaticus*
AT 16-108	360.7	515.75	0.011	Botomian	Kutorgina		*Bergeroniellus asiaticus*
AT 16-107	359.7	515.76	0.011	Botomian	Kutorgina		*Bergeroniellus asiaticus*
AT 16-106	358.7	515.77	0.011	Botomian	Kutorgina		*Bergeroniellus asiaticus*
AT 16-105	357.7	515.78	0.011	Botomian	Kutorgina		*Bergeroniellus asiaticus*
AT 16-103	355.7	515.81	0.011	Botomian	Kutorgina		*Bergeroniellus asiaticus*
AT 16-102	354.7	515.82	0.011	Botomian	Kutorgina		*Bergeroniellus asiaticus*
AT 16-100	352.7	515.84	0.011	Botomian	Kutorgina		*Bergeroniellus asiaticus*
AT 16-99	351.7	515.85	0.011	Botomian	Kutorgina		*Bergeroniellus asiaticus*
AT 16-98	350.7	515.86	0.011	Botomian	Kutorgina		*Bergeroniellus asiaticus*
AT 15-95	349.7	515.87	0.011	Botomian	Sinsk		*Bergeroniellus gurarii*
AT 15-94	348.7	515.88	0.011	Botomian	Sinsk		*Bergeroniellus gurarii*
AT 15-93	347.7	515.90	0.011	Botomian	Sinsk		*Bergeroniellus gurarii*
AT 15-92	346.7	515.91	0.011	Botomian	Sinsk		*Bergeroniellus gurarii*
AT 15-91	345.7	515.92	0.011	Botomian	Sinsk		*Bergeroniellus gurarii*
AT 15-90	344.7	515.93	0.011	Botomian	Sinsk		*Bergeroniellus gurarii*
AT 14-89	343.7	515.94	0.011	Botomian	Sinsk		*Bergeroniellus gurarii*
AT 14-88	342.7	515.95	0.011	Botomian	Sinsk		*Bergeroniellus gurarii*
AT 13-86	341.7	515.96	0.011	Botomian	Sinsk		*Bergeroniellus gurarii*
AT 13-85	340.7	515.97	0.011	Botomian	Sinsk		*Bergeroniellus gurarii*
AT 13-84	339.7	515.99	0.011	Botomian	Sinsk		*Bergeroniellus gurarii*
AT 13-82	337.7	516.01	0.011	Botomian	Sinsk		*Bergeroniellus gurarii*
AT 13-81	336.7	516.02	0.011	Botomian	Sinsk		*Bergeroniellus gurarii*
AT 13-80	335.7	516.03	0.011	Botomian	Sinsk		*Bergeroniellus gurarii*
AT 13-79	334.7	516.04	0.011	Botomian	Sinsk		*Bergeroniellus gurarii*
AT 13-78	333.7	516.05	0.011	Botomian	Sinsk		*Bergeroniellus gurarii*
AT 13-77	332.7	516.06	0.011	Botomian	Sinsk		*Bergeroniellus gurarii*
AT 13-76	331.7	516.07	0.011	Botomian	Sinsk		*Bergeroniellus gurarii*
UT36	330.2	516.09	0.011	Botomian	Sinsk		*Bergeroniellus gurarii*
UT35	329.7	516.10	0.011	Botomian	Sinsk		*Bergeroniellus gurarii*
UT34	329.2	516.10	0.011	Botomian	Sinsk		*Bergeroniellus gurarii*
UT33	328.7	516.11	0.011	Botomian	Sinsk		*Bergeroniellus gurarii*
UT32	328.1	516.11	0.011	Botomian	Sinsk		*Bergeroniellus gurarii*
UT31	327.7	516.12	0.011	Botomian	Sinsk		*Bergeroniellus gurarii*
UT30	326.7	516.13	0.011	Botomian	Sinsk		*Bergeroniellus gurarii*
UT29	325.7	516.14	0.011	Botomian	Sinsk		*Bergeroniellus gurarii*
UT28	325.2	516.15	0.011	Botomian	Sinsk		*Bergeroniellus gurarii*

Sample	Height (m)	Age (Ma)	Sedimentation rate Myr/m	Siberian Stage	Formation	Archaeocyathid biozones	Trilobite and SSFs biozones
UT27	324.2	516.16	0.011	Botomian	Sinsk		*Bergeroniellus gurarii*
UT26	322.9	516.17	0.011	Botomian	Sinsk		*Bergeroniellus gurarii*
UT25	322.2	516.18	0.011	Botomian	Sinsk		*Bergeroniellus gurarii*
UT24	321.2	516.19	0.011	Botomian	Sinsk		*Bergeroniellus gurarii*
UT23	320.2	516.20	0.011	Botomian	Sinsk		*Bergeroniellus gurarii*
UT22	319.2	516.21	0.011	Botomian	Sinsk		*Bergeroniellus gurarii*
UT21	318.2	516.23	0.011	Botomian	Sinsk		*Bergeroniellus gurarii*
UT20	317.2	516.24	0.011	Botomian	Sinsk		*Bergeroniellus gurarii*
UT19	316.2	516.25	0.011	Botomian	Sinsk		*Bergeroniellus gurarii*
UT18	315.2	516.26	0.011	Botomian	Sinsk		*Bergeroniellus gurarii*
UT17	314.2	516.27	0.011	Botomian	Sinsk		*Bergeroniellus gurarii*
UKT102	313.0	516.28	0.011	Botomian	Sinsk		*Bergeroniellus gurarii*
UKT101	312.5	516.29	0.011	Botomian	Sinsk		*Bergeroniellus gurarii*
UKT100	312.0	516.29	0.011	Botomian	Sinsk		*Bergeroniellus gurarii*
UKT099	311.5	516.30	0.011	Botomian	Sinsk		*Bergeroniellus gurarii*
UKT098	311.0	516.31	0.011	Botomian	Sinsk		*Bergeroniellus gurarii*
UKT097	310.5	516.31	0.011	Botomian	Sinsk		*Bergeroniellus gurarii*
UKT096	310.1	516.32	0.011	Botomian	Sinsk		*Bergeroniellus gurarii*
UKT095	309.6	516.32	0.011	Botomian	Sinsk		*Bergeroniellus gurarii*
UKT094	309.0	516.33	0.011	Botomian	Sinsk		*Bergeroniellus gurarii*
UKT093	308.5	516.33	0.011	Botomian	Sinsk		*Bergeroniellus gurarii*
UKT092	308.0	516.34	0.011	Botomian	Sinsk		*Bergeroniellus gurarii*
UKT091	307.5	516.34	0.011	Botomian	Sinsk		*Bergeroniellus gurarii*
UKT090	307.0	516.35	0.011	Botomian	Sinsk		*Bergeroniellus gurarii*
UKT089	302.2	516.40	0.011	Botomian	Sinsk		*Bergeroniellus gurarii*
UKT088	301.7	516.41	0.011	Botomian	Sinsk		*Bergeroniellus gurarii*
UKT087	301.2	516.42	0.011	Botomian	Sinsk		*Bergeroniellus gurarii*
UKT086	300.6	516.42	0.011	Botomian	Sinsk		*Bergeroniellus gurarii*
UKT084	300.0	516.43	0.011	Botomian	Perekhod	*Botomocyathus zelenovi - Porocyathus squamosus*	*Bergeroniellus micmacciformis - Erbiella*
UKT083	299.4	516.44	0.011	Botomian	Perekhod	*Botomocyathus zelenovi - Porocyathus squamosus*	*Bergeroniellus micmacciformis - Erbiella*
UKT082	298.8	516.44	0.011	Botomian	Perekhod	*Botomocyathus zelenovi - Porocyathus squamosus*	*Bergeroniellus micmacciformis - Erbiella*
UKT081	298.7	516.44	0.011	Botomian	Perekhod	*Botomocyathus zelenovi - Porocyathus squamosus*	*Bergeroniellus micmacciformis - Erbiella*
UKT080	298.4	516.45	0.011	Botomian	Perekhod	*Botomocyathus zelenovi - Porocyathus squamosus*	*Bergeroniellus micmacciformis - Erbiella*
UKT079	297.7	516.45	0.011	Botomian	Perekhod	*Botomocyathus zelenovi - Porocyathus squamosus*	*Bergeroniellus micmacciformis - Erbiella*
UKT078	297.2	516.46	0.011	Botomian	Perekhod	*Botomocyathus zelenovi - Porocyathus squamosus*	*Bergeroniellus micmacciformis - Erbiella*
UKT077	296.9	516.46	0.011	Botomian	Perekhod	*Botomocyathus zelenovi - Porocyathus squamosus*	*Bergeroniellus micmacciformis - Erbiella*
UKT076	296.4	516.47	0.011	Botomian	Perekhod	*Botomocyathus zelenovi - Porocyathus squamosus*	*Bergeroniellus micmacciformis - Erbiella*
UKT075	295.9	516.47	0.011	Botomian	Perekhod	*Botomocyathus zelenovi - Porocyathus squamosus*	*Bergeroniellus micmacciformis - Erbiella*
UKT074	295.3	516.48	0.011	Botomian	Perekhod	*Botomocyathus zelenovi - Porocyathus squamosus*	*Bergeroniellus micmacciformis - Erbiella*

Sample	Height (m)	Age (Ma)	Sedimentation rate Myr/m	Siberian Stage	Formation	Archaeocyathid biozones	Trilobite and SSFs biozones
UKT073	294.4	516.49	0.011	Botomian	Perekhod	*Botomocyathus zelenovi - Porocyathus squamosus*	*Bergeroniellus micmacciformis - Erbiella*
UKT072	293.4	516.50	0.011	Botomian	Perekhod	*Botomocyathus zelenovi - Porocyathus squamosus*	*Bergeroniellus micmacciformis - Erbiella*
UKT071	291.9	516.52	0.011	Botomian	Perekhod	*Botomocyathus zelenovi - Porocyathus squamosus*	*Bergeroniellus micmacciformis - Erbiella*
UKT070	290.9	516.53	0.011	Botomian	Perekhod	*Botomocyathus zelenovi - Porocyathus squamosus*	*Bergeroniellus micmacciformis - Erbiella*
UKT069	289.7	516.54	0.011	Botomian	Perekhod	*Botomocyathus zelenovi - Porocyathus squamosus*	*Bergeroniellus micmacciformis - Erbiella*
UKT068	287.7	516.57	0.011	Botomian	Perekhod	*Botomocyathus zelenovi - Porocyathus squamosus*	*Bergeroniellus micmacciformis - Erbiella*
UKT067	286.2	516.58	0.011	Botomian	Perekhod	*Botomocyathus zelenovi - Porocyathus squamosus*	*Bergeroniellus micmacciformis - Erbiella*
UKT066	285.2	516.59	0.011	Botomian	Perekhod	*Botomocyathus zelenovi - Porocyathus squamosus*	*Bergeroniellus micmacciformis - Erbiella*
UKT065	284.2	516.60	0.011	Botomian	Perekhod	*Botomocyathus zelenovi - Porocyathus squamosus*	*Bergeroniellus micmacciformis - Erbiella*
UKT064	283.2	516.62	0.011	Botomian	Perekhod	*Botomocyathus zelenovi - Porocyathus squamosus*	*Bergeroniellus micmacciformis - Erbiella*
UKT063	282.2	516.63	0.011	Botomian	Perekhod	*Botomocyathus zelenovi - Porocyathus squamosus*	*Bergeroniellus micmacciformis - Erbiella*
UKT062	281.2	516.64	0.011	Botomian	Perekhod	*Botomocyathus zelenovi - Porocyathus squamosus*	*Bergeroniellus micmacciformis - Erbiella*
UKT061	279.7	516.66	0.011	Botomian	Perekhod	*Botomocyathus zelenovi - Porocyathus squamosus*	*Bergeroniellus micmacciformis - Erbiella*
UKT060	278.7	516.67	0.011	Botomian	Perekhod	*Botomocyathus zelenovi - Porocyathus squamosus*	*Bergeroniellus micmacciformis - Erbiella*
UKT059	277.7	516.68	0.011	Botomian	Perekhod	*Botomocyathus zelenovi - Porocyathus squamosus*	*Bergeroniellus micmacciformis - Erbiella*
UT16	276.8	516.69	0.011	Botomian	Perekhod	*Botomocyathus zelenovi - Porocyathus squamosus*	*Bergeroniellus micmacciformis - Erbiella*
UT15	275.8	516.70	0.011	Botomian	Perekhod	*Botomocyathus zelenovi - Porocyathus squamosus*	*Bergeroniellus micmacciformis - Erbiella*
UT14	274.8	516.71	0.011	Botomian	Perekhod	*Botomocyathus zelenovi - Porocyathus squamosus*	*Bergeroniellus micmacciformis - Erbiella*
UT13	273.8	516.72	0.011	Botomian	Perekhod	*Botomocyathus zelenovi - Porocyathus squamosus*	*Bergeroniellus micmacciformis - Erbiella*
UT12	272.8	516.73	0.011	Botomian	Perekhod	*Botomocyathus zelenovi - Porocyathus squamosus*	*Bergeroniellus micmacciformis - Erbiella*
UT09	269.8	516.77	0.011	Botomian	Perekhod	*Botomocyathus zelenovi - Porocyathus squamosus*	*Bergeroniellus micmacciformis - Erbiella*
UT08	268.8	516.78	0.011	Botomian	Perekhod	*Botomocyathus zelenovi - Porocyathus squamosus*	*Bergeroniellus micmacciformis - Erbiella*
UT07	268.1	516.78	0.011	Botomian	Perekhod	*Botomocyathus zelenovi - Porocyathus squamosus*	*Bergeroniellus micmacciformis - Erbiella*
UT06	267.6	516.79	0.011	Botomian	Perekhod	*Botomocyathus zelenovi - Porocyathus squamosus*	*Bergeroniellus micmacciformis - Erbiella*
UT05	267.1	516.80	0.011	Botomian	Perekhod	*Botomocyathus zelenovi - Porocyathus squamosus*	*Bergeroniellus micmacciformis - Erbiella*
UT04	266.6	516.80	0.011	Botomian	Perekhod	*Botomocyathus zelenovi - Porocyathus squamosus*	*Bergeroniellus micmacciformis - Erbiella*
UT03	266.2	516.81	0.011	Botomian	Perekhod	*Botomocyathus zelenovi - Porocyathus squamosus*	*Bergeroniellus micmacciformis - Erbiella*
UT02	265.7	516.81	0.011	Botomian	Perekhod	*Botomocyathus zelenovi - Porocyathus squamosus*	*Bergeroniellus micmacciformis - Erbiella*
UT01	264.7	516.82	0.011	Botomian	Perekhod	*Botomocyathus zelenovi - Porocyathus squamosus*	*Bergeroniellus micmacciformis - Erbiella*
UKT054	259.8	516.88	0.011	Botomian	Perekhod	*Botomocyathus zelenovi - Porocyathus squamosus*	*Bergeroniellus micmacciformis - Erbiella*
UKT053	258.8	516.89	0.011	Botomian	Perekhod	*Botomocyathus zelenovi - Porocyathus squamosus*	*Bergeroniellus micmacciformis - Erbiella*
UKT052	258.3	516.89	0.011	Botomian	Perekhod	*Botomocyathus zelenovi - Porocyathus squamosus*	*Bergeroniellus micmacciformis - Erbiella*
UKT051	257.8	516.90	0.011	Botomian	Perekhod	*Botomocyathus zelenovi - Porocyathus squamosus*	*Bergeroniellus micmacciformis - Erbiella*
UKT050	256.7	516.91	0.011	Botomian	Perekhod	*Botomocyathus zelenovi - Porocyathus squamosus*	*Bergeroniellus micmacciformis - Erbiella*
UKT049	255.7	516.92	0.011	Botomian	Perekhod	*Botomocyathus zelenovi - Porocyathus squamosus*	*Bergeroniellus micmacciformis - Erbiella*
UKT048	254.7	516.93	0.011	Botomian	Perekhod	*Botomocyathus zelenovi - Porocyathus squamosus*	*Bergeroniellus micmacciformis - Erbiella*
UKT047	253.7	516.95	0.011	Atdabanian	Perekhod	*Fansycyathus lermontovae*	*Judomia*
UKT046	252.7	516.96	0.011	Atdabanian	Perekhod	*Fansycyathus lermontovae*	*Judomia*
UKT045	251.7	516.97	0.011	Atdabanian	Perekhod	*Fansycyathus lermontovae*	*Judomia*

Sample	Height (m)	Age (Ma)	Sedimentation rate Myr/m	Siberian Stage	Formation	Archaeocyathid biozones	Trilobite and SSFs biozones
UKT044	250.6	516.98	0.011	Atdabanian	Perekhod	*Fansycyathus lermontovae*	*Judomia*
UKT043	249.6	516.99	0.011	Atdabanian	Perekhod	*Fansycyathus lermontovae*	*Judomia*
UKT042	248.8	517.00	0.011	Atdabanian	Perekhod	*Fansycyathus lermontovae*	*Judomia*
UKT041	247.6	517.03	0.024	Atdabanian	Perekhod	*Fansycyathus lermontovae*	*Judomia*
UKT040	247.1	517.04	0.024	Atdabanian	Perekhod	*Fansycyathus lermontovae*	*Judomia*
UKT039	246.1	517.06	0.024	Atdabanian	Perekhod	*Fansycyathus lermontovae*	*Judomia*
UKT038	245.6	517.08	0.024	Atdabanian	Perekhod	*Fansycyathus lermontovae*	*Judomia*
UKT037	244.6	517.10	0.024	Atdabanian	Perekhod	*Fansycyathus lermontovae*	*Judomia*
UKT036	243.6	517.12	0.024	Atdabanian	Perekhod	*Fansycyathus lermontovae*	*Judomia*
UKT035	242.6	517.15	0.024	Atdabanian	Perekhod	*Fansycyathus lermontovae*	*Judomia*
UKT034	241.1	517.18	0.024	Atdabanian	Perekhod	*Fansycyathus lermontovae*	*Judomia*
UKT033	238.6	517.24	0.024	Atdabanian	Perekhod	*Fansycyathus lermontovae*	*Judomia*
UKT032	237.8	517.26	0.024	Atdabanian	Perekhod	*Fansycyathus lermontovae*	*Judomia*
UKT031	236.0	517.30	0.024	Atdabanian	Perekhod	*Fansycyathus lermontovae*	*Judomia*
UKT030	235.3	517.32	0.024	Atdabanian	Perekhod	*Fansycyathus lermontovae*	*Judomia*
UKT028	234.3	517.34	0.024	Atdabanian	Perekhod	*Fansycyathus lermontovae*	*Judomia*
UKT027	232.6	517.38	0.024	Atdabanian	Perekhod	*Fansycyathus lermontovae*	*Judomia*
UKT026	232.4	517.39	0.024	Atdabanian	Perekhod	*Fansycyathus lermontovae*	*Judomia*
UKT025	231.6	517.41	0.024	Atdabanian	Perekhod	*Fansycyathus lermontovae*	*Judomia*
UKT024	226.2	517.53	0.024	Atdabanian	Perekhod	*Fansycyathus lermontovae*	*Judomia*
UKT023	225.8	517.54	0.024	Atdabanian	Perekhod	*Fansycyathus lermontovae*	*Judomia*
UKT022	224.6	517.57	0.024	Atdabanian	Perekhod	*Fansycyathus lermontovae*	*Judomia*
UKT021	223.2	517.61	0.024	Atdabanian	Perekhod	*Fansycyathus lermontovae*	*Judomia*
UKT020	222.2	517.63	0.024	Atdabanian	Perekhod	*Fansycyathus lermontovae*	*Judomia*
UKT019	221.2	517.65	0.024	Atdabanian	Perekhod	*Fansycyathus lermontovae*	*Judomia*
UKT018	216.2	517.77	0.024	Atdabanian	Pestrotsvet	*Nochoroicyathus kokoulini*	*Judomia*
UKT017	213.9	517.82	0.024	Atdabanian	Pestrotsvet	*Nochoroicyathus kokoulini*	*Judomia*
UKT016	213.2	517.84	0.024	Atdabanian	Pestrotsvet	*Nochoroicyathus kokoulini*	*Judomia*
UKT015	212.3	517.86	0.024	Atdabanian	Pestrotsvet	*Nochoroicyathus kokoulini*	*Judomia*
UKT014	211.8	517.87	0.024	Atdabanian	Pestrotsvet	*Nochoroicyathus kokoulini*	*Judomia*
UKT013	211.0	517.89	0.024	Atdabanian	Pestrotsvet	*Nochoroicyathus kokoulini*	*Judomia*
UKT012	208.0	517.96	0.024	Atdabanian	Pestrotsvet	*Nochoroicyathus kokoulini*	*Judomia*
UKT011	206.9	517.99	0.024	Atdabanian	Pestrotsvet	*Nochoroicyathus kokoulini*	*Judomia*
UKT010	206.0	518.01	0.024	Atdabanian	Pestrotsvet	*Nochoroicyathus kokoulini*	*Judomia*
UKT009	205.0	518.04	0.024	Atdabanian	Pestrotsvet	*Nochoroicyathus kokoulini*	*Judomia*
UKT008	204.5	518.05	0.024	Atdabanian	Pestrotsvet	*Nochoroicyathus kokoulini*	*Judomia*
UKT007	203.6	518.07	0.024	Atdabanian	Pestrotsvet	*Nochoroicyathus kokoulini*	*Judomia*
UKT006	202.3	518.10	0.024	Atdabanian	Pestrotsvet	*Carinacyathus pinus*	*Delgadell anabara*
UKT005	201.8	518.11	0.024	Atdabanian	Pestrotsvet	*Carinacyathus pinus*	*Delgadell anabara*

Sample	Height (m)	Age (Ma)	Sedimentation rate Myr/m	Siberian Stage	Formation	Archaeocyathid biozones	Trilobite and SSFs biozones
UKT004	201.7	518.11	0.024	Atdabanian	Pestrotsvet	*Carinacyathus pinus*	*Delgadell anabara*
UKT003	201.3	518.12	0.024	Atdabanian	Pestrotsvet	*Carinacyathus pinus*	*Delgadell anabara*
UKT001	200.7	518.14	0.024	Atdabanian	Pestrotsvet	*Carinacyathus pinus*	*Delgadell anabara*
AKT 7-39	199.7	518.16	0.024	Atdabanian	Pestrotsvet	*Carinacyathus pinus*	*Delgadell anabara*
AKT 7-38	198.7	518.18	0.024	Atdabanian	Pestrotsvet	*Carinacyathus pinus*	*Delgadell anabara*
AKT 7-37	197.7	518.21	0.024	Atdabanian	Pestrotsvet	*Carinacyathus pinus*	*Delgadell anabara*
AKT 7-36	193.7	518.30	0.024	Atdabanian	Pestrotsvet	*Carinacyathus pinus*	*Delgadell anabara*
AKT 6-34	192.7	518.33	0.024	Atdabanian	Pestrotsvet	*Carinacyathus pinus*	*Delgadell anabara*
AKT 5-33	191.7	518.35	0.024	Atdabanian	Pestrotsvet	*Carinacyathus pinus*	*Delgadell anabara*
AKT 5-32	190.7	518.37	0.024	Atdabanian	Pestrotsvet	*Carinacyathus pinus*	*Delgadell anabara*
AKT 4-31	189.7	518.40	0.024	Atdabanian	Pestrotsvet	*Carinacyathus pinus*	*Delgadell anabara*
AKT 4-30	188.7	518.42	0.024	Atdabanian	Pestrotsvet	*Carinacyathus pinus*	*Delgadell anabara*
AKT 4-29	187.7	518.44	0.024	Atdabanian	Pestrotsvet	*Carinacyathus pinus*	*Delgadell anabara*
AKT 4-28	186.7	518.47	0.024	Atdabanian	Pestrotsvet	*Carinacyathus pinus*	*Delgadell anabara*
AKT 3-27	185.7	518.49	0.024	Atdabanian	Pestrotsvet	*Carinacyathus pinus*	*Delgadell anabara*
AKT 3-26	184.7	518.52	0.024	Atdabanian	Pestrotsvet	*Carinacyathus pinus*	*Delgadell anabara*
AKT 3-25	183.7	518.54	0.024	Atdabanian	Pestrotsvet	*Carinacyathus pinus*	*Delgadell anabara*
AKT 3-24	182.7	518.56	0.024	Atdabanian	Pestrotsvet	*Carinacyathus pinus*	*Delgadell anabara*
AKT 3-23	181.7	518.59	0.024	Atdabanian	Pestrotsvet	*Carinacyathus pinus*	*Delgadell anabara*
AKT 2-22	180.7	518.61	0.024	Atdabanian	Pestrotsvet	*Carinacyathus pinus*	*Delgadell anabara*
AKT 2-21	179.7	518.63	0.024	Atdabanian	Pestrotsvet	*Carinacyathus pinus*	*Delgadell anabara*
AKT 2-20	178.7	518.66	0.024	Atdabanian	Pestrotsvet	*Carinacyathus pinus*	*Delgadell anabara*
AKT 1-19	177.7	518.68	0.024	Atdabanian	Pestrotsvet	*Carinacyathus pinus*	*Delgadell anabara*
AKT 1-18	176.7	518.70	0.024	Atdabanian	Pestrotsvet	*Carinacyathus pinus*	*Delgadell anabara*
AKT 1-17	175.7	518.73	0.024	Atdabanian	Pestrotsvet	*Carinacyathus pinus*	*Delgadell anabara*
AKT 1-16	174.7	518.75	0.024	Atdabanian	Pestrotsvet	*Carinacyathus pinus*	*Delgadell anabara*
AKT 1-15	173.7	518.78	0.024	Atdabanian	Pestrotsvet	*Carinacyathus pinus*	*Delgadell anabara*
AKT 1-14	172.7	518.80	0.024	Atdabanian	Pestrotsvet	*Carinacyathus pinus*	*Delgadell anabara*
AKT 1-13	171.7	518.82	0.024	Atdabanian	Pestrotsvet	*Carinacyathus pinus*	*Delgadell anabara*
AKT VG12	166.5	518.95	0.024	Atdabanian	Pestrotsvet	*Carinacyathus pinus*	*Delgadell anabara*
AKT VG11	165.5	518.97	0.024	Atdabanian	Pestrotsvet	*Carinacyathus pinus*	*Delgadell anabara*
AKT VG10	164.5	518.99	0.024	Atdabanian	Pestrotsvet	*Carinacyathus pinus*	*Delgadell anabara*
AKT VG9	163.5	519.02	0.024	Atdabanian	Pestrotsvet	*Carinacyathus pinus*	*Delgadell anabara*
AKT VG8	162.5	519.04	0.024	Atdabanian	Pestrotsvet	*Carinacyathus pinus*	*Delgadell anabara*
AKT B7	161.5	519.06	0.024	Atdabanian	Pestrotsvet	*Carinacyathus pinus*	*Delgadell anabara*
AKT B5	159	519.12	0.024	Atdabanian	Pestrotsvet	*Carinacyathus pinus*	*Delgadell anabara*
AKT B4	158	519.15	0.024	Atdabanian	Pestrotsvet	*Carinacyathus pinus*	*Delgadell anabara*
AKT B3	157	519.17	0.024	Atdabanian	Pestrotsvet	*Carinacyathus pinus*	*Delgadell anabara*
AKT B2	156	519.19	0.024	Atdabanian	Pestrotsvet	*Carinacyathus pinus*	*Delgadell anabara*

Sample	Height (m)	Age (Ma)	Sedimentation rate Myr/m	Siberian Stage	Formation	Archaeocyathid biozones	Trilobite and SSFs biozones
AKT A1	154	519.24	0.024	Atdabanian	Pestrotsvet	*Carinacyathus pinus*	*Delgadell anabara*
Z Mys 54	151.5	519.30	0.024	Atdabanian	Pestrotsvet	*Carinacyathus pinus*	*Delgadell anabara*
Z Mys 53	150	519.34	0.024	Atdabanian	Pestrotsvet	*Carinacyathus pinus*	*Delgadell anabara*
Z Mys 52	149.5	519.35	0.024	Atdabanian	Pestrotsvet	*Carinacyathus pinus*	*Delgadell anabara*
Z Mys 51	149	519.36	0.024	Atdabanian	Pestrotsvet	*Carinacyathus pinus*	*Delgadell anabara*
Z Mys 50	148	519.38	0.024	Atdabanian	Pestrotsvet	*Carinacyathus pinus*	*Delgadell anabara*
Z Mys 49	147	519.41	0.024	Atdabanian	Pestrotsvet	*Carinacyathus pinus*	*Delgadell anabara*
Z Mys 48	146.5	519.42	0.024	Atdabanian	Pestrotsvet	*Carinacyathus pinus*	*Delgadell anabara*
Z Mys 47	145	519.45	0.024	Atdabanian	Pestrotsvet	*Carinacyathus pinus*	*Delgadell anabara*
Z Mys 46	144	519.48	0.024	Atdabanian	Pestrotsvet	*Carinacyathus pinus*	*Delgadell anabara*
Z Mys 45	143	519.50	0.024	Atdabanian	Pestrotsvet	*Carinacyathus pinus*	*Delgadell anabara*
Z Mys 44	142	519.52	0.024	Atdabanian	Pestrotsvet	*Carinacyathus pinus*	*Delgadell anabara*
Z Mys 43	141	519.55	0.024	Atdabanian	Pestrotsvet	*Carinacyathus pinus*	*Delgadell anabara*
Z Mys 42	140	519.57	0.024	Atdabanian	Pestrotsvet	*Carinacyathus pinus*	*Delgadell anabara*
Z Mys 41	139	519.60	0.024	Atdabanian	Pestrotsvet	*Carinacyathus pinus*	*Delgadell anabara*
Z Mys 40	138	519.62	0.024	Atdabanian	Pestrotsvet	*Carinacyathus pinus*	*Delgadell anabara*
Z Mys 39	135	519.69	0.024	Atdabanian	Pestrotsvet	*Carinacyathus pinus*	*Delgadell anabara*
Z Mys 38	134	519.71	0.024	Atdabanian	Pestrotsvet	*Carinacyathus pinus*	*Delgadell anabara*
Z Mys 37	133	519.74	0.024	Atdabanian	Pestrotsvet	*Carinacyathus pinus*	*Delgadell anabara*
Z Mys 36	132	519.76	0.024	Atdabanian	Pestrotsvet	*Carinacyathus pinus*	*Delgadell anabara*
Z Mys 35	129	519.83	0.024	Atdabanian	Pestrotsvet	*Retecoscinus zegebarti*	*Fallotaspis*
Z Mys 34	128	519.86	0.024	Atdabanian	Pestrotsvet	*Retecoscinus zegebarti*	*Fallotaspis*
Z Mys 33	126	519.90	0.024	Atdabanian	Pestrotsvet	*Retecoscinus zegebarti*	*Fallotaspis*
Z Mys 32	125	519.93	0.024	Atdabanian	Pestrotsvet	*Retecoscinus zegebarti*	*Fallotaspis*
Z Mys 31	123	519.97	0.024	Atdabanian	Pestrotsvet	*Retecoscinus zegebarti*	*Fallotaspis*
Z Mys 30	122	520.00	0.024	Atdabanian	Pestrotsvet	*Retecoscinus zegebarti*	*Fallotaspis*
Z Mys 29	121	520.02	0.024	Atdabanian	Pestrotsvet	*Retecoscinus zegebarti*	*Fallotaspis*
Z Mys 28	120	520.04	0.024	Atdabanian	Pestrotsvet	*Retecoscinus zegebarti*	*Fallotaspis*
Z Mys 27	119	520.07	0.024	Atdabanian	Pestrotsvet	*Retecoscinus zegebarti*	*Fallotaspis*
Z Mys 26	118	520.09	0.024	Atdabanian	Pestrotsvet	*Retecoscinus zegebarti*	*Fallotaspis*
Z Mys 25	116	520.14	0.024	Atdabanian	Pestrotsvet	*Retecoscinus zegebarti*	*Fallotaspis*
Z Mys 24	113	520.21	0.024	Atdabanian	Pestrotsvet	*Retecoscinus zegebarti*	*Fallotaspis*
ZHU37	112.0	520.23	0.024	Atdabanian	Pestrotsvet	*Retecoscinus zegebarti*	*Fallotaspis*
ZHU36	111.0	520.26	0.024	Atdabanian	Pestrotsvet	*Retecoscinus zegebarti*	*Fallotaspis*
ZHU35	110.0	520.28	0.024	Atdabanian	Pestrotsvet	*Retecoscinus zegebarti*	*Fallotaspis*
ZHU34	109.0	520.30	0.024	Atdabanian	Pestrotsvet	*Retecoscinus zegebarti*	*Fallotaspis*
ZHU33	97.0	520.59	0.024	Atdabanian	Pestrotsvet	*Retecoscinus zegebarti*	*Profallotaspis jakutensis*
ZHU32	96.0	520.61	0.024	Atdabanian	Pestrotsvet	*Retecoscinus zegebarti*	*Profallotaspis jakutensis*
ZHU31	95.3	520.63	0.024	Atdabanian	Pestrotsvet	*Retecoscinus zegebarti*	*Profallotaspis jakutensis*

Sample	Height (m)	Age (Ma)	Sedimentation rate Myr/m	Siberian Stage	Formation	Archaeocyathid biozones	Trilobite and SSFs biozones
ZHU30	94.8	520.64	0.024	Atdabanian	Pestrotsvet	*Retecoscinus zegebarti*	*Profallotaspis jakutensis*
ZHU29	93.8	520.67	0.029	Atdabanian	Pestrotsvet	*Retecoscinus zegebarti*	*Profallotaspis jakutensis*
ZHU28	92.8	520.70	0.029	Atdabanian	Pestrotsvet	*Retecoscinus zegebarti*	*Profallotaspis jakutensis*
ZHU27	91.8	520.73	0.029	Atdabanian	Pestrotsvet	*Retecoscinus zegebarti*	*Profallotaspis jakutensis*
ZHU26	90.8	520.76	0.029	Atdabanian	Pestrotsvet	*Retecoscinus zegebarti*	*Profallotaspis jakutensis*
ZHU25	89.8	520.79	0.029	Atdabanian	Pestrotsvet	*Retecoscinus zegebarti*	*Profallotaspis jakutensis*
ZHU24	87.8	520.85	0.029	Atdabanian	Pestrotsvet	*Retecoscinus zegebarti*	*Profallotaspis jakutensis*
ZHU23	86.8	520.88	0.029	Atdabanian	Pestrotsvet	*Retecoscinus zegebarti*	*Profallotaspis jakutensis*
ZHU22	85.4	520.92	0.029	Atdabanian	Pestrotsvet	*Retecoscinus zegebarti*	*Profallotaspis jakutensis*
ZHU21	84.7	520.94	0.029	Atdabanian	Pestrotsvet	*Retecoscinus zegebarti*	*Profallotaspis jakutensis*
ZHU20	83.7	520.97	0.029	Atdabanian	Pestrotsvet	*Retecoscinus zegebarti*	*Profallotaspis jakutensis*
ZHU19	82.8	520.99	0.029	Atdabanian	Pestrotsvet	*Retecoscinus zegebarti*	*Profallotaspis jakutensis*
ZHU18	82.2	521.01	0.029	Atdabanian	Pestrotsvet	*Retecoscinus zegebarti*	*Profallotaspis jakutensis*
ZHU17	81.2	521.04	0.029	Atdabanian	Pestrotsvet	*Retecoscinus zegebarti*	*Profallotaspis jakutensis*
ZHU16	80.2	521.07	0.029	Atdabanian	Pestrotsvet	*Retecoscinus zegebarti*	*Profallotaspis jakutensis*
ZHU15	79.5	521.09	0.029	Atdabanian	Pestrotsvet	*Retecoscinus zegebarti*	*Profallotaspis jakutensis*
ZHU14	79.2	521.10	0.029	Atdabanian	Pestrotsvet	*Retecoscinus zegebarti*	*Profallotaspis jakutensis*
ZHU13	78.6	521.12	0.029	Atdabanian	Pestrotsvet	*Retecoscinus zegebarti*	*Profallotaspis jakutensis*
ZHU12	78.4	521.12	0.029	Atdabanian	Pestrotsvet	*Retecoscinus zegebarti*	*Profallotaspis jakutensis*
ZHU11	78.0	521.13	0.029	Atdabanian	Pestrotsvet	*Retecoscinus zegebarti*	*Profallotaspis jakutensis*
ZHU10	77.0	521.16	0.029	Atdabanian	Pestrotsvet	*Retecoscinus zegebarti*	*Profallotaspis jakutensis*
ZHU09	76.4	521.18	0.029	Atdabanian	Pestrotsvet	*Retecoscinus zegebarti*	*Profallotaspis jakutensis*
ZHU08	75.6	521.20	0.029	Atdabanian	Pestrotsvet	*Retecoscinus zegebarti*	*Profallotaspis jakutensis*
ZHU07	73.5	521.27	0.029	Atdabanian	Pestrotsvet	*Retecoscinus zegebarti*	*Profallotaspis jakutensis*
ZHU06	72.7	521.29	0.029	Atdabanian	Pestrotsvet	*Retecoscinus zegebarti*	*Profallotaspis jakutensis*
ZHU05	72.1	521.31	0.029	Atdabanian	Pestrotsvet	*Retecoscinus zegebarti*	*Profallotaspis jakutensis*
ZHU04	71.8	521.32	0.029	Atdabanian	Pestrotsvet	*Retecoscinus zegebarti*	*Profallotaspis jakutensis*
ZHU03	71.2	521.33	0.029	Tommotian	Pestrotsvet	*Dokidocyathus lenaicus*	
ZHU02	70.5	521.35	0.029	Tommotian	Pestrotsvet	*Dokidocyathus lenaicus*	
ZHU01	70.0	521.37	0.029	Tommotian	Pestrotsvet	*Dokidocyathus lenaicus*	
IST50	67.1	521.45	0.029	Tommotian	Pestrotsvet	*Dokidocyathus lenaicus*	
IST49	66.0	521.49	0.029	Tommotian	Pestrotsvet	*Dokidocyathus lenaicus*	
IST48	65.5	521.50	0.029	Tommotian	Pestrotsvet	*Dokidocyathus lenaicus*	
IST47	65.0	521.52	0.029	Tommotian	Pestrotsvet	*Dokidocyathus lenaicus*	
IST46	64.5	521.53	0.029	Tommotian	Pestrotsvet	*Dokidocyathus lenaicus*	
IST45	64.0	521.55	0.029	Tommotian	Pestrotsvet	*Dokidocyathus lenaicus*	
IST44	63.5	521.56	0.029	Tommotian	Pestrotsvet	*Dokidocyathus lenaicus*	
IST43	60.0	521.69	0.037	Tommotian	Pestrotsvet	*Dokidocyathus lenaicus*	
IST42	53.5	521.93	0.037	Tommotian	Pestrotsvet	*Dokidocyathus lenaicus*	

Sample	Height (m)	Age (Ma)	Sedimentation rate Myr/m	Siberian Stage	Formation	Archaeocyathid biozones	Trilobite and SSFs biozones
IST41	52.5	521.97	0.037	Tommotian	Pestrotsvet	*Dokidocyathus lenaicus*	
IST40	51.5	522.01	0.037	Tommotian	Pestrotsvet	*Dokidocyathus lenaicus*	
IST39	49.7	522.08	0.037	Tommotian	Pestrotsvet	*Dokidocyathus lenaicus*	
IST38	47.7	522.15	0.037	Tommotian	Pestrotsvet	*Dokidocyathus lenaicus*	
IST37	47.4	522.16	0.037	Tommotian	Pestrotsvet	*Dokidocyathus lenaicus*	
IST36	46.5	522.20	0.037	Tommotian	Pestrotsvet	*Dokidocyathus lenaicus*	
IST35	46.0	522.21	0.037	Tommotian	Pestrotsvet	*Dokidocyathus lenaicus*	
IST34	45.0	522.25	0.037	Tommotian	Pestrotsvet	*Dokidocyathus lenaicus*	
IST33	44.0	522.29	0.037	Tommotian	Pestrotsvet	*Dokidocyathus lenaicus*	
IST32	43.0	522.33	0.037	Tommotian	Pestrotsvet	*Dokidocyathus lenaicus*	
IST31	42.0	522.36	0.037	Tommotian	Pestrotsvet	*Dokidocyathus lenaicus*	
IST30	41.9	522.37	0.037	Tommotian	Pestrotsvet	*Dokidocyathus lenaicus*	
IST29	41.5	522.38	0.037	Tommotian	Pestrotsvet	*Dokidocyathus lenaicus*	
IST28	41.0	522.40	0.037	Tommotian	Pestrotsvet	*Dokidocyathus regularis*	*Lapworthella bella* (SSFs)
IST27	40.0	522.44	0.037	Tommotian	Pestrotsvet	*Dokidocyathus regularis*	*Lapworthella bella* (SSFs)
IST26	39.0	522.48	0.037	Tommotian	Pestrotsvet	*Dokidocyathus regularis*	*Lapworthella bella* (SSFs)
IST25	38.0	522.51	0.037	Tommotian	Pestrotsvet	*Dokidocyathus regularis*	*Lapworthella bella* (SSFs)
IST24	37.0	522.55	0.037	Tommotian	Pestrotsvet	*Dokidocyathus regularis*	*Lapworthella bella* (SSFs)
IST23	36.0	522.59	0.037	Tommotian	Pestrotsvet	*Dokidocyathus regularis*	*Lapworthella bella* (SSFs)
IST22	35.0	522.63	0.037	Tommotian	Pestrotsvet	*Dokidocyathus regularis*	*Lapworthella bella* (SSFs)
IST21	34.0	522.66	0.037	Tommotian	Pestrotsvet	*Dokidocyathus regularis*	*Lapworthella bella* (SSFs)
IST20	31.0	522.78	0.037	Tommotian	Pestrotsvet	*Dokidocyathus regularis*	*Lapworthella bella* (SSFs)
IST19	29.0	522.85	0.037	Tommotian	Pestrotsvet	*Dokidocyathus regularis*	*Lapworthella bella* (SSFs)
IST18	27.0	522.91	0.030	Tommotian	Pestrotsvet	*Dokidocyathus regularis*	*Lapworthella bella* (SSFs)
IST17	19.9	523.12	0.030	Tommotian	Pestrotsvet	*Dokidocyathus regularis*	*Lapworthella tortuosa* (SSFs)
IST16	19.8	523.12	0.030	Tommotian	Pestrotsvet	*Dokidocyathus regularis*	*Lapworthella tortuosa* (SSFs)
IST15	13.5	523.31	0.030	Tommotian	Pestrotsvet	*Dokidocyathus regularis*	*Lapworthella tortuosa* (SSFs)
IST14	12.5	523.34	0.030	Tommotian	Pestrotsvet	*Dokidocyathus regularis*	*Lapworthella tortuosa* (SSFs)
IST13	11.5	523.37	0.030	Tommotian	Pestrotsvet	*Dokidocyathus regularis*	*Lapworthella tortuosa* (SSFs)
IST12	11.0	523.39	0.030	Tommotian	Pestrotsvet	*Dokidocyathus regularis*	*Lapworthella tortuosa* (SSFs)
IST11	10.2	523.41	0.030	Tommotian	Pestrotsvet	*Dokidocyathus regularis*	*Lapworthella tortuosa* (SSFs)
IST10	9.0	523.44	0.030	Tommotian	Pestrotsvet	*Dokidocyathus regularis*	*Lapworthella tortuosa* (SSFs)
IST09	8.0	523.47	0.030	Tommotian	Pestrotsvet	*Dokidocyathus regularis*	*Lapworthella tortuosa* (SSFs)
IST08	7.0	523.50	0.030	Tommotian	Pestrotsvet	*Dokidocyathus regularis*	*Lapworthella tortuosa* (SSFs)
IST07	6.0	523.53	0.030	Tommotian	Pestrotsvet	*Dokidocyathus regularis*	*Lapworthella tortuosa* (SSFs)
IST06	4.7	523.57	0.030	Nemakit-Dalaynian	Pestrotsvet		*Nochoroicyathus sunnaginicus* (SSFs)
IST05	4.0	523.59	0.030	Nemakit-Dalaynian	Pestrotsvet		*Nochoroicyathus sunnaginicus* (SSFs)
IST04	3.0	523.62	0.030	Nemakit-Dalaynian	Pestrotsvet		*Nochoroicyathus sunnaginicus* (SSFs)
IST03	2.7	523.63	0.030	Nemakit-Dalaynian	Pestrotsvet		*Nochoroicyathus sunnaginicus* (SSFs)

Sample	Height (m)	Age (Ma)	Sedimentation rate Myr/m	Siberian Stage	Formation	Archaeocyathid biozones	Trilobite and SSFs biozones
IST02	2.1	523.65	0.030	Nemakit-Dalaynian	Pestrotsvet		*Nochoroicyathus sunnaginicus* (SSFs)
DVO11	1.5	523.67	0.030	Nemakit-Dalaynian	Pestrotsvet		*Nochoroicyathus sunnaginicus* (SSFs)
DVO10	1.4	523.67	0.030	Nemakit-Dalaynian	Pestrotsvet		*Nochoroicyathus sunnaginicus* (SSFs)
DVO08	1.2	523.68	0.030	Nemakit-Dalaynian	Pestrotsvet		*Nochoroicyathus sunnaginicus* (SSFs)
DVO07	1.1	523.68	0.030	Nemakit-Dalaynian	Yudoma		*Protohertzina anabarica* (SSFs)
DVO06	1.0	523.68	0.030	Nemakit-Dalaynian	Yudoma		*Protohertzina anabarica* (SSFs)
DVO04	0.8	523.69	0.030	Nemakit-Dalaynian	Yudoma		*Protohertzina anabarica* (SSFs)
DVO02	0.0	523.71	0.030	Nemakit-Dalaynian	Yudoma		*Protohertzina anabarica* (SSFs)
DVO01	0.0	523.71	0.030	Nemakit-Dalaynian	Yudoma		*Protohertzina anabarica* (SSFs)

Appendix C

Sulphur, carbon, oxygen isotopes, and elemental data for Aldan-Lena Rivers sections

CAS: carbonate-associated sulphate; Carbonate%: total HCl-leachable carbonate content; TA: Tit-Ary section; LAB: Labaia section; AT: Achchagy-Tuydakh section; UT: Ulakhan-Tyoidukh section; UKT: Ulakhan-Kyyry-Tass section; AKT: AchchagyKyyry-Taas section; Z Myrs and ZHU: Zhurinsky-Mys section; IST: Isit section; DVO: Dvortsy section. Raw carbon and oxygen isotope data of TA, LAB, UT, UKT, ZHU, IST and DVO are analysed by the current study. Carbon isotope data of AT, AKT, Z Mys sections along the Lena river are obtained from pioneering study of Brasier *et al*. (1994) to fill the sampling gap in the current study. Sulphur isotope and elemental concentration were obtained from the current study. Elemental analyses in this Appendix represent total 10% HCl-leachable elemental contents of bulk carbonate samples;

Sample	Height (m)	Age (Ma)	$\delta^{13}C$ (‰)	$\delta^{18}O$ (‰)	$\delta^{34}S_{CAS}$ (‰)	[CAS] ppm	Carbonate % (%)	Mg/Ca (w/w)	Mn/Sr (w/w)
TA40	619.0	512.87	-0.9	-7.5					
TA39	617.0	512.89	-0.8	-7.3	28.1	25.43	87.2	0.005	0.02
TA38	616.0	512.90	-0.9	-7.4					
TA37	615.0	512.91	-0.8	-7.3					
TA36	613.0	512.93	-0.7	-6.8					
TA35	611.0	512.96	-0.8	-7.0	26.7	20.32	88.3	0.005	0.04
TA34	609.0	512.98	-0.8	-7.1					
TA33	608.0	512.99	-0.8	-7.0					
TA32	606.0	513.01	-0.8	-6.5	33.7	35.04	87.1	0.006	0.02
TA31	604.5	513.03	-0.7	-7.2					
TA30	603.0	513.05	-0.8	-7.4					
TA29	601.0	513.07	-0.8	-7.0					
TA28	600.0	513.08	-0.9	-6.7	33.5	37.30	88.1	0.005	0.04
TA27	598.5	513.10	-0.4	-4.2					
TA26	597.0	513.11	-0.4	-4.2					
TA25	596.5	513.12	-0.7	-6.3	30.4	38.43	90.1	0.130	0.20
TA24	592.5	513.16	0.0	-4.3					
TA22	589.1	513.20	-0.3	-4.1					
TA21	588.2	513.21	-1.1	-7.2					
TA20	584.7	513.25	-0.9	-6.4					
TA19	582.7	513.27	-1.0	-7.0	30.2	42.62	87.5	0.009	0.06
TA18	581.4	513.29	-1.1	-6.5	32.5	71.68	88.3	0.004	0.03
TA17	580.2	513.30	-1.4	-6.9	28.1	59.96	87.2	0.004	0.11
TA16	578.7	513.32	-1.0	-4.1					
TA15	575.7	513.35	-0.9	-4.4	25.4	40.98	95.3	0.539	1.23
TA14	574.7	513.36	-1.2	-5.1					
TA13	574.2	513.37	-1.6	-4.5	24.3	171.15	94.6	0.575	3.31
TA12	573.7	513.37	-1.6	-4.7					
TA11	571.7	513.40	-2.0	-6.9					
TA10	569.7	513.42	-1.9	-7.0					
TA09	567.7	513.44	-2.1	-6.8					
TA08	566.7	513.45	-2.0	-7.1	26.7	76.70	88.0	0.031	0.06
TA07	565.9	513.46	-1.6	-7.2					
TA06	564.7	513.47	-2.0	-9.4					
TA05	563.7	513.49	-2.4	-10.6					
TA04	562.7	513.50	-2.1	-9.9					
TA03	561.7	513.51	-1.9	-6.2	28.9	213.47	87.0	0.025	0.04
TA02	560.7	513.52	-1.9	-6.6					
TA01	559.7	513.53	-1.9	-6.4					
LAB92	553.7	513.60	-1.7	-7.0	29.2	59.49	86.7	0.022	0.03
LAB91	551.7	513.62	-1.7	-6.9	33.1	59.77	87.1	0.028	0.04
LAB90	549.7	513.64	-1.7	-7.3					
LAB89	547.7	513.66	-1.8	-7.3					
LAB88	545.7	513.69	-1.8	-7.4					
LAB87	543.7	513.71	-2.3	-7.2					
LAB86	541.7	513.73	-2.1	-7.1					
LAB85	539.7	513.75	-1.8	-7.2					
LAB84	536.7	513.79	-1.9	-7.2					
LAB83	534.7	513.81	-1.5	-7.0	35.2	34.85	88.4	0.045	0.04
LAB82	532.8	513.83	-2.0	-6.7					
LAB81	528.8	513.87	-1.8	-6.6	31.9	41.16	88.5	0.035	0.04
LAB80	526.8	513.90	-1.4	-6.2					
LAB79	524.8	513.92	-2.2	-7.4					
LAB78	522.8	513.94	-2.7	-6.5					
LAB77	520.8	513.96	-1.7	-6.6	20.5	80.62	87.7	0.023	0.03
LAB76	518.8	513.99	-1.5	-6.7					
LAB75	516.3	514.01	-1.7	-6.5					
LAB74	515.3	514.03	-1.8	-6.6	25.7	485.77	86.5	0.055	0.04
LAB73	513.3	514.05	-1.6	-6.2					
LAB72	511.3	514.07	-1.6	-6.5	29.3	65.43	87.0	0.018	0.02
LAB71	509.3	514.09	-1.9	-7.3					
LAB64	507.3	514.11	-1.7	-6.3					
LAB70	505.3	514.14	-1.5	-6.6	28.9	66.07	88.0	0.069	0.05
LAB69	503.3	514.16	-1.4	-6.7					
LAB68	501.3	514.18	-1.6	-6.7					
LAB67	499.3	514.20	-1.6	-6.8	29.5	52.42	87.6	0.033	0.04
LAB66	497.3	514.23	-1.5	-7.0					
LAB65	495.3	514.25	-1.1	-6.5					
LAB63	494.0	514.26	-1.9	-7.2					
LAB62	492.0	514.29	-1.5	-7.1	31.5	49.75	87.5	0.053	0.04

Sample	Height (m)	Age (Ma)	$\delta^{13}C$ (‰)	$\delta^{18}O$ (‰)	$\delta^{34}S_{cas}$ (‰)	[CAS] ppm	Carbonate % (%)	Mg/Ca (w/w)	Mn/Sr (w/w)
LAB61	490.0	514.31	-1.3	-6.1					
LAB60	488.0	514.33	-1.3	-7.0					
LAB59	486.0	514.35	-1.3	-7.0	27.3	64.66	87.3	0.047	0.03
LAB58	484.0	514.37	-1.5	-7.5					
LAB57	483.2	514.38	-1.2	-6.4					
LAB56	482.2	514.39	-1.4	-7.2	22.0	81.96	87.7	0.022	0.04
LAB55	479.7	514.42	-1.5	-7.1					
LAB54	478.7	514.43	-1.1	-6.5		36.39			
LAB53	477.7	514.45	-1.4	-7.1					
LAB51	473.7	514.49	-1.4	-7.1					
LAB50	471.7	514.51	-1.4	-7.4					
LAB48	467.7	514.56	-1.1	-5.7					
LAB47	465.7	514.58	-1.5	-7.2		39.30			
LAB46	463.7	514.60	-1.6	-7.3					
LAB45	462.7	514.61	-1.1	-6.5	18.0	72.66	88.6	0.061	0.06
LAB44	459.7	514.65	-1.3	-7.1	17.9	124.60	87.7	0.070	0.06
LAB43	457.7	514.67	-1.1	-6.6	19.6	10.11	86.1	0.010	0.10
LAB42	455.7	514.69	-1.1	-6.6	25.7	144.78	87.2	0.040	0.06
LAB41	453.0	514.72	-1.3	-6.3	28.1	204.61	87.5	0.024	0.02
LAB40	451.0	514.74	-1.3	-6.7					
LAB39	449.0	514.77	-1.2	-6.4					
LAB38	447.0	514.79	-1.2	-6.8		44.86			
LAB37	446.0	514.80	-1.3	-6.5					
LAB36	445.0	514.81	-1.3	-6.6					
LAB35	444.0	514.82	-1.4	-6.7		103.20	86.9	0.020	0.03
LAB34	442.0	514.84	-1.3	-7.0					
LAB33	440.0	514.87	-1.3	-7.4		44.41			
LAB32	438.0	514.89	-1.3	-7.7					
LAB30	434.0	514.93	-1.4	-7.5					
LAB29	432.0	514.96	-1.4	-7.3					
LAB28	430.0	514.98	-1.3	-7.0		47.76			
LAB27	428.0	515.00	-1.1	-7.1					
LAB26	426.0	515.02	-0.7	-6.0		49.46			
LAB25	424.0	515.04	-1.0	-6.6					
LAB24	421.9	515.07	-1.1	-6.4	30.3	134.41	86.2	0.039	0.03
LAB23	419.9	515.09	-1.2	-6.5					
LAB22	417.9	515.11	-1.0	-6.3					
LAB21	415.9	515.13	-1.9	-9.3	25.6	307.58	84.0	0.018	0.03
LAB20	414.9	515.15	-1.1	-6.3	27.4	56.98	88.3	0.049	0.03
LAB19	412.9	515.17	-1.0	-6.4					
LAB18	410.9	515.19	-1.4	-6.9					
LAB17	408.9	515.21	-1.3	-7.0	28.0	96.17	87.3	0.036	0.05
LAB16	407.9	515.22	-1.2	-7.1					
LAB15	406.7	515.24	-1.2	-6.7		36.20			
LAB13	404.7	515.26	-1.4	-8.0					
LAB12	403.7	515.27	-1.2	-6.8		59.50			
LAB11	402.4	515.29	-1.0	-6.5	27.2	44.96	88.2	0.084	0.03
LAB10	402.2	515.29	-1.3	-7.2					
LAB09	401.7	515.29	-1.1	-6.7					
LAB08	401.3	515.30	-1.1	-6.7		34.91			
LAB07	401.0	515.30	-1.0	-6.8					
LAB06	400.5	515.31	-1.2	-6.8		62.77	88.0	0.043	0.03
LAB05	400.0	515.31	-1.1	-6.7					
LAB04	399.7	515.32	-1.1	-7.1		59.53			
LAB03	399.5	515.32	-1.2	-7.1					
LAB02	399.2	515.32	-1.1	-7.0					
LAB01	398.7	515.33	-0.8	-6.2		41.05			
AT 20-141	395.2	515.37	0.5						
AT 20-140	394.2	515.38	1.5						
AT 20-139	393.2	515.39	1.2						
AT 20-138	392.2	515.40	1.6						
AT 20-137	391.2	515.41	1.8						
AT 20-136	390.2	515.42	1.9						
AT 20-135	389.2	515.43	2.3						
AT 20-134	388.2	515.44	1.6						
AT 20-133	387.2	515.46	1.6						
AT 20-132	386.2	515.47	2.0						
AT 19-131	385.2	515.48	1.7						
AT 19-130	384.2	515.49	1.9						
AT 19-129	383.2	515.50	1.4						

Sample	Height (m)	Age (Ma)	$\delta^{13}C$ (‰)	$\delta^{18}O$ (‰)	$\delta^{34}S_{CAS}$ (‰)	[CAS] ppm	Carbonate % (%)	Mg/Ca (w/w)	Mn/Sr (w/w)
AT 19-128	382.2	515.51	1.8						
AT 18-127	381.2	515.52	2.1						
AT 18-126	380.2	515.53	2.6						
AT 18-125	379.2	515.54	2.2						
AT 18-124	378.2	515.56	2.0						
AT 18-123	377.2	515.57	1.5						
AT 18-122	376.2	515.58	1.2						
AT 17-121	373.7	515.61	1.6						
AT 17-120	372.7	515.62	1.8						
AT 17-119	371.7	515.63	1.9						
AT 17-118	370.7	515.64	1.9						
AT 17-117	369.7	515.65	2.0						
AT 17-116	368.7	515.66	1.8						
AT 17-115	367.7	515.67	2.6						
AT 16-114	366.7	515.68	2.7						
AT 16-113	365.7	515.70	2.1						
AT 16-112	364.7	515.71	1.6						
AT 16-111	363.7	515.72	2.1						
AT 16-109	361.7	515.74	2.2						
AT 16-108	360.7	515.75	2.1						
AT 16-107	359.7	515.76	2.1						
AT 16-106	358.7	515.77	2.1						
AT 16-105	357.7	515.78	2.1						
AT 16-103	355.7	515.81	2.0						
AT 16-102	354.7	515.82	1.6						
AT 16-100	352.7	515.84	2.0						
AT 16-99	351.7	515.85	1.9						
AT 16-98	350.7	515.86	2.1						
AT 15-95	349.7	515.87	1.8						
AT 15-94	348.7	515.88	1.8						
AT 15-93	347.7	515.90	2.0						
AT 15-92	346.7	515.91	1.6						
AT 15-91	345.7	515.92	1.3						
AT 15-90	344.7	515.93	1.6						
AT 14-89	343.7	515.94	1.4						
AT 14-88	342.7	515.95	1.4						
AT 13-86	341.7	515.96	1.8						
AT 13-85	340.7	515.97	1.7						
AT 13-84	339.7	515.99	1.4						
AT 13-82	337.7	516.01	1.3						
AT 13-81	336.7	516.02	0.2						
AT 13-80	335.7	516.03	1.2						
AT 13-79	334.7	516.04	1.2						
AT 13-78	333.7	516.05	1.1						
AT 13-77	332.7	516.06	1.0						
AT 13-76	331.7	516.07	1.1						
UT36	330.2	516.09	0.8	-6.1		40.08	88.0	0.048	0.05
UT35	329.7	516.10	0.6	-6.4	30.8	41.81	87.6	0.028	0.11
UT34	329.2	516.10	0.9	-6.3					
UT33	328.7	516.11	0.8	-6.6					
UT32	328.1	516.11	0.7	-6.3					
UT31	327.7	516.12	0.8	-6.3		37.78			
UT30	326.7	516.13	0.8	-6.4		53.57			
UT29	325.7	516.14	0.8	-5.8					
UT28	325.2	516.15	0.9	-5.9					
UT27	324.2	516.16	0.6	-6.1	35.9	25.69	87.8	0.034	0.05
UT26	322.9	516.17	0.7	-5.8					
UT25	322.2	516.18	0.7	-5.6					
UT24	321.2	516.19	1.0	-6.8					
UT23	320.2	516.20	1.0	-7.2	35.3	33.39	87.7	0.056	0.07
UT22	319.2	516.21	0.7	-6.3					
UT21	318.2	516.23	0.8	-6.2	28.8	42.22	88.9	0.061	0.23
UT20	317.2	516.24	0.8	-7.0					
UT19	316.2	516.25	0.7	-6.3		44.04	88.5	0.020	0.09
UT18	315.2	516.26	0.7	-5.9	32.5	1658.37	89.2	0.088	0.07
UT17	314.2	516.27	0.5	-6.2					
UKT102	313.0	516.28	0.2	-6.0					
UKT101	312.5	516.29	0.5	-5.9	33.9	37.17	88.8	0.087	0.05
UKT100	312.0	516.29	0.3	-6.6					
UKT099	311.5	516.30	0.5	-5.9					

Sample	Height (m)	Age (Ma)	$\delta^{13}C$ (‰)	$\delta^{18}O$ (‰)	$\delta^{34}S_{CAS}$ (‰)	[CAS] ppm	Carbonate % (%)	Mg/Ca (w/w)	Mn/Sr (w/w)
UKT098	311.0	516.31	0.4	-6.2					
UKT097	310.5	516.31	0.3	-6.6					
UKT096	310.1	516.32	0.3	-6.8	31.2	27.95	88.8	0.059	0.14
UKT095	309.6	516.32	0.1	-6.3					
UKT094	309.0	516.33	0.4	-6.4					
UKT093	308.5	516.33	0.3	-6.9		40.22			
UKT092	308.0	516.34	0.5	-6.5					
UKT091	307.5	516.34	0.3	-6.5					
UKT090	307.0	516.35	0.3	-6.1		53.14	87.5	0.055	0.07
UKT089	302.2	516.40	0.3	-7.1	25.3	45.67	87.8	0.021	0.08
UKT088	301.7	516.41	0.5	-6.0					
UKT087	301.2	516.42	0.3	-5.9					
UKT086	300.6	516.42	0.3	-5.8	27.2	120.19	85.1	0.048	0.06
UKT084	300.0	516.43	0.5	-5.9					
UKT083	299.4	516.44	0.0	-7.1	30.7	38.56	87.3	0.025	0.07
UKT082	298.8	516.44	0.5	-5.7					
UKT081	298.7	516.44	0.5	-6.3					
UKT080	298.4	516.45	0.3	-5.7	18.2	74.72	86.6	0.033	0.07
UKT079	297.7	516.45	0.1	-6.1					
UKT078	297.2	516.46	0.3	-6.6	25.4	43.86	87.7	0.035	0.09
UKT077	296.9	516.46	0.3	-6.5					
UKT076	296.4	516.47	0.3	-6.6		52.09			
UKT075	295.9	516.47	0.3	-6.3					
UKT074	295.3	516.48	0.6	-5.8					
UKT073	294.4	516.49	0.4	-5.7	21.8	48.36	86.7	0.043	0.04
UKT072	293.4	516.50	0.2	-6.6					
UKT071	291.9	516.52	0.5	-6.2	15.8	107.71	87.5	0.061	0.06
UKT070	290.9	516.53	0.3	-6.7					
UKT069	289.7	516.54	0.4	-5.8					
UKT068	287.7	516.57	0.2	-6.3		32.41	88.0	0.026	0.06
UKT067	286.2	516.58	0.2	-6.5	26.6	34.59	86.5	0.081	0.13
UKT066	285.2	516.59	0.3	-6.6		37.33	87.2	0.024	0.08
UKT065	284.2	516.60	0.4	-6.9	23.5	71.76	86.9	0.083	0.15
UKT064	283.2	516.62	0.5	-6.1					
UKT063	282.2	516.63	0.8	-7.1	21.8	39.63	91.9	0.467	0.46
UKT062	281.2	516.64	0.9	-7.1	28.2	56.65	87.2	0.012	0.05
UKT061	279.7	516.66	1.2	-7.2		45.71	87.2	0.024	0.09
UKT060	278.7	516.67	1.4	-7.1		37.27			
UKT059	277.7	516.68	1.5	-7.2	28.9	60.60	89.2	0.021	0.07
UT16	276.8	516.69	1.4	-6.7					
UT15	275.8	516.70	1.8	-6.6					
UT14	274.8	516.71	1.8	-6.5					
UT13	273.8	516.72	2.1	-6.6		1789.28	87.1	0.008	0.05
UT12	272.8	516.73	2.0	-5.9	31.5	999.92	87.2	0.018	0.06
UT09	269.8	516.77	2.2	-5.3	32.9	1640.59	86.9	0.006	0.32
UT08	268.8	516.78	2.4	-5.4	30.6	1060.31	89.0	0.046	0.35
UT07	268.1	516.78	2.8	-5.6					
UT06	267.6	516.79	2.8	-7.3					
UT05	267.1	516.80	3.1	-7.4					
UT04	266.6	516.80	3.2	-6.5					
UT03	266.2	516.81	3.7	-6.5	33.3	4884.84	87.3	0.020	0.21
UT02	265.7	516.81	2.9	-6.3	32.3	2808.17	88.0	0.130	0.82
UT01	264.7	516.82	2.7	-5.1	32.2	12163.30	73.2	0.285	0.64
UKT054	259.8	516.88	2.6	-4.4	31.5	4525.04	82.7	0.038	0.73
UKT053	258.8	516.89	2.7	-4.3	30.7	4955.60	79.8	0.063	0.91
UKT052	258.3	516.89	2.2	-4.4					
UKT051	257.8	516.90	2.1	-4.2			77.1	0.170	1.10
UKT050	256.7	516.91	1.3	-4.9	29.8	133.67	78.9	0.130	0.88
UKT049	255.7	516.92	1.0	-4.5					
UKT048	254.7	516.93	0.7	-5.1	30.2	66.90	78.1	0.053	0.63
UKT047	253.7	516.95	0.7	-4.7	28.4	161.38	76.2	0.174	0.84
UKT046	252.7	516.96	0.1	-5.1					
UKT045	251.7	516.97	0.3	-5.1			73.0	0.094	1.00
UKT044	250.6	516.98	-1.0	-5.3					
UKT043	249.6	516.99	-0.7	-5.7	26.4	91.51	81.6	0.142	0.27
UKT042	248.8	517.00	-1.1	-5.2					
UKT041	247.6	517.03	-1.0	-5.5	26.4	56.16	80.3	0.047	0.36
UKT040	247.1	517.04	-0.8	-6.3					
UKT039	246.1	517.06	-1.0	-5.2	26.7	87.83	76.9	0.043	0.42
UKT038	245.6	517.08	-0.9	-5.0					

Sample	Height (m)	Age (Ma)	$\delta^{13}C$ (‰)	$\delta^{18}O$ (‰)	$\delta^{34}S_{CAS}$ (‰)	[CAS] ppm	Carbonate % (%)	Mg/Ca (w/w)	Mn/Sr (w/w)
UKT037	244.6	517.10	-0.8	-5.6	26.7	113.08	79.0	0.050	0.32
UKT036	243.6	517.12	-0.8	-5.1	27.5	70.63	80.3	0.015	0.33
UKT035	242.6	517.15	-0.8	-5.2					
UKT034	241.1	517.18	-0.7	-5.7	24.5	109.32	78.8	0.081	0.33
UKT033	238.6	517.24	-0.1	-5.1	25.3	44.00	82.4	0.010	0.42
UKT032	237.8	517.26	0.0	-5.7	28.7	60.97	82.1	0.096	0.50
UKT031	236.0	517.30	0.2	-5.2	28.3	42.68	82.0	0.026	0.43
UKT030	235.3	517.32	0.6	-4.3					
UKT028	234.3	517.34	0.6	-4.6					
UKT027	232.6	517.38	1.1	-5.3					
UKT026	232.4	517.39	1.1	-5.4	29.0	83.51	77.9	0.076	0.26
UKT025	231.6	517.41	1.2	-5.5	29.6	103.91	68.1	0.163	0.63
UKT024	226.2	517.53	0.4	-5.4	31.5	32.72	80.6	0.011	0.54
UKT023	225.8	517.54	0.4	-5.7	31.2	139.25	76.4	0.065	0.37
UKT022	224.6	517.57	0.3	-6.9					
UKT021	223.2	517.61	0.3	-5.2					
UKT020	222.2	517.63	0.4	-5.7	28.9	141.44	74.6	0.110	0.92
UKT019	221.2	517.65	0.2	-5.9					
UKT018	216.2	517.77	-0.2	-6.3	30.2	75.16	76.6	0.026	0.36
UKT017	213.9	517.82	-0.3	-6.2					
UKT016	213.2	517.84	-0.1	-6.2	29.6	62.85	75.4	0.023	0.23
UKT015	212.3	517.86	0.1	-6.1	30.6	9.37	83.7	0.005	0.30
UKT014	211.8	517.87	-0.1	-6.0					
UKT013	211.0	517.89	0.0	-5.8	29.6	27.63	77.5	0.023	0.61
UKT012	208.0	517.96	0.9	-5.6					
UKT011	206.9	517.99	1.2	-5.6					
UKT010	206.0	518.01	1.3	-5.5	27.0	63.84	75.7	0.093	0.98
UKT009	205.0	518.04	1.5	-5.8	29.7	53.72	80.8	0.023	0.15
UKT008	204.5	518.05	1.9	-5.4	30.4	0.79	82.0	0.014	0.15
UKT007	203.6	518.07	1.8	-5.3	31.8	33.49	78.4	0.018	0.80
UKT006	202.3	518.10	2.2	-5.7			82.9	0.013	0.14
UKT005	201.8	518.11	2.2	-5.1					
UKT004	201.7	518.11	2.6	-5.0	32.8	72.38	74.9	0.079	0.80
UKT003	201.3	518.12	2.7	-5.6					
UKT001	200.7	518.14	2.8	-5.1	33.9	42.10	77.2	0.018	0.81
AKT 7-39	199.7	518.16	3.1						
AKT 7-38	198.7	518.18	3.0						
AKT 7-37	197.7	518.21	3.2						
AKT 7-36	193.7	518.30	2.9						
AKT 6-34	192.7	518.33	2.9						
AKT 5-33	191.7	518.35	2.6						
AKT 5-32	190.7	518.37	2.4						
AKT 4-31	189.7	518.40	2.3						
AKT 4-30	188.7	518.42	2.0						
AKT 4-29	187.7	518.44	1.9						
AKT 4-28	186.7	518.47	1.6						
AKT 3-27	185.7	518.49	1.7						
AKT 3-26	184.7	518.52	1.1						
AKT 3-25	183.7	518.54	1.3						
AKT 3-24	182.7	518.56	1.1						
AKT 3-23	181.7	518.59	1.2						
AKT 2-22	180.7	518.61	1.2						
AKT 2-21	179.7	518.63	1.0						
AKT 2-20	178.7	518.66	1.0						
AKT 1-19	177.7	518.68	1.4						
AKT 1-18	176.7	518.70	1.2						
AKT 1-17	175.7	518.73	1.1						
AKT 1-16	174.7	518.75	1.0						
AKT 1-15	173.7	518.78	1.4						
AKT 1-14	172.7	518.80	1.1						
AKT 1-13	171.7	518.82	1.1						
AKT VG12	166.5	518.95	1.1						
AKT VG11	165.5	518.97	1.0						
AKT VG10	164.5	518.99	1.0						
AKT VG9	163.5	519.02	1.0						
AKT VG8	162.5	519.04	0.8						
AKT B7	161.5	519.06	0.7						
AKT B5	159.0	519.12	0.9						
AKT B4	158.0	519.15	0.8						
AKT B3	157.0	519.17	0.9						

Sample	Height (m)	Age (Ma)	$\delta^{13}C$ (‰)	$\delta^{18}O$ (‰)	$\delta^{34}S_{cas}$ (‰)	[CAS] ppm	Carbonate % (%)	Mg/Ca (w/w)	Mn/Sr (w/w)
AKT B2	156.0	519.19	0.7						
AKT A1	154.0	519.24	0.0						
Z Mys 54	151.5	519.30	-0.5						
Z Mys 53	150.0	519.34	-0.1						
Z Mys 52	149.5	519.35	-0.3						
Z Mys 51	149.0	519.36	-0.4						
Z Mys 50	148.0	519.38	-0.5						
Z Mys 49	147.0	519.41	-0.5						
Z Mys 48	146.5	519.42	-0.4						
Z Mys 47	145.0	519.45	-0.5						
Z Mys 46	144.0	519.48	-0.5						
Z Mys 45	143.0	519.50	-0.9						
Z Mys 44	142.0	519.52	-0.5						
Z Mys 43	141.0	519.55	-0.6						
Z Mys 42	140.0	519.57	-0.4						
Z Mys 41	139.0	519.60	-0.3						
Z Mys 40	138.0	519.62	0.0						
Z Mys 39	135.0	519.69	0.3						
Z Mys 38	134.0	519.71	-0.2						
Z Mys 37	133.0	519.74	-0.1						
Z Mys 36	132.0	519.76	-0.1						
Z Mys 35	129.0	519.83	-0.1						
Z Mys 34	128.0	519.86	0.3						
Z Mys 33	126.0	519.90	0.5						
Z Mys 32	125.0	519.93	1.0						
Z Mys 31	123.0	519.97	0.8						
Z Mys 30	122.0	520.00	1.2						
Z Mys 29	121.0	520.02	0.5						
Z Mys 28	120.0	520.04	1.5						
Z Mys 27	119.0	520.07	1.3						
Z Mys 26	118.0	520.09	1.3						
Z Mys 25	116.0	520.14	1.5						
Z Mys 24	113.0	520.21	1.4						
ZHU37	112.0	520.23	1.1	-6.2					
ZHU36	111.0	520.26	1.2	-6.2					
ZHU35	110.0	520.28	1.2	-6.2			80.0	0.029	0.06
ZHU34	109.0	520.30	1.4	-6.4					
ZHU33	97.0	520.59	1.3	-6.0	35.3	158.27	77.0	0.246	0.64
ZHU32	96.0	520.61	1.3	-5.8					
ZHU31	95.3	520.63	1.5	-5.2					
ZHU30	94.8	520.64	1.8	-5.7	35.4	166.52	79.9	0.223	0.83
ZHU29	93.8	520.67	1.2	-5.8	34.7	179.78	71.7	0.262	0.82
ZHU28	92.8	520.70	0.8	-6.2	35.3	205.30	77.1	0.244	0.73
ZHU27	91.8	520.73	0.8	-5.9	34.4	28.02	75.6	0.278	0.79
ZHU26	90.8	520.76	0.7	-5.7	34.4	180.95	72.4	0.224	0.60
ZHU25	89.8	520.79	0.5	-6.1	34.6	195.57	75.7	0.138	0.43
ZHU24	87.8	520.85	0.4	-6.3	33.7	111.91	77.6	0.050	0.28
ZHU23	86.8	520.88	0.3	-6.5	33.9	126.88	75.8	0.042	0.28
ZHU22	85.4	520.92	0.2	-6.3					
ZHU21	84.7	520.94	0.0	-6.5					
ZHU20	83.7	520.97	0.0	-7.0	34.5	210.08	74.1	0.035	0.14
ZHU19	82.8	520.99	-0.1	-6.9	34.0	177.92	72.8	0.037	0.21
ZHU18	82.2	521.01	0.1	-6.2	34.5	106.13	80.5	0.037	0.24
ZHU17	81.2	521.04	0.0	-6.0					
ZHU16	80.2	521.07	-0.2	-6.6					
ZHU15	79.5	521.09	-0.2	-6.2		158.04			
ZHU14	79.2	521.10	-0.2	-6.1					
ZHU13	78.6	521.12	-0.2	-6.5	34.1	68.73	80.9	0.008	0.17
ZHU12	78.4	521.12	-0.1	-6.8					
ZHU11	78.0	521.13	-0.3	-6.1					
ZHU10	77.0	521.16	-0.3	-6.3					
ZHU09	76.4	521.18	-0.1	-6.3	34.2	47.74	83.2	0.009	0.14
ZHU08	75.6	521.20	-0.2	-6.6	31.3	181.44	74.5	0.044	0.16
ZHU07	73.5	521.27	-1.4	-6.8	29.4	83.53	81.4	0.012	0.65
ZHU06	72.7	521.29	-1.3	-6.9	29.8	87.99	78.7	0.012	0.12
ZHU05	72.1	521.31	-1.4	-6.3					
ZHU04	71.8	521.32	-1.4	-6.6	28.6	173.99	58.1	0.010	0.15
ZHU03	71.2	521.33	-1.6	-6.7	27.7	204.17	69.0	0.282	0.85
ZHU02	70.5	521.35	-1.6	-6.7					
ZHU01	70.0	521.37	-1.6	-6.6	28.8	129.90	72.8	0.158	0.53

Sample	Height (m)	Age (Ma)	$\delta^{13}C$ (‰)	$\delta^{18}O$ (‰)	$\delta^{34}S_{CAS}$ (‰)	[CAS] ppm	Carbonate % (%)	Mg/Ca (w/w)	Mn/Sr (w/w)
IST50	67.1	521.45	-1.7	-7.4	27.4	91.30	77.9	0.011	0.12
IST49	66.0	521.49	-1.7	-7.2					
IST48	65.5	521.50	-1.8	-7.0	26.8	74.55	76.0	0.091	0.29
IST47	65.0	521.52	-2.0	-6.9	26.8	67.21	73.7	0.128	0.28
IST46	64.5	521.53	-1.9	-6.2					
IST45	64.0	521.55	-2.0	-7.1					
IST44	63.5	521.56	-2.0	-6.3					
IST43	60.0	521.69	-2.0	-7.1	27.0	134.51	72.6	0.135	0.41
IST42	53.5	521.93	-2.0	-7.2	28.8	179.16	73.1	0.114	0.40
IST41	52.5	521.97	-1.9	-6.8	28.1	68.34	79.6	0.010	0.53
IST40	51.5	522.01	-1.5	-7.3	28.9	53.56	68.7	0.177	0.27
IST39	49.7	522.08	-1.5	-7.0	28.9	19.39	69.9	0.077	0.48
IST38	47.7	522.15	-1.4	-7.1					
IST37	47.4	522.16	-1.4	-6.7					
IST36	46.5	522.20	-1.4	-7.3					
IST35	46.0	522.21	-1.4	-6.9	29.0	75.64	79.2	0.010	0.40
IST34	45.0	522.25	-1.3	-6.6	29.8	154.67	80.7	0.008	0.23
IST33	44.0	522.29	-1.4	-7.1	28.0	75.19	67.2	0.083	0.47
IST32	43.0	522.33	-1.3	-6.7	28.6	121.58	71.7	0.172	0.47
IST31	42.0	522.36	-1.3	-7.1					
IST30	41.9	522.37	-1.3	-7.1	28.9	20.70	73.1	0.047	0.24
IST29	41.5	522.38	-0.8	-6.4					
IST28	41.0	522.40	-1.1	-5.8	28.2	89.80	70.0	0.311	0.92
IST27	40.0	522.44	-1.2	-6.7					
IST26	39.0	522.48	-0.8	-6.6	28.7	109.50	72.7	0.096	0.52
IST25	38.0	522.51	-0.6	-6.7	29.5	195.56	74.1	0.135	0.43
IST24	37.0	522.55	-0.5	-6.9	30.6	86.18	79.3	0.020	0.22
IST23	36.0	522.59	0.0	-6.3	29.8	71.60	74.0	0.170	0.70
IST22	35.0	522.63	-0.2	-6.8					
IST21	34.0	522.66	-0.2	-7.1	31.1	43.69	72.6	0.064	0.36
IST20	31.0	522.78	0.8	-6.8	30.7	91.68	67.9	0.148	0.54
IST19	29.0	522.85	1.0	-6.7	32.2	98.10	70.1	0.131	0.69
IST18	27.0	522.91	0.9	-6.6					
IST17	19.9	523.12	0.6	-6.8					
IST16	19.8	523.12	0.6	-6.6	32.5	61.78	69.0	0.179	0.63
IST15	13.5	523.31	0.5	-7.0	28.8	121.53	62.9	0.216	0.90
IST14	12.5	523.34	0.3	-6.5	28.0	11.22	67.6	0.139	0.99
IST13	11.5	523.37	0.4	-6.7	29.1	323.31	69.4	0.255	0.94
IST12	11.0	523.39	0.1	-6.8	28.5	20.35	73.6	0.084	0.68
IST11	10.2	523.41	-0.5	-6.5	28.1	115.74	61.8	0.220	1.08
IST10	9.0	523.44	-1.2	-7.1	24.5	106.28	64.7	0.093	0.97
IST09	8.0	523.47	-1.1	-7.1	24.5	39.65	67.1	0.069	0.87
IST08	7.0	523.50	-1.0	-6.5		52.64	76.2	0.019	0.34
IST07	6.0	523.53	-1.3	-6.9	25.0	76.92	71.3	0.033	0.64
IST06	4.7	523.57	-1.8	-7.0					
IST05	4.0	523.59	-1.7	-7.2					
IST04	3.0	523.62	-2.1	-6.8		40.05			
IST03	2.7	523.63	-2.6	-6.2	27.5	73.71	81.3	0.012	0.05
DVO13	2.8	523.63	-2.6	-6.6					
DVO11	1.5	523.67	-2.2	-6.7		144.69			
DVO10	1.4	523.67	-1.8	-6.5	27.5	17.60	69.2	0.058	0.61
DVO08	1.2	523.68	-1.8	-6.4	29.7	85.95	77.3	0.012	0.85
DVO07	1.1	523.68	-1.5	-6.7					
DVO06	1.0	523.68	-0.3	-5.5					
DVO04	0.8	523.69	-0.5	-7.3					
DVO02	0.0	523.71	0.5	-7.4					
DVO01	0.0	523.71	0.5	-6.5	29.6	19.04	85.9	0.134	0.95

Appendix D

Strontium isotopes, and elemental data for Aldan-Lena Rivers sections

HCl-leachable: total 10% HCl-leachable elemental contents of bulk carbonate samples; 2nd leach: elemental concentration in acetic leachate solution from 2nd leaching step (see method details in section 4.2.2). TA: Tit-Ary section; LAB: Labaia section; UT: Ulakhan-Tyoidukh section; UKT: Ulakhan-Kyyry-Tass section; ZHU: Zhurinsky-Mys section; IST: Isit section; DVO: Dvortsy section. normalised: analysed $^{87}Sr/^{86}Sr$ data are adjusted to international standard NIST SRM 987, which gives $^{87}Sr/^{86}Sr$ ratios of 0.710248 (McArthur, Howarth and Shields-Zhou, 2012).

Sample	Height (m)	Age (Ma)	$\delta^{13}C$ (‰)	$\delta^{18}O$ (‰)	HCl-leachable carbonate% %	[Sr] ppm	[Al] ppm	[Rb] ppm	Rb/Sr w/w	Mn/Sr w/w	2nd leach [Sr] ppb	Sr/Ca w/w	Mg/Ca w/w	Mn/Sr w/w	Rb/Sr w/w	$^{87}Sr/^{86}Sr$ analysed	$^{87}Sr/^{86}Sr$ normalised
TA28	600.0	513.08	-0.9	-6.7	88.1	604.26	0.00	2.83	0.00468	0.04	3.46	1.34	0.00	0.02	0.00009	0.708562	0.708576
LAB81	528.8	513.87	-1.8	-6.6	88.5	465.43	98.36	4.15	0.00891	0.04	2.82	1.06	0.01	0.01	0.00013	0.708544	0.708558
LAB56	482.2	514.39	-1.4	-7.2	87.7	410.83	46.86	5.23	0.01273	0.04	2.96	1.11	0.01	0.01	0.00015	0.708553	0.708567
LAB35	444.0	514.82	-1.4	-6.7	86.9	716.10	94.64	0.87	0.00122	0.03	3.91	1.49	0.01	0.02	0.00010	0.708531	0.708545
LAB24	421.9	515.07	-1.1	-6.4	86.2	763.28	247.16	3.54	0.00464	0.03	4.26	1.64	0.02	0.02	0.00030	0.708538	0.708552
LAB20	414.9	515.15	-1.1	-6.3	88.3	740.42	143.53	5.68	0.00767	0.03	4.72	1.78	0.02	0.01	0.00013	0.708541	0.708555
LAB11	402.4	515.29	-1.0	-6.5	88.2	520.53	167.06	2.76	0.00530	0.03	3.34	1.28	0.01	0.02	0.00012	0.708536	0.708550
LAB06	400.5	515.31	-1.2	-6.8	88.0	549.27	126.43	5.59	0.01018	0.03	3.31	1.26	0.02	0.01	0.00019	0.708545	0.708559
UT36	330.2	516.09	0.8	-6.1	88.0	502.67	115.17	4.02	0.00800	0.05	3.10	1.08	0.01	0.02	0.00012	0.708518	0.708532
UT27	324.2	516.16	0.6	-6.1	87.8	662.18	111.39	7.86	0.01187	0.05	4.43	1.57	0.01	0.04	0.00001	0.708523	0.708537
UT19	316.2	516.25	0.7	-6.3	88.5	510.89	66.88	3.78	0.00740	0.09	2.77	1.00	0.02	0.04	0.00016	0.708529	0.708543
UKT101	312.5	516.29	0.5	-5.9	88.8	644.94	187.79	3.99	0.00619	0.05	4.37	1.50	0.04	0.04	0.00007	0.708531	0.708545
UKT090	307.0	516.35	0.3	-6.1	87.5	664.80	138.86	3.43	0.00516	0.07	3.87	1.46	0.02	0.02	0.00019	0.708534	0.708548
UKT083	299.4	516.44	0.0	-7.1	87.3	476.66	75.78	5.07	0.01064	0.07	3.22	1.07	0.01	0.03	0.00006	0.708552	0.708566
UKT068	287.7	516.57	0.2	-6.3	88.0	649.27	88.33	1.70	0.00263	0.06	4.00	1.53	0.02	0.01	0.00024	0.708591	0.708605
UKT066	285.2	516.59	0.3	-6.6	87.2	529.70	78.55	4.17	0.00788	0.08	3.03	1.12	0.01	0.02	0.00024	0.708564	0.708578
UKT061	279.7	516.66	1.2	-7.2	87.2	400.28	55.34	3.24	0.00809	0.09	2.54	0.84	0.01	0.03	0.00035	0.708554	0.708568
UT13	273.8	516.72	2.1	-6.6	87.1	313.56	0.00	0.00	0.00000	0.05	1.90	0.65	0.01	0.02	0.00012	0.708519	0.708533
UT12	272.8	516.73	2.0	-5.9	87.2	281.15	2.41	2.61	0.00930	0.06	1.58	0.58	0.01	0.02	0.00013	0.708522	0.708536
UT03	266.2	516.81	3.7	-6.5	87.3	196.12	0.00	3.30	0.01683	0.21	0.90	0.30	0.01	0.07	0.00032	0.708547	0.708561
UT02	265.7	516.81	2.9	-6.3	88.0	135.43	145.37	3.09	0.02278	0.82	0.73	0.25	0.01	0.31	0.00044	0.708611	0.708625
UKT054	259.8	516.88	2.6	-4.4	82.7	238.43	534.84	3.83	0.01608	0.73	1.56	0.61	0.02	0.32	0.00349	0.708880	0.708894
UKT051	257.8	516.90	2.1	-4.2	77.1	197.27	1178.45	7.01	0.03552	1.10	1.28	0.46	0.08	1.11	0.00934	0.709380	0.709394
UKT045	251.7	516.97	0.3	-5.1	73.0	259.75	1241.70	4.76	0.01834	1.00	2.02	0.71	0.02	0.55	0.00599	0.709023	0.709037
UKT043	249.6	516.99	-0.7	-5.7	81.6	297.78	303.41	4.15	0.01393	0.27	1.14	0.48	0.12	0.15	0.00168	0.708740	0.708754
UKT036	243.6	517.12	-0.8	-5.1	80.3	285.75	340.17	3.73	0.01305	0.33	1.83	0.63	0.01	0.21	0.00152	0.708723	0.708737
UKT033	238.6	517.24	-0.1	-5.1	82.4	280.15	72.14	1.42	0.00506	0.42	2.72	0.70	0.01	0.01	0.00003	0.708602	0.708616
UKT032	237.8	517.26	0.0	-5.7	82.1	364.36	214.08	0.00	0.00000	0.50	2.44	0.88	0.05	0.16	0.00092	0.708660	0.708674
UKT026	232.4	517.39	1.1	-5.4	77.9	546.03	539.04	1.94	0.00356	0.26	4.20	1.61	0.02	0.09	0.00178	0.708713	0.708727
UKT020	222.2	517.63	0.4	-5.7	74.6	268.52	773.65	5.10	0.01900	0.92	1.92	0.61	0.04	0.59	0.00405	0.708850	0.708864
UKT016	213.2	517.84	-0.1	-6.2	75.4	467.80	391.67	0.60	0.00128	0.23	3.64	1.32	0.01	0.16	0.00177	0.708629	0.708643
UKT009	205.0	518.04	1.5	-5.8	80.8	402.57	190.80	3.06	0.00761	0.15	2.80	1.03	0.01	0.01	0.00041	0.708552	0.708566
UKT006	202.3	518.10	2.2	-5.7	82.9	330.05	40.04	3.06	0.00928	0.14	1.94	0.69	0.00	0.07	0.00027	0.708475	0.708489
ZHU35	110.0	520.28	1.2	-6.2	80.0	605.67	411.15	4.12	0.00680	0.06	2.63	0.97	0.01	0.06	0.00085	0.708334	0.708348
ZHU28	92.8	520.70	0.8	-6.2	77.1	180.75	788.79	1.78	0.00987	0.73	0.79	0.30	0.18	0.29	0.00856	0.708943	0.708957
ZHU24	87.8	520.85	0.4	-6.3	77.6	322.54	545.45	5.45	0.01690	0.28	2.69	0.89	0.01	0.14	0.00167	0.708440	0.708454

Sample	Height (m)	Age (Ma)	$\delta^{13}C$ (‰)	$\delta^{18}O$ (‰)	HCl-leachable carbonate% %	[Sr] ppm	[Al] ppm	[Rb] ppm	Rb/Sr w/w	Mn/Sr w/w	2nd leach [Sr] ppb	Sr/Ca w/w	Mg/Ca w/w	Mn/Sr w/w	Rb/Sr w/w	$^{87}Sr/^{86}Sr$ analysed	$^{87}Sr/^{86}Sr$ normalised
ZHU20	83.7	520.97	0.0	-7.0	74.1	472.96	633.38	8.05	0.01703	0.14	2.11	0.80	0.01	0.15	0.00166	0.708371	0.708385
ZHU13	78.6	521.12	-0.2	-6.5	80.9	294.79	177.85	1.56	0.00530	0.17	2.38	0.83	0.01	0.11	0.00103	0.708352	0.708366
ZHU09	76.4	521.18	-0.1	-6.3	83.2	371.04	12.67	2.89	0.00779	0.14	2.19	0.81	0.01	0.03	0.00005	0.708238	0.708252
ZHU01	70.0	521.37	-1.6	-6.6	72.8	227.66	1145.99	6.08	0.02671	0.53	1.69	0.55	0.06	0.23	0.00668	0.708767	0.708781
IST47	65.0	521.52	-2.0	-6.9	73.7	393.88	1151.26	7.36	0.01869	0.28	3.30	1.21	0.03	0.14	0.00307	0.708481	0.708495
IST42	53.5	521.93	-2.0	-7.2	73.1	293.35	1017.70	7.37	0.02513	0.40	2.12	0.67	0.04	0.13	0.00436	0.708497	0.708511
IST35	46.0	522.21	-1.4	-6.9	79.2	270.42	363.91	5.82	0.02154	0.40	1.62	0.61	0.01	0.25	0.00192	0.708396	0.708410
IST26	39.0	522.48	-0.8	-6.6	72.7	217.38	1024.62	2.23	0.01025	0.52	1.34	0.40	0.03	0.25	0.00638	0.708736	0.708750
IST24	37.0	522.55	-0.5	-6.9	79.3	363.23	487.88	3.22	0.00887	0.22	2.82	0.97	0.01	0.15	0.00104	0.708268	0.708282
IST19	29.0	522.85	1.0	-6.7	70.1	224.44	1373.15	5.59	0.02490	0.69	1.66	0.51	0.06	0.30	0.00973	0.708940	0.708954
IST12	11.0	523.39	0.1	-6.8	73.6	231.40	1051.44	3.58	0.01549	0.68	1.92	0.75	0.05	0.26	0.00594	0.708740	0.708754
IST03	2.7	523.63	-2.6	-6.2	81.3	1296.37	190.69	3.00	0.00231	0.05	9.73	3.57	0.01	0.02	0.00010	0.708104	0.708118

Appendix E

Latest Ediacaran–early Cambrian seawater $^{87}Sr/^{86}Sr$ database of least-altered carbonate

$^{87}Sr/^{86}Sr$ data have been adjusted to international standard NIST SRM 987, which gives $^{87}Sr/^{86}Sr$ ratios of 0.710248 (McArthur, Howarth and Shields-Zhou, 2012). Age model correlation between sections is discussed in section 4.2.3. Database references: data from Appendix D of this study; Derry *et al*. (1994); Maloof *et al*. (2010); Li *et al*. (2013); Brasier *et al*. (1996).

Sample	$^{87}Sr/^{86}Sr$	Age (Ma)	Fm./Mb.	Biozones	Region/State	Stage in reference	International Stage	Source
TA28	0.70858	513.1	Keteme	*Bergeroniellus ketemensis*	Aldan-Lena Rivers, Siberia	Toyonian	Stage 4	This study
LAB81	0.70856	513.9	Kutorgina	*Bergeroniaspis ornata*	Aldan-Lena Rivers, Siberia	Botomian	Stage 4	This study
LAB56	0.70857	514.4	Kutorgina	*Bergeroniaspis ornata*	Aldan-Lena Rivers, Siberia	Botomian	Stage 3	This study
LAB35	0.70855	514.8	Kutorgina	*Bergeroniellus asiaticus*	Aldan-Lena Rivers, Siberia	Botomian	Stage 3	This study
LAB24	0.70855	515.1	Kutorgina	*Bergeroniellus asiaticus*	Aldan-Lena Rivers, Siberia	Botomian	Stage 3	This study
LAB20	0.70856	515.1	Kutorgina	*Bergeroniellus asiaticus*	Aldan-Lena Rivers, Siberia	Botomian	Stage 3	This study
LAB11	0.70855	515.3	Kutorgina	*Bergeroniellus asiaticus*	Aldan-Lena Rivers, Siberia	Botomian	Stage 3	This study
LAB06	0.70856	515.3	Kutorgina	*Bergeroniellus asiaticus*	Aldan-Lena Rivers, Siberia	Botomian	Stage 3	This study
UT36	0.70853	516.1	Sinsk	*Bergeroniellus gurarii*	Aldan-Lena Rivers, Siberia	Botomian	Stage 3	This study
UT27	0.70854	516.2	Sinsk	*Bergeroniellus gurarii*	Aldan-Lena Rivers, Siberia	Botomian	Stage 3	This study
UT19	0.70854	516.2	Sinsk	*Bergeroniellus gurarii*	Aldan-Lena Rivers, Siberia	Botomian	Stage 3	This study
UKT101	0.70855	516.3	Sinsk	*Bergeroniellus gurarii*	Aldan-Lena Rivers, Siberia	Botomian	Stage 3	This study
UKT090	0.70855	516.4	Sinsk	*Bergeroniellus gurarii*	Aldan-Lena Rivers, Siberia	Botomian	Stage 3	This study
UKT083	0.70857	516.4	Perekhod	*B. zelenovi - P. squamosu/B. micmacciformis - Erbiella*	Aldan-Lena Rivers, Siberia	Botomian	Stage 3	This study
UKT068	0.70861	516.6	Perekhod	*B. zelenovi - P. squamosu/B. micmacciformis - Erbiella*	Aldan-Lena Rivers, Siberia	Botomian	Stage 3	This study
UKT066	0.70858	516.6	Perekhod	*B. zelenovi - P. squamosu/B. micmacciformis - Erbiella*	Aldan-Lena Rivers, Siberia	Botomian	Stage 3	This study
UKT061	0.70857	516.7	Perekhod	*B. zelenovi - P. squamosu/B. micmacciformis - Erbiella*	Aldan-Lena Rivers, Siberia	Botomian	Stage 3	This study
UT13	0.70853	516.7	Perekhod	*B. zelenovi - P. squamosu/B. micmacciformis - Erbiella*	Aldan-Lena Rivers, Siberia	Botomian	Stage 3	This study
UT12	0.70854	516.7	Perekhod	*B. zelenovi - P. squamosu/B. micmacciformis - Erbiella*	Aldan-Lena Rivers, Siberia	Botomian	Stage 3	This study
UT03	0.70856	516.8	Perekhod	*B. zelenovi - P. squamosu/B. micmacciformis - Erbiella*	Aldan-Lena Rivers, Siberia	Botomian	Stage 3	This study
UKT033	0.70862	517.2	Perekhod	*Fansycyathus lermontovae/Judomia*	Aldan-Lena Rivers, Siberia	Atdabanian	Stage 3	This study
UKT032	0.70867	517.3	Perekhod	*Fansycyathus lermontovae/Judomia*	Aldan-Lena Rivers, Siberia	Atdabanian	Stage 3	This study
UKT026	0.70873	517.4	Perekhod	*Fansycyathus lermontovae/Judomia*	Aldan-Lena Rivers, Siberia	Atdabanian	Stage 3	This study
UKT016	0.70864	517.8	Pestrotsvet	*Nochoroicyathus Kokoulini/Judomia*	Aldan-Lena Rivers, Siberia	Atdabanian	Stage 3	This study
UKT009	0.70857	518.0	Pestrotsvet	*Nochoroicyathus Kokoulini/Judomia*	Aldan-Lena Rivers, Siberia	Atdabanian	Stage 3	This study
UKT006	0.70849	518.1	Pestrotsvet	*Nochoroicyathus Kokoulini/Judomia*	Aldan-Lena Rivers, Siberia	Atdabanian	Stage 3	This study
ZHU35	0.70835	520.3	Pestrotsvet	*Retecoscinus zegebarti/Repinaella*	Aldan-Lena Rivers, Siberia	Atdabanian	Stage 3	This study
ZHU24	0.70845	520.8	Pestrotsvet	*Retecoscinus zegebarti/Profallotaspis jakutensis*	Aldan-Lena Rivers, Siberia	Atdabanian	Stage 3	This study
ZHU20	0.70839	521.0	Pestrotsvet	*Retecoscinus zegebarti/Profallotaspis jakutensis*	Aldan-Lena Rivers, Siberia	Atdabanian	Stage 3	This study
ZHU13	0.70837	521.1	Pestrotsvet	*Retecoscinus zegebarti/Profallotaspis jakutensis*	Aldan-Lena Rivers, Siberia	Atdabanian	Stage 2	This study
ZHU09	0.70825	521.2	Pestrotsvet	*Retecoscinus zegebarti/Profallotaspis jakutensis*	Aldan-Lena Rivers, Siberia	Atdabanian	Stage 2	This study
IST24	0.70828	522.6	Pestrotsvet	*Dokidocyathus regularis/Lapworthella bella*	Aldan-Lena Rivers, Siberia	Tommotian	Stage 2	This study
IST03	0.70812	523.6	Pestrotsvet	*Nochoroicyathus sunnaginicus*	Aldan-Lena Rivers, Siberia	Tommotian	Stage 2	This study
Elanka 20	0.70883	511.1	Elanka	*Anabaraspis splendens*	Aldan-Lena Rivers, Siberia	Amgan	Stage 4	Derry et al., 1994
tary W 55/32g	0.70861	512.1	Titary	*L. grandis*	Aldan-Lena Rivers, Siberia	Toyonian	Stage 4	Derry et al., 1994
Tit W 56/11a	0.70863	512.5	Keteme	*L. grandis*	Aldan-Lena Rivers, Siberia	Toyonian	Stage 4	Derry et al., 1994
Tit W 56/1z	0.70858	512.9	Keteme	*L. grandis*	Aldan-Lena Rivers, Siberia	Toyonian	Stage 4	Derry et al., 1994
Tit W 43/1a	0.70853	514.4	Kutorgina	*Bergeroniaspis ornata*	Aldan-Lena Rivers, Siberia	Botomian	Stage 3	Derry et al., 1994
Lab 15	0.70854	514.9	Kutorgina	*Bergeroniellus asiaticus*	Aldan-Lena Rivers, Siberia	Botomian	Stage 3	Derry et al., 1994
Lab 9	0.70852	515.3	Kutorgina	*Bergeroniellus asiaticus*	Aldan-Lena Rivers, Siberia	Botomian	Stage 3	Derry et al., 1994
Lab 1	0.70852	515.7	Kutorgina	*Bergeroniellus asiaticus*	Aldan-Lena Rivers, Siberia	Botomian	Stage 3	Derry et al., 1994
AKT 20-77	0.70857	517.2	Perekhod	*Fansycyathus lermontovae*	Aldan-Lena Rivers, Siberia	Atdabanian	Stage 3	Derry et al., 1994
ZUR BASE BD 2	0.70814	522.9	Pestrotsvet	*Lapworthella bella*	Aldan-Lena Rivers, Siberia	Tommotian	Stage 2	Derry et al., 1994
M304	0.70829	520.5			M304 section, Morocco	Atdabanian	Stage 3	Maloof et al., 2010
XT-115	0.70838	527.1	Dahai Mb.	*Watsonella crosbyi*	Xiaotan section, South China	Meishucunian	Stage 2	Li et al., 2013
XT-117	0.70831	527.2	Dahai Mb.	*Watsonella crosbyi*	Xiaotan section, South China	Meishucunian	Stage 2	Li et al., 2013

Sample	$^{87}Sr/^{86}Sr$	Age (Ma)	Fm./Mb.	Biozones	Region/State	Stage in reference	International Stage	Source
XT-120	0.70826	527.3	Dahai Mb.	*Watsonella crosbyi*	Xiaotan section, South China	Meishucunian	Stage 2	Li et al., 2013
XT-125	0.70834	527.5	Dahai Mb.	*Watsonella crosbyi*	Xiaotan section, South China	Meishucunian	Stage 2	Li et al., 2013
XT-130	0.70828	527.7	Dahai Mb.	*Watsonella crosbyi*	Xiaotan section, South China	Meishucunian	Stage 2	Li et al., 2013
XT-135	0.70828	527.9	Dahai Mb.	*Watsonella crosbyi*	Xiaotan section, South China	Meishucunian	Stage 2	Li et al., 2013
XT-139	0.70827	528.1	Dahai Mb.	*Watsonella crosbyi*	Xiaotan section, South China	Meishucunian	Stage 2	Li et al., 2013
XT-140	0.70857	528.1	Dahai Mb.	*Watsonella crosbyi*	Xiaotan section, South China	Meishucunian	Stage 2	Li et al., 2013
XT-143	0.70831	528.2	Dahai Mb.	*Watsonella crosbyi*	Xiaotan section, South China	Meishucunian	Stage 2	Li et al., 2013
XT-145	0.70827	528.3	Dahai Mb.	*Watsonella crosbyi*	Xiaotan section, South China	Meishucunian	Stage 2	Li et al., 2013
XT-148	0.70828	528.5	Dahai Mb.	*Watsonella crosbyi*	Xiaotan section, South China	Meishucunian	Stage 2	Li et al., 2013
Sal KH	0.70829	522.7	Khayrkhan		Mongolia	Atdabanian	Stage 3	Brasier et al., 1996
Sal SG3	0.70813	523.1	Salaany Gol		Mongolia	Atdabanian	Stage 3	Brasier et al., 1996
Bay 21-B73	0.70850	532.3	Bayan Gol		Mongolia	Nemakit-Daldynian	Stage 2	Brasier et al., 1996
Bay 21-B66	0.70855	533.1	Bayan Gol		Mongolia	Nemakit-Daldynian	Stage 2	Brasier et al., 1996
Sal By 26	0.70845	533.2	Bayan Gol		Mongolia	Nemakit-Daldynian	Stage 2	Brasier et al., 1996
Bay 21-B64	0.70844	533.3	Bayan Gol		Mongolia	Nemakit-Daldynian	Stage 2	Brasier et al., 1996
Sal By 25	0.70848	533.4	Bayan Gol		Mongolia	Nemakit-Daldynian	Stage 2	Brasier et al., 1996
Sal By 22b	0.70847	535.3	Bayan Gol		Mongolia	Nemakit-Daldynian	Fortunian	Brasier et al., 1996
Sal By 21	0.70846	535.4	Bayan Gol		Mongolia	Nemakit-Daldynian	Fortunian	Brasier et al., 1996
Bay 56	0.70849	536.4	Bayan Gol		Mongolia	Nemakit-Daldynian	Fortunian	Brasier et al., 1996
Tsag 31	0.70854	538.2	Bayan Gol		Mongolia	Nemakit-Daldynian	Fortunian	Brasier et al., 1996
Tsag 28	0.70843	539.4	Bayan Gol		Mongolia	Nemakit-Daldynian	Fortunian	Brasier et al., 1996
Bay 33	0.70846	539.8	Tsagaan Oloom		Mongolia	Nemakit-Daldynian	Fortunian	Brasier et al., 1996
Tsag 25	0.70848	539.8	Tsagaan Oloom		Mongolia	Nemakit-Daldynian	Late Ediacaran	Brasier et al., 1996
Tsag 24	0.70855	541.1	Tsagaan Oloom		Mongolia	Nemakit-Daldynian	Late Ediacaran	Brasier et al., 1996
Bay S5	0.70842	545.3	Tsagaan Oloom		Mongolia	Nemakit-Daldynian	Late Ediacaran	Brasier et al., 1996
Bay S4	0.70853	545.5	Tsagaan Oloom		Mongolia	Nemakit-Daldynian	Late Ediacaran	Brasier et al., 1996
Tsag 20	0.70842	545.5	Tsagaan Oloom		Mongolia	Nemakit-Daldynian	Late Ediacaran	Brasier et al., 1996
Bay S0	0.70853	545.9	Tsagaan Oloom		Mongolia	Nemakit-Daldynian	Late Ediacaran	Brasier et al., 1996

Appendix F

Sample descriptions, sampling GPS locations and U-Pb detrital zircon ages for Tonian–Cambrian successions of North China Craton

Sampling stratigraphic horizons for individual sample is marked in Fig. 5.1. Disc: discordance; Del: deleted. Ying Zhou (University College London) provided data of JSZG2 and JSZG3.

† Age discordance was calculated by ($^{206}Pb/^{238}U$ age)/($^{207}Pb/^{235}U$ age)*100-100 if $^{206}Pb/^{238}U$ age <1100 Ma, otherwise by ($^{206}Pb/^{238}U$ age)/($^{207}Pb/^{206}Pb$ age)*100-100;
§ Del: Analysis is discarded due to large age discordance (not between +5% and -15%);
# Use $^{206}Pb/^{238}U$ age if the age is younger than 1100 Ma, otherwise use $^{207}Pb/^{206}Pb$ age.

Analysis No.	U (ppm)	Pb (ppm)	Th/U	Measured isotopic ratios						Calculated isotopic ages (Ma)						Disc.† (%)	Comment§	Preferred age (Ma)#	
				$^{207}Pb/^{206}Pb$	1σ	$^{207}Pb/^{235}U$	1σ	$^{206}Pb/^{238}U$	1σ	$^{207}Pb/^{206}Pb$	1σ	$^{207}Pb/^{235}U$	1σ	$^{206}Pb/^{238}U$	1σ			Age	1σ
Sample GT01/2014, quartz sandstone, Lower Getun Formation, Manjiantan section of Dalian region, GPS: 39°04'37"N 122°03'36"E																			
GT01/2014_G001	145.5	24.6	0.2844	0.0720	0.0010	1.6511	0.0243	0.1664	0.0020	985.1	9.1	990	11.8	992.5	10.8	0.3		992.5	10.8
GT01/2014_G002	85.4	36	3.9141	0.0787	0.0011	2.1647	0.0320	0.1995	0.0024	1164.9	10	1169.8	13	1172.8	12.8	0.7		1164.9	10
GT01/2014_G003	158.6	28.4	0.25	0.0767	0.0010	1.8819	0.0254	0.1781	0.0021	1112.4	8.8	1074.7	11.5	1056.6	11.2	-1.7		1056.6	11.2
GT01/2014_G004	108.1	17.6	0.2416	0.0731	0.0011	1.6438	0.0245	0.1631	0.0019	1017.6	9.4	987.2	11.9	973.8	10.7	-1.4		973.8	10.7
GT01/2014_G005	129.8	50.7	0.955	0.1128	0.0014	4.9289	0.0619	0.3170	0.0036	1845.5	10.2	1807.2	14	1774.8	17.8	-3.8		1845.5	10.2
GT01/2014_G006	342.5	63.6	0.2492	0.0754	0.0009	1.9162	0.0238	0.1844	0.0021	1078.7	7.8	1086.8	10.9	1091.1	11.3	0.4		1091.1	11.3
GT01/2014_G007	285	147.4	0.4872	0.1685	0.0019	10.6644	0.1252	0.4592	0.0051	2542.7	10.2	2494.3	14.5	2436	22.7	-4.2		2542.7	10.2
GT01/2014_G008	70.6	17.2	0.3635	0.0871	0.0013	2.7993	0.0413	0.2331	0.0028	1363.4	10.8	1355.3	14.1	1350.7	14.7	-0.9		1363.4	10.8
GT01/2014_G009	156	34.6	0.6698	0.0795	0.0010	2.1416	0.0287	0.1955	0.0023	1183.9	9.1	1162.3	12	1151.2	12.1	-2.8		1183.9	9.1
GT01/2014_G010	330.3	64.6	0.2956	0.0775	0.0009	2.0469	0.0255	0.1915	0.0022	1134.9	8.1	1131.2	11.1	1129.7	11.6	-0.5		1134.9	8.1
GT01/2014_G011	92.4	20.3	0.4796	0.0800	0.0012	2.2516	0.0333	0.2042	0.0024	1197.5	10.2	1197.3	13.2	1197.6	13.1	0.0		1197.5	10.2
GT01/2014_G012	80.2	18.8	0.3936	0.0844	0.0013	2.5825	0.0389	0.2221	0.0027	1300.9	10.9	1295.7	14	1292.9	14.2	-0.6		1300.9	10.9
GT01/2014_G013	154.2	32.9	0.3326	0.0801	0.0010	2.2747	0.0307	0.2061	0.0024	1199	9.1	1204.5	12.3	1207.9	12.7	0.7		1199	9.1
GT01/2014_G014	174.3	33.6	0.4231	0.0771	0.0010	1.9574	0.0264	0.1842	0.0021	1123.3	8.9	1101	11.7	1090	11.5	-1.0		1090	11.5
GT01/2014_G015	121.1	23.7	0.4663	0.1019	0.0014	2.6003	0.0357	0.1852	0.0022	1658.3	10.9	1300.7	13.1	1095.4	11.9	-15.8	Del.		
GT01/2014_G016	73.2	41	0.3901	0.1761	0.0021	12.0815	0.1517	0.4978	0.0058	2616.2	11.1	2610.7	15.6	2604.5	25	-0.4		2616.2	11.1
GT01/2014_G017	156.9	33.3	0.4091	0.0773	0.0010	2.1354	0.0288	0.2005	0.0023	1128.4	8.9	1160.3	12.1	1178	12.4	4.4		1128.4	8.9
GT01/2014_G018	52.3	13.6	0.6747	0.0834	0.0014	2.6184	0.0438	0.2279	0.0029	1277.9	12	1305.8	15.3	1323.3	15.1	3.6		1277.9	12
GT01/2014_G019	119.4	32	0.5637	0.0905	0.0012	3.0227	0.0409	0.2423	0.0028	1436.3	10	1413.4	13.3	1398.6	14.6	-2.6		1436.3	10
GT01/2014_G020	130.7	25	0.8021	0.0718	0.0010	1.6207	0.0239	0.1639	0.0019	978.9	9.1	978.2	11.8	978.2	10.7	0.0		978.2	10.7
GT01/2014_G021	173.4	32	0.5302	0.0734	0.0010	1.7224	0.0240	0.1702	0.0020	1025.3	8.8	1016.9	11.5	1013.4	10.9	-0.3		1013.4	10.9
GT01/2014_G022	137.7	42.4	0.5635	0.1026	0.0013	3.9267	0.0507	0.2776	0.0032	1672.2	10.1	1619.2	13.7	1579.3	16.1	-5.6		1672.2	10.1
GT01/2014_G023	481	117.4	0.2595	0.0924	0.0010	3.0574	0.0366	0.2401	0.0027	1475	8.8	1422.1	12.1	1387.4	13.9	-5.9		1475	8.8
GT01/2014_G024	132.5	28.4	0.6002	0.0776	0.0011	2.0647	0.0296	0.1930	0.0023	1136.9	9.6	1137.2	12.5	1137.7	12.3	0.1		1136.9	9.6
GT01/2014_G025	82.8	16	0.5447	0.0752	0.0011	1.8568	0.0272	0.1791	0.0021	1074.4	9.5	1065.9	12.3	1062.1	11.6	-0.4		1062.1	11.6
GT01/2014_G026	310.2	54.6	0.2678	0.0758	0.0009	1.8227	0.0235	0.1744	0.0020	1090.3	8.3	1053.7	11	1036.4	10.9	-1.6		1036.4	10.9
GT01/2014_G027	129.8	31	0.6053	0.0860	0.0012	2.5389	0.0354	0.2141	0.0025	1339.1	10	1283.2	13	1250.6	13.3	-6.6		1339.1	10
GT01/2014_G028	90.6	18.2	0.3129	0.0802	0.0015	2.1561	0.0397	0.1951	0.0026	1201.4	13	1167	15.7	1148.9	13.9	-4.4		1201.4	13
GT01/2014_G029	58.4	11.7	0.4082	0.0786	0.0013	2.0600	0.0350	0.1902	0.0024	1161.3	11.7	1135.6	14.4	1122.6	13	-3.3		1161.3	11.7
GT01/2014_G030	112.4	27.6	0.5384	0.0878	0.0012	2.7272	0.0379	0.2253	0.0027	1378.8	10.1	1335.9	13.3	1309.7	13.9	-5.0		1378.8	10.1
GT01/2014_G031	150.8	26.3	0.5202	0.0706	0.0010	1.5680	0.0227	0.1611	0.0019	946.1	8.7	957.6	11.4	962.9	10.5	0.6		962.9	10.5
GT01/2014_G032	117.6	88.4	1.6021	0.1823	0.0021	12.9518	0.1583	0.5153	0.0059	2674.3	10.8	2676.2	15.3	2679.4	25.2	0.2		2674.3	10.8
GT01/2014_G033	247.5	49.7	0.5182	0.0764	0.0010	1.9495	0.0255	0.1851	0.0021	1106.4	8.5	1098.3	11.4	1094.6	11.5	-0.3		1094.6	11.5
GT01/2014_G034	42.7	11.5	1.2891	0.0797	0.0015	2.2353	0.0429	0.2035	0.0027	1189.3	13.5	1192.2	16.5	1194.1	14.6	0.4		1189.3	13.5
GT01/2014_G035	172.5	40.4	0.4556	0.0833	0.0011	2.5038	0.0335	0.2182	0.0025	1275.3	9.3	1273.1	12.5	1272.3	13.3	-0.2		1275.3	9.3
GT01/2014_G036	44.4	11	0.6741	0.0792	0.0015	2.3799	0.0447	0.2180	0.0029	1176.9	13.1	1236.6	16.5	1271.5	15.3	8.0	Del.		
GT01/2014_G037	150.8	27.8	0.3296	0.0717	0.0011	1.7694	0.0266	0.1790	0.0021	978.3	9.3	1034.3	12.3	1061.3	11.6	2.6		1061.3	11.6
GT01/2014_G038	142	35.9	0.5097	0.0892	0.0012	2.8452	0.0390	0.2315	0.0027	1408	10.1	1367.5	13.3	1342.1	14.2	-4.7		1408	10.1
GT01/2014_G039	104.6	21.6	0.6302	0.0753	0.0012	1.9110	0.0300	0.1841	0.0022	1076.5	10.3	1084.9	13.2	1089.5	12.2	0.4		1089.5	12.2
GT01/2014_G040	303.3	70.7	0.5638	0.0802	0.0010	2.3396	0.0300	0.2115	0.0024	1202.9	8.6	1224.4	11.9	1237	12.8	2.8		1202.9	8.6
GT01/2014_G041	312.9	62	0.3887	0.0758	0.0010	1.9764	0.0257	0.1892	0.0022	1089.3	8.4	1107.5	11.4	1117.2	11.7	2.6		1089.3	8.4
GT01/2014_G042	132.5	25.3	0.3449	0.0740	0.0011	1.8835	0.0282	0.1847	0.0022	1040.9	9.6	1075.3	12.6	1092.7	12	1.6		1092.7	12
GT01/2014_G043	244	45.4	0.3367	0.0727	0.0010	1.8060	0.0244	0.1802	0.0021	1006.2	8.3	1047.6	11.4	1068	11.3	1.9		1068	11.3
GT01/2014_G044	225.7	42.6	0.5259	0.0724	0.0010	1.7323	0.0237	0.1737	0.0020	996.1	8.4	1020.6	11.3	1032.4	11	1.2		1032.4	11
GT01/2014_G045	99.3	22.9	0.9327	0.0776	0.0012	2.0324	0.0325	0.1901	0.0023	1136.4	10.8	1126.4	13.6	1121.6	12.6	-1.3		1136.4	10.8
GT01/2014_G046	180.4	55.8	0.9234	0.0904	0.0011	3.1851	0.0419	0.2557	0.0030	1433.6	9.7	1453.5	13.2	1467.7	15.1	2.4		1433.6	9.7
GT01/2014_G047	47.1	8.2	0.351	0.0762	0.0016	1.7825	0.0362	0.1697	0.0023	1100.9	13.8	1039.1	16	1010.3	12.7	-2.8		1010.3	12.7

Analysis No.	U (ppm)	Pb (ppm)	Th/U	Measured isotopic ratios						Calculated isotopic ages (Ma)						Disc.† (%)	Comment§	Preferred age (Ma)#	
				$^{207}Pb/^{206}Pb$	1σ	$^{206}Pb/^{238}U$	1σ	$^{206}Pb/^{238}U$	1σ	$^{207}Pb/^{206}Pb$	1σ	$^{206}Pb/^{238}U$	1σ	$^{206}Pb/^{238}U$	1σ			Age	1σ
Sample GT01/2014, quartz sandstone, Lower Getun Formation, Manjiantan section of Dalian region, GPS: 39°04'37"N 122°03'36"E																			
GT01/2014_G048	387.8	67.8	0.3574	0.0726	0.0009	1.6891	0.0216	0.1687	0.0019	1003.6	7.8	1004.4	10.6	1005.1	10.5	0.1		1005.1	10.5
GT01/2014_G049	22.7	4	0.6354	0.0697	0.0022	1.4992	0.0460	0.1561	0.0026	919.2	19.1	930.1	21.7	935	14.4	0.5		935	14.4
GT01/2014_G050	163	47.7	0.7342	0.0902	0.0012	3.1513	0.0421	0.2535	0.0029	1429.3	9.9	1445.3	13.4	1456.6	15.1	1.9		1429.3	9.9
GT01/2014_G051	63.6	12.8	0.9432	0.0735	0.0014	1.6928	0.0317	0.1670	0.0022	1028.9	12.1	1005.8	14.6	995.6	12	-1.0		995.6	12
GT01/2014_G052	88	24.1	0.5537	0.0929	0.0013	3.1819	0.0470	0.2486	0.0030	1485.2	11.3	1452.8	14.6	1431.1	15.6	-3.6		1485.2	11.3
GT01/2014_G053	60.1	16.5	0.6839	0.0870	0.0014	2.8739	0.0478	0.2398	0.0031	1359.4	12.3	1375.1	15.7	1385.7	15.9	1.9		1359.4	12.3
GT01/2014_G054	199.6	53.7	0.744	0.0873	0.0011	2.8021	0.0370	0.2328	0.0027	1367.6	9.6	1356.1	12.8	1349.2	14	-1.3		1367.6	9.6
GT01/2014_G055	433.1	86	0.4289	0.0748	0.0009	1.9321	0.0244	0.1873	0.0021	1064.2	7.9	1092.2	11	1106.7	11.5	4.0		1064.2	7.9
GT01/2014_G056	648.4	102.4	0.1209	0.0764	0.0009	1.7347	0.0222	0.1648	0.0019	1104.8	8.3	1021.5	10.8	983.5	10.3	-3.7		983.5	10.3
GT01/2014_G057	188.2	60.2	0.7882	0.0973	0.0012	3.6501	0.0474	0.2722	0.0031	1572.8	9.9	1560.5	13.5	1551.9	15.9	-1.3		1572.8	9.9
GT01/2014_G058	206.5	52.7	1.0834	0.0783	0.0011	2.1999	0.0305	0.2038	0.0024	1155	9.2	1181	12.4	1195.6	12.7	3.5		1155	9.2
GT01/2014_G059	278	48.7	0.18	0.0749	0.0010	1.8394	0.0247	0.1781	0.0021	1066.9	8.5	1059.6	11.4	1056.5	11.2	-0.3		1056.5	11.2
GT01/2014_G060	48.8	10.2	0.5951	0.0752	0.0015	1.9431	0.0391	0.1874	0.0025	1074.9	13.5	1096.1	16.4	1107.2	13.8	3.0		1074.9	13.5
GT01/2014_G061	53.2	11	0.5604	0.0777	0.0015	2.0174	0.0394	0.1884	0.0025	1138.7	13.5	1121.4	16.2	1112.8	13.7	-2.3		1138.7	13.5
GT01/2014_G062	121.1	30.7	0.4346	0.0873	0.0013	2.8494	0.0417	0.2369	0.0029	1366.9	10.8	1368.6	14.1	1370.3	14.9	0.2		1366.9	10.8
GT01/2014_G063	15.7	3.2	1.1401	0.0744	0.0030	1.6683	0.0650	0.1628	0.0032	1051.5	26.4	996.5	28.4	972.1	17.5	-2.5		972.1	17.5
GT01/2014_G064	219.6	38.6	0.5939	0.0694	0.0010	1.5261	0.0223	0.1595	0.0019	911.2	8.6	940.9	11.3	954.1	10.4	1.4		954.1	10.4
GT01/2014_G065	161.2	42.7	0.8228	0.0818	0.0012	2.5169	0.0364	0.2233	0.0027	1240.5	10.1	1276.9	13.4	1299.1	14	4.7		1240.5	10.1
GT01/2014_G066	282.4	97.9	0.523	0.1060	0.0013	4.5735	0.0574	0.3130	0.0036	1732.1	9.9	1744.5	13.7	1755.4	17.5	1.3		1732.1	9.9
GT01/2014_G067	48.8	10.9	0.3994	0.0808	0.0016	2.3582	0.0453	0.2118	0.0028	1216.1	13.7	1230.1	16.8	1238.5	15.1	1.8		1216.1	13.7
GT01/2014_G068	60.1	26.8	1.1726	0.1139	0.0017	5.3977	0.0811	0.3438	0.0043	1862.9	12.4	1884.5	16.5	1904.8	20.7	2.2		1862.9	12.4
GT01/2014_G069	427	78.1	0.3108	0.0712	0.0009	1.7564	0.0229	0.1789	0.0020	963.7	7.8	1029.5	10.9	1061.2	11.2	3.1		1061.2	11.2
GT01/2014_G070	126.4	46.2	0.4607	0.1114	0.0014	5.1249	0.0692	0.3337	0.0040	1822.5	10.9	1840.2	14.9	1856.5	19.1	1.9		1822.5	10.9
GT01/2014_G071	62.7	32	4.3366	0.0697	0.0013	2.1551	0.0394	0.2244	0.0029	918.9	11	1166.7	15.5	1305	15.3	42.0	Del.		
GT01/2014_G072	527.2	91	0.3498	0.0944	0.0011	2.1634	0.0271	0.1662	0.0019	1516.9	9.4	1169.4	11.4	991.2	10.4	-15.2	Del.		
GT01/2014_G073	95	17.9	0.3975	0.0749	0.0012	1.8556	0.0304	0.1797	0.0022	1066.4	10.7	1065.4	13.5	1065.4	12.1	0.0		1065.4	12.1
GT01/2014_G074	68	14	0.5158	0.0773	0.0014	2.0210	0.0354	0.1898	0.0024	1127.9	11.9	1122.6	14.7	1120.3	13.1	-0.7		1127.9	11.9
GT01/2014_G075	108.1	25.9	1.1211	0.0764	0.0012	1.9876	0.0307	0.1887	0.0023	1105.8	10.2	1111.3	13.1	1114.5	12.4	0.8		1105.8	10.2
GT01/2014_G076	32.2	8.2	0.3321	0.0777	0.0017	2.6030	0.0553	0.2432	0.0034	1137.9	14.6	1301.5	18.8	1403.4	17.8	23.3	Del.		
GT01/2014_G077	56.6	13.1	0.7957	0.0762	0.0015	2.0682	0.0399	0.1970	0.0026	1099.3	13	1138.3	16.1	1159.3	14.1	5.5	Del.		
GT01/2014_G078	110.7	19.8	0.2852	0.0746	0.0012	1.8155	0.0296	0.1765	0.0022	1058.3	10.7	1051.1	13.3	1048	11.9	-0.3		1048	11.9
GT01/2014_G079	194.3	87.9	1.0927	0.1153	0.0014	5.6333	0.0722	0.3544	0.0041	1885	10.5	1921.2	14.5	1955.6	19.5	3.7		1885	10.5
GT01/2014_G080	213.5	45.8	0.4366	0.0818	0.0011	2.2688	0.0322	0.2011	0.0024	1241.7	9.9	1202.7	12.8	1181.4	12.7	-4.9		1241.7	9.9
GT01/2014_G081	225.7	63.8	0.6499	0.0902	0.0012	3.1054	0.0413	0.2498	0.0029	1430	9.8	1434	13.2	1437.2	14.9	0.5		1430	9.8
GT01/2014_G082	370.4	74.2	0.614	0.0750	0.0010	1.8664	0.0249	0.1805	0.0021	1069.3	8.5	1069.3	11.4	1069.7	11.3	0.0		1069.7	11.3
GT01/2014_G083	81.9	15.8	0.3579	0.0756	0.0013	1.9470	0.0342	0.1868	0.0024	1085.3	11.7	1097.4	14.6	1103.9	12.9	1.7		1085.3	11.7
GT01/2014_G084	102.8	19.3	0.5479	0.0736	0.0013	1.7432	0.0301	0.1719	0.0022	1030	11.2	1024.6	13.8	1022.5	11.9	-0.2		1022.5	11.9
GT01/2014_G085	212.6	82.4	0.9298	0.1060	0.0013	4.6331	0.0600	0.3171	0.0037	1732.1	10.3	1755.3	14.1	1775.4	17.9	2.5		1732.1	10.3
GT01/2014_G086	129.8	23.6	0.3973	0.0732	0.0012	1.7521	0.0282	0.1738	0.0021	1018.4	10.3	1027.9	13	1032.7	11.7	0.5		1032.7	11.7
GT01/2014_G087	210	43.6	0.6621	0.0737	0.0010	1.8772	0.0270	0.1848	0.0022	1033.8	9.1	1073.1	12.2	1092.9	11.8	1.8		1092.9	11.8
GT01/2014_G088	536.8	100.4	0.342	0.0761	0.0009	1.9025	0.0245	0.1814	0.0021	1096.9	8.3	1082	11.2	1074.8	11.2	-0.7		1074.8	11.2
GT01/2014_G089	203.9	43.8	0.4711	0.0784	0.0011	2.1700	0.0309	0.2008	0.0024	1157.8	9.6	1171.5	12.7	1179.3	12.7	1.9		1157.8	9.6
GT01/2014_G090	163	36.5	0.6857	0.0790	0.0012	2.1533	0.0320	0.1978	0.0024	1171.6	10.1	1166.1	13.1	1163.5	12.7	-0.7		1171.6	10.1
GT01/2014_G091	149	28.6	0.3144	0.0782	0.0012	2.0485	0.0314	0.1901	0.0023	1151.5	10.4	1131.8	13.2	1121.9	12.4	-2.6		1151.5	10.4
GT01/2014_G092	81	16.2	0.4649	0.0796	0.0014	2.0519	0.0365	0.1870	0.0024	1187.1	12.5	1132.9	15	1105.2	13	-6.9		1187.1	12.5
GT01/2014_G093	181.3	37.7	0.3976	0.0757	0.0011	2.0694	0.0305	0.1982	0.0024	1088.2	9.6	1138.7	12.8	1165.8	12.7	7.1	Del.		
GT01/2014_G094	74.1	18.1	0.4085	0.0865	0.0014	2.7475	0.0462	0.2304	0.0029	1349.8	12.4	1341.4	15.6	1336.5	15.4	-1.0		1349.8	12.4

Analysis No.	U (ppm)	Pb (ppm)	Th/U	Measured isotopic ratios						Calculated isotopic ages (Ma)						Disc.† (%)	Comment§	Preferred age (Ma)#	
				$^{207}Pb/^{206}Pb$	1σ	$^{207}Pb/^{235}U$	1σ	$^{206}Pb/^{238}U$	1σ	$^{207}Pb/^{206}Pb$	1σ	$^{207}Pb/^{235}U$	1σ	$^{206}Pb/^{238}U$	1σ			Age	1σ
Sample GT01/2014, quartz sandstone, Lower Getun Formation, Manjiantan section of Dalian region, GPS: 39°04'37"N 122°03'36"E																			
GT01/2014_G095	115.9	23.9	0.3744	0.0770	0.0012	2.1050	0.0329	0.1982	0.0024	1122.2	10.5	1150.4	13.5	1165.8	13	3.9		1122.2	10.5
GT01/2014_G096	150.8	34.5	0.2932	0.0830	0.0012	2.5566	0.0367	0.2236	0.0027	1268.3	10.1	1288.3	13.4	1300.8	14	2.6		1268.3	10.1
GT01/2014_G097	102.8	24.6	1.0238	0.0770	0.0013	2.0671	0.0340	0.1949	0.0024	1120.4	11.1	1138	14.1	1147.6	13.1	2.4		1120.4	11.1
GT01/2014_G098	124.6	24.4	0.5642	0.0738	0.0012	1.8231	0.0297	0.1792	0.0022	1036.6	10.5	1053.8	13.3	1062.5	12	0.8		1062.5	12
GT01/2014_G099	35.7	7	0.4033	0.0759	0.0018	1.9389	0.0456	0.1855	0.0027	1091.4	16	1094.6	18.8	1096.7	14.8	0.2		1096.7	14.8
GT01/2014_G100	174.3	32	0.3174	0.0731	0.0011	1.8050	0.0269	0.1793	0.0021	1015.6	9.4	1047.3	12.3	1062.9	11.6	1.5		1062.9	11.6
GT01/2014_G101	264.9	61.9	0.3706	0.0838	0.0011	2.5791	0.0349	0.2233	0.0026	1287.4	9.6	1294.7	12.8	1299.5	13.6	0.9		1287.4	9.6
GT01/2014_G102	67.1	43.3	3.8106	0.1147	0.0017	4.9755	0.0767	0.3149	0.0040	1874.5	12.9	1815.2	16.6	1764.5	19.5	-5.9		1874.5	12.9
GT01/2014_G103	213.5	43.1	0.7072	0.0745	0.0010	1.8213	0.0258	0.1773	0.0021	1055.6	9.1	1053.1	11.9	1052.3	11.3	-0.1		1052.3	11.3
GT01/2014_G104	89.8	33.1	0.4908	0.1152	0.0016	5.3229	0.0751	0.3353	0.0040	1882.9	11.7	1872.5	15.6	1863.9	19.5	-1.0		1882.9	11.7
GT01/2014_G105	673.6	91.1	0.5205	0.0705	0.0010	1.2268	0.0182	0.1263	0.0015	941.8	9	812.9	10.5	766.8	8.5	-5.7		766.8	8.5
GT01/2014_G106	211.8	47	0.712	0.0786	0.0011	2.1156	0.0297	0.1952	0.0023	1162.8	9.4	1153.9	12.4	1149.5	12.3	-1.1		1162.8	9.4
GT01/2014_G107	350.3	83	0.5211	0.0834	0.0010	2.5018	0.0326	0.2178	0.0025	1277.7	9.1	1272.6	12.3	1270	13.2	-0.6		1277.7	9.1
GT01/2014_G108	209.1	41.4	0.4297	0.0759	0.0011	1.9631	0.0278	0.1878	0.0022	1091.1	9.3	1102.9	12.2	1109.4	11.9	1.7		1091.1	9.3
GT01/2014_G109	179.5	48.3	0.9766	0.0832	0.0011	2.5352	0.0356	0.2211	0.0026	1273.7	9.9	1282.2	13.1	1287.7	13.7	1.1		1273.7	9.9
GT01/2014_G110	142	25.2	0.5438	0.0730	0.0011	1.6446	0.0259	0.1635	0.0020	1013.4	10	987.5	12.5	976.3	11	-1.1		976.3	11
GT01/2014_G111	201.3	51	0.8538	0.0837	0.0012	2.4705	0.0356	0.2141	0.0025	1286.5	10.3	1263.4	13.3	1250.4	13.5	-2.8		1286.5	10.3
GT01/2014_G112	351.2	77.4	0.3013	0.0821	0.0010	2.4360	0.0322	0.2154	0.0025	1247.2	9.1	1253.3	12.3	1257.3	13.1	0.8		1247.2	9.1
GT01/2014_G113	235.3	47.7	0.6487	0.0755	0.0011	1.8840	0.0270	0.1812	0.0021	1080.8	9.3	1075.5	12.1	1073.3	11.6	-0.2		1073.3	11.6
GT01/2014_G114	71.5	18.2	0.683	0.0855	0.0015	2.6507	0.0464	0.2248	0.0029	1327.8	12.9	1314.8	16	1307.3	15.3	-1.5		1327.8	12.9
GT01/2014_G115	82.8	56.8	1.2447	0.1840	0.0024	12.9293	0.1741	0.5098	0.0062	2689.3	12.1	2674.5	16.6	2655.8	26.3	-1.2		2689.3	12.1
GT01/2014_G116	165.6	43.7	1.2589	0.0807	0.0012	2.2703	0.0345	0.2042	0.0025	1213.2	10.6	1203.1	13.6	1197.9	13.2	-1.3		1213.2	10.6
GT01/2014_G117	363.4	64.8	0.2848	0.0741	0.0010	1.7984	0.0248	0.1762	0.0020	1042.8	8.7	1044.9	11.5	1046.2	11.2	0.1		1046.2	11.2
GT01/2014_G118	95	17.6	0.365	0.0758	0.0014	1.8688	0.0335	0.1790	0.0023	1088.7	12	1070.1	14.6	1061.3	12.5	-0.8		1061.3	12.5
GT01/2014_G119	159.5	37.1	0.2605	0.0853	0.0012	2.6956	0.0402	0.2294	0.0028	1321.5	10.7	1327.2	14	1331.2	14.5	0.7		1321.5	10.7
GT01/2014_G120	205.7	44.2	0.2795	0.0800	0.0012	2.3261	0.0342	0.2110	0.0025	1196.2	10.1	1220.3	13.3	1234.3	13.4	3.2		1196.2	10.1
GT01/2014_G121	186.5	43.9	0.4462	0.0831	0.0012	2.5305	0.0372	0.2209	0.0026	1271.6	10.5	1280.9	13.6	1286.8	13.9	1.2		1271.6	10.5
GT01/2014_G122	118.5	48	0.7149	0.1207	0.0016	5.8047	0.0812	0.3488	0.0042	1967.2	11.7	1947.1	15.7	1929	20	-1.9		1967.2	11.7
GT01/2014_G123	226.6	44.9	0.6876	0.1004	0.0014	2.4658	0.0347	0.1782	0.0021	1631.9	11.2	1262.1	13.1	1056.9	11.5	-16.3	Del.		
GT01/2014_G124	293.7	65.3	0.3658	0.0855	0.0011	2.5184	0.0344	0.2138	0.0025	1326.2	9.8	1277.3	12.8	1248.9	13.2	-5.8		1326.2	9.8
GT01/2014_G125	121.1	24.4	0.2829	0.0731	0.0012	1.9976	0.0325	0.1984	0.0024	1015.9	10.4	1114.7	13.7	1166.5	13.1	14.8	Del.		
GT01/2014_G126	391.3	82.2	1.1657	0.0722	0.0010	1.6528	0.0227	0.1662	0.0019	990.7	8.4	990.6	11.1	991	10.6	0.0		991	10.6
GT01/2014_G127	100.2	19.7	0.3615	0.0775	0.0013	2.0248	0.0341	0.1896	0.0024	1133.6	11.5	1123.9	14.2	1119.3	12.8	-1.3		1133.6	11.5
GT01/2014_G128	380.8	71.7	0.4637	0.0729	0.0010	1.7763	0.0243	0.1768	0.0020	1010.9	8.4	1036.8	11.4	1049.5	11.2	1.2		1049.5	11.2
GT01/2014_G129	197.8	64.5	1.5015	0.0901	0.0012	2.9573	0.0412	0.2381	0.0028	1428.3	10.4	1396.7	13.6	1376.6	14.5	-3.6		1428.3	10.4
GT01/2014_G130	117.6	27.2	1.0362	0.0783	0.0013	2.0291	0.0330	0.1881	0.0023	1154	11.1	1125.3	13.8	1110.9	12.6	-3.7		1154	11.1
GT01/2014_G131	-681.5	-177.4	0.4104	0.0892	0.0012	3.0233	0.0409	0.2460	0.0029	1407.8	9.9	1413.5	13.3	1417.9	14.7	0.7		1407.8	9.9
GT01/2014_G132	258	53.8	0.7208	0.0753	0.0011	1.9027	0.0278	0.1833	0.0022	1077.6	9.5	1082	12.4	1084.7	11.8	0.2		1084.7	11.8
GT01/2014_G133	77.6	24.8	0.7675	0.0968	0.0016	3.6295	0.0591	0.2721	0.0035	1563	12.9	1556	16.3	1551.6	17.5	-0.7		1563	12.9
GT01/2014_G134	508.1	174.6	0.477	0.1060	0.0013	4.5921	0.0590	0.3143	0.0036	1732.1	10.2	1747.8	14	1761.6	17.6	1.7		1732.1	10.2
GT01/2014_G135	590	107.1	0.2201	0.0756	0.0010	1.9013	0.0252	0.1825	0.0021	1084.5	8.6	1081.6	11.4	1080.5	11.3	-0.1		1080.5	11.3
GT01/2014_G136	330.3	86.4	0.4388	0.0887	0.0012	2.9979	0.0408	0.2453	0.0029	1397	10	1407.1	13.4	1414.2	14.8	1.2		1397	10
GT01/2014_G137	269.3	69.2	0.6514	0.0867	0.0012	2.7358	0.0386	0.2291	0.0027	1352.9	10.3	1338.2	13.4	1329.6	14.1	-1.7		1352.9	10.3
GT01/2014_G138	173.4	68	0.3928	0.1237	0.0016	6.1976	0.0848	0.3635	0.0043	2010.3	11.5	2004.1	15.5	1998.8	20.3	-0.6		2010.3	11.5
GT01/2014_G139	174.3	40	0.9334	0.0793	0.0012	2.0916	0.0327	0.1915	0.0023	1178.6	10.7	1146	13.5	1129.3	12.6	-4.2		1178.6	10.7
GT01/2014_G140	210.9	56.3	0.5324	0.0889	0.0012	2.9902	0.0422	0.2442	0.0029	1400.9	10.4	1405.1	13.8	1408.4	14.9	0.5		1400.9	10.4
GT01/2014_G141	643.1	110.2	0.3533	0.0718	0.0009	1.6453	0.0221	0.1663	0.0019	979.4	8.1	987.7	10.9	991.8	10.5	0.4		991.8	10.5

Analysis No.	U (ppm)	Pb (ppm)	Th/U	Measured isotopic ratios						Calculated isotopic ages (Ma)						Disc.† (%)	Comment§	Preferred age (Ma)#	
				$^{207}Pb/^{206}Pb$	1σ	$^{206}Pb/^{238}U$	1σ	$^{206}Pb/^{238}U$	1σ	$^{207}Pb/^{206}Pb$	1σ	$^{207}Pb/^{235}U$	1σ	$^{206}Pb/^{238}U$	1σ			Age	1σ
Sample GT01/2014, quartz sandstone, Lower Getun Formation, Manjiantan section of Dalian region, GPS: 39°04'37"N 122°03'36"E																			
GT01/2014_G142	182.1	42.9	0.4166	0.0822	0.0012	2.5228	0.0370	0.2226	0.0027	1250.8	10.3	1278.6	13.6	1295.7	14	3.6		1250.8	10.3
GT01/2014_G143	94.1	17	0.481	0.0742	0.0013	1.7249	0.0310	0.1687	0.0022	1046.6	11.8	1017.9	14.2	1004.9	11.9	-1.3		1004.9	11.9
GT01/2014_G144	391.3	73.2	0.3509	0.0744	0.0010	1.8588	0.0261	0.1814	0.0021	1051.5	8.9	1066.6	11.8	1074.3	11.5	0.7		1074.3	11.5
GT01/2014_G145	55.8	15.5	0.5221	0.0917	0.0017	3.2177	0.0605	0.2546	0.0035	1461	14.6	1461.4	18	1462.4	17.8	0.1		1461	14.6
GT01/2014_G146	135.1	26.5	0.5048	0.0753	0.0012	1.8929	0.0309	0.1824	0.0023	1076.3	10.8	1078.6	13.5	1080.2	12.3	0.1		1080.2	12.3
GT01/2014_G147	87.1	26.6	1.2065	0.0884	0.0015	2.9025	0.0499	0.2382	0.0031	1391.2	12.9	1382.6	16.2	1377.5	16	-1.0		1391.2	12.9
GT01/2014_G148	413.1	76.5	0.4117	0.0743	0.0010	1.8088	0.0252	0.1767	0.0021	1048.8	8.8	1048.7	11.6	1049	11.2	0.0		1049	11.2
GT01/2014_G149	298	69.5	1.0265	0.0786	0.0011	2.0675	0.0297	0.1909	0.0022	1161.3	9.7	1138.1	12.5	1126.4	12.1	-3.0		1161.3	9.7
GT01/2014_G150	147.3	31.1	0.7161	0.0711	0.0012	1.8191	0.0298	0.1856	0.0023	960.9	10	1052.4	13.3	1097.4	12.4	4.3		1097.4	12.4

Analysis No.	U (ppm)	Pb (ppm)	Th/U	Measured isotopic ratios						Calculated isotopic ages (Ma)						Disc.† (%)	Comment§	Preferred age (Ma)#	
				$^{208}Pb/^{206}Pb$	1σ	$^{207}Pb/^{235}U$	1σ	$^{206}Pb/^{238}U$	1σ	$^{208}Pb/^{206}Pb$	1σ	$^{207}Pb/^{235}U$	1σ	$^{206}Pb/^{238}U$	1σ			Age	1σ
Sample GTC1/2013, quartz sandstone, Middle Getun Formation, brick factory at Longwangmiaon section, Dalian city, GPS: 39°07'57"N 121°42'41"E																			
GTC1/2013_G001	132	23.4	0.6742	0.0679	0.0015	1.4350	0.0395	0.1563	0.0017	866.1	13	903.6	15.1	936	9.7	3.6		936	9.7
GTC1/2013_G002	153.8	27.5	0.7526	0.0708	0.0013	1.4903	0.0339	0.1546	0.0017	951.6	11.4	926.5	13.1	926.8	9.4	0.0		926.8	9.4
GTC1/2013_G003	85.8	15.5	0.6701	0.0693	0.0019	1.5571	0.0531	0.1592	0.0018	906.8	16.3	953.3	18	952.5	10	-0.1		952.5	10
GTC1/2013_G004	108.6	19.7	0.644	0.0715	0.0016	1.5185	0.0427	0.1603	0.0018	971.7	14.3	937.9	15.8	958.4	9.9	2.2		958.4	9.9
GTC1/2013_G005	65.2	10.9	0.5642	0.0692	0.0024	1.4325	0.0608	0.1522	0.0018	903.8	20.8	902.6	22	913.2	9.8	1.2		913.2	9.8
GTC1/2013_G006	469.1	84.2	0.2584	0.0824	0.0011	2.0306	0.0304	0.1809	0.0019	1255.3	9.3	1125.8	11.4	1072.1	10.6	-4.8		1072.1	10.6
GTC1/2013_G007	148.8	26	0.7647	0.0693	0.0014	1.4674	0.0377	0.1503	0.0017	906.8	12.5	917.1	14.1	902.5	9.3	-1.6		902.5	9.3
GTC1/2013_G008	110.3	19.7	0.7391	0.0722	0.0019	1.5843	0.0519	0.1555	0.0018	992.7	16.2	964.1	17.3	931.4	9.8	-3.4		931.4	9.8
GTC1/2013_G009	106.4	18.5	0.5664	0.0698	0.0017	1.4958	0.0443	0.1573	0.0018	921.3	14.5	928.7	16.2	942	9.8	1.4		942	9.8
GTC1/2013_G010	93	22.3	0.7164	0.0776	0.0016	2.2108	0.0649	0.2069	0.0023	1135.6	14.5	1184.5	16.7	1212.3	12.3	6.8	Del.		
GTC1/2013_G011	137.6	24.1	0.6058	0.0692	0.0015	1.4679	0.0379	0.1571	0.0017	903.5	12.5	917.3	14.4	940.4	9.7	2.5		940.4	9.7
GTC1/2013_G012	144.9	25.5	0.6912	0.0698	0.0014	1.5000	0.0360	0.1542	0.0017	923.1	11.9	930.4	13.6	924.3	9.4	-0.7		924.3	9.4
GTC1/2013_G013	89.1	15.3	0.6144	0.0706	0.0019	1.4386	0.0465	0.1533	0.0017	945.3	16.2	905.2	17.4	919.5	9.6	1.6		919.5	9.6
GTC1/2013_G014	66.9	11.4	0.4681	0.0702	0.0023	1.5235	0.0611	0.1593	0.0018	932.7	19.7	939.9	21.1	953.1	10.1	1.4		953.1	10.1
GTC1/2013_G015	159.3	29.2	0.7856	0.0696	0.0013	1.4709	0.0347	0.1568	0.0017	915.7	11.6	918.5	13.5	938.7	9.6	2.2		938.7	9.6
GTC1/2013_G016	127.6	23.2	0.7267	0.0697	0.0015	1.5103	0.0410	0.1578	0.0018	918.9	13.1	934.6	14.9	944.8	9.7	1.1		944.8	9.7
GTC1/2013_G017	179.4	30.8	0.7021	0.0875	0.0015	1.8847	0.0394	0.1515	0.0017	1370.4	12.5	1075.7	13	909.5	9.3	-15.4	Del.		
GTC1/2013_G018	60.7	10.3	0.521	0.0727	0.0026	1.5092	0.0661	0.1557	0.0018	1005.6	22.6	934.1	23	932.9	10.1	-0.1		932.9	10.1
GTC1/2013_G019	68	22.3	0.8162	0.0982	0.0018	3.6242	0.1045	0.2742	0.0031	1590.8	14.5	1554.8	16.9	1561.9	15.4	-1.8		1590.8	14.5
GTC1/2013_G020	86.4	14.5	0.6487	0.0703	0.0019	1.4065	0.0454	0.1487	0.0017	937.1	16.3	891.7	17.3	893.7	9.4	0.2		893.7	9.4
GTC1/2013_G021	117	19.8	0.7325	0.0701	0.0016	1.4217	0.0384	0.1471	0.0016	929.8	13.5	898.1	14.7	884.9	9.2	-1.5		884.9	9.2
GTC1/2013_G022	145.4	25.6	0.7065	0.0700	0.0014	1.4750	0.0352	0.1541	0.0017	927.2	11.9	920.2	13.6	923.8	9.4	0.4		923.8	9.4
GTC1/2013_G023	74.7	12.9	0.6134	0.0772	0.0021	1.6183	0.0569	0.1545	0.0018	1125.1	18.9	977.3	18.9	926.4	9.8	-5.2		926.4	9.8
GTC1/2013_G024	138.2	24.5	0.7355	0.0709	0.0015	1.4967	0.0396	0.1542	0.0017	955.1	13.2	929	14.7	924.2	9.6	-0.5		924.2	9.6
GTC1/2013_G025	139.8	25.1	0.7331	0.0671	0.0014	1.4253	0.0369	0.1554	0.0017	840.3	12	899.6	14.2	931.3	9.6	3.5		931.3	9.6
GTC1/2013_G026	157.7	25.9	0.6817	0.0704	0.0013	1.3750	0.0313	0.1446	0.0016	939.8	11.6	878.3	13	870.7	9	-0.9		870.7	9
GTC1/2013_G027	105.3	18.7	0.7395	0.0717	0.0017	1.5528	0.0467	0.1533	0.0017	976.6	15	951.6	16.1	919.4	9.6	-3.4		919.4	9.6
GTC1/2013_G028	165.5	29.4	0.772	0.0682	0.0013	1.4017	0.0319	0.1525	0.0017	873.1	11.1	889.7	13.1	915.2	9.3	2.9		915.2	9.3
GTC1/2013_G029	148.8	24.3	0.5869	0.0689	0.0015	1.3618	0.0356	0.1480	0.0017	896	12.7	872.6	14.3	889.5	9.3	1.9		889.5	9.3
GTC1/2013_G030	83	14.5	0.6564	0.0740	0.0020	1.5465	0.0523	0.1540	0.0017	1041.2	17.6	949.1	18.2	923.2	9.7	-2.7		923.2	9.7
GTC1/2013_G031	205	32.5	0.7291	0.0698	0.0012	1.3056	0.0279	0.1386	0.0015	921.9	10.8	848.2	12.1	836.7	8.6	-1.4		836.7	8.6
GTC1/2013_G032	109.2	19.1	0.6642	0.0684	0.0016	1.3916	0.0399	0.1543	0.0017	880.7	13.9	885.4	15.7	925.1	9.6	4.5		925.1	9.6
GTC1/2013_G033	90.8	15	0.5825	0.0706	0.0020	1.3912	0.0486	0.1496	0.0017	946.4	17.5	885.2	18.5	898.9	9.6	1.6		898.9	9.6

Analysis No.	U (ppm)	Pb (ppm)	Th/U	Measured isotopic ratios						Calculated isotopic ages (Ma)						Disc.† (%)	Comment§	Preferred age (Ma)#	
				$^{208}Pb/^{206}Pb$	1σ	$^{207}Pb/^{235}U$	1σ	$^{206}Pb/^{238}U$	1σ	$^{208}Pb/^{206}Pb$	1σ	$^{207}Pb/^{235}U$	1σ	$^{206}Pb/^{238}U$	1σ			Age	1σ
Sample GTC1/2013, quartz sandstone, Middle Getun Formation, brick factory at Longwangmiaon section, Dalian city, GPS: 39°07'57"N 121°42'41"E																			
GTC1/2013_G034	237.3	37.6	0.7496	0.1167	0.0017	2.1458	0.0407	0.1348	0.0015	1906.4	12.8	1163.7	12.9	815	8.4	-30.0	Del.		
GTC1/2013_G035	352.7	98	0.7998	0.0891	0.0012	2.8641	0.0455	0.2359	0.0025	1407	10	1372.5	12.8	1365.5	13.2	-2.9		1407	10
GTC1/2013_G036	139.3	33.9	0.7693	0.0877	0.0014	2.4585	0.0547	0.2098	0.0023	1376.8	12.4	1259.9	14.4	1228	12.3	-10.8		1376.8	12.4
GTC1/2013_G037	175.5	28.5	0.5411	0.0684	0.0013	1.3897	0.0322	0.1483	0.0016	879.5	11.2	884.6	13	891.4	9.2	0.8		891.4	9.2
GTC1/2013_G038	79.1	13.4	0.5403	0.0770	0.0021	1.6252	0.0560	0.1550	0.0018	1121.4	18.4	980	18.6	929	9.8	-5.2		929	9.8
GTC1/2013_G039	75.2	12.6	0.6075	0.0705	0.0028	1.5036	0.0728	0.1513	0.0018	943.5	24.1	931.8	24.8	908	9.9	-2.6		908	9.9
GTC1/2013_G040	198.9	34.7	0.7787	0.0694	0.0012	1.4271	0.0307	0.1499	0.0016	910.1	10.7	900.3	12.5	900.2	9.2	0.0		900.2	9.2
GTC1/2013_G041	331.5	179.2	0.6135	0.1648	0.0020	10.4795	0.1590	0.4652	0.0050	2505.9	11.4	2478.1	15.1	2462.7	21.9	-1.7		2505.9	11.4
GTC1/2013_G042	106.4	18.8	0.6418	0.0673	0.0016	1.4298	0.0421	0.1575	0.0018	847.7	13.7	901.5	15.9	943	9.8	4.6		943	9.8
GTC1/2013_G043	132.6	22.3	0.7385	0.0712	0.0015	1.4144	0.0373	0.1460	0.0016	964	13.4	895	14.5	878.4	9.1	-1.9		878.4	9.1
GTC1/2013_G044	149.9	23.8	0.6465	0.0679	0.0015	1.2773	0.0330	0.1415	0.0016	864.6	12.5	835.7	14	853.1	8.9	2.1		853.1	8.9
GTC1/2013_G045	96.9	15.2	0.5834	0.0733	0.0019	1.3458	0.0435	0.1415	0.0016	1021.2	17.1	865.7	17.2	853.1	9.1	-1.5		853.1	9.1
GTC1/2013_G046	164.4	24.6	0.7522	0.0722	0.0015	1.3056	0.0327	0.1308	0.0015	990.7	13	848.2	13.4	792.4	8.3	-6.6		792.4	8.3
GTC1/2013_G047	118.7	18.6	0.5631	0.0687	0.0016	1.3180	0.0370	0.1423	0.0016	888.2	13.8	853.6	15.1	857.5	9	0.5		857.5	9
GTC1/2013_G048	133.7	20.6	0.5245	0.0812	0.0017	1.5527	0.0414	0.1409	0.0016	1226	15	951.6	14.8	849.5	8.9	-10.7		849.5	8.9
GTC1/2013_G049	110.3	16.6	0.8674	0.0693	0.0020	1.2078	0.0430	0.1285	0.0015	907.7	17.7	804.2	17.7	779.1	8.5	-3.1		779.1	8.5
GTC1/2013_G050	82.5	13.6	0.6745	0.0709	0.0021	1.3798	0.0510	0.1466	0.0017	953.4	18.7	880.4	19.3	882	9.5	0.2		882	9.5
GTC1/2013_G051	88.6	21.5	0.5619	0.0941	0.0019	2.9328	0.0907	0.2216	0.0025	1510.9	15.9	1390.4	17.5	1290.4	13.4	-14.6		1510.9	15.9
GTC1/2013_G052	242.9	34.2	0.6449	0.0691	0.0013	1.1623	0.0251	0.1264	0.0014	901.7	10.9	783	11.8	767.5	8	-2.0		767.5	8
GTC1/2013_G053	102.5	13.6	0.6481	0.0691	0.0027	1.0881	0.0502	0.1203	0.0015	902.6	23.1	747.6	22	732.1	8.6	-2.1		732.1	8.6
GTC1/2013_G054	91.4	12.4	0.6998	0.0736	0.0025	1.1566	0.0479	0.1211	0.0015	1031.3	22.3	780.4	20.4	736.7	8.3	-5.6		736.7	8.3
GTC1/2013_G055	220.6	29.9	0.7798	0.0752	0.0020	1.1753	0.0382	0.1176	0.0014	1072.8	17.2	789.1	15.9	716.6	8.1	-9.2		716.6	8.1
GTC1/2013_G056	190.5	27.3	0.7743	0.0855	0.0019	1.3681	0.0379	0.1233	0.0014	1327.4	16.3	875.3	14.9	749.6	8.1	-14.4		749.6	8.1
GTC1/2013_G057	146	20.2	0.7739	0.0745	0.0018	1.2073	0.0348	0.1211	0.0014	1054.5	15.6	804	14.8	736.6	7.9	-8.4		736.6	7.9
GTC1/2013_G058	255.7	75.2	0.4561	0.1146	0.0016	4.3662	0.0782	0.2752	0.0030	1873	11.6	1706	14.3	1567	15.1	-16.3	Del.		
GTC1/2013_G059	131.5	19.8	0.7499	0.0727	0.0016	1.2806	0.0344	0.1318	0.0015	1004.5	14.2	837.1	14.4	798.3	8.4	-4.6		798.3	8.4
GTC1/2013_G060	92.5	14	0.7193	0.0699	0.0022	1.2399	0.0461	0.1331	0.0015	925.4	18.7	818.8	18.8	805.6	8.8	-1.6		805.6	8.8
GTC1/2013_G061	152.1	21.5	0.8045	0.0686	0.0018	1.1375	0.0353	0.1222	0.0014	887.9	15.2	771.3	15.3	743.3	8	-3.6		743.3	8
GTC1/2013_G062	76.3	10.7	0.6735	0.0687	0.0029	1.2166	0.0611	0.1254	0.0016	890.6	24.7	808.2	23.9	761.7	8.9	-5.8		761.7	8.9
GTC1/2013_G063	249	39.2	0.7562	0.0698	0.0012	1.3192	0.0273	0.1378	0.0015	921.9	10.5	854.1	11.9	832.3	8.6	-2.6		832.3	8.6
GTC1/2013_G064	69.1	11.2	0.6345	0.0757	0.0025	1.5156	0.0619	0.1442	0.0017	1086.6	21.8	936.7	21.1	868.5	9.5	-7.3		868.5	9.5
GTC1/2013_G065	139.3	23.8	0.7525	0.0679	0.0015	1.3664	0.0363	0.1481	0.0017	864.9	12.7	874.6	14.4	890.5	9.3	1.8		890.5	9.3
GTC1/2013_G066	120.3	16	0.7609	0.0726	0.0022	1.2108	0.0449	0.1170	0.0014	1001.7	19.2	805.6	17.8	713.2	8	-11.5		713.2	8
GTC1/2013_G067	213.4	30.1	0.6974	0.0737	0.0015	1.2376	0.0293	0.1246	0.0014	1033.8	12.8	817.8	12.8	756.8	8	-7.5		756.8	8
GTC1/2013_G068	96.4	13.5	0.7479	0.0761	0.0024	1.2457	0.0477	0.1231	0.0015	1097.4	20.9	821.5	19.1	748.4	8.4	-8.9		748.4	8.4
GTC1/2013_G069	284.2	37.4	0.616	0.0735	0.0015	1.2012	0.0294	0.1197	0.0014	1028.6	12.8	801.1	12.7	729.1	7.8	-9.0		729.1	7.8
GTC1/2013_G070	150.4	22.4	0.6989	0.0678	0.0015	1.2184	0.0335	0.1322	0.0015	862.8	13.2	809	14.2	800.1	8.4	-1.1		800.1	8.4
GTC1/2013_G071	279.7	88.3	0.3475	0.1142	0.0015	4.6028	0.0765	0.3008	0.0032	1867	11.4	1749.8	14.4	1695.3	16.1	-9.2		1867	11.4
GTC1/2013_G072	70.8	10.4	0.5841	0.0705	0.0024	1.2232	0.0500	0.1333	0.0016	943.2	21.1	811.3	20.8	806.8	8.9	-0.6		806.8	8.9
GTC1/2013_G073	187.2	26	0.4967	0.0837	0.0016	1.4478	0.0349	0.1307	0.0015	1285.6	14.2	908.9	13.7	791.8	8.3	-12.9		791.8	8.3
GTC1/2013_G074	92.5	14.6	0.6519	0.0685	0.0021	1.2923	0.0475	0.1409	0.0016	883.7	17.8	842.3	18.8	849.7	9.2	0.9		849.7	9.2
GTC1/2013_G075	81.9	11.1	0.4944	0.0749	0.0025	1.2448	0.0498	0.1269	0.0015	1066.9	21.9	821.1	20.2	770.3	8.6	-6.2		770.3	8.6
GTC1/2013_G076	179.4	26.4	0.7757	0.0700	0.0014	1.1816	0.0281	0.1275	0.0014	928.6	12.2	792.1	12.8	773.5	8.1	-2.3		773.5	8.1
GTC1/2013_G077	186.6	28	0.7778	0.0692	0.0014	1.2238	0.0284	0.1303	0.0014	904.4	11.7	811.5	12.6	789.7	8.2	-2.7		789.7	8.2
GTC1/2013_G078	139.3	20.6	0.6361	0.0706	0.0015	1.2601	0.0330	0.1334	0.0015	944.4	13.4	828	14.1	807.3	8.5	-2.5		807.3	8.5
GTC1/2013_G079	146	22.6	0.7028	0.0707	0.0016	1.2573	0.0332	0.1365	0.0015	948.5	13.6	826.7	14.3	825	8.7	-0.2		825	8.7
GTC1/2013_G080	147.1	25.6	0.8618	0.0699	0.0015	1.3768	0.0367	0.1475	0.0017	924.8	13.2	879.1	14.6	886.8	9.3	0.9		886.8	9.3

Analysis No.	U (ppm)	Pb (ppm)	Th/U	Measured isotopic ratios						Calculated isotopic ages (Ma)						Disc.† (%)	Comment§	Preferred age (Ma)#	
				$^{208}Pb/^{206}Pb$	1σ	$^{207}Pb/^{235}U$	1σ	$^{206}Pb/^{238}U$	1σ	$^{208}Pb/^{206}Pb$	1σ	$^{207}Pb/^{206}U$	1σ	$^{206}Pb/^{238}U$	1σ			Age	1σ
Sample GTC1/2013, quartz sandstone, Middle Getun Formation, brick factory at Longwangmiaon section, Dalian city, GPS: 39°07'57"N 121°42'41"E																			
GTC1/2013_G081	129.3	39.5	1.988	0.0803	0.0015	2.1344	0.0514	0.1999	0.0022	1203.9	13	1160	15	1174.5	11.9	-2.4		1203.9	13
GTC1/2013_G082	239	37.1	0.4502	0.0727	0.0013	1.4585	0.0313	0.1466	0.0016	1004.5	11.2	913.4	12.5	881.7	9.1	-3.5		881.7	9.1
GTC1/2013_G083	90.3	16	0.7172	0.0745	0.0019	1.5074	0.0484	0.1559	0.0018	1054.2	17	933.4	17.7	934.1	9.8	0.1		934.1	9.8
GTC1/2013_G084	81.9	13.4	0.57	0.1002	0.0039	1.9045	0.1024	0.1472	0.0020	1628.2	31.3	1082.7	27.8	885.1	11.2	-18.2	Del.		
GTC1/2013_G085	151	26.1	0.7798	0.0702	0.0015	1.3765	0.0343	0.1487	0.0017	935.4	12.6	878.9	14	893.4	9.3	1.6		893.4	9.3
GTC1/2013_G086	131.5	23.3	0.6807	0.0712	0.0017	1.4901	0.0429	0.1559	0.0018	963.7	14.4	926.4	15.8	933.8	9.8	0.8		933.8	9.8
GTC1/2013_G087	99.7	27.2	0.4058	0.0941	0.0017	3.4230	0.0897	0.2567	0.0029	1510.7	13.8	1509.7	16.2	1472.7	14.6	-2.5		1510.7	13.8
GTC1/2013_G088	123.1	27.3	2.4828	0.0921	0.0020	1.7203	0.0473	0.1404	0.0016	1470.3	16.7	1016.1	15.8	846.7	9	-16.7	Del.		
GTC1/2013_G089	107.5	16.9	0.6494	0.0668	0.0019	1.2548	0.0434	0.1398	0.0016	831.9	16.2	825.6	17.6	843.6	9.1	2.2		843.6	9.1
GTC1/2013_G090	109.8	18.3	0.6131	0.0727	0.0018	1.4737	0.0456	0.1501	0.0017	1004.2	15.9	919.6	16.7	901.3	9.5	-2.0		901.3	9.5
GTC1/2013_G091	182.7	39.1	0.2665	0.0787	0.0014	2.2446	0.0504	0.2094	0.0023	1164.1	11.9	1195.1	14.4	1225.5	12.3	5.3	Del.		
GTC1/2013_G092	144.9	22	0.7284	0.0747	0.0016	1.3295	0.0350	0.1341	0.0015	1061.5	14.3	858.6	14.4	811.2	8.5	-5.5		811.2	8.5
GTC1/2013_G093	80.2	12.9	0.6732	0.0726	0.0023	1.4084	0.0544	0.1428	0.0017	1003.9	19.9	892.5	19.9	860.6	9.4	-3.6		860.6	9.4
GTC1/2013_G094	207.3	32.7	0.7217	0.0829	0.0015	1.5232	0.0342	0.1372	0.0015	1267.3	13.3	939.8	13.3	828.8	8.6	-11.8		828.8	8.6
GTC1/2013_G095	225.1	33.3	0.6623	0.0713	0.0013	1.2425	0.0275	0.1327	0.0015	966.9	11.6	820	12.4	803.1	8.3	-2.1		803.1	8.3
GTC1/2013_G096	89.7	15.1	0.9535	0.0701	0.0021	1.3424	0.0501	0.1395	0.0016	932.2	18.6	864.3	19	841.8	9.2	-2.6		841.8	9.2
GTC1/2013_G097	134.3	21.1	0.7557	0.0740	0.0016	1.3426	0.0360	0.1365	0.0015	1040.6	14.4	864.3	14.7	825	8.7	-4.6		825	8.7
GTC1/2013_G098	177.7	30	0.812	0.0699	0.0014	1.3732	0.0319	0.1440	0.0016	925.7	11.8	877.5	13.2	867.2	9	-1.2		867.2	9
GTC1/2013_G099	101.4	16	0.738	0.0706	0.0019	1.2963	0.0431	0.1384	0.0016	945.3	16.9	844.1	17.3	835.4	8.9	-1.0		835.4	8.9
GTC1/2013_G100	89.7	13.1	0.7315	0.0699	0.0025	1.1520	0.0485	0.1280	0.0015	926.3	21.5	778.2	20.9	776.5	8.7	-0.2		776.5	8.7
GTC1/2013_G101	92.5	12.7	0.6623	0.0675	0.0026	1.0826	0.0490	0.1234	0.0015	851.7	22.1	744.9	21.8	750.2	8.5	0.7		750.2	8.5
GTC1/2013_G102	73	10.2	0.5629	0.0739	0.0028	1.2440	0.0560	0.1285	0.0016	1039	24.4	820.7	22.7	779.4	8.9	-5.0		779.4	8.9
GTC1/2013_G103	201.1	29.7	0.6585	0.0689	0.0013	1.2678	0.0290	0.1325	0.0015	894.8	11.4	831.4	12.5	801.9	8.3	-3.5		801.9	8.3
GTC1/2013_G104	138.2	20.6	0.9226	0.0669	0.0018	1.0964	0.0351	0.1252	0.0014	835.9	15.3	751.6	15.9	760.5	8.2	1.2		760.5	8.2
GTC1/2013_G105	132.6	22.9	0.7047	0.0722	0.0015	1.5105	0.0386	0.1515	0.0017	991	13.2	934.6	14.5	909.3	9.4	-2.7		909.3	9.4
GTC1/2013_G106	239.6	37.4	0.7786	0.0689	0.0013	1.2528	0.0274	0.1354	0.0015	894.5	11	824.7	12.3	818.7	8.5	-0.7		818.7	8.5
GTC1/2013_G107	65.2	8.6	0.5677	0.0799	0.0030	1.3773	0.0643	0.1221	0.0015	1193.8	26.7	879.3	23.2	742.6	8.4	-15.5	Del.		
GTC1/2013_G108	210.6	27.6	0.6753	0.0716	0.0014	1.1285	0.0259	0.1176	0.0013	975.7	12.3	767	12.3	716.9	7.5	-6.5		716.9	7.5
GTC1/2013_G109	105.3	14.5	0.7021	0.0705	0.0022	1.1414	0.0423	0.1227	0.0014	941.8	19.2	773.2	18.4	746	8.3	-3.5		746	8.3
GTC1/2013_G110	174.4	28.2	0.5539	0.0703	0.0014	1.4470	0.0355	0.1483	0.0017	937.4	12.3	908.6	13.7	891.5	9.3	-1.9		891.5	9.3
GTC1/2013_G111	73	11.8	0.6794	0.0680	0.0024	1.3023	0.0557	0.1451	0.0017	868.6	20.7	846.7	21.9	873.5	9.6	3.2		873.5	9.6
GTC1/2013_G112	83	12.1	0.651	0.0735	0.0024	1.2476	0.0488	0.1315	0.0015	1027.8	21.1	822.3	20.1	796.5	8.8	-3.1		796.5	8.8
GTC1/2013_G113	203.9	30.5	0.667	0.0702	0.0014	1.2689	0.0289	0.1335	0.0015	934.5	11.7	831.9	12.7	807.9	8.4	-2.9		807.9	8.4
GTC1/2013_G114	107	19.8	0.8203	0.0735	0.0018	1.4804	0.0447	0.1578	0.0018	1028.9	15.8	922.4	16.8	944.4	9.9	2.4		944.4	9.9
GTC1/2013_G115	234	33.4	0.7209	0.0702	0.0014	1.1653	0.0270	0.1262	0.0014	933.9	12	784.4	12.6	766.4	8	-2.3		766.4	8
GTC1/2013_G116	197.8	31.5	0.8424	0.0693	0.0014	1.2497	0.0295	0.1361	0.0015	907.4	11.9	823.3	13.1	822.3	8.6	-0.1		822.3	8.6
GTC1/2013_G117	76.9	11.6	0.5677	0.0746	0.0025	1.3730	0.0570	0.1390	0.0017	1058.8	22.2	877.4	21.4	838.8	9.3	-4.4		838.8	9.3
GTC1/2013_G118	84.1	15	0.744	0.0704	0.0020	1.5056	0.0539	0.1556	0.0018	939.2	17.8	932.6	19	932.4	9.9	0.0		932.4	9.9
GTC1/2013_G119	113.1	18.3	0.7283	0.0692	0.0018	1.3030	0.0398	0.1422	0.0016	904.1	15.2	847	16.3	857.1	9.1	1.2		857.1	9.1
GTC1/2013_G120	169.9	27.7	0.6897	0.0707	0.0014	1.3447	0.0325	0.1446	0.0016	948.5	12.5	865.3	13.7	870.3	9	0.6		870.3	9
GTC1/2013_G121	198.9	32.4	0.769	0.0683	0.0014	1.2964	0.0307	0.1415	0.0016	876.2	11.7	844.1	13.2	852.9	8.9	1.0		852.9	8.9
GTC1/2013_G122	67.4	39.2	0.4764	0.1703	0.0026	12.2791	0.3587	0.5014	0.0056	2560.8	14.2	2626	17.6	2619.7	23.8	2.3		2560.8	14.2
GTC1/2013_G123	104.7	24.4	1.3864	0.0763	0.0017	1.7617	0.0506	0.1755	0.0020	1103.5	15.2	1031.5	16.6	1042.2	10.9	1.0		1042.2	10.9
GTC1/2013_G124	158.8	24.6	0.5848	0.0719	0.0016	1.3876	0.0368	0.1411	0.0016	982.8	13.8	883.7	14.5	851.1	8.9	-3.7		851.1	8.9
GTC1/2013_G125	221.7	32.8	0.7299	0.0711	0.0014	1.2570	0.0283	0.1304	0.0014	959.4	11.9	826.5	12.6	789.9	8.2	-4.4		789.9	8.2
GTC1/2013_G126	128.1	23.1	0.6482	0.0704	0.0015	1.4422	0.0379	0.1607	0.0018	940.6	13.3	906.6	15.1	960.6	9.9	6.0	Del.		
GTC1/2013_G127	192.8	26.6	0.5685	0.0710	0.0015	1.2194	0.0315	0.1271	0.0014	958	13.4	809.5	13.7	771.4	8.2	-4.7		771.4	8.2

Analysis No.	U (ppm)	Pb (ppm)	Th/U	Measured isotopic ratios						Calculated isotopic ages (Ma)						Disc.† (%)	Comment§	Preferred age (Ma)#	
				$^{208}Pb/^{206}Pb$	1σ	$^{207}Pb/^{235}U$	1σ	$^{206}Pb/^{238}U$	1σ	$^{208}Pb/^{206}Pb$	1σ	$^{207}Pb/^{235}U$	1σ	$^{206}Pb/^{238}U$	1σ			Age	1σ
Sample GTC1/2013, quartz sandstone, Middle Getun Formation, brick factory at Longwangmiaon section, Dalian city, GPS: 39°07'57"N 121°42'41"E																			
GTC1/2013_G128	128.7	18.7	0.7399	0.0713	0.0019	1.2256	0.0404	0.1278	0.0015	966.9	17	812.3	16.7	775.2	8.5	-4.6		775.2	8.5
GTC1/2013_G129	161	25.9	0.7084	0.0713	0.0016	1.4126	0.0385	0.1415	0.0016	967.2	13.8	894.3	14.7	853.3	9	-4.6		853.3	9
GTC1/2013_G130	134.8	23.2	0.7658	0.0699	0.0016	1.3881	0.0379	0.1493	0.0017	925.4	13.6	883.9	15	896.9	9.4	1.5		896.9	9.4
GTC1/2013_G131	129.3	21.5	0.841	0.0705	0.0017	1.3335	0.0378	0.1421	0.0016	943.5	14.5	860.4	15.4	856.5	9	-0.5		856.5	9
GTC1/2013_G132	174.4	39.5	2.7867	0.0746	0.0016	1.3764	0.0345	0.1375	0.0015	1056.7	13.7	878.9	14	830.6	8.7	-5.5		830.6	8.7
GTC1/2013_G133	406.2	67	0.8768	0.0694	0.0012	1.2895	0.0246	0.1396	0.0015	910.4	10	841.1	11.5	842.6	8.6	0.2		842.6	8.6
GTC1/2013_G134	146.5	23.6	0.6639	0.0701	0.0016	1.3060	0.0352	0.1439	0.0016	931.9	13.7	848.4	14.9	866.5	9.1	2.1		866.5	9.1
GTC1/2013_G135	128.7	21.7	0.6238	0.0698	0.0016	1.4682	0.0421	0.1513	0.0017	923.1	14.2	917.4	15.7	908	9.5	-1.0		908	9.5
GTC1/2013_G136	164.9	29.5	0.9177	0.0714	0.0015	1.4640	0.0360	0.1495	0.0017	969.2	12.8	915.6	14.1	898.4	9.3	-1.9		898.4	9.3
GTC1/2013_G137	358.8	56.2	0.7736	0.0697	0.0012	1.2757	0.0258	0.1368	0.0015	919.2	10.6	834.9	11.9	826.4	8.5	-1.0		826.4	8.5
GTC1/2013_G138	150.4	25.8	0.729	0.0684	0.0015	1.4011	0.0370	0.1498	0.0017	879.5	12.9	889.4	14.6	899.6	9.4	1.1		899.6	9.4
GTC1/2013_G139	146	22.9	0.7701	0.0697	0.0016	1.2783	0.0361	0.1364	0.0015	918.9	14.1	836.1	15	824.4	8.7	-1.4		824.4	8.7
GTC1/2013_G140	221.2	35.9	0.887	0.0710	0.0014	1.3001	0.0309	0.1374	0.0015	957.4	12.4	845.8	13.3	829.8	8.7	-1.9		829.8	8.7
GTC1/2013_G141	70.8	11.1	0.6039	0.0684	0.0023	1.3742	0.0573	0.1428	0.0017	881.6	20.1	877.9	21.1	860.3	9.4	-2.0		860.3	9.4
GTC1/2013_G142	98.1	16.8	0.7125	0.0738	0.0019	1.5193	0.0495	0.1500	0.0017	1036.8	16.9	938.2	17.4	901.2	9.6	-3.9		901.2	9.6
GTC1/2013_G143	135.9	24.1	0.7192	0.0706	0.0016	1.4467	0.0394	0.1554	0.0017	944.7	13.7	908.5	15.2	931.2	9.7	2.5		931.2	9.7
GTC1/2013_G144	172.2	29.5	0.7269	0.0696	0.0015	1.3977	0.0350	0.1506	0.0017	917.5	12.6	887.9	14.2	904.1	9.4	1.8		904.1	9.4
GTC1/2013_G145	261.3	39.5	0.8043	0.0690	0.0013	1.2156	0.0276	0.1317	0.0015	899.9	11.6	807.8	12.6	797.5	8.3	-1.3		797.5	8.3
GTC1/2013_G146	134.8	19.1	0.8029	0.0704	0.0020	1.1447	0.0393	0.1225	0.0014	939.2	17.5	774.7	17	745.2	8.2	-3.8		745.2	8.2
GTC1/2013_G147	203.4	34	0.7381	0.0712	0.0014	1.3950	0.0330	0.1463	0.0016	962.9	12.3	886.8	13.6	879.9	9.1	-0.8		879.9	9.1
GTC1/2013_G148	74.7	11.6	0.6118	0.0731	0.0025	1.3457	0.0558	0.1408	0.0017	1016.2	21.8	865.7	21.4	849.2	9.4	-1.9		849.2	9.4
GTC1/2013_G149	143.7	24.4	1.0339	0.0757	0.0016	1.4158	0.0367	0.1408	0.0016	1086.1	14.4	895.6	14.7	849.3	8.9	-5.2		849.3	8.9
GTC1/2013_G150	146.5	22.6	0.5978	0.0706	0.0016	1.3062	0.0355	0.1403	0.0016	945.6	13.9	848.5	14.8	846.4	8.9	-0.2		846.4	8.9
GTC1/2013_G151	148.8	22.9	0.7611	0.0714	0.0016	1.2969	0.0354	0.1345	0.0015	969.2	14.3	844.3	14.7	813.7	8.6	-3.6		813.7	8.6
GTC1/2013_G152	122	18.4	0.7043	0.0701	0.0018	1.2322	0.0385	0.1336	0.0015	931.3	15.9	815.4	16.3	808.6	8.7	-0.8		808.6	8.7
GTC1/2013_G153	213.9	31.6	0.7546	0.0717	0.0015	1.2429	0.0305	0.1294	0.0014	978.6	13	820.2	13.4	784.4	8.2	-4.4		784.4	8.2
GTC1/2013_G154	70.2	11.9	0.6377	0.0666	0.0023	1.4048	0.0593	0.1521	0.0018	825.9	19.6	891	21.6	912.6	9.9	2.4		912.6	9.9
GTC1/2013_G155	322.6	77.8	0.3691	0.1075	0.0017	3.3874	0.0673	0.2337	0.0026	1757	13.5	1501.5	15.4	1353.8	13.4	-22.9	Del.		
GTC1/2013_G156	163.2	21.7	0.6618	0.0707	0.0017	1.1344	0.0312	0.1196	0.0014	947.9	14.4	769.8	14.2	728.2	7.8	-5.4		728.2	7.8
GTC1/2013_G157	90.8	13.6	0.6356	0.0686	0.0021	1.2759	0.0461	0.1354	0.0016	887.6	17.8	835	18.3	818.4	8.9	-2.0		818.4	8.9
GTC1/2013_G158	128.7	18.3	0.5901	0.0717	0.0019	1.2125	0.0373	0.1301	0.0015	977.2	16.2	806.3	16.1	788.2	8.5	-2.3		788.2	8.5
GTC1/2013_G159	89.7	12.5	0.7073	0.0687	0.0023	1.0924	0.0421	0.1232	0.0015	889.7	19.5	749.7	19.1	749	8.3	-0.1		749	8.3
GTC1/2013_G160	167.1	23.7	0.5894	0.0715	0.0015	1.2290	0.0310	0.1297	0.0014	972.3	13.5	813.9	13.8	786	8.2	-3.4		786	8.2
GTC1/2013_G161	179.4	26.7	0.7455	0.0763	0.0016	1.3195	0.0338	0.1310	0.0015	1101.6	14.5	854.3	14.3	793.6	8.4	-7.1		793.6	8.4
GTC1/2013_G162	105.3	15.1	0.7543	0.0653	0.0021	1.0350	0.0379	0.1257	0.0015	785.3	17.2	721.4	18.1	763.1	8.4	5.8	Del.		
GTC1/2013_G163	81.9	11.3	0.5426	0.0688	0.0025	1.1257	0.0473	0.1277	0.0015	893.9	21.2	765.7	21	774.5	8.7	1.2		774.5	8.7
GTC1/2013_G164	131.5	18.5	0.7229	0.0728	0.0019	1.2300	0.0386	0.1247	0.0014	1008.7	16.8	814.3	16.2	757.8	8.2	-6.9		757.8	8.2
GTC1/2013_G165	168.3	25.4	0.7458	0.0698	0.0016	1.2076	0.0334	0.1324	0.0015	923.4	14.1	804.1	14.7	801.8	8.5	-0.3		801.8	8.5

Analysis No.	U (ppm)	Pb (ppm)	Th/U	Measured isotopic ratios						Calculated isotopic ages (Ma)						Disc.† (%)	Comment§	Preferred age (Ma)#	
				$^{208}Pb/^{206}Pb$	1σ	$^{207}Pb/^{235}U$	1σ	$^{206}Pb/^{238}U$	1σ	$^{208}Pb/^{206}Pb$	1σ	$^{207}Pb/^{235}U$	1σ	$^{206}Pb/^{238}U$	1σ			Age	1σ
Sample DLZ03/2014, quartz sandstone, Lower Dalinzi Formation, Manjiantan section of Dalian region, GPS: 39°04'51"N 122°03'16"E																			
DLZ03/2014_G001	228.6	80	0.2933	0.11593	0.00139	5.33048	0.06805	0.33362	0.00384	1894.4	10.3	1873.8	14.2	1855.9	18.6	-2.0		1894.4	10.3
DLZ03/2014_G002	286	112.1	0.6259	0.11551	0.00137	5.45466	0.06906	0.34263	0.00392	1887.9	10.2	1893.5	14.1	1899.3	18.8	0.6		1887.9	10.2
DLZ03/2014_G003	36.3	22.7	1.0742	0.1964	0.00271	13.26077	0.19312	0.48989	0.00637	2796.5	13.1	2698.4	17.9	2570.2	27.6	-8.1		2796.5	13.1
DLZ03/2014_G004	328.8	114.7	0.4541	0.11608	0.00137	5.15732	0.06488	0.32235	0.00368	1896.7	10.1	1845.6	14	1801.2	17.9	-5.0		1896.7	10.1

Analysis No.	U (ppm)	Pb (ppm)	Th/U	Measured isotopic ratios						Calculated isotopic ages (Ma)						Disc.† (%)	Comment§	Preferred age (Ma)#	
				$^{208}Pb/^{206}Pb$	1σ	$^{207}Pb/^{235}U$	1σ	$^{206}Pb/^{238}U$	1σ	$^{207}Pb/^{206}Pb$	1σ	$^{207}Pb/^{235}U$	1σ	$^{206}Pb/^{238}U$	1σ			Age	1σ
Sample DLZ03/2014, quartz sandstone, Lower Dalinzi Formation, Manjiantan section of Dalian region, GPS: 39°04'51"N 122°03'16"E																			
DLZ03/2014_G005	74	17	1.0131	0.07978	0.00149	2.05323	0.03839	0.18672	0.00246	1191.6	13.1	1133.4	15.6	1103.6	13.4	-7.4		1191.6	13.1
DLZ03/2014_G006	140.5	51.6	0.4564	0.11611	0.00148	5.37885	0.07213	0.3361	0.00396	1897.2	10.9	1881.5	14.9	1867.9	19.1	-1.5		1897.2	10.9
DLZ03/2014_G007	144	84.6	0.7212	0.1624	0.00197	10.79358	0.14002	0.48222	0.00568	2480.8	11.2	2505.5	15.7	2536.9	24.7	2.3		2480.8	11.2
DLZ03/2014_G008	111.3	82.4	0.8308	0.20601	0.00244	16.26943	0.20671	0.573	0.00672	2874.4	11.3	2892.8	15.9	2920.1	27.5	1.6		2874.4	11.3
DLZ03/2014_G009	130.4	59.3	0.6289	0.13654	0.00169	7.41309	0.09728	0.39392	0.00463	2183.8	11.1	2162.6	15.3	2141	21.4	-2.0		2183.8	11.1
DLZ03/2014_G010	116.3	67.9	0.5404	0.16578	0.002	11.3413	0.14658	0.49637	0.00584	2515.5	11.2	2551.6	15.7	2598.2	25.2	3.3		2515.5	11.2
DLZ03/2014_G011	93.7	34.6	0.5191	0.11735	0.00157	5.3606	0.07511	0.33143	0.004	1916.3	11.5	1878.6	15.4	1845.3	19.4	-3.7		1916.3	11.5
DLZ03/2014_G012	208.5	105.7	0.256	0.15839	0.00185	10.2382	0.12802	0.46898	0.00539	2438.5	10.8	2456.5	15.2	2479.1	23.7	1.7		2438.5	10.8
DLZ03/2014_G013	68.5	9.9	0.8742	0.06496	0.00146	1.09277	0.02425	0.12205	0.00166	773	12.2	749.8	13.9	742.4	9.5	-1.0		742.4	9.5
DLZ03/2014_G014	77.5	47.3	0.4387	0.18776	0.00232	13.69396	0.18111	0.52914	0.00637	2722.6	11.7	2728.8	16.3	2737.8	26.9	0.6		2722.6	11.7
DLZ03/2014_G015	169.7	79.3	0.6682	0.1424	0.00171	7.84215	0.10038	0.39956	0.00464	2256.6	10.9	2213.1	15	2167	21.4	-4.0		2256.6	10.9
DLZ03/2014_G016	107.2	69	0.6647	0.1885	0.00226	13.76763	0.17728	0.5299	0.00625	2729.1	11.3	2733.9	15.9	2741	26.3	0.4		2729.1	11.3
DLZ03/2014_G017	25.2	21	2.1377	0.1717	0.00261	12.0111	0.19193	0.50755	0.00701	2574.3	14.2	2605.3	19.3	2646.2	30	2.8		2574.3	14.2
DLZ03/2014_G018	217	44.7	0.5004	0.07717	0.00105	2.02131	0.02847	0.19004	0.00223	1125.6	9.3	1122.7	12.2	1121.6	12.1	-0.4		1125.6	9.3
DLZ03/2014_G019	253.3	37.5	0.7574	0.06448	0.00094	1.14343	0.01712	0.12865	0.00152	757.4	7.8	774.1	10.2	780.2	8.7	0.8		780.2	8.7
DLZ03/2014_G020	80.1	42.7	1.0805	0.14731	0.0019	8.39405	0.11445	0.41342	0.005	2314.9	11.8	2274.5	16	2230.5	22.8	-3.6		2314.9	11.8
DLZ03/2014_G021	121.8	80.7	1.5317	0.16816	0.00203	10.82557	0.13939	0.46707	0.00548	2539.4	11.3	2508.3	15.6	2470.7	24.1	-2.7		2539.4	11.3
DLZ03/2014_G022	473.8	144	0.3879	0.11859	0.00138	4.72373	0.05865	0.289	0.00328	1935.1	10.1	1771.5	13.6	1636.5	16.4	-15.4	Del.		
DLZ03/2014_G023	153.1	33.5	0.934	0.07721	0.00113	1.91898	0.02889	0.18032	0.00217	1126.6	10	1087.7	12.6	1068.7	11.9	-1.7		1068.7	11.9
DLZ03/2014_G024	137.5	59.7	1.0942	0.1124	0.00143	5.25054	0.07067	0.3389	0.004	1838.6	10.8	1860.9	14.8	1881.4	19.3	2.3		1838.6	10.8
DLZ03/2014_G025	378.6	101.9	0.5713	0.11703	0.00139	3.96876	0.0501	0.24604	0.00281	1911.4	10.2	1627.8	13.4	1418	14.5	-25.8	Del.		
DLZ03/2014_G026	318.7	111.6	0.612	0.10873	0.00129	4.63182	0.05868	0.30908	0.00354	1778.2	10	1755	13.8	1736.2	17.4	-2.4		1778.2	10
DLZ03/2014_G027	66.5	27.7	0.9835	0.11497	0.00166	5.30994	0.07941	0.3351	0.00419	1879.4	12.4	1870.5	16.3	1863.1	20.2	-0.9		1879.4	12.4
DLZ03/2014_G028	171.7	95.1	0.5983	0.16929	0.002	11.0498	0.13999	0.47355	0.0055	2550.6	11	2527.3	15.4	2499.1	24.1	-2.0		2550.6	11
DLZ03/2014_G029	113.3	44.8	0.4494	0.12091	0.00155	5.99751	0.08116	0.35987	0.00428	1969.7	11.1	1975.5	15.2	1981.6	20.3	0.6		1969.7	11.1
DLZ03/2014_G030	194.9	5.5	0.1216	0.11803	0.00289	0.44728	0.01025	0.02749	0.00042	1926.6	21.1	375.4	9.1	174.8	2.6	-53.4	Del.		
DLZ03/2014_G031	156.6	21.6	0.712	0.06462	0.00111	1.08086	0.01876	0.12136	0.0015	762	9.2	744.1	11.2	738.4	8.6	-3.1		738.4	8.6
DLZ03/2014_G032	254.8	69.7	0.8506	0.09761	0.00123	3.07459	0.04076	0.22854	0.00265	1579	10.1	1426.4	13.1	1326.8	13.9	-16.0	Del.		
DLZ03/2014_G033	412.4	113.1	0.3131	0.10126	0.0012	3.67705	0.04647	0.26345	0.00301	1647.3	9.7	1566.4	13.1	1507.5	15.4	-8.5		1647.3	9.7
DLZ03/2014_G034	159.6	52.9	0.7744	0.09972	0.00129	3.87664	0.05283	0.28206	0.00333	1618.9	10.5	1608.8	14.1	1601.7	16.7	-1.1		1618.9	10.5
DLZ03/2014_G035	135.9	58.7	0.7523	0.13113	0.00164	6.60767	0.0874	0.3656	0.00431	2113.2	11.1	2060.4	15.2	2008.7	20.3	-4.9		2113.2	11.1
DLZ03/2014_G036	239.2	94.4	0.7537	0.11454	0.00138	5.30046	0.06812	0.33573	0.00388	1872.7	10.3	1868.9	14.3	1866.1	18.7	-0.4		1872.7	10.3
DLZ03/2014_G037	202.9	87.9	1.2041	0.11391	0.00139	5.20383	0.06756	0.33144	0.00385	1862.7	10.4	1853.2	14.3	1845.4	18.6	-0.9		1862.7	10.4
DLZ03/2014_G038	118.8	35.2	0.798	0.12931	0.00175	4.5216	0.06361	0.2537	0.00308	2088.6	12	1735	15.1	1457.5	15.8	-30.2	Del.		
DLZ03/2014_G039	158.1	63.5	0.9225	0.11405	0.00144	5.16085	0.06883	0.3283	0.00386	1864.9	10.8	1846.2	14.7	1830.1	18.7	-1.9		1864.9	10.8
DLZ03/2014_G040	304.1	184.1	1.3997	0.16564	0.0019	10.10255	0.12483	0.44249	0.00505	2514.1	10.7	2444.2	15	2361.8	22.6	-6.1		2514.1	10.7
DLZ03/2014_G041	152.6	100.4	0.7765	0.18874	0.00222	13.77421	0.17424	0.52949	0.00617	2731.2	11.1	2734.3	15.7	2739.3	26	0.3		2731.2	11.1
DLZ03/2014_G042	252.3	48.2	0.4075	0.08023	0.00106	2.00296	0.02764	0.18112	0.00212	1202.6	9.3	1116.5	12	1073.1	11.6	-3.9		1073.1	11.6
DLZ03/2014_G043	37.3	15.2	0.9673	0.11205	0.0019	5.09957	0.08815	0.3302	0.00448	1832.9	14.4	1836	18.4	1839.4	21.7	0.4		1832.9	14.4
DLZ03/2014_G044	299.6	87.4	0.7017	0.09854	0.00121	3.43952	0.04462	0.25325	0.00292	1596.7	9.9	1513.5	13.3	1455.2	15	-8.9		1596.7	9.9
DLZ03/2014_G045	86.6	36.1	1.011	0.11628	0.00159	5.34623	0.07651	0.33357	0.00408	1899.8	11.7	1876.3	15.7	1855.7	19.7	-2.3		1899.8	11.7
DLZ03/2014_G046	89.6	50.1	0.6675	0.16258	0.00204	10.52231	0.14064	0.46955	0.00565	2482.7	11.6	2481.9	16.1	2481.6	24.8	0.0		2482.7	11.6
DLZ03/2014_G047	345.4	109.1	0.4433	0.11287	0.00133	4.6499	0.05867	0.2989	0.00342	1846.1	10	1758.3	13.7	1685.9	17	-8.7		1846.1	10
DLZ03/2014_G048	79.1	48	0.9785	0.16861	0.00213	11.07423	0.14894	0.47652	0.00577	2543.9	11.8	2529.4	16.3	2512.1	25.2	-1.3		2543.9	11.8
DLZ03/2014_G049	45.3	23.5	0.8474	0.14831	0.00211	8.6587	0.12914	0.42357	0.00545	2326.5	13	2302.7	17.5	2276.7	24.7	-2.1		2326.5	13
DLZ03/2014_G050	131.4	71.7	2.3714	0.11569	0.00149	5.28836	0.07165	0.33165	0.00394	1890.7	11	1867	15	1846.4	19.1	-2.3		1890.7	11
DLZ03/2014_G051	87.1	51.9	0.7449	0.17129	0.00213	11.53854	0.15321	0.48871	0.00587	2570.3	11.6	2567.7	16.2	2565.1	25.4	-0.2		2570.3	11.6

Analysis No.	U (ppm)	Pb (ppm)	Th/U	Measured isotopic ratios						Calculated isotopic ages (Ma)						Disc.† (%)	Comment§	Preferred age (Ma)#	
				$^{207}Pb/^{206}Pb$	1σ	$^{207}Pb/^{235}U$	1σ	$^{206}Pb/^{238}U$	1σ	$^{207}Pb/^{206}Pb$	1σ	$^{207}Pb/^{235}U$	1σ	$^{206}Pb/^{238}U$	1σ			Age	1σ
Sample DLZ03/2014, quartz sandstone, Lower Dalinzi Formation, Manjiantan section of Dalian region, GPS: 39°04'51"N 122°03'16"E																			
DLZ03/2014_G052	169.2	91.9	0.4882	0.16711	0.00197	10.9715	0.13889	0.47632	0.00553	2528.9	11	2520.7	15.4	2511.2	24.1	-0.7		2528.9	11
DLZ03/2014_G053	83.1	46.1	0.7704	0.18477	0.00231	11.81446	0.15762	0.46389	0.00561	2696.2	11.8	2589.8	16.3	2456.7	24.7	-8.9		2696.2	11.8
DLZ03/2014_G054	232.1	85.1	0.3763	0.11506	0.0014	5.41026	0.06991	0.34114	0.00396	1880.8	10.4	1886.5	14.4	1892.2	19	0.6		1880.8	10.4
DLZ03/2014_G055	41.3	26.5	0.7566	0.18624	0.00255	13.37439	0.19454	0.52101	0.00675	2709.2	12.9	2706.5	17.8	2703.5	28.6	-0.2		2709.2	12.9
DLZ03/2014_G056	215	115.2	0.3486	0.1733	0.00202	11.62416	0.14564	0.48663	0.00561	2589.8	10.9	2574.6	15.3	2556.1	24.3	-1.3		2589.8	10.9
DLZ03/2014_G057	58.9	24.7	1.206	0.11104	0.00169	4.91036	0.07726	0.32082	0.00411	1816.5	12.9	1804	16.8	1793.7	20.1	-1.3		1816.5	12.9
DLZ03/2014_G058	133.4	28	0.5459	0.07653	0.00116	2.02531	0.03143	0.19199	0.00234	1109	10.2	1124	13.2	1132.1	12.7	2.1		1109	10.2
DLZ03/2014_G059	142.5	72	0.7822	0.14263	0.00175	8.23396	0.10776	0.41883	0.00494	2259.4	11.1	2257.1	15.4	2255.2	22.4	-0.2		2259.4	11.1
DLZ03/2014_G060	182.3	110.8	0.9389	0.16709	0.00197	11.05226	0.13975	0.47987	0.00556	2528.7	11	2527.5	15.4	2526.7	24.2	-0.1		2528.7	11
DLZ03/2014_G061	109.8	40.9	0.3733	0.11603	0.00152	5.55824	0.07687	0.34755	0.00418	1895.9	11.2	1909.7	15.3	1922.9	20	1.4		1895.9	11.2
DLZ03/2014_G062	69.5	43.7	0.6404	0.19068	0.00241	13.78391	0.18623	0.52445	0.00642	2748	12	2735	16.7	2718	27.1	-1.1		2748	12
DLZ03/2014_G063	282	114	0.5631	0.1248	0.00147	6.16109	0.07794	0.35815	0.00412	2026	10.3	1998.9	14.4	1973.4	19.6	-2.6		2026	10.3
DLZ03/2014_G064	54.4	17.4	1.1158	0.09143	0.00156	3.17896	0.05512	0.25224	0.00331	1455.6	13.2	1452.1	16.6	1450	17	-0.4		1455.6	13.2
DLZ03/2014_G065	95.7	38.3	0.6471	0.11409	0.00153	5.45555	0.07667	0.34691	0.0042	1865.6	11.4	1893.6	15.5	1919.8	20.1	2.9		1865.6	11.4
DLZ03/2014_G066	126.9	73.1	0.8184	0.16765	0.00203	10.84046	0.14072	0.46911	0.00554	2534.3	11.3	2509.5	15.7	2479.7	24.3	-2.2		2534.3	11.3
DLZ03/2014_G067	166.7	78.5	0.2338	0.15912	0.0019	9.76526	0.12491	0.44524	0.00519	2446.3	11	2412.9	15.4	2374.1	23.1	-3.0		2446.3	11
DLZ03/2014_G068	68.5	14.2	0.4473	0.0801	0.00144	2.1466	0.03875	0.19442	0.00253	1199.5	12.7	1164	15.4	1145.3	13.7	-4.5		1199.5	12.7
DLZ03/2014_G069	175.7	64.7	0.5139	0.11598	0.00145	5.30996	0.07024	0.33217	0.0039	1895.2	10.7	1870.5	14.7	1848.9	18.9	-2.4		1895.2	10.7
DLZ03/2014_G070	126.9	57.5	0.4487	0.1356	0.0017	7.60491	0.10127	0.40689	0.00483	2171.7	11.2	2185.4	15.5	2200.7	22.1	1.3		2171.7	11.2
DLZ03/2014_G071	50.4	30.7	1.0249	0.16905	0.00229	11.05539	0.15853	0.47446	0.00602	2548.3	12.6	2527.8	17.3	2503.1	26.3	-1.8		2548.3	12.6
DLZ03/2014_G072	185.3	67.9	0.5207	0.11321	0.00141	5.13788	0.06796	0.32925	0.00386	1851.6	10.6	1842.4	14.5	1834.7	18.7	-0.9		1851.6	10.6
DLZ03/2014_G073	69.5	37.9	0.9193	0.16445	0.00216	10.08554	0.14021	0.44493	0.0055	2501.9	12.2	2442.6	16.7	2372.7	24.5	-5.2		2501.9	12.2
DLZ03/2014_G074	94.2	36.8	0.7391	0.11219	0.00153	5.13208	0.07316	0.33188	0.00404	1835.2	11.6	1841.4	15.5	1847.5	19.6	0.7		1835.2	11.6
DLZ03/2014_G075	165.7	118.3	0.9374	0.20701	0.00242	15.83622	0.19981	0.555	0.00646	2882.3	11.2	2867	15.8	2845.9	26.8	-1.3		2882.3	11.2
DLZ03/2014_G076	177.2	95.4	0.5053	0.1668	0.00198	10.84368	0.13825	0.47165	0.0055	2525.8	11.1	2509.8	15.5	2490.8	24.1	-1.4		2525.8	11.1
DLZ03/2014_G077	110.3	49.5	0.5035	0.13586	0.00173	7.47512	0.10083	0.39918	0.00478	2175.1	11.4	2170	15.7	2165.3	22	-0.5		2175.1	11.4
DLZ03/2014_G078	225.6	92	0.894	0.11415	0.00139	5.25984	0.06834	0.33431	0.00389	1866.5	10.4	1862.4	14.4	1859.2	18.8	-0.4		1866.5	10.4
DLZ03/2014_G079	60.9	27.5	0.6337	0.13176	0.00185	7.07825	0.104	0.38974	0.0049	2121.6	12.5	2121.3	16.8	2121.6	22.7	0.0		2121.6	12.5
DLZ03/2014_G080	438.1	104.5	1.2004	0.08485	0.00105	2.17627	0.02847	0.18608	0.00214	1312.1	9.1	1173.5	11.8	1100.1	11.6	-16.2	Del.		
DLZ03/2014_G081	297.6	107	0.6061	0.11485	0.00138	5.0599	0.06477	0.31963	0.00369	1877.5	10.3	1829.4	14.1	1787.9	18	-4.8		1877.5	10.3
DLZ03/2014_G082	444.1	141.1	0.2568	0.1158	0.00136	4.96076	0.0624	0.31079	0.00356	1892.4	10.1	1812.7	13.9	1744.6	17.5	-7.8		1892.4	10.1
DLZ03/2014_G083	184.8	69.3	0.5574	0.11478	0.00142	5.29399	0.06946	0.3346	0.00391	1876.4	10.6	1867.9	14.5	1860.6	18.9	-0.8		1876.4	10.6
DLZ03/2014_G084	244.2	166.9	0.8747	0.19464	0.00225	14.43688	0.17986	0.53811	0.00619	2781.8	11	2778.9	15.5	2775.5	25.9	-0.2		2781.8	11
DLZ03/2014_G085	44.8	18.8	1.1329	0.11153	0.00177	5.00457	0.08156	0.32553	0.00426	1824.5	13.4	1820.1	17.4	1816.7	20.7	-0.4		1824.5	13.4
DLZ03/2014_G086	180.8	76.6	0.4248	0.13061	0.00158	6.94455	0.08991	0.38575	0.0045	2106.2	10.7	2104.4	14.9	2103.1	20.9	-0.1		2106.2	10.7
DLZ03/2014_G087	88.6	51.4	0.7608	0.1713	0.00213	11.27724	0.1502	0.47762	0.00574	2570.4	11.6	2546.3	16.1	2516.9	25	-2.1		2570.4	11.6
DLZ03/2014_G088	39.3	13.9	0.8025	0.1071	0.00183	4.41858	0.07692	0.29932	0.00404	1750.6	14.3	1715.8	18	1687.9	20	-3.6		1750.6	14.3
DLZ03/2014_G089	76.5	44.5	0.7075	0.168	0.00215	11.18394	0.1525	0.48295	0.0059	2537.8	11.9	2538.6	16.5	2540.1	25.6	0.1		2537.8	11.9
DLZ03/2014_G090	116.8	48.9	0.7012	0.11868	0.00154	5.84269	0.0803	0.35717	0.00428	1936.4	11.2	1952.8	15.3	1968.7	20.3	1.7		1936.4	11.2
DLZ03/2014_G091	103.7	15.4	1.0342	0.06536	0.00128	1.08326	0.02111	0.12025	0.00156	785.9	10.7	745.2	12.4	732	9	-1.8		732	9
DLZ03/2014_G092	80.1	43.9	0.4587	0.16557	0.00211	10.97118	0.14924	0.48072	0.00586	2513.4	11.9	2520.7	16.4	2530.4	25.5	0.7		2513.4	11.9
DLZ03/2014_G093	122.4	49.9	0.8953	0.11413	0.00149	5.25958	0.07238	0.33433	0.004	1866.2	11.1	1862.3	15.1	1859.3	19.3	-0.4		1866.2	11.1
DLZ03/2014_G094	51.9	19.1	0.6597	0.1093	0.00171	4.82081	0.07745	0.31998	0.00415	1787.8	13.2	1788.5	17.1	1789.6	20.3	0.1		1787.8	13.2
DLZ03/2014_G095	61.4	19.6	0.6639	0.1102	0.0017	4.24278	0.0671	0.27932	0.00357	1802.7	13	1682.3	16.5	1587.9	18	-11.9		1802.7	13
DLZ03/2014_G096	130.9	48.9	0.5141	0.1139	0.00147	5.27474	0.07206	0.33596	0.004	1862.5	11	1864.8	15	1867.2	19.3	0.2		1862.5	11
DLZ03/2014_G097	128.4	57.1	0.8417	0.119	0.00152	5.70751	0.07738	0.34797	0.00414	1941.3	11.1	1932.5	15.1	1924.9	19.8	-0.8		1941.3	11.1
DLZ03/2014_G098	435.5	82.1	0.0941	0.08379	0.00103	2.28265	0.02971	0.19763	0.00227	1287.7	9	1206.9	11.9	1162.6	12.2	-9.7		1287.7	9

Analysis No.	U (ppm)	Pb (ppm)	Th/U	Measured isotopic ratios						Calculated isotopic ages (Ma)						Disc.† (%)	Comment§	Preferred age (Ma)#	
				$^{207}Pb/^{206}Pb$	1σ	$^{207}Pb/^{235}U$	1σ	$^{206}Pb/^{238}U$	1σ	$^{207}Pb/^{206}Pb$	1σ	$^{207}Pb/^{235}U$	1σ	$^{206}Pb/^{238}U$	1σ			Age	1σ
Sample DLZ03/2014, quartz sandstone, Lower Dalinzi Formation, Manjiantan section of Dalian region, GPS: 39°04'51"N 122°03'16"E																			
DLZ03/2014_G099	65.5	26.3	0.9436	0.11379	0.00166	5.12443	0.07769	0.32672	0.00411	1860.8	12.4	1840.2	16.4	1822.5	20	-2.1		1860.8	12.4
DLZ03/2014_G100	59.9	35.9	1.5845	0.15163	0.00208	8.80367	0.12719	0.4212	0.0053	2364.4	12.6	2317.9	17	2265.9	24	-4.2		2364.4	12.6
DLZ03/2014_G101	174.2	66.5	0.6357	0.11523	0.00145	5.2965	0.07056	0.33347	0.00393	1883.5	10.8	1868.3	14.7	1855.2	19	-1.5		1883.5	10.8
DLZ03/2014_G102	448.1	151.5	0.2684	0.11586	0.00136	5.21672	0.06591	0.32664	0.00375	1893.3	10.1	1855.4	14	1822.1	18.2	-3.8		1893.3	10.1
DLZ03/2014_G103	106.7	45.8	1.0098	0.12429	0.00163	5.84929	0.08095	0.34142	0.00412	2018.7	11.5	1953.7	15.5	1893.5	19.8	-6.2		2018.7	11.5
DLZ03/2014_G104	182.8	70.4	0.6483	0.11569	0.00144	5.33785	0.07067	0.33472	0.00393	1890.7	10.7	1874.9	14.6	1861.2	19	-1.6		1890.7	10.7
DLZ03/2014_G105	86.6	37.2	0.9976	0.11388	0.00156	5.37361	0.07733	0.34231	0.00419	1862.2	11.7	1880.7	15.7	1897.8	20.1	1.9		1862.2	11.7
DLZ03/2014_G106	40.8	14.4	0.5237	0.11	0.00185	4.78834	0.0821	0.31579	0.00424	1799.4	14.2	1782.9	18.1	1769.1	20.8	-1.7		1799.4	14.2
DLZ03/2014_G107	287	112.6	0.413	0.14735	0.00175	7.42906	0.0947	0.36577	0.00423	2315.4	10.8	2164.5	14.8	2009.5	20	-13.2		2315.4	10.8
DLZ03/2014_G108	183.8	38.7	0.3308	0.07853	0.00109	2.20657	0.03189	0.20385	0.00243	1160.3	9.6	1183.1	12.8	1196	13	3.1		1160.3	9.6
DLZ03/2014_G109	81.6	34	1.0056	0.11146	0.00156	5.11537	0.07486	0.33294	0.00411	1823.4	11.9	1838.7	15.9	1852.6	19.9	1.6		1823.4	11.9
DLZ03/2014_G110	152.1	153	1.4725	0.25818	0.00302	23.46505	0.29758	0.65936	0.00771	3235.6	11.4	3246.4	16.1	3264.7	30	0.9		3235.6	11.4
DLZ03/2014_G111	198.4	69.8	0.7247	0.11263	0.00142	4.70533	0.06275	0.30309	0.00356	1842.3	10.7	1768.2	14.4	1706.6	17.6	-7.4		1842.3	10.7
DLZ03/2014_G112	55.9	22.1	0.8776	0.11036	0.00168	4.97128	0.07824	0.3268	0.00419	1805.3	12.8	1814.5	16.8	1822.9	20.4	1.0		1805.3	12.8
DLZ03/2014_G113	168.2	23.7	0.8035	0.0657	0.00107	1.09955	0.01825	0.12141	0.00149	796.8	9	753.1	10.8	738.7	8.6	-1.9		738.7	8.6
DLZ03/2014_G114	75.5	42.1	0.5781	0.16392	0.00211	10.74121	0.14742	0.47537	0.00581	2496.5	12	2501	16.5	2507.1	25.4	0.4		2496.5	12
DLZ03/2014_G115	97.2	55.6	0.5858	0.16319	0.00204	10.90605	0.1461	0.48482	0.00583	2489	11.6	2515.2	16.1	2548.2	25.3	2.4		2489	11.6
DLZ03/2014_G116	94.7	52.5	0.6244	0.165	0.00208	10.71249	0.14399	0.47102	0.00567	2507.6	11.7	2498.5	16.2	2488	24.8	-0.8		2507.6	11.7
DLZ03/2014_G117	234.1	138.8	1.0943	0.16267	0.00192	10.24892	0.13037	0.45707	0.0053	2483.6	10.9	2457.5	15.3	2426.6	23.4	-2.3		2483.6	10.9
DLZ03/2014_G118	342.9	122.8	0.3507	0.11565	0.00138	5.36181	0.06852	0.33634	0.00388	1890	10.2	1878.8	14.2	1869	18.7	-1.1		1890	10.2
DLZ03/2014_G119	470.3	166.5	0.2704	0.1146	0.00135	5.36341	0.06781	0.33954	0.00389	1873.6	10.1	1879	14.1	1884.5	18.7	0.6		1873.6	10.1
DLZ03/2014_G120	63.4	36.5	0.887	0.17123	0.00224	10.94633	0.15223	0.46377	0.00573	2569.7	12.2	2518.6	16.7	2456.2	25.2	-4.4		2569.7	12.2
DLZ03/2014_G121	203.9	104	1.08	0.13734	0.00166	7.52674	0.09741	0.39759	0.00463	2193.9	10.9	2176.2	15	2157.9	21.4	-1.6		2193.9	10.9
DLZ03/2014_G122	94.7	39.1	0.3668	0.16179	0.00207	8.64265	0.1174	0.38753	0.00468	2474.5	11.9	2301.1	16	2111.4	21.7	-14.7		2474.5	11.9
DLZ03/2014_G123	91.1	22.6	1.2124	0.07994	0.0013	2.1162	0.03494	0.19206	0.00241	1195.5	11.4	1154.1	14.2	1132.5	13	-5.3		1195.5	11.4
DLZ03/2014_G124	1003	131.3	0.6317	0.06361	0.00078	1.03115	0.01348	0.1176	0.00135	728.7	6.4	719.5	8.7	716.7	7.8	-0.4		716.7	7.8
DLZ03/2014_G125	169.7	61.2	0.459	0.11614	0.00146	5.28612	0.07074	0.33021	0.00389	1897.6	10.8	1866.6	14.7	1839.4	18.9	-3.1		1897.6	10.8
DLZ03/2014_G126	416.4	115.6	0.3989	0.11544	0.00138	4.22201	0.05413	0.26532	0.00306	1886.8	10.2	1678.3	13.6	1517	15.6	-19.6	Del.		
DLZ03/2014_G127	543.8	77.2	0.8303	0.06475	0.00088	1.08156	0.0153	0.12117	0.00142	766.2	7.3	744.4	9.5	737.3	8.2	-1.0		737.3	8.2
DLZ03/2014_G128	214.5	130.8	0.8963	0.16805	0.002	11.21532	0.14362	0.48417	0.00563	2538.3	11.1	2541.2	15.5	2545.4	24.5	0.3		2538.3	11.1
DLZ03/2014_G129	21.7	16.4	2.0324	0.16273	0.00266	10.62522	0.18159	0.4737	0.00681	2484.2	15.2	2490.9	20.2	2499.8	29.8	0.6		2484.2	15.2
DLZ03/2014_G130	290	95.5	0.6734	0.10111	0.00125	4.00153	0.05275	0.28711	0.00334	1644.6	10.1	1634.5	13.8	1627.1	16.7	-1.1		1644.6	10.1
DLZ03/2014_G131	75.5	41	0.8026	0.1676	0.00217	10.41214	0.14353	0.4507	0.00552	2533.8	12.1	2472.1	16.5	2398.4	24.5	-5.3		2533.8	12.1
DLZ03/2014_G132	181.8	66.4	0.6106	0.11045	0.0014	4.90119	0.066	0.32194	0.0038	1806.8	10.7	1802.5	14.6	1799.2	18.5	-0.4		1806.8	10.7
DLZ03/2014_G133	69	33	0.7379	0.13279	0.00181	7.35663	0.10589	0.40192	0.00499	2135.2	12.2	2155.7	16.5	2177.9	22.9	2.0		2135.2	12.2
DLZ03/2014_G134	277.4	100.3	0.2648	0.11511	0.0014	5.49246	0.07147	0.34614	0.00402	1881.6	10.4	1899.4	14.4	1916.1	19.3	1.8		1881.6	10.4
DLZ03/2014_G135	146.5	42.4	0.3985	0.09813	0.00131	3.67455	0.05168	0.27166	0.00325	1588.9	10.7	1565.9	14.3	1549.2	16.5	-2.5		1588.9	10.7
DLZ03/2014_G136	72	37.2	0.472	0.16734	0.00219	10.5679	0.14681	0.45815	0.00564	2531.2	12.2	2485.9	16.7	2431.4	24.9	-3.9		2531.2	12.2
DLZ03/2014_G137	130.9	61	1.4589	0.11473	0.00149	5.34647	0.07366	0.33806	0.00404	1875.6	11.1	1876.3	15.1	1877.3	19.5	0.1		1875.6	11.1
DLZ03/2014_G138	153.1	44.6	0.722	0.09041	0.00123	3.1409	0.04483	0.25202	0.00302	1434.2	10.4	1442.8	14	1448.9	15.5	1.0		1434.2	10.4
DLZ03/2014_G139	136.5	69.7	0.472	0.15922	0.00197	9.94033	0.13153	0.45293	0.00537	2447.4	11.4	2429.3	15.8	2408.3	23.8	-1.6		2447.4	11.4
DLZ03/2014_G140	333.8	114.6	0.3041	0.11483	0.00139	5.18574	0.06717	0.32762	0.0038	1877.2	10.4	1850.3	14.3	1826.8	18.5	-2.7		1877.2	10.4
DLZ03/2014_G141	291.5	40.7	0.6854	0.08262	0.00124	1.40244	0.02159	0.12315	0.0015	1260.3	10.8	890	11.5	748.7	8.6	-15.9	Del.		
DLZ03/2014_G142	77	44.6	0.8607	0.1657	0.00215	10.68441	0.14792	0.46779	0.00574	2514.7	12.1	2496.1	16.6	2473.9	25.2	-1.6		2514.7	12.1
DLZ03/2014_G143	177.7	96.2	1.2291	0.13662	0.00169	7.6616	0.10125	0.40684	0.00479	2184.8	11.1	2192.1	15.3	2200.5	21.9	0.7		2184.8	11.1
DLZ03/2014_G144	183.8	79.8	0.9802	0.12448	0.00156	6.00087	0.0802	0.34972	0.00413	2021.4	11	1976	15	1933.3	19.7	-4.4		2021.4	11
DLZ03/2014_G145	215	77.1	0.8038	0.10259	0.0013	4.26887	0.05755	0.30187	0.00355	1671.5	10.4	1687.4	14.2	1700.6	17.6	1.7		1671.5	10.4

Analysis No.	U (ppm)	Pb (ppm)	Th/U	Measured isotopic ratios						Calculated isotopic ages (Ma)						Disc.† (%)	Comment§	Preferred age (Ma)#	
				$^{207}Pb/^{206}Pb$	1σ	$^{207}Pb/^{235}U$	1σ	$^{206}Pb/^{238}U$	1σ	$^{207}Pb/^{206}Pb$	1σ	$^{207}Pb/^{235}U$	1σ	$^{206}Pb/^{238}U$	1σ			Age	1σ
Sample DLZ03/2014, quartz sandstone, Lower Dalinzi Formation, Manjiantan section of Dalian region, GPS: 39°04'51"N 122°03'16"E																			
DLZ03/2014_G146	114.3	66.4	0.6756	0.16742	0.00209	11.18297	0.14975	0.48459	0.00581	2532	11.6	2538.5	16.1	2547.2	25.2	0.6		2532	11.6
DLZ03/2014_G147	208.5	77.3	0.5554	0.11258	0.00142	5.138	0.06887	0.3311	0.0039	1841.5	10.7	1842.4	14.7	1843.7	18.9	0.1		1841.5	10.7
DLZ03/2014_G148	362.5	116.9	0.4613	0.1144	0.00139	4.72542	0.0614	0.29965	0.00347	1870.5	10.4	1771.8	14.1	1689.6	17.2	-9.7		1870.5	10.4

Analysis No.	U (ppm)	Pb (ppm)	Th/U	Measured isotopic ratios						Calculated isotopic ages (Ma)						Disc.† (%)	Comment§	Preferred age (Ma)#	
				$^{207}Pb/^{206}Pb$	1σ	$^{207}Pb/^{235}U$	1σ	$^{206}Pb/^{238}U$	1σ	$^{207}Pb/^{206}Pb$	1σ	$^{207}Pb/^{235}U$	1σ	$^{206}Pb/^{238}U$	1σ			Age	1σ
Sample DLZ1/2013, quartz sandstone, Middle Dalinzi Formation, Longwangmiao, Dalian city, GPS: 39°07'26"N 121°41'21"E																			
DLZ1/2013_G001	66.7	30	1.2552	0.1104	0.0015	5.0759	0.1133	0.3427	0.0041	1805.3	11.5	1832.1	15.4	1899.5	19.7	5.2	Del.		
DLZ1/2013_G002	147.7	64.6	0.9568	0.1102	0.0013	5.3286	0.0910	0.3527	0.0042	1802.9	10	1873.5	14.3	1947.6	19.8	8.0	Del.		
DLZ1/2013_G003	325.9	45.4	0.5971	0.0638	0.0009	1.1070	0.0178	0.1271	0.0015	734	7	756.7	9.5	771.2	8.5	1.9		771.2	8.5
DLZ1/2013_G004	74.5	12.2	1.2456	0.0654	0.0014	1.1603	0.0319	0.1283	0.0016	787.6	12	782.1	13.7	778.1	9	-0.5		778.1	9
DLZ1/2013_G005	140.7	60.3	1.5613	0.1135	0.0014	5.0957	0.0906	0.3132	0.0037	1856.7	10.4	1835.4	14.3	1756.4	18.1	-5.4		1856.7	10.4
DLZ1/2013_G006	373.4	137.7	0.402	0.1106	0.0012	5.1749	0.0734	0.3412	0.0040	1809	9.5	1848.5	13.8	1892.4	19.1	4.6		1809	9.5
DLZ1/2013_G007	237.9	81.5	0.5939	0.1106	0.0013	4.5449	0.0717	0.3080	0.0036	1809.8	9.9	1739.2	13.9	1730.8	17.8	-4.4		1809.8	9.9
DLZ1/2013_G008	234.9	110.5	1.5776	0.1127	0.0013	5.2154	0.0796	0.3380	0.0040	1842.8	9.7	1855.1	14	1877.1	19	1.9		1842.8	9.7
DLZ1/2013_G009	414.4	68.3	1.1893	0.0940	0.0012	1.8286	0.0282	0.1406	0.0017	1508.9	9.7	1055.8	11.2	847.9	9.3	-19.7	Del.		
DLZ1/2013_G010	16.1	8.7	0.8258	0.1631	0.0030	10.0411	0.4741	0.4449	0.0060	2488.2	17	2438.6	21	2372.3	26.7	-4.7		2488.2	17
DLZ1/2013_G011	173.9	65.2	0.5425	0.1117	0.0013	5.1566	0.0834	0.3362	0.0039	1827.9	9.9	1845.5	14.1	1868.4	19	2.2		1827.9	9.9
DLZ1/2013_G012	106.8	30	0.7999	0.0857	0.0012	2.8136	0.0546	0.2402	0.0029	1330.3	10.2	1359.2	13.6	1387.7	14.8	4.3		1330.3	10.2
DLZ1/2013_G013	27	12.2	0.5167	0.1960	0.0028	10.4597	0.3290	0.3808	0.0047	2793.5	13.6	2476.4	17.5	2080.1	22.1	-25.5	Del.		
DLZ1/2013_G014	69.7	40.2	0.8248	0.1663	0.0020	11.0449	0.2366	0.4711	0.0056	2520.4	11.3	2526.9	15.8	2488.3	24.5	-1.3		2520.4	11.3
DLZ1/2013_G015	290.6	102.5	0.2478	0.1121	0.0013	5.2305	0.0764	0.3401	0.0040	1833.9	9.6	1857.6	13.9	1886.9	19	2.9		1833.9	9.6
DLZ1/2013_G016	247.1	78.8	0.7064	0.1150	0.0014	4.4303	0.0704	0.2800	0.0033	1880.2	10.1	1718	13.8	1591.3	16.5	-15.4	Del.		
DLZ1/2013_G017	198.3	69.8	0.3427	0.1115	0.0013	5.0949	0.0786	0.3317	0.0039	1824.7	9.8	1835.3	13.9	1846.6	18.7	1.2		1824.7	9.8
DLZ1/2013_G018	54.9	21.4	1.9405	0.0946	0.0015	3.3721	0.0871	0.2575	0.0032	1520.7	12.8	1497.9	15.9	1477	16.1	-2.9		1520.7	12.8
DLZ1/2013_G019	125.9	42.2	0.6144	0.1126	0.0014	4.5287	0.0850	0.3028	0.0036	1841.6	10.8	1736.2	14.5	1705.1	17.7	-7.4		1841.6	10.8
DLZ1/2013_G020	196.1	65.3	0.251	0.1114	0.0014	4.8601	0.0834	0.3233	0.0038	1822.1	10.3	1795.4	14.3	1806	18.5	-0.9		1822.1	10.3
DLZ1/2013_G021	342.5	116.2	0.398	0.1139	0.0013	4.9611	0.0705	0.3166	0.0037	1862.9	9.6	1812.7	13.7	1773	18	-4.8		1862.9	9.6
DLZ1/2013_G022	319.8	93	0.4044	0.1121	0.0013	4.2496	0.0630	0.2783	0.0032	1834.1	9.8	1683.7	13.5	1582.7	16.3	-13.7		1834.1	9.8
DLZ1/2013_G023	125.5	48.4	0.8563	0.1100	0.0013	4.8203	0.0826	0.3195	0.0038	1798.6	10.2	1788.4	14.2	1787.1	18.3	-0.6		1798.6	10.2
DLZ1/2013_G024	362.1	119.4	0.257	0.1122	0.0013	4.8993	0.0690	0.3188	0.0037	1835.7	9.5	1802.1	13.6	1784	18.1	-2.8		1835.7	9.5
DLZ1/2013_G025	567.8	74.6	0.7627	0.0627	0.0008	0.9963	0.0143	0.1141	0.0013	698.1	6.2	701.9	8.5	696.7	7.7	-0.7		696.7	7.7
DLZ1/2013_G026	198.3	68.6	0.3797	0.1117	0.0013	4.9946	0.0770	0.3245	0.0038	1827.4	9.9	1818.4	13.9	1811.5	18.4	-0.9		1827.4	9.9
DLZ1/2013_G027	132.5	48.7	0.6527	0.1114	0.0013	4.9392	0.0837	0.3205	0.0038	1822.7	10.2	1809	14.2	1792	18.3	-1.7		1822.7	10.2
DLZ1/2013_G028	226.6	76.1	0.2191	0.1117	0.0013	5.1311	0.0781	0.3277	0.0038	1827.4	9.8	1841.3	13.9	1827	18.5	0.0		1827.4	9.8
DLZ1/2013_G029	58.8	24.9	0.8416	0.1204	0.0016	6.0496	0.1358	0.3505	0.0042	1961.4	11.6	1983	15.5	1936.8	20	-1.3		1961.4	11.6
DLZ1/2013_G030	30.5	14.4	0.7117	0.1601	0.0023	9.1577	0.2654	0.4112	0.0050	2456.6	13.1	2353.9	17.1	2220.3	23	-9.6		2456.6	13.1
DLZ1/2013_G031	97.6	37.2	0.7606	0.1095	0.0014	4.7617	0.0890	0.3236	0.0038	1790.6	10.7	1778.2	14.6	1807.3	18.6	0.9		1790.6	10.7
DLZ1/2013_G032	343.8	98.6	0.2618	0.1123	0.0013	4.3810	0.0630	0.2817	0.0033	1836.5	9.8	1708.8	13.5	1600	16.4	-12.9		1836.5	9.8
DLZ1/2013_G033	238.3	67.1	0.3666	0.1119	0.0014	4.1467	0.0715	0.2739	0.0032	1831.1	10.5	1663.6	14	1560.4	16.2	-14.8		1831.1	10.5
DLZ1/2013_G034	279.7	94.4	0.5847	0.1129	0.0013	4.7089	0.0701	0.3035	0.0035	1847.3	9.9	1768.8	13.7	1708.5	17.4	-7.5		1847.3	9.9
DLZ1/2013_G035	332	92.4	0.5195	0.1039	0.0012	3.5831	0.0520	0.2538	0.0029	1695.3	9.6	1545.8	13.1	1458.1	15.1	-14.0		1695.3	9.6
DLZ1/2013_G036	141.6	18.9	0.879	0.0653	0.0011	0.9961	0.0203	0.1122	0.0013	782.4	9.2	701.8	10.5	685.6	7.8	-2.3		685.6	7.8
DLZ1/2013_G037	130.3	21.2	1.1183	0.0710	0.0011	1.2894	0.0260	0.1300	0.0016	956.8	10	841	11.4	787.6	8.8	-6.4		787.6	8.8
DLZ1/2013_G038	203.9	69.5	0.3566	0.1115	0.0013	4.8188	0.0749	0.3212	0.0037	1824.5	9.9	1788.2	14	1795.7	18.2	-1.6		1824.5	9.9
DLZ1/2013_G039	909.8	105.9	0.9125	0.0942	0.0011	1.2268	0.0166	0.0944	0.0011	1511.7	9.2	812.9	9.2	581.6	6.4	-28.4	Del.		

Analysis No.	U (ppm)	Pb (ppm)	Th/U	Measured isotopic ratios						Calculated isotopic ages (Ma)						Disc.† (%)	Comment§	Preferred age (Ma)#	
				$^{207}Pb/^{206}Pb$	1σ	$^{207}Pb/^{235}U$	1σ	$^{206}Pb/^{238}U$	1σ	$^{207}Pb/^{206}Pb$	1σ	$^{207}Pb/^{235}U$	1σ	$^{206}Pb/^{238}U$	1σ			Age	1σ
Sample DLZ1/2013, quartz sandstone, Middle Dalinzi Formation, Longwangmiao, Dalian city, GPS: 39°07'26"N 121°41'21"E																			
DLZ1/2013_G040	366	98.8	0.5893	0.0973	0.0011	3.2528	0.0468	0.2434	0.0028	1573.6	9.3	1469.9	12.8	1404.6	14.6	-10.7		1573.6	9.3
DLZ1/2013_G041	187.4	77	1.159	0.1122	0.0013	4.9910	0.0812	0.3212	0.0037	1835.4	10.1	1817.8	14.1	1795.4	18.2	-2.2		1835.4	10.1
DLZ1/2013_G042	148.6	35.6	1.1051	0.0775	0.0011	2.0632	0.0396	0.1909	0.0023	1133.3	9.8	1136.7	12.6	1126.2	12.2	-0.6		1133.3	9.8
DLZ1/2013_G043	390	134.8	0.472	0.1134	0.0013	4.9439	0.0705	0.3166	0.0037	1855.1	9.8	1809.8	13.8	1773.3	17.9	-4.4		1855.1	9.8
DLZ1/2013_G044	117.6	36.1	0.7191	0.1118	0.0015	4.0567	0.0775	0.2674	0.0032	1829.2	11.1	1645.6	14.4	1527.8	16.1	-16.5	Del.		
DLZ1/2013_G045	66.2	22.7	0.7061	0.0982	0.0014	4.0556	0.0904	0.2951	0.0035	1590.8	11.5	1645.4	15.2	1666.8	17.5	4.8		1590.8	11.5
DLZ1/2013_G046	68	30.6	0.862	0.1305	0.0017	6.5679	0.1403	0.3717	0.0044	2104.4	11.6	2055	15.6	2037.5	20.7	-3.2		2104.4	11.6
DLZ1/2013_G047	200.4	77.7	0.6864	0.1127	0.0013	5.1622	0.0819	0.3343	0.0039	1842.8	10.1	1846.4	14.1	1859	18.7	0.9		1842.8	10.1
DLZ1/2013_G048	120.3	17.1	0.5829	0.0689	0.0012	1.2687	0.0273	0.1291	0.0015	896	10.2	831.8	11.7	782.8	8.8	-5.9		782.8	8.8
DLZ1/2013_G049	132.5	43.9	0.759	0.0940	0.0012	3.6678	0.0657	0.2826	0.0033	1507.9	10.1	1564.4	13.9	1604.6	16.6	6.4	Del.		
DLZ1/2013_G050	214.8	110.8	0.5303	0.1492	0.0017	9.4240	0.1441	0.4479	0.0052	2336.2	10.5	2380.2	14.9	2386.1	23.1	2.1		2336.2	10.5
DLZ1/2013_G051	132.9	34.6	0.4347	0.0844	0.0011	2.8464	0.0512	0.2413	0.0028	1300.6	9.7	1367.9	13.3	1393.7	14.7	7.2	Del.		
DLZ1/2013_G052	222.2	79.1	0.2958	0.1142	0.0014	5.3290	0.0833	0.3387	0.0039	1866.8	10.1	1873.5	14.2	1880.4	18.9	0.7		1866.8	10.1
DLZ1/2013_G053	280.6	87.1	0.4019	0.1140	0.0014	4.5606	0.0692	0.2942	0.0034	1863.5	10.1	1742.1	13.8	1662.3	17	-10.8		1863.5	10.1
DLZ1/2013_G054	52.3	17.3	1.3746	0.1100	0.0017	4.1106	0.1066	0.2581	0.0031	1799.2	13.3	1656.4	16.1	1480.2	16	-17.7	Del.		
DLZ1/2013_G055	122.9	50.7	0.2915	0.1260	0.0015	6.5872	0.1154	0.3867	0.0045	2042.8	10.7	2057.6	14.9	2107.4	21	3.2		2042.8	10.7
DLZ1/2013_G056	155.1	53.3	0.6412	0.1202	0.0015	5.0781	0.0909	0.3096	0.0036	1958.4	10.9	1832.5	14.6	1738.9	17.8	-11.2		1958.4	10.9
DLZ1/2013_G057	111.1	64.7	0.8531	0.1643	0.0020	10.3252	0.1825	0.4698	0.0055	2499.9	11	2464.4	15.4	2482.6	24	-0.7		2499.9	11
DLZ1/2013_G058	174.7	71.8	0.7745	0.1411	0.0017	6.7274	0.1095	0.3547	0.0041	2240.9	10.8	2076.2	14.8	1957	19.6	-12.7		2240.9	10.8
DLZ1/2013_G059	385.2	121.5	0.4486	0.1636	0.0019	6.6572	0.0997	0.2971	0.0034	2492.9	10.8	2067	14.5	1677	17.1	-32.7	Del.		
DLZ1/2013_G060	95.9	35.9	0.5675	0.1129	0.0015	5.1212	0.0970	0.3322	0.0039	1846.9	10.9	1839.6	14.8	1849.2	18.9	0.1		1846.9	10.9
DLZ1/2013_G061	185.6	27.2	0.9535	0.0641	0.0010	1.0601	0.0200	0.1212	0.0014	744.3	8.1	733.9	10.2	737.2	8.2	0.5		737.2	8.2
DLZ1/2013_G062	117.2	39.7	0.645	0.1013	0.0013	4.0652	0.0738	0.2966	0.0035	1648.3	10.5	1647.4	14.3	1674.6	17.3	1.6		1648.3	10.5
DLZ1/2013_G063	85.4	34.3	0.8089	0.1112	0.0015	5.1735	0.1027	0.3357	0.0040	1819.8	11.1	1848.3	15	1865.8	19.1	2.5		1819.8	11.1
DLZ1/2013_G064	98.5	64	1.0904	0.1709	0.0021	11.4004	0.2063	0.4933	0.0058	2566.4	11.2	2556.5	15.6	2584.8	24.8	0.7		2566.4	11.2
DLZ1/2013_G065	270.2	91.3	0.7195	0.0999	0.0012	4.0468	0.0618	0.2910	0.0034	1622.6	9.7	1643.7	13.5	1646.5	16.8	1.5		1622.6	9.7
DLZ1/2013_G066	168.2	61.6	0.567	0.1126	0.0014	5.0711	0.0836	0.3260	0.0038	1842.3	10.4	1831.3	14.3	1819.1	18.4	-1.3		1842.3	10.4
DLZ1/2013_G067	63.2	10	0.9457	0.0669	0.0015	1.2310	0.0349	0.1316	0.0016	835.9	12.8	814.8	14.3	797	9.2	-2.2		797	9.2
DLZ1/2013_G068	274.1	37.6	0.6091	0.0643	0.0009	1.0903	0.0182	0.1240	0.0014	749.9	7.3	748.6	9.6	753.5	8.3	0.7		753.5	8.3
DLZ1/2013_G069	229.2	87	0.9656	0.1025	0.0013	4.3399	0.0682	0.3066	0.0036	1669.5	10	1701	13.9	1723.8	17.5	3.3		1669.5	10
DLZ1/2013_G070	69.7	39.6	1.2953	0.1461	0.0019	8.5124	0.1752	0.4199	0.0049	2300.2	11.6	2287.2	15.7	2260.1	22.4	-1.7		2300.2	11.6
DLZ1/2013_G071	139	53.1	0.5084	0.1135	0.0014	5.2279	0.0895	0.3430	0.0040	1856.7	10.6	1857.2	14.6	1901.3	19.2	2.4		1856.7	10.6
DLZ1/2013_G072	32.2	20	0.9653	0.1632	0.0023	11.0043	0.3069	0.4830	0.0058	2488.6	12.8	2523.5	17	2540.3	25.3	2.1		2488.6	12.8
DLZ1/2013_G073	268	94.6	0.4143	0.1131	0.0014	5.2212	0.0794	0.3335	0.0039	1849.8	10.2	1856.1	14.2	1855.5	18.6	0.3		1849.8	10.2
DLZ1/2013_G074	248.4	35.4	0.7689	0.0639	0.0009	1.0924	0.0189	0.1237	0.0014	739.6	7.6	749.7	9.8	751.5	8.3	0.3		751.5	8.3
DLZ1/2013_G075	139	55.2	0.5223	0.1187	0.0015	5.7844	0.0993	0.3557	0.0041	1936.4	10.7	1944.1	14.7	1961.8	19.6	1.3		1936.4	10.7
DLZ1/2013_G076	283.2	100.9	0.399	0.1141	0.0014	5.1718	0.0782	0.3309	0.0038	1865.1	10.3	1848	14.2	1842.8	18.5	-1.2		1865.1	10.3
DLZ1/2013_G077	59.7	9.7	0.5722	0.0707	0.0015	1.4735	0.0395	0.1489	0.0018	948.8	12.7	919.6	14.4	894.7	10.2	-2.7		894.7	10.2
DLZ1/2013_G078	222.2	80.7	0.2967	0.1119	0.0014	5.3770	0.0848	0.3442	0.0040	1830.5	10.3	1881.2	14.3	1907	19.1	4.2		1830.5	10.3
DLZ1/2013_G079	254	75.7	1.0946	0.0981	0.0012	3.2448	0.0512	0.2392	0.0028	1588.9	10.1	1467.9	13.2	1382.5	14.4	-13.0		1588.9	10.1
DLZ1/2013_G080	149.9	66.1	0.5424	0.1273	0.0016	6.8904	0.1171	0.3891	0.0045	2061.3	10.9	2097.4	15	2118.4	20.9	2.8		2061.3	10.9
DLZ1/2013_G081	107.2	43.7	0.7711	0.1131	0.0015	5.3118	0.0986	0.3432	0.0040	1849.8	11	1870.8	14.9	1902.2	19.2	2.8		1849.8	11
DLZ1/2013_G082	342	120.5	0.3692	0.1130	0.0014	5.1745	0.0767	0.3299	0.0038	1848.5	10.2	1848.4	14.2	1838.1	18.4	-0.6		1848.5	10.2
DLZ1/2013_G083	128.5	30.3	0.4893	0.0816	0.0012	2.4496	0.0462	0.2175	0.0026	1236.2	10.2	1257.3	13.3	1268.4	13.5	2.6		1236.2	10.2
DLZ1/2013_G084	74.1	27.8	0.5831	0.1136	0.0016	5.0742	0.1051	0.3325	0.0039	1858.3	11.7	1831.8	15.4	1850.7	18.9	-0.4		1858.3	11.7
DLZ1/2013_G085	240.5	67.3	0.4923	0.0909	0.0012	3.2205	0.0516	0.2569	0.0030	1444.5	9.7	1462.1	13.3	1473.7	15.2	2.0		1444.5	9.7
DLZ1/2013_G086	240.5	33.3	0.6998	0.0638	0.0009	1.0467	0.0184	0.1224	0.0014	734.7	7.7	727.2	9.9	744.4	8.2	2.4		744.4	8.2

Analysis No.	U (ppm)	Pb (ppm)	Th/U	Measured isotopic ratios						Calculated isotopic ages (Ma)						Disc.† (%)	Comment§	Preferred age (Ma)#	
				$^{207}Pb/^{206}Pb$	1σ	$^{207}Pb/^{235}U$	1σ	$^{206}Pb/^{238}U$	1σ	$^{207}Pb/^{206}Pb$	1σ	$^{207}Pb/^{235}U$	1σ	$^{206}Pb/^{238}U$	1σ			Age	1σ
Sample DLZ1/2013, quartz sandstone, Middle Dalinzi Formation, Longwangmiao, Dalian city, GPS: 39°07'26"N 121°41'21"E																			
DLZ1/2013_G087	136.4	31.7	0.8246	0.0780	0.0011	2.1230	0.0400	0.1971	0.0023	1147.9	9.9	1156.3	12.8	1159.9	12.4	1.0		1147.9	9.9
DLZ1/2013_G088	191.3	69.6	0.4702	0.1153	0.0014	5.3078	0.0873	0.3317	0.0038	1884.7	10.7	1870.1	14.5	1846.8	18.6	-2.0		1884.7	10.7
DLZ1/2013_G089	68.8	27.2	0.8183	0.1104	0.0016	4.9947	0.1077	0.3301	0.0039	1806.2	11.8	1818.4	15.5	1838.8	18.9	1.8		1806.2	11.8
DLZ1/2013_G090	231.8	78.8	0.2772	0.1153	0.0014	5.2359	0.0832	0.3268	0.0038	1884.1	10.6	1858.5	14.4	1822.9	18.3	-3.2		1884.1	10.6
DLZ1/2013_G091	16.6	2.3	0.6116	0.0783	0.0040	1.3687	0.0872	0.1253	0.0018	1153.7	35.6	875.6	31.3	761.2	10.4	-13.1		761.2	10.4
DLZ1/2013_G092	73.2	41.6	0.8633	0.1633	0.0021	10.4655	0.2165	0.4585	0.0054	2489.6	11.9	2476.9	16.1	2432.8	23.7	-2.3		2489.6	11.9
DLZ1/2013_G093	155.1	57.8	0.6459	0.1125	0.0014	5.0122	0.0863	0.3246	0.0038	1840.7	10.9	1821.4	14.6	1812.2	18.3	-1.5		1840.7	10.9
DLZ1/2013_G094	248.8	46.8	0.193	0.0771	0.0010	2.0328	0.0340	0.1898	0.0022	1124.6	9.2	1126.6	12.1	1120.3	11.9	-0.4		1124.6	9.2
DLZ1/2013_G095	153.8	63.8	0.8558	0.1111	0.0014	5.1778	0.0902	0.3409	0.0040	1817.2	10.9	1849	14.8	1890.8	19	4.1		1817.2	10.9
DLZ1/2013_G096	42.7	24.4	0.8785	0.1652	0.0023	10.9469	0.2849	0.4608	0.0055	2509.4	12.8	2518.6	16.9	2443.2	24.3	-2.6		2509.4	12.8
DLZ1/2013_G097	126.8	53.1	0.9565	0.1112	0.0015	5.1709	0.0944	0.3349	0.0039	1819.3	11.1	1847.8	14.9	1862	18.8	2.3		1819.3	11.1
DLZ1/2013_G098	53.2	30	0.9566	0.1624	0.0022	10.5015	0.2528	0.4486	0.0053	2480.5	12.6	2480	16.6	2388.9	23.6	-3.7		2480.5	12.6
DLZ1/2013_G099	154.7	79.7	0.7919	0.1726	0.0022	10.2076	0.1735	0.4310	0.0050	2583.2	11.7	2453.8	15.7	2310.1	22.4	-10.6		2583.2	11.7
DLZ1/2013_G100	67.5	33	1.2371	0.1228	0.0017	6.1456	0.1331	0.3658	0.0043	1997.9	12.1	1996.7	15.9	2009.5	20.3	0.6		1997.9	12.1
DLZ1/2013_G101	27	4.1	0.7663	0.0712	0.0027	1.2734	0.0588	0.1322	0.0018	962.6	23.3	833.9	22.8	800.1	10	-4.1		800.1	10
DLZ1/2013_G102	72.3	30.2	0.8236	0.1267	0.0017	5.8138	0.1206	0.3401	0.0040	2052.4	12.1	1948.5	15.7	1887.3	19.2	-8.0		2052.4	12.1
DLZ1/2013_G103	253.6	89.2	0.3178	0.1139	0.0014	5.1775	0.0819	0.3328	0.0038	1863.2	10.7	1848.9	14.5	1852	18.5	-0.6		1863.2	10.7
DLZ1/2013_G104	53.6	7.7	0.6501	0.0674	0.0017	1.1366	0.0345	0.1282	0.0016	849.9	14.2	770.9	15.2	777.3	9	0.8		777.3	9
DLZ1/2013_G105	188.2	68.4	0.4181	0.1149	0.0015	5.3396	0.0903	0.3346	0.0039	1877.7	11	1875.2	14.8	1860.4	18.6	-0.9		1877.7	11
DLZ1/2013_G106	115.9	42.8	0.4286	0.1141	0.0015	5.2910	0.0996	0.3391	0.0039	1865.9	11.4	1867.4	15.2	1882.3	19	0.9		1865.9	11.4
DLZ1/2013_G107	137.3	53.8	0.5237	0.1147	0.0015	5.4627	0.0973	0.3491	0.0040	1874.9	11.2	1894.7	15	1930.4	19.3	3.0		1874.9	11.2
DLZ1/2013_G108	98.5	32	0.7728	0.1001	0.0014	3.7823	0.0748	0.2751	0.0032	1626.5	11.4	1589	14.7	1566.8	16.3	-3.7		1626.5	11.4
DLZ1/2013_G109	129.8	26.3	0.3047	0.0804	0.0012	2.1946	0.0425	0.1971	0.0023	1206.3	10.5	1179.3	13.1	1159.9	12.4	-3.8		1206.3	10.5
DLZ1/2013_G110	258.4	86.9	0.2547	0.1139	0.0015	5.0446	0.0804	0.3253	0.0037	1862.5	10.9	1826.8	14.6	1815.6	18.2	-2.5		1862.5	10.9
DLZ1/2013_G111	171.2	88.6	0.5643	0.1616	0.0020	9.7551	0.1624	0.4488	0.0052	2472.3	11.7	2411.9	15.8	2389.9	23	-3.3		2472.3	11.7
DLZ1/2013_G112	118.5	44.2	0.6955	0.1142	0.0015	4.9912	0.0923	0.3210	0.0037	1867.5	11.5	1817.8	15.1	1794.8	18.2	-3.9		1867.5	11.5
DLZ1/2013_G113	125.9	44.6	0.6194	0.1099	0.0015	4.6872	0.0855	0.3110	0.0036	1797.4	11.3	1765	14.9	1745.7	17.8	-2.9		1797.4	11.3
DLZ1/2013_G114	279.3	98.3	0.4762	0.1139	0.0015	5.0183	0.0791	0.3204	0.0037	1862.1	10.9	1822.4	14.5	1791.7	18	-3.8		1862.1	10.9
DLZ1/2013_G115	81.9	37.9	0.5732	0.1484	0.0020	8.2814	0.1652	0.4052	0.0047	2327	12.2	2262.3	16.1	2192.7	21.7	-5.8		2327	12.2
DLZ1/2013_G116	152.5	51.3	0.3795	0.1176	0.0016	4.9675	0.0858	0.3140	0.0036	1919.6	11.4	1813.8	14.9	1760.1	17.8	-8.3		1919.6	11.4
DLZ1/2013_G117	76.7	18.9	0.7223	0.0872	0.0014	2.4918	0.0560	0.2161	0.0026	1365.1	12.4	1269.7	14.9	1261	13.6	-7.6		1365.1	12.4
DLZ1/2013_G118	117.6	72.8	0.9511	0.1648	0.0021	10.7220	0.1959	0.4818	0.0056	2505.2	12	2499.3	16.1	2535.3	24.2	1.2		2505.2	12
DLZ1/2013_G119	129	48.8	0.7292	0.1132	0.0015	4.9746	0.0913	0.3215	0.0037	1852.1	11.5	1815	15.1	1797.2	18.2	-3.0		1852.1	11.5
DLZ1/2013_G120	90.6	34.5	0.7709	0.1116	0.0016	5.0229	0.1009	0.3207	0.0037	1826.3	11.9	1823.2	15.4	1793	18.3	-1.8		1826.3	11.9
DLZ1/2013_G121	67.5	45	1.3511	0.1730	0.0023	11.3804	0.2428	0.4809	0.0056	2586.8	12.6	2554.8	16.7	2531.1	24.5	-2.2		2586.8	12.6
DLZ1/2013_G122	281.5	38.6	0.7688	0.0632	0.0009	1.0031	0.0176	0.1177	0.0014	714.3	7.6	705.4	9.7	717.1	7.8	1.7		717.1	7.8
DLZ1/2013_G123	43.1	16	0.5039	0.1169	0.0018	5.4392	0.1410	0.3330	0.0040	1908.9	13.5	1891.1	16.9	1853	19.2	-2.9		1908.9	13.5
DLZ1/2013_G124	180.4	70.3	0.8458	0.1139	0.0015	4.9565	0.0846	0.3221	0.0037	1863	11.4	1811.9	14.9	1800.2	18.1	-3.4		1863	11.4
DLZ1/2013_G125	172.1	56.7	0.5852	0.1006	0.0014	4.0903	0.0712	0.2909	0.0034	1635	11	1652.4	14.5	1645.9	16.8	0.7		1635	11
DLZ1/2013_G126	125.9	17.2	0.5895	0.0650	0.0012	1.1221	0.0243	0.1230	0.0015	773.7	9.7	764	11.4	747.5	8.3	-2.2		747.5	8.3
DLZ1/2013_G127	61.9	17.3	1.1758	0.0816	0.0014	2.4122	0.0589	0.2137	0.0025	1235	12.5	1246.2	15.2	1248.4	13.5	1.1		1235	12.5
DLZ1/2013_G128	431.4	57.7	0.4882	0.0641	0.0009	1.1045	0.0179	0.1240	0.0014	746.3	7.4	755.5	9.6	753.4	8.2	-0.3		753.4	8.2
DLZ1/2013_G129	72.8	39.4	1.7639	0.1508	0.0021	8.8358	0.1855	0.4215	0.0049	2354.5	12.6	2321.2	16.5	2267.1	22.3	-3.7		2354.5	12.6
DLZ1/2013_G130	67.5	27.4	0.7118	0.1134	0.0017	5.4220	0.1183	0.3420	0.0040	1854.6	12.5	1888.3	16	1896.3	19.3	2.2		1854.6	12.5
DLZ1/2013_G131	138.1	27.5	2.6135	0.0905	0.0015	1.5053	0.0321	0.1182	0.0014	1435.5	13.1	932.6	12.5	720.3	8.1	-22.8	Del.		
DLZ1/2013_G132	80.2	34.3	0.4242	0.1267	0.0018	6.5465	0.1347	0.3847	0.0045	2052.3	12.4	2052.2	16.1	2098.1	20.9	2.2		2052.3	12.4
DLZ1/2013_G133	134.6	19	0.78	0.0665	0.0012	1.0938	0.0233	0.1203	0.0014	820.9	9.9	750.3	11.3	732.5	8.2	-2.4		732.5	8.2

Analysis No.	U (ppm)	Pb (ppm)	Th/U	Measured isotopic ratios						Calculated isotopic ages (Ma)						Disc.† (%)	Comment§	Preferred age (Ma)#	
				$^{207}Pb/^{206}Pb$	1σ	$^{207}Pb/^{235}U$	1σ	$^{206}Pb/^{238}U$	1σ	$^{207}Pb/^{206}Pb$	1σ	$^{207}Pb/^{235}U$	1σ	$^{206}Pb/^{238}U$	1σ			Age	1σ
Sample DLZ1/2013, quartz sandstone, Middle Dalinzi Formation, Longwangmiao, Dalian city, GPS: 39°07'26"N 121°41'21"E																			
DLZ1/2013_G134	252.7	82.6	0.1834	0.1147	0.0015	5.0583	0.0828	0.3229	0.0037	1874.4	11.3	1829.1	14.9	1803.7	18	-3.8		1874.4	11.3
DLZ1/2013_G135	125.5	34.2	0.5627	0.0905	0.0013	3.0012	0.0566	0.2433	0.0028	1436.1	11.1	1407.9	14.2	1403.8	14.6	-2.2		1436.1	11.1
DLZ1/2013_G136	196.1	59.2	0.6686	0.0963	0.0013	3.4165	0.0587	0.2621	0.0030	1554	11	1508.2	14.2	1500.4	15.4	-3.5		1554	11
DLZ1/2013_G137	295	98.3	0.3519	0.1141	0.0015	4.8498	0.0784	0.3158	0.0036	1865.1	11.4	1793.6	14.9	1769	17.7	-5.2		1865.1	11.4
DLZ1/2013_G138	43.1	6.9	0.6458	0.0677	0.0018	1.2828	0.0419	0.1392	0.0017	858.5	15.2	838.1	16.6	840	9.7	0.2		840	9.7
DLZ1/2013_G139	184.7	64.3	0.2344	0.1143	0.0016	5.2894	0.0923	0.3362	0.0039	1868.9	11.7	1867.2	15.3	1868.5	18.7	0.0		1868.9	11.7
DLZ1/2013_G140	150.3	56.2	0.4904	0.1143	0.0016	5.3764	0.0977	0.3360	0.0039	1869.2	11.8	1881.1	15.4	1867.4	18.7	-0.1		1869.2	11.8
DLZ1/2013_G141	93.2	34.9	0.8993	0.1133	0.0017	4.7092	0.0956	0.3048	0.0036	1852.2	12.4	1768.9	15.7	1715.2	17.5	-7.4		1852.2	12.4
DLZ1/2013_G142	318.5	104.3	0.3136	0.1132	0.0015	4.8153	0.0777	0.3134	0.0036	1851.4	11.4	1787.6	14.9	1757.5	17.6	-5.1		1851.4	11.4
DLZ1/2013_G143	59.3	8.3	0.6387	0.0636	0.0015	1.0631	0.0311	0.1238	0.0015	729	12.5	735.3	14.3	752.5	8.7	2.3		752.5	8.7
DLZ1/2013_G144	126.4	20.8	1.2138	0.0633	0.0011	1.0861	0.0236	0.1246	0.0015	719.3	9.3	746.6	11.4	757	8.4	1.4		757	8.4
DLZ1/2013_G145	237	73.9	0.3273	0.1131	0.0016	4.6707	0.0791	0.3020	0.0035	1849.2	11.7	1762	15	1701.1	17.2	-8.0		1849.2	11.7
DLZ1/2013_G146	27.5	3.7	0.5805	0.0757	0.0027	1.2815	0.0563	0.1226	0.0016	1086.6	23.5	837.5	21.5	745.7	9.3	-11.0		745.7	9.3
DLZ1/2013_G147	163	60.9	0.324	0.1132	0.0016	5.4862	0.0985	0.3492	0.0040	1851.7	11.9	1898.4	15.5	1930.7	19.2	4.3		1851.7	11.9
DLZ1/2013_G148	255.3	83.2	0.1803	0.1136	0.0016	5.0020	0.0851	0.3216	0.0037	1857.1	11.7	1819.7	15.2	1797.6	18	-3.2		1857.1	11.7

Analysis No.	U (ppm)	Pb (ppm)	Th/U	Measured isotopic ratios						Calculated isotopic ages (Ma)						Disc.† (%)	Comment§	Preferred age (Ma)#	
				$^{207}Pb/^{206}Pb$	1σ	$^{207}Pb/^{235}U$	1σ	$^{206}Pb/^{238}U$	1σ	$^{207}Pb/^{206}Pb$	1σ	$^{207}Pb/^{235}U$	1σ	$^{206}Pb/^{238}U$	1σ			Age	1σ
Sample DLZ2/2013, quartz sandstone, Middle Dalinzi Formation, Longwangmiao, Dalian city, GPS: 39°07'26"N 121°41'21"E																			
DLZ2/2013_G001	187.5	63.4	0.3002	0.1151	0.0014	4.8415	0.0828	0.3240	0.0020	1880.7	10.7	1792.1	11.8	1809.4	9.5	-3.8		1880.7	10.7
DLZ2/2013_G002	258.7	94	0.1839	0.1142	0.0014	5.3786	0.0847	0.3547	0.0021	1867.3	10.3	1881.4	11.6	1956.9	10	4.8		1867.3	10.3
DLZ2/2013_G003	71.8	10.3	0.5161	0.0642	0.0019	1.1426	0.0403	0.1319	0.0009	747.2	15.9	773.7	16.9	798.6	5.3	3.2		798.6	5.3
DLZ2/2013_G004	38.4	5.7	0.7716	0.0597	0.0032	1.0335	0.0625	0.1281	0.0010	592	24.1	720.7	28.2	776.8	5.8	7.8	Del.		
DLZ2/2013_G005	111.3	82.7	1.1293	0.1791	0.0021	12.9594	0.2355	0.5392	0.0032	2644.2	11.2	2676.7	12.6	2780.2	13.6	5.1	Del.		
DLZ2/2013_G006	165.5	60.8	0.3383	0.1147	0.0014	5.2656	0.0860	0.3447	0.0021	1874.7	10.5	1863.3	11.7	1909.1	9.8	1.8		1874.7	10.5
DLZ2/2013_G007	220.4	82.1	0.3276	0.1158	0.0014	5.3687	0.0823	0.3505	0.0021	1892.4	10.3	1879.9	11.5	1937	9.9	2.4		1892.4	10.3
DLZ2/2013_G008	181.4	63.9	0.4906	0.1158	0.0014	5.1248	0.0842	0.3212	0.0019	1892.2	10.6	1840.2	11.7	1795.8	9.4	-5.1		1892.2	10.6
DLZ2/2013_G009	152.9	37.1	0.1896	0.0895	0.0012	2.8778	0.0486	0.2427	0.0015	1415.3	10.1	1376.1	11	1400.8	7.6	-1.0		1415.3	10.1
DLZ2/2013_G010	207.8	71.5	0.266	0.1146	0.0014	5.0691	0.0774	0.3310	0.0020	1873.4	10.3	1831	11.4	1843	9.4	-1.6		1873.4	10.3
DLZ2/2013_G011	325.6	43.3	0.6679	0.0648	0.0009	1.0214	0.0163	0.1178	0.0007	769.1	7.5	714.6	7.9	717.8	4	0.5		717.8	4
DLZ2/2013_G012	125	40.5	0.6908	0.0994	0.0013	3.5933	0.0670	0.2809	0.0017	1613.4	10.9	1548.1	11.9	1596	8.7	-1.1		1613.4	10.9
DLZ2/2013_G013	31.8	9.5	0.9768	0.0994	0.0026	3.1933	0.1353	0.2440	0.0018	1612.5	21	1455.5	21.1	1407.7	9.5	-12.7		1612.5	21
DLZ2/2013_G014	100.9	15.3	0.8656	0.0671	0.0015	1.1605	0.0305	0.1283	0.0008	839.3	12.7	782.2	12.8	778.2	4.8	-0.5		778.2	4.8
DLZ2/2013_G015	220.9	77.9	0.172	0.1150	0.0014	5.3042	0.0806	0.3460	0.0020	1879.1	10.3	1869.5	11.5	1915.3	9.7	1.9		1879.1	10.3
DLZ2/2013_G016	196.8	74.3	0.4784	0.1142	0.0014	5.1670	0.0842	0.3431	0.0020	1867.9	10.5	1847.2	11.7	1901.5	9.8	1.8		1867.9	10.5
DLZ2/2013_G017	167.7	65.7	0.6146	0.1139	0.0014	5.2317	0.0838	0.3428	0.0020	1862.4	10.5	1857.8	11.7	1900	9.7	2.0		1862.4	10.5
DLZ2/2013_G018	142.5	52.8	0.434	0.1157	0.0015	5.1919	0.0929	0.3404	0.0021	1890.5	11	1851.3	12.1	1888.7	9.9	-0.1		1890.5	11
DLZ2/2013_G019	310.3	111.2	0.2222	0.1153	0.0014	5.3721	0.0781	0.3472	0.0020	1884.9	10.2	1880.4	11.4	1921.4	9.7	1.9		1884.9	10.2
DLZ2/2013_G020	137.6	58.9	0.8653	0.1166	0.0015	5.4562	0.0948	0.3516	0.0021	1904.4	10.8	1893.7	12	1942.4	10.1	2.0		1904.4	10.8
DLZ2/2013_G021	205	64.6	0.6078	0.1156	0.0015	4.4534	0.0731	0.2885	0.0017	1888.5	10.8	1722.3	11.6	1634.2	8.7	-13.5		1888.5	10.8
DLZ2/2013_G022	195.7	75	0.5868	0.1159	0.0014	5.2039	0.0853	0.3391	0.0020	1894.5	10.7	1853.3	11.8	1882.3	9.7	-0.6		1894.5	10.7
DLZ2/2013_G023	186.9	75	0.5957	0.1148	0.0014	5.3455	0.0828	0.3515	0.0021	1876.3	10.4	1876.2	11.7	1941.8	9.9	3.5		1876.3	10.4
DLZ2/2013_G024	622.2	106.7	0.7742	0.1144	0.0014	2.5541	0.0353	0.1597	0.0009	1870.9	10.3	1287.6	9.7	954.9	5.2	-25.8	Del.		
DLZ2/2013_G025	173.2	54.1	0.5077	0.1022	0.0013	3.8634	0.0656	0.2850	0.0017	1663.6	10.6	1606.1	11.6	1616.3	8.6	-2.8		1663.6	10.6
DLZ2/2013_G026	48.2	18.1	0.677	0.1186	0.0019	5.0577	0.1370	0.3288	0.0022	1934.6	13.5	1829	14.5	1832.5	10.5	-5.3		1934.6	13.5
DLZ2/2013_G027	218.7	72.7	0.3805	0.1179	0.0014	5.0044	0.0770	0.3163	0.0019	1925.1	10.5	1820.1	11.5	1771.7	9.1	-8.0		1925.1	10.5

Analysis No.	U (ppm)	Pb (ppm)	Th/U	Measured isotopic ratios						Calculated isotopic ages (Ma)						Disc.† (%)	Comment§	Preferred age (Ma)#	
				$^{207}Pb/^{206}Pb$	1σ	$^{207}Pb/^{235}U$	1σ	$^{206}Pb/^{238}U$	1σ	$^{207}Pb/^{206}Pb$	1σ	$^{207}Pb/^{235}U$	1σ	$^{206}Pb/^{238}U$	1σ			Age	1σ
Sample DLZ2/2013, quartz sandstone, Middle Dalinzi Formation, Longwangmiao, Dalian city, GPS: 39°07'26"N 121°41'21"E																			
DLZ2/2013_G028	58.7	8.2	0.9115	0.0715	0.0024	1.1156	0.0429	0.1166	0.0009	971.2	20.6	760.9	18.4	710.9	4.9	-6.6		710.9	4.9
DLZ2/2013_G029	130.5	51.2	1.02	0.1154	0.0015	4.8076	0.0844	0.3165	0.0019	1885.8	11.1	1786.2	12.1	1772.5	9.4	-6.0		1885.8	11.1
DLZ2/2013_G030	214.3	75.2	0.2038	0.1135	0.0014	5.2625	0.0811	0.3419	0.0020	1856	10.4	1862.8	11.6	1895.6	9.7	2.1		1856	10.4
DLZ2/2013_G031	209.9	67	0.3912	0.1323	0.0016	5.3841	0.0840	0.3025	0.0018	2128.1	11	1882.3	11.8	1703.9	8.9	-19.9	Del.		
DLZ2/2013_G032	58.7	34.5	0.8097	0.1710	0.0022	10.6723	0.2539	0.4823	0.0030	2567.6	12.2	2495	13.5	2537.3	13.2	-1.2		2567.6	12.2
DLZ2/2013_G033	418.8	103.6	0.2615	0.1126	0.0014	3.8280	0.0538	0.2464	0.0014	1841.8	10.3	1598.7	10.8	1419.8	7.4	-22.9	Del.		
DLZ2/2013_G034	374.9	110.4	0.3509	0.1143	0.0014	4.4508	0.0670	0.2854	0.0017	1869	10.5	1721.8	11.4	1618.3	8.4	-13.4		1869	10.5
DLZ2/2013_G035	165.5	47.9	0.3723	0.1176	0.0015	4.3254	0.0741	0.2774	0.0017	1920.1	11.1	1698.2	11.8	1578.1	8.4	-17.8	Del.		
DLZ2/2013_G036	81.7	20.5	0.5301	0.0853	0.0014	2.5402	0.0541	0.2293	0.0014	1321.9	11.7	1283.6	12.6	1330.7	7.5	0.7		1321.9	11.7
DLZ2/2013_G037	138.7	62.8	0.6796	0.1370	0.0017	7.1152	0.1210	0.3899	0.0023	2190	11.2	2125.9	12.4	2122.2	10.8	-3.1		2190	11.2
DLZ2/2013_G038	40	18.3	0.4709	0.1498	0.0022	7.7831	0.2302	0.4126	0.0028	2343.4	13.7	2206.3	14.9	2226.8	12.7	-5.0		2343.4	13.7
DLZ2/2013_G039	81.1	32.6	0.6948	0.1130	0.0016	5.1275	0.1053	0.3444	0.0021	1847.9	11.7	1840.7	12.9	1907.7	10.2	3.2		1847.9	11.7
DLZ2/2013_G040	384.8	105	0.1648	0.1130	0.0014	4.1344	0.0625	0.2759	0.0016	1848.1	10.6	1661.1	11.4	1570.7	8.2	-15.0	Del.		
DLZ2/2013_G041	65.8	23.2	0.5292	0.1146	0.0017	4.7397	0.1106	0.3189	0.0020	1872.8	12.7	1774.3	13.7	1784.3	10	-4.7		1872.8	12.7
DLZ2/2013_G042	55.9	7.7	0.8235	0.0821	0.0023	1.2846	0.0439	0.1181	0.0008	1248.9	20.5	838.9	17.1	719.7	4.8	-14.2		719.7	4.8
DLZ2/2013_G043	256.5	82.6	0.3415	0.1143	0.0014	4.7686	0.0711	0.3083	0.0018	1868.1	10.5	1779.4	11.5	1732.1	8.9	-7.3		1868.1	10.5
DLZ2/2013_G044	37.8	20.9	0.538	0.1687	0.0023	10.3627	0.2809	0.4781	0.0031	2544.9	12.8	2467.7	14.1	2519.2	13.4	-1.0		2544.9	12.8
DLZ2/2013_G045	229.7	79.7	0.1812	0.1143	0.0014	5.2081	0.0785	0.3404	0.0020	1869.2	10.6	1853.9	11.7	1888.5	9.6	1.0		1869.2	10.6
DLZ2/2013_G046	331.6	71	1.2714	0.1075	0.0014	2.5148	0.0390	0.1698	0.0010	1757	10.9	1276.3	10.4	1011	5.6	-20.8	Del.		
DLZ2/2013_G047	213.8	32.3	0.993	0.0681	0.0011	1.0986	0.0207	0.1232	0.0008	871	9.4	752.7	9.4	748.8	4.4	-0.5		748.8	4.4
DLZ2/2013_G048	97.6	25.3	1.2237	0.0818	0.0013	2.1985	0.0455	0.2019	0.0013	1240	11.5	1180.6	12.1	1185.6	6.8	-4.4		1240	11.5
DLZ2/2013_G049	60.3	30.8	0.4361	0.1678	0.0022	10.1325	0.2190	0.4603	0.0028	2536	12.2	2446.9	13.4	2440.9	12.5	-3.7		2536	12.2
DLZ2/2013_G050	131.6	82	1.0884	0.1605	0.0020	10.1546	0.1702	0.4749	0.0028	2461.4	11.6	2449	12.8	2505	12.2	1.8		2461.4	11.6
DLZ2/2013_G051	128.3	71.6	0.5107	0.1634	0.0021	10.5805	0.1798	0.4826	0.0029	2491.6	11.6	2487	12.9	2538.4	12.4	1.9		2491.6	11.6
DLZ2/2013_G052	120	44.8	0.9604	0.1137	0.0015	4.5355	0.0837	0.3060	0.0019	1859.1	11.6	1737.5	12.5	1720.8	9.2	-7.4		1859.1	11.6
DLZ2/2013_G053	339.3	85.6	1.6482	0.1869	0.0024	5.2372	0.0793	0.2090	0.0012	2715.2	11.9	1858.7	11.9	1223.6	6.6	-54.9	Del.		
DLZ2/2013_G054	196.8	94.3	0.7118	0.1621	0.0020	8.9830	0.1435	0.4146	0.0024	2477.9	11.6	2336.3	12.7	2236.1	11.1	-9.8		2477.9	11.6
DLZ2/2013_G055	106.9	57	0.8453	0.1681	0.0021	9.9302	0.1770	0.4436	0.0027	2538.8	11.9	2428.3	13	2366.7	11.8	-6.8		2538.8	11.9
DLZ2/2013_G056	201.7	63.5	0.2802	0.1186	0.0015	4.9000	0.0773	0.3077	0.0018	1935.5	11.1	1802.3	11.9	1729.3	8.9	-10.7		1935.5	11.1
DLZ2/2013_G057	270.2	79.5	0.2769	0.1165	0.0015	4.4927	0.0684	0.2894	0.0017	1903.7	10.9	1729.6	11.7	1638.4	8.4	-13.9		1903.7	10.9
DLZ2/2013_G058	82.8	49.8	1.1305	0.1650	0.0021	10.0648	0.1858	0.4613	0.0028	2508	12	2440.7	13.2	2445.4	12.2	-2.5		2508	12
DLZ2/2013_G059	275.7	88.4	0.2122	0.1144	0.0015	4.9390	0.0754	0.3160	0.0018	1869.7	10.9	1808.9	11.9	1770.3	9	-5.3		1869.7	10.9
DLZ2/2013_G060	207.2	72.5	0.3443	0.1147	0.0015	5.0872	0.0809	0.3316	0.0020	1874.7	11.1	1834	12.2	1845.9	9.4	-1.5		1874.7	11.1
DLZ2/2013_G061	149.7	57.4	0.4351	0.1146	0.0015	5.3754	0.0902	0.3510	0.0021	1873.6	11.3	1880.9	12.4	1939.5	9.9	3.5		1873.6	11.3
DLZ2/2013_G062	101.4	50.6	0.6429	0.1462	0.0019	8.2006	0.1451	0.4263	0.0025	2302.2	11.9	2253.4	13.1	2289.2	11.5	-0.6		2302.2	11.9
DLZ2/2013_G063	88.3	43.5	0.7035	0.1407	0.0019	7.5065	0.1416	0.4166	0.0025	2236.3	12.1	2173.8	13.2	2244.8	11.4	0.4		2236.3	12.1
DLZ2/2013_G064	261.5	80	0.2088	0.1178	0.0015	4.7391	0.0733	0.3024	0.0018	1922.7	11.2	1774.2	12	1703	8.8	-11.4		1922.7	11.2
DLZ2/2013_G065	122.2	15.8	0.5318	0.0651	0.0013	1.0352	0.0238	0.1197	0.0008	776.9	10.8	721.5	10.9	728.9	4.4	1.0		728.9	4.4
DLZ2/2013_G066	115.7	45.2	0.7006	0.1159	0.0016	4.9928	0.0891	0.3346	0.0020	1893.3	11.6	1818.1	12.7	1860.7	9.7	-1.7		1893.3	11.6
DLZ2/2013_G067	254.4	77.1	0.3582	0.1164	0.0015	4.6877	0.0733	0.2929	0.0017	1901	11.2	1765	12	1655.9	8.5	-12.9		1901	11.2
DLZ2/2013_G068	139.2	18.5	0.785	0.0703	0.0012	1.0773	0.0220	0.1137	0.0007	938.3	10.8	742.3	10	694	4.1	-6.5		694	4.1
DLZ2/2013_G069	65.8	42.4	0.463	0.1893	0.0025	13.8274	0.2896	0.5452	0.0033	2736.3	12.6	2738	13.8	2805.1	13.8	2.5		2736.3	12.6
DLZ2/2013_G070	31.2	6.7	0.8817	0.0746	0.0025	1.7881	0.0770	0.1808	0.0013	1056.4	21.8	1041.1	22.4	1071.1	7.2	2.9		1071.1	7.2
DLZ2/2013_G071	52.6	11.8	0.9236	0.0764	0.0017	1.8450	0.0529	0.1867	0.0012	1106.1	15	1061.6	15.6	1103.5	6.7	-0.2		1106.1	15
DLZ2/2013_G072	226.4	72	0.2312	0.1158	0.0015	4.7967	0.0748	0.3116	0.0018	1892.4	11.3	1784.3	12.2	1748.3	8.9	-7.6		1892.4	11.3
DLZ2/2013_G073	79.5	14	0.536	0.0715	0.0015	1.5560	0.0401	0.1609	0.0011	971.7	12.9	952.9	13.5	961.8	5.8	0.9		961.8	5.8
DLZ2/2013_G074	372.2	84.3	0.5097	0.1170	0.0016	3.4676	0.0526	0.2177	0.0013	1910.9	11.4	1519.9	11.4	1269.8	6.7	-33.6	Del.		

Analysis No.	U (ppm)	Pb (ppm)	Th/U	Measured isotopic ratios						Calculated isotopic ages (Ma)						Disc.† (%)	Comment§	Preferred age (Ma)#	
				$^{207}Pb/^{206}Pb$	1σ	$^{207}Pb/^{235}U$	1σ	$^{206}Pb/^{238}U$	1σ	$^{207}Pb/^{206}Pb$	1σ	$^{207}Pb/^{235}U$	1σ	$^{206}Pb/^{238}U$	1σ			Age	1σ
Sample DLZ2/2013, quartz sandstone, Middle Dalinzi Formation, Longwangmiao, Dalian city, GPS: 39°07'26"N 121°41'21"E																			
DLZ2/2013_G075	179.3	62.3	0.2244	0.1144	0.0015	5.1085	0.0843	0.3374	0.0020	1870.9	11.5	1837.5	12.6	1874.1	9.6	0.2		1870.9	11.5
DLZ2/2013_G076	42.2	16.2	1.3987	0.1244	0.0021	4.7551	0.1310	0.2927	0.0020	2019.8	14.8	1777	15.4	1654.8	9.7	-18.1	Del.		
DLZ2/2013_G077	99.2	53.3	0.3862	0.1753	0.0023	11.2981	0.2063	0.4834	0.0029	2609.1	12.5	2548	13.7	2542.2	12.5	-2.6		2609.1	12.5
DLZ2/2013_G078	26.3	17.2	1.5005	0.1664	0.0026	9.6256	0.3148	0.4637	0.0031	2522.2	14.5	2399.6	15.7	2455.8	13.7	-2.6		2522.2	14.5
DLZ2/2013_G079	41.7	6.5	1.1309	0.0658	0.0025	1.0757	0.0477	0.1235	0.0009	799.4	21.4	741.5	21.1	750.7	5.3	1.2		750.7	5.3
DLZ2/2013_G080	300.4	100.3	0.2668	0.1129	0.0015	4.8154	0.0740	0.3224	0.0019	1846.6	11.4	1787.6	12.3	1801.4	9.1	-2.4		1846.6	11.4
DLZ2/2013_G081	162.3	22.2	0.5125	0.0637	0.0011	1.0689	0.0209	0.1271	0.0008	732	8.9	738.2	9.7	771.4	4.4	4.5		771.4	4.4
DLZ2/2013_G082	701.1	91.3	0.532	0.0551	0.0008	0.8798	0.0137	0.1204	0.0007	415.1	4.9	640.9	7.5	732.7	4	14.3	Del.		
DLZ2/2013_G083	199.5	64.8	0.3566	0.1130	0.0016	4.6825	0.0782	0.3092	0.0018	1847.9	11.7	1764.1	12.6	1736.8	9	-6.0		1847.9	11.7
DLZ2/2013_G084	54.3	33	0.9872	0.1615	0.0023	10.1249	0.2273	0.4729	0.0029	2471.4	13.1	2446.2	14.3	2496.4	12.8	1.0		2471.4	13.1
DLZ2/2013_G085	26.9	3.8	0.5908	0.0642	0.0034	1.0670	0.0642	0.1286	0.0010	749.2	28.1	737.3	29	780	5.9	5.8	Del.		
DLZ2/2013_G086	296	97.2	0.116	0.1132	0.0015	5.0097	0.0788	0.3295	0.0019	1850.6	11.6	1821	12.6	1835.9	9.3	-0.8		1850.6	11.6
DLZ2/2013_G087	269.2	37.7	0.8433	0.0637	0.0010	1.0066	0.0183	0.1195	0.0007	731.7	8.4	707.2	9	727.6	4.1	2.9		727.6	4.1
DLZ2/2013_G088	157.3	56	0.2567	0.1135	0.0016	5.2160	0.0912	0.3419	0.0020	1856.8	11.9	1855.2	13	1895.6	9.8	2.1		1856.8	11.9
DLZ2/2013_G089	139.8	46.3	0.5426	0.1150	0.0016	4.6426	0.0825	0.3050	0.0018	1879.9	12.2	1757	13	1716	9	-8.7		1879.9	12.2
DLZ2/2013_G090	64.1	21.2	2.5974	0.0846	0.0016	2.0481	0.0502	0.1957	0.0013	1306.8	13.9	1131.7	14.1	1152	6.9	-11.9		1306.8	13.9
DLZ2/2013_G091	86.1	11.5	0.679	0.0654	0.0016	1.0380	0.0287	0.1200	0.0008	787.6	13.1	722.9	13.1	730.4	4.5	1.0		730.4	4.5
DLZ2/2013_G092	52.6	22.3	0.845	0.1195	0.0019	5.3118	0.1233	0.3513	0.0022	1948.2	13.5	1870.8	14.5	1940.8	10.5	-0.4		1948.2	13.5
DLZ2/2013_G093	163.9	53.9	0.2391	0.1137	0.0016	4.8590	0.0839	0.3199	0.0019	1859.9	12.1	1795.2	13.1	1789.2	9.2	-3.8		1859.9	12.1
DLZ2/2013_G094	51.5	17.2	1.8652	0.0885	0.0017	2.5277	0.0660	0.2252	0.0015	1392.3	14.6	1280	15.1	1309.1	7.8	-6.0		1392.3	14.6
DLZ2/2013_G095	161.7	56.7	0.2941	0.1158	0.0017	5.1976	0.0895	0.3350	0.0020	1891.9	12.2	1852.2	13.2	1862.6	9.6	-1.5		1891.9	12.2
DLZ2/2013_G096	41.1	6.6	1.238	0.0657	0.0024	1.0326	0.0426	0.1239	0.0009	798.1	20	720.2	19.8	752.7	5.1	4.5		752.7	5.1
DLZ2/2013_G097	418.8	52	0.5312	0.0644	0.0010	0.9922	0.0163	0.1146	0.0007	754.1	8	699.8	8.3	699.6	3.9	0.0		699.6	3.9
DLZ2/2013_G098	88.8	29.4	0.8523	0.1146	0.0018	4.1982	0.0924	0.2848	0.0018	1873.3	13.6	1673.7	14.2	1615.3	9	-13.8		1873.3	13.6
DLZ2/2013_G099	52.6	19.1	0.6607	0.1166	0.0019	4.8936	0.1182	0.3158	0.0020	1904.9	13.9	1801.2	14.8	1769.3	9.8	-7.1		1904.9	13.9
DLZ2/2013_G100	276.8	93.9	0.3139	0.1138	0.0016	4.8698	0.0792	0.3245	0.0019	1861	12.1	1797.1	13.1	1811.6	9.2	-2.7		1861	12.1
DLZ2/2013_G101	14.3	NaN	1.5959	0.1968	0.0056	4.0850	0.2073	0.1781	0.0016	2800	27.2	1651.3	25.2	1056.3	8.8	-36.0	Del.		
DLZ2/2013_G102	233	82.3	0.244	0.1150	0.0017	5.2218	0.0871	0.3410	0.0020	1879.7	12.3	1856.2	13.3	1891.6	9.6	0.6		1879.7	12.3
DLZ2/2013_G103	142.5	59.6	0.3825	0.1286	0.0019	6.6146	0.1167	0.3849	0.0023	2079.5	12.8	2061.3	13.8	2099.2	10.6	1.0		2079.5	12.8
DLZ2/2013_G104	98.7	21.2	0.7409	0.0797	0.0014	1.9319	0.0419	0.1882	0.0012	1188.3	12.3	1092.2	12.8	1111.7	6.4	-6.4		1188.3	12.3
DLZ2/2013_G105	70.2	10.3	0.8591	0.0848	0.0019	1.3896	0.0370	0.1248	0.0008	1311	16.3	884.5	13.9	758.2	4.8	-14.3		758.2	4.8
DLZ2/2013_G106	304.8	95.8	0.3692	0.1143	0.0016	4.6413	0.0748	0.3020	0.0018	1869.2	12.3	1756.7	13	1701.3	8.7	-9.0		1869.2	12.3
DLZ2/2013_G107	295.5	84.5	0.1413	0.1150	0.0017	4.4102	0.0726	0.2895	0.0017	1880.5	12.4	1714.3	13	1639	8.4	-12.8		1880.5	12.4
DLZ2/2013_G108	368.9	81.6	0.5243	0.1254	0.0018	3.5126	0.0566	0.2057	0.0012	2034.5	12.7	1530.1	12.4	1205.9	6.4	-40.7	Del.		
DLZ2/2013_G109	23	8.3	0.5225	0.1147	0.0023	4.6668	0.1653	0.3250	0.0023	1875.8	17.4	1761.3	18.3	1814.2	10.9	-3.3		1875.8	17.4
DLZ2/2013_G110	13.2	4.8	0.6686	0.1136	0.0031	4.5236	0.2408	0.3169	0.0025	1857.8	23.6	1735.3	24.3	1774.5	12.1	-4.5		1857.8	23.6
DLZ2/2013_G111	70.7	27.6	0.6938	0.1137	0.0018	5.0137	0.1063	0.3360	0.0021	1860	13.4	1821.6	14.4	1867.4	9.9	0.4		1860	13.4
DLZ2/2013_G112	38.4	16.9	0.6877	0.1235	0.0020	6.2266	0.1634	0.3755	0.0024	2006.7	14.5	2008.2	15.5	2055.3	11.2	2.4		2006.7	14.5
DLZ2/2013_G113	36.2	17.4	1.0094	0.1296	0.0022	6.4548	0.1752	0.3825	0.0025	2092	14.8	2039.8	15.8	2087.7	11.4	-0.2		2092	14.8
DLZ2/2013_G114	241.2	84	0.2928	0.1149	0.0017	5.1141	0.0866	0.3339	0.0020	1877.8	12.7	1838.5	13.6	1857.4	9.4	-1.1		1877.8	12.7
DLZ2/2013_G115	142.5	56	0.6457	0.1122	0.0017	5.0606	0.0908	0.3426	0.0020	1835.5	12.8	1829.5	13.8	1899.4	9.7	3.5		1835.5	12.8
DLZ2/2013_G116	100.9	27.9	0.3732	0.0921	0.0015	3.1384	0.0624	0.2623	0.0016	1469.4	12.5	1442.2	13.4	1501.6	8.1	2.2		1469.4	12.5
DLZ2/2013_G117	149.7	47.8	0.4148	0.1133	0.0017	4.4731	0.0819	0.3033	0.0018	1853	13	1726	13.7	1707.4	9	-7.9		1853	13
DLZ2/2013_G118	176	79.5	0.6173	0.1558	0.0023	8.1097	0.1403	0.3959	0.0023	2410.8	13.7	2243.3	14.5	2150.1	10.7	-10.8		2410.8	13.7
DLZ2/2013_G119	25.2	3.8	0.8917	0.0946	0.0037	1.4950	0.0709	0.1261	0.0010	1520.5	30.5	928.3	25	765.8	5.8	-17.5	Del.		
DLZ2/2013_G120	210.5	73.7	0.2663	0.1135	0.0017	5.1239	0.0901	0.3371	0.0020	1855.9	13	1840.1	14	1872.6	9.6	0.9		1855.9	13
DLZ2/2013_G121	56.5	26.1	0.5722	0.1358	0.0022	7.2193	0.1622	0.4037	0.0025	2173.8	14.3	2138.9	15.3	2186.2	11.4	0.6		2173.8	14.3

Analysis No.	U (ppm)	Pb (ppm)	Th/U	Measured isotopic ratios						Calculated isotopic ages (Ma)						Disc.† (%)	Comment§	Preferred age (Ma)#	
				$^{207}Pb/^{206}Pb$	1σ	$^{207}Pb/^{235}U$	1σ	$^{206}Pb/^{238}U$	1σ	$^{207}Pb/^{206}Pb$	1σ	$^{207}Pb/^{235}U$	1σ	$^{206}Pb/^{238}U$	1σ			Age	1σ
Sample DLZ2/2013, quartz sandstone, Middle Dalinzi Formation, Longwangmiao, Dalian city, GPS: 39°07'26"N 121°41'21"E																			
DLZ2/2013_G122	183.6	25.2	0.6476	0.0637	0.0012	1.0586	0.0214	0.1235	0.0008	732.3	9.4	733.1	10.1	750.7	4.3	2.4		750.7	4.3
DLZ2/2013_G123	17	2.2	0.5956	0.1543	0.0057	2.3873	0.1246	0.1214	0.0011	2393.9	33.7	1238.8	27.7	738.4	6.3	-40.4	Del.		
DLZ2/2013_G124	71.8	15.3	0.4142	0.0804	0.0015	2.1750	0.0525	0.2030	0.0013	1206.6	13.5	1173.1	14.2	1191.3	6.9	-1.3		1206.6	13.5
DLZ2/2013_G125	167.2	57.1	0.2025	0.1130	0.0018	4.8936	0.0873	0.3344	0.0020	1848.4	13.2	1801.1	14.1	1859.5	9.5	0.6		1848.4	13.2
DLZ2/2013_G126	133.8	46.5	0.4165	0.1137	0.0018	4.8747	0.0901	0.3237	0.0019	1859.5	13.3	1797.9	14.2	1807.7	9.4	-2.8		1859.5	13.3
DLZ2/2013_G127	54.3	28.4	0.8786	0.1655	0.0027	9.2210	0.2154	0.4353	0.0027	2512.1	14.9	2360.2	15.9	2329.7	12.2	-7.3		2512.1	14.9
DLZ2/2013_G128	189.1	65.8	0.2649	0.1174	0.0018	5.3205	0.0961	0.3367	0.0020	1916.4	13.4	1872.2	14.3	1870.9	9.6	-2.4		1916.4	13.4
DLZ2/2013_G129	98.1	35.1	0.6708	0.1155	0.0019	4.8058	0.0962	0.3188	0.0019	1887.5	13.9	1785.9	14.7	1783.9	9.4	-5.5		1887.5	13.9
DLZ2/2013_G130	179.8	62.8	0.3269	0.1123	0.0018	4.8979	0.0874	0.3316	0.0020	1837.3	13.3	1801.9	14.2	1846.1	9.4	0.5		1837.3	13.3
DLZ2/2013_G131	34	22.6	0.7771	0.1874	0.0031	13.6752	0.3840	0.5340	0.0034	2719.6	15.4	2727.5	16.6	2758.2	14.3	1.4		2719.6	15.4
DLZ2/2013_G132	121.7	45.2	0.464	0.1156	0.0018	5.2359	0.0994	0.3401	0.0020	1888.6	13.7	1858.5	14.6	1887	9.8	-0.1		1888.6	13.7
DLZ2/2013_G133	115.7	42.3	0.3538	0.1195	0.0019	5.5496	0.1086	0.3446	0.0021	1948.3	13.9	1908.3	14.8	1908.7	9.9	-2.0		1948.3	13.9
DLZ2/2013_G134	120.6	30.1	0.379	0.0862	0.0015	2.6968	0.0537	0.2373	0.0014	1342.2	12.5	1327.6	13.4	1372.4	7.5	2.3		1342.2	12.5
DLZ2/2013_G135	102	36.1	0.553	0.1059	0.0017	4.4153	0.0888	0.3173	0.0019	1729.1	13.7	1715.2	14.6	1776.7	9.4	2.7		1729.1	13.7
DLZ2/2013_G136	57.6	13.3	0.5672	0.0925	0.0018	2.5560	0.0635	0.2081	0.0013	1478.1	15.1	1288.2	15	1218.6	7.2	-17.6	Del.		
DLZ2/2013_G137	143.1	50.4	0.4146	0.1130	0.0018	4.9748	0.0935	0.3299	0.0020	1848.7	13.7	1815.1	14.6	1837.8	9.5	-0.6		1848.7	13.7
DLZ2/2013_G138	83.9	33.4	0.6781	0.1129	0.0019	5.1461	0.1074	0.3441	0.0021	1845.8	14.2	1843.8	15.2	1906.4	10.1	3.3		1845.8	14.2
DLZ2/2013_G139	27.4	6.7	1.1035	0.0793	0.0023	1.9695	0.0743	0.1950	0.0014	1180.6	20.1	1105.1	20.6	1148.4	7.5	-2.7		1180.6	20.1
DLZ2/2013_G140	168.8	61.9	0.2564	0.1164	0.0019	5.4847	0.1015	0.3517	0.0021	1902	13.9	1898.2	14.8	1942.6	9.9	2.1		1902	13.9
DLZ2/2013_G141	24.1	15.1	0.7632	0.1612	0.0028	10.7334	0.3514	0.5018	0.0033	2468.4	16.3	2500.3	17.5	2621.4	14.2	6.2	Del.		
DLZ2/2013_G142	238.5	70.9	0.3763	0.1129	0.0018	4.2894	0.0761	0.2859	0.0017	1846.3	13.7	1691.3	14.2	1620.8	8.4	-12.2		1846.3	13.7
DLZ2/2013_G143	48.2	24.1	0.7254	0.1546	0.0026	8.4468	0.1939	0.4238	0.0026	2397.4	15.4	2280.2	16.3	2277.9	11.9	-5.0		2397.4	15.4
DLZ2/2013_G144	23	15.3	0.9847	0.1788	0.0031	11.7786	0.3864	0.5148	0.0034	2641.9	16.4	2587	17.6	2677.1	14.4	1.3		2641.9	16.4
DLZ2/2013_G145	70.7	27.5	0.7868	0.1132	0.0019	4.9077	0.1057	0.3277	0.0020	1851.9	14.6	1803.6	15.5	1827.4	9.8	-1.3		1851.9	14.6
DLZ2/2013_G146	42.8	10.7	1.0189	0.0858	0.0019	2.3018	0.0654	0.2027	0.0013	1334.6	16.3	1212.8	16.4	1189.8	7.2	-10.9		1334.6	16.3
DLZ2/2013_G147	114.6	65.3	1.1172	0.1646	0.0027	9.7991	0.1877	0.4448	0.0026	2503.4	15.2	2416.1	16.1	2372	11.8	-5.2		2503.4	15.2
DLZ2/2013_G148	103.1	40.5	1.1747	0.1156	0.0019	4.9945	0.0990	0.3170	0.0019	1889.3	14.4	1818.4	15.1	1775	9.3	-6.0		1889.3	14.4

Analysis No.	U (ppm)	Pb (ppm)	Th/U	Measured isotopic ratios						Calculated isotopic ages (Ma)						Disc.† (%)	Comment§	Preferred age (Ma)#	
				$^{207}Pb/^{206}Pb$	1σ	$^{207}Pb/^{235}U$	1σ	$^{206}Pb/^{238}U$	1σ	$^{207}Pb/^{206}Pb$	1σ	$^{207}Pb/^{235}U$	1σ	$^{206}Pb/^{238}U$	1σ			Age	1σ
Sample GH03/2014, quartz sandstone (interbedded with dolostone), Middle Gouhou Formation, Gouhou section of Huaibei region, GPS: 33°59'32"N 117°17'46"E																			
GH03/2014_G001	680.4	79.0	1.1461	0.11166	0.00141	1.51052	0.01872	0.09813	0.00108	1826.6	10.7	934.6	10.2	603.4	6.3	-35.4	Del.		
GH03/2014_G002	98.0	57.6	0.9500	0.15997	0.00196	10.32731	0.12798	0.46835	0.00534	2455.3	11.3	2464.6	15.5	2476.3	23.4	0.9		2455.3	11.3
GH03/2014_G003	184.6	23.9	0.5372	0.06168	0.00100	1.02660	0.01633	0.12075	0.00140	663.0	7.9	717.2	10.3	734.9	8.1	2.5		734.9	8.1
GH03/2014_G004	290.6	123.3	0.4454	0.15854	0.00181	8.69620	0.09983	0.39795	0.00430	2440.1	10.5	2306.7	14.3	2159.6	19.8	-11.5		2440.1	10.5
GH03/2014_G005	193.9	69.0	0.7397	0.14688	0.00178	6.21176	0.07508	0.30683	0.00340	2309.9	11.0	2006.1	14.4	1725.1	16.8	-25.3	Del.		
GH03/2014_G006	204.6	69.7	0.5647	0.10993	0.00135	4.64557	0.05690	0.30660	0.00338	1798.2	10.3	1757.5	13.8	1724.0	16.7	-4.1		1798.2	10.3
GH03/2014_G007	376.5	76.9	0.4145	0.08110	0.00101	2.19721	0.02718	0.19659	0.00214	1223.9	8.9	1180.2	11.5	1157.0	11.5	-5.5		1223.9	8.9
GH03/2014_G008	823.7	94.6	0.8726	0.16093	0.00189	2.31207	0.02691	0.10425	0.00113	2465.5	10.9	1216.0	11.3	639.3	6.6	-47.4	Del.		
GH03/2014_G009	413.8	98.8	0.4457	0.14648	0.00171	4.54938	0.05299	0.22536	0.00244	2305.2	10.6	1740.0	13.3	1310.1	12.8	-43.2	Del.		
GH03/2014_G010	41.3	13.6	0.7030	0.11773	0.00197	4.68162	0.07713	0.28855	0.00378	1922.1	14.4	1764.0	17.8	1634.3	18.9	-15.0		1922.1	14.4
GH03/2014_G011	203.3	46.1	1.2766	0.07680	0.00107	1.85140	0.02537	0.17492	0.00197	1116.0	9.4	1063.9	11.8	1039.2	10.8	-2.3		1039.2	10.8
GH03/2014_G012	460.5	160.1	0.9745	0.11642	0.00137	4.69752	0.05559	0.29280	0.00318	1902.0	10.1	1766.8	13.4	1655.5	15.9	-13.0		1902.0	10.1
GH03/2014_G013	88.0	36.1	0.4859	0.12726	0.00168	6.51626	0.08620	0.37159	0.00433	2060.5	11.6	2048.1	15.5	2036.9	20.4	-1.1		2060.5	11.6
GH03/2014_G014	91.3	31.6	1.5036	0.10496	0.00156	3.72439	0.05482	0.25750	0.00310	1713.6	12.3	1576.6	15.3	1477.0	15.9	-13.8		1713.6	12.3
GH03/2014_G015	381.2	128.5	0.6638	0.12019	0.00140	4.93143	0.05760	0.29775	0.00322	1959.0	10.1	1807.7	13.4	1680.1	16.0	-14.2		1959.0	10.1

Analysis No.	U (ppm)	Pb (ppm)	Th/U	Measured isotopic ratios						Calculated isotopic ages (Ma)						Disc.† (%)	Comment§	Preferred age (Ma)#	
				$^{208}Pb/^{206}Pb$	1σ	$^{207}Pb/^{235}U$	1σ	$^{206}Pb/^{238}U$	1σ	$^{207}Pb/^{206}Pb$	1σ	$^{208}Pb/^{232}U$	1σ	$^{206}Pb/^{238}U$	1σ			Age	1σ
Sample GH03/2014, quartz sandstone (interbedded with dolostone), Middle Gouhou Formation, Gouhou section of Huaibei region, GPS: 33°59'32"N 117°17'46"E																			
GH03/2014_G016	172.6	67.5	0.6432	0.16464	0.00200	8.01173	0.09767	0.35315	0.00396	2503.9	11.3	2232.3	14.9	1949.6	18.9	-22.1	Del.		
GH03/2014_G017	296.6	93.1	0.3558	0.11798	0.00139	4.89759	0.05814	0.30128	0.00328	1925.9	10.2	1801.8	13.5	1697.7	16.2	-11.8		1925.9	10.2
GH03/2014_G018	153.3	48.0	0.5293	0.10893	0.00140	4.36517	0.05603	0.29083	0.00328	1781.6	10.8	1705.8	14.1	1645.7	16.4	-7.6		1781.6	10.8
GH03/2014_G019	68.0	18.4	0.6118	0.10910	0.00171	3.61283	0.05566	0.24033	0.00297	1784.4	13.2	1552.4	15.9	1388.4	15.4	-22.2	Del.		
GH03/2014_G020	310.5	113.0	1.7117	0.12884	0.00152	5.08171	0.06041	0.28626	0.00312	2082.2	10.4	1833.1	13.6	1622.8	15.6	-22.1	Del.		
GH03/2014_G021	287.9	91.2	0.2420	0.12270	0.00148	5.29698	0.06423	0.31333	0.00345	1995.9	10.5	1868.4	14.0	1757.1	16.9	-12.0		1995.9	10.5
GH03/2014_G022	179.9	63.9	0.5589	0.11060	0.00138	4.87590	0.06102	0.32000	0.00357	1809.3	10.5	1798.1	14.1	1789.7	17.4	-1.1		1809.3	10.5
GH03/2014_G023	169.3	34.2	0.7420	0.07164	0.00106	1.74589	0.02548	0.17690	0.00203	975.7	9.3	1025.6	12.1	1050.0	11.1	2.4		1050.0	11.1
GH03/2014_G024	241.9	81.7	0.8180	0.11212	0.00137	4.55422	0.05592	0.29485	0.00325	1834.1	10.4	1740.9	13.7	1665.7	16.2	-9.2		1834.1	10.4
GH03/2014_G025	552.4	202.1	2.5137	0.12301	0.00146	4.11442	0.04920	0.24280	0.00264	2000.3	10.4	1657.2	13.2	1401.2	13.7	-29.9	Del.		
GH03/2014_G026	194.6	76.9	0.8902	0.11222	0.00140	5.07915	0.06400	0.32853	0.00368	1835.7	10.6	1832.6	14.2	1831.3	17.9	-0.2		1835.7	10.6
GH03/2014_G027	416.5	116.5	0.3464	0.17926	0.00210	6.72844	0.07937	0.27246	0.00298	2646.0	11.0	2076.4	14.2	1553.3	15.1	-41.3	Del.		
GH03/2014_G028	210.6	65.4	0.5639	0.12381	0.00157	5.06503	0.06450	0.29698	0.00335	2011.8	11.1	1830.3	14.4	1676.3	16.7	-16.7	Del.		
GH03/2014_G029	102.6	43.3	1.3887	0.22300	0.00286	10.21422	0.13154	0.33251	0.00393	3002.5	12.3	2454.4	16.1	1850.5	19.0	-38.4	Del.		
GH03/2014_G030	234.6	31.1	0.6579	0.06618	0.00102	1.07207	0.01631	0.11760	0.00135	812.1	8.6	739.8	10.1	716.7	7.8	-3.1		716.7	7.8
GH03/2014_G031	1804.0	152.4	0.7694	0.12183	0.00144	1.29654	0.01533	0.07726	0.00083	1983.2	10.3	844.2	9.2	479.7	5.0	-43.2	Del.		
GH03/2014_G032	562.4	120.7	1.5103	0.11862	0.00142	3.09693	0.03724	0.18953	0.00207	1935.5	10.3	1431.9	12.4	1118.8	11.2	-42.2	Del.		
GH03/2014_G033	425.8	124.2	0.7410	0.13208	0.00157	4.89290	0.05864	0.26895	0.00294	2125.8	10.6	1801.0	13.6	1535.5	14.9	-27.8	Del.		
GH03/2014_G034	259.9	89.2	0.4704	0.12213	0.00149	5.33769	0.06562	0.31729	0.00351	1987.6	10.6	1874.9	14.1	1776.5	17.2	-10.6		1987.6	10.6
GH03/2014_G035	116.6	42.5	0.5281	0.11053	0.00149	5.01841	0.06789	0.32962	0.00382	1808.1	11.4	1822.4	15.1	1836.5	18.5	1.6		1808.1	11.4
GH03/2014_G036	561.1	112.5	0.6190	0.14384	0.00172	3.70698	0.04451	0.18711	0.00205	2273.9	10.8	1572.9	13.0	1105.7	11.1	-51.4	Del.		
GH03/2014_G037	505.1	154.5	2.0711	0.14176	0.00169	4.32086	0.05205	0.22129	0.00242	2248.8	10.8	1697.3	13.3	1288.7	12.8	-42.7	Del.		
GH03/2014_G038	96.0	48.1	0.7499	0.13741	0.00179	7.96157	0.10503	0.42066	0.00490	2194.8	11.7	2226.7	15.8	2263.5	22.2	3.1		2194.8	11.7
GH03/2014_G039	49.3	6.7	0.4357	0.06777	0.00172	1.20642	0.02962	0.12925	0.00184	861.5	14.7	803.5	16.2	783.6	10.5	-2.5		783.6	10.5
GH03/2014_G040	477.8	175.1	2.1900	0.13716	0.00163	4.85369	0.05833	0.25693	0.00281	2191.6	10.7	1794.3	13.6	1474.1	14.4	-32.7	Del.		
GH03/2014_G041	241.2	24.5	0.7989	0.07417	0.00128	0.89274	0.01494	0.08739	0.00105	1046.1	11.3	647.8	10.1	540.1	6.2	-16.6	Del.		
GH03/2014_G042	509.1	135.4	1.7511	0.16008	0.00191	4.88987	0.05883	0.22179	0.00243	2456.5	11.0	1800.5	13.7	1291.3	12.8	-47.4	Del.		
GH03/2014_G043	92.0	62.8	1.9644	0.16525	0.00213	10.07502	0.13192	0.44268	0.00518	2510.1	12.0	2441.7	16.1	2362.6	23.1	-5.9		2510.1	12.0
GH03/2014_G044	200.6	17.3	0.6765	0.06692	0.00128	0.72845	0.01356	0.07904	0.00098	835.3	10.9	555.6	9.8	490.4	5.9	-11.7		490.4	5.9
GH03/2014_G045	489.1	130.7	0.5741	0.15107	0.00179	5.39034	0.06469	0.25908	0.00283	2358.1	10.9	1883.3	13.8	1485.1	14.5	-37.0	Del.		
GH03/2014_G046	393.2	135.2	0.2384	0.11244	0.00134	5.16541	0.06276	0.33357	0.00365	1839.2	10.1	1846.9	13.8	1855.7	17.6	0.9		1839.2	10.1
GH03/2014_G047	110.6	47.1	0.4837	0.16315	0.00208	8.90701	0.11519	0.39641	0.00458	2488.6	11.8	2328.5	15.7	2152.5	21.1	-13.5		2488.6	11.8
GH03/2014_G048	599.8	101.9	0.5791	0.07525	0.00095	1.64196	0.02092	0.15844	0.00174	1075.2	8.4	986.5	10.6	948.1	9.7	-3.9		948.1	9.7
GH03/2014_G049	155.9	54.1	0.8456	0.10093	0.00138	4.19051	0.05791	0.30150	0.00345	1641.3	11.1	1672.2	14.6	1698.7	17.1	3.5		1641.3	11.1
GH03/2014_G050	172.6	55.7	0.6650	0.09981	0.00132	3.91325	0.05229	0.28470	0.00324	1620.5	10.7	1616.4	14.1	1615.0	16.3	-0.3		1620.5	10.7
GH03/2014_G051	198.6	43.5	0.6496	0.08592	0.00121	2.38415	0.03350	0.20150	0.00232	1336.4	10.5	1237.9	13.0	1183.4	12.4	-11.4		1336.4	10.5
GH03/2014_G052	260.6	85.1	0.3568	0.11832	0.00148	5.05930	0.06431	0.31050	0.00348	1931.0	10.8	1829.3	14.2	1743.2	17.1	-9.7		1931.0	10.8
GH03/2014_G053	379.9	125.2	0.2597	0.11639	0.00142	5.13019	0.06370	0.32008	0.00354	1901.5	10.5	1841.1	14.0	1790.1	17.3	-5.9		1901.5	10.5
GH03/2014_G054	361.2	123.3	0.3635	0.11613	0.00142	5.16462	0.06420	0.32295	0.00357	1897.5	10.5	1846.8	14.0	1804.1	17.4	-4.9		1897.5	10.5
GH03/2014_G055	224.6	23.4	1.2082	0.12299	0.00208	1.39349	0.02263	0.08228	0.00103	2000.0	14.8	886.2	12.4	509.7	6.1	-42.5	Del.		
GH03/2014_G056	156.6	41.5	0.8385	0.20013	0.00260	6.55990	0.08565	0.23803	0.00276	2827.3	12.4	2054.0	15.3	1376.4	14.4	-51.3	Del.		
GH03/2014_G057	283.2	NaN	1.5718	0.36594	0.00454	10.70871	0.13358	0.21251	0.00243	3774.7	12.3	2498.2	15.7	1242.2	12.9	-67.1	Del.		
GH03/2014_G058	714.4	66.0	0.7900	0.06967	0.00097	0.77767	0.01085	0.08106	0.00091	918.6	8.4	584.2	8.0	502.4	5.4	-14.0		502.4	5.4
GH03/2014_G059	441.8	144.1	0.6713	0.20394	0.00246	8.11956	0.09984	0.28913	0.00320	2858.0	11.5	2244.4	14.8	1637.2	16.0	-42.7	Del.		
GH03/2014_G060	92.0	39.6	0.7045	0.13213	0.00182	6.81839	0.09523	0.37476	0.00446	2126.5	12.3	2088.1	16.1	2051.8	20.9	-3.5		2126.5	12.3
GH03/2014_G061	47.3	13.7	0.9063	0.30618	0.00460	11.43804	0.16931	0.27129	0.00364	3501.8	14.8	2559.5	18.8	1547.3	18.5	-55.8	Del.		
GH03/2014_G062	86.6	34.7	0.7490	0.12607	0.00183	5.88186	0.08620	0.33882	0.00413	2043.9	12.8	1958.6	16.5	1881.0	19.9	-8.0		2043.9	12.8

Analysis No.	U (ppm)	Pb (ppm)	Th/U	Measured isotopic ratios						Calculated isotopic ages (Ma)						Disc.† (%)	Comment§	Preferred age (Ma)#	
				$^{207}Pb/^{206}Pb$	1σ	$^{206}Pb/^{238}U$	1σ	$^{208}Pb/^{232}Th$	1σ	$^{207}Pb/^{206}Pb$	1σ	$^{206}Pb/^{238}U$	1σ	$^{208}Pb/^{232}Th$	1σ			Age	1σ
Sample GH03/2014, quartz sandstone (interbedded with dolostone), Middle Gouhou Formation, Gouhou section of Huaibei region, GPS: 33°59'32"N 117°17'46"E																			
GH03/2014_G063	401.8	134.5	1.1941	0.16304	0.00202	6.58343	0.08289	0.29324	0.00327	2487.4	11.5	2057.1	14.7	1657.7	16.3	-33.4	Del.		
GH03/2014_G064	470.5	238.0	0.7811	0.25569	0.00309	16.88792	0.20909	0.47967	0.00534	3220.3	11.8	2928.5	15.8	2525.8	23.3	-21.6	Del.		
GH03/2014_G065	134.6	65.8	0.8343	0.13404	0.00176	7.43720	0.09960	0.40294	0.00466	2151.6	11.7	2165.5	15.7	2182.6	21.4	1.4		2151.6	11.7
GH03/2014_G066	70.6	20.1	1.6322	0.07970	0.00166	2.23557	0.04554	0.20371	0.00279	1189.6	14.6	1192.3	17.5	1195.2	14.9	0.5		1189.6	14.6
GH03/2014_G067	233.2	82.6	1.0209	0.13843	0.00178	5.61457	0.07342	0.29455	0.00334	2207.7	11.6	1918.3	14.8	1664.2	16.6	-24.6	Del.		
GH03/2014_G068	361.2	122.3	1.1256	0.13051	0.00164	5.19768	0.06657	0.28924	0.00324	2104.8	11.2	1852.2	14.3	1637.7	16.2	-22.2	Del.		
GH03/2014_G069	417.2	54.5	0.4974	0.06754	0.00096	1.13890	0.01621	0.12245	0.00139	854.5	8.2	772.0	9.8	744.6	8.0	-3.5		744.6	8.0
GH03/2014_G070	235.9	48.3	0.6267	0.10445	0.00145	2.64784	0.03683	0.18410	0.00212	1704.7	11.5	1314.0	13.3	1089.3	11.5	-17.1	Del.		
GH03/2014_G071	257.2	94.3	0.5533	0.11532	0.00148	5.28704	0.06924	0.33296	0.00376	1884.9	11.0	1866.8	14.6	1852.7	18.2	-1.7		1884.9	11.0
GH03/2014_G072	174.6	41.8	0.9939	0.07774	0.00116	2.10848	0.03156	0.19698	0.00231	1140.2	10.2	1151.6	13.1	1159.1	12.4	1.7		1140.2	10.2
GH03/2014_G073	76.0	10.7	0.8341	0.06424	0.00148	1.06191	0.02389	0.12004	0.00162	749.5	12.2	734.8	14.0	730.8	9.3	-0.5		730.8	9.3
GH03/2014_G074	401.2	103.1	0.7205	0.14638	0.00187	4.71689	0.06142	0.23402	0.00264	2304.1	11.6	1770.2	14.3	1355.5	13.8	-41.2	Del.		
GH03/2014_G075	140.6	51.4	0.8055	0.11244	0.00155	4.85281	0.06780	0.31345	0.00365	1839.2	11.7	1794.1	15.2	1757.7	17.9	-4.4		1839.2	11.7
GH03/2014_G076	172.6	90.8	3.1626	0.16671	0.00220	6.89667	0.09248	0.30044	0.00347	2524.9	12.3	2098.2	15.6	1693.5	17.2	-32.9	Del.		
GH03/2014_G077	217.9	75.5	0.3028	0.11145	0.00147	5.08921	0.06843	0.33163	0.00378	1823.2	11.2	1834.3	14.8	1846.3	18.3	1.3		1823.2	11.2
GH03/2014_G078	88.0	31.9	0.9228	0.11683	0.00175	4.75531	0.07180	0.29559	0.00361	1908.3	12.9	1777.0	16.2	1669.4	18.0	-12.5		1908.3	12.9
GH03/2014_G079	723.7	137.4	1.2709	0.12361	0.00158	2.77741	0.03617	0.16318	0.00182	2009.0	11.2	1349.5	12.7	974.4	10.1	-27.8	Del.		
GH03/2014_G080	213.9	74.5	1.0827	0.10491	0.00142	4.00905	0.05513	0.27753	0.00319	1712.7	11.2	1636.0	14.4	1578.9	16.1	-7.8		1712.7	11.2
GH03/2014_G081	60.6	22.5	1.3728	0.11755	0.00190	4.73233	0.07672	0.29237	0.00372	1919.3	13.9	1773.0	17.2	1653.4	18.6	-13.9		1919.3	13.9
GH03/2014_G082	108.6	42.0	0.8898	0.11454	0.00165	5.05449	0.07363	0.32047	0.00382	1872.7	12.3	1828.5	15.9	1792.0	18.6	-4.3		1872.7	12.3
GH03/2014_G083	243.2	77.0	0.6732	0.12785	0.00169	4.96256	0.06704	0.28189	0.00322	2068.6	11.7	1813.0	14.8	1600.9	16.2	-22.6	Del.		
GH03/2014_G084	347.9	105.8	2.2100	0.14162	0.00189	4.18908	0.05669	0.21482	0.00246	2247.1	12.1	1671.9	14.4	1254.4	13.1	-44.2	Del.		
GH03/2014_G085	725.7	136.2	0.1486	0.09669	0.00125	2.57057	0.03392	0.19306	0.00216	1561.2	10.3	1292.3	12.5	1137.9	11.7	-27.1	Del.		
GH03/2014_G086	270.6	102.6	1.5486	0.11919	0.00158	4.84354	0.06576	0.29512	0.00337	1944.1	11.5	1792.5	14.7	1667.1	16.8	-14.3		1944.1	11.5
GH03/2014_G087	343.2	111.7	0.3901	0.12624	0.00165	5.38030	0.07197	0.30950	0.00351	2046.3	11.5	1881.7	14.8	1738.2	17.3	-15.1	Del.		
GH03/2014_G088	186.6	26.6	0.7727	0.06407	0.00111	1.09711	0.01885	0.12435	0.00150	743.9	9.1	752.0	11.2	755.6	8.6	0.5		755.6	8.6
GH03/2014_G089	410.5	40.0	0.9198	0.07710	0.00123	0.87375	0.01390	0.08229	0.00098	1123.8	10.8	637.6	9.4	509.8	5.8	-20.0	Del.		
GH03/2014_G090	175.9	59.3	1.0638	0.09548	0.00136	3.56507	0.05177	0.27115	0.00317	1537.6	11.3	1541.8	14.6	1546.6	16.1	0.6		1537.6	11.3
GH03/2014_G091	787.7	200.3	0.5231	0.15006	0.00192	4.92245	0.06476	0.23821	0.00267	2346.6	11.7	1806.1	14.4	1377.4	13.9	-41.3	Del.		
GH03/2014_G092	137.3	50.6	2.9196	0.20338	0.00287	6.44714	0.09177	0.23020	0.00276	2853.5	13.5	2038.7	16.3	1335.5	14.5	-53.2	Del.		
GH03/2014_G093	128.6	40.5	2.1382	0.12142	0.00184	3.63980	0.05549	0.21769	0.00264	1977.2	13.2	1558.3	15.5	1269.7	14.0	-35.8	Del.		
GH03/2014_G094	186.6	74.4	1.2481	0.14097	0.00198	6.40647	0.09192	0.33001	0.00392	2239.2	12.7	2033.2	16.2	1838.4	19.0	-17.9	Del.		
GH03/2014_G095	201.9	94.3	0.7848	0.16490	0.00221	9.17617	0.12618	0.40408	0.00468	2506.5	12.5	2355.7	16.2	2187.8	21.5	-12.7		2506.5	12.5
GH03/2014_G096	181.9	64.3	1.0220	0.11456	0.00161	4.64724	0.06646	0.29458	0.00344	1873.0	12.0	1757.8	15.3	1664.4	17.1	-11.1		1873.0	12.0
GH03/2014_G097	102.6	48.2	0.8777	0.14637	0.00209	8.04519	0.11744	0.39913	0.00481	2303.9	13.0	2236.1	16.9	2165.0	22.2	-6.0		2303.9	13.0
GH03/2014_G098	489.1	129.3	3.3067	0.12293	0.00169	2.53489	0.03540	0.14973	0.00172	1999.2	12.0	1282.1	13.0	899.4	9.6	-29.8	Del.		
GH03/2014_G099	138.6	53.3	0.8264	0.11867	0.00170	5.36735	0.07840	0.32842	0.00389	1936.3	12.4	1879.7	15.9	1830.7	18.9	-5.5		1936.3	12.4
GH03/2014_G100	376.5	84.8	1.4883	0.19165	0.00259	4.93778	0.06804	0.18708	0.00216	2756.4	12.8	1808.7	15.0	1105.5	11.7	-59.9	Del.		
GH03/2014_G101	321.9	32.8	1.0676	0.06176	0.00106	0.70028	0.01197	0.08233	0.00099	665.8	8.4	539.0	8.8	510.0	5.9	-5.4		510.0	5.9
GH03/2014_G102	378.5	51.9	0.6979	0.06587	0.00109	1.10271	0.01825	0.12155	0.00145	802.2	9.2	754.7	10.9	739.5	8.3	-2.0		739.5	8.3
GH03/2014_G103	240.6	106.2	0.5900	0.14680	0.00199	7.98778	0.11176	0.39506	0.00457	2309.0	12.3	2229.6	16.1	2146.3	21.1	-7.0		2309.0	12.3
GH03/2014_G104	124.6	47.3	0.7723	0.11331	0.00168	5.11376	0.07731	0.32767	0.00394	1853.2	12.6	1838.4	16.2	1827.1	19.1	-1.4		1853.2	12.6
GH03/2014_G105	200.6	30.4	1.0131	0.06631	0.00123	1.12068	0.02061	0.12270	0.00153	816.2	10.4	763.3	12.0	746.1	8.8	-2.3		746.1	8.8
GH03/2014_G106	899.6	220.8	0.3787	0.14289	0.00190	4.77754	0.06561	0.24275	0.00275	2262.5	12.0	1781.0	14.7	1401.0	14.3	-38.1	Del.		
GH03/2014_G107	199.9	90.1	0.9098	0.14529	0.00202	7.52239	0.10772	0.37589	0.00440	2291.2	12.6	2175.7	16.3	2057.1	20.6	-10.2		2291.2	12.6
GH03/2014_G108	272.6	85.5	0.3538	0.12212	0.00171	5.10910	0.07349	0.30373	0.00354	1987.4	12.2	1837.6	15.5	1709.8	17.5	-14.0		1987.4	12.2
GH03/2014_G109	96.6	48.1	1.4144	0.20885	0.00300	11.77317	0.17379	0.40925	0.00499	2896.6	13.7	2586.5	17.6	2211.5	22.8	-23.7	Del.		

Analysis No.	U (ppm)	Pb (ppm)	Th/U	Measured isotopic ratios						Calculated isotopic ages (Ma)						Disc.† (%)	Comment§	Preferred age (Ma)#	
				$^{207}Pb/^{206}Pb$	1σ	$^{207}Pb/^{235}U$	1σ	$^{206}Pb/^{238}U$	1σ	$^{207}Pb/^{206}Pb$	1σ	$^{207}Pb/^{235}U$	1σ	$^{206}Pb/^{238}U$	1σ			Age	1σ
Sample GH03/2014, quartz sandstone (interbedded with dolostone), Middle Gouhou Formation, Gouhou section of Huaibei region, GPS: 33°59'32"N 117°17'46"E																			
GH03/2014_G110	299.9	105.7	0.6451	0.12116	0.00168	5.38665	0.07707	0.32277	0.00374	1973.4	12.1	1882.7	15.5	1803.2	18.2	-8.6		1973.4	12.1
GH03/2014_G111	377.2	144.7	0.9790	0.16084	0.00219	7.33381	0.10322	0.33102	0.00381	2464.5	12.6	2152.9	15.9	1843.3	18.5	-25.2	Del.		
GH03/2014_G112	256.6	88.7	0.2979	0.11429	0.00161	5.23938	0.07596	0.33279	0.00388	1868.7	12.0	1859.0	15.6	1851.9	18.8	-0.9		1868.7	12.0
GH03/2014_G113	147.3	21.6	0.7520	0.07932	0.00161	1.38042	0.02752	0.12634	0.00167	1180.1	14.2	880.6	14.3	767.0	9.6	-12.9		767.0	9.6
GH03/2014_G114	430.5	138.6	0.4846	0.11918	0.00165	4.98332	0.07116	0.30354	0.00350	1944.0	12.0	1816.5	15.2	1708.8	17.3	-12.1		1944.0	12.0
GH03/2014_G115	48.0	17.5	0.7318	0.13255	0.00252	5.78198	0.11022	0.31665	0.00451	2132.0	16.9	1943.7	20.6	1773.3	22.1	-16.8	Del.		
GH03/2014_G116	250.6	74.2	1.0550	0.12263	0.00178	4.29847	0.06398	0.25444	0.00300	1994.8	12.7	1693.1	15.4	1461.3	15.4	-26.7	Del.		
GH03/2014_G117	335.9	106.0	0.2084	0.11066	0.00157	4.76010	0.06947	0.31223	0.00363	1810.3	12.0	1777.9	15.4	1751.7	17.8	-3.2		1810.3	12.0
GH03/2014_G118	320.5	108.6	0.5956	0.12606	0.00180	5.49385	0.08066	0.31635	0.00369	2043.7	12.6	1899.6	15.8	1771.9	18.1	-13.3		2043.7	12.6
GH03/2014_G119	743.0	160.6	0.5172	0.16379	0.00228	4.82858	0.06930	0.21398	0.00247	2495.2	12.9	1789.9	15.2	1250.0	13.1	-49.9	Del.		
GH03/2014_G120	669.7	57.6	0.3634	0.05833	0.00092	0.67410	0.01080	0.08388	0.00099	542.2	6.6	523.2	8.1	519.2	5.9	-0.8		519.2	5.9
GH03/2014_G121	244.6	56.4	0.5271	0.10126	0.00154	2.94451	0.04560	0.21105	0.00252	1647.3	12.4	1393.4	14.7	1234.4	13.4	-25.1	Del.		
GH03/2014_G122	32.7	9.7	0.9318	0.10394	0.00232	3.54572	0.07830	0.24758	0.00371	1695.6	18.4	1537.5	21.3	1426.0	19.2	-15.9	Del.		
GH03/2014_G123	229.9	32.6	0.7279	0.06523	0.00115	1.12095	0.01981	0.12472	0.00153	781.8	9.6	763.4	11.5	757.7	8.8	-0.8		757.7	8.8
GH03/2014_G124	139.3	71.7	0.6266	0.16014	0.00233	9.80156	0.14782	0.44420	0.00533	2457.1	13.5	2416.3	17.4	2369.4	23.8	-3.6		2457.1	13.5
GH03/2014_G125	269.2	82.0	0.4803	0.12890	0.00191	5.11384	0.07786	0.28791	0.00343	2083.0	13.1	1838.4	16.1	1631.1	17.2	-21.7	Del.		
GH03/2014_G126	635.8	247.8	1.3470	0.12749	0.00181	5.52795	0.08142	0.31465	0.00366	2063.6	12.5	1905.0	15.8	1763.5	17.9	-14.5		2063.6	12.5
GH03/2014_G127	205.9	69.2	0.6420	0.12711	0.00195	5.39819	0.08518	0.30818	0.00376	2058.4	13.5	1884.6	16.8	1731.7	18.5	-15.9	Del.		
GH03/2014_G128	200.6	87.3	0.3227	0.16089	0.00243	9.29889	0.14530	0.41940	0.00515	2465.0	14.0	2367.9	17.8	2257.8	23.4	-8.4		2465.0	14.0
GH03/2014_G129	441.2	127.5	0.8183	0.12516	0.00185	4.56686	0.06949	0.26478	0.00314	2031.1	13.0	1743.2	15.8	1514.3	16.0	-25.4	Del.		
GH03/2014_G130	375.2	109.1	0.8017	0.12849	0.00194	4.59634	0.07127	0.25956	0.00311	2077.4	13.3	1748.6	16.1	1487.6	15.9	-28.4	Del.		
GH03/2014_G131	394.5	108.6	1.4276	0.12423	0.00188	3.80526	0.05902	0.22225	0.00266	2017.8	13.3	1593.9	15.5	1293.8	14.0	-35.9	Del.		
GH03/2014_G132	117.3	52.3	0.8582	0.12843	0.00199	6.55373	0.10482	0.37026	0.00455	2076.6	13.7	2053.1	17.4	2030.6	21.4	-2.2		2076.6	13.7
GH03/2014_G133	363.2	119.2	0.3183	0.12200	0.00179	5.33347	0.08111	0.31719	0.00374	1985.7	12.8	1874.2	16.1	1776.0	18.3	-10.6		1985.7	12.8
GH03/2014_G134	163.9	77.6	0.8425	0.16543	0.00248	9.25104	0.14371	0.40572	0.00492	2511.9	13.9	2363.2	17.7	2195.3	22.6	-12.6		2511.9	13.9
GH03/2014_G135	326.5	112.2	0.2087	0.11485	0.00170	5.31499	0.08172	0.33575	0.00398	1877.5	12.7	1871.3	16.2	1866.2	19.2	-0.6		1877.5	12.7
GH03/2014_G136	111.3	53.7	0.0038	0.16578	0.00252	10.90950	0.17196	0.47743	0.00585	2515.5	14.1	2515.4	18.2	2516.1	25.5	0.0		2515.5	14.1
GH03/2014_G137	128.6	50.3	0.8748	0.11665	0.00186	5.20765	0.08532	0.32386	0.00400	1905.5	13.7	1853.9	17.2	1808.6	19.5	-5.1		1905.5	13.7
GH03/2014_G138	115.3	25.9	0.9850	0.07595	0.00143	1.92086	0.03631	0.18347	0.00236	1093.8	12.6	1088.4	15.2	1085.9	12.9	-0.2		1085.9	12.9
GH03/2014_G139	168.6	83.0	0.2465	0.16227	0.00243	10.32342	0.16075	0.46151	0.00556	2479.5	13.9	2464.2	17.8	2446.2	24.5	-1.3		2479.5	13.9
GH03/2014_G140	247.9	78.3	0.1779	0.13052	0.00197	5.76909	0.09039	0.32062	0.00384	2105.0	13.4	1941.8	16.7	1792.8	18.7	-14.8		2105.0	13.4
GH03/2014_G141	379.2	147.6	0.9359	0.11661	0.00174	5.57783	0.08625	0.34696	0.00410	1904.9	12.8	1912.7	16.4	1920.1	19.6	0.8		1904.9	12.8
GH03/2014_G142	248.6	92.7	0.4744	0.11215	0.00171	5.23711	0.08294	0.33871	0.00406	1834.5	12.9	1858.7	16.5	1880.5	19.6	2.5		1834.5	12.9
GH03/2014_G143	225.9	68.4	1.4265	0.10592	0.00167	3.57655	0.05817	0.24491	0.00297	1730.3	13.1	1544.3	15.8	1412.2	15.4	-18.4	Del.		
GH03/2014_G144	106.0	44.3	0.7059	0.11717	0.00192	5.72573	0.09669	0.35443	0.00445	1913.5	14.1	1935.3	17.8	1955.7	21.2	2.2		1913.5	14.1
GH03/2014_G145	102.0	35.0	1.1791	0.12317	0.00210	4.62515	0.08055	0.27233	0.00349	2002.6	14.9	1753.8	17.8	1552.6	17.7	-22.5	Del.		
GH03/2014_G146	134.6	89.8	0.5724	0.20321	0.00309	15.60310	0.24751	0.55685	0.00679	2852.2	14.5	2852.8	18.6	2853.6	28.1	0.1		2852.2	14.5
GH03/2014_G147	344.5	98.1	1.4601	0.14528	0.00224	4.66000	0.07425	0.23262	0.00279	2291.1	14.0	1760.1	16.3	1348.2	14.6	-41.2	Del.		
GH03/2014_G148	216.6	133.9	0.7956	0.16690	0.00253	11.41769	0.18064	0.49610	0.00597	2526.8	14.1	2557.9	18.1	2597.0	25.7	2.8		2526.8	14.1
GH03/2014_G149	212.6	29.8	0.7524	0.06495	0.00124	1.09276	0.02097	0.12200	0.00154	772.7	10.3	749.8	12.1	742.1	8.8	-1.0		742.1	8.8

Analysis No.	U (ppm)	Pb (ppm)	Th/U	Measured isotopic ratios						Calculated isotopic ages (Ma)						Disc.† (%)	Comment§	Preferred age (Ma)#	
				$^{207}Pb/^{206}Pb$	1σ	$^{207}Pb/^{235}U$	1σ	$^{206}Pb/^{238}U$	1σ	$^{207}Pb/^{206}Pb$	1σ	$^{207}Pb/^{235}U$	1σ	$^{206}Pb/^{238}U$	1σ			Age	1σ
Sample GH02/2014, quartz sandstone, Lower Gouhou Formation, Jinshanzhai section of Huaibei region, GPS: 33°54'56"N 117°16'57"E																			
GH02/2014_G001	147.6	35.3	0.4832	0.13513	0.00175	3.92594	0.05355	0.21077	0.00255	2165.7	11.6	1619.0	14.3	1232.9	13.6	-43.1	Del.		
GH02/2014_G002	201.0	62.4	0.5998	0.09659	0.00121	3.66072	0.04891	0.27493	0.00326	1559.3	10.0	1562.8	13.8	1565.8	16.5	0.4		1559.3	10.0

Analysis No.	U (ppm)	Pb (ppm)	Th/U	Measured isotopic ratios						Calculated isotopic ages (Ma)						Disc.† (%)	Comment§	Preferred age (Ma)#	
				$^{207}Pb/^{206}Pb$	1σ	$^{206}Pb/^{238}U$	1σ	$^{208}Pb/^{232}Th$	1σ	$^{208}Pb/^{206}Pb$	1σ	$^{207}Pb/^{235}U$	1σ	$^{206}Pb/^{238}U$	1σ			Age	1σ
Sample GH02/2014, quartz sandstone, Lower Gouhou Formation, Jinshanzhai section of Huaibei region, GPS: 33°54'56"N 117°16'57"E																			
GH02/2014_G003	126.7	46.4	0.5681	0.11870	0.00155	5.28538	0.07306	0.32304	0.00394	1936.7	11.3	1866.5	15.3	1804.6	19.2	-6.8		1936.7	11.3
GH02/2014_G004	102.9	44.0	1.2298	0.11605	0.00151	5.14862	0.07106	0.32186	0.00391	1896.2	11.2	1844.2	15.1	1798.8	19.1	-5.1		1896.2	11.2
GH02/2014_G005	610.3	98.8	0.2977	0.10461	0.00126	2.23251	0.02879	0.15482	0.00181	1707.5	10.0	1191.3	11.8	927.9	10.1	-22.1	Del.		
GH02/2014_G006	179.2	64.8	0.9141	0.10811	0.00134	4.33348	0.05758	0.29080	0.00346	1767.8	10.4	1699.8	14.2	1645.5	17.3	-6.9		1767.8	10.4
GH02/2014_G007	280.1	126.9	0.7216	0.14587	0.00175	7.59446	0.09831	0.37770	0.00448	2298.1	10.9	2184.2	15.1	2065.5	21.0	-10.1		2298.1	10.9
GH02/2014_G008	490.4	48.5	0.9224	0.06342	0.00092	0.71321	0.01075	0.08158	0.00098	722.3	7.5	546.7	8.0	505.5	5.8	-7.5		505.5	5.8
GH02/2014_G009	165.6	91.3	0.9556	0.16084	0.00192	9.65956	0.12474	0.43569	0.00518	2464.5	11.1	2402.9	15.5	2331.3	23.3	-5.4		2464.5	11.1
GH02/2014_G010	404.4	99.3	0.5232	0.08989	0.00112	2.76721	0.03668	0.22334	0.00263	1423.2	9.5	1346.7	12.8	1299.5	13.9	-8.7		1423.2	9.5
GH02/2014_G011	247.1	81.1	0.5129	0.13471	0.00162	5.48598	0.07082	0.29544	0.00348	2160.3	10.8	1898.4	14.5	1668.7	17.3	-22.8	Del.		
GH02/2014_G012	53.9	12.5	0.5640	0.14506	0.00234	3.96659	0.06463	0.19837	0.00267	2288.5	14.7	1627.4	17.0	1166.6	14.4	-49.0	Del.		
GH02/2014_G013	171.9	69.4	0.4940	0.17585	0.00211	8.37417	0.10811	0.34548	0.00410	2614.1	11.3	2272.4	15.3	1913.0	19.6	-26.8	Del.		
GH02/2014_G014	191.8	92.5	0.7318	0.14293	0.00170	8.00082	0.10292	0.40611	0.00479	2263.0	10.8	2231.1	15.1	2197.1	22.0	-2.9		2263.0	10.8
GH02/2014_G015	226.3	82.1	0.3363	0.11377	0.00137	5.32854	0.06918	0.33978	0.00400	1860.5	10.3	1873.5	14.4	1885.6	19.2	1.4		1860.5	10.3
GH02/2014_G016	80.6	14.1	0.6068	0.07469	0.00129	1.60414	0.02799	0.15581	0.00201	1060.2	11.4	971.8	13.5	933.4	11.2	-3.9		933.4	11.2
GH02/2014_G017	142.7	53.1	0.2533	0.11890	0.00147	5.81926	0.07718	0.35507	0.00423	1939.8	10.7	1949.3	14.9	1958.8	20.1	1.0		1939.8	10.7
GH02/2014_G018	78.2	29.4	1.1752	0.09976	0.00141	3.94985	0.05836	0.28724	0.00357	1619.6	11.4	1624.0	15.3	1627.7	17.9	0.5		1619.6	11.4
GH02/2014_G019	106.8	19.4	0.8963	0.07129	0.00115	1.48258	0.02437	0.15088	0.00189	965.7	10.1	923.3	12.4	905.9	10.6	-1.9		905.9	10.6
GH02/2014_G020	84.5	44.5	0.2101	0.16407	0.00203	11.02228	0.14726	0.48739	0.00592	2498.0	11.5	2525.0	16.1	2559.4	25.7	2.5		2498.0	11.5
GH02/2014_G021	146.6	98.7	0.6512	0.20041	0.00235	15.23060	0.19453	0.55135	0.00652	2829.5	11.2	2829.8	15.9	2830.8	27.1	0.0		2829.5	11.2
GH02/2014_G022	95.2	21.9	0.4428	0.08287	0.00122	2.45200	0.03747	0.21467	0.00266	1266.2	10.7	1258.0	13.9	1253.6	14.1	-1.0		1266.2	10.7
GH02/2014_G023	102.0	20.7	0.6103	0.08623	0.00130	2.14570	0.03324	0.18053	0.00225	1343.3	11.2	1163.7	13.5	1069.9	12.3	-8.1		1069.9	12.3
GH02/2014_G024	568.1	126.8	0.2313	0.12109	0.00143	3.69736	0.04708	0.22152	0.00258	1972.3	10.3	1570.8	13.3	1289.9	13.6	-34.6	Del.		
GH02/2014_G025	227.2	155.4	0.5961	0.26012	0.00302	21.27783	0.26955	0.59346	0.00699	3247.4	11.3	3151.3	16.0	3003.4	28.3	-7.5		3247.4	11.3
GH02/2014_G026	412.7	156.4	0.2838	0.11857	0.00138	5.85989	0.07424	0.35854	0.00417	1934.8	10.1	1955.3	14.3	1975.2	19.8	2.1		1934.8	10.1
GH02/2014_G027	211.2	48.7	1.0546	0.08107	0.00108	2.02828	0.02843	0.18150	0.00217	1223.1	9.5	1125.0	12.2	1075.2	11.8	-4.4		1075.2	11.8
GH02/2014_G028	165.6	89.5	0.4218	0.16420	0.00195	10.76308	0.13844	0.47556	0.00562	2499.4	11.0	2502.9	15.6	2507.9	24.6	0.3		2499.4	11.0
GH02/2014_G029	82.5	48.8	0.8330	0.16764	0.00209	10.94628	0.14677	0.47372	0.00576	2534.2	11.6	2518.6	16.2	2499.9	25.2	-1.4		2534.2	11.6
GH02/2014_G030	333.6	111.2	0.9871	0.14203	0.00170	5.27277	0.06787	0.26934	0.00316	2252.1	10.8	1864.5	14.3	1537.5	16.0	-31.7	Del.		
GH02/2014_G031	313.6	106.5	0.4108	0.13154	0.00161	5.69888	0.07498	0.31433	0.00373	2118.6	10.9	1931.2	14.7	1762.0	18.3	-16.8	Del.		
GH02/2014_G032	124.3	22.8	0.8566	0.06916	0.00107	1.46639	0.02337	0.15383	0.00190	903.5	9.3	916.6	12.0	922.4	10.6	0.6		922.4	10.6
GH02/2014_G033	127.2	39.1	0.9012	0.13856	0.00181	4.75225	0.06549	0.24883	0.00303	2209.3	11.8	1776.5	15.0	1432.4	15.6	-35.2	Del.		
GH02/2014_G034	130.1	74.9	0.5077	0.16518	0.00200	11.21167	0.14675	0.49243	0.00588	2509.4	11.3	2540.9	15.9	2581.2	25.4	2.9		2509.4	11.3
GH02/2014_G035	78.7	29.6	0.4326	0.12982	0.00173	6.19251	0.08755	0.34607	0.00427	2095.5	11.8	2003.4	15.9	1915.8	20.4	-8.6		2095.5	11.8
GH02/2014_G036	102.4	45.8	1.0683	0.11619	0.00151	5.58319	0.07743	0.34863	0.00424	1898.4	11.2	1913.5	15.3	1928.1	20.3	1.6		1898.4	11.2
GH02/2014_G037	117.5	30.6	0.4582	0.08434	0.00119	2.79943	0.04130	0.24082	0.00295	1300.4	10.3	1355.4	14.0	1391.0	15.3	7.0	Del.		
GH02/2014_G038	402.0	108.3	1.0325	0.13300	0.00161	3.99383	0.05192	0.21786	0.00256	2137.9	10.8	1632.9	13.7	1270.6	13.6	-40.6	Del.		
GH02/2014_G039	130.1	77.1	0.5560	0.16490	0.00201	11.32598	0.14905	0.49832	0.00596	2506.5	11.3	2550.3	15.9	2606.6	25.6	4.0		2506.5	11.3
GH02/2014_G040	113.1	24.2	1.2752	0.10008	0.00152	2.21567	0.03458	0.16063	0.00202	1625.6	12.3	1186.0	13.8	960.3	11.2	-19.0	Del.		
GH02/2014_G041	187.9	56.0	0.4875	0.14434	0.00180	5.41211	0.07207	0.27203	0.00325	2279.9	11.3	1886.8	14.8	1551.1	16.5	-32.0	Del.		
GH02/2014_G042	59.2	34.3	0.8859	0.16204	0.00213	10.31119	0.14484	0.46167	0.00576	2477.1	12.2	2463.1	16.8	2446.9	25.4	-1.2		2477.1	12.2
GH02/2014_G043	195.2	87.7	0.5521	0.12657	0.00155	6.85346	0.09025	0.39285	0.00465	2050.9	10.8	2092.7	15.1	2136.0	21.5	4.2		2050.9	10.8
GH02/2014_G044	88.9	44.3	0.8336	0.13489	0.00175	7.55878	0.10458	0.40655	0.00497	2162.6	11.6	2180.0	16.0	2199.1	22.8	1.7		2162.6	11.6
GH02/2014_G045	298.6	98.7	0.8453	0.11510	0.00141	4.34089	0.05725	0.27361	0.00323	1881.5	10.5	1701.2	14.0	1559.1	16.3	-17.1	Del.		
GH02/2014_G046	349.6	70.7	0.7315	0.08878	0.00113	2.16024	0.02936	0.17654	0.00209	1399.4	9.7	1168.3	12.1	1048.0	11.5	-10.3		1048.0	11.5
GH02/2014_G047	130.6	75.4	0.8350	0.29160	0.00352	18.56133	0.24242	0.46181	0.00553	3426.2	11.8	3019.3	16.4	2447.5	24.4	-28.6	Del.		
GH02/2014_G048	169.4	35.0	0.5252	0.08626	0.00120	2.22787	0.03247	0.18738	0.00228	1344.0	10.4	1189.8	13.0	1107.2	12.4	-17.6	Del.		
GH02/2014_G049	157.8	89.0	0.8327	0.15532	0.00190	9.73215	0.12860	0.45459	0.00541	2405.3	11.3	2409.8	15.7	2415.6	24.0	0.4		2405.3	11.3

Analysis No.	U (ppm)	Pb (ppm)	Th/U	Measured isotopic ratios						Calculated isotopic ages (Ma)						Disc.† (%)	Comment§	Preferred age (Ma)#	
				$^{207}Pb/^{206}Pb$	1σ	$^{206}Pb/^{238}U$	1σ	$^{208}Pb/^{232}Th$	1σ	$^{207}Pb/^{206}Pb$	1σ	$^{206}Pb/^{238}U$	1σ	$^{208}Pb/^{232}Th$	1σ			Age	1σ
Sample GH02/2014, quartz sandstone, Lower Gouhou Formation, Jinshanzhai section of Huaibei region, GPS: 33°54'56"N 117°16'57"E																			
GH02/2014_G050	65.1	30.5	0.8093	0.12957	0.00177	6.88885	0.09979	0.38573	0.00482	2092.1	12.1	2097.2	16.4	2103.0	22.4	0.5		2092.1	12.1
GH02/2014_G051	134.5	26.7	0.9520	0.16064	0.00223	3.45206	0.04974	0.15591	0.00194	2462.4	12.8	1516.3	14.7	934.0	10.8	-38.4	Del.		
GH02/2014_G052	198.1	55.1	0.0203	0.09945	0.00128	3.97223	0.05455	0.28978	0.00347	1613.8	10.4	1628.5	14.3	1640.4	17.3	1.6		1613.8	10.4
GH02/2014_G053	472.4	89.2	0.4224	0.33300	0.00401	7.66780	0.09922	0.16706	0.00197	3630.9	11.9	2192.8	15.1	995.9	10.9	-54.6	Del.		
GH02/2014_G054	303.9	106.3	0.8393	0.14816	0.00185	5.86059	0.07845	0.28699	0.00342	2324.8	11.4	1955.4	15.0	1626.5	17.1	-30.0	Del.		
GH02/2014_G055	161.2	61.7	0.7307	0.12156	0.00158	5.48304	0.07597	0.32724	0.00396	1979.2	11.3	1897.9	15.3	1825.0	19.2	-7.8		1979.2	11.3
GH02/2014_G056	74.3	25.9	1.0253	0.10046	0.00157	3.83269	0.06206	0.27680	0.00358	1632.6	12.7	1599.6	16.3	1575.2	18.1	-3.5		1632.6	12.7
GH02/2014_G057	203.4	113.1	0.8674	0.18570	0.00229	11.52376	0.15335	0.45023	0.00538	2704.4	11.6	2566.5	16.0	2396.3	23.9	-11.4		2704.4	11.6
GH02/2014_G058	119.4	18.6	0.8212	0.09631	0.00168	1.71619	0.03012	0.12928	0.00170	1553.8	13.9	1014.6	14.0	783.8	9.7	-22.8	Del.		
GH02/2014_G059	91.8	62.2	1.3821	0.16533	0.00217	11.01992	0.15479	0.48358	0.00599	2510.9	12.2	2524.8	16.8	2542.8	26.0	1.3		2510.9	12.2
GH02/2014_G060	58.3	28.8	1.7286	0.11781	0.00180	5.44985	0.08683	0.33562	0.00438	1923.3	13.2	1892.7	17.2	1865.6	21.1	-3.0		1923.3	13.2
GH02/2014_G061	129.6	46.4	1.0945	0.09788	0.00138	3.79830	0.05615	0.28155	0.00347	1584.1	11.3	1592.4	15.1	1599.2	17.5	0.9		1584.1	11.3
GH02/2014_G062	275.3	92.7	0.9023	0.16614	0.00210	6.15890	0.08300	0.26895	0.00322	2519.1	11.8	1998.6	15.2	1535.5	16.4	-39.0	Del.		
GH02/2014_G063	188.9	112.8	0.6963	0.16784	0.00209	11.38189	0.15291	0.49200	0.00589	2536.2	11.6	2554.9	16.1	2579.3	25.4	1.7		2536.2	11.6
GH02/2014_G064	86.9	19.3	0.3598	0.14751	0.00222	4.01517	0.06200	0.19748	0.00255	2317.3	13.7	1637.3	16.1	1161.8	13.7	-49.9	Del.		
GH02/2014_G065	93.7	20.0	0.6180	0.07711	0.00126	2.01149	0.03378	0.18926	0.00241	1124.0	11.1	1119.4	14.1	1117.4	13.1	-0.6		1124.0	11.1
GH02/2014_G066	137.9	41.4	0.7301	0.08880	0.00125	3.15369	0.04656	0.25768	0.00315	1399.8	10.7	1445.9	14.4	1478.0	16.1	5.6	Del.		
GH02/2014_G067	84.0	36.1	1.0398	0.19392	0.00264	8.79831	0.12621	0.32918	0.00413	2775.7	12.9	2317.3	16.9	1834.4	20.0	-33.9	Del.		
GH02/2014_G068	30.1	17.7	0.6797	0.16885	0.00254	11.35068	0.18074	0.48773	0.00663	2546.3	14.0	2552.4	18.9	2560.8	28.7	0.6		2546.3	14.0
GH02/2014_G069	210.2	46.9	0.9391	0.20141	0.00269	4.91281	0.06873	0.17698	0.00217	2837.7	12.7	1804.5	15.3	1050.5	11.9	-41.8	Del.		
GH02/2014_G070	249.1	97.8	0.3834	0.12127	0.00153	6.03291	0.08181	0.36094	0.00429	1975.0	11.0	1980.6	15.1	1986.6	20.3	0.6		1975.0	11.0
GH02/2014_G071	32.0	21.1	1.2485	0.16718	0.00247	11.12455	0.17369	0.48280	0.00644	2529.6	13.8	2533.6	18.5	2539.5	28.0	0.4		2529.6	13.8
GH02/2014_G072	246.2	34.9	0.6796	0.06614	0.00103	1.13841	0.01821	0.12488	0.00154	810.8	8.7	771.8	10.7	758.6	8.8	-1.7		758.6	8.8
GH02/2014_G073	190.3	77.4	0.5502	0.18488	0.00236	8.73428	0.11911	0.34275	0.00412	2697.1	12.1	2310.7	16.0	1899.9	19.8	-29.6	Del.		
GH02/2014_G074	579.2	87.3	0.6162	0.08644	0.00117	1.58071	0.02259	0.13268	0.00159	1348.0	10.1	962.6	11.2	803.1	9.0	-16.6	Del.		
GH02/2014_G075	36.9	15.8	0.9250	0.10908	0.00182	5.18987	0.08921	0.34519	0.00466	1784.1	14.0	1851.0	18.3	1911.6	22.3	7.1	Del.		
GH02/2014_G076	137.9	34.8	0.2439	0.10189	0.00143	3.45326	0.05081	0.24591	0.00301	1658.8	11.5	1516.6	14.7	1417.3	15.6	-14.6		1658.8	11.5
GH02/2014_G077	56.3	33.4	0.8686	0.16478	0.00226	10.70630	0.15638	0.47140	0.00594	2505.3	12.7	2498.0	17.3	2489.7	26.0	-0.6		2505.3	12.7
GH02/2014_G078	125.8	42.9	0.7035	0.09840	0.00136	3.95816	0.05787	0.29184	0.00357	1594.0	11.1	1625.7	15.0	1650.7	17.8	3.6		1594.0	11.1
GH02/2014_G079	152.9	69.4	1.0597	0.11520	0.00152	5.60834	0.07901	0.35322	0.00426	1883.0	11.3	1917.4	15.4	1950.0	20.3	3.6		1883.0	11.3
GH02/2014_G080	123.3	72.1	0.7794	0.16347	0.00212	10.68326	0.14842	0.47416	0.00574	2491.9	12.0	2496.0	16.5	2501.8	25.1	0.4		2491.9	12.0
GH02/2014_G081	147.1	53.6	1.2132	0.09576	0.00133	3.65638	0.05349	0.27704	0.00338	1543.1	11.0	1561.9	14.7	1576.4	17.1	2.2		1543.1	11.0
GH02/2014_G082	189.4	71.3	0.2458	0.11760	0.00154	5.83424	0.08144	0.35994	0.00432	1920.1	11.3	1951.5	15.4	1981.9	20.5	3.2		1920.1	11.3
GH02/2014_G083	67.5	12.4	0.7624	0.06793	0.00133	1.48139	0.02911	0.15822	0.00211	866.4	11.4	922.8	14.4	946.9	11.7	2.6		946.9	11.7
GH02/2014_G084	114.1	31.3	0.6453	0.09124	0.00135	3.01457	0.04648	0.23972	0.00298	1451.6	11.4	1411.3	14.7	1385.2	15.5	-4.6		1451.6	11.4
GH02/2014_G085	82.1	15.0	0.7043	0.06849	0.00125	1.50577	0.02788	0.15951	0.00208	883.4	10.8	932.7	13.7	954.1	11.6	2.3		954.1	11.6
GH02/2014_G086	100.0	40.2	1.5338	0.10201	0.00149	4.01619	0.06139	0.28564	0.00356	1661.0	11.9	1637.5	15.6	1619.7	17.9	-2.5		1661.0	11.9
GH02/2014_G087	137.9	58.3	0.8405	0.11269	0.00153	5.39866	0.07775	0.34757	0.00423	1843.2	11.5	1884.6	15.6	1923.0	20.2	4.3		1843.2	11.5
GH02/2014_G088	119.0	39.3	0.9307	0.09464	0.00138	3.52357	0.05371	0.27013	0.00335	1520.9	11.5	1532.5	15.1	1541.5	17.0	1.4		1520.9	11.5
GH02/2014_G089	125.8	51.0	0.7837	0.11389	0.00157	5.33494	0.07782	0.33985	0.00416	1862.4	11.8	1874.5	15.8	1885.9	20.0	1.3		1862.4	11.8
GH02/2014_G090	142.3	31.7	0.7986	0.07910	0.00120	2.06688	0.03246	0.18958	0.00235	1174.6	10.6	1137.9	13.4	1119.1	12.7	-4.7		1174.6	10.6
GH02/2014_G091	279.7	113.3	0.4422	0.13307	0.00173	6.71101	0.09299	0.36591	0.00436	2138.9	11.6	2074.1	15.6	2010.1	20.6	-6.0		2138.9	11.6
GH02/2014_G092	281.1	89.6	0.5516	0.12646	0.00166	5.04027	0.07038	0.28918	0.00345	2049.3	11.6	1826.1	15.0	1637.4	17.3	-20.1	Del.		
GH02/2014_G093	136.4	29.6	0.3160	0.07964	0.00119	2.30076	0.03575	0.20960	0.00259	1188.1	10.5	1212.5	13.7	1226.7	13.8	3.2		1188.1	10.5
GH02/2014_G094	97.6	24.5	1.0185	0.08412	0.00133	2.33240	0.03794	0.20116	0.00253	1295.3	11.6	1222.2	14.4	1181.5	13.6	-8.8		1295.3	11.6
GH02/2014_G095	193.2	24.5	0.6814	0.34972	0.00482	5.32576	0.07597	0.11049	0.00138	3705.8	13.6	1873.0	15.9	675.6	8.0	-63.9	Del.		
GH02/2014_G096	108.8	47.3	1.0542	0.11376	0.00160	5.33330	0.07898	0.34015	0.00419	1860.3	12.0	1874.2	16.0	1887.4	20.2	1.5		1860.3	12.0

Analysis No.	U (ppm)	Pb (ppm)	Th/U	Measured isotopic ratios						Calculated isotopic ages (Ma)						Disc.† (%)	Comment§	Preferred age (Ma)#	
				$^{207}Pb/^{206}Pb$	1σ	$^{207}Pb/^{235}U$	1σ	$^{206}Pb/^{238}U$	1σ	$^{206}Pb/^{204}Pb$	1σ	$^{207}Pb/^{235}U$	1σ	$^{206}Pb/^{238}U$	1σ			Age	1σ
Sample GH02/2014, quartz sandstone, Lower Gouhou Formation, Jinshanzhai section of Huaibei region, GPS: 33°54'56"N 117°16'57"E																			
GH02/2014_G097	145.2	60.0	0.9389	0.11338	0.00156	5.19106	0.07544	0.33219	0.00404	1854.3	11.7	1851.2	15.6	1849.0	19.5	-0.3		1854.3	11.7
GH02/2014_G098	55.3	22.3	0.9268	0.13810	0.00216	6.13446	0.09944	0.32229	0.00424	2203.5	14.1	1995.2	17.8	1800.9	20.7	-18.3	Del.		
GH02/2014_G099	67.5	18.1	1.2120	0.13115	0.00222	3.66066	0.06283	0.20252	0.00272	2113.4	15.0	1562.8	17.2	1188.8	14.6	-43.7	Del.		
GH02/2014_G100	169.4	34.2	0.9431	0.08816	0.00139	1.99437	0.03242	0.16414	0.00206	1386.0	11.9	1113.6	13.6	979.7	11.4	-12.0		979.7	11.4
GH02/2014_G101	93.2	16.4	0.6100	0.08547	0.00151	1.82399	0.03262	0.15484	0.00203	1326.2	13.1	1054.1	14.4	928.0	11.3	-12.0		928.0	11.3
GH02/2014_G102	150.5	53.7	0.8170	0.21874	0.00298	8.57952	0.12343	0.28458	0.00349	2971.4	13.1	2294.4	16.7	1614.4	17.5	-45.7	Del.		
GH02/2014_G103	198.6	60.6	0.6300	0.09909	0.00138	3.64788	0.05370	0.26710	0.00324	1607.1	11.2	1560.0	14.7	1526.1	16.5	-5.0		1607.1	11.2
GH02/2014_G104	78.7	13.6	0.4725	0.11185	0.00188	2.38579	0.04069	0.15476	0.00202	1829.7	14.3	1238.3	15.2	927.6	11.3	-25.1	Del.		
GH02/2014_G105	120.4	65.2	0.4317	0.16828	0.00228	11.09872	0.16021	0.47852	0.00584	2540.6	12.6	2531.5	17.0	2520.8	25.5	-0.8		2540.6	12.6
GH02/2014_G106	93.7	35.3	0.6982	0.11201	0.00164	4.98318	0.07657	0.32277	0.00403	1832.3	12.4	1816.5	16.3	1803.2	19.6	-1.6		1832.3	12.4
GH02/2014_G107	26.2	15.0	0.6184	0.17781	0.00280	11.73599	0.19387	0.47888	0.00655	2632.5	14.8	2583.6	19.5	2522.4	28.6	-4.2		2632.5	14.8
GH02/2014_G108	171.4	35.6	0.5584	0.07733	0.00117	2.00597	0.03147	0.18820	0.00232	1129.7	10.3	1117.5	13.2	1111.6	12.6	-1.6		1129.7	10.3
GH02/2014_G109	203.9	49.5	0.6715	0.11714	0.00167	3.35374	0.05004	0.20771	0.00254	1913.0	12.3	1493.7	14.7	1216.6	13.6	-36.4	Del.		
GH02/2014_G110	79.6	15.0	0.8419	0.07008	0.00130	1.53991	0.02882	0.15942	0.00209	930.7	11.3	946.5	14.0	953.6	11.6	0.7		953.6	11.6
GH02/2014_G111	254.9	60.7	0.2785	0.11730	0.00163	3.61232	0.05300	0.22342	0.00270	1915.5	12.0	1552.2	14.6	1299.9	14.2	-32.1	Del.		
GH02/2014_G112	170.4	109.6	1.0385	0.16695	0.00226	11.24455	0.16216	0.48866	0.00591	2527.3	12.6	2543.6	16.9	2564.9	25.6	1.5		2527.3	12.6
GH02/2014_G113	384.0	94.7	1.2917	0.07586	0.00107	1.93463	0.02868	0.18503	0.00223	1091.4	9.4	1093.1	12.4	1094.4	12.1	0.1		1094.4	12.1
GH02/2014_G114	123.8	49.9	0.7930	0.11326	0.00162	5.24544	0.07903	0.33602	0.00413	1852.4	12.2	1860.0	16.1	1867.5	19.9	0.8		1852.4	12.2
GH02/2014_G115	244.7	77.6	0.7740	0.14150	0.00196	5.07065	0.07410	0.25998	0.00315	2245.6	12.5	1831.2	15.6	1489.7	16.1	-33.7	Del.		
GH02/2014_G116	135.5	48.6	0.6663	0.10601	0.00153	4.55976	0.06923	0.31208	0.00384	1731.9	12.0	1741.9	15.8	1750.9	18.9	1.1		1731.9	12.0
GH02/2014_G117	79.6	32.1	0.8050	0.11355	0.00172	5.26389	0.08313	0.33635	0.00425	1857.0	12.9	1863.0	16.8	1869.1	20.5	0.7		1857.0	12.9
GH02/2014_G118	236.5	22.2	0.7236	0.06170	0.00109	0.69672	0.01246	0.08192	0.00104	663.7	8.6	536.8	9.1	507.6	6.2	-5.4		507.6	6.2
GH02/2014_G119	341.3	133.4	0.4600	0.14490	0.00198	7.01940	0.10164	0.35146	0.00422	2286.6	12.4	2113.9	16.2	1941.6	20.1	-15.1	Del.		
GH02/2014_G120	111.2	24.7	0.6009	0.08187	0.00133	2.26840	0.03796	0.20102	0.00254	1242.4	11.6	1202.5	14.5	1180.8	13.6	-5.0		1242.4	11.6
GH02/2014_G121	148.1	43.4	0.7637	0.09360	0.00140	3.21920	0.05013	0.24954	0.00308	1500.1	11.7	1461.8	15.0	1436.1	15.9	-4.3		1500.1	11.7
GH02/2014_G122	109.7	47.8	0.9551	0.15482	0.00224	7.59289	0.11527	0.35581	0.00442	2399.9	13.3	2184.0	17.1	1962.3	21.0	-18.2	Del.		
GH02/2014_G123	201.0	67.2	1.2606	0.10135	0.00147	3.49641	0.05322	0.25029	0.00306	1649.0	11.8	1526.4	15.0	1440.0	15.8	-12.7		1649.0	11.8
GH02/2014_G124	68.0	33.2	1.6015	0.11371	0.00177	5.31752	0.08626	0.33928	0.00434	1859.5	13.3	1871.7	17.2	1883.2	20.9	1.3		1859.5	13.3
GH02/2014_G125	59.2	37.9	1.1890	0.16641	0.00246	10.95290	0.17072	0.47752	0.00608	2521.9	13.8	2519.1	18.2	2516.5	26.5	-0.2		2521.9	13.8
GH02/2014_G126	27.7	18.4	0.5668	0.20298	0.00319	15.53866	0.25772	0.55540	0.00760	2850.3	15.0	2848.9	19.9	2847.6	31.5	-0.1		2850.3	15.0
GH02/2014_G127	350.1	35.6	0.9764	0.06313	0.00103	0.72192	0.01213	0.08296	0.00103	712.6	8.4	551.8	8.7	513.8	6.1	-6.9		513.8	6.1
GH02/2014_G128	83.5	32.3	0.7384	0.11983	0.00184	5.41634	0.08655	0.32792	0.00415	1953.7	13.3	1887.4	17.1	1828.3	20.1	-6.4		1953.7	13.3
GH02/2014_G129	59.2	8.0	2.1929	0.08641	0.00211	1.00254	0.02383	0.08418	0.00125	1347.4	18.2	705.1	14.5	521.0	7.4	-26.1	Del.		
GH02/2014_G130	273.8	48.1	0.4797	0.10136	0.00151	2.22077	0.03455	0.15895	0.00195	1649.2	12.1	1187.6	13.5	950.9	10.8	-19.9	Del.		
GH02/2014_G131	174.3	105.6	0.6850	0.16682	0.00236	11.42932	0.17070	0.49707	0.00606	2526.0	13.2	2558.8	17.4	2601.2	26.1	3.0		2526.0	13.2
GH02/2014_G132	362.7	127.9	0.2105	0.11622	0.00164	5.49781	0.08189	0.34321	0.00414	1898.9	12.1	1900.3	15.9	1902.1	19.9	0.2		1898.9	12.1
GH02/2014_G133	693.3	240.0	1.1937	0.12969	0.00182	4.76652	0.07046	0.26666	0.00320	2093.8	12.4	1779.0	15.5	1523.8	16.3	-27.2	Del.		
GH02/2014_G134	72.8	17.5	0.3827	0.08356	0.00145	2.62801	0.04677	0.22818	0.00297	1282.3	12.6	1308.5	16.0	1325.0	15.6	3.3		1282.3	12.6
GH02/2014_G135	167.0	27.2	1.2357	0.06480	0.00112	1.11756	0.01980	0.12512	0.00158	767.8	9.3	761.8	11.5	760.0	9.1	-0.2		760.0	9.1
GH02/2014_G136	69.4	13.5	0.8928	0.07020	0.00139	1.56572	0.03127	0.16182	0.00217	934.2	12.1	956.7	14.8	966.9	12.0	1.1		966.9	12.0
GH02/2014_G137	134.5	71.2	0.2745	0.16413	0.00237	10.94774	0.16699	0.48391	0.00597	2498.7	13.4	2518.7	17.7	2544.3	25.9	1.8		2498.7	13.4
GH02/2014_G138	220.9	52.7	0.7227	0.09273	0.00141	2.60110	0.04114	0.20350	0.00251	1482.4	11.9	1300.9	14.4	1194.1	13.4	-19.4	Del.		
GH02/2014_G139	134.5	55.6	1.1962	0.13645	0.00210	5.97899	0.09567	0.31790	0.00402	2182.6	13.8	1972.8	17.3	1779.5	19.7	-18.5	Del.		
GH02/2014_G140	57.8	13.4	0.9412	0.29938	0.00511	7.84485	0.13377	0.19011	0.00268	3467.0	16.8	2213.4	19.9	1122.0	14.5	-67.6	Del.		
GH02/2014_G141	134.5	31.0	0.8934	0.11169	0.00199	2.69989	0.04917	0.17537	0.00222	1827.1	15.1	1328.4	16.2	1041.6	12.2	-21.6	Del.		
GH02/2014_G142	192.8	53.0	1.0360	0.16161	0.00250	4.72672	0.07565	0.21219	0.00268	2472.6	14.3	1772.0	16.7	1240.5	14.3	-49.8	Del.		
GH02/2014_G143	164.6	67.8	0.5246	0.12759	0.00190	6.41508	0.09996	0.36478	0.00451	2065.0	13.1	2034.3	17.0	2004.8	21.3	-2.9		2065.0	13.1

Analysis No.	U (ppm)	Pb (ppm)	Th/U	Measured isotopic ratios						Calculated isotopic ages (Ma)						Disc.† (%)	Comment§	Preferred age (Ma)#	
				$^{207}Pb/^{206}Pb$	1σ	$^{206}Pb/^{238}U$	1σ	$^{208}Pb/^{232}Th$	1σ	$^{207}Pb/^{206}Pb$	1σ	$^{207}Pb/^{235}U$	1σ	$^{206}Pb/^{238}U$	1σ			Age	1σ
Sample GH02/2014, quartz sandstone, Lower Gouhou Formation, Jinshanzhai section of Huaibei region, GPS: 33°54'56"N 117°16'57"E																			
GH02/2014_G144	283.1	102.3	0.2448	0.13925	0.00202	6.51941	0.09955	0.33966	0.00414	2217.9	13.1	2048.5	16.7	1885.0	19.9	-15.0	Del.		
GH02/2014_G145	295.7	106.4	0.8775	0.16636	0.00243	6.63655	0.10163	0.28942	0.00354	2521.4	13.6	2064.2	16.8	1638.6	17.7	-35.0	Del.		
GH02/2014_G146	52.0	34.2	1.1907	0.17488	0.00271	11.72998	0.19044	0.48662	0.00629	2604.9	14.5	2583.1	18.9	2556.0	27.3	-1.9		2604.9	14.5
GH02/2014_G147	80.1	23.7	0.8080	0.09932	0.00167	3.42708	0.05916	0.25033	0.00324	1611.4	13.6	1510.6	16.7	1440.2	16.7	-10.6		1611.4	13.6
GH02/2014_G148	107.3	67.9	1.1767	0.16434	0.00246	10.72798	0.16846	0.47359	0.00591	2500.8	13.9	2499.9	18.1	2499.3	25.9	-0.1		2500.8	13.9

Analysis No.	U (ppm)	Pb (ppm)	Th/U	Measured isotopic ratios						Calculated isotopic ages (Ma)						Disc.† (%)	Comment§	Preferred age (Ma)#	
				$^{207}Pb/^{206}Pb$	1σ	$^{206}Pb/^{238}U$	1σ	$^{208}Pb/^{232}Th$	1σ	$^{207}Pb/^{206}Pb$	1σ	$^{207}Pb/^{235}U$	1σ	$^{206}Pb/^{238}U$	1σ			Age	1σ
Sample JSZG2, quartz sandstone, Lower Gouhou Formation, Jinshanzhai section of Huaibei region																			
JSZG2_G001	70.4	41.2	0.5901	0.16457	0.00210	11.14961	0.14150	0.49151	0.00543	2503.2	11.9	2535.7	15.7	2577.2	23.5	-3.0		2503.2	11.9
JSZG2_G002	127.7	48.5	0.4694	0.10998	0.00144	5.19878	0.06678	0.34291	0.00371	1799.1	11.0	1852.4	14.5	1900.7	17.8	-5.6		1799.1	11.0
JSZG2_G003	115.2	33.0	0.4589	0.09030	0.00124	3.28123	0.04427	0.26359	0.00288	1431.9	10.5	1476.6	13.7	1508.2	14.7	-5.3		1431.9	10.5
JSZG2_G004	164.0	56.5	0.3573	0.10706	0.00136	4.75118	0.05916	0.32194	0.00342	1750.0	10.6	1776.3	13.9	1799.2	16.7	-2.8		1750.0	10.6
JSZG2_G005	119.2	47.7	0.5941	0.11318	0.00146	5.44178	0.06887	0.34877	0.00374	1851.1	11.0	1891.5	14.4	1928.7	17.9	-4.2		1851.1	11.0
JSZG2_G006	82.3	15.9	0.7977	0.07172	0.00121	1.63054	0.02668	0.16492	0.00190	978.0	10.6	982.1	12.9	984.1	10.5	-0.2		984.1	10.5
JSZG2_G007	198.1	36.8	0.3679	0.12637	0.00175	3.02420	0.04056	0.17359	0.00191	2048.1	12.2	1413.7	13.5	1031.9	10.5	27.0	Del.		
JSZG2_G008	295.1	105.1	0.3708	0.12089	0.00151	5.53030	0.06781	0.33182	0.00350	1969.4	10.9	1905.3	14.1	1847.2	16.9	6.2	Del.		
JSZG2_G009	295.1	133.2	0.2248	0.14140	0.00169	8.31055	0.09775	0.42632	0.00441	2244.4	10.8	2265.5	14.3	2289.1	19.9	-2.0		2244.4	10.8
JSZG2_G010	116.4	46.7	0.6367	0.11198	0.00145	5.34252	0.06810	0.34604	0.00372	1831.8	11.0	1875.7	14.4	1915.7	17.8	-4.6		1831.8	11.0
JSZG2_G011	128.8	74.9	0.5221	0.16537	0.00202	11.26165	0.13582	0.49393	0.00522	2511.3	11.4	2545.0	15.1	2587.7	22.5	-3.0		2511.3	11.4
JSZG2_G012	59.6	22.6	0.5190	0.11281	0.00160	5.25745	0.07335	0.33802	0.00382	1845.2	12.1	1862.0	15.5	1877.1	18.4	-1.7		1845.2	12.1
JSZG2_G013	129.4	49.5	0.8429	0.11382	0.00147	5.04083	0.06383	0.32121	0.00343	1861.3	11.0	1826.2	14.2	1795.6	16.7	3.5		1861.3	11.0
JSZG2_G014	306.5	40.9	0.2776	0.06288	0.00087	1.14626	0.01538	0.13220	0.00139	704.2	7.0	775.5	9.4	800.4	7.9	-3.2		800.4	7.9
JSZG2_G015	132.8	36.4	0.4170	0.09098	0.00124	3.19662	0.04248	0.25482	0.00275	1446.2	10.5	1456.3	13.4	1463.3	14.1	-1.2		1446.2	10.5
JSZG2_G016	21.0	12.8	0.7951	0.16680	0.00256	11.20878	0.17217	0.48737	0.00624	2525.8	14.3	2540.6	18.6	2559.3	27.0	-1.3		2525.8	14.3
JSZG2_G017	103.9	17.9	0.5793	0.06945	0.00113	1.51109	0.02372	0.15779	0.00177	912.1	9.8	934.9	12.1	944.5	9.9	-1.0		944.5	9.9
JSZG2_G018	151.5	29.1	0.2637	0.07513	0.00108	1.96067	0.02726	0.18925	0.00204	1072.0	9.5	1102.1	12.1	1117.3	11.1	-4.2		1072.0	9.5
JSZG2_G019	158.9	63.6	0.6140	0.11254	0.00142	5.38471	0.06656	0.34699	0.00365	1840.8	10.7	1882.4	14.1	1920.2	17.5	-4.3		1840.8	10.7
JSZG2_G020	111.2	46.7	0.3461	0.12941	0.00167	6.90171	0.08696	0.38675	0.00414	2090.0	11.4	2098.9	14.9	2107.7	19.2	-0.9		2090.0	11.4
JSZG2_G021	101.6	57.2	0.5197	0.18144	0.00226	12.33542	0.15090	0.49302	0.00526	2666.1	11.7	2630.3	15.4	2583.7	22.7	3.1		2666.1	11.7
JSZG2_G022	26.7	14.7	0.2785	0.17853	0.00260	12.39223	0.17999	0.50336	0.00619	2639.3	13.7	2634.6	17.9	2628.2	26.5	0.4		2639.3	13.7
JSZG2_G023	117.5	44.0	0.3632	0.11311	0.00148	5.41508	0.06917	0.34716	0.00371	1850.0	11.1	1887.2	14.5	1921.0	17.8	-3.8		1850.0	11.1
JSZG2_G024	236.7	95.6	0.5146	0.12177	0.00150	6.03432	0.07268	0.35935	0.00373	1982.3	10.7	1980.8	14.0	1979.1	17.7	0.2		1982.3	10.7
JSZG2_G025	249.7	66.1	0.5206	0.10506	0.00134	3.64787	0.04518	0.25177	0.00263	1715.4	10.6	1560.0	13.1	1447.6	13.5	15.6	Del.		
JSZG2_G026	33.5	15.0	0.4738	0.12374	0.00206	6.79105	0.11171	0.39794	0.00508	2010.8	14.6	2084.6	18.6	2159.5	23.4	-7.4		2010.8	14.6
JSZG2_G027	91.4	26.6	0.3172	0.09100	0.00131	3.48089	0.04867	0.27737	0.00305	1446.6	11.1	1522.9	14.3	1578.1	15.4	-9.1		1446.6	11.1
JSZG2_G028	64.1	24.4	0.6418	0.11203	0.00160	5.08466	0.07090	0.32909	0.00369	1832.6	12.1	1833.5	15.4	1834.0	17.9	-0.1		1832.6	12.1
JSZG2_G029	200.9	55.1	0.7550	0.08416	0.00112	2.70939	0.03490	0.23343	0.00245	1296.3	9.7	1331.0	12.6	1352.5	12.8	-4.3		1296.3	9.7
JSZG2_G030	73.2	43.7	0.6394	0.16891	0.00220	11.52994	0.14721	0.49493	0.00542	2546.9	12.1	2567.0	15.9	2592.0	23.4	-1.8		2546.9	12.1
JSZG2_G031	144.2	26.0	0.6815	0.06960	0.00108	1.51934	0.02284	0.15827	0.00174	916.6	9.4	938.2	11.6	947.2	9.7	-1.0		947.2	9.7
JSZG2_G032	56.2	33.7	0.7747	0.17036	0.00225	11.40296	0.14775	0.48531	0.00537	2561.2	12.3	2556.7	16.1	2550.4	23.3	0.4		2561.2	12.3
JSZG2_G033	133.4	70.2	0.2365	0.16508	0.00205	11.03716	0.13367	0.48475	0.00507	2508.4	11.5	2526.3	15.1	2547.9	22.0	-1.6		2508.4	11.5
JSZG2_G034	73.2	43.7	0.8363	0.16492	0.00214	10.78497	0.13718	0.47415	0.00515	2506.7	12.1	2504.8	15.7	2501.7	22.5	0.2		2506.7	12.1
JSZG2_G035	134.0	47.6	0.4642	0.11447	0.00149	5.08264	0.06429	0.32192	0.00340	1871.6	11.1	1833.2	14.2	1799.1	16.6	3.9		1871.6	11.1
JSZG2_G036	107.8	48.7	0.3886	0.13357	0.00173	7.51584	0.09466	0.40794	0.00434	2145.4	11.6	2174.9	15.0	2205.5	19.9	-2.8		2145.4	11.6
JSZG2_G037	73.8	12.0	0.4976	0.07482	0.00131	1.53804	0.02591	0.14904	0.00172	1063.7	11.5	945.7	12.9	895.6	9.6	5.3	Del.		

Analysis No.	U (ppm)	Pb (ppm)	Th/U	Measured isotopic ratios						Calculated isotopic ages (Ma)						Disc.† (%)	Comment§	Preferred age (Ma)#	
				$^{207}Pb/^{206}Pb$	1σ	$^{207}Pb/^{235}U$	1σ	$^{206}Pb/^{238}U$	1σ	$^{207}Pb/^{206}Pb$	1σ	$^{207}Pb/^{235}U$	1σ	$^{206}Pb/^{238}U$	1σ			Age	1σ
Sample JSZG2, quartz sandstone, Lower Gouhou Formation, Jinshanzhai section of Huaibei region																			
JSZG2_G038	91.4	33.3	0.3931	0.11272	0.00152	5.20174	0.06813	0.33456	0.00360	1843.7	11.5	1852.9	14.7	1860.4	17.4	-0.9		1843.7	11.5
JSZG2_G039	140.8	58.4	0.4535	0.13155	0.00167	6.88371	0.08499	0.37936	0.00397	2118.8	11.3	2096.6	14.6	2073.3	18.6	2.1		2118.8	11.3
JSZG2_G040	80.6	34.3	0.3866	0.12643	0.00170	6.76476	0.08831	0.38791	0.00420	2048.9	11.8	2081.1	15.3	2113.1	19.5	-3.1		2048.9	11.8
JSZG2_G041	88.0	31.9	0.4499	0.12061	0.00164	5.46391	0.07205	0.32843	0.00356	1965.3	11.8	1894.9	14.9	1830.8	17.3	6.8	Del.		
JSZG2_G042	91.9	55.8	0.9648	0.16552	0.00211	10.70609	0.13309	0.46889	0.00498	2512.8	11.9	2498.0	15.4	2478.7	21.9	1.4		2512.8	11.9
JSZG2_G043	230.4	78.1	0.2300	0.11953	0.00151	5.41685	0.06604	0.32853	0.00339	1949.2	10.9	1887.5	14.0	1831.3	16.4	6.1	Del.		
JSZG2_G044	99.3	74.9	0.2733	0.26654	0.00334	24.14505	0.29689	0.65670	0.00705	3285.8	12.2	3274.3	16.1	3254.3	27.4	1.0		3285.8	12.2
JSZG2_G045	133.4	25.8	0.3828	0.07463	0.00110	1.88516	0.02680	0.18312	0.00197	1058.6	9.7	1075.9	12.1	1084.0	10.7	-0.8		1084.0	10.7
JSZG2_G046	68.1	36.4	0.5672	0.16419	0.00217	10.38197	0.13397	0.45837	0.00500	2499.3	12.3	2469.4	15.9	2432.4	22.1	2.7		2499.3	12.3
JSZG2_G047	193.0	62.7	0.3718	0.10498	0.00136	4.40121	0.05497	0.30391	0.00316	1714.0	10.7	1712.6	13.7	1710.7	15.6	0.2		1714.0	10.7
JSZG2_G048	70.9	26.5	0.5784	0.11421	0.00162	5.13820	0.07039	0.32611	0.00359	1867.5	12.1	1842.4	15.3	1819.5	17.5	2.6		1867.5	12.1
JSZG2_G049	96.5	39.1	0.4398	0.12629	0.00168	6.34026	0.08137	0.36391	0.00387	2047.0	11.7	2024.0	14.9	2000.7	18.3	2.3		2047.0	11.7
JSZG2_G050	151.0	55.6	0.2895	0.12531	0.00167	5.99212	0.07727	0.34662	0.00370	2033.2	11.7	1974.7	14.9	1918.4	17.7	5.6	Del.		
JSZG2_G051	173.7	31.1	0.6009	0.06896	0.00101	1.51758	0.02135	0.15951	0.00169	897.5	8.7	937.5	11.1	954.1	9.4	-1.8		954.1	9.4
JSZG2_G052	101.0	24.0	0.7710	0.08928	0.00134	2.50873	0.03610	0.20368	0.00223	1410.2	11.4	1274.6	13.5	1195.1	11.9	15.3	Del.		
JSZG2_G053	78.3	34.8	0.5931	0.13184	0.00180	6.99949	0.09260	0.38481	0.00418	2122.6	12.1	2111.4	15.5	2098.7	19.5	1.1		2122.6	12.1
JSZG2_G054	116.9	42.5	0.3523	0.11478	0.00153	5.36371	0.06901	0.33871	0.00358	1876.4	11.4	1879.1	14.6	1880.5	17.2	-0.2		1876.4	11.4
JSZG2_G055	68.1	26.0	0.5732	0.11349	0.00162	5.23932	0.07206	0.33464	0.00368	1856.0	12.2	1859.0	15.4	1860.8	17.8	-0.3		1856.0	12.2
JSZG2_G056	163.5	70.3	0.9479	0.11589	0.00151	5.50713	0.06890	0.34443	0.00358	1893.8	11.2	1901.7	14.3	1907.9	17.2	-0.7		1893.8	11.2
JSZG2_G057	103.3	27.5	0.3025	0.09003	0.00130	3.17682	0.04400	0.25576	0.00275	1426.2	11.1	1451.5	13.9	1468.1	14.1	-2.9		1426.2	11.1
JSZG2_G058	65.3	37.5	0.5570	0.16301	0.00216	10.92218	0.14054	0.48566	0.00524	2487.1	12.3	2516.5	15.9	2551.9	22.7	-2.6		2487.1	12.3
JSZG2_G059	207.7	88.7	0.3299	0.12692	0.00161	6.89480	0.08405	0.39374	0.00403	2055.7	11.2	2098.0	14.5	2140.2	18.6	-4.1		2055.7	11.2
JSZG2_G060	88.0	30.8	0.3964	0.11133	0.00156	4.94383	0.06644	0.32187	0.00347	1821.2	11.9	1809.8	14.9	1798.9	16.9	1.2		1821.2	11.9
JSZG2_G061	72.1	47.8	1.4455	0.16000	0.00214	10.20787	0.13196	0.46240	0.00499	2455.7	12.4	2453.8	15.9	2450.1	22.0	0.2		2455.7	12.4
JSZG2_G062	66.4	16.4	0.3496	0.08606	0.00137	2.79620	0.04264	0.23551	0.00264	1339.5	11.8	1354.5	14.6	1363.3	13.8	-1.8		1339.5	11.8
JSZG2_G063	102.7	44.7	1.2000	0.11734	0.00161	5.30984	0.06992	0.32799	0.00350	1916.1	11.8	1870.4	14.9	1828.6	17.0	4.6		1916.1	11.8
JSZG2_G064	94.8	56.9	0.6226	0.16599	0.00216	11.37777	0.14260	0.49681	0.00524	2517.6	12.1	2554.6	15.6	2600.1	22.6	-3.3		2517.6	12.1
JSZG2_G065	157.2	40.8	0.8154	0.08164	0.00116	2.45235	0.03338	0.21772	0.00230	1236.9	10.2	1258.1	12.8	1269.8	12.2	-2.7		1236.9	10.2
JSZG2_G066	84.6	39.4	0.4803	0.13478	0.00182	7.64234	0.09947	0.41097	0.00440	2161.2	12.1	2189.8	15.5	2219.4	20.1	-2.7		2161.2	12.1
JSZG2_G067	48.8	37.1	0.3199	0.22348	0.00297	19.09605	0.24767	0.61929	0.00684	3005.9	12.8	3046.7	16.7	3107.1	27.2	-3.4		3005.9	12.8
JSZG2_G068	59.6	36.9	0.8177	0.16711	0.00225	11.34439	0.14803	0.49202	0.00535	2528.9	12.5	2551.9	16.1	2579.4	23.1	-2.0		2528.9	12.5
JSZG2_G069	135.7	37.2	0.6047	0.08947	0.00126	2.99404	0.04028	0.24254	0.00256	1414.2	10.7	1406.1	13.4	1399.9	13.3	1.0		1414.2	10.7
JSZG2_G070	46.0	8.8	0.3679	0.07537	0.00144	1.90464	0.03489	0.18314	0.00220	1078.4	12.7	1082.7	15.0	1084.1	12.0	-0.1		1084.1	12.0
JSZG2_G071	46.0	20.9	0.5436	0.13082	0.00191	7.15386	0.10110	0.39632	0.00447	2109.0	13.0	2130.8	16.4	2152.1	20.6	-2.0		2109.0	13.0
JSZG2_G072	110.7	41.4	0.3610	0.11540	0.00169	5.54642	0.07788	0.34833	0.00385	1886.1	12.5	1907.8	15.8	1926.6	18.4	-2.1		1886.1	12.5
JSZG2_G073	62.4	22.3	0.3768	0.12054	0.00189	5.50222	0.08301	0.33081	0.00385	1964.2	13.6	1900.9	16.8	1842.3	18.6	6.2	Del.		
JSZG2_G074	116.4	77.2	0.4579	0.19880	0.00255	15.35724	0.18880	0.55987	0.00581	2816.4	12.2	2837.7	15.7	2866.1	24.0	-1.8		2816.4	12.2
JSZG2_G075	107.3	75.0	1.2203	0.16639	0.00217	11.54028	0.14395	0.50265	0.00524	2521.7	12.1	2567.8	15.6	2625.2	22.5	-4.1		2521.7	12.1
JSZG2_G076	59.6	44.0	0.6202	0.21567	0.00285	17.57148	0.22497	0.59046	0.00639	2948.6	12.7	2966.6	16.4	2991.3	25.9	-1.4		2948.6	12.7
JSZG2_G077	63.6	35.3	0.6344	0.15810	0.00215	10.13210	0.13265	0.46444	0.00502	2435.4	12.6	2446.9	16.1	2459.1	22.1	-1.0		2435.4	12.6
JSZG2_G078	55.1	12.9	0.3847	0.08125	0.00140	2.47243	0.04064	0.22054	0.00253	1227.5	12.3	1264.0	15.0	1284.7	13.4	-4.7		1227.5	12.3
JSZG2_G079	73.2	42.0	0.5086	0.16715	0.00224	11.33567	0.14568	0.49148	0.00524	2529.3	12.5	2551.1	16.0	2577.1	22.6	-1.9		2529.3	12.5
JSZG2_G080	26.1	15.0	0.4156	0.17040	0.00256	11.71910	0.17196	0.49841	0.00597	2561.6	14.0	2582.2	18.0	2607.0	25.7	-1.8		2561.6	14.0
JSZG2_G081	200.9	68.4	0.1985	0.11704	0.00160	5.38281	0.07010	0.33330	0.00350	1911.5	11.8	1882.1	14.8	1854.4	16.9	3.0		1911.5	11.8
JSZG2_G082	34.6	6.7	0.2878	0.07639	0.00160	1.99308	0.03985	0.18909	0.00238	1105.3	14.1	1113.2	16.5	1116.4	12.9	-1.0		1105.3	14.1
JSZG2_G083	757.7	135.3	0.4645	0.13667	0.00179	3.24949	0.04021	0.17231	0.00175	2185.4	11.8	1469.1	12.9	1024.8	9.6	30.2	Del.		
JSZG2_G084	131.7	50.0	0.2891	0.11499	0.00155	5.67795	0.07272	0.35784	0.00371	1879.7	11.5	1928.0	14.7	1971.9	17.6	-4.9		1879.7	11.5

Analysis No.	U (ppm)	Pb (ppm)	Th/U	Measured isotopic ratios						Calculated isotopic ages (Ma)						Disc.† (%)	Comment§	Preferred age (Ma)#	
				$^{207}Pb/^{206}Pb$	1σ	$^{206}Pb/^{238}U$	1σ	$^{208}Pb/^{232}Th$	1σ	$^{207}Pb/^{206}Pb$	1σ	$^{206}Pb/^{238}U$	1σ	$^{208}Pb/^{232}Th$	1σ			Age	1σ
Sample JSZG2, quartz sandstone, Lower Gouhou Formation, Jinshanzhai section of Huaibei region																			
JSZG2_G085	65.8	42.0	0.6924	0.16691	0.00226	11.80333	0.15323	0.51248	0.00550	2526.9	12.6	2588.9	16.2	2667.2	23.4	-5.6		2526.9	12.6
JSZG2_G086	88.0	20.1	0.4146	0.08303	0.00135	2.45617	0.03804	0.21438	0.00238	1269.9	11.8	1259.2	14.2	1252.1	12.6	1.4		1269.9	11.8
JSZG2_G087	91.4	34.0	0.5200	0.11259	0.00158	5.15977	0.06886	0.33212	0.00352	1841.6	11.9	1846.0	15.0	1848.6	17.0	-0.4		1841.6	11.9
JSZG2_G088	79.5	31.3	0.4892	0.11519	0.00167	5.59299	0.07768	0.35189	0.00384	1882.9	12.4	1915.0	15.6	1943.6	18.3	-3.2		1882.9	12.4
JSZG2_G089	53.9	29.9	0.3784	0.16703	0.00232	11.27603	0.15065	0.48924	0.00536	2528.1	12.9	2546.2	16.5	2567.4	23.2	-1.6		2528.1	12.9
JSZG2_G090	145.3	60.9	0.7157	0.11411	0.00153	5.57039	0.07080	0.35377	0.00364	1865.9	11.4	1911.5	14.5	1952.6	17.3	-4.6		1865.9	11.4
JSZG2_G091	195.8	91.3	0.7153	0.13100	0.00172	7.05344	0.08767	0.39021	0.00397	2111.4	11.7	2118.2	14.8	2123.8	18.4	-0.6		2111.4	11.7
JSZG2_G092	118.1	37.7	0.4846	0.09741	0.00137	3.89511	0.05199	0.28980	0.00303	1575.1	11.3	1612.7	14.2	1640.5	15.1	-4.2		1575.1	11.3
JSZG2_G093	84.6	38.4	0.6827	0.13300	0.00184	7.04072	0.09249	0.38365	0.00406	2137.9	12.3	2116.6	15.5	2093.3	18.9	2.1		2137.9	12.3
JSZG2_G094	68.7	32.0	0.3213	0.14789	0.00206	8.77346	0.11641	0.42992	0.00462	2321.7	12.7	2314.7	16.0	2305.4	20.8	0.7		2321.7	12.7
JSZG2_G095	73.8	39.1	0.4205	0.16775	0.00229	10.88080	0.14151	0.47008	0.00501	2535.3	12.7	2513.0	16.1	2483.9	22.0	2.0		2535.3	12.7
JSZG2_G096	36.3	8.3	0.7753	0.07583	0.00157	2.03639	0.04017	0.19462	0.00242	1090.6	13.8	1127.8	16.4	1146.4	13.1	-5.1		1090.6	13.8
JSZG2_G097	57.9	35.6	0.7143	0.21107	0.00291	15.03849	0.19868	0.51636	0.00566	2913.8	13.2	2817.7	16.8	2683.7	24.1	7.9	Del.		
JSZG2_G098	107.8	71.3	1.6309	0.16755	0.00229	10.49064	0.13606	0.45376	0.00481	2533.3	12.7	2479.1	16.0	2411.9	21.3	4.8		2533.3	12.7
JSZG2_G099	57.9	17.7	0.8324	0.09325	0.00173	3.25965	0.05785	0.25334	0.00310	1493.0	14.5	1471.5	17.3	1455.7	15.9	2.5		1493.0	14.5
JSZG2_G100	42.6	12.0	0.9029	0.08944	0.00163	2.84780	0.04933	0.23076	0.00275	1413.6	13.9	1368.2	16.4	1338.5	14.4	5.3	Del.		
JSZG2_G101	140.2	66.0	0.5428	0.13800	0.00185	7.80452	0.09870	0.40987	0.00420	2202.3	12.1	2208.7	15.2	2214.3	19.2	-0.5		2202.3	12.1
JSZG2_G102	32.4	12.0	0.6474	0.11262	0.00190	4.98110	0.08035	0.32054	0.00381	1842.1	14.3	1816.1	17.4	1792.4	18.6	2.7		1842.1	14.3
JSZG2_G103	107.3	40.0	0.5227	0.11260	0.00158	5.15272	0.06823	0.33165	0.00346	1841.8	11.9	1844.8	14.9	1846.4	16.7	-0.2		1841.8	11.9
JSZG2_G104	124.3	23.8	0.5091	0.08266	0.00126	2.08732	0.02994	0.18301	0.00194	1261.2	11.0	1144.6	12.7	1083.4	10.6	5.4	Del.		
JSZG2_G105	140.8	62.3	0.5532	0.13090	0.00177	6.98339	0.08872	0.38664	0.00396	2110.1	12.0	2109.3	15.1	2107.2	18.4	0.1		2110.1	12.0
JSZG2_G106	200.9	70.0	0.1423	0.11615	0.00155	5.52813	0.06942	0.34494	0.00348	1897.8	11.5	1905.0	14.4	1910.4	16.7	-0.7		1897.8	11.5
JSZG2_G107	58.5	32.2	0.4712	0.16611	0.00233	10.99993	0.14658	0.47991	0.00518	2518.8	13.1	2523.1	16.5	2526.9	22.6	-0.3		2518.8	13.1
JSZG2_G108	157.2	56.3	0.3363	0.11637	0.00161	5.39057	0.07026	0.33571	0.00347	1901.2	11.9	1883.4	14.8	1866.0	16.7	1.9		1901.2	11.9
JSZG2_G109	70.9	40.0	0.4684	0.16820	0.00232	11.33950	0.14828	0.48860	0.00518	2539.8	12.9	2551.5	16.2	2564.6	22.4	-1.0		2539.8	12.9
JSZG2_G110	73.8	42.2	0.6344	0.16056	0.00221	10.54446	0.13739	0.47596	0.00501	2461.6	12.7	2483.8	16.1	2509.6	21.9	-2.0		2461.6	12.7
JSZG2_G111	56.8	37.5	0.9157	0.18284	0.00254	12.92587	0.17064	0.51235	0.00550	2678.8	13.1	2674.3	16.5	2666.7	23.4	0.5		2678.8	13.1
JSZG2_G112	109.0	23.9	0.6456	0.07929	0.00123	2.10901	0.03087	0.19278	0.00205	1179.4	10.8	1151.8	13.0	1136.4	11.1	3.6		1179.4	10.8
JSZG2_G113	170.8	60.7	0.1764	0.11774	0.00160	5.64901	0.07177	0.34772	0.00353	1922.2	11.7	1923.6	14.6	1923.7	16.9	-0.1		1922.2	11.7
JSZG2_G114	82.9	48.7	0.5524	0.18117	0.00247	12.52616	0.16088	0.50110	0.00523	2663.6	12.8	2644.7	16.1	2618.5	22.5	1.7		2663.6	12.8
JSZG2_G115	27.2	16.2	0.6432	0.17948	0.00277	12.18185	0.18109	0.49191	0.00588	2648.1	14.5	2618.5	18.3	2578.9	25.4	2.6		2648.1	14.5
JSZG2_G116	28.9	16.7	0.5974	0.16816	0.00257	11.26091	0.16577	0.48533	0.00570	2539.4	14.2	2545.0	18.0	2550.4	24.7	-0.4		2539.4	14.2
JSZG2_G117	45.4	29.5	0.6867	0.16706	0.00240	11.93986	0.16322	0.51799	0.00569	2528.4	13.4	2599.7	16.9	2690.7	24.2	-6.4		2528.4	13.4
JSZG2_G118	81.2	13.4	0.5076	0.07623	0.00142	1.59387	0.02793	0.15153	0.00174	1101.1	12.5	967.8	13.6	909.5	9.7	6.0	Del.		
JSZG2_G119	36.9	15.1	0.7107	0.11552	0.00190	5.51733	0.08652	0.34614	0.00403	1888.0	14.1	1903.3	17.3	1916.1	19.3	-1.5		1888.0	14.1
JSZG2_G120	76.6	30.2	0.5187	0.11858	0.00173	5.73295	0.07862	0.35041	0.00373	1934.9	12.6	1936.3	15.6	1936.6	17.8	-0.1		1934.9	12.6
JSZG2_G121	182.2	45.9	0.5893	0.08290	0.00119	2.57204	0.03462	0.22486	0.00230	1266.9	10.4	1292.7	12.9	1307.5	12.1	-3.2		1266.9	10.4
JSZG2_G122	169.7	42.4	0.4113	0.08400	0.00121	2.70298	0.03625	0.23324	0.00238	1292.6	10.5	1329.3	13.1	1351.5	12.4	-4.6		1292.6	10.5
JSZG2_G123	40.9	12.9	0.8056	0.10222	0.00208	3.73615	0.07235	0.26492	0.00348	1664.8	16.7	1579.1	19.4	1515.0	17.7	9.0	Del.		
JSZG2_G124	101.0	53.1	0.4640	0.15243	0.00209	9.64218	0.12407	0.45849	0.00472	2373.4	12.6	2401.2	15.8	2432.9	20.9	-2.5		2373.4	12.6
JSZG2_G125	55.6	24.5	0.4331	0.13379	0.00198	7.30147	0.10180	0.39555	0.00429	2148.3	13.2	2149.0	16.4	2148.5	19.8	0.0		2148.3	13.2
JSZG2_G126	97.1	21.7	0.3089	0.08251	0.00129	2.46458	0.03623	0.21649	0.00230	1257.6	11.3	1261.7	13.7	1263.3	12.2	-0.4		1257.6	11.3
JSZG2_G127	68.1	24.6	0.4065	0.11736	0.00175	5.36535	0.07531	0.33136	0.00356	1916.4	12.8	1879.3	15.7	1845.0	17.2	3.7		1916.4	12.8
JSZG2_G128	51.7	18.3	0.4699	0.11171	0.00176	4.96720	0.07365	0.32230	0.00357	1827.4	13.4	1813.8	16.3	1801.0	17.4	1.4		1827.4	13.4
JSZG2_G129	118.6	28.8	0.8068	0.08348	0.00129	2.35118	0.03391	0.20415	0.00215	1280.5	11.2	1227.9	13.3	1197.6	11.5	6.5	Del.		
JSZG2_G130	20.4	11.6	0.5807	0.17392	0.00286	11.51115	0.18286	0.47974	0.00603	2595.7	15.4	2565.5	19.3	2526.1	26.3	2.7		2595.7	15.4
JSZG2_G131	42.6	9.5	0.3331	0.08123	0.00156	2.40458	0.04375	0.21456	0.00255	1227.0	13.7	1244.0	16.2	1253.1	13.5	-2.1		1227.0	13.7

Analysis No.	U (ppm)	Pb (ppm)	Th/U	Measured isotopic ratios						Calculated isotopic ages (Ma)						Disc.† (%)	Comment§	Preferred age (Ma)#	
				$^{207}Pb/^{206}Pb$	1σ	$^{207}Pb/^{235}U$	1σ	$^{206}Pb/^{238}U$	1σ	$^{207}Pb/^{206}Pb$	1σ	$^{207}Pb/^{235}U$	1σ	$^{206}Pb/^{238}U$	1σ			Age	1σ
Sample JSZG2, quartz sandstone, Lower Gouhou Formation, Jinshanzhai section of Huaibei region																			
JSZG2_G132	61.3	22.4	0.4346	0.11116	0.00169	5.12065	0.07329	0.33389	0.00361	1818.5	12.9	1839.5	15.8	1857.2	17.4	-2.1		1818.5	12.9
JSZG2_G133	48.2	17.0	0.4482	0.11003	0.00178	4.86760	0.07413	0.32066	0.00361	1799.9	13.6	1796.7	16.6	1793.0	17.6	0.4		1799.9	13.6
JSZG2_G134	157.2	51.6	0.6498	0.09790	0.00140	3.83792	0.05090	0.28418	0.00289	1584.5	11.5	1600.7	14.1	1612.4	14.5	-1.8		1584.5	11.5
JSZG2_G135	82.3	31.9	0.4206	0.11397	0.00168	5.53639	0.07625	0.35211	0.00371	1863.7	12.6	1906.3	15.6	1944.7	17.7	-4.3		1863.7	12.6
JSZG2_G136	68.1	27.1	0.5563	0.11313	0.00171	5.45305	0.07727	0.34940	0.00375	1850.3	12.9	1893.2	15.9	1931.7	17.9	-4.4		1850.3	12.9
JSZG2_G137	57.9	22.0	0.4815	0.11602	0.00178	5.46871	0.07871	0.34169	0.00371	1895.8	13.2	1895.7	16.1	1894.8	17.8	0.1		1895.8	13.2
JSZG2_G138	159.5	21.9	0.4472	0.06543	0.00108	1.16347	0.01797	0.12891	0.00136	788.2	9.0	783.6	10.7	781.6	7.8	0.2		781.6	7.8
JSZG2_G139	144.7	51.5	0.2711	0.11685	0.00165	5.49966	0.07194	0.34118	0.00347	1908.6	12.1	1900.5	15.0	1892.3	16.7	0.9		1908.6	12.1
JSZG2_G140	123.2	69.4	0.5331	0.16737	0.00231	11.15653	0.14270	0.48320	0.00491	2531.5	12.9	2536.3	16.0	2541.2	21.3	-0.4		2531.5	12.9
JSZG2_G141	131.7	46.8	0.2141	0.11673	0.00166	5.54446	0.07286	0.34433	0.00351	1906.7	12.2	1907.5	15.1	1907.5	16.8	0.0		1906.7	12.2
JSZG2_G142	16.5	11.1	1.4340	0.17497	0.00301	11.39229	0.18954	0.47199	0.00616	2605.8	16.1	2555.8	20.2	2492.3	27.0	4.4		2605.8	16.1
JSZG2_G143	49.4	19.5	0.6914	0.11348	0.00180	5.26159	0.07826	0.33612	0.00372	1855.9	13.5	1862.7	16.5	1868.0	17.9	-0.7		1855.9	13.5
JSZG2_G144	178.2	64.8	0.1550	0.11668	0.00163	5.74027	0.07399	0.35664	0.00358	1906.0	12.0	1937.5	14.9	1966.2	17.0	-3.2		1906.0	12.0
JSZG2_G145	64.1	38.0	0.7354	0.17168	0.00245	11.50392	0.15343	0.48576	0.00512	2574.1	13.3	2564.9	16.6	2552.3	22.2	0.8		2574.1	13.3
JSZG2_G146	115.2	61.9	0.2652	0.17057	0.00236	11.53968	0.14799	0.49047	0.00498	2563.2	12.9	2567.8	16.0	2572.7	21.5	-0.4		2563.2	12.9
JSZG2_G147	225.3	29.8	0.3294	0.06677	0.00104	1.18523	0.01709	0.12869	0.00132	830.6	8.8	793.7	10.3	780.4	7.5	1.7		780.4	7.5
JSZG2_G148	117.5	16.4	0.4402	0.06604	0.00115	1.19601	0.01933	0.13129	0.00140	807.6	9.7	798.7	11.3	795.2	8.0	0.4		795.2	8.0
JSZG2_G149	53.9	20.4	0.4703	0.11176	0.00173	5.22560	0.07574	0.33899	0.00367	1828.2	13.1	1856.8	16.1	1881.8	17.7	-2.9		1828.2	13.1
JSZG2_G150	158.4	35.2	0.5385	0.08209	0.00126	2.28405	0.03233	0.20173	0.00208	1247.7	11.0	1207.4	13.1	1184.6	11.2	5.1			

Analysis No.	U (ppm)	Pb (ppm)	Th/U	Measured isotopic ratios						Calculated isotopic ages (Ma)						Disc.† (%)	Comment§	Preferred age (Ma)#	
				$^{207}Pb/^{206}Pb$	1σ	$^{207}Pb/^{235}U$	1σ	$^{206}Pb/^{238}U$	1σ	$^{207}Pb/^{206}Pb$	1σ	$^{207}Pb/^{235}U$	1σ	$^{206}Pb/^{238}U$	1σ			Age	1σ
Sample JSZG3, quartz sandstone, Lower Gouhou Formation, Jinshanzhai section of Huaibei region																			
JSZG3_G001	144.2	55.2	0.6162	0.10831	0.00129	4.95986	0.06179	0.33485	0.00385	1771.2	10.0	1812.5	14.0	1861.8	18.6	-5.1		1771.2	10.0
JSZG3_G002	178.8	74.5	0.9637	0.11043	0.00129	5.07226	0.06208	0.33585	0.00383	1806.5	9.9	1831.5	13.9	1866.7	18.5	-3.3		1806.5	9.9
JSZG3_G003	151.0	58.0	0.5705	0.11000	0.00131	5.10929	0.06357	0.33960	0.00390	1799.4	10.0	1837.7	14.1	1884.7	18.8	-4.7		1799.4	10.0
JSZG3_G004	137.9	50.8	1.1237	0.09580	0.00122	3.77445	0.04993	0.28802	0.00337	1543.9	10.1	1587.3	13.9	1631.6	16.9	-5.7		1543.9	10.1
JSZG3_G005	198.1	78.5	0.6283	0.10837	0.00125	5.09985	0.06175	0.34401	0.00390	1772.2	9.7	1836.1	13.7	1905.9	18.7	-7.5		1772.2	9.7
JSZG3_G006	152.7	89.2	0.6921	0.15747	0.00177	10.37450	0.12366	0.48158	0.00549	2428.7	10.4	2468.8	14.8	2534.1	23.9	-4.3		2428.7	10.4
JSZG3_G007	56.8	13.3	1.0562	0.07640	0.00140	1.96753	0.03590	0.18823	0.00245	1105.6	12.3	1104.5	15.2	1111.8	13.3	-0.6		1105.6	12.3
JSZG3_G008	145.9	78.1	0.2790	0.15829	0.00178	10.52872	0.12546	0.48615	0.00554	2437.5	10.4	2482.5	14.9	2554.0	24.0	-4.8		2437.5	10.4
JSZG3_G009	43.7	22.9	1.5204	0.18756	0.00249	9.78354	0.13443	0.38122	0.00481	2720.9	12.6	2414.6	16.9	2082.0	22.4	23.5	Del.		
JSZG3_G010	166.9	35.9	0.6414	0.08493	0.00115	2.23743	0.03095	0.19252	0.00226	1313.9	10.0	1192.9	12.6	1135.0	12.2	13.6	Del.		
JSZG3_G011	135.1	72.4	0.4263	0.15847	0.00179	10.27773	0.12272	0.47391	0.00540	2439.4	10.4	2460.1	14.9	2500.7	23.6	-2.5		2439.4	10.4
JSZG3_G012	65.8	45.5	1.4766	0.15973	0.00195	10.57394	0.13558	0.48371	0.00577	2452.8	11.3	2486.4	15.8	2543.4	25.1	-3.7		2452.8	11.3
JSZG3_G013	91.9	49.8	0.4160	0.15626	0.00183	10.21580	0.12629	0.47767	0.00555	2415.6	10.8	2454.5	15.3	2517.1	24.2	-4.2		2415.6	10.8
JSZG3_G014	225.3	78.9	0.1926	0.11130	0.00127	5.20410	0.06213	0.34161	0.00384	1820.8	9.7	1853.3	13.7	1894.4	18.5	-4.0		1820.8	9.7
JSZG3_G015	94.2	36.8	0.8043	0.11021	0.00139	4.95002	0.06465	0.32810	0.00384	1802.9	10.6	1810.8	14.6	1829.2	18.6	-1.5		1802.9	10.6
JSZG3_G016	86.8	23.1	1.1696	0.12938	0.00179	3.77311	0.05267	0.21304	0.00258	2089.6	12.3	1587.0	14.8	1245.0	13.7	40.4	Del.		
JSZG3_G017	53.4	29.7	0.7412	0.15702	0.00201	9.84351	0.13123	0.45791	0.00558	2423.8	11.8	2420.2	16.3	2430.3	24.7	-0.3		2423.8	11.8
JSZG3_G018	237.8	56.2	0.3297	0.08240	0.00101	2.56582	0.03250	0.22743	0.00257	1255.0	8.8	1291.0	12.2	1321.0	13.5	-5.3		1255.0	8.8
JSZG3_G019	97.6	41.8	0.6151	0.15697	0.00189	8.26023	0.10364	0.38432	0.00448	2423.3	11.1	2260.0	15.2	2096.4	20.9	13.5	Del.		
JSZG3_G020	152.1	57.9	0.5518	0.11177	0.00133	5.18796	0.06428	0.33895	0.00386	1828.4	10.1	1850.6	14.0	1881.6	18.6	-2.9		1828.4	10.1
JSZG3_G021	98.8	56.1	0.6568	0.16454	0.00192	10.74214	0.13173	0.47672	0.00551	2502.9	10.8	2501.1	15.3	2513.0	24.1	-0.4		2502.9	10.8
JSZG3_G022	129.4	26.6	0.2776	0.07955	0.00113	2.21420	0.03176	0.20322	0.00239	1185.9	9.9	1185.5	12.9	1192.6	12.8	-0.6		1185.9	9.9
JSZG3_G023	159.5	90.5	0.5931	0.15964	0.00179	10.48872	0.12399	0.47970	0.00540	2451.9	10.4	2478.9	14.7	2526.0	23.5	-3.0		2451.9	10.4

Analysis No.	U (ppm)	Pb (ppm)	Th/U	Measured isotopic ratios						Calculated isotopic ages (Ma)						Disc.† (%)	Comment§	Preferred age (Ma)#	
				$^{207}Pb/^{206}Pb$	1σ	$^{206}Pb/^{238}U$	1σ	$^{208}Pb/^{232}Th$	1σ	$^{207}Pb/^{206}Pb$	1σ	$^{206}Pb/^{238}U$	1σ	$^{208}Pb/^{232}Th$	1σ			Age	1σ
Sample JSZG3, quartz sandstone, Lower Gouhou Formation, Jinshanzhai section of Huaibei region																			
JSZG3_G024	94.2	54.0	0.6915	0.16212	0.00191	10.58972	0.13057	0.47687	0.00552	2477.9	10.9	2487.8	15.3	2513.6	24.1	-1.4		2477.9	10.9
JSZG3_G025	141.9	53.4	0.4034	0.11250	0.00134	5.34437	0.06628	0.34682	0.00395	1840.2	10.1	1876.0	14.1	1919.4	18.9	-4.3		1840.2	10.1
JSZG3_G026	88.0	23.8	1.0509	0.13320	0.00181	3.98911	0.05469	0.21862	0.00262	2140.6	12.1	1632.0	14.7	1274.6	13.9	40.5	Del.		
JSZG3_G027	159.5	122.7	0.5835	0.22875	0.00253	19.28600	0.22531	0.61541	0.00694	3043.3	10.7	3056.2	15.3	3091.6	27.7	-1.6		3043.3	10.7
JSZG3_G028	183.9	31.7	0.2556	0.07281	0.00098	1.70884	0.02345	0.17131	0.00197	1008.7	8.6	1011.9	11.4	1019.3	10.8	-0.7		1019.3	10.8
JSZG3_G029	85.7	34.5	1.0430	0.11098	0.00145	4.87412	0.06534	0.32053	0.00378	1815.5	11.0	1797.8	14.8	1792.3	18.5	1.3		1815.5	11.0
JSZG3_G030	221.9	79.0	0.4540	0.11182	0.00128	5.01158	0.05996	0.32710	0.00365	1829.2	9.7	1821.3	13.5	1824.3	17.7	0.3		1829.2	9.7
JSZG3_G031	333.2	117.3	0.2107	0.11156	0.00124	5.22977	0.06084	0.34209	0.00377	1825.0	9.4	1857.5	13.4	1896.7	18.1	-3.9		1825.0	9.4
JSZG3_G032	204.9	84.8	0.5237	0.12548	0.00143	6.30293	0.07488	0.36654	0.00409	2035.6	10.0	2018.9	14.0	2013.1	19.3	1.1		2035.6	10.0
JSZG3_G033	235.5	106.3	0.6210	0.15594	0.00173	8.52385	0.09918	0.39884	0.00442	2412.1	10.2	2288.5	14.3	2163.7	20.4	10.3	Del.		
JSZG3_G034	83.4	29.5	0.4635	0.10894	0.00144	4.81286	0.06519	0.32235	0.00380	1781.8	11.1	1787.1	14.9	1801.2	18.5	-1.1		1781.8	11.1
JSZG3_G035	65.3	36.7	0.7080	0.15398	0.00192	9.82597	0.12717	0.46558	0.00552	2390.6	11.5	2418.6	15.9	2464.1	24.3	-3.1		2390.6	11.5
JSZG3_G036	166.3	30.4	0.2423	0.07369	0.00101	1.84302	0.02564	0.18247	0.00210	1033.0	8.9	1060.9	11.8	1080.5	11.4	-1.8		1080.5	11.4
JSZG3_G037	254.8	96.8	0.6114	0.11049	0.00126	5.04147	0.05973	0.33285	0.00369	1807.5	9.6	1826.3	13.5	1852.2	17.8	-2.5		1807.5	9.6
JSZG3_G038	212.8	47.5	0.4041	0.07820	0.00099	2.26401	0.02941	0.21118	0.00238	1152.0	8.7	1201.2	12.0	1235.1	12.7	-7.2		1152.0	8.7
JSZG3_G039	109.0	41.2	0.7210	0.10781	0.00136	4.77549	0.06187	0.32311	0.00372	1762.7	10.6	1780.6	14.4	1804.9	18.1	-2.4		1762.7	10.6
JSZG3_G040	241.2	93.2	0.8048	0.10874	0.00125	4.82572	0.05775	0.32368	0.00359	1778.4	9.6	1789.4	13.4	1807.7	17.5	-1.6		1778.4	9.6
JSZG3_G041	229.9	93.7	0.5604	0.16668	0.00188	8.85628	0.10390	0.38753	0.00431	2524.6	10.5	2323.3	14.5	2111.4	20.0	16.4	Del.		
JSZG3_G042	281.0	75.9	0.6107	0.09140	0.00108	3.03089	0.03685	0.24183	0.00268	1455.0	9.1	1415.4	12.4	1396.2	13.9	4.0		1455.0	9.1
JSZG3_G043	296.3	79.6	0.5575	0.11919	0.00142	4.14337	0.05084	0.25350	0.00284	1944.1	10.3	1662.9	13.4	1456.5	14.6	25.1	Del.		
JSZG3_G044	149.8	47.2	0.5738	0.09536	0.00119	3.68422	0.04717	0.28174	0.00319	1535.2	9.9	1568.0	13.5	1600.1	16.0	-4.2		1535.2	9.9
JSZG3_G045	182.2	105.3	0.7777	0.16420	0.00184	10.64142	0.12455	0.47256	0.00524	2499.4	10.4	2492.3	14.6	2494.8	22.9	0.2		2499.4	10.4
JSZG3_G046	67.5	49.7	0.8870	0.17971	0.00218	13.64195	0.17348	0.55348	0.00654	2650.2	11.4	2725.2	16.0	2839.6	27.1	-7.1		2650.2	11.4
JSZG3_G047	115.8	17.8	1.0246	0.06049	0.00107	1.03253	0.01806	0.12444	0.00151	621.1	8.2	720.2	11.1	756.1	8.7	-5.0		756.1	8.7
JSZG3_G048	196.4	107.5	0.3361	0.16761	0.00187	11.31026	0.13170	0.49196	0.00544	2533.9	10.4	2549.1	14.7	2579.2	23.5	-1.8		2533.9	10.4
JSZG3_G049	325.2	52.2	0.5910	0.06642	0.00086	1.32681	0.01740	0.14563	0.00162	819.6	7.3	857.5	9.9	876.4	9.1	-2.2		876.4	9.1
JSZG3_G050	164.6	86.7	0.6077	0.15650	0.00178	9.66732	0.11440	0.45024	0.00501	2418.2	10.5	2403.6	14.6	2396.3	22.3	0.9		2418.2	10.5
JSZG3_G051	44.3	23.3	0.5095	0.15901	0.00218	10.04075	0.14204	0.46022	0.00578	2445.2	12.7	2438.5	17.2	2440.5	25.5	0.2		2445.2	12.7
JSZG3_G052	65.3	36.4	0.6743	0.16277	0.00203	10.45546	0.13472	0.46816	0.00552	2484.6	11.6	2476.0	15.9	2475.5	24.2	0.4		2484.6	11.6
JSZG3_G053	52.8	28.3	0.6198	0.16014	0.00210	10.04419	0.13582	0.45710	0.00556	2457.1	12.1	2438.9	16.5	2426.7	24.6	1.2		2457.1	12.1
JSZG3_G054	90.2	44.3	0.8014	0.14210	0.00182	7.92189	0.10411	0.40627	0.00479	2253.0	11.6	2222.2	15.7	2197.8	22.0	2.4		2253.0	11.6
JSZG3_G055	200.4	32.2	0.4358	0.06760	0.00097	1.41077	0.02028	0.15206	0.00174	856.3	8.3	893.5	10.9	912.5	9.7	-2.1		912.5	9.7
JSZG3_G056	139.1	23.1	0.5487	0.07087	0.00108	1.48897	0.02254	0.15309	0.00179	953.7	9.4	925.9	11.7	918.3	10.0	0.8		918.3	10.0
JSZG3_G057	85.1	51.1	1.0280	0.16364	0.00199	10.47458	0.13148	0.46639	0.00539	2493.6	11.3	2477.7	15.6	2467.7	23.7	1.0		2493.6	11.3
JSZG3_G058	125.4	46.7	0.4655	0.11299	0.00143	5.25664	0.06788	0.33896	0.00388	1848.1	10.8	1861.9	14.6	1881.7	18.7	-1.8		1848.1	10.8
JSZG3_G059	194.7	42.8	0.8672	0.07599	0.00102	1.92750	0.02607	0.18479	0.00209	1094.8	9.0	1090.7	11.8	1093.1	11.4	-0.2		1093.1	11.4
JSZG3_G060	114.7	38.1	0.6214	0.11227	0.00142	4.55414	0.05866	0.29551	0.00336	1836.5	10.7	1740.9	14.2	1669.0	16.7	9.1	Del.		
JSZG3_G061	123.7	68.4	0.5682	0.16223	0.00190	10.55209	0.12797	0.47383	0.00534	2479.0	10.9	2484.5	15.1	2500.3	23.4	-0.9		2479.0	10.9
JSZG3_G062	131.7	35.0	1.0841	0.08381	0.00119	2.43372	0.03457	0.21153	0.00245	1288.1	10.4	1252.6	13.2	1237.0	13.0	4.0		1288.1	10.4
JSZG3_G063	208.9	99.1	0.3190	0.15000	0.00171	9.00463	0.10600	0.43726	0.00481	2345.9	10.4	2338.5	14.5	2338.4	21.6	0.3		2345.9	10.4
JSZG3_G064	166.3	66.7	0.5555	0.12675	0.00151	6.24117	0.07620	0.35864	0.00400	2053.4	10.5	2010.2	14.3	1975.7	19.0	3.8		2053.4	10.5
JSZG3_G065	144.2	63.7	0.2044	0.14127	0.00167	8.20283	0.09988	0.42289	0.00473	2242.8	10.7	2253.7	14.7	2273.6	21.4	-1.4		2242.8	10.7
JSZG3_G066	42.0	23.0	0.5135	0.16132	0.00220	10.52433	0.14745	0.47512	0.00591	2469.5	12.6	2482.1	17.1	2506.0	25.8	-1.5		2469.5	12.6
JSZG3_G067	28.9	10.7	0.7224	0.10846	0.00200	4.71033	0.08648	0.31627	0.00439	1773.7	15.5	1769.1	19.3	1771.5	21.5	0.1		1773.7	15.5
JSZG3_G068	152.7	27.2	0.3103	0.07203	0.00104	1.72451	0.02481	0.17435	0.00200	986.8	9.1	1017.7	11.9	1036.0	11.0	-1.8		1036.0	11.0
JSZG3_G069	428.0	69.1	0.0829	0.07559	0.00093	1.77202	0.02208	0.17071	0.00187	1084.2	8.2	1035.3	10.7	1016.0	10.3	1.9		1016.0	10.3
JSZG3_G070	207.2	77.1	0.4500	0.13154	0.00153	6.20036	0.07384	0.34323	0.00377	2118.6	10.3	2004.5	14.0	1902.2	18.1	10.2	Del.		

Analysis No.	U (ppm)	Pb (ppm)	Th/U	Measured isotopic ratios						Calculated isotopic ages (Ma)						Disc.† (%)	Comment§	Preferred age (Ma)#	
				$^{207}Pb/^{206}Pb$	1σ	$^{207}Pb/^{235}U$	1σ	$^{206}Pb/^{238}U$	1σ	$^{207}Pb/^{206}Pb$	1σ	$^{207}Pb/^{235}U$	1σ	$^{206}Pb/^{238}U$	1σ			Age	1σ
Sample JSZG3, quartz sandstone, Lower Gouhou Formation, Jinshanzhai section of Huaibei region																			
JSZG3_G071	257.1	88.4	0.1928	0.11264	0.00131	5.20777	0.06213	0.33663	0.00368	1842.4	9.9	1853.9	13.6	1870.4	17.7	-1.5		1842.4	9.9
JSZG3_G072	73.8	25.1	0.6016	0.11356	0.00160	4.74309	0.06727	0.30409	0.00363	1857.1	12.0	1774.9	15.5	1711.6	17.9	7.8	Del.		
JSZG3_G073	166.9	62.5	0.6057	0.11119	0.00135	5.02113	0.06220	0.32876	0.00366	1819.0	10.3	1822.9	14.0	1832.4	17.8	-0.7		1819.0	10.3
JSZG3_G074	112.4	42.2	0.5480	0.11159	0.00143	5.11569	0.06646	0.33375	0.00380	1825.5	10.9	1838.7	14.6	1856.5	18.4	-1.7		1825.5	10.9
JSZG3_G075	183.9	97.7	0.6889	0.16536	0.00194	10.27117	0.12360	0.45216	0.00504	2511.2	10.9	2459.5	15.0	2404.8	22.4	4.2		2511.2	10.9
JSZG3_G076	172.0	95.5	0.3495	0.18059	0.00206	12.40126	0.14556	0.49988	0.00549	2658.3	10.7	2635.3	14.9	2613.3	23.6	1.7		2658.3	10.7
JSZG3_G077	103.3	52.5	0.4974	0.14512	0.00194	8.85930	0.12086	0.44435	0.00534	2289.2	12.1	2323.6	16.4	2370.1	23.8	-3.5		2289.2	12.1
JSZG3_G078	227.0	119.7	0.5754	0.16271	0.00184	10.16904	0.11795	0.45491	0.00494	2484.0	10.5	2450.3	14.5	2417.0	21.9	2.7		2484.0	10.5
JSZG3_G079	80.0	41.7	0.3756	0.16769	0.00205	10.83582	0.13599	0.47030	0.00539	2534.7	11.4	2509.1	15.6	2484.9	23.6	2.0		2534.7	11.4
JSZG3_G080	114.7	42.8	0.7687	0.11264	0.00143	4.89068	0.06305	0.31599	0.00357	1842.4	10.8	1800.7	14.3	1770.1	17.5	3.9		1842.4	10.8
JSZG3_G081	98.2	16.7	0.6405	0.06740	0.00115	1.40103	0.02357	0.15127	0.00181	850.2	9.8	889.4	12.4	908.1	10.1	-2.1		908.1	10.1
JSZG3_G082	44.8	25.6	0.7445	0.16126	0.00216	10.39713	0.14250	0.46918	0.00570	2468.9	12.4	2470.8	16.8	2480.0	25.0	-0.4		2468.9	12.4
JSZG3_G083	72.1	9.0	0.3320	0.06642	0.00141	1.11461	0.02307	0.12211	0.00158	819.6	11.9	760.4	13.3	742.7	9.1	2.3		742.7	9.1
JSZG3_G084	80.6	44.0	0.5004	0.16574	0.00204	10.83848	0.13657	0.47585	0.00546	2515.1	11.4	2509.4	15.6	2509.2	23.8	0.2		2515.1	11.4
JSZG3_G085	12.5	4.7	0.6743	0.10709	0.00267	4.71691	0.11621	0.32049	0.00539	1750.5	20.8	1770.2	25.2	1792.1	26.3	-2.4		1750.5	20.8
JSZG3_G086	116.4	61.5	0.5416	0.16328	0.00203	10.32461	0.13120	0.46009	0.00530	2489.9	11.5	2464.3	15.7	2440.0	23.4	2.0		2489.9	11.5
JSZG3_G087	55.6	38.7	0.7561	0.16392	0.00221	12.09791	0.16798	0.53697	0.00661	2496.5	12.5	2612.0	17.1	2770.8	27.7	-11.0		2496.5	12.5
JSZG3_G088	64.1	33.0	0.3833	0.16088	0.00205	10.24403	0.13328	0.46324	0.00541	2464.9	11.8	2457.1	16.0	2453.8	23.8	0.4		2464.9	11.8
JSZG3_G089	92.5	45.6	0.4573	0.15883	0.00203	9.65088	0.12572	0.44203	0.00516	2443.2	11.8	2402.0	15.9	2359.7	23.1	3.4		2443.2	11.8
JSZG3_G090	135.1	49.8	0.5975	0.11224	0.00141	4.99639	0.06334	0.32384	0.00362	1836.0	10.7	1818.7	14.2	1808.5	17.6	1.5		1836.0	10.7
JSZG3_G091	155.5	58.6	0.3922	0.11970	0.00145	5.74478	0.07082	0.34912	0.00386	1951.7	10.5	1938.1	14.2	1930.4	18.4	1.1		1951.7	10.5
JSZG3_G092	27.2	9.5	0.5496	0.10780	0.00207	4.62813	0.08809	0.31230	0.00440	1762.6	16.1	1754.4	19.9	1752.0	21.6	0.6		1762.6	16.1
JSZG3_G093	94.2	27.7	0.6673	0.11760	0.00208	4.28645	0.07449	0.26512	0.00355	1920.1	15.2	1690.8	18.3	1516.0	18.1	21.0	Del.		
JSZG3_G094	144.2	74.1	0.5060	0.15301	0.00180	9.46384	0.11366	0.44988	0.00495	2379.8	10.8	2384.0	14.8	2394.7	22.0	-0.6		2379.8	10.8
JSZG3_G095	122.6	26.1	0.3489	0.08152	0.00118	2.29875	0.03297	0.20509	0.00235	1234.0	10.3	1211.9	13.1	1202.6	12.6	2.5		1234.0	10.3
JSZG3_G096	98.2	36.1	0.8560	0.10747	0.00144	4.51614	0.06094	0.30563	0.00350	1757.0	11.2	1733.9	14.7	1719.2	17.3	2.2		1757.0	11.2
JSZG3_G097	161.8	70.9	0.4958	0.13330	0.00159	7.16436	0.08668	0.39086	0.00429	2141.9	10.6	2132.1	14.4	2126.8	19.9	0.7		2141.9	10.6
JSZG3_G098	253.1	56.7	0.5159	0.09282	0.00116	2.63736	0.03317	0.20663	0.00226	1484.2	9.7	1311.1	12.2	1210.8	12.1	18.4	Del.		
JSZG3_G099	61.9	9.2	0.4620	0.07743	0.00157	1.48418	0.02910	0.13939	0.00181	1132.3	13.8	923.9	14.6	841.2	10.2	9.0	Del.		
JSZG3_G100	682.8	101.8	0.3188	0.12086	0.00143	2.52043	0.03008	0.15165	0.00163	1969.0	10.3	1277.9	11.6	910.2	9.1	28.8	Del.		
JSZG3_G101	93.1	32.2	0.4950	0.10866	0.00146	4.67838	0.06296	0.31305	0.00358	1777.1	11.3	1763.4	14.8	1755.7	17.6	1.2		1777.1	11.3
JSZG3_G102	97.6	33.0	0.7655	0.10042	0.00138	3.95188	0.05415	0.28612	0.00327	1631.9	11.2	1624.4	14.5	1622.1	16.4	0.6		1631.9	11.2
JSZG3_G103	182.2	64.6	0.4388	0.11318	0.00138	5.07220	0.06234	0.32580	0.00356	1851.1	10.4	1831.5	13.9	1818.0	17.3	1.8		1851.1	10.4
JSZG3_G104	199.8	112.0	0.6878	0.16315	0.00188	10.48735	0.12269	0.46730	0.00504	2488.6	10.7	2478.8	14.6	2471.7	22.1	0.7		2488.6	10.7
JSZG3_G105	165.7	88.3	0.4473	0.16028	0.00187	10.35675	0.12277	0.46972	0.00510	2458.6	10.8	2467.2	14.8	2482.3	22.4	-1.0		2458.6	10.8
JSZG3_G106	207.2	125.4	0.8017	0.16418	0.00190	10.98151	0.12941	0.48623	0.00526	2499.2	10.7	2521.6	14.7	2554.3	22.8	-2.2		2499.2	10.7
JSZG3_G107	223.6	39.2	0.4422	0.07197	0.00098	1.62872	0.02197	0.16451	0.00181	985.1	8.6	981.4	11.0	981.8	10.0	0.0		981.8	10.0
JSZG3_G108	177.7	54.4	0.3697	0.11240	0.00151	4.51927	0.06061	0.29225	0.00333	1838.6	11.4	1734.5	14.7	1652.8	16.6	10.1	Del.		
JSZG3_G109	120.9	62.2	0.5007	0.16140	0.00194	10.13689	0.12328	0.45649	0.00504	2470.4	11.1	2447.3	15.1	2424.0	22.3	1.9		2470.4	11.1
JSZG3_G110	105.6	34.0	0.6171	0.10310	0.00138	4.02832	0.05382	0.28398	0.00320	1680.7	11.0	1639.9	14.2	1611.4	16.1	4.1		1680.7	11.0
JSZG3_G111	181.6	70.4	0.7439	0.11211	0.00136	5.06305	0.06184	0.32821	0.00356	1833.9	10.3	1829.9	13.8	1829.7	17.3	0.2		1833.9	10.3
JSZG3_G112	285.5	115.9	0.3316	0.12610	0.00146	6.56425	0.07685	0.37833	0.00403	2044.3	10.2	2054.6	13.9	2068.5	18.8	-1.2		2044.3	10.2
JSZG3_G113	198.1	71.0	0.4839	0.11546	0.00139	5.15418	0.06245	0.32441	0.00351	1887.1	10.3	1845.1	13.8	1811.2	17.1	4.0		1887.1	10.3
JSZG3_G114	165.7	74.9	0.3785	0.13716	0.00163	7.76670	0.09307	0.41149	0.00445	2191.6	10.7	2204.4	14.5	2221.7	20.3	-1.4		2191.6	10.7
JSZG3_G115	74.9	45.6	1.0224	0.16542	0.00207	10.70988	0.13594	0.47049	0.00534	2511.8	11.6	2498.3	15.7	2485.7	23.4	1.0		2511.8	11.6
JSZG3_G116	106.7	16.8	0.3240	0.06905	0.00115	1.45395	0.02369	0.15300	0.00179	900.2	9.9	911.5	12.3	917.8	10.0	-0.7		917.8	10.0
JSZG3_G117	172.5	74.3	0.2972	0.13843	0.00165	7.68348	0.09210	0.40329	0.00436	2207.7	10.7	2194.7	14.5	2184.2	20.0	1.1		2207.7	10.7

Analysis No.	U (ppm)	Pb (ppm)	Th/U	Measured isotopic ratios						Calculated isotopic ages (Ma)						Disc.† (%)	Comment§	Preferred age (Ma)#	
				$^{207}Pb/^{206}Pb$	1σ	$^{206}Pb/^{238}U$	1σ	$^{208}Pb/^{232}Th$	1σ	$^{207}Pb/^{206}Pb$	1σ	$^{207}Pb/^{235}U$	1σ	$^{206}Pb/^{238}U$	1σ			Age	1σ
Sample JSZG3, quartz sandstone, Lower Gouhou Formation, Jinshanzhai section of Huaibei region																			
JSZG3_G118	207.2	59.1	0.6912	0.08845	0.00113	3.01702	0.03845	0.24785	0.00270	1392.3	9.7	1411.9	12.8	1427.4	13.9	-2.5		1392.3	9.7
JSZG3_G119	101.6	35.7	0.4471	0.11156	0.00148	4.94978	0.06553	0.32236	0.00363	1825.0	11.2	1810.8	14.7	1801.2	17.7	1.3		1825.0	11.2
JSZG3_G120	125.4	52.0	0.4355	0.12911	0.00159	6.69267	0.08299	0.37662	0.00413	2085.9	10.9	2071.7	14.6	2060.5	19.3	1.2		2085.9	10.9
JSZG3_G121	186.2	71.2	0.7092	0.11317	0.00138	5.09860	0.06222	0.32732	0.00353	1850.9	10.4	1835.9	13.8	1825.4	17.1	1.4		1850.9	10.4
JSZG3_G122	77.8	35.8	0.2870	0.14865	0.00190	8.78965	0.11305	0.42957	0.00487	2330.5	11.7	2316.4	15.6	2303.8	22.0	1.1		2330.5	11.7
JSZG3_G123	35.2	14.1	0.9876	0.10978	0.00201	4.85199	0.08794	0.32108	0.00436	1795.8	15.4	1794.0	19.2	1795.0	21.3	0.0		1795.8	15.4
JSZG3_G124	30.6	14.4	0.6462	0.14095	0.00220	7.79624	0.12199	0.40180	0.00518	2238.9	14.1	2207.8	18.2	2177.3	23.8	2.8		2238.9	14.1
JSZG3_G125	198.1	60.4	1.0546	0.11426	0.00150	3.98742	0.05199	0.25351	0.00282	1868.2	11.2	1631.6	14.0	1456.6	14.5	22.0	Del.		
JSZG3_G126	331.5	110.4	0.2439	0.11424	0.00139	5.10841	0.06239	0.32481	0.00350	1867.9	10.4	1837.5	13.8	1813.2	17.0	2.9		1867.9	10.4
JSZG3_G127	111.8	39.4	0.4329	0.11530	0.00150	5.15349	0.06712	0.32467	0.00362	1884.6	11.1	1845.0	14.6	1812.5	17.6	3.8		1884.6	11.1
JSZG3_G128	183.9	62.5	0.3381	0.11021	0.00139	4.86949	0.06137	0.32092	0.00351	1802.9	10.6	1797.0	14.1	1794.2	17.1	0.5		1802.9	10.6
JSZG3_G129	223.1	75.5	0.2510	0.11193	0.00140	5.05053	0.06318	0.32772	0.00357	1831.0	10.6	1827.8	14.1	1827.3	17.3	0.2		1831.0	10.6
JSZG3_G130	154.4	53.6	0.3903	0.11525	0.00146	5.14136	0.06489	0.32401	0.00355	1883.8	10.9	1843.0	14.2	1809.3	17.3	4.0		1883.8	10.9
JSZG3_G131	30.6	19.0	1.4307	0.16171	0.00289	9.84457	0.17757	0.44215	0.00654	2473.6	16.6	2420.3	21.4	2360.3	29.2	4.6		2473.6	16.6
JSZG3_G132	94.2	47.5	0.6196	0.15058	0.00189	8.94221	0.11290	0.43128	0.00481	2352.5	11.5	2332.1	15.3	2311.5	21.7	1.7		2352.5	11.5
JSZG3_G133	138.5	48.9	0.5338	0.11475	0.00145	5.00979	0.06289	0.31705	0.00346	1876.0	10.8	1821.0	14.1	1775.3	16.9	5.4	Del.		
JSZG3_G134	25.0	9.5	0.7655	0.10950	0.00203	4.85760	0.08898	0.32216	0.00438	1791.1	15.6	1794.9	19.4	1800.3	21.4	-0.5		1791.1	15.6
JSZG3_G135	346.2	60.7	0.2628	0.07660	0.00097	1.83596	0.02298	0.17406	0.00185	1110.8	8.6	1058.4	10.9	1034.4	10.2	2.3		1034.4	10.2
JSZG3_G136	210.0	126.1	0.4913	0.18041	0.00209	12.80799	0.14932	0.51552	0.00546	2656.6	10.9	2665.6	14.8	2680.2	23.2	-0.9		2656.6	10.9
JSZG3_G137	137.9	41.5	0.5126	0.09706	0.00127	3.65317	0.04733	0.27331	0.00299	1568.4	10.5	1561.2	13.6	1557.6	15.1	0.7		1568.4	10.5
JSZG3_G138	183.9	75.0	0.2565	0.14486	0.00178	7.80163	0.09570	0.39105	0.00425	2286.1	11.2	2208.4	14.8	2127.7	19.7	6.9	Del.		
JSZG3_G139	132.2	29.9	0.6222	0.07881	0.00113	2.18265	0.03083	0.20109	0.00224	1167.4	9.9	1175.5	12.6	1181.2	12.0	-1.2		1167.4	9.9
JSZG3_G140	93.7	38.2	0.5487	0.12607	0.00163	6.26301	0.08060	0.36070	0.00400	2043.9	11.4	2013.3	14.9	1985.5	19.0	2.9		2043.9	11.4
JSZG3_G141	211.7	67.7	0.6923	0.11544	0.00150	4.52698	0.05843	0.28473	0.00313	1886.8	11.1	1735.9	14.2	1615.1	15.7	14.4	Del.		
JSZG3_G142	173.1	43.3	0.3763	0.08903	0.00119	2.92268	0.03845	0.23833	0.00260	1404.8	10.2	1387.8	13.1	1378.0	13.5	1.9		1404.8	10.2
JSZG3_G143	34.6	18.3	0.2097	0.17133	0.00240	11.62772	0.16459	0.49272	0.00603	2570.7	13.1	2574.9	17.4	2582.4	26.0	-0.5		2570.7	13.1
JSZG3_G144	112.4	48.3	0.2902	0.13625	0.00169	7.56030	0.09377	0.40284	0.00439	2180.1	11.1	2180.2	14.8	2182.1	20.2	-0.1		2180.1	11.1
JSZG3_G145	129.4	36.0	0.3843	0.09032	0.00121	3.25397	0.04320	0.26155	0.00287	1432.3	10.3	1470.1	13.5	1497.8	14.7	-4.6		1432.3	10.3
JSZG3_G146	27.2	5.7	0.2707	0.07379	0.00174	2.09045	0.04786	0.20565	0.00288	1035.7	15.3	1145.7	18.8	1205.6	15.4	-16.4	Del.		
JSZG3_G147	99.3	47.1	0.5582	0.14249	0.00180	8.12500	0.10242	0.41393	0.00456	2257.7	11.4	2245.0	15.2	2232.9	20.8	1.1		2257.7	11.4
JSZG3_G148	105.6	54.1	0.5738	0.16348	0.00201	10.01618	0.12291	0.44475	0.00484	2492.0	11.4	2436.3	15.2	2371.9	21.6	4.8		2492.0	11.4
JSZG3_G149	56.8	20.5	0.5966	0.11183	0.00163	4.90022	0.07059	0.31807	0.00371	1829.4	12.4	1802.3	15.7	1780.3	18.1	2.7		1829.4	12.4
JSZG3_G150	264.5	24.6	0.6433	0.05863	0.00094	0.67181	0.01044	0.08317	0.00092	553.4	6.8	521.8	8.0	515.0	5.5	1.3		515.0	5.5

Analysis No.	U (ppm)	Pb (ppm)	Th/U	Measured isotopic ratios						Calculated isotopic ages (Ma)						Disc.† (%)	Comment§	Preferred age (Ma)#	
				$^{208}Pb/^{232}Th$	1σ	$^{207}Pb/^{235}U$	1σ	$^{206}Pb/^{238}U$	1σ	$^{207}Pb/^{206}Pb$	1σ	$^{207}Pb/^{235}U$	1σ	$^{206}Pb/^{238}U$	1σ			Age	1σ
Sample JSZ01/2013, quartz sandstone, Middle Jinshanzhai Formation, Jinshanzhai section of Huaibei region																			
JSZ01/2013_G001	80.6	28.6	0.6353	0.12838	0.0018	5.29446	0.12443	0.30661	0.00388	2075.9	12.4	1868.0	16.2	1724.0	19.1	-17.0	Del.		
JSZ01/2013_G002	77.2	32.6	0.9407	0.11107	0.00148	5.23863	0.11216	0.33865	0.00422	1817.0	11.3	1858.9	15.5	1880.2	20.3	3.5		1817.0	11.3
JSZ01/2013_G003	81.8	38.8	0.6787	0.13761	0.00172	7.64569	0.15804	0.40198	0.00499	2197.3	11.2	2190.2	15.8	2178.2	22.9	-0.9		2197.3	11.2
JSZ01/2013_G004	399.8	170.9	1.4186	0.13362	0.00151	6.54057	0.09851	0.35542	0.00433	2146.1	10.1	2051.4	14.6	1960.4	20.6	-8.7		2146.1	10.1
JSZ01/2013_G005	215.4	94.9	0.5883	0.12825	0.00147	6.97514	0.11273	0.39039	0.00477	2074.1	10.1	2108.3	14.9	2124.6	22.1	2.4		2074.1	10.1
JSZ01/2013_G006	70.9	30.4	0.7937	0.11353	0.0015	5.43252	0.11645	0.35638	0.00445	1856.7	11.3	1890.0	15.7	1965.0	21.1	5.8	Del.		
JSZ01/2013_G007	68.5	27.2	0.7181	0.11008	0.00149	5.19556	0.1145	0.33675	0.00421	1800.7	11.4	1851.9	15.6	1871.0	20.3	3.9		1800.7	11.4
JSZ01/2013_G008	44.4	26.8	0.6062	0.17214	0.00217	12.43628	0.3035	0.50392	0.00634	2578.6	11.8	2637.9	16.7	2630.6	27.2	2.0		2578.6	11.8
JSZ01/2013_G009	85.3	23.9	1.3157	0.09367	0.00136	3.01782	0.0654	0.22853	0.00287	1501.5	11.4	1412.1	14.6	1326.8	15.1	-11.6		1501.5	11.4
JSZ01/2013_G010	331.8	86.5	0.9937	0.12651	0.00147	3.92714	0.05976	0.22703	0.00277	2050.0	10.2	1619.3	13.7	1318.9	14.6	-35.7	Del.		

Analysis No.	U (ppm)	Pb (ppm)	Th/U	Measured isotopic ratios						Calculated isotopic ages (Ma)						Disc.† (%)	Comment§	Preferred age (Ma)#	
				$^{208}Pb/^{206}Pb$	1σ	$^{207}Pb/^{235}U$	1σ	$^{206}Pb/^{238}U$	1σ	$^{208}Pb/^{206}Pb$	1σ	$^{207}Pb/^{235}U$	1σ	$^{206}Pb/^{238}U$	1σ			Age	1σ
Sample JSZ01/2013, quartz sandstone, Middle Jinshanzhai Formation, Jinshanzhai section of Huaibei region																			
JSZ01/2013_G011	91.0	17.6	0.9773	0.09085	0.00151	1.95143	0.04574	0.1631	0.00208	1443.5	12.8	1098.9	14.3	974.0	11.5	-11.4		974.0	11.5
JSZ01/2013_G012	110.6	28.4	0.7136	0.08418	0.00118	2.56014	0.05075	0.22435	0.00279	1296.7	10.3	1289.3	13.7	1304.8	14.7	0.6		1296.7	10.3
JSZ01/2013_G013	350.8	125.5	1.7101	0.13618	0.00154	5.67907	0.08403	0.3053	0.00372	2179.2	10.1	1928.2	14.4	1717.5	18.4	-21.2	Del.		
JSZ01/2013_G014	22.5	8.3	1.0064	0.09888	0.00198	4.18265	0.15035	0.29208	0.00394	1603.1	16.1	1670.6	19.6	1651.9	19.7	3.0		1603.1	16.1
JSZ01/2013_G015	78.3	19.3	0.9174	0.08444	0.00135	2.31195	0.05337	0.20243	0.00256	1302.7	11.7	1216.0	14.5	1188.4	13.7	-8.8		1302.7	11.7
JSZ01/2013_G016	256.9	55.9	0.4147	0.0893	0.0011	2.5743	0.04152	0.20873	0.00256	1410.6	9.4	1293.4	12.7	1222.0	13.7	-13.4		1410.6	9.4
JSZ01/2013_G017	144.0	33.4	0.3828	0.08339	0.00112	2.56262	0.04781	0.22119	0.00274	1278.4	9.8	1290.0	13.3	1288.2	14.5	0.8		1278.4	9.8
JSZ01/2013_G018	107.1	22.1	0.4198	0.07658	0.00115	2.0588	0.04301	0.19432	0.00243	1110.3	10.1	1135.2	13.3	1144.7	13.1	3.1		1110.3	10.1
JSZ01/2013_G019	258.6	91.3	1.1664	0.10996	0.00128	4.4601	0.07017	0.30106	0.00368	1798.7	9.8	1723.6	14.1	1696.6	18.2	-5.7		1798.7	9.8
JSZ01/2013_G020	107.7	21.8	0.4536	0.07589	0.00114	1.99374	0.04157	0.18879	0.00236	1092.2	10.1	1113.4	13.2	1114.8	12.8	2.1		1092.2	10.1
JSZ01/2013_G021	140.0	47.8	0.2820	0.1113	0.00136	5.01807	0.08971	0.3279	0.00404	1820.8	10.3	1822.4	14.7	1828.2	19.6	0.4		1820.8	10.3
JSZ01/2013_G022	200.5	76.7	1.4548	0.11348	0.00138	4.4707	0.07699	0.29378	0.00361	1855.9	10.4	1725.5	14.4	1660.4	18.0	-10.5		1855.9	10.4
JSZ01/2013_G023	46.1	11.2	0.3929	0.08542	0.00152	2.66627	0.07286	0.23069	0.00298	1325.1	13.2	1319.2	16.3	1338.1	15.6	1.0		1325.1	13.2
JSZ01/2013_G024	235.0	73.2	2.2141	0.10763	0.00135	3.08547	0.05262	0.21054	0.00259	1759.7	10.5	1429.1	13.5	1231.7	13.8	-30.0	Del.		
JSZ01/2013_G025	138.3	47.0	0.6860	0.09806	0.00128	3.82833	0.07336	0.29362	0.00364	1587.6	10.5	1598.7	14.6	1659.6	18.1	4.5		1587.6	10.5
JSZ01/2013_G026	307.6	134.7	0.4384	0.13042	0.00149	7.06219	0.11084	0.39434	0.00482	2103.6	10.1	2119.3	14.9	2142.9	22.3	1.9		2103.6	10.1
JSZ01/2013_G027	182.6	80.5	0.4028	0.12765	0.00149	6.88337	0.11503	0.39903	0.00489	2065.9	10.3	2096.5	15.0	2164.6	22.5	4.8		2065.9	10.3
JSZ01/2013_G028	255.8	110.8	0.4307	0.12813	0.00147	6.78863	0.10615	0.39134	0.00478	2072.5	10.1	2084.2	14.9	2129.0	22.1	2.7		2072.5	10.1
JSZ01/2013_G029	131.9	57.3	0.3368	0.1278	0.00153	7.1124	0.12909	0.39945	0.00492	2067.9	10.6	2125.6	15.3	2166.5	22.7	4.8		2067.9	10.6
JSZ01/2013_G030	134.8	40.0	1.0867	0.09108	0.00121	3.0812	0.05784	0.25049	0.0031	1448.3	10.2	1428.0	14.0	1441.0	16.0	-0.5		1448.3	10.2
JSZ01/2013_G031	79.5	39.6	0.8705	0.12892	0.00164	7.01885	0.14714	0.40232	0.00501	2083.3	11.3	2113.8	15.9	2179.7	23.0	4.6		2083.3	11.3
JSZ01/2013_G032	679.2	166.7	2.1837	0.12961	0.00147	3.14669	0.0445	0.17442	0.00213	2092.7	10.0	1444.2	12.8	1036.4	11.7	-28.2	Del.		
JSZ01/2013_G033	50.7	16.8	0.9168	0.09315	0.00151	3.44996	0.0895	0.2712	0.00347	1490.9	12.7	1515.9	16.3	1546.9	17.6	3.8		1490.9	12.7
JSZ01/2013_G034	213.1	88.6	0.8722	0.13108	0.00153	6.43656	0.10615	0.35662	0.00437	2112.5	10.4	2037.3	14.9	1966.1	20.8	-6.9		2112.5	10.4
JSZ01/2013_G035	233.9	99.0	0.4439	0.12928	0.0015	6.74327	0.10859	0.38306	0.00469	2088.2	10.3	2078.3	14.9	2090.6	21.9	0.1		2088.2	10.3
JSZ01/2013_G036	288.0	73.2	1.2989	0.09113	0.00112	2.60942	0.04215	0.20895	0.00256	1449.3	9.5	1303.3	12.8	1223.2	13.7	-15.6	Del.		
JSZ01/2013_G037	87.6	38.4	1.4889	0.11233	0.00149	4.87881	0.10134	0.31888	0.00398	1837.5	11.3	1798.6	15.4	1784.3	19.5	-2.9		1837.5	11.3
JSZ01/2013_G038	200.5	56.1	0.7632	0.08857	0.00112	2.89454	0.04968	0.24341	0.003	1394.9	9.6	1380.5	13.4	1404.4	15.6	0.7		1394.9	9.6
JSZ01/2013_G039	108.9	38.0	0.7882	0.10191	0.00136	4.10243	0.08294	0.29362	0.00366	1659.2	10.9	1654.8	14.9	1659.6	18.2	0.0		1659.2	10.9
JSZ01/2013_G040	216.6	71.0	1.0299	0.10614	0.00131	4.03534	0.06979	0.27737	0.00342	1734.1	10.3	1641.3	14.2	1578.1	17.3	-9.0		1734.1	10.3
JSZ01/2013_G041	625.6	163.7	2.3780	0.12567	0.00144	3.05727	0.04358	0.17714	0.00216	2038.3	10.1	1422.1	12.8	1051.3	11.8	-26.1	Del.		
JSZ01/2013_G042	103.1	25.8	0.7028	0.0847	0.00124	2.48239	0.05191	0.21784	0.00273	1308.7	10.8	1266.9	14.0	1270.5	14.5	-2.9		1308.7	10.8
JSZ01/2013_G043	365.8	62.8	0.4317	0.08626	0.0011	1.88134	0.03063	0.16006	0.00197	1344.0	9.5	1074.5	11.8	957.1	-28.8			957.1	10.9
JSZ01/2013_G044	246.5	105.0	0.6251	0.12949	0.0015	6.72906	0.1079	0.37041	0.00453	2091.1	10.3	2076.4	14.9	2031.3	21.3	-2.9		2091.1	10.3
JSZ01/2013_G045	146.3	60.0	1.1368	0.10842	0.00135	4.66379	0.08421	0.31799	0.00393	1773.0	10.4	1760.8	14.7	1779.9	19.2	0.4		1773.0	10.4
JSZ01/2013_G046	129.6	29.6	0.4573	0.08052	0.00114	2.37373	0.04673	0.21258	0.00265	1209.8	10.0	1234.7	13.5	1242.5	14.1	2.7		1209.8	10.0
JSZ01/2013_G047	406.7	70.1	1.1952	0.08134	0.00102	1.63807	0.02561	0.14631	0.00179	1229.7	8.9	985.0	11.1	880.2	10.1	-10.6		880.2	10.1
JSZ01/2013_G048	65.7	44.8	1.8244	0.1647	0.00208	9.71473	0.21366	0.44662	0.00559	2504.5	11.7	2408.1	16.4	2380.2	24.9	-5.0		2504.5	11.7
JSZ01/2013_G049	340.4	60.0	1.1678	0.0727	0.00096	1.4404	0.02406	0.14695	0.00181	1005.6	8.4	905.9	10.9	883.8	10.2	-2.4		883.8	10.2
JSZ01/2013_G050	225.2	80.8	0.5685	0.1091	0.00131	4.78112	0.07859	0.32469	0.00398	1784.4	10.1	1781.6	14.5	1812.6	19.4	1.6		1784.4	10.1
JSZ01/2013_G051	69.1	22.1	0.5411	0.10755	0.0016	4.21683	0.10149	0.29487	0.00375	1758.3	12.4	1677.3	16.2	1665.8	18.7	-5.3		1758.3	12.4
JSZ01/2013_G052	41.5	17.4	0.9890	0.11258	0.00176	5.11162	0.14078	0.33444	0.00431	1841.5	13.3	1838.0	17.2	1859.9	20.8	1.0		1841.5	13.3
JSZ01/2013_G053	214.3	36.2	0.6488	0.07427	0.00105	1.57347	0.0288	0.15719	0.00195	1048.8	9.2	959.8	11.8	941.1	10.9	-1.9		941.1	10.9
JSZ01/2013_G054	183.2	69.1	0.9945	0.10155	0.00127	4.22218	0.07404	0.30246	0.00373	1652.6	10.2	1678.3	14.4	1703.5	18.5	3.1		1652.6	10.2
JSZ01/2013_G055	211.4	43.9	0.9859	0.07631	0.00107	1.85305	0.03441	0.17445	0.00217	1103.2	9.4	1064.5	12.3	1036.6	11.9	-2.6		1036.6	11.9
JSZ01/2013_G056	211.4	64.9	1.4655	0.09713	0.00126	3.17881	0.05683	0.23593	0.00292	1569.7	10.4	1452.0	13.8	1365.5	15.2	-13.0		1569.7	10.4
JSZ01/2013_G057	282.8	120.4	0.4320	0.12809	0.00149	6.76069	0.10598	0.38641	0.00473	2071.9	10.3	2080.6	15.0	2106.2	22.0	1.7		2071.9	10.3
JSZ01/2013_G058	140.0	35.8	1.0909	0.0792	0.00114	2.13548	0.04176	0.20206	0.00252	1177.1	10.0	1160.4	13.3	1186.4	13.5	0.8		1177.1	10.0
JSZ01/2013_G059	51.8	12.1	0.5263	0.0772	0.00147	2.29072	0.06491	0.21242	0.00276	1126.4	13.0	1209.4	16.2	1241.7	14.7	10.2	Del.		
JSZ01/2013_G060	183.2	37.2	0.6222	0.07406	0.00105	1.81635	0.03387	0.18106	0.00225	1043.1	9.2	1051.4	12.4	1072.8	12.3	2.0		1072.8	12.3
JSZ01/2013_G061	103.1	17.4	0.4832	0.07011	0.0012	1.48865	0.03408	0.15721	0.002	931.6	10.4	925.8	13.1	941.3	11.1	1.7		941.3	11.1

Analysis No.	U (ppm)	Pb (ppm)	Th/U	Measured isotopic ratios						Calculated isotopic ages (Ma)						Disc.† (%)	Comment§	Preferred age (Ma)#	
				$^{208}Pb/^{206}Pb$	1σ	$^{207}Pb/^{235}U$	1σ	$^{206}Pb/^{238}U$	1σ	$^{208}Pb/^{206}Pb$	1σ	$^{207}Pb/^{235}U$	1σ	$^{206}Pb/^{238}U$	1σ			Age	1σ
Sample JSZ01/2013, quartz sandstone, Middle Jinshanzhai Formation, Jinshanzhai section of Huaibei region																			
JSZ01/2013_G062	254.0	39.8	0.2803	0.07071	0.00098	1.47236	0.02606	0.15476	0.00192	949.0	8.5	919.1	11.4	927.6	10.7	0.9		927.6	10.7
JSZ01/2013_G063	187.2	57.0	1.6843	0.10372	0.00143	3.29556	0.06547	0.2328	0.00291	1691.7	11.4	1480.0	14.5	1349.2	15.2	-20.2	Del.		
JSZ01/2013_G064	144.6	45.0	0.9784	0.09326	0.00125	3.3197	0.06346	0.253	0.00314	1493.2	10.5	1485.7	14.2	1453.9	16.2	-2.6		1493.2	10.5
JSZ01/2013_G065	42.6	16.3	0.4947	0.11854	0.00185	5.63096	0.15692	0.34509	0.00446	1934.3	13.5	1920.9	17.5	1911.1	21.4	-1.2		1934.3	13.5
JSZ01/2013_G066	540.9	170.7	0.1952	0.12914	0.00149	5.56741	0.08132	0.31289	0.00382	2086.3	10.2	1911.1	14.5	1754.9	18.8	-15.9	Del.		
JSZ01/2013_G067	193.0	58.7	1.5336	0.09886	0.00128	3.17255	0.05618	0.23771	0.00294	1602.7	10.4	1450.5	13.9	1374.8	15.3	-14.2		1602.7	10.4
JSZ01/2013_G068	587.6	213.7	2.0924	0.13703	0.00158	4.79499	0.06934	0.25972	0.00317	2190.0	10.4	1784.0	14.2	1488.4	16.2	-32.0	Del.		
JSZ01/2013_G069	88.1	15.1	0.5300	0.08004	0.0014	1.68895	0.04024	0.15682	0.00201	1198.0	12.3	1004.4	14.0	939.1	11.2	-6.5		939.1	11.2
JSZ01/2013_G070	285.1	121.2	0.5064	0.12849	0.00151	6.86048	0.10931	0.38281	0.00469	2077.4	10.4	2093.6	15.0	2089.4	21.9	0.6		2077.4	10.4
JSZ01/2013_G071	178.0	62.8	0.5718	0.10602	0.00133	4.66711	0.08266	0.31285	0.00386	1732.1	10.4	1761.4	14.7	1754.7	19.0	1.3		1732.1	10.4
JSZ01/2013_G072	473.5	183.4	2.6119	0.16055	0.00187	5.54917	0.08282	0.25126	0.00308	2461.5	10.8	1908.2	14.6	1445.0	15.9	-41.3	Del.		
JSZ01/2013_G073	153.8	45.8	1.4321	0.09392	0.00127	2.98884	0.05602	0.23401	0.00291	1506.5	10.6	1404.8	14.0	1355.5	15.2	-10.0		1506.5	10.6
JSZ01/2013_G074	582.4	159.2	2.1152	0.18108	0.0021	5.03789	0.07266	0.1998	0.00244	2662.8	10.9	1825.7	14.2	1174.2	13.1	-55.9	Del.		
JSZ01/2013_G075	262.7	110.0	0.4465	0.12913	0.00153	6.69006	0.10748	0.37915	0.00465	2086.2	10.5	2071.3	15.1	2072.3	21.7	-0.7		2086.2	10.5
JSZ01/2013_G076	144.0	49.3	1.2217	0.11112	0.00148	4.10107	0.07958	0.27256	0.0034	1817.8	11.3	1654.5	14.9	1553.8	17.2	-14.5		1817.8	11.3
JSZ01/2013_G077	116.9	47.9	0.4947	0.12833	0.00163	6.53563	0.12698	0.36789	0.00457	2075.2	11.2	2050.7	15.6	2019.5	21.5	-2.7		2075.2	11.2
JSZ01/2013_G078	452.2	175.7	2.0029	0.13602	0.00161	5.16941	0.07828	0.2782	0.00341	2177.1	10.6	1847.6	14.5	1582.3	17.2	-27.3	Del.		
JSZ01/2013_G079	280.0	91.1	1.1043	0.13017	0.00158	4.97404	0.08103	0.28513	0.00351	2100.3	10.8	1814.9	14.7	1617.1	17.6	-23.0	Del.		
JSZ01/2013_G080	551.3	123.4	1.8628	0.11481	0.00142	3.0063	0.0476	0.18815	0.00231	1876.9	10.6	1409.2	13.2	1111.3	12.5	-40.8	Del.		
JSZ01/2013_G081	227.0	48.4	1.0430	0.07774	0.00107	1.91416	0.03452	0.1811	0.00225	1140.2	9.4	1086.0	12.4	1073.0	12.3	-1.2		1073.0	12.3
JSZ01/2013_G082	58.8	25.8	1.0534	0.11582	0.00171	5.53512	0.13944	0.34687	0.00442	1892.7	12.7	1906.1	16.8	1919.6	21.2	1.4		1892.7	12.7
JSZ01/2013_G083	201.0	42.9	1.4245	0.09556	0.00133	2.1637	0.03985	0.16635	0.00207	1539.1	11.0	1169.5	13.0	992.0	11.4	-15.2	Del.		
JSZ01/2013_G084	227.5	38.8	0.4482	0.07162	0.00103	1.56546	0.0289	0.16074	0.002	975.2	9.0	956.6	11.8	960.9	11.1	0.4		960.9	11.1
JSZ01/2013_G085	380.2	164.5	1.8927	0.14082	0.00168	5.9392	0.09222	0.30807	0.00378	2237.3	10.8	1967.0	14.9	1731.2	18.6	-22.6	Del.		
JSZ01/2013_G086	52.4	20.3	0.9772	0.1061	0.00167	4.74303	0.12597	0.31133	0.004	1733.5	13.1	1774.9	16.9	1747.2	19.7	0.8		1733.5	13.1
JSZ01/2013_G087	204.5	33.1	0.3302	0.07166	0.00104	1.54059	0.02875	0.15754	0.00196	976.3	9.1	946.7	11.8	943.1	10.9	-0.4		943.1	10.9
JSZ01/2013_G088	168.8	68.4	0.3476	0.12506	0.00156	6.4761	0.11574	0.37636	0.00465	2029.6	10.9	2042.7	15.4	2059.3	21.8	1.5		2029.6	10.9
JSZ01/2013_G089	43.2	12.7	0.8892	0.09142	0.00169	3.08835	0.0908	0.24529	0.00322	1455.4	14.3	1429.8	17.4	1414.1	16.7	-2.8		1455.4	14.3
JSZ01/2013_G090	134.8	33.8	1.7451	0.09776	0.00147	2.57163	0.05473	0.1964	0.00248	1581.8	12.1	1292.6	14.5	1156.0	13.4	-26.9	Del.		
JSZ01/2013_G091	145.7	53.4	0.6337	0.1119	0.00147	4.79194	0.09142	0.32121	0.00399	1830.5	11.1	1783.5	15.3	1795.6	19.5	-1.9		1830.5	11.1
JSZ01/2013_G092	253.5	114.1	0.6215	0.12776	0.00159	6.81037	0.12061	0.39376	0.00486	2067.4	11.0	2087.1	15.6	2140.2	22.5	3.5		2067.4	11.0
JSZ01/2013_G093	95.6	20.0	0.8432	0.07506	0.00126	1.78614	0.04092	0.17621	0.00224	1070.1	11.1	1040.4	13.8	1046.2	12.3	0.6		1046.2	12.3
JSZ01/2013_G094	271.9	54.5	0.6128	0.08657	0.00115	2.17464	0.03711	0.18079	0.00224	1350.9	9.9	1173.0	12.6	1071.3	12.2	-8.7		1071.3	12.2
JSZ01/2013_G095	169.9	30.1	0.5856	0.0729	0.0011	1.57299	0.03089	0.16052	0.00201	1011.2	9.7	959.6	12.3	959.7	11.2	0.0		959.7	11.2
JSZ01/2013_G096	189.5	66.7	0.3729	0.10665	0.00136	4.61308	0.08086	0.32837	0.00406	1742.9	10.6	1751.6	14.9	1830.5	19.7	5.0	Del.		
JSZ01/2013_G097	228.1	43.9	0.6850	0.07273	0.00103	1.66894	0.03032	0.16968	0.00211	1006.4	9.0	996.8	12.1	1010.3	11.6	1.4		1010.3	11.6
JSZ01/2013_G098	374.4	73.3	0.0775	0.07946	0.00102	2.17014	0.03492	0.20437	0.00252	1183.6	9.0	1171.5	12.5	1198.8	13.5	1.3		1183.6	9.0
JSZ01/2013_G099	143.4	62.6	0.7703	0.13046	0.00166	6.65558	0.12228	0.37437	0.00464	2104.2	11.3	2066.7	15.7	2049.9	21.8	-2.6		2104.2	11.3
JSZ01/2013_G100	190.1	78.9	0.4758	0.12825	0.0016	6.55566	0.11437	0.3808	0.0047	2074.1	11.0	2053.4	15.5	2080.0	21.9	0.3		2074.1	11.0
JSZ01/2013_G101	32.8	16.3	1.8284	0.11325	0.00198	5.08969	0.15994	0.32907	0.00435	1852.2	14.9	1834.4	18.6	1833.9	21.1	-1.0		1852.2	14.9
JSZ01/2013_G102	1118.7	217.7	4.3374	0.11419	0.00149	1.27184	0.01985	0.08095	0.001	1867.1	11.1	833.2	10.2	501.8	6.0	-39.8	Del.		
JSZ01/2013_G103	334.7	113.3	0.7606	0.09969	0.00124	3.96855	0.06397	0.28853	0.00355	1618.3	10.1	1627.8	14.2	1634.2	17.8	1.0		1618.3	10.1
JSZ01/2013_G104	545.5	81.7	2.3078	0.09093	0.00122	1.31758	0.02149	0.10463	0.00129	1445.1	10.3	853.5	10.5	641.5	7.5	-24.8	Del.		
JSZ01/2013_G105	250.0	101.8	1.1623	0.12828	0.00159	6.00776	0.10004	0.34683	0.00428	2074.5	11.0	1977.0	15.3	1919.4	20.5	-7.5		2074.5	11.0
JSZ01/2013_G106	182.6	73.9	0.3862	0.13125	0.00165	6.43371	0.11222	0.3749	0.00463	2114.8	11.2	2036.9	15.6	2052.4	21.7	-2.9		2114.8	11.2
JSZ01/2013_G107	93.9	17.9	0.4317	0.07458	0.00129	1.85773	0.04455	0.1786	0.00228	1057.2	11.4	1066.2	14.1	1059.3	12.5	-0.6		1059.3	12.5
JSZ01/2013_G108	347.4	101.5	0.8815	0.12168	0.00151	4.39345	0.07028	0.26475	0.00326	1981.0	10.8	1711.1	14.5	1514.1	16.6	-23.6	Del.		
JSZ01/2013_G109	141.7	49.2	0.4567	0.1068	0.00142	4.5029	0.08473	0.31798	0.00395	1745.5	11.1	1731.5	15.2	1779.9	19.3	2.0		1745.5	11.1
JSZ01/2013_G110	307.0	127.7	0.6319	0.12945	0.00159	6.45488	0.10423	0.36302	0.00447	2090.5	10.9	2039.8	15.3	1996.5	21.1	-4.5		2090.5	10.9
JSZ01/2013_G111	167.1	69.5	0.5942	0.12745	0.00163	6.31211	0.11417	0.36573	0.00453	2063.1	11.3	2020.1	15.6	2009.3	21.4	-2.6		2063.1	11.3
JSZ01/2013_G112	346.8	57.1	1.2092	0.07547	0.0011	1.4057	0.02585	0.13611	0.0017	1081.0	9.7	891.3	11.4	822.6	9.6	-7.7		822.6	9.6

Analysis No.	U (ppm)	Pb (ppm)	Th/U	Measured isotopic ratios						Calculated isotopic ages (Ma)						Disc.† (%)	Comment§	Preferred age (Ma)#	
				$^{208}Pb/^{206}Pb$	1σ	$^{207}Pb/^{235}U$	1σ	$^{206}Pb/^{238}U$	1σ	$^{208}Pb/^{206}Pb$	1σ	$^{207}Pb/^{235}U$	1σ	$^{206}Pb/^{238}U$	1σ			Age	1σ
Sample JSZ01/2013, quartz sandstone, Middle Jinshanzhai Formation, Jinshanzhai section of Huaibei region																			
JSZ01/2013_G113	178.6	76.8	0.6925	0.12785	0.00163	6.3858	0.11399	0.37085	0.00459	2068.6	11.3	2030.3	15.6	2033.4	21.6	-1.7		2068.6	11.3
JSZ01/2013_G114	277.1	114.1	0.3906	0.12855	0.0016	6.57929	0.10828	0.37854	0.00466	2078.2	11.0	2056.6	15.5	2069.5	21.8	-0.4		2078.2	11.0
JSZ01/2013_G115	324.3	96.3	1.0430	0.13075	0.00164	4.7506	0.07743	0.26497	0.00327	2108.1	11.1	1776.2	14.8	1515.2	16.7	-28.1	Del.		
JSZ01/2013_G116	642.9	155.3	1.8118	0.13667	0.0017	3.53265	0.05417	0.18984	0.00234	2185.4	11.2	1534.6	13.9	1120.5	12.7	-48.7	Del.		
JSZ01/2013_G117	49.0	16.5	1.4209	0.09357	0.00169	2.95759	0.08248	0.24535	0.00321	1499.5	14.2	1396.8	17.2	1414.5	16.6	-5.7		1499.5	14.2
JSZ01/2013_G118	1050.7	264.5	2.1365	0.12317	0.00151	2.93829	0.04308	0.17449	0.00214	2002.6	10.7	1391.8	13.2	1036.8	11.7	-25.5	Del.		
JSZ01/2013_G119	100.2	36.7	1.0166	0.10362	0.00149	4.1094	0.08759	0.29143	0.00367	1689.9	11.8	1656.2	15.6	1648.7	18.3	-2.4		1689.9	11.8
JSZ01/2013_G120	286.9	97.0	0.4956	0.10977	0.0014	4.63883	0.07758	0.31155	0.00385	1795.6	10.7	1756.3	14.9	1748.3	18.9	-2.6		1795.6	10.7
JSZ01/2013_G121	278.2	114.6	0.4614	0.12964	0.00164	6.64711	0.11289	0.37359	0.00461	2093.1	11.2	2065.6	15.6	2046.3	21.6	-2.2		2093.1	11.2
JSZ01/2013_G122	235.6	54.4	1.1613	0.07999	0.00119	2.13879	0.04254	0.1944	0.00244	1196.7	10.5	1161.4	13.5	1145.2	13.2	-4.3		1196.7	10.5
JSZ01/2013_G123	109.4	22.7	1.3355	0.0716	0.00128	1.553	0.03701	0.15601	0.002	974.6	11.2	951.7	13.5	934.6	11.2	-1.8		934.6	11.2
JSZ01/2013_G124	211.4	59.8	1.1878	0.10336	0.00142	3.34956	0.06242	0.23941	0.00298	1685.3	11.3	1492.7	14.6	1383.6	15.5	-17.9	Del.		
JSZ01/2013_G125	147.5	49.7	0.6825	0.10205	0.00141	4.08648	0.0796	0.29247	0.00365	1661.7	11.3	1651.6	15.2	1653.9	18.2	-0.5		1661.7	11.3
JSZ01/2013_G126	369.8	151.0	2.2326	0.11887	0.00156	4.32089	0.07547	0.27119	0.00336	1939.3	11.4	1697.4	15.0	1546.8	17.0	-20.2	Del.		
JSZ01/2013_G127	936.1	136.2	0.9743	0.14756	0.00186	2.71461	0.04123	0.13394	0.00165	2317.8	11.5	1332.5	13.1	810.3	9.4	-39.2	Del.		
JSZ01/2013_G128	293.2	109.1	0.8879	0.11434	0.00148	5.04965	0.08581	0.31689	0.00392	1869.5	11.1	1827.7	15.1	1774.5	19.2	-5.1		1869.5	11.1
JSZ01/2013_G129	154.4	76.9	0.7554	0.16243	0.00211	9.15668	0.17271	0.42171	0.00525	2481.1	12.0	2353.8	16.5	2268.2	23.8	-8.6		2481.1	12.0
JSZ01/2013_G130	419.4	176.3	1.6485	0.18532	0.00232	8.8975	0.14244	0.36016	0.00444	2701.1	11.8	2327.5	16.1	1982.9	21.0	-26.6	Del.		
JSZ01/2013_G131	788.0	252.6	2.1017	0.15428	0.00193	4.90046	0.07511	0.23108	0.00284	2393.9	11.5	1802.3	14.8	1340.2	14.9	-44.0	Del.		
JSZ01/2013_G132	121.5	44.2	0.5094	0.1086	0.00153	4.76159	0.09791	0.3269	0.0041	1776.1	11.8	1778.2	15.9	1823.3	19.9	2.7		1776.1	11.8
JSZ01/2013_G133	461.4	172.7	2.1760	0.1413	0.0018	4.92637	0.07926	0.25966	0.00321	2243.2	11.5	1806.8	15.0	1488.1	16.4	-33.7	Del.		
JSZ01/2013_G134	66.8	11.5	0.4771	0.07087	0.00145	1.53533	0.04266	0.15997	0.0021	953.7	12.7	944.6	15.1	956.6	11.7	1.3		956.6	11.7
JSZ01/2013_G135	244.8	89.9	0.8396	0.11534	0.00156	4.93554	0.09238	0.31961	0.00398	1885.2	11.6	1808.4	15.6	1787.8	19.4	-5.2		1885.2	11.6
JSZ01/2013_G136	706.2	108.2	2.5767	0.13017	0.0017	1.78148	0.02775	0.10046	0.00124	2100.3	11.6	1038.7	11.7	617.1	7.3	-40.6	Del.		
JSZ01/2013_G137	267.9	71.2	0.9742	0.07995	0.00114	2.32034	0.04318	0.21606	0.00269	1195.8	10.0	1218.5	13.5	1261.0	14.3	5.5	Del.		
JSZ01/2013_G138	511.5	108.6	1.2162	0.11579	0.00154	2.81573	0.04657	0.18141	0.00225	1892.2	11.4	1359.7	13.7	1074.7	12.3	-21.0	Del.		
JSZ01/2013_G139	197.6	88.6	0.5723	0.12919	0.0017	6.83806	0.12308	0.39187	0.00486	2087.0	11.7	2090.7	16.1	2131.5	22.5	2.1		2087.0	11.7
JSZ01/2013_G140	121.5	39.1	0.9543	0.10071	0.00147	3.78029	0.07873	0.27187	0.00342	1637.2	11.9	1588.6	15.5	1550.3	17.3	-5.3		1637.2	11.9
JSZ01/2013_G141	158.4	43.7	0.5516	0.08843	0.00128	2.95611	0.05799	0.24882	0.00312	1391.8	11.0	1396.4	14.6	1432.4	16.1	2.9		1391.8	11.0
JSZ01/2013_G142	268.4	43.4	0.3098	0.06986	0.00104	1.52042	0.02823	0.15847	0.00198	924.2	9.0	938.6	11.9	948.3	11.0	1.0		948.3	11.0
JSZ01/2013_G143	181.5	78.8	0.4784	0.12921	0.00172	6.72086	0.12393	0.38822	0.00483	2087.2	11.8	2075.4	16.2	2114.6	22.4	1.3		2087.2	11.8
JSZ01/2013_G144	313.4	80.1	1.6780	0.09678	0.00136	2.54975	0.04623	0.19751	0.00246	1563.0	11.2	1286.4	13.8	1161.9	13.2	-25.7	Del.		
JSZ01/2013_G145	422.8	130.5	0.2926	0.1032	0.00135	4.14487	0.06746	0.30021	0.00371	1682.5	10.7	1663.2	14.8	1692.3	18.4	0.6		1682.5	10.7
JSZ01/2013_G146	305.3	56.6	0.7717	0.07769	0.00112	1.76252	0.03189	0.16646	0.00207	1139.0	9.9	1031.8	12.4	992.6	11.4	-3.8		992.6	11.4
JSZ01/2013_G147	385.4	154.5	1.1377	0.13231	0.00171	6.21222	0.10154	0.34701	0.00429	2128.8	11.5	2006.2	15.7	1920.3	20.5	-9.8		2128.8	11.5
JSZ01/2013_G148	270.2	41.2	0.8815	0.07569	0.00115	1.3549	0.02558	0.13222	0.00166	1086.9	10.1	869.7	11.6	800.5	9.5	-8.0		800.5	9.5
JSZ01/2013_G149	1074.9	231.8	1.7863	0.186	0.00238	4.53812	0.06894	0.17571	0.00217	2707.1	12.1	1738.0	14.8	1043.5	11.9	-40.0	Del.		

Analysis No.	U (ppm)	Pb (ppm)	Th/U	Measured isotopic ratios						Calculated isotopic ages (Ma)						Disc.† (%)	Comment§	Preferred age (Ma)#	
				$^{208}Pb/^{206}Pb$	1σ	$^{207}Pb/^{235}U$	1σ	$^{206}Pb/^{238}U$	1σ	$^{208}Pb/^{206}Pb$	1σ	$^{207}Pb/^{235}U$	1σ	$^{206}Pb/^{238}U$	1σ			Age	1σ
Sample JSZ02/2014, Conglomerate, Lower Jinshanzhai Formation, close to the contact with Wangshan Fm, Jinshanzhai section of Huaibei region, GPS: 33°54'58"N 117°17'03"E																			
JSZ02/2014_G001	295.1	89.4	0.4517	0.09947	0.00124	3.83986	0.05105	0.28005	0.00327	1614.2	10.1	1601.1	13.8	1591.6	16.5	-1.4		1614.2	10.1
JSZ02/2014_G002	424.5	122.5	0.3257	0.12883	0.00155	4.92851	0.06356	0.27753	0.00321	2082.1	10.6	1807.2	14.1	1578.9	16.2	-24.2	Del.		
JSZ02/2014_G003	108.3	61.6	0.6826	0.16735	0.0021	10.98422	0.14754	0.47618	0.00571	2531.3	11.7	2521.8	16.2	2510.6	24.9	-0.8		2531.3	11.7
JSZ02/2014_G004	103.2	38.7	0.6767	0.11402	0.00154	5.09653	0.07221	0.32426	0.00393	1864.5	11.5	1835.5	15.4	1810.5	19.1	-2.9		1864.5	11.5
JSZ02/2014_G005	373.6	138.4	0.2241	0.11954	0.00144	5.89458	0.0761	0.35772	0.00414	1949.4	10.4	1960.4	14.5	1971.4	19.7	1.1		1949.4	10.4
JSZ02/2014_G006	361.5	148.7	0.6160	0.12747	0.00155	6.34151	0.08263	0.3609	0.0042	2063.4	10.7	2024.2	14.8	1986.4	19.9	-3.7		2063.4	10.7
JSZ02/2014_G007	189.3	87.2	0.7813	0.12788	0.00161	6.7743	0.09067	0.38432	0.00454	2069.0	11.1	2082.4	15.3	2096.4	21.1	1.3		2069.0	11.1
JSZ02/2014_G008	105.7	58.8	0.5487	0.16925	0.00212	11.18986	0.15026	0.47964	0.00575	2550.2	11.7	2539.1	16.2	2525.7	25.1	-1.0		2550.2	11.7
JSZ02/2014_G009	54.9	17.0	0.3207	0.1008	0.00159	4.09753	0.06662	0.29491	0.0038	1638.9	12.8	1653.8	16.6	1666.0	18.9	1.7		1638.9	12.8

Analysis No.	U (ppm)	Pb (ppm)	Th/U	Measured isotopic ratios						Calculated isotopic ages (Ma)						Disc.† (%)	Comment§	Preferred age (Ma)#	
				$^{207}Pb/^{206}Pb$	1σ	$^{207}Pb/^{235}U$	1σ	$^{206}Pb/^{238}U$	1σ	$^{207}Pb/^{206}Pb$	1σ	$^{207}Pb/^{235}U$	1σ	$^{206}Pb/^{238}U$	1σ			Age	1σ
Sample JSZ02/2014, Conglomerate, Lower Jinshanzhai Formation, close to the contact with Wangshan Fm, Jinshanzhai section of Huaibei region, GPS: 33°54'58"N 117°17'03"E																			
JSZ02/2014_G010	397.8	167.5	0.6256	0.12865	0.00154	6.49762	0.08363	0.36642	0.00423	2079.6	10.6	2045.6	14.6	2012.5	20.0	-3.2		2079.6	10.6
JSZ02/2014_G011	331.8	132.9	0.4335	0.12834	0.00155	6.47179	0.08385	0.36583	0.00424	2075.4	10.7	2042.1	14.7	2009.7	20.0	-3.2		2075.4	10.7
JSZ02/2014_G012	256.8	120.3	0.8431	0.12864	0.00158	6.82475	0.08957	0.38487	0.0045	2079.5	10.9	2088.9	15.0	2099.0	20.9	0.9		2079.5	10.9
JSZ02/2014_G013	149.5	88.2	0.6892	0.16813	0.00208	11.3231	0.15014	0.4886	0.00579	2539.1	11.5	2550.1	16.0	2564.6	25.1	1.0		2539.1	11.5
JSZ02/2014_G014	248.7	105.4	0.4415	0.12858	0.00158	6.8011	0.08934	0.38375	0.00448	2078.6	10.9	2085.9	15.0	2093.8	20.9	0.7		2078.6	10.9
JSZ02/2014_G015	1439.0	249.7	0.2892	0.12557	0.00149	2.96167	0.03782	0.17111	0.00196	2036.8	10.4	1397.8	12.5	1018.2	10.8	-27.2	Del.		
JSZ02/2014_G016	159.1	68.2	0.5082	0.12979	0.00165	6.83734	0.09258	0.38219	0.00455	2095.1	11.3	2090.6	15.4	2086.5	21.2	-0.4		2095.1	11.3
JSZ02/2014_G017	378.6	113.7	0.3357	0.10263	0.00127	4.03811	0.05329	0.28545	0.00332	1672.2	10.1	1641.9	13.8	1618.8	16.6	-3.2		1672.2	10.1
JSZ02/2014_G018	100.7	43.1	0.4870	0.12909	0.00172	6.81008	0.09588	0.38272	0.00466	2085.6	11.8	2087.0	16.0	2089.0	21.7	0.2		2085.6	11.8
JSZ02/2014_G019	188.8	79.7	0.4763	0.12799	0.0016	6.68143	0.08921	0.37873	0.00446	2070.5	11.0	2070.2	15.2	2070.3	20.9	0.0		2070.5	11.0
JSZ02/2014_G020	316.7	141.5	0.5833	0.12842	0.00156	6.88349	0.08949	0.38887	0.00452	2076.5	10.7	2096.5	14.9	2117.6	21.0	2.0		2076.5	10.7
JSZ02/2014_G021	379.6	152.6	0.6609	0.16713	0.00204	8.13112	0.1064	0.35296	0.00413	2529.1	11.4	2245.7	15.3	1948.7	19.7	-22.9	Del.		
JSZ02/2014_G022	184.8	93.0	0.3082	0.16008	0.00196	10.18377	0.134	0.46152	0.00542	2456.5	11.3	2451.6	15.7	2446.3	23.9	-0.4		2456.5	11.3
JSZ02/2014_G023	385.2	201.2	0.3903	0.16689	0.00199	10.8131	0.13901	0.47005	0.00544	2526.7	11.1	2507.2	15.4	2483.8	23.9	-1.7		2526.7	11.1
JSZ02/2014_G024	200.9	89.9	0.6497	0.12821	0.00161	6.78957	0.09075	0.38419	0.00453	2073.6	11.1	2084.4	15.2	2095.8	21.1	1.1		2073.6	11.1
JSZ02/2014_G025	41.8	20.1	0.7922	0.14141	0.00215	7.79623	0.12363	0.39996	0.00529	2244.5	13.7	2207.8	18.1	2168.9	24.4	-3.4		2244.5	13.7
JSZ02/2014_G026	95.2	22.8	0.8378	0.07913	0.00129	2.19846	0.03657	0.20156	0.00254	1175.4	11.4	1180.6	14.4	1183.7	13.6	0.7		1175.4	11.4
JSZ02/2014_G027	282.5	114.5	0.2832	0.12807	0.00157	6.74972	0.08851	0.38234	0.00446	2071.6	10.8	2079.2	15.0	2087.2	20.8	0.8		2071.6	10.8
JSZ02/2014_G028	255.8	128.3	0.2616	0.15984	0.00194	10.23978	0.1334	0.46475	0.00542	2454.0	11.2	2456.7	15.6	2460.5	23.9	0.3		2454.0	11.2
JSZ02/2014_G029	129.4	57.2	0.9080	0.11996	0.00156	5.92386	0.08179	0.35825	0.00429	1955.6	11.3	1964.7	15.4	1973.9	20.4	0.9		1955.6	11.3
JSZ02/2014_G030	128.4	50.0	0.3017	0.12297	0.0016	6.22059	0.0857	0.36699	0.00439	1999.8	11.4	2007.3	15.5	2015.2	20.7	0.8		1999.8	11.4
JSZ02/2014_G031	187.8	69.7	0.1934	0.12825	0.00162	6.39959	0.08621	0.36201	0.00428	2074.1	11.2	2032.2	15.2	1991.7	20.3	-4.0		2074.1	11.2
JSZ02/2014_G032	96.2	37.0	0.7249	0.11154	0.00155	5.0466	0.07375	0.32823	0.00403	1824.7	11.8	1827.2	15.7	1829.8	19.6	0.3		1824.7	11.8
JSZ02/2014_G033	142.0	62.3	0.5915	0.12926	0.00167	6.83013	0.09369	0.38333	0.00458	2087.9	11.4	2089.6	15.6	2091.8	21.3	0.2		2087.9	11.4
JSZ02/2014_G034	131.4	59.2	0.6876	0.12955	0.00168	6.84395	0.09434	0.38326	0.0046	2091.9	11.5	2091.4	15.7	2091.5	21.4	0.0		2091.9	11.5
JSZ02/2014_G035	276.9	102.0	0.3750	0.12875	0.00159	6.09602	0.08059	0.34351	0.00402	2081.0	10.9	1989.7	14.8	1903.5	19.3	-8.5		2081.0	10.9
JSZ02/2014_G036	469.3	132.0	0.1460	0.10411	0.00128	4.05747	0.05329	0.28274	0.00328	1698.6	10.1	1645.8	13.8	1605.1	16.5	-5.5		1698.6	10.1
JSZ02/2014_G037	54.4	20.2	0.4704	0.11421	0.00179	5.30694	0.08585	0.33709	0.0044	1867.5	13.4	1870.0	17.4	1872.7	21.2	0.3		1867.5	13.4
JSZ02/2014_G038	63.4	29.2	3.6270	0.15534	0.00238	5.16254	0.08085	0.24111	0.00315	2405.6	14.1	1846.5	17.1	1392.5	16.4	-42.1	Del.		
JSZ02/2014_G039	266.9	110.8	0.4062	0.12985	0.00161	6.80717	0.09026	0.38032	0.00446	2095.9	11.0	2086.7	15.1	2077.8	20.8	-0.9		2095.9	11.0
JSZ02/2014_G040	1206.4	233.2	0.2859	0.16559	0.00199	4.37214	0.0564	0.19155	0.00221	2513.6	11.2	1707.1	13.8	1129.8	12.0	-55.1			
JSZ02/2014_G041	162.6	68.7	0.3689	0.13032	0.00166	6.98376	0.09501	0.38879	0.00462	2102.3	11.3	2109.4	15.5	2117.2	21.4	0.7		2102.3	11.3
JSZ02/2014_G042	145.5	57.9	0.4595	0.12015	0.00156	5.96507	0.08234	0.36018	0.0043	1958.4	11.3	1970.8	15.3	1983.0	20.4	1.3		1958.4	11.3
JSZ02/2014_G043	925.9	187.2	0.4305	0.12773	0.00156	3.41009	0.04445	0.19368	0.00224	2067.0	10.8	1506.7	13.2	1141.3	12.1	-44.8	Del.		
JSZ02/2014_G044	198.9	101.2	0.2601	0.15821	0.00196	10.23755	0.13568	0.46945	0.00552	2436.6	11.4	2456.5	15.8	2481.1	24.2	1.8		2436.6	11.4
JSZ02/2014_G045	194.4	84.2	0.5058	0.12929	0.00164	6.86824	0.09291	0.38539	0.00456	2088.3	11.2	2094.6	15.4	2101.4	21.2	0.6		2088.3	11.2
JSZ02/2014_G046	313.7	134.4	0.4264	0.12861	0.00159	6.88829	0.09106	0.38856	0.00454	2079.1	10.9	2097.2	15.1	2116.1	21.1	1.8		2079.1	10.9
JSZ02/2014_G047	129.9	44.2	0.5863	0.10093	0.00139	4.20307	0.0609	0.30211	0.00367	1641.3	11.2	1674.6	15.1	1701.8	18.2	3.7		1641.3	11.2
JSZ02/2014_G048	181.3	83.9	0.6202	0.13314	0.00169	7.31492	0.09893	0.3986	0.00472	2139.8	11.3	2150.6	15.5	2162.6	21.8	1.1		2139.8	11.3
JSZ02/2014_G049	167.7	79.0	0.9097	0.1277	0.00165	6.70193	0.09199	0.38075	0.00454	2066.6	11.4	2072.9	15.5	2079.8	21.2	0.6		2066.6	11.4
JSZ02/2014_G050	220.5	93.2	0.4257	0.12857	0.00162	6.78368	0.09115	0.38278	0.00451	2078.5	11.1	2083.6	15.3	2089.3	21.0	0.5		2078.5	11.1
JSZ02/2014_G051	358.5	85.8	0.4744	0.08838	0.00114	2.69264	0.03687	0.22103	0.0026	1390.8	9.8	1326.4	12.9	1287.3	13.7	-7.4		1390.8	9.8
JSZ02/2014_G052	206.4	78.0	0.6358	0.11989	0.00153	5.47367	0.07448	0.33123	0.00392	1954.6	11.1	1896.5	14.9	1844.3	19.0	-5.6		1954.6	11.1
JSZ02/2014_G053	402.3	172.6	0.5133	0.12838	0.00158	6.73841	0.08865	0.38078	0.00443	2075.9	10.9	2077.7	15.0	2079.9	20.7	0.2		2075.9	10.9
JSZ02/2014_G054	1523.1	91.0	0.3817	0.07765	0.00101	0.59712	0.00821	0.05579	0.00065	1137.9	8.9	475.4	6.6	350.0	4.0	-26.4	Del.		
JSZ02/2014_G055	223.6	109.1	0.1464	0.17097	0.00212	11.06304	0.14687	0.46944	0.00552	2567.2	11.6	2528.5	15.9	2481.1	24.2	-3.4		2567.2	11.6
JSZ02/2014_G056	221.5	107.3	1.0439	0.13803	0.00174	7.21297	0.09694	0.3791	0.00447	2202.6	11.3	2138.1	15.4	2072.1	20.9	-5.9		2202.6	11.3
JSZ02/2014_G057	115.3	73.1	0.7840	0.17143	0.00218	11.98205	0.16327	0.50708	0.00608	2571.7	11.9	2603.0	16.4	2644.2	26.0	2.8		2571.7	11.9
JSZ02/2014_G058	333.8	96.0	0.2249	0.1044	0.00133	4.06918	0.05514	0.28277	0.00332	1703.8	10.5	1648.1	14.1	1605.3	16.7	-5.8		1703.8	10.5
JSZ02/2014_G059	298.6	128.7	0.4751	0.12835	0.0016	6.84191	0.09147	0.38675	0.00454	2075.5	11.0	2091.2	15.2	2107.7	21.1	1.6		2075.5	11.0
JSZ02/2014_G060	140.5	40.6	0.6932	0.09029	0.00126	3.1276	0.04579	0.2513	0.00304	1431.7	10.7	1439.5	14.2	1445.2	15.7	0.9		1431.7	10.7

Analysis No.	U (ppm)	Pb (ppm)	Th/U	Measured isotopic ratios						Calculated isotopic ages (Ma)						Disc.† (%)	Comment§	Preferred age (Ma)#	
				$^{208}Pb/^{206}Pb$	1σ	$^{207}Pb/^{235}U$	1σ	$^{206}Pb/^{238}U$	1σ	$^{207}Pb/^{206}Pb$	1σ	$^{207}Pb/^{235}U$	1σ	$^{206}Pb/^{238}U$	1σ			Age	1σ
Sample JSZ02/2014, Conglomerate, Lower Jinshanzhai Formation, close to the contact with Wangshan Fm, Jinshanzhai section of Huaibei region, GPS: 33°54'58"N 117°17'03"E																			
JSZ02/2014_G061	97.2	27.8	0.7812	0.08958	0.00132	3.00664	0.04597	0.2435	0.003	1416.6	11.3	1409.3	14.6	1404.9	15.6	-0.8		1416.6	11.3
JSZ02/2014_G062	1406.8	95.7	0.6307	0.0852	0.0011	0.74735	0.01021	0.06364	0.00074	1320.1	9.5	566.7	7.5	397.7	4.5	-29.8	Del.		
JSZ02/2014_G063	219.0	85.9	0.3917	0.12778	0.00163	6.36548	0.08645	0.36142	0.00427	2067.7	11.3	2027.5	15.3	1988.9	20.2	-3.8		2067.7	11.3
JSZ02/2014_G064	106.2	48.4	0.6232	0.13112	0.00175	7.0815	0.10007	0.39181	0.00475	2113.0	11.9	2121.7	16.0	2131.2	22.0	0.9		2113.0	11.9
JSZ02/2014_G065	228.6	123.2	0.9714	0.13965	0.00176	8.16625	0.11005	0.42424	0.00501	2222.9	11.4	2249.6	15.6	2279.7	22.7	2.6		2222.9	11.4
JSZ02/2014_G066	147.0	62.7	0.7857	0.15146	0.00197	7.69248	0.10614	0.36848	0.00442	2362.5	11.9	2195.7	15.9	2022.2	20.8	-14.4		2362.5	11.9
JSZ02/2014_G067	126.4	60.6	0.8720	0.12766	0.0017	6.86345	0.09684	0.39004	0.00472	2066.0	11.8	2093.9	15.9	2123.0	21.9	2.8		2066.0	11.8
JSZ02/2014_G068	113.8	49.4	0.4810	0.12857	0.00172	6.88191	0.09743	0.38832	0.00471	2078.5	11.8	2096.3	16.0	2115.0	21.9	1.8		2078.5	11.8
JSZ02/2014_G069	284.0	125.0	0.5226	0.1286	0.00162	6.90393	0.09294	0.3895	0.00458	2078.9	11.1	2099.2	15.3	2120.5	21.2	2.0		2078.9	11.1
JSZ02/2014_G070	198.9	86.2	0.4411	0.13407	0.00172	7.25335	0.09938	0.3925	0.00467	2152.0	11.5	2143.1	15.6	2134.4	21.6	-0.8		2152.0	11.5
JSZ02/2014_G071	465.7	196.5	0.9781	0.1608	0.002	7.5556	0.10056	0.3409	0.00399	2464.1	11.5	2179.6	15.3	1891.0	19.2	-23.3	Del.		
JSZ02/2014_G072	329.3	129.4	0.4364	0.1279	0.0016	6.34791	0.08511	0.36008	0.00422	2069.3	11.0	2025.1	15.0	1982.6	20.0	-4.2		2069.3	11.0
JSZ02/2014_G073	80.1	21.3	0.5823	0.08968	0.00146	2.95793	0.04946	0.23929	0.00307	1418.7	12.4	1396.9	15.7	1383.0	16.0	-2.5		1418.7	12.4
JSZ02/2014_G074	172.7	69.5	0.3999	0.12843	0.00166	6.5574	0.09033	0.37043	0.00441	2076.6	11.4	2053.6	15.5	2031.4	20.7	-2.2		2076.6	11.4
JSZ02/2014_G075	65.5	24.1	0.7834	0.10813	0.00166	4.63489	0.07369	0.31099	0.00398	1768.1	12.9	1755.6	16.7	1745.6	19.6	-1.3		1768.1	12.9
JSZ02/2014_G076	129.4	47.6	0.8004	0.11269	0.00156	4.82266	0.07017	0.31048	0.00379	1843.2	11.8	1788.9	15.5	1743.1	18.6	-5.4		1843.2	11.8
JSZ02/2014_G077	262.3	101.9	0.3236	0.12726	0.00161	6.41441	0.0868	0.36569	0.0043	2060.5	11.2	2034.2	15.2	2009.1	20.3	-2.5		2060.5	11.2
JSZ02/2014_G078	168.2	68.3	0.4660	0.13054	0.00169	6.61609	0.09113	0.36771	0.00438	2105.2	11.5	2061.5	15.5	2018.6	20.6	-4.1		2105.2	11.5
JSZ02/2014_G079	292.0	70.8	0.4925	0.08695	0.00115	2.67296	0.03733	0.22303	0.00264	1359.4	9.9	1321.0	13.1	1297.9	13.9	-4.5		1359.4	9.9
JSZ02/2014_G080	176.2	55.8	0.5005	0.09734	0.00131	3.85449	0.05493	0.28729	0.00344	1573.8	10.8	1604.2	14.5	1628.0	17.2	3.4		1573.8	10.8
JSZ02/2014_G081	125.9	54.6	0.5287	0.1272	0.0017	6.72928	0.09541	0.3838	0.00464	2059.6	11.8	2076.5	15.9	2094.0	21.6	1.7		2059.6	11.8
JSZ02/2014_G082	72.5	30.7	1.1376	0.11088	0.00163	5.01094	0.07691	0.32786	0.00412	1813.9	12.4	1821.2	16.4	1828.0	20.0	0.8		1813.9	12.4
JSZ02/2014_G083	291.0	99.4	0.7081	0.10188	0.00132	4.13449	0.05701	0.29442	0.00348	1658.7	10.6	1661.1	14.3	1663.6	17.3	0.3		1658.7	10.6
JSZ02/2014_G084	68.5	33.5	1.6849	0.11429	0.00168	5.29143	0.08136	0.3359	0.00423	1868.7	12.6	1867.5	16.5	1866.9	20.4	-0.1		1868.7	12.6
JSZ02/2014_G085	329.8	138.2	0.4583	0.12767	0.00162	6.66295	0.09011	0.37864	0.00445	2066.1	11.2	2067.7	15.3	2069.9	20.8	0.2		2066.1	11.2
JSZ02/2014_G086	390.2	145.1	0.9577	0.16011	0.00203	6.8294	0.09245	0.30946	0.00365	2456.8	11.7	2089.5	15.3	1738.0	18.0	-29.3	Del.		
JSZ02/2014_G087	126.4	52.1	0.7571	0.1172	0.00159	5.61409	0.08035	0.34753	0.00421	1914.0	11.7	1918.3	15.7	1922.8	20.1	0.5		1914.0	11.7
JSZ02/2014_G088	155.1	68.9	0.6345	0.12801	0.00168	6.76814	0.09458	0.38359	0.0046	2070.8	11.6	2081.6	15.7	2093.0	21.4	1.1		2070.8	11.6
JSZ02/2014_G089	255.8	110.0	0.7909	0.12613	0.00167	6.27386	0.08794	0.36089	0.00433	2044.7	11.6	2014.8	15.6	1986.4	20.5	-2.9		2044.7	11.6
JSZ02/2014_G090	130.4	40.6	0.6782	0.1121	0.00156	4.13033	0.0603	0.26733	0.00326	1833.7	11.8	1660.3	15.1	1527.2	16.6	-16.7	Del.		
JSZ02/2014_G091	81.6	35.3	0.3664	0.13164	0.00183	7.22491	0.10587	0.39819	0.00492	2120.0	12.4	2139.6	16.6	2160.7	22.7	1.9		2120.0	12.4
JSZ02/2014_G092	154.1	65.3	0.4061	0.12904	0.0017	6.88348	0.09646	0.38701	0.00464	2084.9	11.7	2096.5	15.8	2108.9	21.6	1.2		2084.9	11.7
JSZ02/2014_G093	488.9	109.5	0.2850	0.12665	0.00162	3.83905	0.05234	0.21993	0.00259	2052.0	11.3	1601.0	14.0	1281.5	13.7	-37.5	Del.		
JSZ02/2014_G094	43.3	18.1	0.6886	0.12039	0.0019	5.94736	0.09737	0.3584	0.00471	1962.0	13.7	1968.2	17.9	1974.6	22.4	0.6		1962.0	13.7
JSZ02/2014_G095	255.8	98.4	0.4652	0.13035	0.00168	6.3266	0.08705	0.35215	0.00417	2102.7	11.4	2022.1	15.3	1944.9	19.9	-7.5		2102.7	11.4
JSZ02/2014_G096	215.0	103.9	0.2872	0.15217	0.00195	9.38245	0.12827	0.44733	0.0053	2370.5	11.8	2376.1	16.0	2383.4	23.6	0.5		2370.5	11.8
JSZ02/2014_G097	3136.3	195.9	0.1658	0.10836	0.00137	0.93599	0.01263	0.06267	0.00073	1772.0	10.6	670.8	8.4	391.8	4.4	-77.9	Del.		
JSZ02/2014_G098	535.2	112.8	0.4107	0.12592	0.00162	3.48528	0.04768	0.20081	0.00236	2041.8	11.3	1523.9	13.7	1179.7	12.7	-42.2	Del.		
JSZ02/2014_G099	418.4	169.5	0.4252	0.12892	0.00164	6.5781	0.08931	0.37019	0.00435	2083.3	11.3	2056.4	15.3	2030.3	20.5	-2.5		2083.3	11.3
JSZ02/2014_G100	284.0	123.8	0.5182	0.1291	0.00166	6.88081	0.09441	0.3867	0.00457	2085.8	11.4	2096.2	15.5	2107.5	21.2	1.0		2085.8	11.4
JSZ02/2014_G101	209.5	33.7	0.4024	0.11277	0.0016	2.30204	0.03401	0.14811	0.0018	1844.5	12.1	1212.9	13.2	890.4	10.1	-26.6	Del.		
JSZ02/2014_G102	325.8	126.8	0.4452	0.12836	0.00165	6.28916	0.08608	0.35548	0.00419	2075.6	11.4	2016.9	15.3	1960.7	19.9	-5.5		2075.6	11.4
JSZ02/2014_G103	129.9	74.8	1.1361	0.15557	0.00204	9.41503	0.1318	0.4391	0.00528	2408.1	12.1	2379.3	16.3	2346.6	23.7	-2.6		2408.1	12.1
JSZ02/2014_G104	291.0	98.7	0.6467	0.10225	0.00135	4.18241	0.05852	0.29676	0.00352	1665.4	10.8	1670.6	14.5	1675.2	17.5	0.6		1665.4	10.8
JSZ02/2014_G105	185.3	108.8	2.4758	0.11676	0.00155	5.61701	0.07908	0.34902	0.00417	1907.2	11.4	1918.7	15.4	1929.9	19.9	1.2		1907.2	11.4
JSZ02/2014_G106	223.6	82.0	0.4876	0.12764	0.00168	5.873	0.08228	0.33383	0.00399	2065.7	11.6	1957.3	15.4	1856.9	19.3	-10.1		2065.7	11.6
JSZ02/2014_G107	108.8	65.8	0.7720	0.16914	0.00223	11.43622	0.16107	0.49057	0.00594	2549.2	12.3	2559.4	16.7	2573.1	25.7	0.9		2549.2	12.3
JSZ02/2014_G108	49.8	27.9	1.2519	0.1366	0.00203	7.8473	0.12235	0.4168	0.00537	2184.5	13.3	2213.6	17.7	2245.9	24.4	2.8		2184.5	13.3
JSZ02/2014_G109	263.3	111.9	0.3842	0.12872	0.00167	6.90814	0.09565	0.38939	0.00462	2080.6	11.5	2099.7	15.6	2120.0	21.4	1.9		2080.6	11.5
JSZ02/2014_G110	247.7	102.7	0.3508	0.12787	0.00167	6.76417	0.09383	0.38379	0.00456	2068.9	11.5	2081.0	15.6	2094.0	21.2	1.2		2068.9	11.5
JSZ02/2014_G111	231.6	99.5	0.4459	0.12804	0.00167	6.84498	0.09516	0.38786	0.00461	2071.2	11.5	2091.6	15.6	2112.9	21.4	2.0		2071.2	11.5

Analysis No.	U (ppm)	Pb (ppm)	Th/U	Measured isotopic ratios						Calculated isotopic ages (Ma)						Disc.† (%)	Comment§	Preferred age (Ma)#	
				$^{207}Pb/^{206}Pb$	1σ	$^{207}Pb/^{235}U$	1σ	$^{206}Pb/^{238}U$	1σ	$^{207}Pb/^{206}Pb$	1σ	$^{207}Pb/^{235}U$	1σ	$^{206}Pb/^{238}U$	1σ			Age	1σ
Sample JSZ02/2014, Conglomerate, Lower Jinshanzhai Formation, close to the contact with Wangshan Fm, Jinshanzhai section of Huaibei region, GPS: 33°54'58"N 117°17'03"E																			
JSZ02/2014_G112	231.1	98.7	1.0776	0.11677	0.00154	5.37078	0.07522	0.33371	0.00397	1907.4	11.3	1880.2	15.2	1856.3	19.2	-2.7		1907.4	11.3
JSZ02/2014_G113	95.2	43.9	0.4895	0.13696	0.00189	7.73483	0.11285	0.40974	0.00504	2189.1	12.4	2200.7	16.6	2213.7	23.0	1.1		2189.1	12.4
JSZ02/2014_G114	265.9	107.5	0.4416	0.12858	0.00169	6.53242	0.09113	0.36861	0.00439	2078.6	11.6	2050.3	15.6	2022.9	20.7	-2.7		2078.6	11.6
JSZ02/2014_G115	91.6	27.7	0.6442	0.11732	0.00176	4.21405	0.06558	0.26061	0.00328	1915.8	12.9	1676.8	16.1	1493.0	16.8	-22.1	Del.		
JSZ02/2014_G116	362.5	123.1	0.2284	0.12598	0.00164	5.75958	0.07966	0.33171	0.00392	2042.6	11.5	1940.4	15.2	1846.7	19.0	-9.6		2042.6	11.5
JSZ02/2014_G117	90.1	36.0	0.4639	0.12137	0.00173	6.0526	0.09048	0.36182	0.00448	1976.5	12.4	1983.4	16.5	1990.8	21.2	0.7		1976.5	12.4
JSZ02/2014_G118	235.6	97.1	0.4323	0.12688	0.00167	6.55319	0.09163	0.37474	0.00446	2055.2	11.6	2053.1	15.6	2051.7	20.9	-0.2		2055.2	11.6
JSZ02/2014_G119	247.2	104.1	0.7131	0.118	0.00156	5.82057	0.0817	0.35789	0.00426	1926.2	11.4	1949.5	15.4	1972.2	20.2	2.4		1926.2	11.4
JSZ02/2014_G120	395.3	172.6	0.5495	0.12663	0.00164	6.70595	0.09253	0.38422	0.00454	2051.7	11.4	2073.4	15.5	2096.0	21.1	2.2		2051.7	11.4
JSZ02/2014_G121	243.2	151.5	1.0754	0.16332	0.00212	10.72056	0.14864	0.47626	0.00566	2490.3	12.0	2499.2	16.3	2511.0	24.7	0.8		2490.3	12.0
JSZ02/2014_G122	156.6	91.4	0.9122	0.15627	0.00208	9.97052	0.141	0.46293	0.00558	2415.7	12.3	2432.1	16.6	2452.5	24.6	1.5		2415.7	12.3
JSZ02/2014_G123	256.8	108.5	0.4429	0.12831	0.00169	6.76017	0.09486	0.38228	0.00456	2074.9	11.6	2080.5	15.7	2086.9	21.3	0.6		2074.9	11.6
JSZ02/2014_G124	299.1	121.1	0.4502	0.12758	0.00167	6.46813	0.09031	0.36785	0.00437	2064.9	11.6	2041.6	15.5	2019.3	20.6	-2.2		2064.9	11.6
JSZ02/2014_G125	110.3	40.4	1.7958	0.08827	0.00133	3.02336	0.04727	0.24853	0.00308	1388.4	11.4	1413.5	14.9	1430.9	15.9	3.1		1388.4	11.4
JSZ02/2014_G126	171.2	72.8	0.4287	0.12882	0.00173	6.84987	0.09759	0.38581	0.00464	2081.9	11.9	2092.2	16.0	2103.4	21.6	1.0		2081.9	11.9
JSZ02/2014_G127	36.8	16.7	0.4176	0.13637	0.00214	7.72435	0.12658	0.41098	0.00546	2181.6	14.1	2199.4	18.5	2219.4	24.9	1.7		2181.6	14.1
JSZ02/2014_G128	106.7	47.9	0.6242	0.13093	0.00182	7.00463	0.10301	0.38817	0.00477	2110.5	12.3	2112.0	16.5	2114.3	22.2	0.2		2110.5	12.3
JSZ02/2014_G129	68.5	38.8	1.7599	0.12708	0.00185	6.70951	0.10269	0.38308	0.00482	2058.0	12.8	2073.9	17.0	2090.7	22.5	1.6		2058.0	12.8
JSZ02/2014_G130	54.4	15.9	0.7628	0.09044	0.00161	3.12133	0.05639	0.2504	0.00334	1434.8	13.7	1438.0	17.1	1440.5	17.2	0.4		1434.8	13.7
JSZ02/2014_G131	73.5	47.1	0.6112	0.18563	0.00255	13.61391	0.19874	0.53211	0.00661	2703.8	13.0	2723.2	17.5	2750.3	27.8	1.7		2703.8	13.0
JSZ02/2014_G132	98.2	37.9	0.7065	0.11112	0.00161	5.06508	0.0768	0.33073	0.0041	1817.8	12.3	1830.3	16.2	1841.9	19.9	1.3		1817.8	12.3
JSZ02/2014_G133	113.8	57.2	0.2670	0.16077	0.00219	10.31878	0.14932	0.46569	0.0057	2463.8	12.6	2463.8	17.0	2464.6	25.1	0.0		2463.8	12.6
JSZ02/2014_G134	258.8	98.6	0.3202	0.11775	0.00157	5.80913	0.08236	0.35794	0.00428	1922.4	11.5	1947.8	15.5	1972.4	20.3	2.6		1922.4	11.5
JSZ02/2014_G135	233.6	78.6	0.6178	0.10251	0.00139	4.19063	0.06018	0.29661	0.00355	1670.1	11.1	1672.2	14.8	1674.5	17.6	0.3		1670.1	11.1
JSZ02/2014_G136	344.9	128.7	0.3988	0.12702	0.00167	6.06632	0.08502	0.34653	0.00412	2057.1	11.6	1985.4	15.5	1918.0	19.7	-6.8		2057.1	11.6
JSZ02/2014_G137	109.8	36.2	0.4638	0.10054	0.00149	4.18234	0.06474	0.30181	0.00376	1634.1	12.0	1670.6	15.9	1700.3	18.6	4.1		1634.1	12.0
JSZ02/2014_G138	347.4	134.7	0.2982	0.12256	0.00161	6.18162	0.08671	0.36595	0.00435	1993.8	11.5	2001.9	15.5	2010.3	20.5	0.8		1993.8	11.5
JSZ02/2014_G139	42.3	22.5	1.0439	0.13856	0.00214	7.92061	0.1279	0.41475	0.00545	2209.3	13.9	2222.0	18.3	2236.6	24.8	1.2		2209.3	13.9
JSZ02/2014_G140	74.0	28.9	0.8707	0.11101	0.00168	4.93246	0.07789	0.32239	0.00408	1816.0	12.8	1807.8	16.7	1801.4	19.9	-0.8		1816.0	12.8
JSZ02/2014_G141	99.7	48.6	0.7909	0.13591	0.00192	7.56859	0.1127	0.40406	0.005	2175.7	12.7	2181.1	16.8	2187.7	23.0	0.6		2175.7	12.7
JSZ02/2014_G142	168.2	61.5	0.8374	0.10536	0.00149	4.42448	0.06566	0.3047	0.00371	1720.6	11.7	1716.9	15.5	1714.6	18.3	-0.4		1720.6	11.7
JSZ02/2014_G143	223.6	69.9	0.3306	0.10268	0.00142	4.21024	0.06149	0.29752	0.00359	1673.1	11.3	1676.0	15.1	1679.0	17.8	0.4		1673.1	11.3
JSZ02/2014_G144	172.7	85.1	0.8722	0.138	0.00187	7.63848	0.10982	0.4016	0.00485	2202.3	12.2	2189.4	16.3	2176.4	22.3	-1.2		2202.3	12.2
JSZ02/2014_G145	68.5	39.1	0.5585	0.17285	0.00244	11.66843	0.17449	0.48979	0.00616	2585.4	13.2	2578.2	17.7	2569.8	26.7	-0.6		2585.4	13.2
JSZ02/2014_G146	147.0	65.9	0.8492	0.12834	0.00178	6.54225	0.09586	0.36986	0.00451	2075.4	12.3	2051.6	16.3	2028.7	21.2	-2.2		2075.4	12.3
JSZ02/2014_G147	231.1	87.6	0.4481	0.12818	0.00173	6.13772	0.08795	0.34744	0.00417	2073.2	11.9	1995.6	15.8	1922.4	20.0	-7.3		2073.2	11.9

Analysis No.	U (ppm)	Pb (ppm)	Th/U	Measured isotopic ratios						Calculated isotopic ages (Ma)						Disc.† (%)	Comment§	Preferred age (Ma)#	
				$^{207}Pb/^{206}Pb$	1σ	$^{207}Pb/^{235}U$	1σ	$^{206}Pb/^{238}U$	1σ	$^{207}Pb/^{206}Pb$	1σ	$^{207}Pb/^{235}U$	1σ	$^{206}Pb/^{238}U$	1σ			Age	1σ
Sample SJ01/2014, quartz sandstone, Upper Shijia Formation, close to the contact with Wangshan Fm. Heifengling section of Huaibei region																			
SJ01/2014_G001	211.1	77.2	0.8387	0.10195	0.00161	4.25611	0.06686	0.30289	0.00362	1659.9	12.9	1684.9	16.3	1705.6	17.9	2.8		1659.9	12.9
SJ01/2014_G002	158.6	44.2	0.7551	0.08755	0.00153	2.87956	0.0495	0.23865	0.00294	1372.6	13.2	1376.6	16.1	1379.7	15.3	0.5		1372.6	13.2
SJ01/2014_G003	370.2	70.2	0.7341	0.08349	0.00139	1.98292	0.03248	0.17232	0.00205	1280.7	12.1	1109.7	13.8	1024.9	11.3	-7.6		1024.9	11.3
SJ01/2014_G004	167.4	53	0.3724	0.10332	0.00166	4.23655	0.06763	0.2975	0.00359	1684.6	13.2	1681.1	16.5	1678.9	17.8	-0.3		1684.6	13.2
SJ01/2014_G005	169.4	63.8	0.8853	0.1041	0.00172	4.40054	0.07214	0.30671	0.00377	1698.5	13.6	1712.4	17	1724.5	18.6	1.5		1698.5	13.6
SJ01/2014_G006	755.9	199.9	0.693	0.09865	0.00144	3.17324	0.04602	0.23338	0.00265	1598.8	11.8	1450.7	14.3	1352.2	13.9	-15.4	Del.		
SJ01/2014_G007	160.7	56.7	0.6385	0.09957	0.00209	4.18987	0.08676	0.30533	0.00438	1616.1	17	1672	20.8	1717.7	21.6	6.3	Del.		
SJ01/2014_G008	320.8	87.4	0.7433	0.08653	0.00134	2.80242	0.04293	0.23499	0.00272	1350	11.6	1356.2	14.5	1360.6	14.2	0.8		1350	11.6
SJ01/2014_G009	746.7	188.5	1.3814	0.0905	0.00134	2.42377	0.03573	0.19432	0.00221	1436.1	11.4	1249.7	13.4	1144.7	11.9	-20.3	Del.		

Analysis No.	U (ppm)	Pb (ppm)	Th/U	Measured isotopic ratios						Calculated isotopic ages (Ma)						Disc.† (%)	Comment§	Preferred age (Ma)#	
				$^{207}Pb/^{206}Pb$	1σ	$^{207}Pb/^{235}U$	1σ	$^{206}Pb/^{238}U$	1σ	$^{207}Pb/^{206}Pb$	1σ	$^{207}Pb/^{235}U$	1σ	$^{206}Pb/^{238}U$	1σ			Age	1σ
Sample SJ01/2014, quartz sandstone, Upper Shijia Formation, close to the contact with Wangshan Fm. Heifengling section of Huaibei region																			
SJ01/2014_G010	122.6	32.4	0.4157	0.0904	0.00165	3.07847	0.05518	0.24707	0.00313	1434	14	1427.3	17	1423.3	16.2	-0.7		1434	14
SJ01/2014_G011	671	112.3	0.298	0.07657	0.00114	1.76674	0.02614	0.16742	0.00189	1110	10.1	1033.3	12.1	997.9	10.4	-3.4		997.9	10.4
SJ01/2014_G012	392.9	97.9	0.8168	0.07962	0.00122	2.31332	0.03518	0.2108	0.00242	1187.6	10.7	1216.4	13.6	1233.1	12.9	3.8		1187.6	10.7
SJ01/2014_G013	103.5	25.7	0.9687	0.07837	0.00165	2.19411	0.04509	0.20314	0.0027	1156.3	14.5	1179.2	17.4	1192.2	14.5	3.1		1156.3	14.5
SJ01/2014_G014	378	139	0.8094	0.10904	0.00157	4.64497	0.06666	0.30908	0.00351	1783.4	12.1	1757.4	15.3	1736.2	17.3	-2.6		1783.4	12.1
SJ01/2014_G015	230.2	62.1	1.2864	0.07789	0.00135	2.19585	0.03763	0.20456	0.00247	1144.1	11.9	1179.7	14.7	1199.8	13.2	4.9		1144.1	11.9
SJ01/2014_G016	168.4	44.7	0.3698	0.08846	0.00149	3.06476	0.05092	0.25138	0.00304	1392.5	12.8	1423.9	15.9	1445.6	15.7	3.8		1392.5	12.8
SJ01/2014_G017	384.2	79.9	0.6176	0.07734	0.00123	1.98365	0.03108	0.18609	0.00215	1130	10.8	1110	13.3	1100.2	11.7	-2.6		1130	10.8
SJ01/2014_G018	263.7	90.6	0.4742	0.10715	0.00161	4.63755	0.06939	0.31404	0.00365	1751.5	12.5	1756.1	15.9	1760.6	17.9	0.5		1751.5	12.5
SJ01/2014_G019	303.3	80	0.999	0.082	0.00131	2.42207	0.03843	0.21431	0.00251	1245.5	11.5	1249.2	14.2	1251.7	13.3	0.5		1245.5	11.5
SJ01/2014_G020	307.9	103.9	0.9979	0.10863	0.00162	4.52892	0.06724	0.30249	0.0035	1776.6	12.5	1736.3	15.7	1703.6	17.3	-4.1		1776.6	12.5
SJ01/2014_G021	78.3	21.5	0.5152	0.09468	0.00197	3.25037	0.0661	0.24908	0.00344	1521.7	16.4	1469.3	19.4	1433.7	17.8	-5.8		1521.7	16.4
SJ01/2014_G022	323.4	87	0.456	0.13492	0.00197	4.96993	0.07228	0.26727	0.00307	2163	13.1	1814.2	15.7	1526.9	15.6	-29.4	Del.		
SJ01/2014_G023	315.1	116.5	0.7717	0.10774	0.00159	4.65626	0.06837	0.31358	0.0036	1761.5	12.3	1759.4	15.6	1758.3	17.7	-0.2		1761.5	12.3
SJ01/2014_G024	109.2	63.9	0.6691	0.16958	0.00264	11.38427	0.17888	0.48708	0.00613	2553.5	14.5	2555.1	18.7	2558	26.6	0.2		2553.5	14.5
SJ01/2014_G025	246.7	86.9	0.145	0.11285	0.00168	5.40805	0.08041	0.34771	0.00403	1845.8	12.7	1886.1	16.2	1923.7	19.3	4.2		1845.8	12.7
SJ01/2014_G026	96.3	30.6	0.6256	0.09747	0.00182	3.74809	0.06898	0.27901	0.00364	1576.3	14.9	1581.7	18.3	1586.4	18.3	0.6		1576.3	14.9
SJ01/2014_G027	356.9	108.2	0.676	0.09273	0.00139	3.38532	0.05041	0.26489	0.00303	1482.4	11.7	1501	14.8	1514.8	15.4	2.2		1482.4	11.7
SJ01/2014_G028	469.6	102.1	0.4975	0.07991	0.00122	2.22476	0.03366	0.20201	0.00231	1194.8	10.7	1188.9	13.4	1186.1	12.4	-0.7		1194.8	10.7
SJ01/2014_G029	358.9	105	0.7408	0.08831	0.00134	3.06314	0.04617	0.25166	0.00289	1389.2	11.5	1423.5	14.6	1447	14.9	4.2		1389.2	11.5
SJ01/2014_G030	241.5	73	0.8554	0.09467	0.00149	3.29241	0.05155	0.25233	0.00297	1521.5	12.4	1479.3	15.3	1450.5	15.3	-4.7		1521.5	12.4
SJ01/2014_G031	177.7	45.5	0.9949	0.08139	0.00145	2.32927	0.04072	0.20764	0.00254	1230.9	12.7	1221.3	15.4	1216.2	13.6	-1.2		1230.9	12.7
SJ01/2014_G032	90.1	28.7	0.4767	0.11012	0.00201	4.45922	0.08017	0.2938	0.00383	1801.4	15.4	1723.4	18.6	1660.5	19.1	-7.8		1801.4	15.4
SJ01/2014_G033	328	85.2	0.8057	0.08647	0.00137	2.62876	0.04121	0.22056	0.00257	1348.7	11.8	1308.7	14.5	1284.8	13.6	-4.7		1348.7	11.8
SJ01/2014_G034	201.3	50	0.9292	0.08184	0.00143	2.31546	0.03973	0.20527	0.00249	1241.7	12.5	1217	15.1	1203.6	13.3	-3.1		1241.7	12.5
SJ01/2014_G035	277	67.8	1.0054	0.079	0.00132	2.15333	0.03548	0.19776	0.00234	1172.1	11.6	1166.1	14.2	1163.3	12.6	-0.8		1172.1	11.6
SJ01/2014_G036	408.9	114.6	0.6669	0.0902	0.00137	3.05796	0.04604	0.24596	0.00282	1429.8	11.6	1422.2	14.6	1417.6	14.6	-0.9		1429.8	11.6
SJ01/2014_G037	257.5	66.6	1.1095	0.07955	0.00133	2.23138	0.03692	0.20352	0.00242	1185.9	11.7	1191	14.4	1194.2	13	0.7		1185.9	11.7
SJ01/2014_G038	413.5	190.5	1.2522	0.1575	0.00225	8.21993	0.11728	0.37867	0.00429	2429	13.2	2255.5	16.5	2070.1	20.1	-14.8		2429	13.2
SJ01/2014_G039	69	19.8	0.4234	0.09413	0.00196	3.46241	0.07096	0.26688	0.00369	1510.7	16.4	1518.7	19.7	1524.9	18.8	0.9		1510.7	16.4
SJ01/2014_G040	231.2	139	1.2072	0.156	0.00229	9.66095	0.14204	0.44931	0.00522	2412.8	13.5	2403	17.2	2392.2	23.2	-0.9		2412.8	13.5
SJ01/2014_G041	429	90.1	0.2347	0.08318	0.00129	2.38007	0.03663	0.20759	0.00238	1273.4	11.3	1236.6	13.8	1216	12.7	-4.5		1273.4	11.3
SJ01/2014_G042	279.6	75.9	0.3123	0.09118	0.00144	3.27087	0.05126	0.26029	0.00304	1450.4	12.2	1474.2	15.3	1491.3	15.5	2.8		1450.4	12.2
SJ01/2014_G043	382.6	120.7	0.6664	0.11145	0.00166	4.44906	0.06605	0.28963	0.00332	1823.2	12.6	1721.5	15.6	1639.7	16.6	-10.1		1823.2	12.6
SJ01/2014_G044	1278.6	212.1	0.1637	0.07748	0.00113	1.81216	0.02631	0.16969	0.00189	1133.6	10	1049.9	12	1010.4	10.4	-3.8		1010.4	10.4
SJ01/2014_G045	270.9	86.3	0.8276	0.09532	0.00151	3.52118	0.05523	0.26802	0.00314	1534.4	12.5	1532	15.6	1530.7	16	-0.2		1534.4	12.5
SJ01/2014_G046	460.4	131.1	1.1403	0.09702	0.00148	3.09662	0.04696	0.23158	0.00266	1567.6	12.2	1431.9	14.7	1342.8	13.9	-14.3		1567.6	12.2
SJ01/2014_G047	335.2	165.7	0.6309	0.14537	0.00212	8.48053	0.12372	0.42327	0.00484	2292.2	13.3	2283.8	16.8	2275.3	21.9	-0.7		2292.2	13.3
SJ01/2014_G048	235.8	59.2	0.4567	0.0853	0.00145	2.73656	0.04582	0.23277	0.00279	1322.4	12.6	1338.4	15.5	1349	14.6	2		1322.4	12.6
SJ01/2014_G049	92.7	29.6	0.8414	0.09271	0.00182	3.37856	0.06522	0.2644	0.0035	1482	15.3	1499.4	18.6	1512.3	17.8	2		1482	15.3
SJ01/2014_G050	19.1	4.5	0.0652	0.09333	0.00347	3.16792	0.11435	0.24626	0.00502	1494.6	29.1	1449.4	32.7	1419.2	26	-5		1494.6	29.1
SJ01/2014_G051	473.8	80.2	0.3028	0.07665	0.00126	1.79394	0.02919	0.16981	0.00198	1112.1	11.1	1043.3	13.1	1011.1	10.9	-3.1		1011.1	10.9
SJ01/2014_G052	297.1	89.5	0.4726	0.10062	0.00159	3.89719	0.0611	0.28101	0.00329	1635.6	12.8	1613.1	15.9	1596.4	16.6	-2.4		1635.6	12.8
SJ01/2014_G053	732.3	211.5	0.2173	0.11202	0.00165	4.42892	0.06482	0.28686	0.00323	1832.4	12.5	1717.8	15.4	1625.8	16.2	-11.3		1832.4	12.5
SJ01/2014_G054	336.3	106.8	0.933	0.09514	0.00151	3.39955	0.05334	0.25926	0.00302	1530.8	12.5	1504.3	15.4	1486.1	15.5	-2.9		1530.8	12.5
SJ01/2014_G055	835.2	222.6	0.6552	0.09646	0.00144	3.13674	0.04658	0.23593	0.00266	1556.7	11.9	1441.8	14.4	1365.5	13.9	-12.3		1556.7	11.9
SJ01/2014_G056	163.2	41.1	1.2037	0.09773	0.00177	2.83358	0.05034	0.21037	0.00263	1581.3	14.5	1364.5	16.5	1230.8	14	-22.2	Del.		

Analysis No.	U (ppm)	Pb (ppm)	Th/U	Measured isotopic ratios						Calculated isotopic ages (Ma)						Disc.† (%)	Comment§	Preferred age (Ma)#	
				$^{207}Pb/^{206}Pb$	1σ	$^{207}Pb/^{235}U$	1σ	$^{206}Pb/^{238}U$	1σ	$^{207}Pb/^{206}Pb$	1σ	$^{207}Pb/^{235}U$	1σ	$^{206}Pb/^{238}U$	1σ			Age	1σ
Sample SJ01/2014, quartz sandstone, Upper Shijia Formation, close to the contact with Wangshan Fm. Heifengling section of Huaibei region																			
SJ01/2014_G057	351.7	65	0.4661	0.07549	0.00129	1.80273	0.03036	0.17327	0.00205	1081.6	11.4	1046.4	13.6	1030.1	11.3	-1.6		1030.1	11.3
SJ01/2014_G058	670.5	104.2	0.4603	0.08101	0.0013	1.69335	0.02687	0.15167	0.00175	1221.7	11.4	1006	12.6	910.3	9.8	-9.5		910.3	9.8
SJ01/2014_G059	208	43.7	0.4093	0.08856	0.00157	2.45114	0.04278	0.2008	0.00245	1394.7	13.4	1257.8	15.5	1179.6	13.2	-15.4	Del.		
SJ01/2014_G060	172	43	1.0419	0.08001	0.00151	2.211	0.04087	0.2005	0.0025	1197.2	13.3	1184.5	15.8	1178	13.4	-1.6		1197.2	13.3
SJ01/2014_G061	327	101.8	0.2325	0.10449	0.00164	4.37212	0.06805	0.30358	0.00352	1705.4	13	1707.1	16.1	1709	17.4	0.2		1705.4	13
SJ01/2014_G062	135.4	70.4	0.0937	0.20739	0.00338	14.68373	0.24057	0.51371	0.00658	2885.3	15.6	2795	19.7	2672.4	28	-7.4		2885.3	15.6
SJ01/2014_G063	318.8	93.1	0.7939	0.10081	0.00162	3.55019	0.05642	0.2555	0.00299	1639.1	13.1	1538.5	15.8	1466.8	15.4	-10.5		1639.1	13.1
SJ01/2014_G064	739.5	270.9	0.3359	0.16547	0.00245	8.24496	0.12176	0.36152	0.00408	2512.3	13.8	2258.3	16.9	1989.4	19.3	-20.8	Del.		
SJ01/2014_G065	156.5	56.1	0.1974	0.11516	0.00198	5.53221	0.09442	0.34853	0.00434	1882.4	14.7	1905.6	18.3	1927.6	20.7	2.4		1882.4	14.7
SJ01/2014_G066	976.3	239.3	0.3615	0.11952	0.00181	4.01081	0.06025	0.24347	0.00275	1949.1	13.1	1636.4	15.4	1404.7	14.3	-27.9	Del.		
SJ01/2014_G067	287.3	76.2	0.6226	0.09424	0.00157	3.08703	0.05082	0.23766	0.00282	1512.9	13.1	1429.5	15.7	1374.5	14.7	-9.1		1512.9	13.1
SJ01/2014_G068	176.6	98.7	0.3052	0.18167	0.00296	12.76791	0.20831	0.50992	0.00638	2668.2	15.3	2662.7	19.3	2656.3	27.2	-0.4		2668.2	15.3
SJ01/2014_G069	280.1	57.9	0.8915	0.07739	0.00137	1.86537	0.03251	0.17488	0.0021	1131.3	12.1	1068.9	14.1	1038.9	11.5	-2.8		1038.9	11.5
SJ01/2014_G070	160.7	40	1.0014	0.08311	0.00179	2.30498	0.04829	0.20122	0.00271	1271.8	15.6	1213.8	18	1181.9	14.5	-7.1		1271.8	15.6
SJ01/2014_G071	79.8	58.1	1.4339	0.1826	0.00313	12.86171	0.22193	0.51103	0.00675	2676.6	16.2	2669.6	20.4	2661	28.8	-0.6		2676.6	16.2
SJ01/2014_G072	192.6	42.5	0.4075	0.08003	0.00151	2.30633	0.04277	0.20909	0.00261	1197.7	13.3	1214.2	16	1224	13.9	2.2		1197.7	13.3
SJ01/2014_G073	106.6	28.3	0.6818	0.08893	0.00182	2.83083	0.05679	0.23096	0.00306	1402.7	15.6	1363.7	18.3	1339.5	16	-4.5		1402.7	15.6
SJ01/2014_G074	582.9	142.5	0.9036	0.08789	0.00147	2.49521	0.04124	0.20598	0.00242	1380.1	12.6	1270.6	14.8	1207.4	12.9	-12.5		1380.1	12.6
SJ01/2014_G075	55.6	15.7	0.9762	0.07483	0.00217	2.37918	0.06738	0.23067	0.00372	1063.9	19.1	1236.4	23.7	1338	19.5	25.8	Del.		
SJ01/2014_G076	359.9	196	0.3284	0.18594	0.00298	12.86123	0.20579	0.50184	0.00606	2706.6	15.1	2669.5	18.9	2621.7	26	-3.1		2706.6	15.1
SJ01/2014_G077	164.3	43.1	0.563	0.08481	0.00166	2.76732	0.05337	0.23674	0.00306	1311.2	14.4	1346.8	17.5	1369.7	16	4.5		1311.2	14.4
SJ01/2014_G078	1112.8	210.2	0.1278	0.07154	0.00116	1.91232	0.03064	0.19395	0.00221	972.9	10.1	1085.4	13.2	1142.7	11.9	17.5	Del.		
SJ01/2014_G079	241	48.6	0.3734	0.07621	0.00143	2.02719	0.03735	0.193	0.00238	1100.6	12.6	1124.7	15.3	1137.6	12.9	3.4		1100.6	12.6
SJ01/2014_G080	129.8	37	0.6049	0.09219	0.00179	3.22805	0.06143	0.25405	0.00327	1471.3	15.1	1463.9	18.1	1459.3	16.8	-0.8		1471.3	15.1
SJ01/2014_G081	216.3	59.5	0.4674	0.0918	0.00166	3.22019	0.05745	0.2545	0.00314	1463.3	14	1462	17	1461.6	16.1	-0.1		1463.3	14
SJ01/2014_G082	274.5	55	0.4042	0.07521	0.00146	1.96854	0.03732	0.18991	0.00237	1074.1	12.9	1104.8	15.5	1120.9	12.8	4.4		1074.1	12.9
SJ01/2014_G083	281.2	62.8	0.4472	0.07825	0.00139	2.25503	0.03947	0.20909	0.00251	1153.2	12.2	1198.4	15.1	1224	13.4	6.1	Del.		
SJ01/2014_G084	192.1	72.3	0.6349	0.11257	0.00194	5.08189	0.08668	0.32753	0.00397	1841.3	14.6	1833.1	17.9	1826.4	19.3	-0.8		1841.3	14.6
SJ01/2014_G085	167.4	35.2	0.4598	0.08221	0.00164	2.2305	0.0434	0.19685	0.00251	1250.5	14.3	1190.7	16.6	1158.4	13.5	-7.4		1250.5	14.3
SJ01/2014_G086	201.9	44	0.4032	0.07689	0.00147	2.18148	0.04097	0.20584	0.00256	1118.3	13	1175.2	15.9	1206.6	13.7	7.9	Del.		
SJ01/2014_G087	139	32.7	0.8288	0.07815	0.00167	2.152	0.04491	0.19978	0.00264	1150.7	14.7	1165.7	17.4	1174.1	14.2	2		1150.7	14.7
SJ01/2014_G088	241.5	67.1	0.5302	0.0924	0.00163	3.20897	0.05579	0.25196	0.00304	1475.6	13.7	1459.3	16.5	1448.6	15.7	-1.8		1475.6	13.7
SJ01/2014_G089	249.8	57.4	0.849	0.08308	0.00153	2.2746	0.04112	0.19864	0.00243	1271.1	13.4	1204.4	15.6	1168	13.1	-8.1		1271.1	13.4
SJ01/2014_G090	160.7	37.1	0.7229	0.08279	0.00164	2.30727	0.0446	0.20219	0.00257	1264.3	14.3	1214.5	16.7	1187.1	13.8	-6.1		1264.3	14.3
SJ01/2014_G091	251.8	55.9	0.2806	0.08038	0.00149	2.40352	0.04385	0.21694	0.00266	1206.3	13.1	1243.7	15.9	1265.7	14.1	4.9		1206.3	13.1
SJ01/2014_G092	317.7	73.1	0.3069	0.08499	0.00151	2.61787	0.04585	0.22347	0.00268	1315.3	13.1	1305.7	15.8	1300.2	14.1	-1.2		1315.3	13.1
SJ01/2014_G093	174.1	50.4	0.3364	0.09799	0.00181	3.71373	0.06734	0.27496	0.00342	1586.2	14.8	1574.3	17.8	1565.9	17.3	-1.3		1586.2	14.8
SJ01/2014_G094	164.3	35.4	0.5228	0.07652	0.00156	2.08646	0.0416	0.19783	0.00253	1108.7	13.8	1144.4	16.5	1163.7	13.6	5		1108.7	13.8
SJ01/2014_G095	189.5	69.2	0.7969	0.11521	0.00214	4.91594	0.08991	0.30958	0.00394	1883.2	15.9	1805	19	1738.6	19.4	-7.7		1883.2	15.9
SJ01/2014_G096	207.5	47.1	1.1229	0.09049	0.00218	2.40828	0.05607	0.19309	0.0028	1435.9	18.5	1245.1	20.2	1138.1	15.1	-20.7	Del.		
SJ01/2014_G097	120	41.3	0.7583	0.10576	0.00211	4.27666	0.08395	0.29339	0.0039	1727.6	16.6	1688.9	19.7	1658.4	19.4	-4		1727.6	16.6
SJ01/2014_G098	376.4	146.8	0.1652	0.12757	0.00215	6.68572	0.11157	0.38023	0.0045	2064.8	14.9	2070.7	18.2	2077.4	21	0.6		2064.8	14.9
SJ01/2014_G099	298.2	135	0.1354	0.16153	0.00271	9.82695	0.16319	0.44139	0.00525	2471.7	15.5	2418.7	19	2356.9	23.5	-4.6		2471.7	15.5
SJ01/2014_G100	69	22.6	0.8973	0.10023	0.00227	3.73951	0.08267	0.27069	0.00389	1628.4	18.4	1579.9	21.5	1544.3	19.7	-5.2		1628.4	18.4
SJ01/2014_G101	29.9	6.7	0.938	0.07325	0.00277	1.853	0.06777	0.18353	0.00343	1020.9	24.3	1064.5	27.8	1086.2	18.7	2		1086.2	18.7
SJ01/2014_G102	288.9	81.6	0.5919	0.216	0.00391	7.09793	0.12556	0.23841	0.00304	2951.1	17.4	2123.8	19.7	1378.4	15.8	-53.3	Del.		
SJ01/2014_G103	186.4	43.3	0.5465	0.08718	0.00172	2.57124	0.04953	0.21397	0.0027	1364.5	14.8	1292.5	17.1	1249.9	14.3	-8.4		1364.5	14.8

Analysis No.	U (ppm)	Pb (ppm)	Th/U	Measured isotopic ratios						Calculated isotopic ages (Ma)						Disc.† (%)	Comment§	Preferred age (Ma)#	
				$^{207}Pb/^{206}Pb$	1σ	$^{207}Pb/^{235}U$	1σ	$^{206}Pb/^{238}U$	1σ	$^{207}Pb/^{206}Pb$	1σ	$^{207}Pb/^{235}U$	1σ	$^{206}Pb/^{238}U$	1σ			Age	1σ
Sample SJ01/2014, quartz sandstone, Upper Shijia Formation, close to the contact with Wangshan Fm. Heifengling section of Huaibei region																			
SJ01/2014_G104	442.9	103.6	0.5049	0.08586	0.00154	2.51904	0.04427	0.21285	0.00254	1335	13.3	1277.5	15.7	1244	13.5	-6.8		1335	13.3
SJ01/2014_G105	553.1	184.6	0.7318	0.09862	0.0017	3.88149	0.06595	0.28556	0.00335	1598.2	13.9	1609.8	16.8	1619.3	16.8	1.3		1598.2	13.9
SJ01/2014_G106	132.3	46	1.0699	0.09703	0.00192	3.67231	0.0714	0.27458	0.00354	1567.8	15.8	1565.4	18.8	1564	17.9	-0.2		1567.8	15.8
SJ01/2014_G107	78.3	18.7	0.8702	0.07829	0.00196	2.15145	0.05223	0.19938	0.00287	1154.2	17.3	1165.5	20	1172	15.4	1.5		1154.2	17.3
SJ01/2014_G108	433.1	96.5	0.4358	0.08361	0.00152	2.4148	0.04305	0.20954	0.00251	1283.5	13.2	1247	15.6	1226.4	13.4	-4.5		1283.5	13.2
SJ01/2014_G109	343	69.3	0.4307	0.07599	0.00145	1.99652	0.03722	0.19062	0.00232	1094.8	12.8	1114.3	15.3	1124.7	12.6	2.7		1094.8	12.8
SJ01/2014_G110	420.2	93.7	0.9496	0.08816	0.00163	2.254	0.04078	0.1855	0.00224	1386	14	1198	15.5	1097	12.2	-8.4		1097	12.2
SJ01/2014_G111	127.2	57.3	0.2911	0.1352	0.0025	7.77693	0.14238	0.41732	0.00528	2166.6	16.6	2205.5	20.2	2248.3	24	3.8		2166.6	16.6
SJ01/2014_G112	23.2	5.7	1.489	0.08006	0.0033	2.00838	0.07964	0.18199	0.00374	1198.5	29	1118.3	31.2	1077.8	20.4	-3.6		1077.8	20.4
SJ01/2014_G113	192.6	112.1	3.2076	0.10823	0.00203	4.59154	0.08469	0.30779	0.00383	1769.8	15.7	1747.7	18.8	1729.8	18.9	-2.3		1769.8	15.7
SJ01/2014_G114	272.9	65.7	0.667	0.093	0.00177	2.74567	0.05116	0.2142	0.00264	1487.9	14.9	1340.9	16.9	1251.2	14	-15.9	Del.		
SJ01/2014_G115	211.6	74.3	1.4429	0.10377	0.00196	3.97124	0.0738	0.27766	0.00345	1692.6	15.6	1628.3	18.3	1579.6	17.4	-6.7		1692.6	15.6
SJ01/2014_G116	133.9	58.8	0.66	0.13612	0.00257	7.14799	0.13295	0.38097	0.00485	2178.4	16.9	2130	20.3	2080.8	22.6	-4.5		2178.4	16.9
SJ01/2014_G117	176.6	36.5	0.4337	0.07516	0.00169	2.01521	0.04417	0.19452	0.0026	1072.8	14.9	1120.6	17.8	1145.8	14	6.8	Del.		
SJ01/2014_G118	38.1	8.9	0.9127	0.07809	0.00255	2.07711	0.06548	0.19297	0.00332	1149.2	22.5	1141.3	25.3	1137.4	17.9	-1		1149.2	22.5
SJ01/2014_G119	339.4	90.1	0.2398	0.09757	0.00181	3.50051	0.06381	0.26028	0.00316	1578.2	14.9	1527.3	17.5	1491.3	16.2	-5.5		1578.2	14.9
SJ01/2014_G120	255.4	55.2	0.3965	0.07915	0.00158	2.235	0.04368	0.20487	0.00256	1175.9	13.9	1192.1	16.5	1201.4	13.7	2.2		1175.9	13.9
SJ01/2014_G121	142.1	46.5	0.9975	0.09581	0.00196	3.47501	0.0697	0.26314	0.00342	1544	16.2	1521.6	19.1	1505.9	17.5	-2.5		1544	16.2
SJ01/2014_G122	123.1	37.7	0.044	0.10458	0.00211	4.53608	0.08994	0.31468	0.0041	1706.9	16.7	1737.6	20	1763.7	20.1	3.3		1706.9	16.7
SJ01/2014_G123	161.7	46.1	0.394	0.08634	0.00176	3.16979	0.0633	0.26635	0.00341	1345.8	15.2	1449.8	18.6	1522.2	17.4	13.1	Del.		
SJ01/2014_G124	137.5	49.6	3.1822	0.07994	0.00179	2.10149	0.04591	0.19073	0.00255	1195.5	15.7	1149.3	17.9	1125.3	13.8	-5.9		1195.5	15.7
SJ01/2014_G125	704.5	205.3	1.2477	0.09584	0.00176	3.01807	0.05425	0.22847	0.00272	1544.6	14.6	1412.2	16.7	1326.5	14.3	-14.1		1544.6	14.6
SJ01/2014_G126	475.8	112	0.3653	0.09048	0.0017	2.90877	0.0536	0.23323	0.00282	1435.7	14.4	1384.2	16.9	1351.4	14.7	-5.9		1435.7	14.4
SJ01/2014_G127	836.8	172.8	0.1685	0.08431	0.00155	2.43204	0.04397	0.20929	0.00249	1299.7	13.5	1252.1	15.8	1225	13.3	-5.7		1299.7	13.5
SJ01/2014_G128	362	102.2	0.5769	0.09007	0.00172	3.14248	0.05874	0.25311	0.00308	1427	14.6	1443.2	17.4	1454.5	15.8	1.9		1427	14.6
SJ01/2014_G129	91.1	35.9	3.5272	0.07664	0.00191	2.08387	0.0506	0.19728	0.0028	1111.8	16.8	1143.5	19.7	1160.7	15.1	4.4		1111.8	16.8
SJ01/2014_G130	61.8	11.2	0.4656	0.07471	0.00219	1.75765	0.04978	0.17069	0.00266	1060.7	19.3	1030	21.5	1015.9	14.6	-1.4		1015.9	14.6
SJ01/2014_G131	133.9	42.6	1.1204	0.09046	0.00194	3.10001	0.06494	0.24863	0.00328	1435.3	16.5	1432.7	19.3	1431.4	16.9	-0.3		1435.3	16.5
SJ01/2014_G132	147.8	48.4	0.6699	0.10237	0.0021	4.02098	0.08084	0.28496	0.00369	1667.5	16.8	1638.4	19.7	1616.3	18.5	-3.1		1667.5	16.8
SJ01/2014_G133	45.3	17.6	1.2055	0.10215	0.00261	4.16579	0.10388	0.29588	0.0046	1663.6	20.9	1667.3	24.5	1670.8	22.9	0.4		1663.6	20.9
SJ01/2014_G134	609.7	125.1	0.4315	0.07924	0.00153	2.17747	0.04116	0.19936	0.00242	1178.1	13.5	1173.9	15.9	1171.9	13	-0.5		1178.1	13.5
SJ01/2014_G135	77.2	26.2	1.0614	0.09392	0.00219	3.47554	0.07906	0.26847	0.00379	1506.5	18.3	1521.7	21.5	1533	19.3	1.8		1506.5	18.3
SJ01/2014_G136	356.3	128.1	1.0842	0.11122	0.00214	4.44835	0.0839	0.29016	0.00355	1819.4	16.3	1721.4	18.9	1642.3	17.7	-9.7		1819.4	16.3
SJ01/2014_G137	247.7	82.9	0.2441	0.10874	0.00213	4.85489	0.09344	0.32391	0.00404	1778.4	16.4	1794.5	19.6	1808.8	19.7	1.7		1778.4	16.4
SJ01/2014_G138	245.1	80	0.7657	0.1102	0.00219	4.24835	0.0826	0.27968	0.00351	1802.7	16.8	1683.4	19.3	1589.8	17.7	-11.8		1802.7	16.8
SJ01/2014_G139	212.7	58.9	1.59	0.07921	0.00171	2.13398	0.0448	0.19545	0.00252	1177.4	15	1159.9	17.4	1150.8	13.6	-2.3		1177.4	15
SJ01/2014_G140	154	36.5	0.8382	0.09414	0.0021	2.58331	0.05556	0.19909	0.0027	1510.9	17.5	1295.9	19.1	1170.4	14.5	-22.5	Del.		
SJ01/2014_G141	105.6	25.7	1.2166	0.07917	0.00196	2.08476	0.05008	0.19104	0.00269	1176.4	17.2	1143.8	19.5	1127	14.6	-4.2		1176.4	17.2
SJ01/2014_G142	213.7	49.7	0.8069	0.08314	0.0018	2.27347	0.04784	0.19839	0.00257	1272.5	15.7	1204.1	17.8	1166.7	13.8	-8.3		1272.5	15.7
SJ01/2014_G143	187.4	61.2	0.5464	0.10307	0.00212	4.13843	0.08347	0.29129	0.00373	1680.1	16.9	1661.9	19.8	1648	18.6	-1.9		1680.1	16.9
SJ01/2014_G144	113.3	42.6	0.5189	0.11076	0.00239	5.12777	0.10829	0.33588	0.00452	1811.9	18.2	1840.7	21.6	1866.8	21.8	3		1811.9	18.2
SJ01/2014_G145	76.7	24.3	0.5221	0.10288	0.00243	4.06284	0.09353	0.28651	0.0041	1676.7	19.4	1646.9	22.5	1624.1	20.5	-3.1		1676.7	19.4
SJ01/2014_G146	155	33.5	0.3646	0.07795	0.00179	2.22121	0.04958	0.20672	0.00276	1145.6	15.8	1187.8	18.6	1211.3	14.7	5.7	Del.		
SJ01/2014_G147	143.2	34.5	0.5662	0.08305	0.0019	2.48304	0.05544	0.2169	0.00292	1270.4	16.6	1267.1	19.2	1265.5	15.5	-0.4		1270.4	16.6
SJ01/2014_G148	495.4	95.2	0.316	0.07559	0.00154	1.94553	0.03879	0.18672	0.00231	1084.2	13.6	1096.9	16	1103.6	12.5	1.8		1084.2	13.6
SJ01/2014_G149	334.2	106.1	0.7645	0.09558	0.00195	3.55369	0.07083	0.26975	0.00337	1539.5	16.2	1539.3	19	1539.5	17.1	0		1539.5	16.2
SJ01/2014_G150	390.8	124.3	0.195	0.10679	0.00213	4.61035	0.09011	0.3132	0.00387	1745.3	16.6	1751.1	19.6	1756.4	19	0.6		1745.3	16.6

Analysis No.	U (ppm)	Pb (ppm)	Th/U	Measured isotopic ratios						Calculated isotopic ages (Ma)						Disc.†	Comment§	Preferred age (Ma)#	
				$^{207}Pb/^{206}Pb$	1σ	$^{207}Pb/^{235}U$	1σ	$^{206}Pb/^{238}U$	1σ	$^{207}Pb/^{206}Pb$	1σ	$^{207}Pb/^{235}U$	1σ	$^{206}Pb/^{238}U$	1σ	(%)		Age	1σ
Sample SJ02/2014, quartz sandstone, Lower Shijia Formation, Heifengling section of Huaibei region, GPS: 33°52'49"N 117°19'56"E																			
SJ02/2014_G001	423	105.6	1.5625	0.0906	0.0011	2.30791	0.02892	0.18483	0.00206	1438.2	9.3	1214.7	11.7	1093.3	11.2	-10		1093.3	11.2
SJ02/2014_G002	155	38.1	1.1156	0.08279	0.00114	2.24047	0.03134	0.19636	0.00228	1264.3	10	1193.8	12.6	1155.7	12.3	-8.6		1264.3	10
SJ02/2014_G003	305	73.8	0.8995	0.07295	0.00093	2.09335	0.02731	0.20822	0.00235	1012.6	8.2	1146.6	11.7	1219.3	12.5	20.4	Del.		
SJ02/2014_G004	110.1	37.5	1.5796	0.10205	0.00141	3.49066	0.04915	0.2482	0.00294	1661.7	11.3	1525.1	14.4	1429.2	15.2	-14		1661.7	11.3
SJ02/2014_G005	755.6	140	0.7796	0.0833	0.00099	1.95946	0.02408	0.17068	0.00189	1276.3	8.6	1101.7	10.9	1015.9	10.4	-7.8		1015.9	10.4
SJ02/2014_G006	151.1	37.6	1.4006	0.08033	0.00124	2.08811	0.03226	0.18862	0.00227	1205.1	10.9	1144.9	13.4	1113.9	12.3	-7.6		1205.1	10.9
SJ02/2014_G007	127.5	28.1	0.3195	0.083	0.00118	2.48552	0.03583	0.21729	0.00255	1269.2	10.3	1267.8	13.3	1267.5	13.5	-0.1		1269.2	10.3
SJ02/2014_G008	157.3	47.2	0.9311	0.0933	0.00123	3.1854	0.04306	0.24774	0.00286	1494	10.3	1453.6	13.5	1426.8	14.8	-4.5		1494	10.3
SJ02/2014_G009	642.1	146	1.5979	0.08187	0.00098	1.92443	0.02391	0.17057	0.00189	1242.4	8.6	1089.6	10.9	1015.3	10.4	-6.8		1015.3	10.4
SJ02/2014_G010	177.5	40.1	0.7481	0.08552	0.00116	2.35684	0.03261	0.19997	0.00231	1327.4	10	1229.6	12.7	1175.2	12.4	-11.5		1327.4	10
SJ02/2014_G011	483.1	92.6	0.7968	0.08268	0.00102	1.94775	0.02471	0.17094	0.00191	1261.7	8.9	1097.7	11.2	1017.3	10.5	-7.3		1017.3	10.5
SJ02/2014_G012	412.3	104.1	0.441	0.08994	0.00109	2.98602	0.03733	0.24091	0.00269	1424.3	9.3	1404.1	12.5	1391.4	14	-2.3		1424.3	9.3
SJ02/2014_G013	131.5	33.6	0.5781	0.09757	0.00133	3.15599	0.04381	0.23471	0.00275	1578.2	10.9	1446.5	13.9	1359.1	14.4	-13.9		1578.2	10.9
SJ02/2014_G014	133.7	30.5	0.8503	0.07591	0.00113	2.03108	0.0305	0.19414	0.0023	1092.7	10	1126	12.9	1143.8	12.4	4.7		1092.7	10
SJ02/2014_G015	298.3	81.6	1.4082	0.08408	0.00106	2.42157	0.03153	0.20898	0.00236	1294.4	9.2	1249	12.2	1223.4	12.6	-5.5		1294.4	9.2
SJ02/2014_G016	378.6	81	0.4978	0.07769	0.00097	2.14238	0.02754	0.20009	0.00225	1139	8.5	1162.6	11.6	1175.8	12.1	3.2		1139	8.5
SJ02/2014_G017	590.4	147.3	1.0486	0.08207	0.00099	2.29477	0.02857	0.20288	0.00226	1247.2	8.7	1210.7	11.6	1190.8	12.1	-4.5		1247.2	8.7
SJ02/2014_G018	500.5	157.9	0.6121	0.10696	0.00126	4.22591	0.05165	0.2867	0.00319	1748.3	9.8	1679.1	13.3	1625	16	-7		1748.3	9.8
SJ02/2014_G019	175.8	60	0.6085	0.10644	0.00134	4.44743	0.05783	0.3032	0.00347	1739.3	10.5	1721.2	14.1	1707.2	17.2	-1.8		1739.3	10.5
SJ02/2014_G020	223.6	50	0.7649	0.07985	0.00107	2.16579	0.02959	0.19681	0.00226	1193.3	9.4	1170.1	12.3	1158.2	12.2	-2.9		1193.3	9.4
SJ02/2014_G021	375.3	90.7	1.4119	0.0869	0.00109	2.23781	0.02891	0.18685	0.00211	1358.3	9.4	1193	11.8	1104.3	11.5	-18.7	Del.		
SJ02/2014_G022	796	191.4	0.0989	0.09357	0.00109	3.19133	0.03882	0.24748	0.00274	1499.5	9.1	1455.1	12.4	1425.5	14.2	-4.9		1499.5	9.1
SJ02/2014_G023	437.1	106.5	0.5344	0.08352	0.00102	2.5662	0.03245	0.22297	0.0025	1281.4	8.9	1291.1	12.1	1297.5	13.2	1.3		1281.4	8.9
SJ02/2014_G024	227.5	56.3	1.2876	0.08186	0.0011	2.14974	0.02941	0.19057	0.00219	1242.2	9.6	1165	12.3	1124.5	11.9	-9.5		1242.2	9.6
SJ02/2014_G025	254.5	62.1	1.2898	0.07735	0.00102	1.9978	0.02698	0.18741	0.00214	1130.2	9	1114.8	11.8	1107.3	11.6	-2		1130.2	9
SJ02/2014_G026	767.4	253.3	0.4065	0.10944	0.00127	4.66502	0.0564	0.30932	0.00342	1790.1	9.8	1761	13.4	1737.4	16.8	-2.9		1790.1	9.8
SJ02/2014_G027	482	128	1.3398	0.09234	0.00112	2.60212	0.03272	0.20449	0.00229	1474.4	9.4	1301.2	12.1	1199.4	12.3	-18.7	Del.		
SJ02/2014_G028	792.1	170.3	0.7658	0.08493	0.00101	2.29136	0.02833	0.19577	0.00217	1313.9	8.8	1209.6	11.5	1152.6	11.7	-12.3		1313.9	8.8
SJ02/2014_G029	441.5	97.4	1.5	0.08167	0.00102	1.97237	0.02547	0.17524	0.00197	1237.6	8.9	1106.1	11.3	1040.9	10.8	-5.9		1040.9	10.8
SJ02/2014_G030	197.7	40.9	0.6013	0.07733	0.00107	1.98964	0.02813	0.18669	0.00216	1129.7	9.4	1112	12.2	1103.4	11.7	-2.3		1129.7	9.4
SJ02/2014_G031	751.1	263.4	0.2592	0.15509	0.00179	7.56231	0.09118	0.35382	0.00391	2402.8	10.6	2180.4	14.3	1952.8	18.6	-18.7	Del.		
SJ02/2014_G032	48.9	20.3	1.9295	0.09825	0.00164	3.70456	0.06224	0.27361	0.00353	1591.2	13.4	1572.4	16.9	1559.1	17.9	-2		1591.2	13.4
SJ02/2014_G033	585.9	146.8	0.0992	0.09854	0.00117	3.51899	0.04351	0.25913	0.00288	1596.7	9.6	1531.5	12.9	1485.4	14.7	-7		1596.7	9.6
SJ02/2014_G034	98.9	21.5	0.1539	0.09281	0.00138	2.87706	0.04332	0.22496	0.00272	1484	11.6	1375.9	14.4	1308	14.3	-11.9		1484	11.6
SJ02/2014_G035	505	135.7	0.4604	0.09002	0.00109	3.09504	0.03878	0.24949	0.00279	1426	9.3	1431.5	12.7	1435.8	14.4	0.7		1426	9.3
SJ02/2014_G036	711.2	139.3	0.4599	0.0904	0.00109	2.40714	0.03006	0.19323	0.00215	1434	9.3	1244.7	11.8	1138.8	11.6	-20.6	Del.		
SJ02/2014_G037	93.3	34.4	0.3074	0.14112	0.00185	6.9759	0.09442	0.35869	0.00424	2241	11.8	2108.4	15.7	1976	20.1	-11.8		2241	11.8
SJ02/2014_G038	830.3	183.6	0.8199	0.10989	0.0013	3.14605	0.03874	0.20774	0.00231	1797.6	10	1444	12.5	1216.8	12.3	-32.3	Del.		
SJ02/2014_G039	325.8	69.4	0.5282	0.07963	0.00103	2.15853	0.02866	0.1967	0.00223	1187.8	9.1	1167.8	11.9	1157.6	12	-2.5		1187.8	9.1
SJ02/2014_G040	224.7	50.8	2.0438	0.07875	0.00113	1.72904	0.02521	0.15933	0.00187	1165.9	9.9	1019.4	11.9	953.1	10.4	-6.5		953.1	10.4
SJ02/2014_G041	252.8	51.5	0.4905	0.08921	0.00118	2.32875	0.03157	0.18944	0.00217	1408.7	10.1	1221.1	12.4	1118.3	11.8	-20.6	Del.		
SJ02/2014_G042	484.8	101.1	0.6147	0.08332	0.00104	2.15169	0.02776	0.18738	0.00211	1276.7	9.1	1165.6	11.7	1107.2	11.5	-13.3		1276.7	9.1
SJ02/2014_G043	324.7	103.5	0.6649	0.0988	0.00122	3.82918	0.0491	0.28123	0.00318	1601.6	9.9	1598.9	13.5	1597.6	16	-0.3		1601.6	9.9
SJ02/2014_G044	292.1	87	0.646	0.10384	0.00129	3.84771	0.04965	0.26889	0.00305	1693.9	10.2	1602.8	13.6	1535.2	15.5	-9.4		1693.9	10.2
SJ02/2014_G045	375.8	105.6	1.0798	0.08485	0.00107	2.63529	0.03423	0.22537	0.00254	1312.1	9.3	1310.5	12.5	1310.2	13.4	-0.1		1312.1	9.3

Analysis No.	U (ppm)	Pb (ppm)	Th/U	Measured isotopic ratios						Calculated isotopic ages (Ma)						Disc.† (%)	Comment§	Preferred age (Ma)#	
				$^{207}Pb/^{206}Pb$	1σ	$^{207}Pb/^{235}U$	1σ	$^{206}Pb/^{238}U$	1σ	$^{207}Pb/^{206}Pb$	1σ	$^{207}Pb/^{235}U$	1σ	$^{206}Pb/^{238}U$	1σ			Age	1σ
Sample SJ02/2014, quartz sandstone, Lower Shijia Formation, Heifengling section of Huaibei region, GPS: 33°52'49"N 117°19'56"E																			
SJ02/2014_G046	171.9	48.3	0.8534	0.08128	0.00112	2.6477	0.03733	0.23638	0.00275	1228.2	9.8	1314	13.3	1367.9	14.3	11.4	Del.		
SJ02/2014_G047	578.6	117.8	0.3696	0.07727	0.00096	2.08083	0.02674	0.19542	0.00219	1128.2	8.5	1142.5	11.5	1150.7	11.8	2		1128.2	8.5
SJ02/2014_G048	414	137.7	0.8201	0.10039	0.00123	3.90076	0.04957	0.28196	0.00317	1631.3	9.9	1613.8	13.4	1601.2	15.9	-1.8		1631.3	9.9
SJ02/2014_G049	378.1	68	0.2341	0.08238	0.00106	2.1065	0.028	0.18556	0.00211	1254.6	9.3	1150.9	11.8	1097.3	11.5	-4.7		1097.3	11.5
SJ02/2014_G050	322.5	73.8	0.7725	0.07652	0.001	2.077	0.02804	0.19696	0.00224	1108.7	8.8	1141.2	11.9	1159	12.1	4.5		1108.7	8.8
SJ02/2014_G051	434.2	96.6	0.8525	0.09121	0.00115	2.50263	0.03258	0.19911	0.00225	1451	9.7	1272.8	12.3	1170.5	12.1	-19.3	Del.		
SJ02/2014_G052	144.9	39.6	0.7909	0.08719	0.00124	2.80391	0.04079	0.23337	0.00276	1364.7	10.7	1356.6	13.8	1352.1	14.4	-0.9		1364.7	10.7
SJ02/2014_G053	401.7	85.6	0.5354	0.08123	0.00104	2.21295	0.02936	0.1977	0.00224	1227	9.1	1185.1	12	1163	12.1	-5.2		1227	9.1
SJ02/2014_G054	402.2	95.1	0.9049	0.08751	0.00112	2.41927	0.03198	0.20061	0.00228	1371.7	9.6	1248.3	12.3	1178.6	12.2	-14.1		1371.7	9.6
SJ02/2014_G055	483.7	110.1	0.2493	0.08515	0.00106	2.64906	0.03433	0.22576	0.00254	1319	9.2	1314.4	12.4	1312.2	13.4	-0.5		1319	9.2
SJ02/2014_G056	108.4	31.3	0.6499	0.09138	0.00134	3.21031	0.04798	0.25494	0.00306	1454.5	11.3	1459.6	14.7	1463.9	15.7	0.6		1454.5	11.3
SJ02/2014_G057	397.2	116.6	0.2283	0.10227	0.00127	4.07962	0.05249	0.28946	0.00327	1665.7	10.2	1650.2	13.7	1638.8	16.3	-1.6		1665.7	10.2
SJ02/2014_G058	435.9	101	0.7672	0.06725	0.00091	1.85273	0.02571	0.19992	0.00227	845.5	7.8	1064.4	11.7	1174.9	12.2	39	Del.		
SJ02/2014_G059	759.5	160	0.7235	0.08011	0.00101	2.10124	0.02735	0.19033	0.00214	1199.7	8.9	1149.2	11.6	1123.2	11.6	-6.4		1199.7	8.9
SJ02/2014_G060	463.5	115.7	1.2682	0.09315	0.00119	2.52548	0.0332	0.19675	0.00223	1490.9	10	1279.4	12.4	1157.8	12	-22.3			
SJ02/2014_G061	243.8	47	0.301	0.07499	0.00105	1.95657	0.028	0.18934	0.0022	1068.2	9.3	1100.7	12.2	1117.8	11.9	4.6		1068.2	9.3
SJ02/2014_G062	485.4	155.7	0.8845	0.0953	0.00119	3.50409	0.04535	0.26681	0.00301	1534	9.9	1528.1	13.3	1524.6	15.3	-0.6		1534	9.9
SJ02/2014_G063	357.3	74.3	0.7564	0.08052	0.00108	2.12628	0.0292	0.19163	0.0022	1209.8	9.5	1157.4	12.2	1130.2	11.9	-6.6		1209.8	9.5
SJ02/2014_G064	553.3	142.8	0.9894	0.07518	0.00096	2.18916	0.02883	0.21129	0.00238	1073.3	8.5	1177.6	11.9	1235.7	12.7	15.1	Del.		
SJ02/2014_G065	134.8	44.4	0.9033	0.09928	0.00139	3.85862	0.05551	0.28203	0.00334	1610.6	11.3	1605.1	14.8	1601.6	16.8	-0.6		1610.6	11.3
SJ02/2014_G066	229.8	75.7	0.9775	0.09734	0.00128	3.61221	0.04901	0.26928	0.0031	1573.8	10.5	1552.2	13.9	1537.1	15.7	-2.3		1573.8	10.5
SJ02/2014_G067	539.3	211.8	0.5461	0.14357	0.00175	6.97528	0.08865	0.35256	0.00396	2270.7	11.1	2108.3	14.7	1946.8	18.9	-14.3		2270.7	11.1
SJ02/2014_G068	348.3	106.6	1.3387	0.09088	0.00118	2.96117	0.03971	0.23646	0.0027	1444.1	10	1397.7	13.1	1368.3	14.1	-5.3		1444.1	10
SJ02/2014_G069	174.1	43.7	0.7267	0.08501	0.00121	2.54699	0.03698	0.21742	0.00255	1315.8	10.5	1285.6	13.4	1268.2	13.5	-3.6		1315.8	10.5
SJ02/2014_G070	224.1	72.1	0.9603	0.09415	0.00125	3.4574	0.04743	0.26648	0.00308	1511.1	10.4	1517.6	13.9	1522.9	15.7	0.8		1511.1	10.4
SJ02/2014_G071	409	110.7	0.388	0.08992	0.00115	3.15412	0.04181	0.25453	0.00289	1423.8	9.8	1446	13.2	1461.8	14.9	2.7		1423.8	9.8
SJ02/2014_G072	233.7	76.3	0.493	0.10678	0.0014	4.39962	0.05961	0.29899	0.00345	1745.2	10.9	1712.3	14.5	1686.3	17.1	-3.4		1745.2	10.9
SJ02/2014_G073	995.4	271.6	0.1503	0.11176	0.00137	4.30239	0.05501	0.27935	0.00313	1828.2	10.4	1693.8	13.7	1588.1	15.8	-13.1		1828.2	10.4
SJ02/2014_G074	250.5	67	0.8314	0.09454	0.00127	3.01307	0.04157	0.23128	0.00267	1518.9	10.6	1410.9	13.5	1341.2	14	-11.7		1518.9	10.6
SJ02/2014_G075	234.8	53.4	0.8133	0.08616	0.0012	2.35706	0.03352	0.19852	0.00231	1341.8	10.4	1229.7	12.9	1167.4	12.4	-13		1341.8	10.4
SJ02/2014_G076	479.7	103.9	0.155	0.08224	0.00106	2.49465	0.03337	0.22012	0.0025	1251.2	9.3	1270.5	12.5	1282.5	13.2	2.5		1251.2	9.3
SJ02/2014_G077	123	49.7	1.0536	0.11009	0.00153	4.8685	0.06973	0.32091	0.00381	1800.9	11.7	1796.8	15.4	1794.2	18.6	-0.4		1800.9	11.7
SJ02/2014_G078	301.7	66	0.8263	0.07997	0.0011	2.08377	0.02945	0.18907	0.00219	1196.2	9.7	1143.5	12.3	1116.3	11.9	-6.7		1196.2	9.7
SJ02/2014_G079	274.7	60.7	0.7565	0.07765	0.00108	2.05811	0.02941	0.19234	0.00223	1137.9	9.5	1135	12.4	1134	12.1	-0.3		1137.9	9.5
SJ02/2014_G080	96.1	38.8	1.0748	0.10947	0.00159	4.80343	0.07159	0.31842	0.00386	1790.6	12.2	1785.5	15.9	1782	18.9	-0.5		1790.6	12.2
SJ02/2014_G081	990.9	269.7	0.2997	0.11519	0.00143	4.34162	0.05613	0.27349	0.00307	1882.9	10.6	1701.3	13.8	1558.5	15.5	-17.2	Del.		
SJ02/2014_G082	531.4	234.9	0.6536	0.1677	0.00209	9.0109	0.11682	0.38991	0.0044	2534.8	11.6	2339.1	15.4	2122.4	20.4	-16.3	Del.		
SJ02/2014_G083	230.9	51.9	0.6466	0.07955	0.00113	2.19418	0.0319	0.20015	0.00234	1185.9	9.9	1179.2	12.8	1176.1	12.6	-0.8		1185.9	9.9
SJ02/2014_G084	282.6	77.8	1.0626	0.08315	0.00114	2.52742	0.03554	0.22057	0.00255	1272.7	9.9	1280	13	1284.9	13.5	1		1272.7	9.9
SJ02/2014_G085	93.3	30.1	0.799	0.10009	0.00153	3.81435	0.05931	0.27654	0.00339	1625.8	12.4	1595.8	15.8	1573.9	17.1	-3.2		1625.8	12.4
SJ02/2014_G086	227.5	51.8	0.6509	0.08183	0.00117	2.2843	0.03343	0.20257	0.00237	1241.5	10.2	1207.4	13	1189.1	12.7	-4.2		1241.5	10.2
SJ02/2014_G087	92.7	22.2	1.3553	0.08688	0.00149	2.16469	0.03717	0.1808	0.00228	1357.8	12.8	1169.8	14.8	1071.3	12.4	-8.4		1071.3	12.4
SJ02/2014_G088	191	65.9	0.9104	0.0995	0.00138	3.9221	0.05585	0.28604	0.00335	1614.8	11.2	1618.3	14.7	1621.7	16.8	0.4		1614.8	11.2
SJ02/2014_G089	608.4	299.2	0.2404	0.17517	0.00219	11.24149	0.14657	0.46569	0.00526	2607.7	11.7	2543.4	15.7	2464.6	23.1	-5.5		2607.7	11.7
SJ02/2014_G090	128.6	40.9	1.5194	0.10502	0.00155	3.41336	0.05137	0.23585	0.00284	1714.7	12.2	1507.5	15	1365.1	14.8	-20.4	Del.		
SJ02/2014_G091	168	77.5	2.2057	0.10543	0.00147	4.21446	0.06034	0.29007	0.00341	1721.8	11.6	1676.8	15	1641.9	17	-4.6		1721.8	11.6
SJ02/2014_G092	243.8	90.8	1.5949	0.09147	0.00126	3.32859	0.04727	0.26405	0.00307	1456.4	10.7	1487.8	14.1	1510.5	15.7	3.7		1456.4	10.7

Analysis No.	U (ppm)	Pb (ppm)	Th/U	Measured isotopic ratios						Calculated isotopic ages (Ma)						Disc.† (%)	Comment§	Preferred age (Ma)#	
				$^{207}Pb/^{206}Pb$	1σ	$^{207}Pb/^{235}U$	1σ	$^{206}Pb/^{238}U$	1σ	$^{207}Pb/^{206}Pb$	1σ	$^{207}Pb/^{235}U$	1σ	$^{206}Pb/^{238}U$	1σ			Age	1σ
Sample SJ02/2014, quartz sandstone, Lower Shijia Formation, Heifengling section of Huaibei region, GPS: 33°52'49"N 117°19'56"E																			
SJ02/2014_G093	307.8	98.5	0.5402	0.09753	0.00131	3.88125	0.05371	0.28876	0.00333	1577.4	10.8	1609.8	14.3	1635.3	16.7	3.7		1577.4	10.8
SJ02/2014_G094	201.1	69.7	0.4994	0.10694	0.00146	4.63107	0.06531	0.31424	0.00367	1747.9	11.4	1754.9	15	1761.5	18	0.8		1747.9	11.4
SJ02/2014_G095	409	129.8	1.1662	0.10997	0.00145	4.01209	0.05464	0.26473	0.00303	1798.9	11.1	1636.6	14.2	1514	15.4	-15.8	Del.		
SJ02/2014_G096	183.7	62.6	0.9617	0.09865	0.00139	3.7712	0.05457	0.27739	0.00327	1598.8	11.3	1586.6	14.7	1578.2	16.5	-1.3		1598.8	11.3
SJ02/2014_G098	848.8	176.5	0.291	0.08423	0.0011	2.37768	0.03228	0.20483	0.00233	1297.9	9.6	1235.9	12.4	1201.2	12.5	-7.4		1297.9	9.6
SJ02/2014_G099	929.7	170.4	0.5343	0.08269	0.00109	1.95111	0.02658	0.17122	0.00195	1261.9	9.5	1098.8	11.7	1018.8	10.7	-7.3		1018.8	10.7
SJ02/2014_G100	268.5	70.2	0.6738	0.08473	0.00121	2.67692	0.03905	0.22926	0.00268	1309.4	10.5	1322.1	13.6	1330.6	14.1	1.6		1309.4	10.5
SJ02/2014_G101	87.1	24	0.5285	0.08803	0.00147	3.02982	0.051	0.24973	0.00314	1383.1	12.6	1415.2	16	1437.1	16.2	3.9		1383.1	12.6
SJ02/2014_G102	153.9	40.2	1.3219	0.0972	0.0015	2.68984	0.042	0.2008	0.00244	1571.1	12.3	1325.7	14.5	1179.6	13.1	-24.9	Del.		
SJ02/2014_G103	334.2	74.9	0.3692	0.08003	0.00113	2.36076	0.03423	0.21404	0.00249	1197.7	9.9	1230.8	13.1	1250.3	13.2	4.4		1197.7	9.9
SJ02/2014_G104	142.7	69.6	1.252	0.12007	0.0017	6.07879	0.08863	0.36737	0.00438	1957.3	12.3	1987.2	16.1	2017	20.6	3.1		1957.3	12.3
SJ02/2014_G105	417.4	110.5	0.9205	0.08459	0.00117	2.57688	0.03664	0.22104	0.00255	1306.2	10.2	1294.1	13.2	1287.4	13.5	-1.4		1306.2	10.2
SJ02/2014_G106	271.9	86.7	0.8233	0.09166	0.00129	3.38555	0.04889	0.268	0.00313	1460.4	10.9	1501.1	14.3	1530.6	15.9	4.8		1460.4	10.9
SJ02/2014_G107	329.8	72.7	0.5469	0.07776	0.00112	2.14826	0.03164	0.20048	0.00234	1140.7	9.9	1164.5	12.8	1177.9	12.6	3.3		1140.7	9.9
SJ02/2014_G108	378.6	104.9	0.5978	0.09656	0.00133	3.37969	0.04785	0.25396	0.00294	1558.7	11	1499.7	14.1	1458.9	15.1	-6.4		1558.7	11
SJ02/2014_G109	242.7	121.7	0.8103	0.13114	0.00178	7.42203	0.10434	0.41066	0.00478	2113.3	12.1	2163.6	16	2217.9	21.8	5		2113.3	12.1
SJ02/2014_G110	100	27.8	0.7438	0.0655	0.00115	2.1689	0.03855	0.24025	0.00301	790.4	9.6	1171.1	15	1388	15.6	75.6	Del.		
SJ02/2014_G111	504.5	126.4	0.6659	0.09195	0.00126	2.81007	0.03977	0.22175	0.00256	1466.4	10.6	1358.2	13.4	1291.1	13.5	-12		1466.4	10.6
SJ02/2014_G112	385.9	90.1	0.3502	0.08749	0.00123	2.73768	0.03944	0.22706	0.00263	1371.3	10.6	1338.7	13.5	1319.1	13.8	-3.8		1371.3	10.6
SJ02/2014_G113	298.3	97.5	0.7885	0.09726	0.00136	3.72616	0.05378	0.27799	0.00324	1572.2	11.2	1577	14.6	1581.2	16.3	0.6		1572.2	11.2
SJ02/2014_G114	102.8	24.2	0.4869	0.10288	0.0017	3.11699	0.05143	0.21983	0.0028	1676.7	13.6	1436.9	16	1281	14.8	-23.6	Del.		
SJ02/2014_G115	210.1	58.7	0.4905	0.09175	0.00134	3.23888	0.04855	0.25615	0.00303	1462.2	11.3	1466.5	14.6	1470.1	15.5	0.5		1462.2	11.3
SJ02/2014_G116	204.5	47.4	0.7419	0.08033	0.00124	2.22096	0.03476	0.20061	0.0024	1205.1	10.9	1187.7	13.7	1178.6	12.9	-2.2		1205.1	10.9
SJ02/2014_G117	41	9.8	1.0233	0.07698	0.00182	2.04328	0.04741	0.19258	0.00279	1120.7	16	1130.1	18.9	1135.3	15.1	1.3		1120.7	16
SJ02/2014_G118	164	51.7	0.5496	0.09635	0.00144	3.75743	0.05748	0.28296	0.00339	1554.6	11.9	1583.7	15.4	1606.3	17	3.3		1554.6	11.9
SJ02/2014_G119	121.3	24.1	0.733	0.07269	0.0013	1.73404	0.03097	0.17308	0.00217	1005.3	11.4	1021.3	14.1	1029.1	11.9	0.8		1029.1	11.9
SJ02/2014_G120	181.4	60	0.3317	0.10869	0.00157	4.69598	0.06988	0.31348	0.00372	1777.6	12.1	1766.5	15.7	1757.8	18.3	-1.1		1777.6	12.1
SJ02/2014_G121	314	65.8	0.4585	0.0757	0.00113	2.03873	0.03097	0.19541	0.0023	1087.1	10	1128.5	13	1150.6	12.4	5.8	Del.		
SJ02/2014_G122	180.3	62.1	0.7368	0.09939	0.00147	4.03865	0.06112	0.29484	0.00351	1612.7	11.9	1642	15.5	1665.7	17.5	3.3		1612.7	11.9
SJ02/2014_G123	487	133	0.5899	0.09241	0.00129	3.13046	0.04507	0.24579	0.00284	1475.8	10.9	1440.2	13.9	1416.7	14.7	-4		1475.8	10.9
SJ02/2014_G124	515.7	116.5	0.5847	0.08014	0.00114	2.24549	0.03275	0.20329	0.00236	1200.4	10	1195.4	12.9	1193	12.6	-0.6		1200.4	10
SJ02/2014_G125	340.4	62.9	0.4819	0.08751	0.0013	2.05293	0.03104	0.17022	0.00201	1371.7	11.2	1133.3	13	1013.3	11.1	-10.6		1013.3	11.1
SJ02/2014_G126	432.6	153.4	0.3753	0.11377	0.00157	5.1903	0.07418	0.33102	0.00383	1860.5	11.8	1851	15.3	1843.3	18.5	-0.9		1860.5	11.8
SJ02/2014_G127	426.4	121.1	0.5694	0.09072	0.00128	3.18169	0.04635	0.25446	0.00296	1440.7	10.9	1452.7	14.1	1461.4	15.2	1.4		1440.7	10.9
SJ02/2014_G128	304.5	73.3	1.0091	0.07733	0.00117	2.06952	0.03187	0.19417	0.0023	1129.7	10.3	1138.8	13.2	1143.9	12.4	1.3		1129.7	10.3
SJ02/2014_G129	264	81.9	0.7133	0.09601	0.0014	3.54613	0.05295	0.26798	0.00315	1548	11.6	1537.6	14.8	1530.5	16	-1.1		1548	11.6
SJ02/2014_G130	270.8	96.7	0.7691	0.11744	0.00168	4.93643	0.07265	0.30498	0.00358	1917.6	12.3	1808.5	15.6	1716	17.7	-10.5		1917.6	12.3
SJ02/2014_G131	269.6	83.1	0.0244	0.1046	0.00151	4.58093	0.06799	0.31777	0.00374	1707.3	11.9	1745.8	15.5	1778.8	18.3	4.2		1707.3	11.9
SJ02/2014_G132	1041.5	284.5	0.0903	0.11245	0.00155	4.36054	0.06212	0.28136	0.00323	1839.4	11.7	1704.9	14.8	1598.2	16.2	-13.1		1839.4	11.7
SJ02/2014_G133	282.6	48.7	0.3272	0.08502	0.0013	2.07119	0.03232	0.17675	0.0021	1316	11.3	1139.3	13.3	1049.2	11.5	-7.9		1049.2	11.5
SJ02/2014_G134	119.1	32.5	1.0596	0.08636	0.00145	2.57021	0.04364	0.21594	0.00269	1346.3	12.5	1292.2	15.3	1260.4	14.3	-6.4		1346.3	12.5
SJ02/2014_G135	115.7	29.6	0.8463	0.11109	0.00184	3.07075	0.05115	0.20055	0.00251	1817.3	14	1425.4	15.9	1178.3	13.5	-35.2	Del.		
SJ02/2014_G136	261.8	65.3	0.6651	0.08448	0.0013	2.55222	0.04011	0.2192	0.00262	1303.6	11.3	1287.1	14.2	1277.6	13.9	-2		1303.6	11.3
SJ02/2014_G137	348.9	121.8	1.0045	0.09802	0.00142	3.78117	0.05623	0.27988	0.00328	1586.8	11.6	1588.8	15	1590.8	16.5	0.2		1586.8	11.6
SJ02/2014_G138	296.6	66	0.802	0.07853	0.00121	2.04958	0.03211	0.18935	0.00225	1160.3	10.7	1132.2	13.3	1117.9	12.2	-3.7		1160.3	10.7
SJ02/2014_G139	232.6	51.1	0.3453	0.08403	0.0013	2.45274	0.03875	0.21179	0.00253	1293.2	11.3	1258.2	14.1	1238.3	13.5	-4.2		1293.2	11.3
SJ02/2014_G140	184.8	49	1.2868	0.11615	0.00179	3.5533	0.0557	0.22195	0.00268	1897.8	13.2	1539.2	15.5	1292.2	14.1	-31.9	Del.		

Analysis No.	U (ppm)	Pb (ppm)	Th/U	Measured isotopic ratios						Calculated isotopic ages (Ma)						Disc.† (%)	Comment§	Preferred age (Ma)#	
				$^{207}Pb/^{206}Pb$	1σ	$^{207}Pb/^{235}U$	1σ	$^{206}Pb/^{238}U$	1σ	$^{207}Pb/^{206}Pb$	1σ	$^{207}Pb/^{235}U$	1σ	$^{206}Pb/^{238}U$	1σ			Age	1σ
Sample SJ02/2014, quartz sandstone, Lower Shijia Formation, Heifengling section of Huaibei region, GPS: 33°52'49"N 117°19'56"E																			
SJ02/2014_G141	148.9	37.4	0.9769	0.0794	0.00134	2.23017	0.03805	0.20379	0.00252	1182.1	11.8	1190.6	14.7	1195.6	13.5	1.1		1182.1	11.8
SJ02/2014_G142	92.1	18.3	0.5411	0.0736	0.00143	1.84212	0.03559	0.18159	0.00236	1030.5	12.6	1060.6	15.4	1075.7	12.9	1.4		1075.7	12.9
SJ02/2014_G143	407.8	94.7	1.0767	0.07618	0.00116	1.94592	0.03019	0.18532	0.00219	1099.8	10.2	1097	12.9	1096	11.9	-0.1		1096	11.9
SJ02/2014_G144	129.2	45.3	0.7338	0.10088	0.0016	4.1498	0.06707	0.29846	0.00365	1640.4	12.9	1664.2	16.4	1683.7	18.1	2.6		1640.4	12.9
SJ02/2014_G145	641.5	146.6	0.5554	0.0841	0.00123	2.43442	0.03658	0.21001	0.00245	1294.9	10.7	1252.8	13.5	1228.9	13.1	-5.1		1294.9	10.7
SJ02/2014_G146	149.4	43.6	0.8836	0.08605	0.00141	2.86358	0.04766	0.24142	0.00296	1339.3	12.2	1372.4	15.4	1394.1	15.4	4.1		1339.3	12.2
SJ02/2014_G147	159	42.4	1.0271	0.09548	0.0016	2.81314	0.0476	0.21376	0.00266	1537.6	13.3	1359	15.6	1248.8	14.1	-18.8	Del.		
SJ02/2014_G148	193.8	57.2	0.5959	0.09148	0.00144	3.302	0.05289	0.26187	0.00316	1456.6	12.2	1481.5	15.5	1499.4	16.1	2.9		1456.6	12.2
SJ02/2014_G149	169.1	61.3	0.6014	0.10797	0.00167	4.74154	0.07498	0.31861	0.00385	1765.4	12.9	1774.6	16.5	1782.9	18.8	1		1765.4	12.9
SJ02/2014_G150	180.9	43.7	0.3732	0.0875	0.00142	2.76122	0.04555	0.22894	0.00279	1371.5	12.2	1345.1	15.1	1328.9	14.6	-3.1		1371.5	12.2

Appendix G

Matlab codes for the Coupled Carbon-Sulphur Cycles Model

The description of the model is introduced in section 3.2.3.2. The model is developed based on the modification of source codes of GEOARBSULF model (Berner, 2006).

```
function dy = Equations(t,y)
%%%%%% Simple ODE solver for Matlab
%%%%%% Tianchen He 2017

%%%%%%% setup dy array
dy = zeros(11,1);

%%%%%%% set up global parameters
global stepnumber
global pars
global workingstate
global data


%%%%%%%% d13c data
d13c_time = data.d13c_data(:,1) .* -1e6 ;
d13c_value = data.d13c_data(:,2) ;

d13c_input = interp1(d13c_time,d13c_value,t) ;

%%%%%%%% d34s data
% d34s_time = data.d34s_data(:,1) .* -1e6 ;
% d34s_value = data.d34s_data(:,2) ;
% %
% d34s_input = interp1(d34s_time,d34s_value,t) ;


%%%%%%%%%%%%%%%%%%%%%%%%%%%%%%%%%%%%%%%%%%%%%%%%%%%%%%%%%%%%%%%%%%%%%%%%%%%%
%
%%%%%%%%%%%%%%%%%   Flux
calculations   %%%%%%%%%%%%%%%%%%%%%%%%%%%%%%
%%%%%%%%%%%%%%%%%%%%%%%%%%%%%%%%%%%%%%%%%%%%%%%%%%%%%%%%%%%%%%%%%%%%%%%%%%%%
%

%%%%%%%%%%%%% get variables from Y to make working easier
C = y(1) ;
OC = pars.OC_0  ;
CAR = pars.CAR_0 ;
d13c_oc = pars.d13c_oc_0 ;
d13c_car = pars.d13c_car_0 ;

S = y(6) ;
PY = pars.PY_0 ;
GYP = pars.GYP_0  ;
d34s_py = pars.d34s_py_0 ;
d34s_gyp = pars.d34s_gyp_0 ;

O2 = y(12) ;

%%%%% calculate carbon fluxes here (mol / yr)
% Fwcar = 12.5e12 * (CAR / pars.CAR_0)  ;%%%% deduced CAR weathering
flux
Fwcar = 12e12   ;%%%% deduced CAR weathering flux*2
% Fwcar = 37.5e12 * (CAR / pars.CAR_0)  ;%%%% deduced CAR weathering
flux*3
% Fcar = 12.5e12 * (C/pars.C0) / 10 ;%%%% carbonate sink flux
Fcar = 12e12 ;%%%% carbonate sink flux*2
% Fcar = 37.5e12 * (C/pars.C0) / 10 ;%%%% carbonate sink flux*3
frac = 27 ;%%%% Frac factor carbon
```

```
%%%% oxygen-dependent oxidative weathering
Fwoc = 4e12  ;%%%% deduced OC weathering flux
% Fwoc = 16e12 * (OC / pars.OC_0) * ( (O2/pars.O20)^0.5 )  ;%%%%
deduced OC weathering flux*2
% Fwoc = 24e12 * (OC / pars.OC_0) * ( (O2/pars.O20)^0.5 )  ;%%%%
deduced OC weathering flux*3
% Fwoc = 4.5e12 * (OC / pars.OC_0)   ;%%%% deduced OC weathering
flux

%%%% no oxygen dependence on pyrite weathering at high O2
% Fwpy = 1e12 * (PY / pars.PY_0) ;
Fwpy = 2e12  ;%%%% PY weathering flux
% Fwpy = 16e12 * (PY / pars.PY_0) * ( (O2/pars.O20)^0.5 ) ;%%%% PY
weathering flux*2
% Fwpy = 24e12 * (PY / pars.PY_0) * ( (O2/pars.O20)^0.5 ) ;%%%% PY
weathering flux*3
% Fwpy = 4.5e12 * (PY / pars.PY_0)  ;%%%% PY weathering flux

%%%%% calculate sulfur fluxes here (mol / yr)
% Fwsulf = 1.0e12 * (GYP / pars.GYP_0);%%%% sulf weathering flux
Fwsulf = 1e12 ;%%%% sulf weathering flux
% Fwsulf = 6e12 ;%%%% sulf weathering flux*2
% Fsulf = 1.0e12 * (S/pars.S0) ;%%%% sulf sink flux
% fracS = 40 ;%%%% Frac factor sulfur present-day at -35
fracS = 40 ;%%%% Frac factor sulfur -50



%%%% assume we know ocean value
d13c_ocean = d13c_input ;
% d13c_ocean = 0.5 ;

% d34s_ocean = d34s_input ;
% d34s_ocean = 20 ;
d34s_ocean = y(11)/y(6) ;


%%%%%%% Organic carbon burial form isotope mass balance calculation
Foc = (1/frac) * ( Fwoc*(d13c_ocean - d13c_oc) +  Fwcar*(d13c_ocean
- d13c_car)  ) ;


%%%% Fpy calculated from organic C burial rate and inverse
relationship with O2 as in COPSE
%%%% assumed not limited by low sulphur concentraiton here or flux
would be very low
% Fpy = 0.48e12 * (Foc/3.2e12) * (pars.O20/O2) ;
Fpy = 0.5 * (Foc)  ;

%%%% sulphate deposition assumed to balance inputs and outputs for
constant S
Fsulf = Fwsulf + Fwpy - Fpy ;


%%%% oxygen production rate (the oxygen reservoir is added below as
dy(12)
O2prod = Foc + 2*Fpy ;

%%%% O2mr mixing ratio
```

```
copsek16 = 3.762 ;
mrO2 = 100 .* ( O2/pars.O20 )  /   ( (O2/pars.O20)  + copsek16 ) ;



%%%% find d13c(in) for paper
d13cin = ( Fwcar.*d13c_car + Fwoc.*d13c_oc ) ./ (Fwcar+Fwoc)

%%%%%%%%%%%%%%%%%%%%%%%%%%%%%%%%%%%%%%%%%%%%%%%%%%%%%%%%%%%%%%%%%%%%%%%%%%%%
%
%%%%%%%%%%%%%%%%%   Reservoir
calculations   %%%%%%%%%%%%%%%%%%%%%%%%
%%%%%%%%%%%%%%%%%%%%%%%%%%%%%%%%%%%%%%%%%%%%%%%%%%%%%%%%%%%%%%%%%%%%%%%%%%%%
%

%%%% Ocean CO32-
dy(1) = Fwoc + Fwcar - Foc - Fcar ;

%%%% Organic carbon
% dy(2) =  Foc - Fwoc ;

%%%% Carbonate
% dy(3) = Fcar - Fwcar ;

%%%% Organic carbon * d13C(organic carbon)
% dy(4) =  Foc*(d13c_ocean - frac) - Fwoc*(d13c_oc) ;

%%%% Carbonate * d13C(carbonate)
% dy(5) =  Fcar*(d13c_ocean) - Fwcar*(d13c_car) ;

%%%% Ocean sulfate
dy(6) = Fwpy + Fwsulf - Fpy - Fsulf ;

%%%% Pyrite reservoir
% dy(7) =  Fpy - Fwpy ;

%%%% Gypsum reservoir
% dy(8) = Fsulf - Fwsulf ;

%%%% Pyrite * d34S(pyrite)
% dy(9) =  Fpy*(d34s_ocean - fracS) - Fwpy*(d34s_py) ;

%%%% Gypsum * d34S(gypsum)
% dy(10) =  Fsulf*(d34s_ocean) - Fwsulf*(d34s_gyp) ;

%%%% Ocean sulphate * d34S(sulphate)
dy(11) = Fwpy*(d34s_py) + Fwsulf*(d34s_gyp) - Fpy*(d34s_ocean -
fracS) - Fsulf*(d34s_ocean) ;

%%%% atmosphere+ocean oxygen moles
dy(12) = Foc - Fwoc + 2*(Fpy - Fwpy) ;



%%%%%%%%%%%%%%%%%%%%%%%%%%%%%%%%%%%%%%%%%%%%%%%%%%%%%%%%%%%%%%%%%%%%%%%%%%%%
%
%%%%%%%%%%%%%%%%%   Save output as
working   %%%%%%%%%%%%%%%%%%%%%%%%
%%%%%%%%%%%%%%%%%%%%%%%%%%%%%%%%%%%%%%%%%%%%%%%%%%%%%%%%%%%%%%%%%%%%%%%%%%%%
%
```

```
%%%%%%% record model dy states while working
workingstate.C(stepnumber,1) = C ;
workingstate.OC(stepnumber,1) = OC ;
workingstate.CAR(stepnumber,1) = CAR ;
workingstate.Fwoc(stepnumber,1) = Fwoc ;
workingstate.Fwcar(stepnumber,1) = Fwcar ;
workingstate.Foc(stepnumber,1) = Foc ;
workingstate.Fcar(stepnumber,1) = Fcar ;
workingstate.d13c_oc(stepnumber,1) = d13c_oc ;
workingstate.d13c_car(stepnumber,1) = d13c_car ;
workingstate.d13c_input(stepnumber,1) = d13c_input ;
workingstate.S(stepnumber,1) = S ;
workingstate.PY(stepnumber,1) = PY ;
workingstate.GYP(stepnumber,1) = GYP ;
workingstate.Fwpy(stepnumber,1) = Fwpy ;
workingstate.Fwsulf(stepnumber,1) = Fwsulf ;
workingstate.Fpy(stepnumber,1) = Fpy ;
workingstate.Fsulf(stepnumber,1) = Fsulf ;
workingstate.d34s_py(stepnumber,1) = d34s_py ;
workingstate.d34s_gyp(stepnumber,1) = d34s_gyp ;
workingstate.d34s_ocean(stepnumber,1) = d34s_ocean ;
workingstate.O2(stepnumber,1) = O2 ;
workingstate.O2prod(stepnumber,1) = O2prod ;
workingstate.mrO2(stepnumber,1) = mrO2 ;

%%%%%%%% record time
workingstate.time(stepnumber,1) = t ;
workingstate.time_myr(stepnumber,1) = t / 1e6 ;

%%%% final action: record current model step
stepnumber = stepnumber + 1 ;


end
```

```
%%%%%% Simple ODE solver for Matlab
%%%%%% Tianchen He 2017

%%%%%%%%%%%%%%%%%%%%%%%%%%%%%%%%%%%%%%%%%%%%%%%%%%%%%%%%%%%%%%%%%%%%%%%%%%%
%
%%%%%%%%%%%%%%%%%   Define
parameters   %%%%%%%%%%%%%%%%%%%%%%%%%%%%%
%%%%%%%%%%%%%%%%%%%%%%%%%%%%%%%%%%%%%%%%%%%%%%%%%%%%%%%%%%%%%%%%%%%%%%%%%%%
%
clear all

%%%%%%% set up global structures
global stepnumber
global pars
global workingstate
global data

%%%% The below are present day values to set the system against
%%%% They should not be altered (to decrease sulphate concentration
for example)
%%%% Altering the model sulphate concentration for the Cambrian
should be done below in "model start state"

%%%%%% model parameters carbon cycle
pars.C0 = 3.3e18 ; %%%% present day mols of CO32- in ocean
pars.OC_0 = 13e20 ;%%%% present day mols of OC in sediment
pars.CAR_0 = 52e20 ;%%%% present day mols of CAR in sediment


%%%% Din -8
% pars.d13c_oc_0 = -28.25;%%%% initial value of the calculated
d13c_oc
% pars.d13c_car_0 = -1.25 ;%%%% initial value of the analysed
d13c_car

%%%% Din -5.5
% pars.d13c_oc_0 = -25.8 ;%%%% initial value of the calculated
d13c_oc
% pars.d13c_car_0 = 1.2 ;%%%% initial value of the analysed d13c_car


%%% AVERAGE (-6.75)
pars.d13c_oc_0 = -27;%%%% initial value of the calculated d13c_oc
pars.d13c_car_0 = 0.01 ;%%%% initial value of the analysed d13c_car


%%%%%% model parameters sulphur cycle
% pars.S0 = 42e16 ; %%%% present day mols of sulphate in ocean / 100
pars.S0 = 42e18 ; %%%% present day mols of sulphate in ocean
pars.PY_0 = 2e20 ;%%%% present day mols of pyrite in sediment
pars.GYP_0 = 2e20 ;%%%% present day mols of gypsum in sediment
pars.d34s_py_0 = -10 ;%%%% initial value of the calculated d34s_py
pars.d34s_gyp_0 = 30 ;%%%% initial value of the analysed d34s_cas
pars.d34s_ocean_0 = 30 ;%%%% initial value of the analysed d34s_cas


pars.O20 = 3.7e19 ; %%%% present day O2 moles

%%%%%%%%%%%%%%%%%%%%%%%%%%%%%%%%%%%%%%%%%%%%%%%%%%%%%%%%%%%%%%%%%%%%%%%%%%%
%
```

```
%%%%%%%%%%%%%%%%%   Load
Data   %%%%%%%%%%%%%%%%%%%%%%%%%%%%%%%%%%
%%%%%%%%%%%%%%%%%%%%%%%%%%%%%%%%%%%%%%%%%%%%%%%%%%%%%%%%%%%%%%%%%%%%%%%%%%%%
%

%%%% e.g. an excel file of d13C data
data.d13c_data = xlsread('cmodel.xlsx') ;

%%%% e.g. an excel file of d34S data
data.d34s_data = xlsread('smodel.xlsx') ;
data.d34s_time = data.d34s_data(:,1) .* -1 ; %%%% Myr
data.d34s_value = data.d34s_data(:,2) ;

%%%%%%%%%%%%%%%%%%%%%%%%%%%%%%%%%%%%%%%%%%%%%%%%%%%%%%%%%%%%%%%%%%%%%%%%%%%%
%
%%%%%%%%%%%%%%%%%   Initialise   %%%%%%%%%%%%%%%%%%%%%%%%%%%%%%%%%%%%%%%%%
%
%%%%%%%%%%%%%%%%%%%%%%%%%%%%%%%%%%%%%%%%%%%%%%%%%%%%%%%%%%%%%%%%%%%%%%%%%%%%
%

%%%%%%% set maximum step size for solver
options = odeset('maxstep',1e4) ;

%%%% run beginning
fprintf('Beginning run: \n')

%%%% set stepnumber to 1
stepnumber = 1 ;

%%%%%%% model timeframe in years (0 = present day)
pars.whenstart = -524.5e6 ;
pars.whenend = -516e6 ;

%%%% model start state
pars.startstate(1) = pars.C0 * 10 ; %%% assumed high
atmosphere/ocean CO2
pars.startstate(2) = pars.OC_0;
pars.startstate(3) = pars.CAR_0;
pars.startstate(4) = pars.startstate(2)*pars.d13c_oc_0;
pars.startstate(5) = pars.startstate(3)*pars.d13c_car_0;

%%%% Here is where you change the model sulphate concentration
% pars.startstate(6) = pars.S0 * 0.01 ; %%% 1%
pars.startstate(6) = pars.S0 * 0.0345 ; %%% 1mM
% pars.startstate(6) = pars.S0 * 0.025 ; %%% 0.7mM
% pars.startstate(6) = pars.S0 * 0.05 ; %%% 1.4mM
% pars.startstate(6) = pars.S0 * 0.1 ; %%% 2.8mM
% pars.startstate(6) = pars.S0 * 0.155 ; %%% 5.6mMmM
% pars.startstate(6) = pars.S0 * 0.2 ; %%% 5.6mMmM
% pars.startstate(6) = pars.S0 * 0.5 ; %%% 14mMmM

pars.startstate(7) = pars.PY_0 * 3 ;
pars.startstate(8) = pars.GYP_0 * 0.1 ; %%%% assumed less evaporites
pars.startstate(9) = pars.startstate(7)*pars.d34s_py_0;
pars.startstate(10) = pars.startstate(8)*pars.d34s_gyp_0;
pars.startstate(11) = pars.startstate(6)*pars.d34s_ocean_0;

%%%% Also change the starting O2 level
pars.startstate(12) = pars.O20 * 0.25 ; %%% assumed low oxygen
(0.25PAL)
```

```
%%%%%%% run the system
[rawoutput.T,rawoutput.Y] = ode15s(@Equations,[pars.whenstart
pars.whenend],pars.startstate,options);

%%%%% start time counter
tic




%%%%%%%%%%%%%%%%%%%%%%%%%%%%%%%%%%%%%%%%%%%%%%%%%%%%%%%%%%%%%%%%%%%%%%%%%%%%
%
%%%%%%%%%%%%%%%%%   Postprocessing   %%%%%%%%%%%%%%%%%%%%%%%%%%%%%%%%
%
%%%%%%%%%%%%%%%%%%%%%%%%%%%%%%%%%%%%%%%%%%%%%%%%%%%%%%%%%%%%%%%%%%%%%%%%%%%%
%
%%%%%%%%%%%%%%%%% dont mess with
this! %%%%%%%%%%%%%%%%%%%%%%%%%%%%%%
%%%%%% takes 'workingstate' from model and turns into
'state' %%%%%%%

%%%% size of output
pars.output_length = length(rawoutput.T) ;
%%%%%%%%%% model finished output to screen
fprintf('Integration finished \t') ; fprintf('Total steps: %d \t' ,
stepnumber ) ; fprintf('Output steps: %d \n' , pars.output_length )
toc

%%%%%%%%% print final model states using final state for each
timepoint
%%%%%%%%% during integration
fprintf('assembling state vectors... \t')
tic

for u = 1:pars.output_length

    %%%%% for each T value find accompanying diagnostic values
    trecords = find( workingstate.time == rawoutput.T(u) ) ;
    %%%%% take final model step for this timestep
    finalrecord = max(trecords) ;

    %%%%%% assemble output state vectors
    field_names = fieldnames(workingstate) ;
    for numfields = 1:length(field_names)
        eval([' state.' char( field_names(numfields) ) '(u,1) =
workingstate.' char( field_names(numfields) ) '(finalrecord) ; '])
    end
end
%%%%%% done message
fprintf('Done: ')
endtime = toc ;
fprintf('time (s): %d \n', endtime )
```

```
%%%%%%%%%%%%%%%%%%%%%%%%%%%%%%%%%%%%%%%%%%%%%%%%%%%%%%%%%%%%%%%%%%%%%%%%%%%%
%
%%%%%%%%%%%%%%%%%   Plotting
script   %%%%%%%%%%%%%%%%%%%%%%%%%%%%%%
%%%%%%%%%%%%%%%%%%%%%%%%%%%%%%%%%%%%%%%%%%%%%%%%%%%%%%%%%%%%%%%%%%%%%%%%%%%%
%

%%%% make one figure for everything, use subplots for each plot
figure

%%% first subplot
subplot(4,4,1)
hold on
box on
plot(state.time_myr,state.C)
xlabel('Time (Ma)')
ylabel('C (mol)')


%%% sec subplot
subplot(4,4,2)
hold on
box on
plot(state.time_myr,state.OC)
xlabel('Time (Ma)')
ylabel('OC')

%%% third subplot
subplot(4,4,3)
hold on
box on
plot(state.time_myr,state.CAR)
xlabel('Time (Ma)')
ylabel('CAR')

%%% fourth subplot
subplot(4,4,4)
hold on
box on
plot(state.time_myr,state.Fwoc,'r')
hold on
plot(state.time_myr,state.Foc,'b')
xlabel('Time (Ma)')
ylabel('OC fluxes')

%%% fifth subplot
subplot(4,4,5)
hold on
box on
plot(state.time_myr,state.Fwcar,'r')
hold on
plot(state.time_myr,state.Fcar,'b')
xlabel('Time (Ma)')
ylabel('CAR fluxes')

%%% sixth subplot
subplot(4,4,6)
hold on
box on
```

```
plot(state.time_myr,state.d13c_oc,'r')
hold on
plot(state.time_myr,state.d13c_car,'b')
xlabel('Time (Ma)')
ylabel('d13C values')

%%% seventh subplot
subplot(4,4,7)
hold on
box on
plot(state.time_myr,state.S)
xlabel('Time (Ma)')
ylabel('S (mol)')


%% eighth subplot
subplot(4,4,8)
hold on
box on
plot(state.time_myr,state.PY)
xlabel('Time (Ma)')
ylabel('PY')

%%% nineth subplot
subplot(4,4,9)
hold on
box on
plot(state.time_myr,state.GYP)
xlabel('Time (Ma)')
ylabel('GYP')

%%% tenth subplot
subplot(4,4,10)
hold on
box on
plot(state.time_myr,state.Fwpy,'r')
hold on
plot(state.time_myr,state.Fpy,'b')
xlabel('Time (Ma)')
ylabel('PY fluxes')

%%% eleventh subplot
subplot(4,4,11)
hold on
box on
plot(state.time_myr,state.Fwsulf,'r')
hold on
plot(state.time_myr,state.Fsulf,'b')
xlabel('Time (Ma)')
ylabel('GYP fluxes')

%%% twelve subplot
subplot(4,4,12)
hold on
box on
plot(state.time_myr,state.d34s_py,'r')
hold on
plot(state.time_myr,state.d34s_gyp,'b')
xlabel('Time (Ma)')
ylabel('d34S values')
```

```
%%%% thirteenth subplot
subplot(4,4,13)
hold on
box on
plot(data.d34s_time,data.d34s_value,'b')
hold on
plot(state.time_myr,state.d34s_ocean,'r')
xlabel('Time (Ma)')
ylabel('d34S values')

%%% 14th subplot
subplot(4,4,14)
hold on
box on
plot(state.time_myr,state.O2,'r')
xlabel('Time (Ma)')
ylabel('O2 (mol)')

%%%% 15th subplot
subplot(4,4,15)
hold on
box on
plot(state.time_myr,state.O2prod,'r')
xlabel('Time (Ma)')
ylabel('O2 production (mol/yr)')

%%%% 16th subplot
subplot(4,4,16)
hold on
box on
plot(state.time_myr,state.mrO2,'k')
xlabel('Time (Ma)')
ylabel('O2 (%)')

%%%%%%%%%%%%%%%%%%%%%%%%%%%%%%%%%%%%%%%%%%%%%%%%%%%%%%%%%%%%%%%%%%%%%%%%%%%%
%
%%%%%%%%%%%%%%%%%   Cleanup
workspace   %%%%%%%%%%%%%%%%%%%%%%%%%%%%%%
%%%%%%%%%%%%%%%%%%%%%%%%%%%%%%%%%%%%%%%%%%%%%%%%%%%%%%%%%%%%%%%%%%%%%%%%%%%%
%

%%%% delete parameters you dont need here
clear u
clear trecords
clear stepnumber
clear numfields
clear finalrecords
clear endtime
clear finalrecord
```

Appendix H

Author's publications arising from the thesis

Tianchen He, Ying Zhou, Pieter Vermeesch, Martin Rittner, Lanyun Miao, Maoyan Zhu, Andrew Carter, Philip A. E. Pogge Von Strandmann, Graham A. Shields: *Measuring the 'Great Unconformity' on the North China Craton using new detrital zircon age data*. Geological Society, London, Special Publications 2016; 448., DOI:10.1144/SP448.14

Rosalie Tostevin, **Tianchen He**, Alexandra V Turchyn, Rachel A Wood, Amelia M Penny, Fred Bowyer, Gilad Antler, Graham A Shields: *Constraints on the late Ediacaran sulfur cycle from carbonate associated sulfate*. Precambrian Research 01/2017; 290., DOI:10.1016/j.precamres.2017.01.004

In preparation:

Tianchen He, Maoyan Zhu, Benjamin J. W. Mills, Peter M. Wynn, Andrey Yu. Zhuravlev, Aihua Yang, Rosalie Tostevin, Graham A. Shields: *Extreme redox oscillations due to coupling of the marine sulphur and carbon cycles during the Cambrian Explosion*.

Tianchen He, Benjamin J. W. Mills, Peter M. Wynn, Graham A. Shields: *Constraints on the Cambrian Stage 2 marine sulphur cycle from carbonate-associated sulphate*.

Tianchen He, Matthew F. Thirlwall, Benjamin J. W. Mills, Maoyan Zhu, Christina J. Manning, Philip A. E. Pogge Von Strandmann, Ying Zhou, Graham A. Shields: *Strontium isotope evidence for high continental weathering flux during the Cambrian radiation of animals*.